EMERGING INFECTIOUS DISEASES®

CDC
Centers for Disease Control and Prevention

World TB Day

March 2023

Felix-Joseph Barrias (1822–1907), ***Death of Chopin***, 1885. Oil on canvas. 43.3 in × 51.6 in/ 110 cm × 131 cm. The National Museum in Krakow, Poland. Muzeum Narodowe w Krakowie, digital collection (mnk.pl)

EMERGING INFECTIOUS DISEASES®

Emerging Infectious Diseases is published monthly by the Centers for Disease Control and Prevention, 1600 Clifton Rd NE, Mailstop H16-2, Atlanta, GA 30329-4027, USA. Telephone 404-639-1960; email, eideditor@cdc.gov

EMERGING INFECTIOUS DISEASES®

World TB Day **March 2023**

On the Cover

Félix-Joseph Barrias (1822–1907), *Death of Chopin*, 1885. Oil on canvas. 43.3 in × 51.6 in/110 cm × 131 cm. The National Museum in Krakow, Poland. Muzeum Narodowe w Krakowie, digital collection (https://mnk.pl)

About the Cover p. 674

Synopses

Medscape EDUCATION ACTIVITY

***Bartonella* spp. Infections Identified by Molecular Methods, United States**
Molecular diagnostic testing can identify these pathogens, including uncommon and previously undescribed species.
D.W. McCormick et al. **467**

Risk for Prison-to-Community Tuberculosis Transmission, Thailand, 2017–2020
R. Miyahara et al. **477**

Multicenter Retrospective Study of Vascular Infections and Endocarditis Caused by *Campylobacter* spp., France
C. Tinévez et al. **484**

Yellow Fever Vaccine–Associated Viscerotropic Disease among Siblings, São Paulo State, Brazil
E.G. Fernandes et al. **493**

Research

COVID-19 Test Allocation Strategy to Mitigate SARS-CoV-2 Infections across School Districts
R. Pasco et al. **501**

Using Discarded Facial Tissues to Monitor and Diagnose Viral Respiratory Infections
G. Lagathu et al. **511**

Postacute Sequelae of SARS-CoV-2 in University Setting
M. Landry et al. **519**

Medscape EDUCATION ACTIVITY

Clonal Expansion of Multidrug-Resistant *Streptococcus dysgalactiae* Subspecies *equisimilis* Causing Bacteremia, Japan, 2005–2021
Clones with acquired Tn916-like integrative conjugative elements are associated with increased prevalence.
K. Shinohara et al. **528**

Associations of *Anaplasma phagocytophilum* Bacteria Variants in *Ixodes scapularis* Ticks and Humans, New York, USA
M. Prusinski et al. **540**

Prevalence of *Mycobacterium tuberculosis* Complex among Wild Rhesus Macaques and 2 Subspecies of Long-Tailed Macaques, Thailand, 2018–2022
S. Meesawat et al. **551**

Increase in Colorado Tick Fever Virus Disease Cases and Effect of COVID-19 Pandemic on Behaviors and Testing Practices, Montana, 2020
R.A. Soto et al. **561**

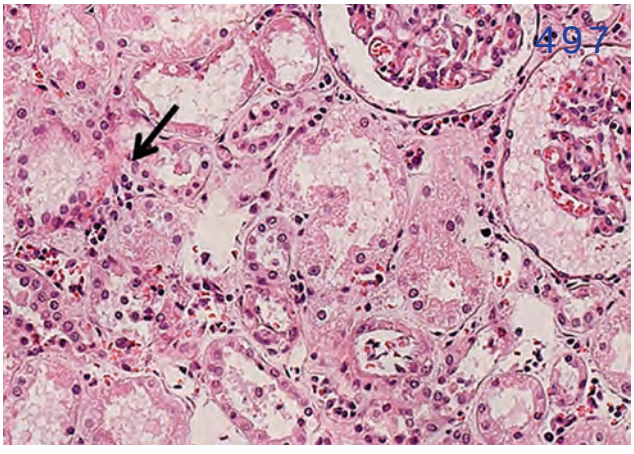

Comparative Effectiveness of COVID-19 Vaccines in Preventing Infections and Disease Progression from SARS-CoV-2 Omicron BA.5 and BA.2, Portugal
I. Kislaya et al. **569**

Clonal Dissemination of Antifungal-Resistant *Candida haemulonii*, China
X. Chen et al. **576**

Dispatches

Extended Viral Shedding of MERS-CoV Clade B Virus in Llamas Compared with African Clade C Strain
J. Rodon et al. **585**

Seroprevalence of Specific SARS-CoV-2 Antibodies during Omicron BA.5 Wave, Portugal, April–June 2022
I. Kislaya et al. **590**

SARS-CoV-2 Incubation Period during the Omicron BA.5–Dominant Period in Japan
T. Ogata, H. Tanaka **595**

EMERGING INFECTIOUS DISEASES®
March 2023

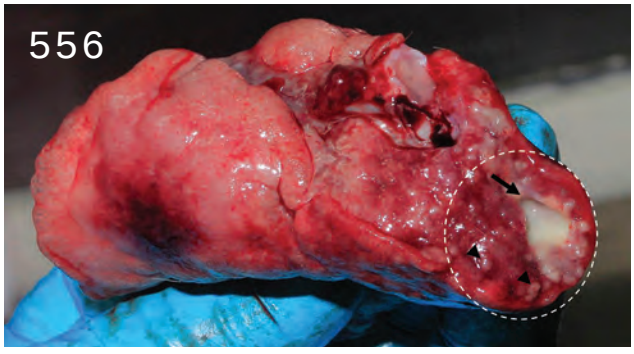

Risk Factors for Reinfection with SARS-CoV-2 Omicron Variant among Previously Infected Frontline Workers
K.D. Ellingson et al. **599**

Correlation of High Seawater Temperature with *Vibrio* and *Shewanella* Infections, Denmark, 2010–2018
Y.M.G. Hounmanou et al. **605**

Tuberculosis Preventive Therapy among Persons Living with HIV, Uganda, 2016–2022
D. Lukoye et al. **609**

Nosocomial Severe Fever with Thrombocytopenia Syndrome in Companion Animals, Japan, 2022
H. Mekata et al. **614**

***Burkholderia thailandensis* Isolated from the Environment, United States**
C.M. Hall et al. **618**

***Mycobacterium leprae* in Armadillo Tissues from Museum Collections, United States**
D. Romero-Alvarez et al. **622**

New Detection of Locally Acquired Japanese Encephalitis Virus Using Clinical Metagenomics, New South Wales, Australia
J. Maamary et al. **627**

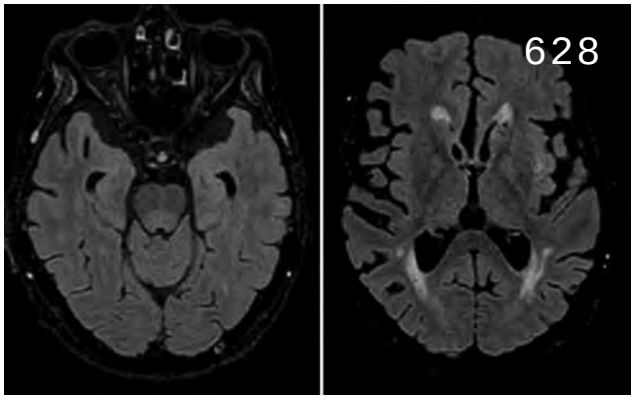

EMERGING INFECTIOUS DISEASES®
March 2023

Reemergence of Lymphocytic Choriomeningitis Mammarenavirus, Germany
C. Mehl et al. **631**

***Emergomyces pasteurianus* in Man Returning to the United States from Liberia and Review of the Literature**
J. Pierce et al. **635**

Research Letters

Recurrent Cellulitis Revealing *Helicobacter cinaedi* in a Patient on Ibrutinib Therapy, France
A.-L. Roupie et al. **640**

***Inquilinus limosus* Bacteremia in Lung Transplant Recipient after SARS-CoV-2 Infection**
E. Farfour et al. **642**

Genomic Analysis of Early Monkeypox Virus Outbreak Strains, Washington, USA
P. Roychoudhury et al. **644**

Sustained Mpox Proctitis with Primary Syphilis and HIV Seroconversion, Australia
R.M. Burdon et al. **647**

Intrahost Monkeypox Virus Genome Variation in Patient with Early Infection, Finland, 2022
H. Vauhkonen et al. **649**

New Postmortem Perspective on Emerging SARS-CoV-2 Variants of Concern, Germany
F. Heinrich et al. **652**

Possible Mpox Protection from Smallpox Vaccine–Generated Antibodies among Older Adults
I. Sanz-Muñoz et al. **656**

SARS-CoV-2 Infection in a Hippopotamus, Hanoi, Vietnam
V.N. Bui et al. **658**

Emergence of *Mycobacterium orygis*–Associated Tuberculosis in Wild Ruminants, India
M. Sharma et al. **661**

SARS-CoV-2 Spillback to Wild Coatis in Sylvatic–Urban Hotspot, Brazil
A.G. Stoffella-Dutra et al. **664**

***Babesia microti* Causing Intravascular Hemolysis in Immunocompetent Child, China**
J. Yao et al. **667**

Tick-Borne Encephalitis in Pregnant Woman and Long-Term Sequelae
A. Velay et al. **669**

Books and Media

Phantom Plague: How Tuberculosis Shaped History
H.M. Blumberg et al. **672**

About the Cover

Ars Longa, Vita Brevis
T. Chorba **674**

Online Report

Interventions to Reduce Risk for Pathogen Spillover and Early Disease Spread to Prevent Outbreaks, Epidemics, and Pandemics
N.M. Vora et al.
https://wwwnc.cdc.gov/eid/article/29/3/22-1079_article

Conference Summary

The 100 Days Mission—2022 Global Pandemic Preparedness Summit
D. Gouglas et al.
https://wwwnc.cdc.gov/eid/article/29/3/22-1142_article

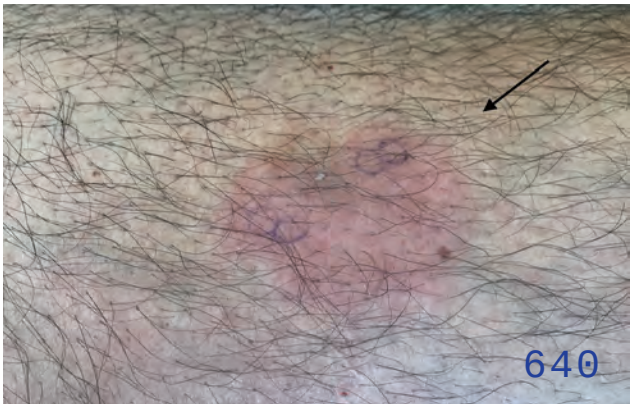

DAVID J. SENCER CDC MUSEUM

History·Legacy·Innovation

Dr. David J. Sencer, Mrs. Mountin and Jim Collins celebrate CDC's 25th anniversary, 1961.

CDC at 75

January 9, 2023–July 28, 2023

TEMPORARY EXHIBITIONS GALLERY

Opening January 9, *CDC at 75* is a commemorative exhibition that tells unique stories about the work of this fabled agency and provides a glimpse into the breadth and depth of CDC's history and vast accomplishments. It features rarely seen objects, documents, and media taken from the CDC Museum's rich collections and archives.

Hours

Monday–Wednesday: 9 a.m.–5 p.m.
Thursday: 9 a.m.–7 p.m.
Friday: 9 a.m.–5 p.m.
Closed weekends and federal holidays

Location

1600 Clifton Road, NE
Atlanta, GA
30329-4021
Phone (404) 639-0830

Admission and parking free • Vehicle inspection required
Government-issued photo ID required for adults over the age of 18
Passport required for non-U.S. citizens

Bartonella spp. Infections Identified by Molecular Methods, United States

David W. McCormick, Sara L. Rassoulian-Barrett, Daniel R. Hoogestraat, Stephen J. Salipante, Dhruba SenGupta, Elizabeth A. Dietrich, Brad T. Cookson, Grace E. Marx,[1] Joshua A. Lieberman[1]

In support of improving patient care, this activity has been planned and implemented by Medscape, LLC and Emerging Infectious Diseases. Medscape, LLC is jointly accredited with commendation by the Accreditation Council for Continuing Medical Education (ACCME), the Accreditation Council for Pharmacy Education (ACPE), and the American Nurses Credentialing Center (ANCC), to provide continuing education for the healthcare team.

Medscape, LLC designates this Journal-based CME activity for a maximum of 1.00 ***AMA PRA Category 1 Credit(s)™***. Physicians should claim only the credit commensurate with the extent of their participation in the activity.

Successful completion of this CME activity, which includes participation in the evaluation component, enables the participant to earn up to 1.0 MOC points in the American Board of Internal Medicine's (ABIM) Maintenance of Certification (MOC) program. Participants will earn MOC points equivalent to the amount of CME credits claimed for the activity. It is the CME activity provider's responsibility to submit participant completion information to ACCME for the purpose of granting ABIM MOC credit.

All other clinicians completing this activity will be issued a certificate of participation. To participate in this journal CME activity: (1) review the learning objectives and author disclosures; (2) study the education content; (3) take the post-test with a 75% minimum passing score and complete the evaluation at http://www.medscape.org/journal/eid; and (4) view/print certificate. For CME questions, see page 677.

Release date: February 22, 2023; Expiration date: February 22, 2024

Learning Objectives

Upon completion of this activity, participants will be able to:

- Assess the microbiologic characteristics of identified bartonellosis cases, based on a series of broad-range and organism-specific molecular assays at a large clinical reference laboratory
- Evaluate demographic and clinical characteristics of patients with bartonellosis, based on a series of broad-range and organism-specific molecular assays at a large clinical reference laboratory
- Determine the clinical implications of the demographic, clinical, and microbiologic characteristics of patients with bartonellosis, based on a series of broad-range and organism-specific molecular assays at a large clinical reference laboratory

CME Editor

Susan Zunino, PhD, Technical Writer/Editor, Emerging Infectious Diseases. *Disclosure: Susan Zunino, PhD, has no relevant financial relationships.*

CME Author

Laurie Barclay, MD, freelance writer and reviewer, Medscape, LLC. *Disclosure: Laurie Barclay, MD, has no relevant financial relationships.*

Authors

David W. McCormick, MD, MPH; Sara L. Rassoulian-Barrett, MS; Daniel R. Hoogestraat, BS, MB(ASCP); Stephen J. Salipante, MD, PhD; Dhruba SenGupta, PhD; Elizabeth A. Dietrich, PhD; Brad T. Cookson, MD, PhD; Grace E. Marx, MD, MPH; Joshua A. Lieberman, MD, PhD.

[1]These senior authors contributed equally to this article.

Molecular methods can enable rapid identification of *Bartonella* spp. infections, which are difficult to diagnose by using culture or serology. We analyzed clinical test results of PCR that targeted bacterial 16S rRNA hypervariable V1–V2 regions only or in parallel with PCR of *Bartonella*-specific *ribC* gene. We identified 430 clinical specimens infected with *Bartonella* spp. from 420 patients in the United States. Median patient age was 37 (range 1–79) years; 62% were male. We identified *B. henselae* in 77%, *B. quintana* in 13%, *B. clarridgeiae* in 1%, *B. vinsonii* in 1%, and *B. washoensis* in 1% of specimens. Eighty-three percent of specimens with *B. quintana* were cardiac specimens; 34% of specimens with *B. henselae* were lymph nodes. We detected novel or uncommon *Bartonella* spp. in 9 patients. Molecular diagnostic testing can identify *Bartonella* spp. infections, including uncommon and undescribed species, and might be particularly useful for patients who have culture-negative endocarditis or lymphadenitis.

Bartonella spp. are fastidious, gram-negative intracellular bacteria that are transmitted to humans by insect vectors. The genus includes 12 species associated with human infection: *B. henselae*, *B. quintana*, *B. bacilliformis*, *B. elizabethae*, *B. vinsonii*, *B. koehlerae*, *B. clarridgieae*, *B. alsatica*, *B. doshiae*, *B. grahamii*, *B. rattimassiliensis*, and *B. tribocorum* (*1*,*2*). Bartonellosis cases are not nationally notifiable in the United States, limiting knowledge of disease epidemiology.

In the United States, *B. henselae* is the most common pathogenic *Bartonella* spp.; ≈12,500 cases of infection and 500 hospitalizations occur annually (*3*). The most common clinical manifestation of *B. henselae* infection is cat-scratch disease (lymphadenopathy and fever after a cat scratch or bite), although infection can also cause hepatic lesions, ocular disease, osteomyelitis, and endocarditis (*4*,*5*). *B. quintana* infection is uncommon and incidence is unknown. Clinically, *B. quintana* infection can manifest as acute febrile illness or subacute endocarditis. *B. quintana* is transmitted by body lice and causes the most frequently reported vectorborne disease among persons experiencing homelessness (PEH); seroprevalence in the PEH population is 5%–15% (*6*–*8*). Manifestations of other *Bartonella* spp. infections are sporadically described in case reports, often as culture-negative endocarditis.

Serology is the diagnostic tool most frequently used to identify *Bartonella* spp. infections. However, serologic diagnosis is complicated by lack of species-specific results, differences in use and interpretation of serologic assays among laboratories, and cross-reactivity with other pathogens, including *Chlamydia* spp. and *Coxiella burnettii* (*9*–*15*), which can lead to misdiagnosis and insufficient treatment. Bacterial cultures of blood or tissue can establish the diagnosis, but sensitivity of cultures is low because of the fastidious nature of *Bartonella* spp. and might result in underdiagnosis of infection. Combining enrichment culture techniques with molecular methods might increase detection of *Bartonella* spp. in blood or other clinical specimens (*16*).

Molecular detection of bacterial pathogens has emerged as an important clinical tool that can increase diagnostic yield compared with culture alone, particularly for detection of fastidious organisms (*17*). *Bartonella* spp. have been detected by using broad-range PCR-based assays that target conserved binding sites flanking regions of the rRNA gene and have species-specific variations (*18*) or by using organism-specific gene targets, such as *gltA* (*19*) and *ribC* (*20*). We describe the demographic, clinical, and microbiologic characteristics of patients with bartonellosis diagnosed by both broad-range and organism-specific molecular assays at a large clinical reference laboratory in Washington, USA.

Materials and Methods

Population

We included information for all patients who had an acceptable clinical specimen submitted to the University of Washington (Seattle, Washington, USA) Molecular Microbiology clinical diagnostic reference laboratory during 2003–2021. Acceptable specimen types were fresh frozen tissue, formalin-fixed paraffin embedded (FFPE) tissues, and body fluids other than blood. To identify *Bartonella* spp., we performed 16S rRNA sequencing by using broad-range PCR primers (PCR-16S) or next-generation sequencing (NGS-16S) or performed a *Bartonella henselae* and *B. quintana* bi-species–targeted PCR (BT-PCR) requested by the ordering clinician.

We evaluated patient information if the specimen had *Bartonella* spp. as the final species assignment, had sufficient material for testing, and was an acceptable specimen type for the assay performed and if the presence of PCR inhibitors was excluded

Author affiliations: Centers for Disease Control and Prevention, Fort Collins, Colorado, USA (D.W. McCormick, E.A. Dietrich, G.E. Marx); University of Washington, Seattle, Washington, USA (S.L. Rassoulian-Barrett, D.R. Hoogestraat, S.J. Salipante, D. SenGupta, B.T. Cookson, J.A. Lieberman)

DOI: https://doi.org/10.3201/eid2902.221223

(inhibitors precluded ruling out *Bartonella* spp.). If a patient had multiple specimens submitted >30 days apart, we included only the information provided with the first positive specimen submission in the analysis. From the specimen submission form, we obtained the patient's sex and age, US state and healthcare facility where the specimen was submitted, specimen collection date, and specimen description (e.g., anatomic location).

Ethics Approval

The study was approved by the University of Washington Institutional Review Board (approval no. STUDY00013877). This study was reviewed in accordance with policies and procedures of the Centers for Disease Control and Prevention and was determined to be exempt from Institutional Review Board requirements.

Molecular Methods for *Bartonella* spp. Identification

The University of Washington Molecular Microbiology laboratory performed all clinical testing pursuant to its high-complexity Clinical Laboratory Improvements Amendments license and College of American Pathologists accreditation. Laboratory-developed processes were validated in accordance with standards set by the Clinical Laboratory Standards Institute and monitored for quality through regular proficiency testing, biannual external inspections by the College of American Pathologists, and incorporation of control reactions as prescribed by the Clinical Laboratory Improvements Amendments.

We performed DNA extraction as previously described for both fresh and FFPE tissue (*21*), except that we also validated and used multiple DNA extraction kits (QIAGEN) in 2021 because of COVID–19-related supply chain disruptions. We performed broad-range PCR amplification of the V1–V2 hypervariable region of the bacterial 16S rRNA gene (PCR-16S) as previously described (18). When sequencing results of 16S PCR products suggested mixed DNA templates, we performed amplicon-based NGS of the V1–V2 16S rRNA locus (NGS-16S) reflexively by using an Illumina Miseq instrument and 250 bp paired-end reads (*22*,*23*). Targeted detection of *Bartonella* spp. by BT-PCR incorporated broad-range 16S primers and 2 primer sets that amplified ribC alleles of *B. quintana* and *B. henselae*. The 16S primers also detect other *Bartonella* spp. but at a higher limit of detection: 100 templates per reaction for other *Bartonella* spp. compared with 5–25 for the *Bartonella* species-specific primers. We sequenced PCR products by using the Sanger method and assigned taxonomic classification after BLAST analysis (*24*) by using both the National Center for Biotechnology Information public databases and a curated database containing type strains and RefSeq (https://www.ncbi.nlm.nih.gov/refseq) records (*21*,*22*). Each case was reviewed by 2 independent certified medical laboratory scientists and a board-certified pathologist (*21*).

Description of Detected *Bartonella* spp.

When available, results from BT-PCR provided specific taxonomic classification of *Bartonella* spp. If BT-PCR results were unavailable, we used results from PCR-16S or NGS-16S. Some 16S rRNA gene V1–V2 sequences lacked sufficient specificity to provide a species-rank classification, either because of close homology to multiple species or lack of homology to any established species. Therefore, we retrospectively analyzed those sequences reported as *Bartonella* spp. by using BLAST to attempt a species-rank classification (defined as 99.7% sequence homology of the V1–V2 sequence). For diagnostic reporting purposes, species with validly published names according to the taxonomic code were identified at the species level in the clinical diagnostic report; otherwise, we identified the genus in accordance with the laboratory's standard operating procedures (Appendix, https://wwwnc.cdc.gov/EID/article/29/3/22-1223-App1.pdf) (*22*,*23*).

Statistical Methods

We used $\chi 2$ tests to compare categorical variables and Mann-Whitney U tests to compare age distributions. For comparisons between patients who had *B. quintana* infections and those who had *B. henselae* infections, we excluded information from patients who had specimen results indicating another *Bartonella* sp. We performed all statistical analyses by using R software version 4.0.3 (*25*).

To examine the proportion of specimens infected with *Bartonella* spp. by year and US state, we only included information for patients who had specimens submitted for BT-PCR. We excluded specimens submitted for PCR-16S that was used to evaluate a diverse array of bacterial pathogens. To calculate percent positivity of BT-PCR results, we collected data on ordering location (US state) and year of specimen submission for all BT-PCR assays, including those in which *Bartonella* spp. was not detected. Similar denominator data for PCR-16S and NGS-16S testing were not available.

Results

We identified 430 clinical specimens from 420 patients that had molecular evidence of *Bartonella* spp.

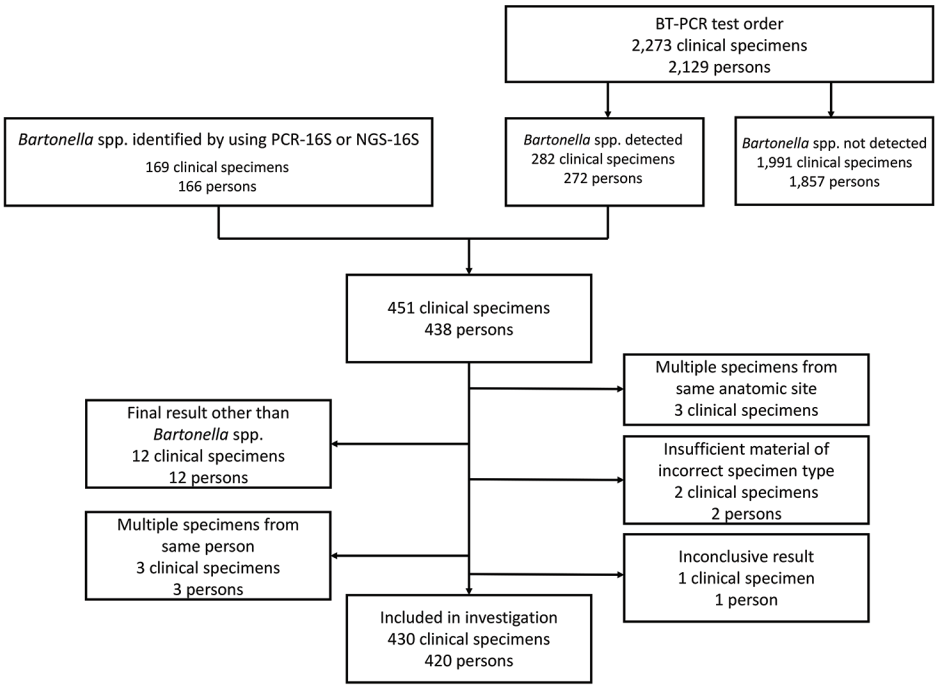

Figure 1. Flow diagram showing clinical specimens included in the analysis in study of *Bartonella* spp. infections identified by molecular methods during 2003–2021 at an academic laboratory in the United States. If a patient had multiple specimens submitted ≥30 days apart, only information from the first *Bartonella*-positive specimen was included. Clinical specimens were tested for *Bartonella* spp. by PCR. A total of 430 specimens from 420 patients were included in the study. BT-PCR, *B. henselae* and *B. quintana* bispecific targeted PCR; NGS-16S, next-generation sequencing of 16S rRNA amplicons; PCR-16S, PCR of 16S rRNA gene followed by Sanger sequencing–based species identification.

infection (Figure 1). We performed molecular testing by using BT-PCR alone on specimens from 149 (35%) patients, PCR-16S alone (no BT-PCR or NGS-16S) on specimens from 143 (34%) patients, reflexive NGS-16S on specimens from 5 (1%) patients for whom PCR-16S detected multiple bacterial DNA templates (precluding identification of *Bartonella* spp.), and both BT-PCR and PCR-16S sequencing on specimens from 121 (28%) patients. We detected *Bartonella* spp. DNA by both BT-PCR and NGS-16S in a specimen from 1 (<1%) patient and by BT-PCR, PCR-16S, and NGS-16S in a specimen from 1 (<1%) patient. We performed species-level identification for 272/272 (100%) specimens on which we performed BT-PCR, 163/265 (62%) specimens on which we performed PCR-16S sequencing, and 5/7 (71%) specimens on which we performed NGS-16S sequencing. Of 2,273 specimens submitted for BT-PCR during 2003–2021, we identified *Bartonella* spp. in 282 (12%) specimens from 272 patients.

We identified *Bartonella* spp. in a higher proportion of specimens submitted as unfixed tissue (187/1,276, 16%) than those submitted as FFPE tissue (97/997, 10%; p = 0.0002). The total number of annual specimens submitted for BT-PCR testing increased over time; an annual median of 18 specimens during 2003–2012 increased to an annual median of 225 during 2013–2021 (Figure 2). Overall, we identified *Bartonella* spp. in 13% (260/1,938) of specimens during 2013–2021; peak detection during this period occurred in 2019, when *Bartonella* spp. were detected in 17% of submitted specimens.

Among the 420 patients with detectable *Bartonella* spp., we identified *B. henselae* in specimens from 338 (80%) patients, *B. quintana* from 54 (13%), *B. clarridgeiae* from 4 (1%), *B. vinsonii* from 2 (1%), and *B. washoensis* (GenBank accession no. ON402466) from 1 (1%). We identified *Bartonella* at the genus level in the remaining 21 (5%) patients; of those, we identified 2 candidate species through subsequent analysis: 1 case of endocarditis caused by *Candidatus* Bartonella mayotimonensis (*19*) (GenBank accession no. ON402516) and a unique 16S sequence (tissue specimen; anatomic site not specified by ordering provider) which might represent a previously undescribed *Bartonella* sp. (GenBank accession no. ON402515) (Appendix Table). Of the 420 patients, 411 (98%) had a single submitted clinical specimen. Among the 9 patients with multiple specimens, only 1 *Bartonella* sp. was identified in each patient.

Among 397 patients who had *Bartonella* spp. detected in ≥1 specimen and available data regarding their sex, 245 (62%) were male (Table 1). A higher proportion of patients who had detectable *B. quintana* (41/50, 82%) were male compared with those who had detectable *B. henselae* (187/321, 58%; p = 0.001). Age at the time of specimen collection was available for 415/420 (99%) patients; median age was

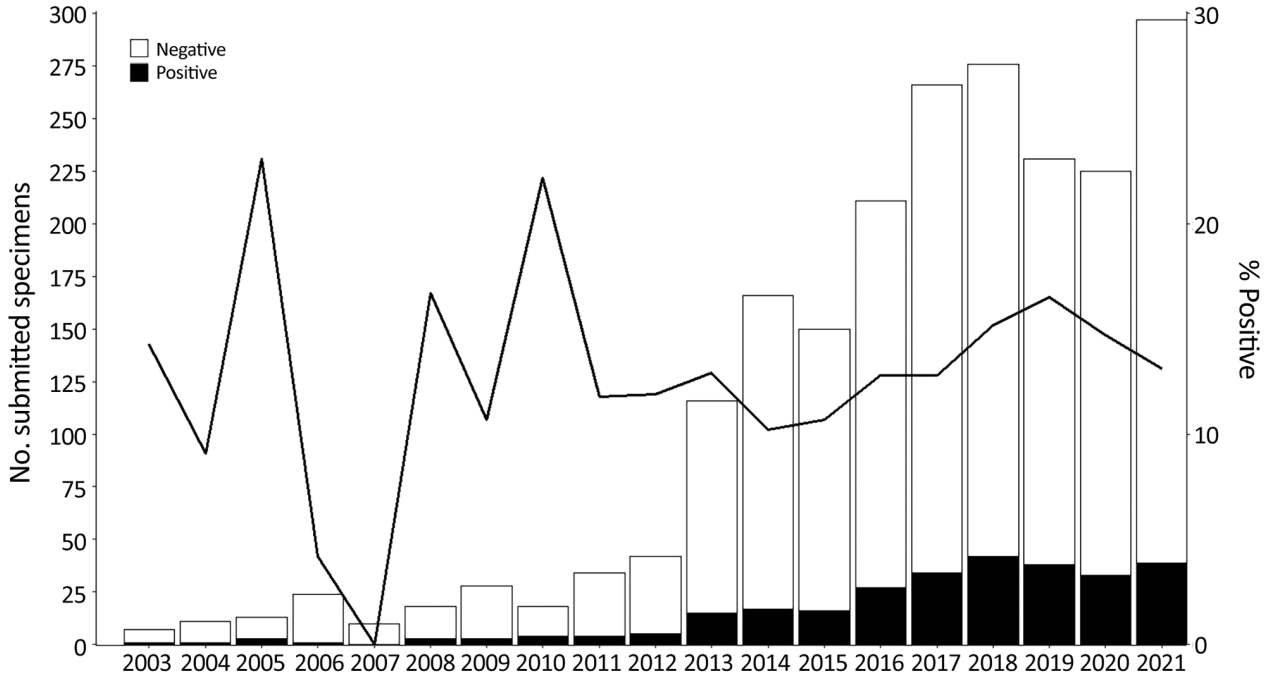

Figure 2. Number and percentage of specimens tested by using *Bartonella*-specific PCR during 2003–2021 in study of *Bartonella* spp. infections identified by molecular methods, United States. A total of 2,273 specimens were submitted for *B. henselae* and *B. quintana* bispecific targeted PCR. Bars indicate total numbers of submitted specimens each year and numbers of *Bartonella*-positive or negative specimens. Line indicates percentage of specimens that were positive for *Bartonella* spp.

37 years (range 1–79 years). Most (235/415, 57%) patients were 18–65 years of age, 134/415 (32%) were <18 years of age, and 45/415 (11%) were ≥65 years of age. Patients who had detectable *B. quintana* in ≥1 specimen (median age 52 years, interquartile range [IQR] 45–60 years) were older than those who had detectable *B. henselae* (median age 32 years, IQR 11–54 years; p<0.0001).

Specimen descriptions were provided for all specimens. The most common specimens submitted were

Table 1. Demographic characteristics and specimen origin for patients who had *Bartonella* spp. detected by PCR in study of *Bartonella* spp. infections identified by molecular methods, United States*

Variable	No. patients†	*B. henselae*, n = 338	*B. quintana*, n = 54	Other *Bartonella* spp.,‡ n = 28
Age, y, median (range)	415	32 (1–79)	52 (9–76)	30 (1–77)
<18	NA	122/335 (36)	2/52 (4)	10/28 (36)
18–65	NA	182/335 (54)	43/52 (83)	11/28 (39)
≥65	NA	31/335 (9)	7/52 (13)	7/28 (25)
Sex	397	NA	NA	NA
M	NA	187/321 (58)	41/50 (82)	17/26 (65)
F	NA	134/321 (42)	9/50 (18)	9/26 (35)
Specimen origin§	361	NA	NA	NA
Texas	48	38/48 (79)	4/48 (8)	6/48 (13)
Washington	46	34/46 (74)	8/46 (17)	4/46 (9)
Ohio	40	36/40 (90)	0/40 (0)	4/40 (10)
California	40	22/40 (55)	16/40 (40)	2/40 (5)
Michigan	30	27/30 (90)	3/30 (10)	0/30 (0)
Florida	27	26/27 (96)	0/27 (0)	1/27 (4)
Oregon	21	17/21 (80)	2/21 (10)	2/21 (10)
Pennsylvania	11	10/11 (91)	0/11 (0)	1/11 (9)
Other¶	NA	78/98 (80)	15/98 (15)	5/98 (5)

*Values are no./total no. (%) unless otherwise indicated. NA, not applicable.
†Total number of patients for each indicated variable.
‡Includes *B. vinsonii* (n = 2), *B. clarridgeiae* (n = 4), *B. washoensis* (n = 1), and *Bartonella* sp. not otherwise specified (n = 21).
§Restricted to states with ≥10 patients who were infected with an identified *Bartonella* spp. to preserve anonymity.
¶Alaska (n = 4), Alabama (n = 5), Arkansas (n = 5), Colorado (n = 5), Connecticut (n = 3), District of Columbia (n = 2), Georgia (n = 5), Hawaii (n = 2), Iowa (n = 3), Idaho (n = 1), Illinois (n = 3), Indiana (n = 6), Kentucky (n = 2), Louisiana (n = 1), Massachusetts (n = 5), Maine (n = 1), Montana (n = 5), Mississippi (n = 1), North Carolina (n = 8), Nebraska (n = 5), New Hampshire (n = 2), New Jersey (n = 1), New York (n = 3), Oklahoma (n = 1), South Carolina (n = 3), Tennessee (n = 5), Utah (n = 1), Virginia (n = 5), and Wisconsin (n = 5).

cardiac (150/430, 35%), lymph node biopsy or aspirate (122/430, 29%), and abscess fluid (38/430, 9%) (Figure 3). We identified *B. quintana* more frequently in cardiac specimens (45/54, 83%) and *B. henselae* more frequently in lymph node specimens (115/338, 34%). We detected *B. henselae* in axillary (29/115, 25%), inguinal (27/115, 23%), and cervical (12/115, 10%) lymph node specimens and in cardiac (82/338, 24%), abscess (35/338, 10%), and liver (14/338, 4%) specimens. We detected *B. washoensis* in 1 lymph node specimen (unspecified anatomic location) and *B. vinsonii* (n = 2) and *B. clarridgeiae* (n = 4) only in cardiac specimens. For patients with *Bartonella* spp. identified in cardiac specimens, the aortic valve (85/140, 61%) was most frequently involved, followed by the mitral valve (23/140, 16%). We detected *Bartonella* spp. in >1 valve from 8 (6%) patients. Of cardiac specimens that had ≥1 valve affected, 105/116 (90%) were from the left side of the heart.

We observed a higher proportion of *Bartonella* spp. in cardiac tissue of male (107/245, 44%) than female (24/152, 16%) patients. However, 57 (38%) female patients had *Bartonella* spp. detected in lymph node specimens compared with 61 (25%) male patients, and 71 (47%) female patients had *Bartonella* spp. detected in other (not cardiac or lymph node) specimen types, compared with 77 (31%) male patients (p<0.0001) (Table 2). For patients <18 years of age, we detected *Bartonella* spp.

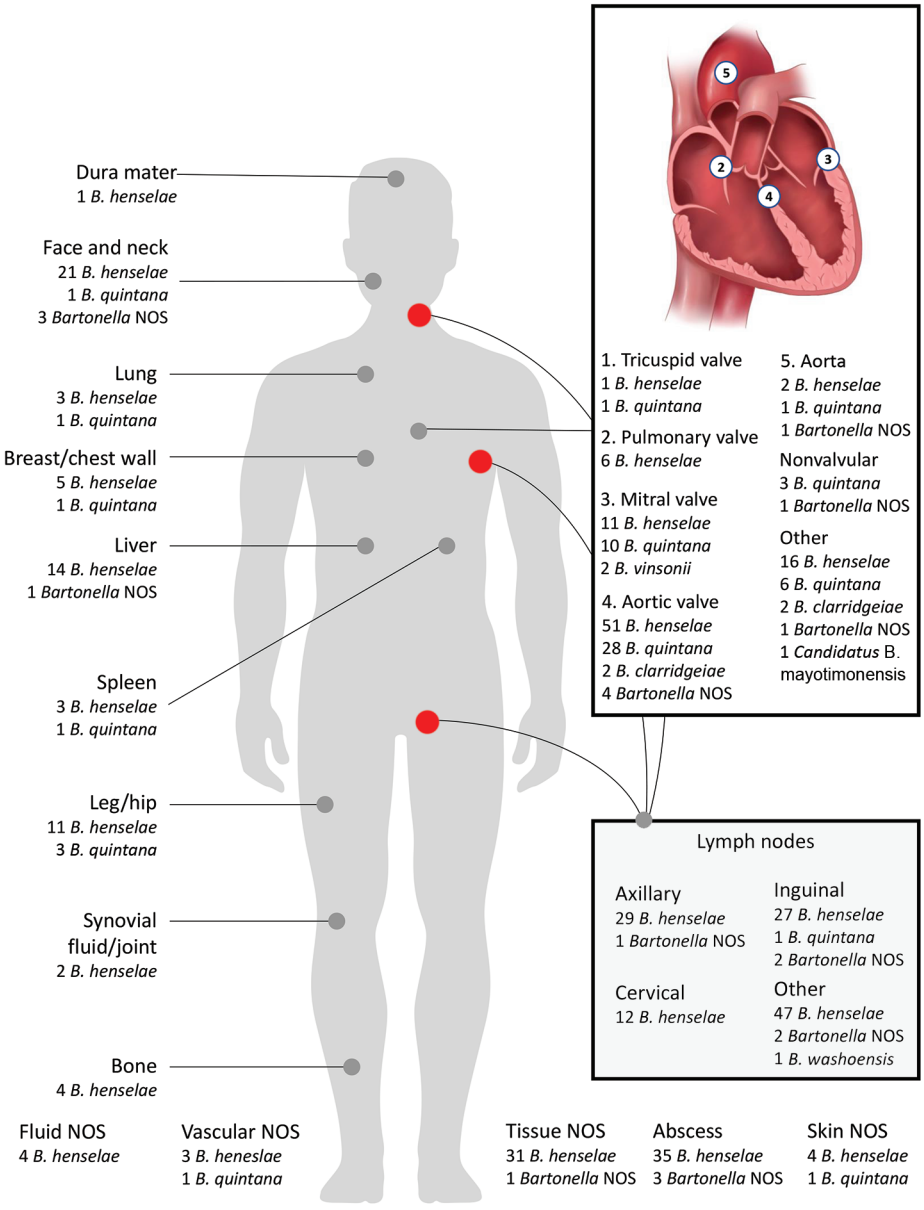

Figure 3. Frequency of *Bartonella* spp. from different anatomic sites identified during 2003–2021 in study of *Bartonella* spp. infections identified by molecular methods, United States. Multiple specimens were submitted for 9 patients. We detected *Bartonella* spp. in both splenic and cardiac specimens from 1 patient, in 2 cardiac specimens each from 7 patients, and in 3 cardiac specimens from 1 patient. If we detected *Bartonella* spp. on multiple valve specimens, those were included in the total count for all involved valves. For the heart valve inset, other sites are cardiac tissue NOS (n = 18), right ventricular outflow tract conduit (n = 3), pacemaker or implantable cardiac device lead (n = 4), and coronary cusp (n = 1). For the lymph node inset, other sites are lymph node NOS (n = 38), supraclavicular (n = 3), submental (n = 2), mesenteric (n = 1), preauricular (n = 1), submandibular (n = 1), epitrochlear (n = 1), jugular (n = 1), iliac (n = 1), and paraspinal (n = 1). NOS, not otherwise specified.

Table 2. Categorical age and sex of infected persons grouped by specimen type in study of *Bartonella* spp. infections identified by molecular methods, United States

Variable	No. (%) specimens			p value†
	Cardiac, n = 140	Lymph node, n = 122	Other,* n = 158	
Age, y				<0.0001
<18, n = 134	5 (4)	52 (39)	77 (57)	
18–65, n = 236	106 (45)	66 (27)	64 (27)	
≥65, n = 45	27 (60)	3 (7)	15 (33)	
Sex				<0.0001
M, n = 245	107 (44)	61 (25)	77 (31)	
F, n = 152	24 (16)	57 (38)	71 (47)	

*Abscess (n = 38), tissue (n = 32), neck/face/arm (n = 25), liver (n = 15), leg/hip (n = 14), breast/chest wall (n = 6), skin (n = 5), lung (n = 4), aorta (n = 2), vascular (n = 2), body fluid NOS (n = 4), bone (n = 4), spleen (n = 4), synovial fluid (n = 2), and dura mater (n = 1).
†By χ^2 test.

more frequently in lymph node (52/134, 39%) or other noncardiac specimen types (77/134, 57%), whereas *Bartonella* spp. was most frequently identified in cardiac specimens from patients who were 18–65 (106/235, 45%) and ≥65 (27/45, 60%) years old (p<0.0001). For patients <18 years of age, *B. henselae* was the most commonly identified species (122/134, 91%).

Information on the origin of specimens was available for 361/420 (86%) patients, representing 36 states and the District of Columbia (Table 1). The states providing the greatest number of specimens were Texas (48/361, 13%) and Washington (46/361, 13%); specimens were provided for ≥10 patients in 8 (22%) states and for <5 patients in 16 states and the District of Columbia (46%). Among states with ≥10 specimens in which we identified *Bartonella* spp., California (16/40, 40%) and Washington (8/46, 17%) had the highest proportion of specimens infected with *B. quintana*; *B. quintana* was not identified in >10% of specimens in any other state.

Discussion

We report 420 cases of bartonellosis in the United States identified by uniform, clinical molecular diagnostic methods at a single reference laboratory during 2003–2021, representing 36 US states and including 140 persons who had endocarditis because of *Bartonella* spp. infections. Those cases highlight the broad clinical spectrum of disease caused by *Bartonella* spp., provide evidence that multiple species can cause bartonellosis, and demonstrate the utility of clinical molecular testing for pathogen identification.

B. henselae was the most frequently identified species causing bartonellosis. Although *B. henselae* was most often detected in lymph node specimens, consistent with cat-scratch disease (*3*), this species was also identified in cardiac specimens, underscoring its potential to cause endocarditis and endovascular disease (*26*). *B. henselae* was also detected in a diverse range of clinical specimens, including liver and bone, indicating the breadth of atypical *B. henselae* infections (*4*,*5*). Although atypical bartonellosis manifestations are rare, ≈25% of pediatric hospitalizations associated with cat-scratch disease are caused by atypical *B. henselae* infections (*27*). A previous study of US insurance claims data found that atypical infections with *B. henselae* accounted for 1.5% of cases; ocular and hepatic lesions were the most common clinical manifestations of atypical *B. henselae* infection (*28*). Overall, *Bartonella* spp. were more frequently found in cardiac specimens in our study, which might reflect the preponderance of certain specimen types submitted for molecular diagnostic tests.

B. quintana was the second most frequently identified species overall and in cardiac specimens, which is consistent with *B. quintana* as a causative agent of subacute endocarditis (*11*,*26*,*29*). California and Washington had the highest proportion of specimens infected with *B. quintana*; a high prevalence of antibodies against *B. quintana* has been described among PEH living in both states (*6*,*7*). Eight states reported ≥10 cases of bartonellosis during the study period, and Texas and Washington reported the highest number of cases. The higher proportion of *B. quintana* infections observed in California and Washington might be from epidemiologic clustering, because *B. quintana* is transmitted by body lice, which can be spread through shared clothing and bedding material, and clusters of *B. quintana* infections have been reported among PEH (*6*,*8*,*30*). The higher number of *B. quintana* infections in California and Washington might reflect geographic differences in the number or type of specimens submitted for molecular testing. Although other studies have reported that *B. henselae* infection is more common in the southeastern region of the United States (*3*,*28*), we did not identify a clear predominance of infections in this region, which might reflect specimen submission patterns. Despite a potential bias from specimen submission patterns, molecular testing methods might identify spatiotemporal clusters of *B. quintana* infections.

Persons who had *B. henselae* infections were younger, and a higher proportion were female compared with those who had *B. quintana* infections. This finding likely reflects the higher incidence of *B. henselae* infection in children, possibly because children might spend more time in close proximity with domesticated cats (*3*). Persons <18 years of age commonly had lymph node or abscess involvement, typical of cat-scratch disease (*5*).

Nearly all patients with endocarditis had left-sided disease, which is consistent with other reports of endocarditis caused by *Bartonella* spp. (*11*,*29*,*31*). We found that *B. henselae* was a more frequent cause of endocarditis in our study than in prior studies that used molecular methods (*26*,*29*). In a study of 685 patients in the United Kingdom who had endocarditis, *B. quintana* was identified in 12/13 cases that had available PCR diagnostic results; *B. henselae* was identified in only 1/13 cases (*29*). A retrospective review of cases using PCR testing on heart valves identified *B. quintana* in 26/45 patients, compared with 19/45 patients who had *B. henselae* infections (*26*). However, the differences observed in our study might be because of differences in sample submission practices; we did not have information from the referring hospitals on the total number of patients with endocarditis caused by *Bartonella* spp. Although previous reviews have recommended the use of serologic testing to diagnose endocarditis caused by *Bartonella* spp. (*31*), our findings, in combination with those of other large studies (*26*,*29*), underscore the improved accuracy of molecular testing methods in obtaining a definitive diagnosis.

We identified 9 patients who had infections from novel or newly emerging *Bartonella* spp., including 2 patients with endocarditis caused by *B. vinsonii* and 4 patients with endocarditis caused by *B. clarridgieae*. Both *B. vinsonii* and *B. clarridgieae* have been reported to cause endocarditis (*20*,*26*,*32*), although only 1 case of endocarditis caused by *B. clarridgieae* infection has been previously reported (*32*); that infection was also confirmed by using molecular methods. We detected *Candidatus* B. mayotimonensis in 1 case of endocarditis, similar to findings for a single case reported previously (*19*). We also detected a case of *B. washoensis* lymphadenitis; this bacterium has been detected in ground squirrels and their fleas and was reported to be the etiologic agent in 2 human cases of myocarditis and meningitis in the United States (*33*) and prosthetic valve endocarditis in a patient in Germany (*34*). We detected a novel 16S rRNA sequence variant of *Bartonella*, most likely representing a previously undescribed species.

Although serology is an important diagnostic method for bartonellosis, case reports have described cross-reactivity of antibodies against *B. clarridgieae*, *B. henselae*, and *B. quintana* (*32*,*35*,*36*) and cross-reactivity between antibodies against *B. vinsonii* and *Coxiella burnetii* (*20*), highlighting the utility of molecular methods for species-specific diagnosis of those pathogens. Because *B. quintana*, *B. henselae*, and other non–*Bartonella* spp. pathogens are often treated with different antimicrobial drugs and for different durations, identification of infecting species can frequently have major effects on treatment, in addition to the epidemiologic value of recognizing novel organisms.

Despite increased specificity of molecular methods compared with serology and potential to detect novel organisms, disparate PCR positivity rates for fresh (16%) and FFPE (8%) tissue specimens highlight how preanalytical factors, such as formalin fixation, can limit assay yield. Other potential factors that can limit sensitivity of molecular methods include specimen selection, organism prevalence, and tissue volume. Formalin fixation damages DNA and can reduce assay sensitivity but has not always reduced positivity rates, perhaps because histopathologic evaluation permits selection of tissue most likely to contain microbial DNA (*21*). In this study, lymph nodes constituted the highest proportion of FFPE specimens. The observed discordant PCR positivity between specimen types might reflect anatomic site of disease, volume of tissue available for PCR, or tissue-specific variations in organism prevalence.

The first limitation of our study is that the analyzed specimens were not representative of all infections caused by *Bartonella* spp. because they represented more severe illness, and submitted specimens were primarily from tissues known to be infected by those pathogens. Second, the specimens did not represent a random sample of persons with bartonellosis; therefore, we could not estimate incidence or perform statistical inference testing. Third, not all geographic regions or states were equally represented, limiting our ability to compare results between different geographic areas. Fourth, we had little information regarding clinical features of the patients from whom specimens were collected, limiting our ability to determine potential risk factors on the basis of medical or social history. Fifth, preanalytical specimen handling can affect diagnostic yield; we could not assess or control variations in storage or transport conditions or tissue processing, such as formalin pH or acid-based decalcification of bone. Sixth, clinical testing might have missed *Bartonella* spp. other than *B. henselae* or *B. quintana* that were

present at levels below the limit of detection for the 16S primers, because the *ribC* primers were designed to increase specificity and sensitivity for detecting *B. henselae* and *B. quintana*. Finally, some specimens might have been misclassified, leading to a higher proportion of specimens categorized as abscesses or tissue if more specific information on anatomic site was not provided on the specimen submission form.

In conclusion, molecular methods provide a powerful diagnostic tool to detect infections caused by *Bartonella* spp. Those methods should be considered for patients who have culture-negative endocarditis or lymphadenitis of unclear etiology, particularly in persons with established risk factors, including exposure to cats or prior homelessness. Broader use of molecular methods in suspected cases of bartonellosis will help elucidate the full clinical spectrum of *Bartonella* infections and increase awareness of this underrecognized pathogen.

Acknowledgments

We thank Mindy Barringer and Alissa Eckert for creating the artwork for Figure 3 and Mary Stewart for helpful discussions on 16S rRNA sequences in *Bartonella* spp.

About the Author

Dr. McCormick is an epidemic intelligence service officer in the Bacterial Diseases Branch, Division of Vector-Borne Diseases, National Center for Emerging and Zoonotic Infectious Diseases, Centers for Disease Control and Prevention, Fort Collins, Colorado, USA. His primary research interests focus on the epidemiology and prevention of vectorborne diseases.

References

1. Cheslock MA, Embers ME. Human bartonellosis: an underappreciated public health problem? Trop Med Infect Dis. 2019;4:69. https://doi.org/10.3390/tropicalmed4020069
2. Krügel M, Król N, Kempf VAJ, Pfeffer M, Obiegala A. Emerging rodent-associated *Bartonella*: a threat for human health? Parasit Vectors. 2022;15:113. https://doi.org/10.1186/s13071-022-05162-5
3. Nelson CA, Saha S, Mead PS. Cat-scratch disease in the United States, 2005–2013. Emerg Infect Dis. 2016;22:1741–6. https://doi.org/10.3201/eid2210.160115
4. Lemos AP, Domingues R, Gouveia C, de Sousa R, Brito MJ. Atypical bartonellosis in children: what do we know? J Paediatr Child Health. 2021;57:653–8. https://doi.org/10.1111/jpc.15304
5. Florin TA, Zaoutis TE, Zaoutis LB. Beyond cat scratch disease: widening spectrum of *Bartonella henselae* infection. Pediatrics. 2008;121:e1413–25. https://doi.org/10.1542/peds.2007-1897
6. Jackson LA, Spach DH, Kippen DA, Sugg NK, Regnery RL, Sayers MH, et al. Seroprevalence to *Bartonella quintana* among patients at a community clinic in downtown Seattle. J Infect Dis. 1996;173:1023–6. https://doi.org/10.1093/infdis/173.4.1023
7. Smith HM, Reporter R, Rood MP, Linscott AJ, Mascola LM, Hogrefe W, et al. Prevalence study of antibody to ratborne pathogens and other agents among patients using a free clinic in downtown Los Angeles. J Infect Dis. 2002;186:1673–6. https://doi.org/10.1086/345377
8. McCormick DW, Rowan SE, Pappert R, Yockey B, Dietrich EA, Petersen JM, et al. *Bartonella* seroreactivity among persons experiencing homelessness during an outbreak of *Bartonella quintana* in Denver, Colorado, 2020. Open Forum Infect Dis. 2021;8:ofab230. https://doi.org/10.1093/ofid/ofab230
9. Spach DH, Koehler JE. *Bartonella*-associated infections. Infect Dis Clin North Am. 1998;12:137–55. https://doi.org/10.1016/S0891-5520(05)70414-1
10. Fournier PE, Mainardi JL, Raoult D. Value of microimmunofluorescence for diagnosis and follow-up of *Bartonella endocarditis*. Clin Diagn Lab Immunol. 2002;9:795–801. https://doi.org/10.1128/cdli.9.4.795-801.2002
11. Fournier PE, Thuny F, Richet H, Lepidi H, Casalta JP, Arzouni JP, et al. Comprehensive diagnostic strategy for blood culture-negative endocarditis: a prospective study of 819 new cases. Clin Infect Dis. 2010;51:131–40. https://doi.org/10.1086/653675
12. Drummond MR, Dos Santos LS, Silva MND, Almeida AR, Diniz PPVP, Angerami R, et al. False negative results in bartonellosis diagnosis. Vector Borne Zoonotic Dis. 2019;19:453–4. https://doi.org/10.1089/vbz.2018.2378
13. Massei F, Messina F, Gori L, Macchia P, Maggiore G. High prevalence of antibodies to *Bartonella henselae* among Italian children without evidence of cat scratch disease. Clin Infect Dis. 2004;38:145–8. https://doi.org/10.1086/379824
14. Okaro U, Addisu A, Casanas B, Anderson B. *Bartonella* species, an emerging cause of blood-culture-negative endocarditis. Clin Microbiol Rev. 2017;30:709–46. https://doi.org/10.1128/CMR.00013-17
15. Vermeulen MJ, Verbakel H, Notermans DW, Reimerink JHJ, Peeters MF. Evaluation of sensitivity, specificity and cross-reactivity in *Bartonella henselae* serology. J Med Microbiol. 2010;59:743–5. https://doi.org/10.1099/jmm.0.015248-0
16. Vaca DJ, Dobler G, Fischer SF, Keller C, Konrad M, von Loewenich FD, et al. Contemporary diagnostics for medically relevant fastidious microorganisms belonging to the genera *Anaplasma, Bartonella, Coxiella, Orientia and Rickettsia*. FEMS Microbiol Rev. 2022;46:fuac013. https://doi.org/10.1093/femsre/fuac013
17. Cummings LA, Hoogestraat DR, Rassoulian-Barrett SL, Rosenthal CA, Salipante SJ, Cookson BT, et al. Comprehensive evaluation of complex polymicrobial specimens using next generation sequencing and standard microbiological culture. Sci Rep. 2020;10:5446. https://doi.org/10.1038/s41598-020-62424-x
18. Lee SA, Plett SK, Luetkemeyer AF, Borgo GM, Ohliger MA, Conrad MB, et al. *Bartonella quintana* aortitis in a man with AIDS, diagnosed by needle biopsy and 16S rRNA gene amplification. J Clin Microbiol. 2015;53:2773–6. https://doi.org/10.1128/JCM.02888-14
19. Lin EY, Tsigrelis C, Baddour LM, Lepidi H, Rolain JM, Patel R, et al. *Candidatus Bartonella mayotimonensis* and endocarditis. Emerg Infect Dis. 2010;16:500–3. https://doi.org/10.3201/eid1603.081673
20. Downey RD, Russo SM, Hauger SB, Murphey DK, Marx G, Huynh T, et al. Identification of an emergent pathogen, *Bartonella vinsonii*, using next-generation sequencing in a patient with culture-negative endocarditis. J Pediatric Infect Dis Soc. 2021;10:213–6. https://doi.org/10.1093/jpids/piaa014

21. Lieberman JA, Bryan A, Mays JA, Stephens K, Kurosawa K, Mathias PC, et al. High clinical impact of broad-range fungal PCR in suspected fungal sinusitis. J Clin Microbiol. 2021;59:e0095521. https://doi.org/10.1128/JCM.00955-21
22. Lieberman JA, Kurosawa K, SenGupta D, Cookson BT, Salipante SJ, Busch D. Identification of *Leptotrichia goodfellowii* infective endocarditis by next-generation sequencing of 16S rDNA amplicons. Cold Spring Harb Mol Case Stud. 2021;7:a005876. https://doi.org/10.1101/mcs.a005876
23. Cummings LA, Kurosawa K, Hoogestraat DR, SenGupta DJ, Candra F, Doyle M, et al. Clinical next generation sequencing outperforms standard microbiological culture for characterizing polymicrobial samples. Clin Chem. 2016; 62:1465–73. https://doi.org/10.1373/clinchem.2016.258806
24. Altschul SF, Gish W, Miller W, Myers EW, Lipman DJ. Basic local alignment search tool. J Mol Biol. 1990;215:403–10. https://doi.org/10.1016/S0022-2836(05)80360-2
25. The R Foundation. The R project for statistical computing, 2020 [cited 2022 Aug 1]. https://www.r-project.org
26. Edouard S, Nabet C, Lepidi H, Fournier PE, Raoult D. *Bartonella*, a common cause of endocarditis: a report on 106 cases and review. J Clin Microbiol. 2015;53:824–9. https://doi.org/10.1128/JCM.02827-14
27. Reynolds MG, Holman RC, Curns AT, O'Reilly M, McQuiston JH, Steiner CA. Epidemiology of cat-scratch disease hospitalizations among children in the United States. Pediatr Infect Dis J. 2005;24:700–4. https://doi.org/10.1097/01.inf.0000172185.01939.fc
28. Nawrocki CC, Max RJ, Marzec NS, Nelson CA. Atypical manifestations of cat-scratch disease, United States, 2005–2014. Emerg Infect Dis. 2020;26:1438–46. https://doi.org/10.3201/eid2607.200034
29. Chaloner GL, Harrison TG, Birtles RJ. *Bartonella* species as a cause of infective endocarditis in the UK. Epidemiol Infect. 2013;141:841–6. https://doi.org/10.1017/S0950268812001185
30. Raoult D, Foucault C, Brouqui P. Infections in the homeless. Lancet Infect Dis. 2001;1:77–84. https://doi.org/10.1016/S1473-3099(01)00062-7
31. Hubers SA, DeSimone DC, Gersh BJ, Anavekar NS. I nfective endocarditis: a contemporary review. Mayo Clin Proc. 2020;95:982–97. https://doi.org/10.1016/j.mayocp.2019.12.008
32. Logan JMJ, Hall JL, Chalker VJ, O'Connell B, Birtles RJ. *Bartonella clarridgeiae* infection in a patient with aortic root abscess and endocarditis. Access Microbiol. 2019;1:e000064. https://doi.org/10.1099/acmi.0.000064
33. Osikowicz LM, Billeter SA, Rizzo MF, Rood MP, Freeman AN, Burns JE, et al. Distribution and diversity of *Bartonella* washoensis strains in ground squirrels from California and their potential link to human cases. Vector Borne Zoonotic Dis. 2016;16:683–90. https://doi.org/10.1089/vbz.2016.2009
34. von Loewenich FD, Seckert C, Dauber E, Kik MJL, de Vries A, Sprong H, et al. Prosthetic valve endocarditis with *Bartonella washoensis* in a human European patient and its detection in red squirrels (Sciurus vulgaris). J Clin Microbiol. 2019;58:e01404-19. https://doi.org/10.1128/JCM.01404-19
35. Margileth AM, Baehren DF. Chest-wall abscess due to cat-scratch disease (CSD) in an adult with antibodies to *Bartonella clarridgeiae*: case report and review of the thoracopulmonary manifestations of CSD. Clin Infect Dis. 1998;27:353–7. https://doi.org/10.1086/514671
36. Kordick DL, Hilyard EJ, Hadfield TL, Wilson KH, Steigerwalt AG, Brenner DJ, et al. *Bartonella clarridgeiae*, a newly recognized zoonotic pathogen causing inoculation papules, fever, and lymphadenopathy (cat scratch disease). J Clin Microbiol. 1997;35:1813–8. https://doi.org/10.1128/jcm.35.7.1813-1818.1997

Address for correspondence: Grace E. Marx, Centers for Disease Control and Prevention, 3156 Rampart Rd, Fort Collins, CO 80521, USA; email: lwx1@cdc.gov

Risk for Prison-to-Community Tuberculosis Transmission, Thailand, 2017–2020

Reiko Miyahara, Pundharika Piboonsiri, Boonchai Chiyasirinroje, Worarat Imsanguan, Supalert Nedsuwan, Hideki Yanai, Katsushi Tokunaga, Prasit Palittapongarnpim, Megan Murray, Surakameth Mahasirimongkol

To determine contributions of previously incarcerated persons to tuberculosis (TB) transmission in the community, we performed a healthcare facility–based cohort study of TB patients in Thailand during 2017–2020. We used whole-genome sequencing of *Mycobacterium tuberculosis* isolates from patients to identify genotypic clusters and assess the association between previous incarceration and TB transmission in the community. We identified 4 large genotype clusters (≥10 TB patients/cluster); 28% (14/50) of the patients in those clusters were formerly incarcerated. Formerly incarcerated TB patients were more likely than nonincarcerated patients to be included in large clusters. TB patients within the large genotype clusters were geographically dispersed throughout Chiang Rai Province. Community TB transmission in the community was associated with the presence of formerly incarcerated individuals in Thailand. To reduce the risk for prison-to-community transmission, we recommend TB screening at the time of entry and exit from prisons and follow-up screening in the community.

Tuberculosis (TB) is a major public health problem in prisons globally. One meta-analysis reported that the incidence of TB among incarcerated persons was 4.1- to 26.9-fold higher than that in the general population (*1*). High levels of TB transmission in prisons have been attributed to crowding (*2*), poorly ventilated facilities (*3*), and lack of access to healthcare (*4*). In addition, several studies have reported a risk for spillover of TB from prisons into communities (*5*) and found that prisons can serve as drivers of population-level incidence (*6*–*8*). Evaluating the risk for TB transmission from prisons to the community is helpful for developing an effective intervention strategy to reduce the risk for spillover to the community.

In Thailand, the TB burden is high (*9*), and the country has the largest inmate population in Southeast Asia (411 inmates/100,000 national population in 2021) (*10*). A previous cross-sectional study conducted in a prison in Bangkok, Thailand, found that 46.5% of the population had latent TB infection diagnosed by tuberculin skin test or interferon-γ release assay (*11*).

Our objective with this study was to identify genotype clusters in the community by using whole-genome sequencing (WGS) data and to assess the contribution of previously incarcerated persons to these transmission clusters. The project was approved by the ethics committees of Chiang Rai Prachanukroh Hospital, Chiang Rai, and the Thai Ministry of Public Health. All TB patients enrolled in the study provided written informed consent.

Methods

Study Population

To evaluate host and pathogen genetic risk factors for TB development and transmission, during December 2017–February 2020, we conducted a healthcare facility–based cohort study in 18 districts in Chiang Rai Province, Thailand. We enrolled persons who had a positive *Mycobacterium tuberculosis* culture, were ≥18 years of age, agreed to participate, provided blood or saliva samples for human DNA extraction, and were HIV negative at the time of TB diagnosis. Trained

Author affiliations: National Institute of Infectious Diseases, Tokyo, Japan (R. Miyahara); National Center for Global Health and Medicine, Tokyo (R. Miyahara, K. Tokunaga); Harvard T.H. Chan School of Public Health, Boston, Massachusetts, USA (R. Miyahara, M. Murray); The University of Tokyo, Tokyo (P. Piboonsiri); Ministry of Public Health, Nonthaburi, Thailand (P. Piboonsiri, S. Mahasirimongkol); TB/HIV Research Foundation, Chiang Rai, Thailand (B. Chiyasirinroje); Chiangrai PrachChanukroh Hospital, Chiang Rai (W. Imsanguan, S. Nedsuwan); Fukujuji Hospital and Research Institute of Tuberculosis, Kiyose, Japan (H. Yanai); National Center Biobank Network, Tokyo (K. Tokunaga): Mahidol University, Bangkok, Thailand (P. Palittapongarnpim); Harvard Medical School, Boston (M. Murray)

DOI: https://doi.org/10.3201/eid2903.221023

research nurses collected baseline demographic and clinical information, including age, sex, ethnicity, date of diagnosis, sputum test results, chest radiograph results, treatment outcome, education level, annual income, and incarceration history (including the year of entry into prison and the duration of incarceration). We did not enroll TB patients who were incarcerated at the time of TB diagnosis.

WGS

We extracted DNA from *M. tuberculosis* culture isolates and then sequenced the whole genomes by using Nextera XT (Illumina, https://www.illumina.com). We applied variant calling methods by using the H37Rv reference genome (GenBank accession no. NC_00962.3) (*12*). We used an in-house Python script to determine the *M. tuberculosis* lineage on the basis of WGS data (*13*). We constructed a phylogenetic tree by using the maximum-likelihood methods in MEGAX (*14*) and visualized the tree with the Interactive Tree of Life (iTOL) online tool, version 6.5.2 (https://itol.embl.de). We also analyzed pairwise single-nucleotide polymorphism (SNP) distances by using MEGA X and the frequency of pairwise SNP distances within sublineages (*12*). We used 2 SNP difference thresholds that have been used internationally to define clusters (*15*–*17*); the main analysis used a 12-SNP cutoff, which enabled inclusion of potentially related isolates, and the secondary analysis used a 5-SNP cutoff to identify highly related isolates. We defined large clusters as those that included >10 isolates linked to ≥1 other isolate by 12 pairwise SNP distances (Figure 1).

Statistical Analyses

For persons for whom we had WGS and incarceration history data, we compared baseline characteristics based on the incarceration status by using χ^2

Figure 1. Phylogenetic tree of patients with pulmonary tuberculosis of *Mycobacterium tuberculosis* lineage in study of risk for prison-to-community tuberculosis transmission, Chiang Rai Province, Thailand, 2017–2020. Scale bar indicates 0.01 substitutions per site SNP, single-nucleotide polymorphism.

tests for categorical variables. We used univariable and multivariable logistic regression models to evaluate the association between incarceration status and the risk for inclusion in a large cluster after adjusting for age, sex, ethnicity, and history of TB treatment. Because the only large clusters were clusters of lineage 2 strains, in the multivariate model adjusting for lineage we included only patients with lineage 2 isolates. We geocoded the patients' addresses at the time of their TB diagnosis and used ArcGIS 10.0 software (Environmental Systems Research Institute, https://www.esri.com) to plot the addresses of patients in the same large clusters on a map. We used the nearest neighbor index (NNI), defined as the ratio of the observed mean distance to the expected mean distance, to assess whether the spatial distribution pattern was random (NNI = 1), dispersed (NNI >1), or clustered (NNI <1) (*18*). We performed statistical analyses by using Stata 16.0 (StataCorp LLC, https://www.stata.com).

Results

A total of 10.1% (n = 60) healthcare facility patients had a history of former incarceration; those persons were more likely than other TB patients to be infected with lineage 2 *M. tuberculosis* strains, unemployed, 40–59 years of age, male, of hill tribe ethnicity, and to have a history of previous TB treatment (Table 1).

TB isolates were classified into 4 lineages: lineage 1 (271 [45.8%]), lineage 2 (236 [39.9%]), lineage 3 (7 [1.2%]), and lineage 4 (78 [13.2%]) (Figure 1). When we used the 12-SNP cutoff, the percentage of clustered cases was 6.6% (18 patients) in lineage 1, 46.2% (109 patients) in lineage 2, and 29.5% (23 patients) in lineage 4 (Appendix Table 1, https://wwwnc.cdc.gov/EID/article/29/3/22-1023-App1.pdf). None of the lineage 3 isolates were clustered. We identified 4 large clusters (≥10 isolates) of strains with 150 (25.3%) isolates by using the 12-SNP cutoff and 1 large cluster with 33 (5.6%) isolates by using the 5-SNP cutoff (Table 2, Figure 1). The percentage of formerly incarcerated persons within the 4 large clusters was 28.0% (n = 14). In the univariate analysis for all lineages, *M. tuberculosis* isolates from previously incarcerated TB patients were 4.19 (95% CI 2.11–8.34-fold) more likely to be members of large clusters. After we adjusted for patient age, ethnicity, sex, and previous TB treatment history, prior incarceration remained associated with inclusion in large clusters (adjusted odds ratio [aOR] 4.47, 95% CI 2.05–9.32) (Table 2). Because the 4 large clusters included only lineage 2 isolates, we restricted our analysis to lineage 2 in the multivariate analysis. The odds ratio for prior incarceration decreased modestly (aOR 3.57, 95% CI 1.56–8.15) among lineage 2 isolates after adjustment for age, ethnicity, sex, and previous TB treatment history. Although there was only 1 large cluster with a cutoff of 5 SNPs, the genomic association with incarceration history was stronger than for persons in the large clusters with a cutoff of 12 SNPs (Appendix Table 2).

The proportion of formerly incarcerated persons in a large cluster with the 12-SNP cutoff ranged from 20.0% through 40.0% (Appendix Table 3). A maximum of 4/14 (28.6%) persons in the large clusters had received a TB diagnosis within 2 years after release. Cluster 3 included the highest percentage of formerly incarcerated persons (40.0%); 3 of the 4 formerly incarcerated patients had been incarcerated during 2014–2018, and TB developed within 2 years after they were released. We found little overlap between the periods of incarceration in clusters 1, 2 and 4. The NNIs were close to 1 or >1 (cluster 1, 1.352; cluster 2, 0.980; cluster 3, 1.350; cluster 4, 1.050), which suggested that the patients in the large clusters were not spatially clustered (Figure 2).

Discussion

Our study found that formerly incarcerated TB patients were 4.7 times more likely than nonincarcerated TB patients to be linked with other patients in large transmission clusters. The association between being in a large cluster and having a previous incarceration history suggests that these genotypes could have circulated in prisons and spread to the community.

The timing of TB diagnosis varied after persons were released from prison. Only 29% of the formerly incarcerated persons in the large clusters received a TB diagnosis within the first 2 years after their release from prison.

Our results suggest that formerly incarcerated persons could be at higher risk for disease progression from latent to active TB for several years after their release from prison. A study from Brazil showed that among 83% of incarcerated persons in whom TB developed, diagnoses were within 2 years of release (*5*), and another study from Brazil estimated that it took 7 years for TB incidence rates among formerly incarcerated persons to decline to community levels (*6*). Because of the long-term risk for active TB development in incarcerated persons after they are released, careful follow-up of such incarcerated persons should be a focus of local public health centers in the community (*19*).

Our study showed that in this setting, formerly incarcerated TB patients were widely distributed

Table 1. Characteristics of nonincarcerated TB patients and formerly incarcerated TB patients, Chiang Rai Province, Thailand, December 2017–February 2020*

Characteristic	Nonincarcerated TB patients, n = 532	Formerly incarcerated TB patients, n = 60	p value
Mycobacterium tuberculosis lineage			0.006
1	256 (48.1)	15 (25.0)	
2	201 (37.8)	35 (58.3)	
3	6 (1.1)	1 (1.7)	
4	69 (13.0)	9 (15.0)	
Age, y			0.047
18–39	101 (19.0)	13 (21.7)	
40–49	99 (18.6)	18 (30.0)	
50-–9	139 (26.1)	17 (28.3)	
≥60	60 (36.3)	12 (20.0)	
Sex			0.001
M	373 (70.1)	54 (90.0)	
F	159 (30.0)	6 (10.0)	
Ethnicity			0.032
Thai	408 (76.7)	37 (61.7)	
Hill tribe	115 (21.6)	15 (36.7)	
Other	9 (1.7)	9 (1.7)	
TB history			0.002
No	508 (95.5)	53 (88.3)	
Yes	24 (4.5)	6 (10.0)	
Unknown	0	1 (1.7)	
Prison year			
Before 1999	NA	11 (18.3)	
2000–2004	NA	5 (8.3)	
2005–2009	NA	15 (25.0)	
2010–2014	NA	16 (26.7)	
After 2015	NA	12 (20.0)	
Unknown	NA	1 (2.9)	
Prison time, y			
<1	NA	35 (58.3)	
1–2	NA	5 (8.3)	
≥2	NA	20 (33.3)	

*NA, not applicable; TB, tuberculosis.

throughout a large geographic area (Figure 2). This result was not consistent with that of a previous study in Lima, Peru, which found higher risk for multidrug-resistant TB among persons living near prisons (*20*). The difference in the spatial distribution of TB observed between the 2 studies is probably associated with the smaller number of more centralized prisons in Chiang Rai than in Lima. Lima has >10 million residents and 7 prisons, and formerly incarcerated persons are likely to reside in areas relatively close to the prisons in which they were incarcerated. In contrast, Chiang Rai Province has only 1.2 million inhabitants dispersed over ≈4,500 square miles and only 2 prisons. In addition, 1 study from Brazil found that prison-related TB genotypes were widely dispersed throughout regions because some inmates were transferred from one prison to another (*21*). With dissemination of the risk for TB infection throughout large areas, it would be challenging to detect links between formerly incarcerated TB patients and community TB patients and to estimate the effect of incarceration history on the community transmission.

Table 2. Association between formerly incarcerated TB patients and *Mycobacterium tuberculosis* genotype clusters, all lineages, Japan, 2022*

Variable	Total	Unclustered	Small cluster, 2–6 cases	Large cluster, ≥10 cases	Unadjusted OR† (95% CI)	Adjusted OR‡ (95% CI)
Cutoff of 5 SNPs						
Total	592	559	22	11		
No history of incarceration	532 (89.9)	508 (91.0)	18 (81.8)	6 (54.6)	Referent	Referent
Formerly incarcerated	60 (10.1)	51 (9.1)	4 (18.2)	5 (45.5)	7.97 (2.36–26.96)	10.32 (2.47–43.09)
Cutoff of 12 SNPs						
Total	592	442	100	50		
No history of incarceration	532 (89.9)	407 (92.1)	89 (89.0)	36 (72.0)	Referent	Referent
Formerly incarcerated	60 (10.1)	35 (7.9)	11 (11.0)	14 (28.0)	4.19 (2.11–8.34)	4.47 (2.05–9.32)

*Values are no. (%) cases except as indicated. OR, odds ratio; SNP, single-nucleotide polymorphism; TB, tuberculosis.
†ORs for the history of incarceration comparing those in large clusters with those unclustered or in small clusters.
‡ORs adjusted for age, ethnicity, sex, and history of TB treatment.

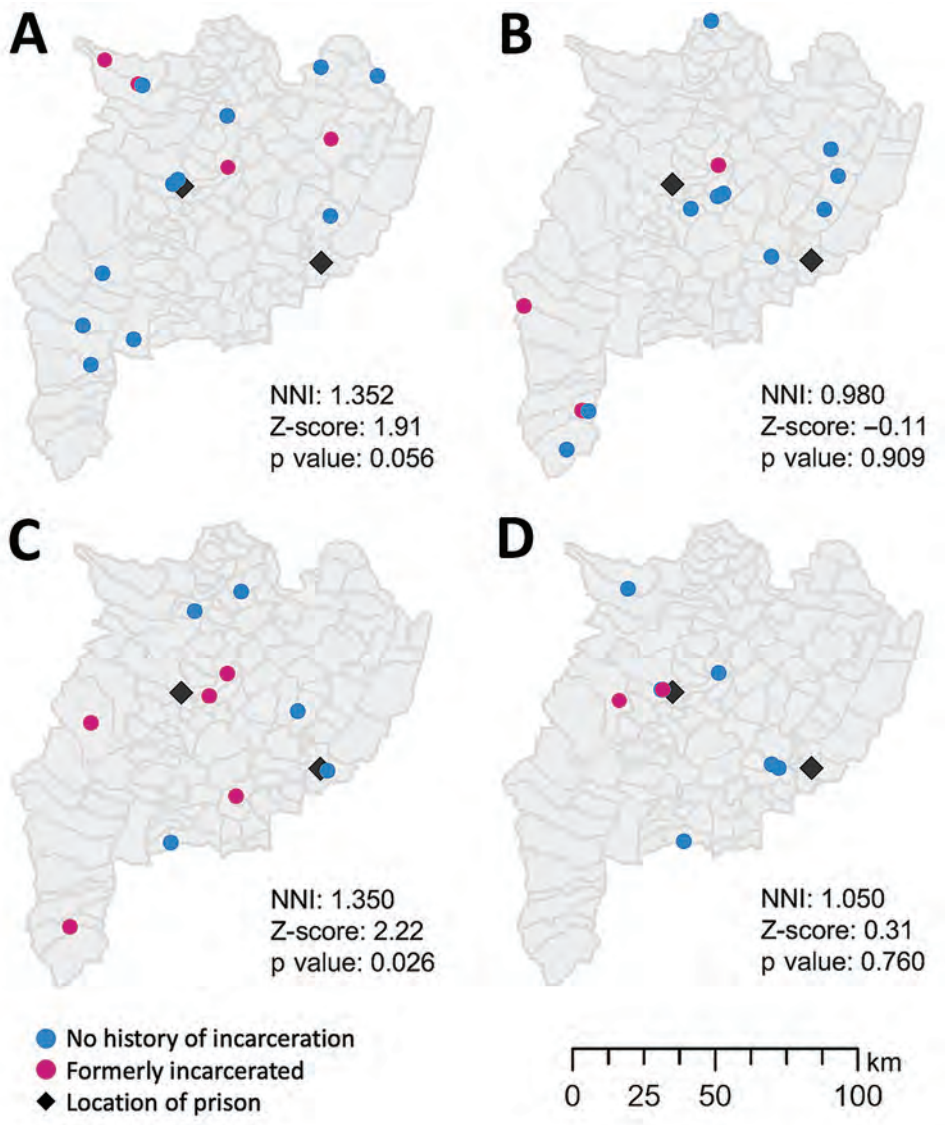

Figure 2. Distribution of clusters of tuberculosis patients in study of risk for prison-to-community tuberculosis transmission, Thailand, 2017–2020. NNI, nearest-neighbor index.

TB control strategies in prisons should focus on not only reducing TB transmission in prison but also on preventing spillover from prison to community. In 2021, the World Health Organization Consolidated Guidelines on Tuberculosis updated the recommendation of systematic screening in prisons from a "conditional recommendation" to a "strong recommendation" but noted that there was "very low certainty of evidence" (*22*). As a recent modeling analysis showed (*6*), combined interventions could reduce TB incidence in prisons and in the general population. Options for preventing TB transmission in prisons include screening at the time of entry into the prison, periodic mass screening of incarcerated persons, or both. To control prison-to-community transmission, exit screening before persons return to their respective residential areas and follow-up testing in the community should also be performed (*6*). Furthermore, although the World Health Organization guidelines conditionally recommend preventive therapy in incarcerated persons depending on resource availability and the local risk for TB (*19*), few countries with low TB burden and high income have implemented preventive therapy programs for incarcerated persons (*23*). To reduce illness and death as well as the risk for TB transmission, the benefits of preventive therapy for incarcerated persons in countries with high TB burden should also be considered (*6*).

Among the limitations of our study, we were not able to establish exact and direct epidemiologic links between incarcerated persons and persons in the general population through contact tracing and are therefore not able to rule out the possibility that formerly

incarcerated persons were infected in the community after release rather than vice versa. In addition, our study did not include all TB patients for whom diagnosis was made at the study site because we excluded patients who did not have culture isolates, who died before we contacted them, and who were co-infected with HIV. Therefore, we missed some links that might have affected the number of clusters, the size of clusters, and the proportion of formerly incarcerated persons in large clusters.

In conclusion, our study determined that large clusters included a high percentage of formerly incarcerated TB patients with variable years of incarceration and residential areas. Because prison-related genotypes are circulating in the community, control strategies such as entry and exit screening at release and follow-up screening in the community should be considered to prevent TB-associated illness and death among incarcerated persons and community transmission.

Acknowledgments

We thank Chiangrai Prachanukroh Hospital, the TB clinics in Chiang Rai Province, and Tuberculosis and HIV Research Foundation for supporting the study.

This study was supported by the Japan Agency for Medical Research and Development/Japan International Cooperation Agency under a Science and Technology Research Partnership for Sustainable Development project (grant no. JP17jm0110010), the Japan Society for the Promotion of Science KAKENHI (grant no. 20K15847), and a Health Research Grant, International Joint Research provided by the Pfizer Health Research Foundation.

About the Author

Dr. Miyahara is a researcher at the Center for Surveillance, Immunization, and Epidemiologic Research, National Institute of Infectious Diseases, Tokyo, Japan. Her primary research interests are the clinical and genetic epidemiology of infectious diseases, including tuberculosis and COVID-19.

Reference

1. Cords O, Martinez L, Warren JL, O'Marr JM, Walter KS, Cohen T, et al. Incidence and prevalence of tuberculosis in incarcerated populations: a systematic review and meta-analysis. Lancet Public Health. 2021;6:e300–8. https://doi.org/10.1016/S2468-2667(21)00025-6
2. Morasert T, Worapas W, Kaewmahit R, Uphala W. Prevalence and risk factors associated with tuberculosis disease in Suratthani Central Prison, Thailand. Int J Tuberc Lung Dis. 2018;22:1203–9. https://doi.org/10.5588/ijtld.17.0654
3. Gebrecherkos T, Gelaw B, Tessema B. Smear positive pulmonary tuberculosis and HIV co-infection in prison settings of North Gondar Zone, Northwest Ethiopia. BMC Public Health. 2016;16:1091. https://doi.org/10.1186/s12889-016-3761-y
4. Rubenstein LS, Amon JJ, McLemore M, Eba P, Dolan K, Lines R, et al. HIV, prisoners, and human rights. Lancet. 2016;388:1202–14. https://doi.org/10.1016/S0140-6736(16)30663-8
5. Sacchi FPC, Praça RM, Tatara MB, Simonsen V, Ferrazoli L, Croda MG, et al. Prisons as reservoir for community transmission of tuberculosis, Brazil. Emerg Infect Dis. 2015;21:452–5. https://doi.org/10.3201/eid2103.140896
6. Mabud TS, de Lourdes Delgado Alves M, Ko AI, Basu S, Walter KS, Cohen T, et al. Evaluating strategies for control of tuberculosis in prisons and prevention of spillover into communities: an observational and modeling study from Brazil. PLoS Med. 2019;16:e1002737. https://doi.org/10.1371/journal.pmed.1002737
7. Basu S, Stuckler D, McKee M. Addressing institutional amplifiers in the dynamics and control of tuberculosis epidemics. Am J Trop Med Hyg. 2011;84:30–7. https://doi.org/10.4269/ajtmh.2011.10-0472
8. Séraphin MN, Didelot X, Nolan DJ, May JR, Khan MSR, Murray ER, et al. Genomic investigation of a *Mycobacterium tuberculosis* outbreak involving prison and community cases in Florida, United States. Am J Trop Med Hyg. 2018;99:867–74. https://doi.org/10.4269/ajtmh.17-0700
9. World Health Organization. Global tuberculosis report 2021 [cited 2022 Sep 14]. https://www.who.int/publications/i/item/9789240037021
10. Institute for Crime and Justice Policy Research, Birbeck University of London. World prison brief data [cited 2022 Sep 14]. https://www.prisonstudies.org/country/thailand
11. Gatechompol S, Harnpariphan W, Supanan R, Suwanpimolkul G, Sophonphan J, Ubolyam S, et al. Prevalence of latent tuberculosis infection and feasibility of TB preventive therapy among Thai prisoners: a cross-sectional study. BMC Public Health. 2021;21:1206. https://doi.org/10.1186/s12889-021-11271-0
12. Disratthakit A, Toyo-Oka L, Thawong P, Paiboonsiri P, Wichukjinda N, Ajawatanawong P, et al. An optimized genomic VCF workflow for precise identification of *Mycobacterium tuberculosis* cluster from cross-platform whole genome sequencing data. Infect Genet Evol. 2020;79:104152. https://doi.org/10.1016/j.meegid.2019.104152
13. Ajawatanawong P, Yanai H, Smittipat N, Disratthakit A, Yamada N, Miyahara R, et al. A novel ancestral Beijing sublineage of *Mycobacterium tuberculosis* suggests the transition site to modern Beijing sublineages. Sci Rep. 2019;9:13718. https://doi.org/10.1038/s41598-019-50078-3
14. Kumar S, Stecher G, Li M, Knyaz C, Tamura K. MEGA X: Molecular Evolutionary Genetics Analysis across computing platforms. Mol Biol Evol. 2018;35:1547–9. https://doi.org/10.1093/molbev/msy096
15. Dale K, Globan M, Horan K, Sherry N, Ballard S, Tay EL, et al. Whole genome sequencing for tuberculosis in Victoria, Australia: a genomic implementation study from 2017 to 2020. Lancet Reg Health West Pac. 2022;28:100556.
16. Walker TM, Lalor MK, Broda A, Ortega LS, Morgan M, Parker L, et al. Assessment of *Mycobacterium tuberculosis* transmission in Oxfordshire, UK, 2007-12, with whole pathogen genome sequences: an observational study. Lancet Respir Med. 2014;2:285–92. https://doi.org/10.1016/S2213-2600(14)70027-X
17. Walker TM, Ip CL, Harrell RH, Evans JT, Kapatai G, Dedicoat MJ, et al. Whole-genome sequencing to delineate

Mycobacterium tuberculosis outbreaks: a retrospective observational study. Lancet Infect Dis. 2013;13:137–46. https://doi.org/10.1016/S1473-3099(12)70277-3
18. Clark PJEF, Evans FC. Distance to nearest neighbor as a measure of spatial relationships in populations. Ecology. 1954;35:445–53. https://doi.org/10.2307/1931034
19. World Health Organization. Prisons and health [cited 2022 Sep 14]. https://apps.who.int/iris/handle/10665/128603
20. Warren JL, Grandjean L, Moore DAJ, Lithgow A, Coronel J, Sheen P, et al. Investigating spillover of multidrug-resistant tuberculosis from a prison: a spatial and molecular epidemiological analysis. BMC Med. 2018;16:122. https://doi.org/10.1186/s12916-018-1111-x
21. Walter KS, Pereira Dos Santos PC, Gonçalves TO, Da Silva BO, Santos ADS, Leite ADC, et al. The role of prisons in disseminating tuberculosis in Brazil: a genomic epidemiology study. Lancet Reg Health Am. 2022;9:100186.
22. World Health Organization. WHO consolidated guidelines on tuberculosis: module 2: screening—systematic screening for tuberculosis disease [cited 2022 Sep 14]. https://www.who.int/publications/i/item/9789240022676
23. Centers for Disease Control and Prevention (CDC); National Center for HIV/AIDS, Viral Hepatitis, STD, and TB Prevention. Prevention and control of tuberculosis in correctional and detention facilities: recommendations from CDC. Endorsed by the Advisory Council for the Elimination of Tuberculosis, the National Commission on Correctional Health Care, and the American Correctional Association. MMWR Recomm Rep. 2006;55(RR-9):1–44.

Address for correspondence: Reiko Miyahara, National Institute of Infectious Diseases, 1-23-1 Toyama, Shinjuku-ku, Tokyo 162-8640, Japan; email: rmiyahara@niid.go.jp

etymologia revisited

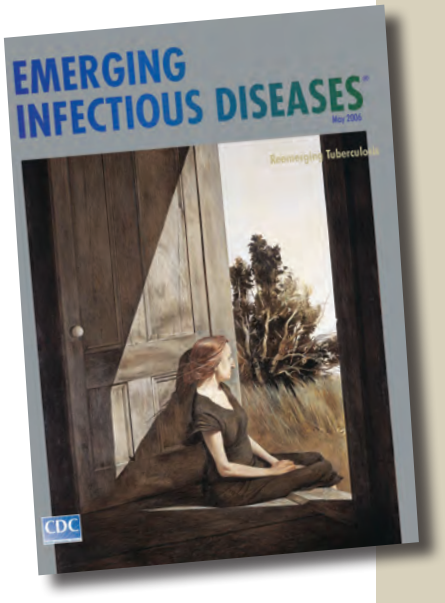

Tuberculosis
[too-ber′′ku-lo′sis]

Any of the infectious diseases of humans or other animals caused by bacteria of the genus *Mycobacterium*. From the Latin *tuberculum*, "small swelling," the diminutive form of *tuber*, "lump." Tuberculosis has existed in humans since antiquity; it is believed to have originated with the first domestication of cattle. Evidence of tuberculosis has been shown in human skeletal remains and mummies from as early as 4000 bc. *Mycobacterium bovis* bacillus Calmette-Guérin has been successfully used to immunize humans since 1921, and treatment (rather than prevention) of tuberculosis has been possible since the introduction of streptomycin in 1946. Hopes of completely eliminating the disease, however, have been diminished since the rise of drug-resistant *M. tuberculosis* strains in the 1980s.

Originally published in May 2006

Source:

Dorland's illustrated medical dictionary. 30th ed. Philadelphia: Saunders; 2003; Merriam-Webster's collegiate dictionary. 11th ed. Springfield (MA): Merriam-Webster Incorporated; 2003; and http://www.wikipedia.org

https://wwwnc.cdc.gov/eid/article/12/5/et-1205_article

Multicenter Retrospective Study of Vascular Infections and Endocarditis Caused by *Campylobacter* spp., France

Claire Tinévez, Philippe Lehours, Anne-Gaëlle Ranc, Yaniss Belaroussi, Fanny Velardo, Damien Dubois, Catherine Neuwirth, Hélène Pailhoriès, Marie Dorel, Genevieve Hery-Arnaud, Olivier Join-Lambert, Emmanuelle Gras, Stéphane Corvec, Cyrielle Codde, Damien Fournier, Hugo Boijout, Violaine Doat, Leslie Bouard, Anne-Sophie Lagneaux, Maxime Pichon, Célia Couzigou, Claire Letellier, Adrien Lemaignen, Emmanuelle Bille, Xavier Bérard, Caroline Caradu, Claire Webster, Didier Neau, Charles Cazanave, Mathilde Puges, for the Campylobacteremia Study Group

The incidence of campylobacteriosis has substantially increased over the past decade, notably in France. Secondary localizations complicating invasive infections are poorly described. We aimed to describe vascular infection or endocarditis caused by *Campylobacter* spp. We included 57 patients from a nationwide 5-year retrospective study on *Campylobacter* spp. bacteremia conducted in France; 44 patients had vascular infections, 12 had endocarditis, and 1 had both conditions. *Campylobacter fetus* was the most frequently involved species (83%). Antibiotic treatment involved a β-lactam monotherapy (54%) or was combined with a fluoroquinolone or an aminoglycoside (44%). The mortality rate was 25%. Relapse occurred in 8% of cases and was associated with delayed initiation of an efficient antimicrobial therapy after the first symptoms, diabetes, and coexistence of an osteoarticular location. Cardiovascular *Campylobacter* spp. infections are associated with a high mortality rate. Systematically searching for those localizations in cases of *C. fetus* bacteremia may be warranted.

Campylobacteriosis is the leading cause of foodborne bacterial gastroenteritis. Its incidence in North America, Europe, and Australia is alarming, and data from Africa, Asia, and the Middle East indicate that campylobacteriosis is endemic in several areas (*1*–*3*). The incidence of campylobacteriosis seems to have increased over recent years but might partially be overestimated because of differences in molecular techniques.

Campylobacter spp. is a gram-negative mobile curved rod. After digestive contamination, it can translocate through the gastrointestinal barrier, leading to

Author affiliations: Centre Hospitalier Universitaire de Bordeaux, Bordeaux, France (C. Tinévez, P. Lehours, Y. Belaroussi, X. Bérard, C. Caradu, D. Neau, C. Cazanave, M. Puges); Centre Hospitalier Universitaire de Lyon, Lyon, France (A.-G. Ranc); Institut National de la Santé et de la Recherche Médicale, Bordeaux (F. Velardo); Centre Hospitalier Universitaire de Toulouse, Toulouse, France (D. Dubois); Centre Hospitalier Universitaire de Dijon, Dijon, France (C. Neuwirth); Centre Hospitalier Universitaire d'Angers, Angers, France (H. Pailhoriès); Centre Hospitalier Universitaire de Rennes, Rennes, France (M. Dorel); Centre Hospitalier Universitaire de Brest, Brest, France (G. Héry-Arnaud); Centre Hospitalier Universitaire de Caen, Caen, France (O. Join-Lambert); Hôpital Européen Georges–Pompidou, Paris, France (E. Gras); Centre Hospitalier Universitaire de Nantes, Nantes, France (S. Corvec); Centre Hospitalier Universitaire de Limoges, Limoges, France (C. Codde); Centre Hospitalier Universitaire de Besançon, Besançon, France (D. Fournier); Centre Hospitalier de Tarbes, Tarbes, France (H. Boijout); Centre Hospitalier Pierre Oudot, Bourguoin-Jallieu, France (V. Doat); Centre Hospitalier Départemental de Vendée, La Roche-Sur-Yon, France (L. Bouard); Centre Hospitalier Universitaire de Nancy, Nancy, France (A.-S. Lagneaux); Centre Hospitalier Universitaire de Poitiers, Poitiers, France (M. Pichon); Centre Hospitalier de Rodez, Rodez, France (C. Couzigou); Centre Hospitalier de Saint-Brieuc, Saint-Brieuc, France (C. Letellier); Centre Hospitalier Universitaire de Tours, Tours, France (A. Lemaignen); Centre Hospitalier de Necker-Enfants Malades, Paris (E. Bille); Imperial College London, London, UK (C. Webster)

DOI: https://doi.org/10.3201/eid2903.221417

bacteremia. This complication is poorly described because of its scarcity, accounting for <1% of *Campylobacter* spp. infections but having substantial mortality rates (3%–28%) (*4*–*6*). Bacteremias can be complicated by secondary localizations in the joints, bones, soft tissues, arterial wall, and valves (*5*,*7*,*8*). Lack of awareness of this risk and a challenging diagnosis caused by tedious culture may be responsible for underdiagnosis.

Vascular infections and endocarditis caused by *Campylobacter* spp. have been poorly described in the literature; therefore, clinical manifestations, treatment, and outcomes remain unclear. Identifying the predisposing underlying conditions for *Campylobacter* spp. vascular infections or endocarditis and recognizing evocative clinical and biologic signs could lead to an earlier effective antibiotic therapy. Our study aimed to describe *Campylobacter* spp.–related vascular infections and endocarditis in France and analyze the factors associated with 3-month mortality rates.

Methods

Study Design and Patients

We conducted an ancillary study from the Campylobacteremia Project (*6*), a multicenter retrospective study conducted in 37 hospitals participating in the surveillance network of France's National Reference Centre for Campylobacters and Helicobacters (NRCCH), along with other hospitals in France. The Campylobacteremia study included all patients with *Campylobacter* spp. bacteremia during January 1, 2015–December 31, 2019. We extracted and analyzed records from patients with vascular localizations or endocarditis for our study. We also included patients with *Campylobacter* spp. identification from a retrospective cohort of vascular infections in Bordeaux University Hospital (BUH; Bordeaux, France) during January 1, 2004–December 31, 2019, excluding patients already included through the NRCCH.

Data Collection

We retrospectively extracted data on demographic characteristics, clinical signs, underlying conditions previously described as risk factors of campylobacteriosis, or cardiovascular infections (*4*–*10*) and medicosurgical treatment from medical records through a standardized questionnaire sent to clinicians and microbiologists. We also extracted microbiologic data, especially identification to species level, results of concomitant stool or any other site culture (e.g., fluid and biopsy), and susceptibility to ampicillin, amoxicillin/clavulanic acid, erythromycin, tetracyclines, gentamicin, fluoroquinolones, and imipenem when tested.

Definitions

We defined endovascular localizations by a positive vascular biopsy, graft, blood culture (or a combination of these) and evocative images on computed tomography, ^{18}F-fluoro-deoxyglucose-positron emission tomography/computed tomography (^{18}F-FDG PET/CT), or leukocyte scan based on the American Heart Association consensus for native infections and Management of Aortic Graft Infection Collaboration (MAGIC) criteria for vascular graft and endograft infections (VGEIs) (*10*,*11*). We defined endocarditis by a positive valvular biopsy, blood culture, or both, associated with evocative images on echocardiography, ^{18}F-FDG PET/CT, or leukocyte scan according to the European Society of Cardiology 2015 modified criteria for diagnosing infective endocarditis (*9*).

We considered antibiotic treatment appropriate if the strain was susceptible to ≥1 of the drugs prescribed, according to the Antibiogram Committee of the French Society of Microbiology and European Committee On Antimicrobial Susceptibility Testing recommendations (*12*). *Campylobacter* spp. are naturally resistant to third-generation cephalosporins, ticarcillin, and piperacillin, so we considered those antibiotics to be inappropriate.

We defined relapse by ≥1 new positive blood culture with *Campylobacter* spp. after clinical sign resolution and apyrexia or negative control blood culture. We defined 3-month mortality as death within 3 months of the first positive blood culture.

Microbiological Diagnosis

All participating laboratories used continually monitored noninvasive blood culture systems (e.g., BacT/Alert and Virtuo [bioMérieux, https://www.biomerieux.com] or Bactec [Becton Dickinson, https://www.bd.com]). Each blood culture set included an aerobic and an anaerobic bottle inoculated with 10 mL of blood and incubated for 5 days. Two sets of blood culture were recommended. We performed Gram staining and fresh examinations for positive samples. We identified curved or spiral-shaped gram-negative rods as *Campylobacter* spp. We inoculated a blood agar plate and incubated it in a microaerobic atmosphere (6% O_2, 7% CO_2, 7% H_2, and 78% N_2) at 35°C. For patients who underwent vascular surgery, we obtained several samples from vascular tissue, thrombus, or grafts; for patients who underwent valvular surgery, we analyzed native or prosthetic valves. We plated intra-operative samples onto polyvitex chocolate agars (bioMérieux) and inoculated them into 10 mL of Schaedler and brain–heart broth. We incubated agar plates at 37°C for 14 days in aerobic atmosphere

with 5% CO_2 and for 14 days in anaerobic atmosphere. We incubated broth at 37°C for 15 days and subsequently plated cloudy broth media on polyvitex chocolate agar plates and incubated them in a 5% CO_2 atmosphere for 7 days. We performed bacterial identification by using matrix-assisted laser desorption/ionization time-of-flight mass spectrometry (*13*) from positive standard bacterial culture. We interpreted susceptibility testing according to Antibiogram Committee of the French Society of Microbiology and European Committee On Antimicrobial Susceptibility Testing recommendations (*12*).

Objectives

Our primary objective was to evaluate the risk factors of 3-month mortality in patients with *Campylobacter* spp. vascular infection, endocarditis, or both. The secondary objectives were to describe the epidemiology, clinical manifestations, and therapeutic management and to evaluate risk factors of relapse.

Ethics Approval

We declared our study to France's National Institute of Health Data (https://www.snds.gouv.fr). We reported our retrospective cohort with France's data protection authority (https://www.cnil.fr).

Statistical Analysis

We expressed descriptive statistics as percentages for categorical variables and as the mean with SD and median with interquartile range (IQR) for continuous variables. We performed univariate analyses using Fisher exact test for count data, Wilcoxon test, and Pearson χ^2 test with Yates' continuity correction to identify the factors associated with a fatal outcome within 3 months. We considered results with p values <0.05 to be statistically significant. We performed statistical analyses with R studio version 1.2.5033 (https://rstudio.com).

Results

Among 592 patients with *Campylobacter* spp. bacteremia, 57 were included in this analysis (Figure 1); 38 had a vascular infection (6.6%) and 12 had endocarditis (2.1%). Seven more patients among the 384 included in the BUH retrospective cohort before 2015 or without bacteremia were included. Overall, most included patients had a vascular infection (n = 44), followed by endocarditis (n = 12). One had both endocarditis and an infectious native aortic aneurysm.

Demographic Data and Clinical Characteristics of Vascular Infection Cases

We compared clinical characteristics of patients with native (n = 30) or prosthetic (n = 15) vascular infections (Table 1). Male (80%) and elderly (64.9% were ≥65 years of age) patients were predominantly affected. Most patients had underlying conditions, mainly cardiovascular, and impairing immunity conditions; 26.7% were active smokers, 24.4% had diabetes, 24.4% had a history of aortic aneurysm, and 22.2% had ischemic cardiomyopathy.

Fever (71.1% of cases) and abdominal or lumbar pain (51.1% of cases) were the most common clinical signs. Diarrhea was quite rare (22.2%).

The infections were heterogeneous. The aorta was the most commonly infected vessel (66.7%); however, peripheral arteries could also be involved, either iliac (n = 2), popliteal (n = 3), gastroduodenal (n = 1), or carotid (n = 1). Some rare venous infections were described, either portal veins (n = 2), jugular-peritoneal shunt (n = 1), sural or femoral veins (n = 1 each),

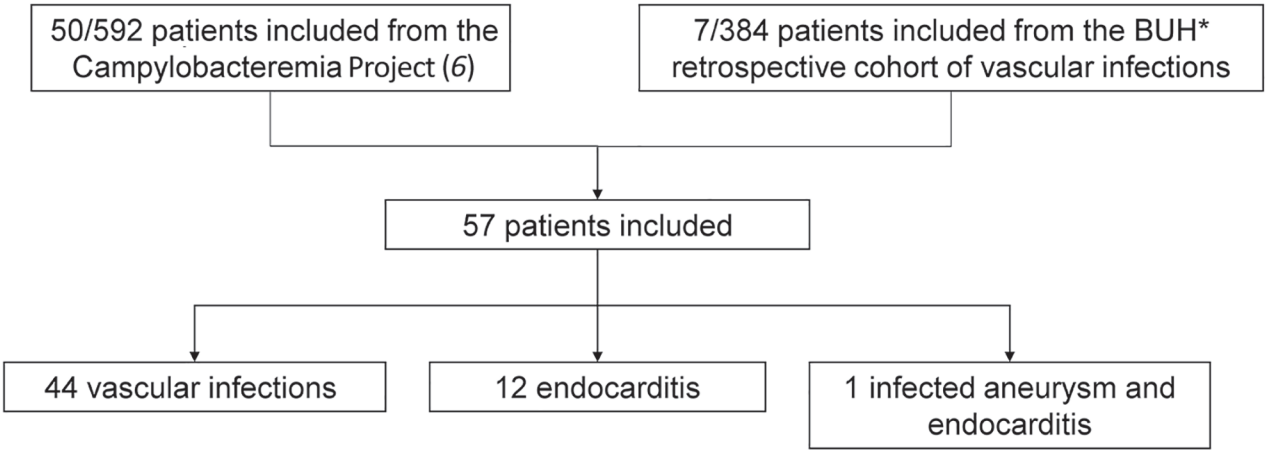

Figure 1. Flowchart of 57 patients with *Campylobacter* spp. vascular infections in a multicenter retrospective study on vascular infections and endocarditis caused by *Campylobacter* spp., France. BUH, Bordeaux University Hospital (Bordeaux, France).

Table 1. Characteristics of 45 patients with *Campylobacter* spp. vascular infections in a multicenter retrospective study on vascular infections and endocarditis caused by *Campylobacter* spp., France*

Characteristic	Vascular infection	Native vascular infection	Vascular graft or endograft infection
All patients	45 (100)	30 (66.7)	15 (33.3)
Age, y, median (interquartile range)	69.5 (61.2–81.3)	69.5 (61.8–81.3)	70 (62–81)
Sex			
M	36 (80)	23 (76.7)	13 (86.7)
F	9 (20)	7 (23.3)	2 (13.3)
Localization			
Aortic	30 (66.7)	17 (56.7)	13 (86.7)
Peripheral artery	7 (15.6)	6 (20)	1 (6.7)
Venous involvement	5 (11.1)	4 (13.3)	1 (6.7)
Lymphatic involvement	1 (2.2)	1 (3.3)	0
Not available	2 (4.4)	2 (6.7)	0
Underlying condition			
Preexisting aortic aneurysm	11 (24.4)	9 (30)	2 (13.3)
Ischemic cardiomyopathy	10 (22.2)	8 (26.7)	2 (13.3)
Tobacco use	12 (26.7)	8 (26.7)	4 (26.7)
Chronic liver disease	5 (11.1)	4 (13.3)	1 (3.3)
Diabetes	11 (24.4)	8 (26.7)	3 (20)
Chronic renal failure	9 (20)	5 (16.7)	4 (26.7)
Hematologic malignancy	2 (4.4)	2 (6.7)	0
Solid neoplasm	11 (24.4)	6 (20)	5 (33.3)
Immunodeficiency	7 (15.6)	6 (20)	1 (6.7)
Clinical manifestations†			
Fever	32 (71.1)	24 (80)	8 (53.3)
Septic shock	1 (2.2)	1 (3.3)	0
Hemorrhagic shock	4 (8.9)	3 (10)	1 (6.7)
Diarrhea	10 (22.2)	6 (20)	4 (26.7)
Gastrointestinal bleeding	6 (13.3)	5 (16.7)	1 (3.3)
Abdominal or lumbar pain	23 (51.1)	16 (53.3)	7 (46.7)
Acute limb ischemia	3 (6.7)	3 (10)	0
Osteoarticular involvement	4 (8.9)	2 (6.7)	2 (13.3)
Campylobacter species			
C. fetus	36 (80)	23 (76.7)	13 (86.7)
C. jejuni	5 (11.1)	4 (13.3)	1 (3.3)
Other *Campylobacter* spp.	4 (8.9)	3 (10)	1 (3.3)

*Values are no. (%) except as indicated.
†Signs and symptoms occurring within the past month were considered.

and finally a lymphangioma of the lower limb (n = 1). One third of these cases occurred on vascular grafts or endografts (33.3%), including 13 aortic, 1 femoropopliteal, and 1 jugular-peritoneal shunt.

Four of these patients also had an osteoarticular infection, 1 had hip arthritis, and 3 had spondylodiscitis, 2 of which occurred in patients with aortitis, suggesting a contiguous infection. One of these 2 patients also had a psoas abscess.

Demographic Data and Clinical Characteristics of Endocarditis Cases

We compared clinical characteristics of patients with endocarditis (Table 2). Again, the clinical manifestations were nonspecific; most patients were febrile (84.6%), and a cardiac murmur was found in only 4 patients.

Valvular infections mostly occurred on the aortic valve (n = 9), and only 2 were on the mitral valve. No right-sided infective endocarditis was found. Those infections involved 7 prosthetic valves, 4 native valves, and 2 intracardiac devices (pacemakers). The time interval between valve or pacemaker implantation and endocarditis was >1 year in all cases.

Diagnostic Imaging Results

All but 1 of the patients with vascular infection had documented imaging procedure data (Table 3). Detailed echography data were reported in 11 cases of endocarditis. All of them had major criteria for endocarditis, either typical oscillating valvular vegetation (n = 11), cardiac abscess (n = 3), valve perforation (n = 1), or prosthetic valve dehiscence (n = 1). One diagnosis was made on ^{18}F-FDG PET/CT, which revealed hypermetabolism around the site of a prosthetic aortic valve associated with a thoracic aorta aneurysm. The last case, a mediastinitis associated with pacemaker infection, was diagnosed intraoperatively.

Microbiologic Diagnosis and Antimicrobial Susceptibility Profiles

C. fetus was the most frequently identified species (82.5%), followed by *C. jejuni* (10.5%) (Figure 2).

Table 2. Characteristics of 13 patients with *Campylobacter* spp. endocarditis in a multicenter retrospective study on vascular infections and endocarditis caused by *Campylobacter* spp., France*

Characteristic	Infective endocarditis	Native valve infective endocarditis	Prosthetic valve infective endocarditis and CIED infection
All patients	13 (100)	4 (30.8)	9 (69.2)
Age, y, median (interquartile range)	67 (60.3–80.8)	64 (57–80)	67 (60.3–80.8)
Sex			
M	13 (100)	4 (30.8)	9 (69.2)
F	0	0	0
Localization			
Aortic valve	9 (69.2)	3	6
Mitral valve	2 (15.4)	1	1
CIED	2 (15.4)	0	2
Underlying condition			
Ischemic cardiomyopathy	2 (15.4)	0	2
Chronic liver disease	2 (15.4)	1	1
Diabetes	4 (30.8)	2	2
Chronic renal failure	4 (30.8)	2	2
Hematologic malignancy	1 (7.7)	0	1
Solid neoplasm	2 (15.4)	1	1
Immunodeficiency	4 (30.8)	1	3
Clinical manifestations†			
Fever	11 (84.6)	3	8
Septic shock	2 (15.4)	1	1
Diarrhea	3 (23.1)	1	2
Gastrointestinal bleeding	1 (7.7)	0	1
Abdominal or lumbar pain	3 (23.1)	2	1
Cardiac murmur	4 (30.8)	1	3
Cardiac failure	1 (7.7)	1	0
Campylobacter species			
C. fetus	12 (92.3)	4	8
C. jejuni	1 (7.7)	0	1

*Values are no. (%) except as indicated. CIED, cardiac implantable electronic device.
†Signs and symptoms occurring within the past month were considered.

C. fetus was responsible for 92.3% of endocarditis and 80% of vascular infections. A *C. rectus* infection occurred on a gastroduodenal artery in a neutropenic patient with diabetes who was co-infected with commensal bacteria of the oral cavity. As comparison, among the initial cohort of patients with bacteremia, *C. jejuni* (42.9%) and *C. fetus* (42.6%) were the most commonly identified species, followed by *C. coli* (6.8%) and *C. ureolyticus* (3.7%) (*6*). Among the 252 patients with *C. fetus* bacteremia, 29 (11.5%) patients had vascular localization, and 11 (4.4.%) had endocarditis. However, secondary vascular localizations were not systematically researched and might have been underdiagnosed in the initial cohort.

Blood cultures were performed in all patients and were positive in 100% of patients with endocarditis and 88.9% of patients with vascular infections. The median time to positive blood samples was rather long, 55.5 hours (IQR 44.95–73 hours). The 5 patients with vascular infections and negative blood cultures were all infected by *C. fetus* species. Intraoperative specimens were positive in 11 vascular infections

Table 3. Imaging results for 44 patients with vascular infections in a multicenter retrospective study on vascular infections and endocarditis caused by *Campylobacter* spp., France*

Radiologic finding	Native vascular infection, no.	Vascular graft and endograft infection, no.
All patients	30	14
Computed tomography	23	12
Perivascular or graft infiltration	5	5
Perivascular or graft gas	2	2
Abscess	1	4
Dissection	2	0
Pseudoaneurysm	3	2
Rupture	6	2
Thrombosis	4	3
Enteric contact with aorta	1	2
^{18}F-FDG PET/CT	10	8
Perivascular or graft abnormal metabolic activity	6	8
Leukocyte scan	1	2
Vascular radiolabeled leukocyte uptake	0	1

^{18}F-FDG PET/CT, ^{18}F-fluoro-deoxyglucose-positron emission tomography/computed tomography.

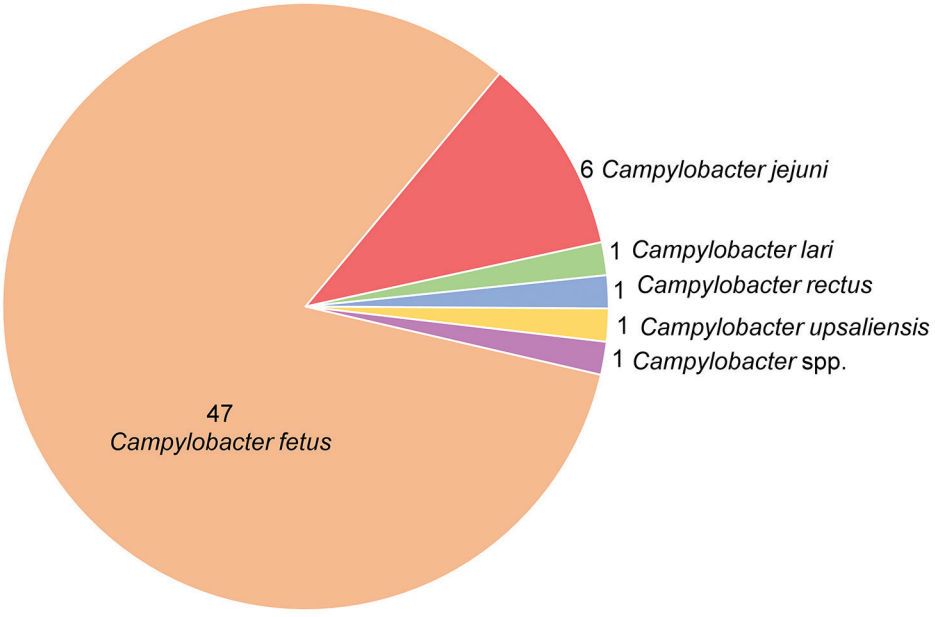

Figure 2. Distribution of *Campylobacter* species among 57 patients with vascular infections and endocarditis in a multicenter retrospective study on vascular infections and endocarditis caused by *Campylobacter* spp., France. Numbers indicate no. cases.

over the 14 cultures performed and 1 of 2 patients with endocarditis. Only 1 patient had a positive stool culture (*C. jejuni*) among the 12 performed.

We assessed antimicrobial-acquired resistance (Table 4). No strain was resistant to amoxicillin/clavulanate or to imipenem among the levels tested. Higher rates of resistance were observed for ampicillin (9.8%), fluoroquinolones (31.4%), and tetracycline (20.5%).

Clinical Outcome

Survival without relapse at 3 months was observed for 67.3% (33/49) of the patients with available data at follow-up; the mortality rate was estimated at 24.5% (12 cases), and estimated relapse rate was 8.2% (4 cases). Two patients with endocarditis and 10 patients with vascular localization died within 3 months.

Among the 56 patients for whom antimicrobial therapy was documented, 54 (96.4%) received an appropriate treatment based on the susceptibility results. Only 2 patients were inefficiently treated (1 by third-generation cephalosporine, 1 by ofloxacin). Regarding antimicrobial therapy regimen among patients with VGEIs or prosthetic valves, 9/24 (37.5%) received single therapy and 15/24 (62.5%) dual therapy, combining a β-lactam with either a fluoroquinolone (9 patients), an aminoglycoside (5 patients), or a macrolide (1 patient). All patients with endocarditis received an initial association of aminoglycoside infusion and a β-lactam, except for 1 who received an aminoglycoside and fluoroquinolone therapy. The median duration of antimicrobial treatment was 42 days (IQR 20–49 days). Five patients received lifelong suppressive antimicrobial therapy (amoxicillin, amoxicillin/clavulanate, or ofloxacin).

We analyzed risks factors for 3-month mortality and relapse. Neither time to efficient therapy, immunosuppression, surgery, nor antimicrobial therapy regimen (single versus dual therapy) was associated with 3-month mortality in multivariate analysis. However, the time to efficient antimicrobial therapy initiation after the first symptoms was much longer in the patients who relapsed compared with relapse-free patients (61 days [IQR 20.3–104.3 days] vs. 9.5

Table 4. Antimicrobial resistance by species of *Campylobacter* spp. identified in a multicenter retrospective study on vascular infections and endocarditis caused by *Campylobacter* spp., France*

Antimicrobial tested	MIC breakpoint, mg/L	No. (%) isolates		
		C. fetus	*C. jejuni*	Other *Campylobacter* spp.
Ampicillin	16	1/44 (2.3)	3/5 (60)	1/2 (50)
Amoxicillin/clavulanate	16	0/40	0/5	0/3
Ciprofloxacin	0.5	11/44 (25)	3/5 (60)	2/2 (100)
Erythromycin	4	1/43 (2.3)	0/5	0/2
Tetracycline	2	5/38 (13.2)	4/5 (80)	0/1
Gentamicin†	2	0/41	0/5	0/2
Imipenem	2	0/7	Not tested	0/1

*Strains susceptible to gentamicin were assumed to be susceptible to amikacin.

days [IQR 2–15 days]; p = 0.006). Relapse patients also more often had diabetes (75% vs. 12%; p = 0.022) and osteoarticular-associated infection (75% vs. 2%; p = 0.001) than did relapse-free patients.

Nine of the 15 patients with VGEIs underwent surgery, and 7 underwent complete graft removal. Two patients with prosthetic valve endocarditis underwent surgery for valve replacement, and 2 underwent infected pacemaker replacement. Two more patients required surgery because of severe valve dysfunction.

Discussion

We examined a comprehensive series of *Campylobacter* spp. cases associated vascular infections and endocarditis among 57 patients identified because of the participation of 37 hospitals in France. Consistent with data on *Campylobacter* spp. bacteremia, male and elderly patients were predominantly affected, and most patients had underlying conditions, particularly cardiovascular conditions, diabetes, solid neoplasm, chronic renal failure, or hepatic failure (*6*). Of interest, although *Campylobacter* spp. is the leading cause of bacterial diarrhea responsible for enteritis mainly occurring before 30 years of age in immunocompetent patients, invasive infections are more likely to affect immunocompromised elderly patients (*7*).

Native vascular infections preferentially affect the infra-renal aorta; *Salmonella* spp. and *Staphylococcus aureus* were the most commonly identified bacteria in previous studies (*14*,*15*). *Campylobacter* spp. involvement is rarely described, even though it represented almost 10% of infective native aortic aneurysms in a recent study in France (*16*). In our study, 66.7% of infections were aortic, and 15.6% occurred on peripheral arteries. Venous infections were also reported, but thrombophlebitis is poorly described so far because only a few case reports are available (*17*–*19*).

The 13 cases of endocarditis included in our study and the 21 case reports previously described in the literature highlight the role of this non-HACEK (species other than *Haemophilus* species, *Actinobacillus actinomycetemcomitans*, *Cardiobacterium hominis*, *Eikenella corrodens*, or *Kingella* spp.) gram-negative bacillus in endocarditis (Appendix, https://wwwnc.cdc.gov/EID/article/29/3/22-1417-App1.pdf). So far, the International Collaboration on Infective Endocarditis Prospective Cohort Study has described 49 (1.8%) endocarditis attributable to non-HACEK gram-negative bacilli among 2,761 patients with definite endocarditis (*20*). Most commonly encountered bacilli were *Escherichia coli* and *Pseudomonas aeruginosa,* but no *Campylobacter* spp. infection was reported. These gram-negative bacilli infections were severe, leading to an increased in-hospital mortality rate of 24% compared with 8% for *Streptococcus* spp. and 33% for *S. aureus*–associated endocarditis (*21*). In our study, the 3-month mortality rate associated with endocarditis was 15.4%, but it remains difficult to conclude given the small number of patients. Non-HACEK gram-negative bacilli endocarditis is usually associated with active injection drug use (up to 93% of cases) and therefore involves native tricuspid valve in most cases (*22*). In our cohort, all endocarditis cases were left-sided, and 69.2% occurred either on prosthetic valves or intracardiac devices. This profile looks more like other foodborne endocarditis, such as *Salmonella* spp. or *Listeria monocytogenes*, which more likely affect older and immunocompromised patients and are associated with higher mortality rates (42.5% for *Salmonella* spp. [*23*] and 41% for *L. monocytogenes* [*24*]).

C. fetus was the most frequently involved species (82.5%), whereas according to the report of NRCCH, this species represents only 1% of the isolates analyzed among the 8,082 isolates received in 2020 (*25*). In our study, the most frequently isolated species are *C. jejuni* (84%) and *C. coli* (13%), and they both are predominantly isolated from stool culture (98.8% of *C. jejuni* and 99.6% of *C. coli*). *C. fetus* is much less common (1%) and is predominantly isolated from blood culture or deep samplings (57%) compared with stool samples (41%) (*25*). *C. fetus* virulence is notably attributable to a protein capsule called the S-layer, which impairs complement activation by a lack of C3b binding (*26*). Different mechanisms have been suggested to explain its tropism for vascular endothelium, especially when the latter is previously damaged, such as the production of procoagulant factors favoring the formation of microthrombi or the presence of a membrane receptor with an affinity for the endothelium (*27*).

Regarding the nonspecific symptoms, because only 22.8% of patients had diarrhea, and because of the lack of awareness of the risk for secondary localizations associated with campylobacteriosis, those complications might be underestimated. Among patients with *C. fetus* bacteremia in the campylobacteremia study, 11.5% had a vascular infection and 4.4% had endocarditis. Furthermore, 11% of the 99 patients who underwent echocardiography had endocarditis, close to the rate described for *S. aureus* bacteremia (*6*,*28*). Those findings warrant the use of systematic transthoracic echocardiography in cases of *C. fetus* bacteremia. Foreign implants and preexisting aneurysms also seemed to be risk factors for bacterial colonization because vascular infections occurred on (endo)grafts in 33.3% of cases and native aneurysms

in 24.4%. Therefore, a systematic computed tomography angiogram should be discussed for these patients. Moreover, the risk for 3-month relapse was associated with osteoarticular involvements, highlighting the paramount importance of a comprehensive diagnosis and treatment of these secondary localizations.

The association of 3-month relapse with delayed initiation of efficient antimicrobial therapy advocates for the necessity of prompt appropriate treatment. The retrospective design of our study did not enable us to make a conclusion on the optimal treatment modality. Nevertheless, considering low acquired resistance rates, which is consistent with NRCCH reports in recent years (*25*), an initial dual bactericidal therapy by amoxicillin/clavulanate and gentamicin could be a good option for empiric therapy. The issue of secondary targeted therapy remains unresolved. Amoxicillin and macrolides could be good options according to the susceptibility profile. Ciprofloxacin could also be of interest; however, the use of fluoroquinolones remains debated given the recent divergent data published on possible excess risks of aneurysmal rupture and aortic dissection (*29*,*30*).

Campylobacter spp. cardiovascular infections are rare but should be considered seriously in light of the high incidence of campylobacteriosis. These infections are associated with high mortality rates and mainly occur in elderly patients with underlying conditions. The relapse rate is also high and correlates with delayed initiation of an efficient antimicrobial therapy, suggesting a need for prompt recognition and treatment. Therefore, systematic transthoracic echocardiography should be performed in cases of *C. fetus* bacteremia. Dedicated imaging might also be indicated for patients with a preexisting aneurysm or vascular (endo)graft, even in the absence of evocative symptoms.

Campylobacteremia Study Group: Corentine Alauzet, Meghann Antoine, Olivier Barraud, Thierry Benoit-Cattin, Emilie Bessède, Renaud Blondé, Pierre Boyer, Lauranne Broutin, Julie Brouty, Christophe Burucoa, Mathilde Carrer, Vincent Cattoir, Laura Courtellemont, Anne Cypierre, Chloé Dominges Martins, Astrid Ducournau, Maïlys Ducours, Bruno Dumoulard, Sibyle Etiévant, Erwan Fayoux, Marguerite Fines-Guyon, Nathalie Grall, Ariane Gross, Thomas Guillard, Jérome Guinard, Cécile Guyonnet, Edgar Horta, Aude Jacquez, Jean-Philippe Lavigne, David Lebeaux, Cécile Le Brun, Cédric Lebreton, Nadine Lemaitre, Marion Leterrier, Jean-Luc Mainardi, Cléa Melenotte, Anne-Laure Michon, Marie-Christine Moulhade, Clémentine Moreau, Laurence Parmeland, Pierre Patoz, Caroline Piau, Jérémy Picard, Nora Poey, Elise Recalt, Louise Sauleau, Eve-marie Takoudju, Pierre Tattevin, Xavier Tessier, Pauline Tirard-Collet, Cong Tri Tran.

Acknowledgments

We thank all of the laboratories that sent *Campylobacter* strains to our reference center and all the participants in the Campylobacteremia Study Group.

This study was financed by internal funding of the French National Reference Centre for Campylobacters and Helicobacters, Bordeaux, France.

This material is original research and has not been previously published or submitted for publication elsewhere. The authors declare no conflict of interest.

About the Author

Dr. Tinévez is a clinician in the Department of Infectious and Tropical Diseases at Bordeaux University Hospital, France. Her research interests include campylobacteriosis and vascular infections. She also works on the cellular response to cytomegalovirus infection in transplant patients.

References

1. Kaakoush NO, Castaño-Rodríguez N, Mitchell HM, Man SM. Global epidemiology of *Campylobacter* infection. Clin Microbiol Rev. 2015;28:687–720. https://doi.org/10.1128/CMR.00006-15
2. Tack DM, Marder EP, Griffin PM, Cieslak PR, Dunn J, Hurd S, et al. Preliminary incidence and trends of infections with pathogens transmitted commonly through food—Foodborne Diseases Active Surveillance Network, 10 U.S. sites, 2015–2018. MMWR Morb Mortal Wkly Rep. 2019;68:369–73. https://doi.org/10.15585/mmwr.mm6816a2
3. European Food Safety Authority; European Centre for Disease Prevention and Control. The European Union One Health 2020 zoonoses report. EFSA J. 2021;19:e06971.
4. Gazaigne L, Legrand P, Renaud B, Bourra B, Taillandier E, Brun-Buisson C, et al. *Campylobacter fetus* bloodstream infection: risk factors and clinical features. Eur J Clin Microbiol Infect Dis. 2008;27:185–9. https://doi.org/10.1007/s10096-007-0415-0
5. Feodoroff B, Lauhio A, Ellström P, Rautelin H. A nationwide study of *Campylobacter jejuni* and *Campylobacter coli* bacteremia in Finland over a 10-year period, 1998–2007, with special reference to clinical characteristics and antimicrobial susceptibility. Clin Infect Dis. 2011;53:e99–106. https://doi.org/10.1093/cid/cir509
6. Tinévez C, Velardo F, Ranc AG, Dubois D, Pailhoriès H, Codde C, et al.; Campylobacteremia Study Group. Retrospective multicentric study on *Campylobacter* spp. bacteremia in France: the Campylobacteremia Study. Clin Infect Dis. 2022;75:702–9. https://doi.org/10.1093/cid/ciab983
7. Pacanowski J, Lalande V, Lacombe K, Boudraa C, Lesprit P, Legrand P, et al.; CAMPYL Study Group. *Campylobacter* bacteremia: clinical features and factors associated with fatal outcome. Clin Infect Dis. 2008;47:790–6. https://doi.org/10.1086/591530
8. Fernández-Cruz A, Muñoz P, Mohedano R, Valerio M, Marín M, Alcalá L, et al. *Campylobacter* bacteremia: clinical characteristics, incidence, and outcome over 23 years. Medicine (Baltimore). 2010;89:319–30. https://doi.org/10.1097/MD.0b013e3181f2638d

9. Habib G, Lancellotti P, Antunes MJ, Bongiorni MG, Casalta JP, Del Zotti F, et al.; ESC Scientific Document Group. 2015 ESC guidelines for the management of infective endocarditis. Eur Heart J. 2015;36:3075–128. https://doi.org/10.1093/eurheartj/ehv319
10. Wilson WR, Bower TC, Creager MA, Amin-Hanjani S, O'Gara PT, Lockhart PB, et al. Vascular graft infections, mycotic aneurysms, and endovascular infections: a scientific statement from the American Heart Association. Circulation. 2016;134:e412–60. https://doi.org/10.1161/CIR.0000000000000457
11. Chakfé N, Diener H, Lejay A, Assadian O, Berard X, Caillon J, et al.; ESVS Guidelines Committee. European Society for Vascular Surgery (ESVS) 2020 clinical practice guidelines on the management of vascular graft and endograft infections. Eur J Vasc Endovasc Surg. 2020;59:339–84. https://doi.org/10.1016/j.ejvs.2019.10.016
12. European Committee on Antimicrobial Susceptibility Testing. Breakpoint tables for interpretation of MICs and zone diameters [cited 2022 Sep 1]. https://www.eucast.org/fileadmin/src/media/PDFs/EUCAST_files/Breakpoint_tables/v_12.0_Breakpoint_Tables.pdf
13. Bessède E, Solecki O, Sifré E, Labadi L, Mégraud F. Identification of *Campylobacter* species and related organisms by matrix assisted laser desorption ionization-time of flight (MALDI-TOF) mass spectrometry. Clin Microbiol Infect. 2011;17:1735–9. https://doi.org/10.1111/j.1469-0691.2011.03468.x
14. Zhu C, Zhao J, Huang B, Yuan D, Yang Y, Wang T. Long-term outcome of endovascular aortic repair for mycotic abdominal aortic aneurysm. ANZ J Surg. 2020;90:1376–80. https://doi.org/10.1111/ans.16122
15. Heinola I, Sörelius K, Wyss TR, Eldrup N, Settembre N, Setacci C, et al. Open repair of mycotic abdominal aortic aneurysms with biological grafts: an international multicenter study. J Am Heart Assoc. 2018;7:e008104. https://doi.org/10.1161/JAHA.117.008104
16. Journeau L, de la Chapelle M, Guimard T, Ferfar Y, Saadoun D, Mahé I, et al. A strobe multicenter descriptive study of 55 infectious aortitis. Medicine (Baltimore). 2020;99:e22422. https://doi.org/10.1097/MD.0000000000022422
17. Jawad II, Chandna A, Morris-Jones S, Logan S. Unusual case of Lemierre's syndrome. BMJ Case Rep. 2018;11:e226948. https://doi.org/10.1136/bcr-2018-226948
18. Morrison VA, Lloyd BK, Chia JKS, Tuazon CU. Cardiovascular and bacteremic manifestations of *Campylobacter fetus* infection: case report and review. Rev Infect Dis. 1990;12:387–92. https://doi.org/10.1093/clinids/12.3.387
19. Carbone KM, Heinrich MC, Quinn TC. Thrombophlebitis and cellulitis due to *Campylobacter fetus* ssp. fetus. Report of four cases and a review of the literature. Medicine (Baltimore). 1985;64:244–50. https://doi.org/10.1097/00005792-198507000-00005
20. Morpeth S, Murdoch D, Cabell CH, Karchmer AW, Pappas P, Levine D, et al.; International Collaboration on Endocarditis Prospective Cohort Study (ICE-PCS) Investigators. Non-HACEK gram-negative bacillus endocarditis. Ann Intern Med. 2007;147:829–35. https://doi.org/10.7326/0003-4819-147-12-200712180-00002
21. Hill EE, Herijgers P, Claus P, Vanderschueren S, Herregods MC, Peetermans WE. Infective endocarditis: changing epidemiology and predictors of 6-month mortality: a prospective cohort study. Eur Heart J. 2007;28:196–203. https://doi.org/10.1093/eurheartj/ehl427
22. Veve MP, McCurry ED, Cooksey GE, Shorman MA. Epidemiology and outcomes of non-HACEK infective endocarditis in the southeast United States. PLoS One. 2020; 15:e0230199. https://doi.org/10.1371/journal.pone.0230199
23. Cheng WL, Li CW, Li MC, Lee NY, Lee CC, Ko WC. *Salmonella* infective endocarditis. J Microbiol Immunol Infect. 2016;49:313–20. https://doi.org/10.1016/j.jmii.2015.02.659
24. Shoai-Tehrani M, Pilmis B, Maury MM, Robineau O, Disson O, Jouvion G, et al.; Listeria Endovascular Infections Study Group. *Listeria monocytogenes*-associated endovascular infections: a study of 71 consecutive cases. J Infect. 2019;79:322–31. https://doi.org/10.1016/j.jinf.2019.07.013
25. Centre National de Référence des Campylobacters et Hélicobacters. Rapport annuel d'activité 2021 Centre National de Référence des Campylobacters et des Hélicobacters année d'exercice 2020 [cited 2022 Sep 01]. https://www.cnrch.fr/bilans-et-publications/bilans-annuels-cnr-ch
26. Sprenger H, Zechner EL, Gorkiewicz G. So close and yet so far—molecular microbiology of *Campylobacter fetus* subspecies. Eur J Microbiol Immunol (Bp). 2012;2:66–75. https://doi.org/10.1556/EuJMI.2.2012.1.10
27. Wagenaar JA, van Bergen MAP, Blaser MJ, Tauxe RV, Newell DG, van Putten JPM. *Campylobacter fetus* infections in humans: exposure and disease. Clin Infect Dis. 2014;58:1579–86. https://doi.org/10.1093/cid/ciu085
28. Le Moing V, Alla F, Doco-Lecompte T, Delahaye F, Piroth L, Chirouze C, et al.; VIRSTA Study Group. *Staphylococcus aureus* bloodstream infection and endocarditis—a prospective cohort study. PLoS One. 2015;10:e0127385. https://doi.org/10.1371/journal.pone.0127385
29. Dong YH, Chang CH, Wang JL, Wu LC, Lin JW, Toh S. Association of infections and use of fluoroquinolones with the risk of aortic aneurysm or aortic dissection. JAMA Intern Med. 2020;180:1587–95. https://doi.org/10.1001/jamainternmed.2020.4192
30. Newton ER, Akerman AW, Strassle PD, Kibbe MR. Association of fluoroquinolone use with short-term risk of development of aortic aneurysm. JAMA Surg. 2021;156:264–72. https://doi.org/10.1001/jamasurg.2020.6165

Address for correspondence: Claire Tinévez, Infectious and Tropical Diseases Department, Bordeaux University Hospital, Place Amélie Raba Léon, 33076 Bordeaux, France; email: claire.tinevez@chu-bordeaux.fr

Yellow Fever Vaccine–Associated Viscerotropic Disease among Siblings, São Paulo State, Brazil

Eder Gatti Fernandes, Victor Bertollo Gomes Porto, Patrícia Mouta Nunes de Oliveira, Amaro Nunes Duarte-Neto, Maria de Lourdes de Sousa Maia, Letícia Kegele Lignani, Juliana Silva Nogueira, Gabriellen Vitiello Teixeira, Silvia D'Andretta Iglezias, Roberta Morozetti Blanco, Helena Keico Sato

We describe 5 cases of yellow fever vaccine–associated viscerotropic disease (YEL-AVD) in 2 familial clusters during the 2017–2018 yellow fever (YF) vaccination campaign in São Paulo state, Brazil. The first case was that of a 40-year-old white man who died of icterohemorrhagic syndrome, which was confirmed to be YEL-AVD by using real-time reverse transcription PCR to detect 17DD YF vaccine in the liver. Ten years previously, his brother died of a clinically similar disease without a confirmed diagnosis 9 days after YF vaccination. The second cluster included 3 of 9 siblings in whom hepatitis developed in the first week after receiving fractionated doses of YF vaccine. Two of them died of hemorrhagic diathesis and renal and respiratory failure, and 17DD-YF vaccine was detected in serum samples from all patients and in the liver in 1 case. Genetic factors might play a substantial role in the incidence of YEL-AVD.

Brazil recently experienced its largest-recorded yellow fever (YF) outbreak in decades; >2,000 human cases and ≈750 deaths occurred during July 2016–June 2018 (*1*). The virus reached the metropolitan areas, where the YF vaccine had not been previously recommended. This situation led to the need for vaccination campaigns in affected areas, which included fractionated doses of the 17DD YF vaccine. In 2017, >5 million persons were vaccinated with the standard dose in the state of São Paulo, Brazil. During January 25–July 3, 2018, the state also used a fractionated-dose vaccine as part of a dose-sparing strategy in 54 municipalities. The fractionated dose consisted of 0.1 mL (one fifth of the standard dose) administered in the subcutaneous tissue to person >2 years of age. This approach was necessary because of insufficient vaccine stock for the entire population at the height of the epidemic. In 2018, a total of 10 million persons were vaccinated; of those, 5.3 million received the standard dose and 4.7 million received the fractionated dose.

During the 2016–2018 YF epidemic, southeastern Brazil was the most affected area; São Paulo state had 559 confirmed cases of YF and 214 deaths attributed to YF (*2*). As a consequence, the YF vaccination coverage rate, which was 5% of the population in 2016, increased to 65% by the end of 2018 in the metropolitan area of the city of São Paulo.

In late 2017, the Health Surveillance Department of the State of São Paulo (Centro de Vigilância Epidemiológica "Prof. Alexandre Vranjac") received a report of a man in the metropolitan area of São Paulo city who died after YF vaccination. The patient's brother had died soon after YF vaccination 10 years previously, but cause of death was undetermined. Two months later, the surveillance team received a report from Natividade da Serra in São Paulo state of 3 temporary adverse events associated with YF vaccination among siblings of 1 family that ended in 2 deaths.

The data resulted in a suspicion of YF vaccine–associated viscerotropic disease (YEL-AVD). They were not the first suspected cases of YEL-AVD during the 2017–2018 vaccination campaign. However, the report of 2 familial clusters of severe adverse events following immunization (AEFI) related to YF vaccine in the state of São Paulo triggered a field epidemiologic

Author affiliations: Instituto de Infectologia Emílio Ribas, São Paulo, Brazil (E.G. Fernandes); Centro de Vigilância Epidemiológica "Prof. Alexandre Vranjac," São Paulo (E.G. Fernandes, H.K. Sato); Programa Nacional de Imunizações, Brasilia, Brazil (V.B.G. Porto); Bio-Manguinhos, Rio de Janeiro, Brazil (P.M.N. de Oliveira, M. de Lourdes de Sousa Maia, L.K. Lignani, G.V. Teixeira); Faculdade de Medicina da Universidade de São Paulo, São Paulo (A.N. Duarte-Neto); Instituto Adolfo Lutz, São Paulo (A.N. Duarte-Neto, J.S. Nogueira, S. D'Andretta Iglezias, R.M. Blanco)

DOI: https://doi.org/10.3201/eid2903.220989

investigation. In this descriptive study, we describe the epidemiologic investigation of the 2 clusters of YEL-AVD among family members.

Methods

We used the AEFI surveillance system of São Paulo state, Brazil, to capture information from January 2017–June 2018. The cases reported are level 1 according to Brighton Collaboration Viscerotropic Disease Working Group case definition in terms of the diagnostic certainty (definite or probable YF vaccine–associated causality) (*3*). All case-patients were first-degree relatives (siblings) with YEL-AVD. We also included 1 previous case-patient who had onset of symptoms before 2017 but was related to a current case-patient.

We obtained information regarding the vaccine and clinical and laboratory findings from the official AEFI passive surveillance system database. A field investigation team reviewed medical records. The team also visited the patients' families to collect clinical and epidemiologic details, in addition to the vaccination status of first-degree relatives, and searched for other suspected cases of AEFI. Last, the team traced the biologic samples for additional and specific laboratory investigations.

We analyzed the available serum and postmortem samples at the Instituto Adolfo Lutz, the central public health laboratory for YF and other notifiable diseases. We extracted the viral RNA from 140 μL of serum by using a QIAamp Viral RNA Minikit (QIAGEN, https://www.qiagen.com) according to the manufacturer's instructions. We tested the viral genome by using the real-time reverse transcription PCR (RT-PCR) protocol as described by Domingo et al. (*4*). Positive samples were submitted to a second RT-PCR reaction, according to Bae et al. (*5*). This reaction can detect 17DD viral genome but cannot amplify viral genome from wild-type strains circulating in the Americas. We considered samples that tested positive by both RT-PCR protocols positive for vaccine-associated virus. We isolated the YF virus from serum samples using cultured cells of *Aedes albopictus*, clone C6/36, and performed viral identification using indirect immunofluorescence assay with polyclonal YF antibodies and conjugated antimouse immunoglobulins. We used the US Centers for Disease Control and Prevention MAC-ELISA protocol for detecting IgM (*6*). The postmortem samples were analyzed by 2 expert pathologists in infectious diseases and YF pathology (S.D'A.I. and A.N.D.N.). We performed immunohistochemistry reactions to detect in situ YF virus antigens using a polyclonal wild YF virus strain primary antibody (*7*). This study was approved by the Research Ethics Committee of the Health Department of the Municipality of São Paulo (approval no. CAAE 37233620.5.0000.0086).

Results

Cluster 1

Case 1 was that of a 40-year-old white man who received the first dose of 17DD YF vaccine (lot 174VFC056Z) on December 16, 2017 (Figure 1). No simultaneous vaccines were administered. On day 3 after vaccination,

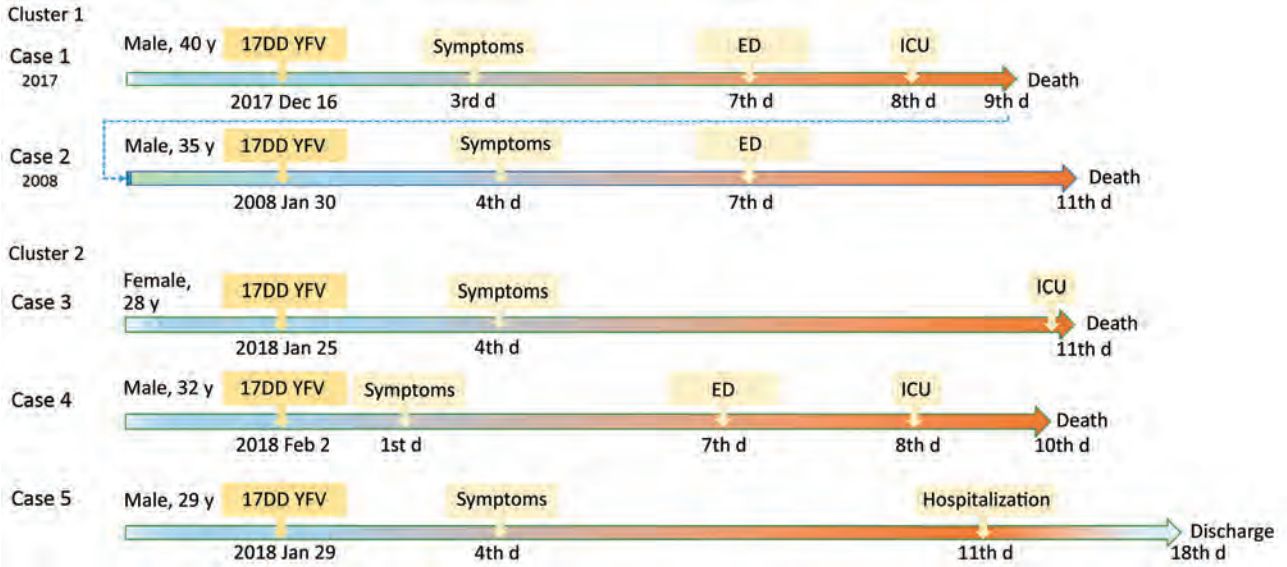

Figure 1. Timelines of reported cases of YFV–associated viscerotropic disease after 17DD vaccination during yellow fever epidemic, São Paulo state, Brazil, 2017–2018. Cases 1–2 were brothers and received standard doses. Cases 3–5 are siblings and received fractionated doses. ED, emergency department; ICU, intensive care unit; YFV, yellow fever vaccine.

headache, malaise, and fever developed, and he took analgesics. After a day of clinical improvement, his symptoms returned, along with a high fever, nausea, and vomiting, for the next 3 days. On day 7 after vaccination, he was admitted to the emergency department for diffuse abdominal pain and hypotension. Initial laboratory tests revealed only thrombocytopenia (platelets 51,000/mm^3 [reference range 150,000–450,000/mm^2]). On day 8 after vaccination, he had fever, jaundice, conjunctival hyperemia, peripheral edema, hypotension, dyspnea, tachycardia, and oliguria. The patient was transferred to a tertiary-care center in critical condition experiencing respiratory distress, shock, and metabolic acidosis (arterial blood gas pH 6.8, bicarbonate 9 mmol/L, carbon dioxide partial pressure 58 mm Hg, and partial pressure of oxygen 50 mm Hg). He was started on mechanical ventilation and was administered antibiotics (piperacillin and tazobactam), fluids, and vasoactive drugs. Chest radiography revealed bilateral pulmonary congestion in the middle-upper lobes. Laboratory tests revealed increased total leukocyte count with left shift (total leukocyte count 34,700 cells/mm^3; promyelocytes 2%, myelocytes 4%, metamyelocytes 8%, rods 34%, and neutrophils 42%), as well as increased serum levels of creatinine, urea, creatine phosphokinase, liver enzymes, and bilirubin. His platelets dropped to 38,000/mm^3, and the international normalized ratio (INR) increased (Table). The serum level of C-reactive protein increased (20.66 mg/dL). The patient died on December 25, 2017, on day 9 after vaccination (Figure 1), day 6 after illness onset.

Autopsy results (Figure 2, panels A–J) revealed microvesicular steatosis with discrete and mixed portal and sinusoidal inflammatory infiltrates in the liver; acute tubular necrosis and interstitial nephritis in the kidneys; edema and interstitial mononuclear infiltrates in the myocardium; pulmonary hemorrhages; mild cerebral edema; and hypoplasia of the white pulp of the spleen. Immunohistochemistry detected YF antigens in the Kupffer cells, rare hepatocytes, and in inflammatory cells in the liver, kidneys, heart, and spleen. The same 17DD strain was identified by RT-PCR in a serum sample collected on December 25 (day 9 after vaccination), and the virus was isolated after inoculation in C6/36 cells.

Case 2 was that of a 35-year-old man who received the first dose of 17DD YF vaccine (lot information unavailable) on January 30, 2008 (Figure 1), because he wished to travel to YF-endemic areas of Brazil. On February 3, 2008 (day 4 after vaccination), he began experiencing fever (38.5°C) and myalgia. The symptoms progressively worsened; 3 days later, he was hospitalized with vomiting, diarrhea, petechiae, and jaundice. He began experiencing oliguria, mental confusion, and generalized clonic-tonic convulsions on day 7 after vaccination and was transferred to a tertiary-care center. Laboratory tests revealed high INR (1.37), increased serum direct and indirect bilirubin levels (8.49 and 7.22 mg/dL), elevated liver enzymes (aspartate aminotransferase [AST] 492 U/L and alanine aminotransferase [ALT] 189 U/L), thrombocytopenia (platelets 52,000/mm^3), leukocytosis (24,300 cells/mm^3) with an increase in neutrophil proportion (6% rods and 81% segmented cells), and acute renal failure (creatinine 4.8 mg/dL, urea 131 mg/dL). The patient was started on mechanical ventilation and administered fluids, platelet transfusions, and ceftriaxone for possible acute meningitis. However, the patient experienced progressive multiple organ dysfunction with worsening liver and renal functions and coagulopathy (Table). The patient died on day 11 after vaccination (Figure 1), day 9 after illness onset.

After the death of the patient in case 1, the surveillance team traced and recovered a serum sample from case 2, which was collected on February 9, 2008 (day 10 after vaccination) and stored at −20°C in the Instituto Adolfo Lutz for 10 years. This sample was sent to Biomanguinhos/Fiocruz (Rio de Janeiro, Brazil) for further analysis, which revealed detectable RNA of 17DD YF with a low viral load. Patients in both cases had 2 siblings and parents who were vaccinated during the YF vaccine campaigns in the state of São Paulo. No AEFI was reported among their relatives.

Cluster 2

Case 3 was that of a 28-year-old white woman who received the first dose of 17DD YF vaccine (fractionated dose, lot 175VFC064Z) on January 25, 2018 (Figure 1). On day 4 after vaccination, she began experiencing abdominal pain, fever (38°C), vomiting, dysuria, and generalized myalgia. She was prescribed analgesics. On day 11 after vaccination, she returned for medical assistance because her condition had worsened and included tachycardia and tachypnea. Laboratory tests revealed leukocyte count of 19,370 cells/mm^3 with 77% neutrophils and 2% rods; hemoglobin 14 g/dL and hematocrit 40.4%; thrombocytopenia (platelets 29,000/mm^3); acute renal failure (creatinine 2.92 U/dL, urea 153 U/dL); and elevated serum liver enzymes (AST 464 U/L and ALT 137 U/L) and creatine phosphokinase (CPK) (99 U/L). Urinalysis revealed proteinuria, leukocyturia, and hematuria. The first differential diagnosis was sepsis caused by urinary tract infection, and the patient was prescribed ceftriaxone. She was transferred to a tertiary-care center for respiratory distress, hypoglycemia, oliguria, metabolic

Table. Clinical findings of cases of adverse events after YF vaccination in siblings from 2 familial clusters, São Paulo state, Brazil, 2017–2018*

	Cluster 1		Cluster 2		
Case information	Case 1	Case 2	Case 3	Case 4	Case 5
Patient age, y/sex	40/M	35/M	28/F	32/M	29/M
Patient race	White	White	White	White	White
Kind of YF vaccine	Standard	Standard	Fractionated	Fractionated	Fractionated
Days from vaccination to symptom onset	3	4	4	1	4
Symptoms	Fever, headache, vomiting, abdominal pain, jaundice, bleeding	Fever, myalgia, vomiting, diarrhea, jaundice, seizures	Fever, myalgia, abdominal pain, dysuria, vomiting, bleeding	Fever, myalgia, abdominal pain, jaundice, bleeding	Fever, vomiting, myalgia, headache
Platelets, per µL†	38,000	29,000	23,000	29,000	75,000
Aspartate transaminase, U/L†	366	2,254	769	1,930	137
Alanine aminotransferase, U/L	166	617	180	503	122
International normalized ratio†	1.94	1.8	1.9	2.0	2.0
Total bilirubin, mg/dL†	8.5	8.5	6.5	7.6	0.6
Creatinine, mg/dL†	6.7	5.9	2.9	5.9	1.4
Creatinine phosphokinase†	428	1,061	13,080	2,770	514
Outcome	Died	Died	Died	Died	Recovered
RT-PCR for YF vaccine in blood	Positive, 9 DAV	Positive, 10 DAV	Positive, 11 DAV	Positive, 10 DAV	Positive, 14 DAV
Viral isolation in serum sample >7 DAV	Positive, 9 DAV	ND	ND	ND	ND
YF IgM	Detected, 9 DAV	ND	ND	Detected, 10 DAV	Negative, 14 DAV
Liver histopathological pattern at autopsy	Typical‡	ND	ND	Typical‡	ND
YF immunohistochemistry in hepatic tissue	Positive	NA	NA	Positive	NA
RT-PCR for YF in liver	ND	ND	ND	Positive	ND

*DAV, days after vaccination; NA, not applicable; ND, not done; RT-PCR, reverse transcription PCR; YF, yellow fever.
†Most altered result.
‡The liver exhibited discrete microvesicular fatty change and mixed sinusoidal inflammatory infiltrate, with no evidence of hepatocellular necrosis in the sample.

acidosis (pH 7.07, bicarbonate 10.3 mmol/L), and progressive shock. In the intensive care unit, she was started on mechanical ventilation and cardiovascular support, but her condition deteriorated. The leukocyte count increased to 31,500 cells/mm^3 with 88% neutrophils, 5% rods, and 5% lymphocytes, as well as a serum C-reactive protein level of 90.4 mg/dL. The levels of platelets, INR, CPK, and liver function parameters worsened (Table). The patient experienced refractory acidosis and died the same day (Figure 1).

Case 4 was that of a 32-year-old white man who was the brother of the patient in case 3. He received the first dose of 17DD YF vaccine (fractionated dose, lot 173VFA013Z) on February 2, 2018 (Figure 1). On day 1 after vaccination, he began experiencing malaise, myalgia, chest pain, epigastric pain, and fever (39.3°C). He sought medical care at the local ED and was prescribed analgesics. On February 9, 2018 (day 7 after vaccination) he again sought medical care; examination revealed tachycardia (130 bpm), thrombocytopenia (platelets 80,000/mm^3), proteinuria, leukocyturia, and hematuria. He was prescribed fluid therapy, antipyretics, and ciprofloxacin and was discharged. On the 8th day of illness (February 10, 2018), he returned to the ED with jaundice, dyspnea, hypotension, and a capillary blood glucose level of 63 mg/dL. At that point, laboratory analysis revealed renal insufficiency (creatinine 3.1 U/dL, urea 82 U/dL); increased liver enzyme levels (AST 214 U/L, ALT 95 U/L), increased serum (6.7 mg/dL) and direct (3.12 mg/dL) bilirubin; and increased INR 1.88. CPK level was unremarkable (194 U/L). The patient was treated with fluids and intravenous glucose and was transferred to a tertiary-care center. In the intensive care unit, the patient experienced hematuria, oliguria, agitation, mental confusion, metabolic acidosis (pH 7.08, bicarbonate 15.2 mmol/L), shock, and hypoxemia. He was prescribed mechanical ventilation, ceftriaxone for possible urinary sepsis, intravenous glucose, fresh frozen plasma, cryoprecipitate, hydrocortisone, vasoactive drugs, and hemodialysis. His medical condition continued to deteriorate despite supportive therapy, and multiple organ failure developed (Table). The patient died on day 10 after vaccination (Figure 1), day 9 after illness onset. A postmortem liver sample was collected, and histopathological analysis (Figure 1, panels K, L) revealed midzonal microvesicular steatosis with scattered acidophilic degeneration of hepatocytes (Councilman bodies) and discrete periportal inflammatory reaction, congestion, and cholestasis. Immunocytochemistry detected YF virus antigens in the Kupffer cells and

mesenchymal cells. RT-PCR detected RNA of 17DD YF in the hepatic tissue.

Case 5 was that of a 29-year-old white man who was a brother of the patients in cases 3 and 4. He received the first dose of 17DD YF vaccine (fractionated dose, lot 173VFA013Z) on January 29, 2018 (Figure 1). On day 4 after vaccination, he began experiencing nausea, vomiting, generalized myalgia, fever, and headache. On February 7, he sought medical care; the first differential diagnosis was urinary tract infection. Initial laboratory tests revealed leukocyte count of 7,000 cells/mm^3 with 80% neutrophils and 11% lymphocytes, hemoglobin 14.8 g/dL, hematocrit 44%, and platelets 92,000/mm^3. Urinalysis revealed hematuria and leukocyturia. The patient was discharged with antipyretics and oral ciprofloxacin. The next day, he began experiencing diffuse abdominal pain and returned to an ED. After normal abdominal ultrasonography, he was administered fluid therapy and antiemetics and discharged. On February 9, 2008, he was admitted to the hospital with the same symptoms, as well as mental confusion and fever. His leukocyte count increased to 22,700/mm^3 and the platelet count dropped to 75,000/mm^3, and other test results showed mild acute renal injury (creatinine 1.4 U/dL) and hepatitis (AST 137 U/L, ALT 121 U/L,

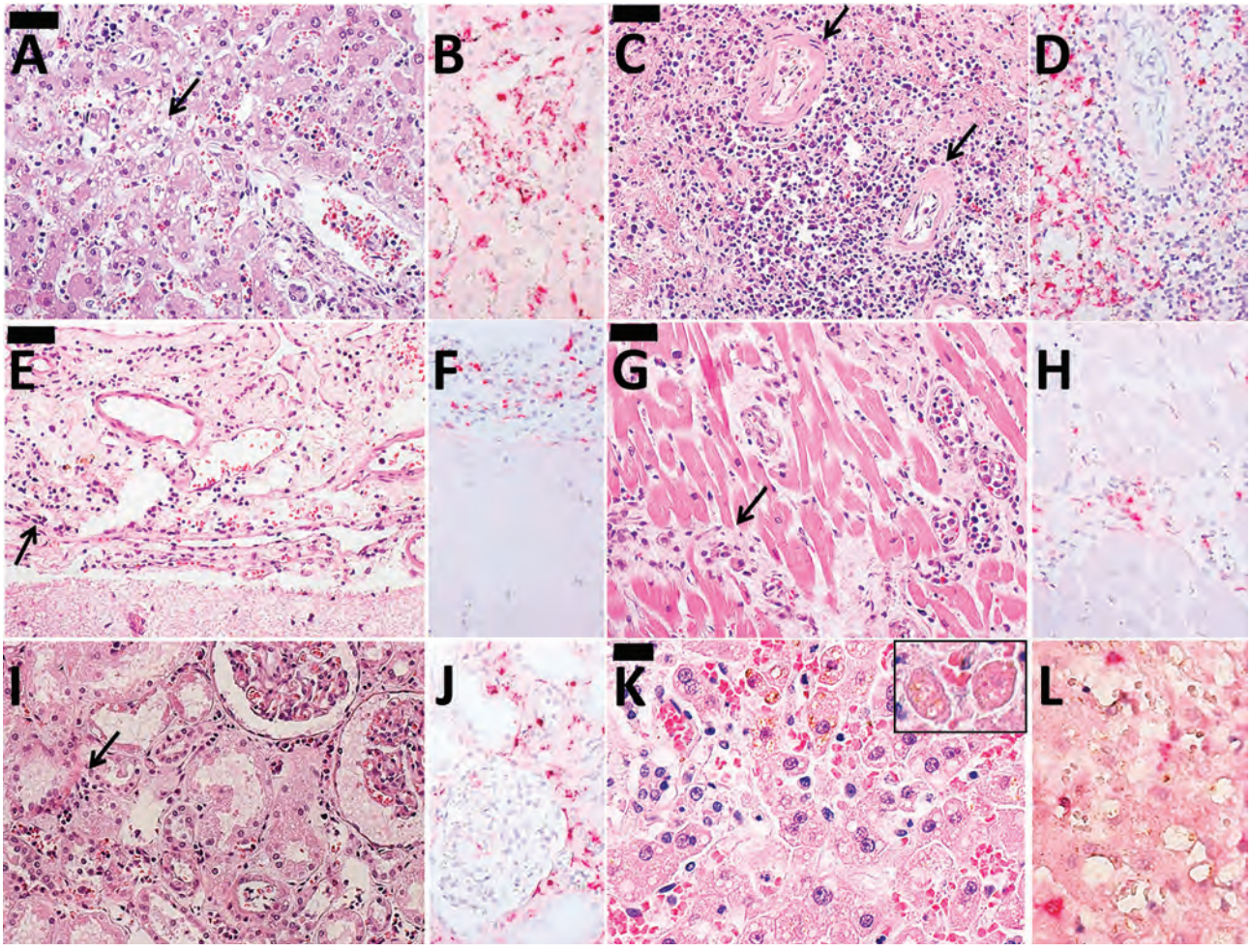

Figure 2. Histopathological findings in 2 case-patients with fatal reaction to 17DD yellow fever (YF) vaccine, São Paolo state, Brazil, 2017–2018. A, B) Liver tissue from case 1: A) steatotic hepatitis (arrow) with scarce inflammatory reaction and rare apoptotic bodies; B) immunostaining for YF antigens in Kuppfer cells and inflammatory cells in the portal tract. C, D) Spleen tissue from case 1: C) lymphoid hypoplasia (arrows); D) YF antigens in cells located on the white pulp and red pulp. E, F) Meningeal tissue from case 1: E) mononuclear meningoencephalitis (arrow); F) YF antigens detected in the cytoplasm of meningeal inflammatory cells. G, H) Cardiac tissue from case 1: G) mononuclear interstitial myocarditis (arrow); H) positive YF antigens detected in the inflammatory cells; I, J) Kidney tissue from case 1: I) acute tubular necrosis and interstitial nephritis (arrow); J) detectable YF antigens in the inflammatory cells. K ,L) Liver tissue from case 2: K) steatotic hepatitis with rare apoptotic bodies (inset); L) scarce immunodetection of YF antigens in the Kuppfer cells. Panels A, C, D, E, G, I, and K are hematoxylin and eosin stained; B, D, F, H, J, and L are immunohistochemistry with alkaline phosphatase conjugated polymer, using a mouse polyclonal YF antibody directed to wild strain (Instituto Adolfo Lutz, São Paolo, Brazil). Scale bars in panels A, C, E, and G indicate 50 μm and in panel K indicates 20 μm. Original magnification ×400.

and INR 2.04). The patient responded well to fluid therapy and antibiotics, and the laboratory parameters returned to normal levels by day 16 after vaccination (Figure 1).

The patients in cases 3–5 were 3 of 11 siblings. Their parents died years before the events reported in this study and their YF vaccination status was unknown. Of the 11 siblings, 9 were vaccinated for YF for the first time during the 2017–2018 campaign. No other AEFI were reported.

The patients in these cases had no recent history of travel, acute medical conditions, or other vaccinations within the previous month. The patient in case 3 was obese, but none of the other patients had relevant medical conditions. In cases 1 and 4, YF IgM was detected using MAC-ELISA. Serum samples from all patients had detectable RNA of 17DD YF strain; samples were collected on the day of death, except in case 5, in which the sample was collected day 14 after vaccination. During hospitalization, all patients had negative results on serologic tests for dengue, leptospirosis, hepatitis B core protein, hepatitis B surface antigen, hepatitis A virus, and HIV, as well as blood and urine cultures.

Discussion

We describe 2 clusters of siblings with YEL-AVD. The clinical characteristics of all the cases match those of YEL-AVD previously described (*8*–*12*). The symptoms began within the first week after vaccination (range 1–4 days); the initial symptoms were nonspecific (fever, headache, myalgia, nausea, and vomiting) and evolved alongside laboratory abnormalities (thrombocytopenia and elevation of serum total bilirubin, hepatic transaminases, and creatinine levels). The patients who died experienced hypotension and hemorrhage, as well as acute renal and respiratory failure and coagulopathy.

In each cluster, at least 1 case was confirmed (*3*,*13*). In case 1, YF was detected in serum >7 days after vaccination with a typical histopathological pattern and in the liver by immunohistochemistry. Case 4 (cluster 2) included a typical histopathological pattern and positive RT-PCR result for YF in the liver. The other cases were characterized as suspected cases because of their clinical characteristics and lack of available histopathologic details.

Considering the Brighton Collaboration criteria for case definition (*3*), 4 patients (cases 1–4) met ≥3 major criteria: hepatic abnormalities (total bilirubin ≥1.5 times the upper limit of normal [ULN] or ALT or AST ≥3 times ULN), renal abnormalities (creatinine ≥1.5 times ULN), musculoskeletal abnormalities (CPK ≥5 times ULN), respiratory abnormalities (oxygen saturation ≤88% on room air or need for mechanical ventilation), platelet count <100,000/μL, and coagulopathy (INR≥1.5). Those patients were classified as level 1 diagnostic certainty according to the case definition of viscerotropic disease (*3*). Case 5 satisfied 2 major criteria (platelet count 75,000/μL and INR 2) with level 2 diagnostic certainty for viscerotropic disease (*3*). However, case 5 had YF 17DD viral RNA in blood samples 14 days after vaccination, which qualifies for diagnosis of a viscerotropic disease and definite yellow fever vaccine–associated causality, according to the Brighton Collaboration (*3*).

Case 2 was identified retrospectively. His clinical manifestations were typical and similar to those of his sibling (case 1). Despite the positive RT-PCR test for YFVV, the viral load was low, and viral isolation was not possible. However, this result does not invalidate the discovery. The serum sample was stored for >10 years, which could have compromised the test to identify the virus.

Ours is not the first report of a viscerotropic disease among siblings in Brazil. A 19-year-old woman experienced YEL-AVD and died; her 12-year-old sister also experienced a severe adverse event after 17DD YF vaccination, which suggested YEL-AVD, but she recovered (*14*). Two siblings 30 and 34 years of age with diagnoses of adrenal insufficiency (Addison's disease) who were receiving physiologic doses of cortisone died of probable YEL-AVD (*15*).

Among the AEFI cases during the 2017–2018 YF vaccination campaign, cases 3 and 5 (cluster 2) received vaccines from the same lot. Case 4 (cluster 2) and case 1 (cluster 1) received vaccines from different lots. The same lots were distributed to >50 cities and were administered to hundreds of thousands of other persons without any reported serious adverse events (data not shown). No changes in the manufacturing methods of the 17DD vaccine in Brazil could account for the adverse events. Genetic mutations in the YF virus do not seem to be the cause of the adverse reactions because the vaccine virus in the previously confirmed YEL-AVD cases revealed no substantial mutation from the original lot (*12*,*16*,*17*). Furthermore, the YF virus isolates recovered from fatal cases of YEL-AVD revealed no reversion to virulence in animal models (*16*). The occurrence of adverse events might have been related to individual, genetically determined host factors, which is strengthened by the incidence of cases among siblings.

The cases we report strengthen the hypothesis of host genetic predisposition to YEL-AVD. Impaired immunologic profiles have suggested that a robust adaptive immune response with abnormalities in the innate

immune system might be involved in the development of YEL-AEFI (*14*,*18*–*21*). The genomic signatures correlated with the immune response to 17DD YF, revealing molecular events observed in the innate immunity against viruses (*22*). Molecules involved in the innate sensing of viruses, such as cytoplasmic receptors of 2,5′-OAS (oligoadenylate synthetase) family members 1, 2, 3 and L, TLR7 (toll-like receptor 7), MDA-5 (melanoma differentiation-associated), and RIG-I (retinoic acid-inducible I), as well as transcription factors that regulate type I interferons (IRF7 [interferon regulatory factor 7] and STAT1 [signal transducer and activator of transcription 1]), are induced (*22*). Genetic variations could result in an impairment of the innate immune response involved in the direct control of viral replication or in mediating viral clearance. The reduced expression of CCR5 (C-C chemokine receptor type 5) because of polymorphism might impair the responsiveness of cells to ligands such as RANTES (Regulated upon Activation, Normal T Cell Expressed and Presumably Secreted) (*20*). Such a breakdown could impair the migration of monocytes to tissue sites of infection with a milder innate response that fails to limit early viral replication (*20*). An investigated fatal case of YEL-AVD revealed genetic variations in the OAS genes that encode essential proteins involved in the innate immune response to viral infections (*17*).

The 17DD YF virus promotes the induction of critical type I interferon (IFN) mediators, such as STAT1 and IRF7 in humans, which lead to the expression of IFN-stimulated genes with antiviral properties, thus effectively mounting an antiviral response in infected and surrounding cells (*22*–*25*). Hernandez et al. (*26*) revealed IFN-αβ receptor 1 deficiency in a 14-year-old girl in whom YEL-AVD was diagnosed without any known risk factors for the disease. In this case, a single-gene inborn error of innate immunity, specifically that of type I IFN cell-intrinsic immunity, was related to the severe adverse reactions to the YF vaccine (*26*). In another study, a case-patient with YEL-AVD had a complete recessive IFN-αβ receptor 2 deficiency (*14*). The patient in case 5 in that study, the only one who survived, underwent exome sequence analysis with other ongoing studies; however, no inborn errors of type I IFN or autoantibodies against IFN I were identified (*14*).

In this study, the siblings in cluster 1 received standard doses of 17DD YF vaccine, whereas the siblings in cluster 2 received fractionated doses. Clinical trials have identified similar viremia and immunogenic responses between the doses. No serious adverse events were identified in these studies, although the sample size was too small for a safety evaluation (*27*–*32*).

Our findings strongly suggest that genetic predispositions in innate immune responses are related to the occurrence of YEL-AVD disease. Future investigations into genetic predispositions to YEL-AVD are warranted. Obtaining a thorough medical history, particularly regarding severe reactions to the vaccine in family members, is advisable before administering the 17DD YF vaccine.

M.L.S.M., P.M.N.O., G.V.T., and L.K.L. are employees of Biomanguinhos, a public and nonprofit producer of the yellow fever vaccine.

About the Author

Dr. Fernandes is a medical doctor and infectious disease specialist at the Emílio Ribas Institute of Infectious Diseases and the Immunization Division of the State of São Paulo. His primary research interests are vaccine safety, infectious diseases, and epidemiology.

References

1. Brazil Ministry of Health. Secretary of Health Surveillance. General coordination for the development of epidemiology in services. Health surveillance guide 2019 [cited 2022 Jun 15]. https://bvsms.saude.gov.br/bvs/publicacoes/guia_vigilancia_saude_3ed.pdf
2. Epidemiological Surveillance Center. "Prof. Alexandre Vranjac." Epidemiological bulletin yellow fever update. 2022 [cited 2022 Jun 16]. https://www.saude.sp.gov.br/cve-centro-de-vigilancia-epidemiologica-prof.-alexandre-vranjac/areas-de-vigilancia/doencas-de-transmisSão-por-vetores-e-zoonoses/agravos/febre-amarela/boletim-epidemiologico
3. Gershman MD, Staples JE, Bentsi-Enchill AD, Breugelmans JG, Brito GS, Camacho LAB, et al.; Brighton Collaboration Viscerotropic Disease Working Group. Viscerotropic disease: case definition and guidelines for collection, analysis, and presentation of immunization safety data. Vaccine. 2012;30:5038–58. https://doi.org/10.1016/j.vaccine.2012.04.067
4. Domingo C, Patel P, Yillah J, Weidmann M, Méndez JA, Nakouné ER, et al. Advanced yellow fever virus genome detection in point-of-care facilities and reference laboratories. J Clin Microbiol. 2012;50:4054–60. https://doi.org/10.1128/JCM.01799-12
5. Bae HG, Nitsche A, Teichmann A, Biel SS, Niedrig M. Detection of yellow fever virus: a comparison of quantitative real-time PCR and plaque assay. J Virol Methods. 2003;110:185–91. https://doi.org/10.1016/S0166-0934(03)00129-0
6. Martin DA, Muth DA, Brown T, Johnson AJ, Karabatsos N, Roehrig JT. Standardization of immunoglobulin M capture enzyme-linked immunosorbent assays for routine diagnosis of arboviral infections. J Clin Microbiol. 2000;38:1823–6.
7. Duarte-Neto AN, Cunha MDP, Marcilio I, Song ATW, de Martino RB, Ho YL, et al. Yellow fever and orthotopic liver transplantation: new insights from the autopsy room for an old but re-emerging disease. Histopathology. 2019;75:638–48. https://doi.org/10.1111/his.13904
8. Khromava AY, Eidex RB, Weld LH, Kohl KS, Bradshaw RD, Chen RT, et al.; Yellow Fever Vaccine Safety Working Group.

Yellow fever vaccine: an updated assessment of advanced age as a risk factor for serious adverse events. Vaccine. 2005; 23:3256–63. https://doi.org/10.1016/j.vaccine.2005.01.089
9. Martin M, Weld LH, Tsai TF, Mootrey GT, Chen RT, Niu M, et al.; GeoSentinel Yellow Fever Working Group1. Advanced age a risk factor for illness temporally associated with yellow fever vaccination. Emerg Infect Dis. 2001;7:945–51. https://doi.org/10.3201/eid0706.010605
10. Lawrence GL, Burgess MA, Kass RB. Age-related risk of adverse events following yellow fever vaccination in Australia. Commun Dis Intell Q Rep. 2004;28:244–8.
11. Martin M, Tsai TF, Cropp B, Chang GJ, Holmes DA, Tseng J, et al. Fever and multisystem organ failure associated with 17D-204 yellow fever vaccination: a report of four cases. Lancet. 2001;358:98–104. https://doi.org/10.1016/S0140-6736(01)05327-2
12. Whittembury A, Ramirez G, Hernández H, Ropero AM, Waterman S, Ticona M, et al. Viscerotropic disease following yellow fever vaccination in Peru. Vaccine. 2009;27:5974–81. https://doi.org/10.1016/j.vaccine.2009.07.082
13. Staples JE, Gershman M, Fischer M; Centers for Disease Control and Prevention (CDC). Yellow fever vaccine: recommendations of the Advisory Committee on Immunization Practices (ACIP). MMWR Recomm Rep. 2010;59(RR-7):1–27.
14. Bastard P, Michailidis E, Hoffmann HH, Chbihi M, Le Voyer T, Rosain J, et al. Auto-antibodies to type I IFNs can underlie adverse reactions to yellow fever live attenuated vaccine. J Exp Med. 2021;218:e20202486. https://doi.org/10.1084/jem.20202486
15. Martins RM, Maia MLS, Santos EM, Cruz RLS, dos Santos PRG, Carvalho SMD, et al. Yellow fever vaccine post-marketing surveillance in Brazil. Procedia Vaccinol. 2010;2:178–83. https://doi.org/10.1016/j.provac.2010.07.012
16. Galler R, Pugachev KV, Santos CL, Ocran SW, Jabor AV, Rodrigues SG, et al. Phenotypic and molecular analyses of yellow fever 17DD vaccine viruses associated with serious adverse events in Brazil. Virology. 2001;290:309–19. https://doi.org/10.1006/viro.2001.1168
17. Belsher JL, Gay P, Brinton M, DellaValla J, Ridenour R, Lanciotti R, et al. Fatal multiorgan failure due to yellow fever vaccine-associated viscerotropic disease. Vaccine. 2007; 25:8480–5. https://doi.org/10.1016/j.vaccine.2007.08.061
18. Bae HG, Domingo C, Tenorio A, de Ory F, Muñoz J, Weber P, et al. Immune response during adverse events after 17D-derived yellow fever vaccination in Europe. J Infect Dis. 2008;197:1577–84. https://doi.org/10.1086/587844
19. Fradico JRB, Campi-Azevedo AC, Peruhype-Magalhães V, Coelho-Dos-Reis JGA, Faria ES, Drumond BP, et al. CCL3, CCL5, IL-15, IL-1Ra and VEGF compose a reliable algorithm to discriminate classes of adverse events following 17DD-YF primary vaccination according to cause-specific definitions. Vaccine. 2021;39:4359–72. https://doi.org/10.1016/j.vaccine.2021.05.101
20. Pulendran B, Miller J, Querec TD, Akondy R, Moseley N, Laur O, et al. Case of yellow fever vaccine—associated viscerotropic disease with prolonged viremia, robust adaptive immune responses, and polymorphisms in CCR5 and RANTES genes. J Infect Dis. 2008;198:500–7. https://doi.org/10.1086/590187
21. Silva ML, Espírito-Santo LR, Martins MA, Silveira-Lemos D, Peruhype-Magalhães V, Caminha RC, et al. Clinical and immunological insights on severe, adverse neurotropic and viscerotropic disease following 17D yellow fever vaccination. Clin Vaccine Immunol. 2010;17:118–26. https://doi.org/10.1128/CVI.00369-09
22. Querec TD, Akondy RS, Lee EK, Cao W, Nakaya HI, Teuwen D, et al. Systems biology approach predicts immunogenicity of the yellow fever vaccine in humans. Nat Immunol. 2009;10:116–25. https://doi.org/10.1038/ni.1688
23. Gaucher D, Therrien R, Kettaf N, Angermann BR, Boucher G, Filali-Mouhim A, et al. Yellow fever vaccine induces integrated multilineage and polyfunctional immune responses. J Exp Med. 2008;205:3119–31. https://doi.org/10.1084/jem.20082292
24. Fernandez-Garcia MD, Meertens L, Chazal M, Hafirassou ML, Dejarnac O, Zamborlini A, et al. Vaccine and wild-type strains of yellow fever virus engage distinct entry mechanisms and differentially stimulate antiviral immune responses. MBio. 2016;7:e01956–15. https://doi.org/10.1128/mBio.01956-15
25. Erickson AK, Pfeiffer JK. Dynamic viral dissemination in mice infected with yellow fever virus strain 17D. J Virol. 2013;87:12392–7. https://doi.org/10.1128/JVI.02149-13
26. Hernandez N, Bucciol G, Moens L, Le Pen J, Shahrooei M, Goudouris E, et al. Inherited IFNAR1 deficiency in otherwise healthy patients with adverse reaction to measles and yellow fever live vaccines. J Exp Med. 2019;216:2057–70. https://doi.org/10.1084/jem.20182295
27. Nnaji CA, Shey MS, Adetokunboh OO, Wiysonge CS. Immunogenicity and safety of fractional dose yellow fever vaccination: a systematic review and meta-analysis. Vaccine. 2020;38:1291–301. https://doi.org/10.1016/j.vaccine.2019.12.018
28. Emi Aikawa N, Andrade Balbi V, Borba EF, Coracini Tonacio A, Maluf Elias Sallum A, Maria Arruda Campos L, et al. Yellow fever vaccination in Brazil: short-term safety and immunogenicity in juvenile autoimmune rheumatic diseases. Vaccine X. 2021;10:100131. https://doi.org/10.1016/j.jvacx.2021.100131
29. Lopes Ode S, Guimarães SS, de Carvalho R. Studies on yellow fever vaccine. III—dose response in volunteers. J Biol Stand. 1988;16:77–82. https://doi.org/10.1016/0092-1157(88)90034-0
30. Campi-Azevedo AC, de Almeida Estevam P, Coelho-Dos-Reis JG, Peruhype-Magalhães V, Villela-Rezende G, Quaresma PF, et al. Subdoses of 17DD yellow fever vaccine elicit equivalent virological/immunological kinetics timeline. BMC Infect Dis. 2014;14:391. https://doi.org/10.1186/1471-2334-14-391
31. Roukens AH, Vossen AC, Bredenbeek PJ, van Dissel JT, Visser LG. Intradermally administered yellow fever vaccine at reduced dose induces a protective immune response: a randomized controlled non-inferiority trial. PLoS One. 2008;3:e1993. https://doi.org/10.1371/journal.pone.0001993
32. Martins RM, Maia ML, Farias RHG, Camacho LAB, Freire MS, Galler R, et al. 17DD yellow fever vaccine: a double blind, randomized clinical trial of immunogenicity and safety on a dose-response study. Hum Vaccin Immunother. 2013;9:879–88. https://doi.org/10.4161/hv.22982

Address for correspondence: Eder Gatti Fernandes, Divisão de Imunização, Centro de Vigilância Epidemiológica "Prof. Alexandre Vranjac," Coordenadoria de Controle de Doenças da Secretaria de Estado da Saúde de São Paulo, Av. Dr Arnaldo, 351, 6° andar, Pacaembu, 01246-000, São Paulo, SP, Brazil; email: edergatti@hotmail.com

COVID-19 Test Allocation Strategy to Mitigate SARS-CoV-2 Infections across School Districts

Remy Pasco, Kaitlyn Johnson, Spencer J. Fox, Kelly A. Pierce, Maureen Johnson-León, Michael Lachmann, David P. Morton, Lauren Ancel Meyers

In response to COVID-19, schools across the United States closed in early 2020; many did not fully reopen until late 2021. Although regular testing of asymptomatic students, teachers, and staff can reduce transmission risks, few school systems consistently used proactive testing to safeguard return to classrooms. Socioeconomically diverse public school districts might vary testing levels across campuses to ensure fair, effective use of limited resources. We describe a test allocation approach to reduce overall infections and disparities across school districts. Using a model of SARS-CoV-2 transmission in schools fit to data from a large metropolitan school district in Texas, we reduced incidence between the highest and lowest risk schools from a 5.6-fold difference under proportional test allocation to 1.8-fold difference under our optimized test allocation. This approach provides a roadmap to help school districts deploy proactive testing and mitigate risks of future SARS-CoV-2 variants and other pathogen threats.

By early January 2023, the COVID-19 pandemic had caused >6.7 million deaths worldwide (*1*), and severe socioeconomic hardship (*2*–*4*), particularly for racial minorities (*5*,*6*). Children experienced pandemic-related school closures that led to substantial losses in learning (*7*–*9*), elevated rates of child abuse (*10*), lack of access to healthy food (*11*), and emotional harm (*12*). By the end of March 2020, all kindergarten through 12th grade (K–12) public schools in the United States had stopped in-person instruction (*13*), affecting 55 million students. Schools in 48 US states remained closed through the end of the school year (*14*). In August and September of 2020, a total of 74% of the 100 largest school districts in the United States started the year with remote-only teaching (*15*). By November 2020, 19% of those districts remained fully remote, and 36% had fully resumed in-person learning (*15*). Schools continued to reopen throughout the year.

By September 2021, a large fraction (70%) of US adults had been vaccinated with highly effective SARS-CoV-2 vaccines (*16*), including an estimated 86% of K–12 teachers and school staff (*17*). However, children <12 years of age were still ineligible for vaccines (*16*,*18*). Because large pockets of the country were still unvaccinated, COVID-19 continued to claim lives, and 100,000 deaths were reported in the United States during July–September 2021, including 246 deaths among children 0–17 years of age (*16*). At the end of October 2021, the United States authorized administration of COVID-19 vaccines for children 5–11 years of age (*19*). In January 2022, schools returned from winter break amidst a major COVID-19 wave fueled by the emergence of the highly transmissible and immune-evasive Omicron variant (F.P. Lyngse, unpub. data, https://doi.org/10.1101/2021.12.27.21268278), and case counts among students and staff reached record numbers despite increasing vaccine coverage in the United States (*16*,*20*).

Schools across the country adopted diverse reopening plans for the 2021–22 school year. Among the largest districts, 96% offered some form of in-person learning (*21*). Although some schools fully returned to prepandemic normal operations without COVID-19 interventions, many adopted policies for using masks, social distancing, quarantine, or testing requirements to safeguard the return to campus. The federal government invested $122 billion to support safe, in-person instruction through screening, improved building ventilation, purchase of personal protective equipment, hiring of additional personnel,

Author affiliations: The University of Texas at Austin, Austin, Texas, USA (R. Pasco, K. Johnson, S.J. Fox, K.A. Pierce, M. Johnson-León, L.A. Meyers); Santa Fe Institute, Santa Fe, New Mexico, USA (M. Lachmann, L.A. Meyers); Northwestern University, Evanston, Illinois, USA (D.P. Morton)

DOI: https://doi.org/10.3201/eid2903.220761

and other measures (*22*,*23*). Within the first 2 months of the school year, ≈1.5% of schools closed temporarily in response to COVID-19 outbreaks (*21*).

Frequent and systematic testing of asymptomatic persons has been shown to be a viable and cost-effective mitigation strategy in communities, universities, and schools (*24*–*29*). However, tests are costly and inaccessible for many school districts in the United States; districts with limited testing resources are forced to determine how to allocate testing across schools to protect their students, staff, and communities. Some districts have opted to restrict testing to symptomatic persons and other districts have apportioned tests according to school enrollment (*30*,*31*).

In this study, we propose a strategy for allocating testing resources across a diverse school district in which the frequency of testing depends on the school's enrollment and grade range, recent COVID-19 cases reported among students and staff, and the estimated prevalence in the surrounding (i.e., catchment) community. Coupling derivative-free constrained optimization and a detailed agent-based simulation of SARS-CoV-2 transmission within and between classrooms, we derived an optimal allocation of tests across a school system that could minimize the maximum risk for cumulative infections on any campus over a 10-week period. We applied our approach to design a testing strategy for the 11 main high schools in the Austin Independent School District (AISD; Austin, Texas, USA), which has 18,500 enrolled students and 1,500 staff (*32*).

Methods

To determine an optimal allocation of tests across schools we developed a 2-step framework in which we first modeled COVID-19 transmission within schools for different levels of surveillance testing and then used those results as an input to an optimization model (Appendix, https://wwwnc.cdc.gov/EID/article/29/3/22-0761-App1.pdf). We first considered a hypothetical school system with 6 schools of 500 students each that differ over 2 parameters: community incidence and in-school transmission rate. For community incidence, we considered low and high scenarios. In the low scenario, the community had 35 new daily cases/100,000 persons; in the high scenario the community had 70 new daily cases/100,000 persons. For the transmission rate, we considered unmitigated R_0 values to be low (1.0), moderate (1.5), or high (2.0).

We then modeled 11 high schools in AISD by using student enrollment based on attendance in early January 2021. We considered 2 different in-school transmission rate scenarios: an unmitigated transmission rate in all schools of with an R_0 of 1.0; and transmission rates of each school estimated by fitting a regression model of the number of cases reported in that school against the estimated enrollment (*33*) (Appendix).

For each school and each scenario, we ran 300 stochastic simulations. We assumed that only students (not adult staff) were tested on Monday mornings and that test results were available instantly (*34*); preliminary analysis suggested that testing adults had minimal effects. During any given week, students in the model were selected for testing evenly across classes rather than testing a subset of entire classes.

In addition to proactive testing, we assumed that 90% of symptomatic persons would seek testing 0.5–1.5 days after symptom onset and then isolate after testing, even before results are available. We assumed 20% of infected students and 57% of infected adults would become symptomatic (*35*,*36*).

In our analysis of a hypothetical school system, we assumed that tests were perfectly accurate and that a positive test immediately triggered a 14-day isolation of the person and a 14-day quarantine of household and classroom members. For our case study of AISD, we assumed lower test accuracy based on estimates for the widely used Abbott BinaxNow antigen tests (https://www.abbott.com), which had 95% sensitivity for symptomatic persons, 80% sensitivity for asymptomatic persons, and 99% specificity (*37*,*38*).

Transmission Model

We built a stochastic agent-based model of COVID-19 transmission within schools that included household transmission for students. We held the average community incidence constant through the simulation and all persons could become infected through outside interactions that were not explicitly modeled. The modeled population included students, teachers, staff, bus drivers, and members of the students' households. We modeled various contacts between agents in schools (Appendix).

We used published estimates for the average SARS-CoV-2 incubation, latent, and infectious periods, as well as a person's infectiousness through time (*39*). We assumed that asymptomatic cases were two thirds as infectious as symptomatic cases (*40*).

We simulated contacts at half-hour intervals and stochastically determined infection events based on the transmission probability between pairs of interacting persons. For each scenario, we derived the transmission rate to produce the specified unmitigated in-school R_0 (Appendix). This R_0 is the basic

reproductive rate we would obtain without any testing, symptomatic or surveillance, and reflects other mitigation measures in place, such as face masks or social distancing.

We ran simulations for 10 weeks. We initiated simulations with everyone susceptible and simulated community and household infections for 10 days before school started.

Optimization Model

The objective of our test-allocation problem was to minimize the maximum risk experienced by any school in the system under consideration. Because of the stochastic nature of our COVID-19 transmission model, we had to choose a measure that summarized the risk for a given school under each possible frequency of surveillance testing. We defined the risk for each school as the expected number of on-campus infections of students plus the 90% conditional value-at-risk (CVaR) of the number of on-campus infections. Here, CVaR represents the expected number of such infections, conditional on restricting attention to the worst 10% of simulated outcomes, and hence accounts for risk aversion. Given 2 candidate allocations with a similar average number of cases, we preferred the allocation that limited the upside tail risk in terms of a large outbreak. We further accounted for risk by taking the worst-case risk measure across all schools. We used on-campus infections, rather than total infections, because total infections are partially driven by community incidence rather than school interventions. We further used the proportion of a school's infected population rather than the absolute number of infections, which enabled us to treat large and small schools equally. Then, we could calculate each school's risk as a function of the number of tests allocated; more tests reduced the risk incurred. Our goal was to allocate tests to schools to minimize the largest risk measure incurred at any school, subject to the constraints that we respect total testing capacity across the school system and that we cannot test all students at a school more than once per week (Appendix Figure 13).

Results

Under all transmission scenarios, we expected proactive testing to greatly reduce the proportion of students infected on campus over a 10-week period (Figure 1, panel A). In the high-risk scenario (in-school R_0 = 2.0), 14-day testing reduced the fraction of students infected from 18.2% to 4.1%; under the lowest risk scenario (in-school R_0 = 1.0), the expected incidence decreased from 4.0% to 1.5%. When we increased testing frequency from every 14 days to every 7 days, the expected incidence in high-risk scenario reduced to 2.1% and expected incidence in low-risk scenario reduced to 1.0%.

The efficacy of testing to mitigate in-school transmission depended on whether quarantine was limited

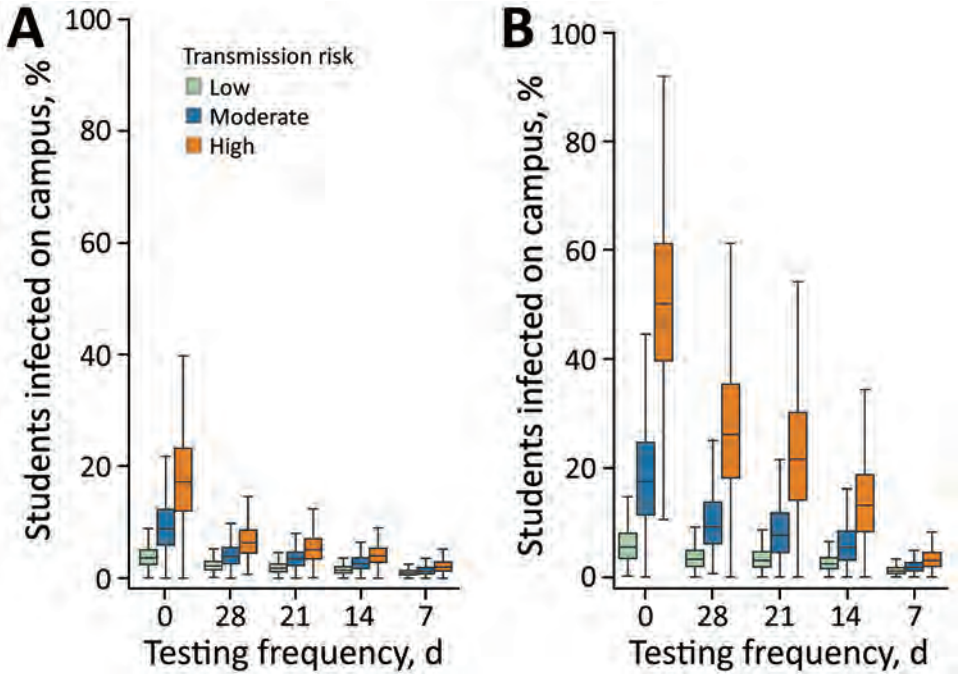

Figure 1. Projected effects of a COVID-19 test allocation strategy to mitigate SARS-CoV-2 infections across 11 school districts in the Austin Independent School District, Austin, Texas, USA. The whisker plots demonstrate projected effects over a 10-week period in a school with 500 students under 2 scenarios: A) assuming the household and classroom of each detected case is quarantined; or B) assuming only households (not entire classrooms) are quarantined. Colors indicate reproduction numbers as low (1.0), moderate (1.5), and high (2.0) in-school transmission risks in the absence of proactive or symptomatic testing, isolation, and quarantine. Whiskers indicate points that lie within 1.5 interquartile ranges of the lower and upper quartiles; boxes indicate interquartile range and horizontal bars indicate median fraction of students infected on-campus depending on the frequency of proactive testing as never (0), or once per every 28, 21, 14, or 7 days. Results are based on 300 stochastic simulations for each scenario.

to the household of the positive case or extended to the entire classroom (Figure 1, panel B). Under a moderate transmission scenario (in-school R_0 = 1.5) in which students are tested every other week, the expected incidence decreased from 6.3% (95% CI 1.0%–15.6%) to 2.9% (95% CI 1.0%–6.2%) when we added classroom quarantine to household quarantine. We also estimated the costs of quarantine in terms of days of in-school education lost over the 10-week projection period, under the moderate transmission risk scenario (Figure 2, panel A; Appendix 11). Without proactive testing, we expected the strategy of quarantining entire classrooms after a positive test to result in an average of 3 (6%) out of 50 school days missed per student. We expected household-only quarantine to reduce that cost by roughly 6.5-fold, to an average 0.9% of school days missed; however, that strategy roughly doubled the days students spent at school while infectious (Figure 2, panel B).

Regardless of quarantine policy, our model showed that proactive testing could reduce in-school exposure, with few to no additional lost days of school. In addition, we found that shortening the quarantine period for classroom contacts from 14 to 7 days would mitigate some of the educational losses without substantially increasing health risks (Appendix Figure 12).

As a sensitivity analysis, we also considered a higher rate of SARS-CoV-2 introductions from the surrounding community by raising daily new cases from 35 cases/100,000 persons to 70 cases/100,000 persons and lowering the accuracy of SARS-CoV-2 tests (*37*,*38*) (Appendix Figures 10, 11). In our sensitivity analysis, we found that our estimates were robust to the assumed sensitivity and specificity of the tests (Appendix).

Case Study—Optimizing Testing across a Large Municipal School District

We applied our model to derive an optimal allocation of testing resources across the 11 high schools in AISD, the largest district in Austin, Texas, which includes 75,000 students, 5,500 teachers, and 5,000 staff. The district operates 125 schools from pre-K–12th grade; 55% of students are Hispanic and 30% White, and >50% come from economically disadvantaged backgrounds (*32*). We estimated the external force of infection for each school by comparing reported COVID-19 incidence in the neighborhood of a school to reported incidence across the entire metropolitan statistical area (MSA) from March 2020–January 2021 (Figure 3, panel A) (*41*). We listed the schools in order of the estimated external risks; the catchment of school A had almost double (195%) the city-wide incidence, and the catchment of school K had only 37%. In general, risk (i.e., COVID-19 incidence) was higher on the east side of Austin.

We estimated on-campus transmission risk for each school by using reported cases from each school during August 16, 2020–March 8, 2021 (Figure 3, panel B). In brief, we scaled the in-school R_0 based on the difference between the cumulative, per student incidence in a school to the cumulative incidence throughout the district. We assumed a baseline R_0 of 1.0; thus, schools with incidence equal to the district-wide incidence had resulting estimates that ranged from 0.70–1.41. Our estimates for on-campus transmission risk and external force of infection were not greatly correlated (Appendix). We also ran scenarios in which all schools had the same transmission risk (Appendix Figures 5, 6).

On the basis of the estimated heterogeneity in risks across the district, we estimated the optimal

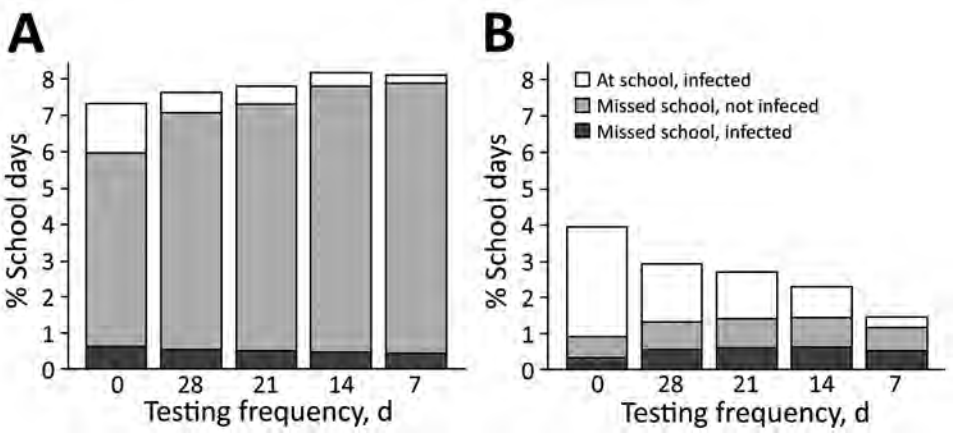

Figure 2. Projected days of school missed in a COVID-19 test allocation strategy to mitigate SARS-CoV-2 infections across 11 school districts in the Austin Independent School District, Austin, Texas, USA. The graphs demonstrate the expected proportion of school days missed due to isolation or quarantine over a 10-week period in a school with 500 students under 2 scenarios: A) assuming the household and classroom of each detected case is quarantined; or B) assuming only households (not entire classrooms) are quarantined. Estimates assume a moderate (reproduction number = 1.5) in-school transmission risk in the absence of proactive or symptomatic testing, isolation, and quarantine. All projections assume that isolation and quarantine periods last 14 days. In addition to on-campus transmission, persons might be exposed in the surrounding community at a rate of 35 new daily infections/100,000 population. The results are based on 300 stochastic simulations for each scenario.

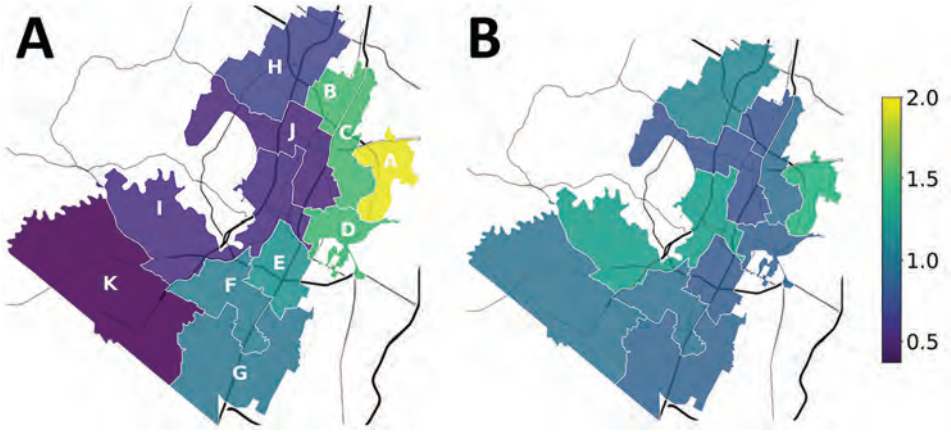

Figure 3. Locations of 11 high schools in the Austin Independent School District, Austin, Texas, USA, used to model a COVID-19 test allocation strategy to mitigate SARS-CoV-2 infections across school districts. A) Daily incidence of COVID-19 infections in late January 2021 in the catchment area of each high school relative to the average incidence across the Austin Metropolitan Statistical Area. Estimates are based on COVID-19 case reports during March 2020–January 2021. A value of one corresponds to the average incidence in the MSA. Schools are listed A through K from highest to lowest estimated daily incidence (Appendix Table 3, https://wwwnc.cdc.gov/EID/article/29/3/22-0761-App1.pdf). B) On-campus transmission risks, estimated from reported COVID-19 cases during August 16, 2020–March 8, 2021. Values are scaled so that 1.0 means that the school reported the expected number of cases, based on a least-squares linear fit of reported cases to school enrollment (Appendix Figure 4).

allocation of testing resources across schools by searching the space of possible allocations. For a given allocation, we projected the outcome for each school by first averaging the expected cumulative incidence (i.e., the mean across 300 simulations) and then the projected tail risk (i.e., the mean across the 10% worst-outcome simulations). We found the maximum value across schools (i.e., the projection for the highest-risk school) and then selected the allocation that minimized this value. Assuming that the average community incidence was 70 new daily cases per 100,000 population, based on estimates from late January 2021 in the Austin area (*42*), and that the district had a total testing budget of 1 test per student every 14 days across the district, the optimized allocation ranged from testing once per 45 days in the lowest-risk school (school K) to once per 7 days in the highest-risk school (school A) (Figure 4, panel A). We assumed that testing could not be administered more frequently than weekly. The optimal allocation

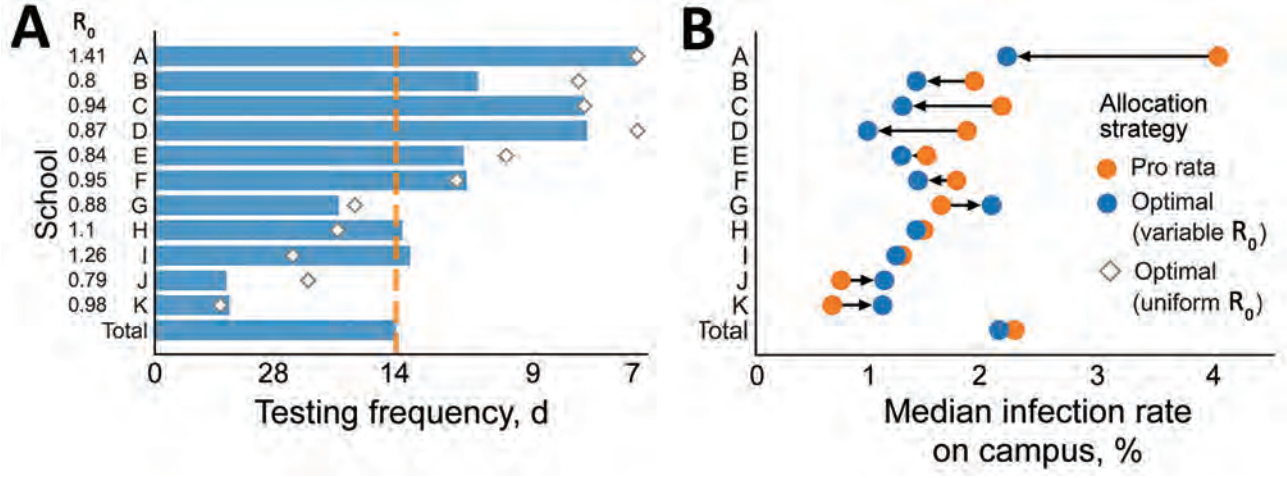

Figure 4. Test allocations and estimated infection rates based on testing frequency in a COVID-19 test allocation strategy to mitigate SARS-CoV-2 infections across 11 school districts in the Austin Independent School District, Austin, Texas, USA. A) Testing allocation for 3 testing strategies. Orange dashed line indicates pro rata strategy; blue bars indicate optimized strategy to minimize the maximum risk; diamonds indicate optimized strategy considering only variation in community transmission risks. Numbers to the left of the y-axis indicate the assumed on-campus reproduction number for each school. B) The median percent of students infected on-campus under the optimized strategy (blue) and pro rata strategy (orange), over a 10-week period; arrows indicate increases or decreases in infection rates. We modeled infections rates by using 3 testing strategies: pro rata, in which all schools test their students once per every 14 days; optimized to minimize the maximum risk of any school, considering variation in both community and in-school transmission risks; optimized considering only variation in community transmission risks. Values are averaged across 300 simulations (Appendix Table 4, https://wwwnc.cdc.gov/EID/article/29/3/22-0761-App1.pdf). The model assumes that classrooms quarantine for 14 days following a positive test.

differed slightly when we assumed instead that schools had the same on-campus R_0 and differences in risk stemmed solely from the community force of infection (Figure 4, panel A).

We projected infection rates under both the optimized allocation and a nonoptimized pro rata allocation in which resources would be allocated proportional to enrollment (Figure 4, panel A). We expected the optimized strategy to slightly reduce the overall infection rate for the district relative to the pro rata strategy and equalize risks across campuses. In the optimized strategy, the median infection rate increased by 0.4% for the lowest-risk school (school K) and decreased by 1.8% for the highest-risk school (school A) (Appendix Table 4).

When we considered total incidence by combining both community-acquired and school-acquired infections, we expected ≈5.8-fold difference between the highest risk and lowest risk schools, in the absence of testing (Figure 5, panel A). Using a 14-day testing budget, we found a pro rata strategy would lower overall incidence but not reduce the disparity (Figure 5, panel B), but an optimized allocation would greatly shrink the gap to a 3.6-fold difference (Figure 5, panel C). Restricting our analysis to infections that occur on campus, the optimized allocation again reduced the disparity in risk across schools (Table).

To provide intuition, we also derived an optimal testing allocation to reduce risks in a hypothetical district containing 6 schools, 1 of each combination of either low or high external risk and either low, moderate, or high internal risk (Appendix Figures 8, 9). We compared 3 possible testing scenarios: no testing, universal testing every 2 weeks, and an optimal testing strategy in which the 2-week testing budget is allocated to schools to minimize the maximum risk experienced by any school in the system. We found that going from no testing to a pro rata allocation decreased the maximum risk for any school from 24.7% (95% CI 11.9–38.0) of students infected to 6.6% (95% CI 3.0–11.4); under the optimal allocation, risk was further reduced to 4.5% (95% CI 1.4–8.3). Using this strategy, the total expected risk across all 6 schools was reduced from 12.8% (95% CI 9.0–16.9) of infections without testing to 3.8% (95% CI 2.5–5.2) with a pro rata allocation, which was further reduced to 3.5% (95% CI 2.4–4.8) under the optimal testing allocation (Appendix Figure 14, panel B).

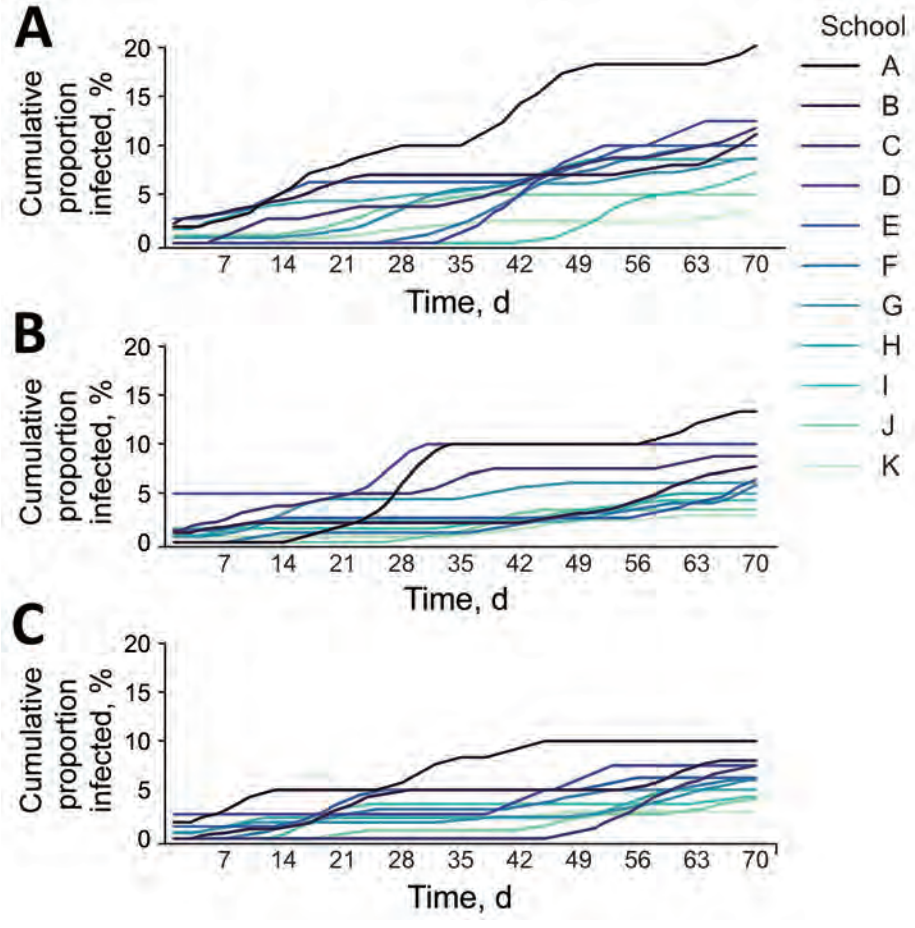

Figure 5. Cumulative infections in schools used to model a COVID-19 test allocation strategy to mitigate SARS-CoV-2 infections across 11 school districts in the Austin Independent School District, Austin, Texas, USA. Graphs represent cumulative COVID-19 infections over a 10-week period under 3 testing scenarios: A) no testing; B) all schools test students every 14 days; and C) optimized allocation of tests based on school-specific transmission risks, assuming a district-wide budget of 1 test per student every 14 days. Schools are ordered from A–K based on community incidence from high to low in the school catchment area. Graphs show 7-day moving averages based on a single simulation for each scenario and school. To show representative projections, we selected the simulation that produced a cumulative attack rate closest to the median across all 300 simulations.

Table. Estimated heterogeneity in COVID-19 incidence and total disease burden across 11 high schools in the Austin Independent School District, Austin, Texas, USA, under 3 testing scenarios in a modeled COVID-19 test allocation strategy to mitigate SARS-CoV-2 infections across school districts*

Infections	Testing allocation		
	No testing	Pro rata testing	Optimal testing
Total infections†			
Risk gap	5.8	4.8	3.6
Gini coefficient (SE)‡	0.23 (0.053)	0.26 (0.057)	0.19 (0.037)
No. infections (95% CI)§	115 (79–158)	70 (50–94)	69 (49–93)
Infection rate (95% CI)§	9.4 (6.5–12.9)	5.7 (4.1–7.7)	5.6 (4–7.6)
On-campus infections#			
Risk gap	6.5	5.6	1.8
Gini coefficient (SE)‡	0.27 (0.098)	0.23 (0.075)	0.13 (0.041)
No. infections (95% CI)§	70 (38–119)	27 (13–49)	26 (12–48)
Infection rate (95% CI)§	5.8 (3.1–9.7)	2.2 (1.1–4.1)	2.1 (1.0–3.9)

*The risk gap is the ratio of the median cumulative incidence across 300 simulations of the school with the highest expected incidence to that of the school with the lowest expected incidence.
†Total student infections, occurring both on and off campus, over the 10-week projection period.
‡Gini coefficients indicate overall disparities in expected burden, where values of 0 correspond to maximum equality and values of 1 correspond to maximum inequality (*43*). Gini coefficients were calculated using the median proportion of students infected across 300 simulations.
§The total median infections in the district over the horizon simulated, expressed as absolute and per capita.
#Infections occurring on campus, over the 10-week projection period.

Discussion

Proactive testing can be an effective strategy for preventing SARS-CoV-2 transmission on school campuses, if test turnaround is short and positive cases are immediately isolated (*44*; A. Bilinski, unpub. data, https://doi.org/10.1101/2021.05.12.21257131).Because testing requires considerable time, resources, and personnel, schools might opt to streamline their efforts as COVID-19 risks change. Our study provides a framework to help school districts allocate limited testing resources across different schools, depending on the in-school and local community transmission risks, while weighing the costs and benefits of classroom quarantine after a positive test. Prioritizing testing based on estimated risks can help mitigate the disproportionate COVID-19 burden falling on lower socioeconomic and racial minority neighborhoods (*45*–*47*).

Our results suggest that the optimal allocation of tests across schools depends on both the in-school transmission rate and the force of infection from the surrounding community. However, estimating in-school risks is difficult without sufficient testing because of overdispersion in the distribution of secondary cases and the small proportion of children that develop symptoms upon SARS-CoV-2 infection (*48*). A modest level of baseline surveillance testing could help determine the relative risks across schools (*49*). Our case study of AISD high schools suggests that even without such information, allocating testing resources based on community risks alone could substantially close gaps among schools (Appendix Figure 7).

Although proactive testing can lower and equalize COVID-19 risks across a heterogeneous school district, disparities are likely to persist. Schools drawing from neighborhoods with high COVID-19 incidence will continue to experience higher case counts and absenteeism. Other intervention measures, including vaccination and use of face masks, are essential for further reducing risks and ensuring equitable access to education.

The optimal allocation of scarce resources across multiple entities, like the number of tests per school, depends on the state of the entire system. A school might receive anywhere from no tests to enough tests for weekly testing of every student, depending on the level of risk relative to other schools. Schools could potentially game the system to gain larger allocations. For example, a school could inflate reported cases or enable higher rates of transmission by allowing high-risk activities or relaxing precautionary measures. If such issues arose, then allocation calculations could be based solely on estimates for the force of infection from the surrounding communities.

This approach can be broadly applied to distributing limited SARS-CoV-2 testing resources across systems with heterogeneous risks, such as workplaces, correctional facilities, or long-term care facilities. Our case study demonstrates that, even within a single city, tailoring control strategies to hyperlocal estimates of risks can reduce transmission overall and mitigate chronic disparities in access to resources and disease burden. On larger geographic scales, spatiotemporal variation in COVID-19 risks has been even more apparent, and cities, states, and countries exhibit highly asynchronous waves of transmission. Dynamic allocation of scarce public health resources based on reliable estimates of risk could substantially reduce the burden of COVID-19 and future pathogen

threats across the United States but requires considerable coordination at the state and federal level.

The first limitation of our study is that we assumed immediate in-school and community risks could be reliably estimated. In practice, the data required to estimate such risks often lag, are biased, or are unavailable. Such uncertainty could be included in our model by using stochastic variables that evolve based on test results from each school. However, the additional complexity would slow computational optimization. Second, we estimated heterogeneity in incidence but did not explicitly consider vaccination, health outcomes other than incidence, or socioeconomic or other factors known to correlate with COVID-19 risks (*50*). Schools drawing from more vulnerable communities might have access to fewer mitigation resources besides testing, lower vaccination coverage, or higher infection hospitalization and mortality rates. Such factors could be explicitly modeled and incorporated into the objective function used to derive equitable allocations. Third, the study derived allocations to minimize infections occurring across a school district. However, other outcomes could be explicitly incorporated into further analyses, including absenteeism and loss of education resulting from isolation and quarantine. The costs and benefits of quarantining entire classrooms, in addition to the households of positive cases, depend on the frequency of testing. Classroom quarantine would always be expected to elevate absenteeism but only substantially reduces exposure risks when testing is infrequent. With frequent testing or low transmission risks, limiting the scope and duration of quarantine might be advisable. Hospitalization risks for school staff and the potential for schools to exacerbate transmission in the surrounding community also could be integrated into allocation calculations. Finally, our model does not consider the potential costs or logistical impediments to dynamically allocating tests among schools. In addition to the challenges of rapidly calculating allocations and distributing tests accordingly, schools might require additional trained staff to administer tests, conduct contact tracing, and ensure the quick and safe isolation and quarantine of affected persons (*30*).

In conclusion, as the United States plans for COVID-19 postpandemic management, proactive testing will remain a highly effective countermeasure that can be tailored to changing risks on a local scale. As tests become more economical and as surveillance within schools and communities improves, our model demonstrates that school systems can optimize testing and quarantine policies to prevent transmission, limit absenteeism, and ensure continuity of operations during future COVID-19 surges.

Acknowledgments

We thank the Texas Advanced Computing Center at The University of Texas (Austin, TX, USA) for providing high performance computing and database resources that contributed to the research results.

This work was supported by grant no. U01IP001136 from the Centers for Disease Control and Prevention, grant no. NIH-R01-AI151176 from the National Institutes of Health, grant no. 17STQAC00001-04-00US from the Department of Homeland Security, and a generous donation from Tito's Handmade Vodka. The funders had no role in the design and conduct of the study; collection, management, analysis, and interpretation of the data; preparation, review, or approval of the manuscript; or decision to submit the manuscript for publication. The views and conclusions contained in this document are those of the authors and should not be interpreted as necessarily representing the official policies, either expressed or implied, of the funding institutions.

About the Author

Mr. Pasco is a PhD candidate at the University of Texas at Austin, Austin, Texas, USA. His research interests include mathematical modeling of infectious diseases and operations research.

References

1. Johns Hopkins Coronavirus Resource Center. COVID-19 map [cited 2023 Jan 13]. https://coronavirus.jhu.edu/map.html
2. United Nations Conference on Trade and Development. COVID-19's economic fallout will long outlive the health crisis, report warns [cited 2021 Apr 13]. https://unctad.org/news/covid-19s-economic-fallout-will-long-outlive-health-crisis-report-warns
3. Czeisler MÉ, Lane RI, Petrosky E, Wiley JF, Christensen A, Njai R, et al. Mental health, substance use, and suicidal ideation during the COVID-19 pandemic—United States, June 24–30, 2020. MMWR Morb Mortal Wkly Rep. 2020; 69:1049–57. https://doi.org/10.15585/mmwr.mm6932a1
4. Vahratian A, Blumberg SJ, Terlizzi EP, Schiller JS. Symptoms of anxiety or depressive disorder and use of mental health care among adults during the COVID-19 pandemic—United States, August 2020–February 2021. MMWR Morb Mortal Wkly Rep. 2021;70:490–4. https://doi.org/10.15585/mmwr.mm7013e2
5. Center on Budget and Policy Priorities. Tracking the COVID-19 recession's effects on food, housing, and employment hardships [cited 2021 Apr 13]. https://www.cbpp.org/research/poverty-and-inequality/tracking-the-covid-19-recessions-effects-on-food-housing-and
6. Parker K, Minkin R, Bennett J. Economic fallout from COVID-19 continues to hit lower-income Americans the hardest. Pew Research Foundation; 2020 Sep 24 [cited 2021 Apr 13]. https://www.pewresearch.org/social-trends/2020/09/24/economic-fallout-from-covid-19-continues-to-hit-lower-income-americans-the-hardest

7. Azevedo JP, Hasan A, Goldemberg D, Geven K, Iqbal SA. Simulating the potential impacts of COVID-19 school closures on schooling and learning outcomes: a set of global estimates [cited 2021 Apr 13]. World Bank Res Obs. 2021;36:1–40. https://academic.oup.com/wbro/article-pdf/36/1/1/36757308/lkab003.pdf.
8. Engzell P, Frey A, Verhagen MD. Learning loss due to school closures during the COVID-19 pandemic. Proc Natl Acad Sci U S A. 2021;118:e2022376118. https://doi.org/10.1073/pnas.2022376118
9. Dorn E, Hancock B, Sarakatsannis J, Viruleg E. COVID-19 and learning loss—disparities grow and students need help. McKinsey & Company. 2020 [cited 2021 Apr 13]. https://www.mckinsey.com/industries/public-and-social-sector/our-insights/covid-19-and-learning-loss-disparities-grow-and-students-need-help
10. Baron EJ, Goldstein EG, Wallace CT. Suffering in silence: How COVID-19 school closures inhibit the reporting of child maltreatment. J Public Econ. 2020;190:104258. https://doi.org/10.1016/j.jpubeco.2020.104258
11. Kinsey EW, Hecht AA, Dunn CG, Levi R, Read MA, Smith C, et al. School closures during COVID-19: opportunities for innovation in meal service. Am J Public Health. 2020;110:1635–43. https://doi.org/10.2105/AJPH.2020.305875
12. Orgilés M, Morales A, Delvecchio E, Mazzeschi C, Espada JP. Immediate psychological effects of the COVID-19 quarantine in youth from Italy and Spain. Front Psychol. 2020;11:579038. https://doi.org/10.3389/fpsyg.2020.579038
13. Honein MA, Barrios LC, Brooks JT. Data and policy to guide opening schools safely to limit the spread of SARS-CoV-2 infection. JAMA. 2021;325:823–4. https://doi.org/10.1001/jama.2021.0374
14. Education Week Staff. A year of COVID-19: what it looked like for schools. Education Week. 2021 Mar 4 [cited 2021 Nov 2]. https://www.edweek.org/leadership/a-year-of-covid-19-what-it-looked-like-for-schools/2021/03
15. Center for American Progress. Remote learning and school reopenings: what worked and what didn't [cited 2021 Nov 2]. https://www.americanprogress.org/issues/education-k-12/reports/2021/07/06/501221/remote-learning-school-reopenings-worked-didnt
16. US Centers for Disease Control and Prevention. COVID data tracker [cited 2021 Aug 12]. https://covid.cdc.gov/covid-data-tracker/#vaccinations_vacc-total-admin-rate-total
17. Busser C. NEA survey finds educators back in classrooms and ready for fall. National Education Association. 2021 Jun 17 [cited 2021 Nov 2]. https://www.nea.org/about-nea/media-center/press-releases/nea-survey-finds-educators-back-classrooms-and-ready-fall
18. Gutman-Wei R. Why is it taking so long to get vaccines for kids? The Atlantic. 2021 Aug 11 [cited 2021 Aug 12]. https://www.theatlantic.com/health/archive/2021/08/covid-vaccination-timeline-children/619729/
19. US Food and Drug Administration. FDA Authorizes Pfizer-BioNTech COVID-19 vaccine for emergency use in children 5 through 11 years of age [cited 2021 Dec 6]. https://www.fda.gov/news-events/press-announcements/fda-authorizes-pfizer-biontech-covid-19-vaccine-emergency-use-children-5-through-11-years-age
20. Goldstein D. Omicron upends return to school in U.S. The New York Times. 2022 Jan 3 [cited 2022 Jan 5]. https://www.nytimes.com/live/2022/01/03/us/school-closings-covid
21. Parks SE, Zviedrite N, Budzyn SE, Panaggio MJ, Raible E, Papazian M, et al. COVID-19–related school closures and learning modality changes—United States, August 1–September 17, 2021. MMWR Morb Mortal Wkly Rep. 2021;70:1374–6. https://doi.org/10.15585/mmwr.mm7039e2
22. US Department of Health and Human Services. Biden administration to invest more than $12 billion to expand COVID-19 testing [cited 2021 Jul 7]. https://www.hhs.gov/about/news/2021/03/17/biden-administration-invest-more-than-12-billion-expand-covid-19-testing.html
23. US Department of Education. Department of Education announces American Rescue Plan funds for all 50 States, Puerto Rico, and the District of Columbia to help schools reopen [cited 2021 Jul 5]. https://www.ed.gov/news/press-releases/department-education-announces-american-rescue-plan-funds-all-50-states-puerto-rico-and-district-columbia-help-schools-reopen
24. Larremore DB, Wilder B, Lester E, Shehata S, Burke JM, Hay JA, et al. Test sensitivity is secondary to frequency and turnaround time for COVID-19 screening. Sci Adv. 2021;7:eabd5393. https://doi.org/10.1126/sciadv.abd5393
25. Du Z, Pandey A, Bai Y, Fitzpatrick MC, Chinazzi M, Pastore Y Piontti A, et al. Comparative cost-effectiveness of SARS-CoV-2 testing strategies in the USA: a modelling study. Lancet Public Health. 2021;6:e184–91. https://doi.org/10.1016/S2468-2667(21)00002-5
26. Paltiel AD, Zheng A, Walensky RP. Assessment of SARS-CoV-2 screening strategies to permit the safe reopening of college campuses in the United States. JAMA Netw Open. 2020;3:e2016818. https://doi.org/10.1001/jamanetworkopen.2020.16818
27. Lanier WA, Babitz KD, Collingwood A, Graul MF, Dickson S, Cunningham L, et al. COVID-19 testing to sustain in-person instruction and extracurricular activities in high schools—Utah, November 2020–March 2021. MMWR Morb Mortal Wkly Rep. 2021;70:785–91. https://doi.org/10.15585/mmwr.mm7021e2
28. Frazier PI, Cashore JM, Duan N, Henderson SG, Janmohamed A, Liu B, et al. Modeling for COVID-19 college reopening decisions: Cornell, a case study. Proc Natl Acad Sci U S A. 2022;119:e2112532119. https://doi.org/10.1073/pnas.2112532119
29. Vohra D, Rowan P, Goyal R, Hotchkiss J, O'Neil S. Early insights and recommendations for implementing a covid-19 antigen testing program in K-12 schools: lessons learned from six pilot sites. New York: The Rockefeller Foundation; 2021 [cited 2021 Apr 13]. https://www.rockefellerfoundation.org/wp-content/uploads/2021/02/Early-Insights-and-Recommendations-for-K-12-Schools-Covid-19-Testing-Lessons-Learned-from-Six-Pilot-Sites.pdf
30. Faherty LJ, Master BK, Steiner ED, Kaufman JH, Predmore Z, Stelitano L, et al. COVID-19 testing in K-12 schools–insights from early adopters. Santa Monica (CA): RAND Corporation; 2021 [cited 2021 Jul 5]. https://www.rockefellerfoundation.org/wp-content/uploads/2021/02/RAND_Covid-19-Testing-in-K-12-Schools_Insights-from-Early-Adopters.pdf
31. Howard J. Debate emerges around Covid-19 testing strategies in schools as districts plan to reopen. CNN. 2021 Jul 19 [cited 2021 Nov 2]. https://www.cnn.com/videos/tv/2021/07/19/lead-erica-hill-live-jake-tapper.cnn
32. Austin Independent School District. About our schools [cited 2021 May 19]. https://www.austinisd.org/schools
33. Austin Independent School District. COVID-19 dashboard [cited 2021 Apr 14]. https://www.austinisd.org/openforlearning/dashboard
34. Abbott. Taking COVID-19 testing to a new level [cited 2021 Apr 14]. https://www.abbott.com/BinaxNOW-Test-NAVICA-App.html

35. Davies NG, Klepac P, Liu Y, Prem K, Jit M, Eggo RM; CMMID COVID-19 working group. Age-dependent effects in the transmission and control of COVID-19 epidemics. Nat Med. 2020;26:1205–11. https://doi.org/10.1038/s41591-020-0962-9
36. Gudbjartsson DF, Helgason A, Jonsson H, Magnusson OT, Melsted P, Norddahl GL, et al. Spread of SARS-CoV-2 in the Icelandic population. N Engl J Med. 2020;382:2302–15. https://doi.org/10.1056/NEJMoa2006100
37. Pollock NR, Jacobs JR, Tran K, Cranston AE, Smith S, O'Kane CY, et al. Performance and implementation evaluation of the Abbott BinaxNOW Rapid Antigen Test in a high-throughput drive-through community testing site in Massachusetts. J Clin Microbiol. 2021;59:e00083-21. https://doi.org/10.1128/JCM.00083-21
38. US Food and Drug Administration. Abbott BinaxNOW COVID-19 Ag CARD instructions for use and characteristics [cited 2021 Apr 19]. https://www.fda.gov/media/141570/download
39. He X, Lau EHY, Wu P, Deng X, Wang J, Hao X, et al. Temporal dynamics in viral shedding and transmissibility of COVID-19. Nat Med. 2020;26:672–5. https://doi.org/10.1038/s41591-020-0869-5
40. He D, Zhao S, Lin Q, Zhuang Z, Cao P, Wang MH, et al. The relative transmissibility of asymptomatic COVID-19 infections among close contacts. Int J Infect Dis. 2020;94:145–7. https://doi.org/10.1016/j.ijid.2020.04.034
41. University of Texas at Austin COVID-19 Modeling Consortium. Heterogeneous burden of the COVID-19 pandemic in central Texas [cited 2021 Apr 25]. https://sites.cns.utexas.edu/sites/default/files/cid/files/austin_covid-19_spatial_burden_report.pdf
42. University of Texas at Austin COVID-19 Modeling Consortium. Austin dashboard [cited 2021 Nov 5]. https://covid-19.tacc.utexas.edu/dashboards/austin
43. Atkinson AB. On the measurement of inequality. J Econ Theory. 1970;2:244–63. https://doi.org/10.1016/0022-0531(70)90039-6
44. Liu Q-H, Zhang J, Peng C, Litvinova M, Huang S, Poletti P, et al. Model-based evaluation of alternative reactive class closure strategies against COVID-19. Nat Commun. 2022;13:322. https://doi.org/10.1038/s41467-021-27939-5
45. Rubin-Miller L, Alban C, Artiga S, Sullivan S. COVID-19 Racial Disparities in Testing, Infection, Hospitalization, and Death: Analysis of Epic Patient Data. Kaiser Family Foundation; 2020 Sep 15 [cited 2021 Jul 5]. https://www.kff.org/coronavirus-covid-19/issue-brief/covid-19-racial-disparities-testing-infection-hospitalization-death-analysis-epic-patient-data
46. Mena GE, Martinez PP, Mahmud AS, Marquet PA, Buckee CO, Santillana M. Socioeconomic status determines COVID-19 incidence and related mortality in Santiago, Chile. Science. 2021;372:eabg5298. https://doi.org/10.1126/science.abg5298
47. Martin CA, Jenkins DR, Minhas JS, Gray LJ, Tang J, Williams C, et al.; Leicester COVID-19 consortium. Socio-demographic heterogeneity in the prevalence of COVID-19 during lockdown is associated with ethnicity and household size: results from an observational cohort study. EClinicalMedicine. 2020;25:100466. https://doi.org/10.1016/j.eclinm.2020.100466
48. Endo A, Abbott S, Kucharski AJ, Funk S; Centre for the Mathematical Modelling of Infectious Diseases COVID-19 Working Group. Estimating the overdispersion in COVID-19 transmission using outbreak sizes outside China. Wellcome Open Res. 2020;5:67. https://doi.org/10.12688/wellcomeopenres.15842.3
49. Leng T, Hill EM, Holmes A, Southall E, Thompson RN, Tildesley MJ, et al. Quantifying pupil-to-pupil SARS-CoV-2 transmission and the impact of lateral flow testing in English secondary schools. Nat Commun. 2022;13:1106. https://doi.org/10.1038/s41467-022-28731-9
50. Woody S, Javan E, Johnson K, Pasco R, Johnson-León M, Lachmann M, et al. Spatial distribution of COVID-19 infections and vaccinations in Austin, Texas. University of Texas at Austin. 2021 [cited 2021 Jul 5]. https://covid-19.tacc.utexas.edu/media/filer_public/fe/f2/fef289f8-800c-4390-ab27-6eff3b229f59/covid_infections_and_vaccinations_-_austin_zip_codes_-_ut_-_041221.pdf

Address for correspondence: Lauren Ancel Meyers, Department of Integrative Biology, 1 University Station C0990, Austin, TX 78712, USA; email: laurenmeyers@austin.utexas.edu

Using Discarded Facial Tissues to Monitor and Diagnose Viral Respiratory Infections

Gisele Lagathu, Claire Grolhier, Juliette Besombes, Anne Maillard, Pauline Comacle, Charlotte Pronier, Vincent Thibault

Molecular biology amplification enables sensitive detection of most respiratory viruses through nasopharyngeal swabbing. We developed an innovative approach to detect viral genomes on used facial tissues. In 2 communities of children, used tissues were collected once weekly for 1 year. Pooled analysis of tissues enabled detection of successive virus circulation in 4 age groups over time and forecasted by several weeks the circulation of influenza in the general population. At the individual level, in a proof-of-concept study of 30 volunteers with influenza-like signs/symptoms, we identified common respiratory viruses. The signals for SARS-CoV-2 obtained in parallel from 15 facial tissues and swab samples were similar and often higher for the tissues (11/15). Individual analysis of tissues offers a noninvasive, sensitive, and affordable alternative to self-sampling without a medical care requirement. Pooled analyses may be used to detect virus spread in specific communities, predict seasonal epidemics, and alert the population to viral infections.

Respiratory viral infections (RVIs) are the most common virus-induced pathologies. Associated signs/symptoms range from common colds with simple rhinorrhea without fever to acute respiratory distress syndrome sometimes leading to death (*1*). In addition to their clinical effects, RVIs have a major economic effect because of not only healthcare resource use (direct costs) but also productivity losses (indirect costs), and they paradoxically receive little attention (*2*,*3*). Moreover, antimicrobial treatments are too often prescribed for RVIs, thereby disseminating antimicrobial resistance.

Author affiliations: Centre Hospitalier Universitaire Rennes, Rennes, France (G. Lagathu, C. Grolhier, J. Besombes, A. Maillard, P. Comacle, C. Pronier, V. Thibault); University of Rennes, Rennes (C. Grolhier, J. Besombes, C. Pronier, V. Thibault)

DOI: https://doi.org/10.3201/eid2903.221416

Respiratory viruses can be detected all year, but they seem to circulate more during winter, when temperature, humidity, and behavioral patterns are favorable for their dissemination (*4*). Although this observation holds true for classical winter RVIs, our recent experience with SARS-CoV-2 and unprecedented observations of several worldwide epidemic waves of COVID-19 independent of the season should also be mentioned. Respiratory virus year-round circulation follows multicomponent rules, still imperfectly understood (*5*). RVIs cause mostly upper respiratory illnesses, particularly in adults, but are also associated with severe lower respiratory tract signs/symptoms, causing a major disease burden among children (*6*).

In recent years, diagnosis of viral infection has largely benefited from progress in molecular biology methods. Several easy-to-perform commercial assays are available, and switching from manual techniques requiring a high level of expertise to highly automated approaches has made simultaneous detection of most common respiratory viruses much easier (*7*). Syndromic panels also offer rapid diagnosis, enabling adapted care for the most severely ill patients (*8*,*9*). As it becomes easier to provide an accurate diagnosis, correct identification of pathogens in RVIs deserves more attention. Associating a virus with a disease, even a simple cold, has several advantages. For children, diagnosing a viral cause of respiratory infection may limit the use of antimicrobial therapy, reassure the parents, and avoid further transmission to the community or even nosocomial infection (*10*,*11*). For adults, diagnosis could help control transmission, particularly to the most vulnerable populations; SARS-CoV-2 is a good example. The main drawback lies in the cost of diagnosing respiratory viruses, but costs may go down in the future.

Detecting respiratory viruses is hampered by the collection method, relying on nasal swab sampling

that is usually considered invasive by patients (*12*). Although nasopharyngeal swab sample testing is considered the most sensitive, alternative approaches have been proposed, particularly for COVID-19 diagnosis. Saliva or oropharyngeal swab samples seem to be reliable in terms of sensitivity, but they have not been extensively tested for all common respiratory viruses. Blaschke et al. have proposed testing used facial tissues to diagnose RVIs in children (*13*). They analyzed only a small surface of the tissue yet obtained relative satisfactory sensitivity (up to 84%). The most sensitive sample type overall was nasal aspirate, but facial tissue tended to be more sensitive for older children.

With this study, we aimed to determine the potential of used facial tissue for documenting RVIs in different settings. We collected data as a population approach after pooling used tissues from different communities of children and as an individual approach among adults or children. All participants either already had a diagnosis of RVI (positive controls) based on a standard nasal swab sample tested by using the same diagnostic assay or had respiratory signs/symptoms consistent with an upper respiratory tract viral infection.

All participants were informed about the purpose of the study. Because nose blowing is an individual act, participation was intentional and voluntary. Most volunteers were either family members, professionals working in the laboratory, or their relatives. This type of research is in agreement with the Jardé law on biomedical research and does not require additional authorization. Nevertheless, we obtained approval from the ethics committee of the University of Rennes.

Material and Methods

Community Testing

We conducted the pooled collection study in 2 parts. The first part was conducted in a daycare center located within the Centre Hospitalier Universitaire (Rennes, France), which hosted mostly employees' children. Collection of used facial tissues started on week 40 of 2018 and continued through week 15 of 2019. The second part was conducted in a preschool (*maternelle*), from week 37 of 2019 through week 10 of 2020. For both locations, parents were informed of the study, and results were regularly communicated by the directors on an informal basis.

In the first part of the study, at the daycare center all used tissues were collected anonymously each week and pooled. The daycare facility could accommodate up to 40 children in each of 2 units, divided by age: youngest (<19 months of age) and oldest (19 months–4 years of age). The daycare staff collected all tissues during the week, and the container was collected each Friday; tissues were used for either nose blowing or, for the younger children, nose washing with a small amount of physiologic solution. For the second part of the study, the preschool comprised 2 classes of 20 pupils each: the first (3 years of age) and the second (4 years of age) grades. Tissues were used only for nose blowing, and the children were asked to throw their tissues in the specific container instead of the garbage. Each Friday, the filled containers were collected and clean empty containers were delivered for the following week.

Individual Collection of Tissue

For 15 volunteers with COVID-19 diagnosed by reverse transcription PCR of a standard nasopharyngeal swab sample, results obtained the same day on individual facial tissues enabled comparison of cycle threshold (Ct) values between both matrices. To enable documentation of secretion kinetics over 5 days, 2 volunteers, after COVID-19 diagnosis, agreed to provide daily nose discharge from nasopharyngeal swab samples.

Processing of Collected Material

To determine the volume of soaking buffer needed, each week, we counted all tissues from each container. Eventually, we chose a volume of 7 mL of Dulbecco's phosphate-buffered saline (DPBS; GIBCO, https://www.thermofisher.com) per tissue. We collected the saturated liquid after the pooled tissues had been gently soaked for few minutes and then pressed with a home-brew device. For individual collections, we introduced the used tissues into a 60-mL syringe soaked with 7 mL of DPBS. We then firmly pressed the syringe plunger onto the soaked tissue and, depending on the tissue absorbing capacity, regularly obtained 5 mL of residual liquid.

Viral Genome Detection

We used commercial kits to detect viral genomes. For pooled collections, we used Allplex Seegene (Eurobio, https://www.eurobio-scientific.com) on the sample of collected liquid, according to the manufacturer's recommendations. The kit detects influenza A virus; influenza A(H1) virus; influenza A(H1N1) pdm09 virus; influenza A(H3) virus; influenza B virus; respiratory syncytial viruses A and B; adenovirus; enterovirus; human metapneumovirus (hMPV); parainfluenza viruses 1–4; bocaviruses 1–4; coronaviruses 229E, NL63, and OC43; and human rhinovirus.

For individual testing, and particularly to detect SARS-CoV-2 RNA, we used TaqPath (ThermoFisher Scientific, https://www.thermofisher.com), Alinity (Abbott, https://www.corelaboratory.abbott), GeneXpert (Cepheid, https://info.cepheid.com), and FilmArray (bioMérieux, https://www.biomerieux.com). To detect cytomegalovirus (CMV), Epstein-Barr virus, and human parvovirus B19 genome, as part of our routine daily workflow we used RealStar assays (Altona, https://www.altona-diagnostics.com). All products were used as recommended by the manufacturers. For the kinetic study on SARS-CoV-2–positive samples and the comparison of signals between nasopharyngeal swab samples and tissues, we obtained all Ct values from a SARS-CoV-2 AMP Kit automatized on Alinity. This test amplifies 2 genome target genes (RNA polymerase and nucleocapsid), and the obtained signal is provided as a single Ct. Concordance between the signals obtained by the different commercial techniques routinely used in our laboratory is excellent. Our laboratory is certified according to COFRAC NF EN ISO 15189.

Statistical Analyses

To compare Ct values obtained from nasopharyngeal swab and tissue samples, we used a Wilcoxon test. We considered $p<0.05$ to be significant.

Results

Pooled Material

For the first study, used facial tissues were not collected when the daycare facility was closed during Christmas break. Rhinovirus and bocavirus were detected all year long, particularly from the youngest children. Other viruses were detected sporadically throughout the study period (Figure 1). Except for rhinovirus and bocavirus, viral infection in the youngest and oldest children was not synchronously detected. Influenza virus was detected as soon as week 1 in 2019, although the peak in the general population occurred only in week 6. In both age groups, parvovirus B19 was regularly but not continuously detected. By contrast, CMV detection was persistent among the youngest and intermittent among the oldest children.

The second study was unexpectedly interrupted by the confinement declared by the government of France after emergence of the COVID-19 pandemic. Rhinovirus was detected at almost all times, but other viruses were sporadically detected (Figure 2). Except for hMPV detected for children in both classes on weeks 47 and 48, viruses seemed to circulate independently among children in both classes.

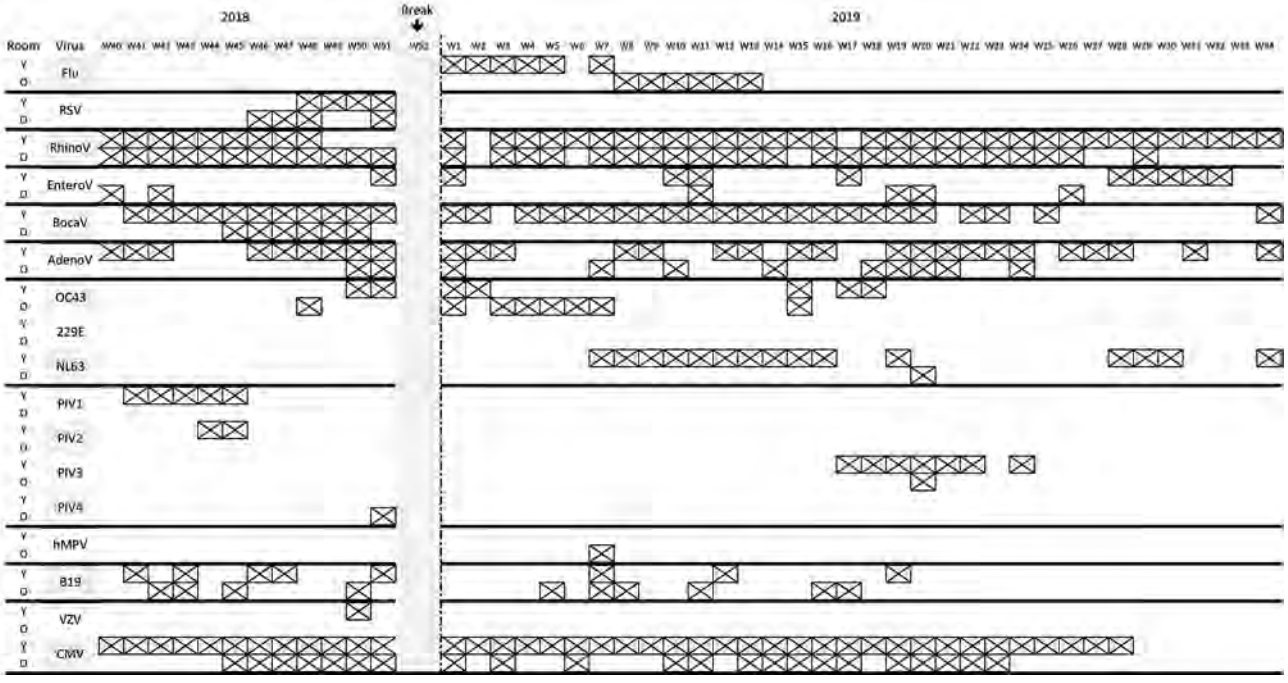

Figure 1. Detection of viruses by age group during study involving used facial tissues to monitor and diagnose viral respiratory infection. Each week is represented by a column, and detection of different viruses is indicated by a crossed cell. 229E, coronavirus 229E; OC43, coronavirus OC43; NL63, coronavirus NL63; AdenoV, adenovirus; BocaV, bocavirus; CMV, cytomegalovirus; EnteroV, enterovirus; Flu, influenza virus; hMPV, human metapneumovirus; O, older age group; PIV, parainfluenza virus; RSV, respiratory syncytial virus; RhinoV, rhinovirus; VZV, varicella zoster virus; W, week; Y, younger age group.

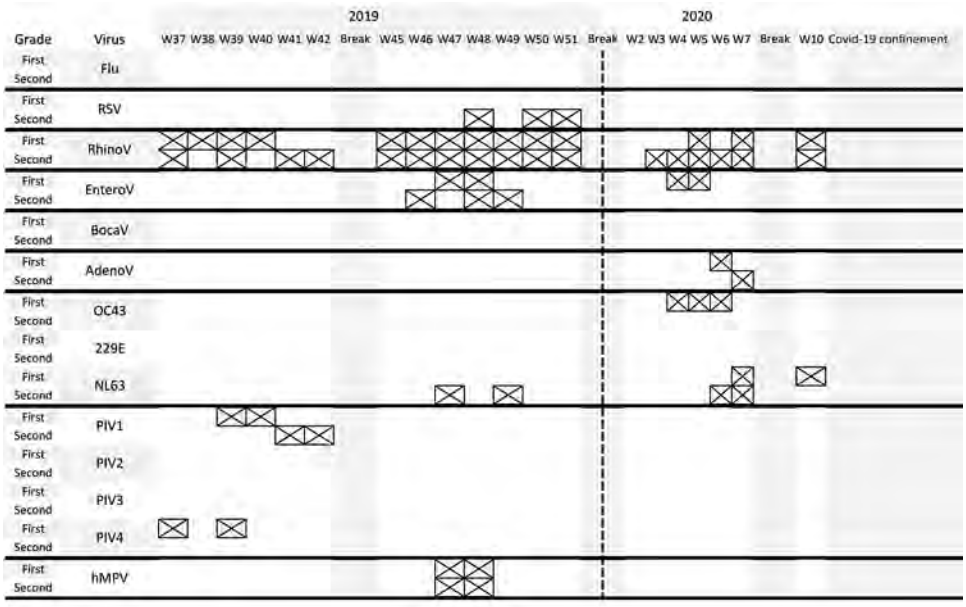

Figure 2. Detection of viruses by grade (first or second) during study of used facial tissues to monitor and diagnose viral respiratory infection. Each week is represented by a column, and detection of different viruses is indicated by a crossed cell. AdenoV, adenovirus; BocaV, bocavirus; EnteroV, enterovirus flu, influenza virus; hMPV, human metapneumovirus; PIV, parainfluenza virus; RSV, respiratory syncytial virus; RhinoV, rhinovirus; W, week.

Individual Collections

After validating pooled collections from the daycare center, we proposed an individual approach to investigators and their relatives as soon as they exhibited influenza-like signs/symptoms. To process single facial tissues, we adapted the process to using a 60-mL syringe and a 7-mL volume of DPBS; after several steps of optimization, we retained these conditions. We sent 22 used tissues to the laboratory, where they were processed accordingly. All but 2 samples were positive for ≥1 virus. Viruses detected during the past 3 years were rhinovirus, bocavirus, influenza B virus, hMPV, coronaviruses 229E and OC43, adenovirus, and SARS-CoV-2. Some diagnoses were performed on samples that had been shipped through regular postal mailing. Most tissues were stored in standard plastic bags at room temperature for several days before being analyzed; there was no noticeable loss of sensitivity.

This in-progress work validates the feasibility of the approach on an individual basis. For most volunteers, tissue analysis enabled identification of the virus responsible for the observed signs/symptoms. As expected, all volunteers recovered from common RVIs within few days.

When we compared signals obtained on both matrices collected from the 15 volunteers on the same day, median Ct was 23 on facial tissues but only reached a median Ct of 26 on nasopharyngeal swab specimens. The difference did not reach statistical significance (Figure 3), but Cts were lower for 11 of the 15 tissues than on swab samples. Values were within the typical standard range for SARS-CoV-2–infected patients.

For the 2 COVID-19–positive volunteers who provided daily facial tissue samples, the Ct obtained from tissues was lower than that from nasopharyngeal swab samples (19 vs. 27 and 23 vs. 27) (Figure 4).

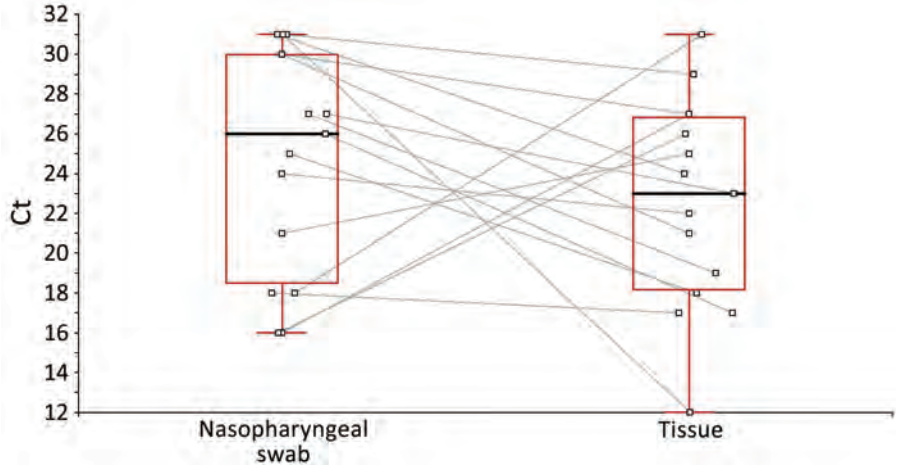

Figure 3. Reverse transcription PCR signal (Ct) obtained from nasopharyngeal swab samples collected from persons with COVID-19 compared with Ct obtained from processed used facial tissues in study of using facial tissues to monitor and diagnose viral respiratory infection. Each square indicates a patient, and observations for the same patient are linked between plots. Black lines within boxes indicate medians; box tops, 75th percentile; box bottoms, 25th percentile; and whiskers, maximums and minimums. Ct, cycle threshold.

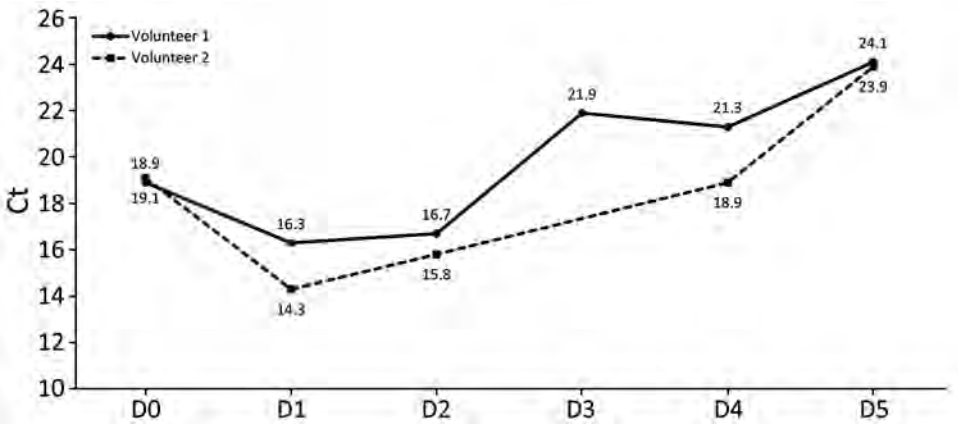

Figure 4. Ct values obtained from used facial tissues collected each morning after the first day from 2 volunteers in study of using facial tissues to monitor and diagnose viral respiratory infection. Volunteer 1 (closed circle, solid line) and volunteer 2 (closed square, dotted line) provided tissues every morning for 5 days (except day 3 for volunteer 2). Each tissue was analyzed as described, and SARS-CoV-2 RNA was detected using an Alinity assay (Abbott, https://www.corelaboratory.abbott). Day 0, the day of COVID-19 diagnosis performed on a typical nasal swab sample. Ct, cycle threshold.

At each time point, the signal was positive; Ct ranged from 14 to 24. For 1 volunteer, at a later time point (11 days after initial diagnosis), Ct was 35.

Discussion

We initially designed this study as a proof-of-concept study; our objective was to describe the circulation of respiratory viruses in communities of children. The results led us to consider a more individual approach, and we were able to gather enough data despite the COVID-19 pandemic. In the first part of the study, using pooled material, we gathered a large amount of data. Collecting used tissues from both institutions, the daycare center and the preschool, did not raise concerns from the professionals or the parents; both groups seemed interested in the study and awaited the weekly results. One objective of the regular monitoring of virus circulation would be to communicate the results on a weekly basis throughout the year to limit the unnecessary use of antimicrobial drugs when a viral infection is identified in a community, to inform the parents about what to do in such circumstances, and to possibly limit general practitioner visits. Parents who are informed about the circulation of a specific virus in a group of children may be less worried and could share their concerns with others. Collecting used tissues is noninvasive, well accepted by children and parents, and provides valuable information about the epidemiology of viruses in a specific community.

Despite proximity, older and younger children were not affected by the same viruses at the same time, which indicates that hygienic rules were probably well applied, particularly in the daycare center, but also that children of different ages are not susceptible to the same infections. That information reflects development of immunity during growth, but collecting data throughout the year demonstrates the susceptibility of children in each age group to viral infection.

Constant circulation of rhinovirus was not unexpected and may indicate rather weak immunity to the virus and highlights the relatively mild signs/symptoms in young children. Detecting parainfluenza virus in autumn in both communities of children fits well with the recent work from Horemheb-Rubio et al. (*14*). The start of the school year, when children gather, certainly plays a role in transmission of those viruses. Of note, parainfluenza virus 3 was also detected in the daycare center after the March break and persisted for several weeks.

Detecting CMV in the daycare center is informative and underlines the limits of our approach. Indeed, and particularly for CMV, detecting viral genome in pooled material may indicate either that the virus is perpetually circulating and propagated among children or that 1 or a few infants, those infected before or at birth, continuously shed virus (*15*). It is not possible to certify if detection comes from a long period of virus shedding, particularly if the level of secretion is high, as seen with CMV after maternofetal infection. For both community studies, we considered it unethical to perform individual analyses. Detecting 1 positive child would have led to possible discrimination or even eviction from the group.

In addition to the possible bias that detecting a virus in a pool of facial tissues may reflect only 1 long-shedding child, it is also possible that 1 child put >1 tissue in the collecting container. Those biases should be taken into consideration, and solutions should be sought to limit their influence in future similar studies.

Another objective of our community testing strategy would be to propose a surveillance model based on few strategically chosen groups. Seasonal virus infections propagate very efficiently among young

children, and monitoring those communities may be useful for predicting emergence of winter seasonal viruses. In the study performed in the daycare center, the first influenza-positive collection was detected 6 weeks before the seasonal peak in the general population. Identifying such emergence early would leave enough time to deliver prevention messages (e.g., mask use) to the population. One may imagine a surveillance model similar to what has been done with sewage water for SARS-CoV-2 (*16*). Information from such surveillance would be communicated to the general population to better convey which preventive measures to take. Depending on the objective, several strategies could be considered. Because RVIs are probably transmitted by children, regular pooled tissue testing in a few representative classrooms would provide valuable information. Another approach would be to rely on a network of collaborative general pediatricians selected according to recruitment, who could collect tissues from children with respiratory signs/symptoms. Such surveillance requires individual participation, as opposed to wastewater testing, yet it may provide much more precise information about a specific population.

Individual testing was not a priority in our study, but detecting viral nucleic acid from numerous different viruses in tissues sent to our laboratory gave us confidence that that strategy could be pertinent. The COVID-19 epidemic gave us the opportunity to validate our approach. When tissues were collected from persons with COVID-19 diagnosed from standard nasopharyngeal swab samples, the signal obtained from tissues was higher in 73% (11/15) of cases (Figure 3). The median Ct value obtained from tissues was 3 units lower than that from classical nasal swab samples, a difference that was not statistically significant, possibly because of the low number of samples tested in parallel.

Blowing in a tissue is an individual action, and its effectiveness largely depends on the person. Nasopharyngeal swabbing also depends on the skill of a professional but may be less subject to variability. One possible way to assess the sampling quality is to quantify a cellular gene, yet this strategy is not routinely applied and lacks consensus among scientists (*17*). Quantifying a cellular gene on each tissue sample might validate the quality of the blowing. We anticipate that a threshold would have to be defined according to the tested population; elderly persons may not be able to blow as vigorously as younger persons. The kinetics performed on samples from the 2 COVID-19–positive volunteers who provided daily tissue samples demonstrate that SARS-CoV-2 nucleic acids are easily detectable on tissues for a long period. Those kinetics resemble kinetics usually described for large cohorts (*18*). The most sensitive approach might be having persons blow their nose in the morning because nasal fluids and dying cells accumulate in the respiratory tract during sleep. The influence of the timing for tissue collection should also be investigated. For the 2 COVID-19–positive volunteers, tissues were collected early in the morning at awakening, and neither person experienced any nasal congestion or rhinorrhea. Vigorous blowing was recommended to both participants. For those kinetics, but also for some individual diagnoses performed on demand, tissues were stored for several days at room temperature or even shipped by mail. Reverse transcription PCR performed on 32 tissues collected from volunteers positive for COVID-19, as documented by an antigen test and stored for a median of 12 days, were all positive, indicating that tissues can be stored and shipped without too much loss of sensitivity (data not shown). Possibly offering at-home sampling and remote diagnosis is a unique asset of this approach. Remotely testing patients should be considered when a viral infection emerges with signs/symptoms not requiring specific medical care. Such was the situation with COVID-19; many patients did not require medical attention. Leaving patients the possibility of collecting the sample themselves without being in contact with medical staff or other persons would limit the risk of propagating any emergent virus. Although the best matrix for performing COVID-19 diagnosis, has been debated, a unique tissue can be loaded first with nasal discharge and then sputum for 1 patient, which may increase sensitivity when nasal discharge is limited (*7*). The possibility of combining 2 matrices on the same sample may increase clinical sensitivity of the used-tissue strategy. Few of the tested tissues had both materials, but we cannot affirm that the performance was improved by such an approach. Because this method was developed to speed access to diagnosis, we made no recommendations regarding the brand or the kind of facial tissue to use. A formal assessment of our method on different tissues is required, yet common sense indicates use of commonly available commercial unperfumed plain white facial tissue.

Of note, $\geq$1 sample positive for $\geq$1 virus was analyzed on the different systems routinely used in our laboratory. A valid result was obtained on all platforms used. Those results probably reflect improved extraction processes for most commercially available automated systems. In particular, no PCR inhibition was observed for the analyzed tissue liquids. Moreover, complete sequences of SARS-CoV-2 can also be obtained from tissues; an example of 1 sequence

obtained from used tissue is referenced in GISAID (https://www.gisaid.org; identification no. EPI_ISL_13050738).

This study reflects major changes in virology that have occurred in recent years. Although growing the virus in cell culture was the reference for diagnosis, we slightly moved to molecular detection of viral nucleic acids. The information gained by each strategy is different: in the first instance, we identified live virus, probably infectious; in the second, we found only the presence of viral components. Yet the overall sensitivity of nucleic acid amplification methods now offers improved clinical sensitivity despite loss of information regarding the viability of the virus and possibly its infectiousness. Detecting viral nucleic acids in used tissues is feasible and possibly as sensitive as classical sampling methods, if not more so. That possibility provides the option for virus testing of pooled samples in communities to provide information on the dissemination of any respiratory-transmitted virus and to propose a noninvasive method for the general population. Situations in which persons need to be repeatedly tested, such as athletes during a several-day event, may also largely benefit from this strategy. Being able to send tissues by regular mail for remote diagnosis is also a real asset with potential application for gaining information about the diffusion of an infection in a population. Although this study should be considered as a proof-of-concept work, we believe that the accumulation of data justifies considering the use of our methods on a larger scale.

Acknowledgments

We are indebted to the directors of the daycare (Ms. Cloarec) and the preschool (Ms. Bernier) and the children who provided their used tissues. We also thank Florence Godey, who collected some tissues in parallel to nasopharyngeal swabs; Bérengère Cador, who also collected tissues; and all volunteers.

Conceptualization and formal analyses were provided by V.T., investigation by L.G., G.C., B.J, M.A., C.P., P.C., and V.T.; acquisition of data by L.G., G.C., B.J., M.A., C.P., P.C., and V.T.; methods by V.T.; resources by V.T. and L.G.; supervision by V.T.; and writing and original draft by V.T. Authors declare no competing interest in the presented work. No specific funding was obtained to conduct this work.

A patent application (PCT/EP2021/081662) has been filed as a result of this work. V.T. is the only applicant on the patent, which describes methods for collecting and processing used tissues before molecular detection of respiratory viral pathogens.

About the Author

Dr. Lagathu is a medical doctor in charge of clinical virology diagnosis in Centre Hospitalier Universitaire of Rennes. Her work focuses mostly on mother-to-child and respiratory infections.

References

1. Jain S, Self WH, Wunderink RG, Fakhran S, Balk R, Bramley AM, et al.; CDC EPIC Study Team. Community-acquired pneumonia requiring hospitalization among U.S. adults. N Engl J Med. 2015;373:415–27. https://doi.org/10.1056/NEJMoa1500245
2. Fendrick AM, Monto AS, Nightengale B, Sarnes M. The economic burden of non-influenza-related viral respiratory tract infection in the United States. Arch Intern Med. 2003;163:487–94. https://doi.org/10.1001/archinte.163.4.487
3. Mizgerd JP. Lung infection—a public health priority. PLoS Med. 2006;3:e76. https://doi.org/10.1371/journal.pmed.0030076
4. Moriyama M, Hugentobler WJ, Iwasaki A. Seasonality of respiratory viral infections. Annu Rev Virol. 2020;7:83–101. https://doi.org/10.1146/annurev-virology-012420-022445
5. Cannell JJ, Zasloff M, Garland CF, Scragg R, Giovannucci E. On the epidemiology of influenza. Virol J. 2008;5:29. https://doi.org/10.1186/1743-422X-5-29
6. Henrickson KJ, Hoover S, Kehl KS, Hua W. National disease burden of respiratory viruses detected in children by polymerase chain reaction. Pediatr Infect Dis J. 2004; 23(Suppl):S11–8. https://doi.org/10.1097/01.inf.0000108188.37237.48
7. Zhang N, Wang L, Deng X, Liang R, Su M, He C, et al. Recent advances in the detection of respiratory virus infection in humans. J Med Virol. 2020;92:408–17. https://doi.org/10.1002/jmv.25674
8. Bouzid D, Zanella M-C, Kerneis S, Visseaux B, May L, Schrenzel J, et al. Rapid diagnostic tests for infectious diseases in the emergency department. Clin Microbiol Infect. 2021;27:182–91. https://doi.org/10.1016/j.cmi.2020.02.024
9. Visseaux B, Collin G, Ichou H, Charpentier C, Bendhafer S, Dumitrescu M, et al. Usefulness of multiplex PCR methods and respiratory viruses' distribution in children below 15 years old according to age, seasons and clinical units in France: a 3 years retrospective study. PLoS One. 2017;12:e0172809. https://doi.org/10.1371/journal.pone. 0172809
10. Pavia AT. Viral infections of the lower respiratory tract: old viruses, new viruses, and the role of diagnosis. Clin Infect Dis. 2011;52(Suppl 4):S284–9. https://doi.org/10.1093/cid/cir043
11. Rogan DT, Kochar MS, Yang S, Quinn JV. Impact of rapid molecular respiratory virus testing on real-time decision making in a pediatric emergency department. J Mol Diagn. 2017;19:460–7. https://doi.org/10.1016/j.jmoldx.2017.01.009
12. Baron EJ, Miller JM, Weinstein MP, Richter SS, Gilligan PH, Thomson RB Jr, et al. A guide to utilization of the microbiology laboratory for diagnosis of infectious diseases: 2013 recommendations by the Infectious Diseases Society of America (IDSA) and the American Society for Microbiology (ASM). Clin Infect Dis. 2013;57:e22–121. https://doi.org/10.1093/cid/cit278
13. Blaschke AJ, Allison MA, Meyers L, Rogatcheva M, Heyrend C, Mallin B, et al. Non-invasive sample collection for respiratory virus testing by multiplex PCR. J Clin Virol. 2011;52:210–4. https://doi.org/10.1016/j.jcv.2011.07.015

14. Horemheb-Rubio G, Eggeling R, Schmeißer N, Pfeifer N, Lengauer T, Gärtner BC, et al.; Respiratory Virus Network. Respiratory viruses dynamics and interactions: ten years of surveillance in central Europe. BMC Public Health. 2022;22:1167. https://doi.org/10.1186/s12889-022-13555-5
15. Cannon MJ, Hyde TB, Schmid DS. Review of cytomegalovirus shedding in bodily fluids and relevance to congenital cytomegalovirus infection. Rev Med Virol. 2011;21:240–55. https://doi.org/10.1002/rmv.695
16. Wurtzer S, Marechal V, Mouchel JM, Maday Y, Teyssou R, Richard E, et al. Evaluation of lockdown effect on SARS-CoV-2 dynamics through viral genome quantification in waste water, Greater Paris, France, 5 March to 23 April 2020. Euro Surveill 2020;25:2000776.
17. Pronier C, Gacouin A, Lagathu G, Le Tulzo Y, Tadié J-M, Thibault V. Respiratory influenza viral load as a marker of poor prognosis in patients with severe symptoms. J Clin Virol. 2021;136:104761. https://doi.org/10.1016/j.jcv.2021.104761
18. Drain PK. Rapid diagnostic testing for SARS-CoV-2. N Engl J Med. 2022;386:264–72. https://doi.org/10.1056/NEJMcp2117115

Address for correspondence: Vincent Thibault, CHU Rennes, University of Rennes, INSERM, EHESP, Irset UMR S1085, 2 Rue Henri le Guilloux, Rennes 35033, France; email: vincent.thibault@chu-rennes.fr

Postacute Sequelae of SARS-CoV-2 in University Setting

Megan Landry, Sydney Bornstein, Nitasha Nagaraj, Gary A. Sardon Jr., Amanda Castel, Amita Vyas, Karen McDonnell, Mira Agneshwar, Alyson Wilkinson, Lynn Goldman

Postacute sequelae of SARS-CoV-2 infection, commonly known as long COVID, is estimated to affect 10% to 80% of COVID-19 survivors. We examined the prevalence and predictors of long COVID from a sample of 1,338 COVID-19 cases among university members in Washington, DC, USA, during July 2021–March 2022. Cases were followed up after 30 days of the initial positive result with confidential electronic surveys including questions about long COVID. The prevalence of long COVID was 36%. Long COVID was more prevalent among those who had underlying conditions, who were not fully vaccinated, who were female, who were former/current smokers, who experienced acute COVID-19 symptoms, who reported higher symptom counts, who sought medical care, or who received antibody treatment. Understanding long COVID among university members is imperative to support persons who have ongoing symptoms and to strengthen existing services or make referrals to other services, such as mental health, exercise programs, or long-term health studies.

It is estimated that 1 in 3 Americans who have SARS-CoV-2 infection will experience symptoms related to postacute sequelae of SARS-CoV-2 (*1*), also referred to as long COVID (other terms include long-haul coronavirus disease, post-–COVID-19 conditions, or chronic COVID-19) (*2*). The length of time that a person must experience symptoms to be considered to have long COVID is not universally accepted; definitions range from 28 days to 6 months after acute SARS-CoV-2 infection (*3*–*7*). A recent World Health Organization working group used a Delphi process to conclude that "a post-COVID-19 condition occurs in individuals with a history of probable or confirmed SARS-CoV-2 infection, usually 3 months from the onset of COVID-19 with symptoms that last for at least 2 months and cannot be explained by an alternative diagnosis" (*8*).

Author affiliation: The George Washington University Milliken Institute School of Public Health, Washington DC, USA

DOI: https://doi.org/10.3201/eid2903.221522

Regardless of a universally agreed upon length of time a person must experience symptoms to be characterized as long COVID, this sequela has been suggested to be the "next national health disaster" (*9*), and because of discrepancies in symptoms and long-term effects on quality of life, there seem to be more questions than answers. Although long COVID manifests differently in each person, nearly 50 signs and symptoms have been linked to the condition (*10*). The most common signs and symptoms are fatigue, shortness of breath, muscle pain, joint pain, headache, cough, chest pain, altered smell, altered taste, and diarrhea (*11*). Other reported signs and symptoms include cognitive impairment (known as brain fog), memory loss, palpitations, anxiety, sore throat, sleep disorders, runny nose, sneezing, hoarseness, ear pain, thoughts of self-harm and suicide, seizures, and bladder incontinence (*8*,*11*), as well as cardiac effects, such as myocardial inflammation (*12*).

Although some investigators have reported that long COVID occurs at rates that are independent of symptom severity (*11*–*13*), others have found long COVID is more common among patients hospitalized for COVID-19 or those who experienced moderate-to-severe symptoms (*6*,*11*,*14*–*20*). However, long COVID has been observed in patients who were asymptomatic (*2*) or only experienced mild symptoms, and it has been reported that symptoms can fluctuate or relapse (*7*–*8*,*21*–*23*). Furthermore, little is known about long COVID signs and symptoms and predictors on a college campus, where most of the population is young and healthy, but among whom potential complications of long COVID could be detrimental to academic learning and overall quality of life.

Long COVID signs and symptoms might vary by sex, age, and initial illness severity. For example, nervous system symptoms such as headaches and dizziness are more common among women, but men are more likely to have musculoskeletal system symptoms such as pain in the muscles or joints and numbness of the limbs (*24*). Younger patients have reported

more headaches, abdominal symptoms, and anxiety/depression, and older patients were more likely to have breathing difficulties, cognitive symptoms, pain, and fatigue (*19*).

Aside from the medical illness long COVID poses, persistent signs and symptoms can negatively affect leisure and work, causing further strain on one's quality of life. Persons who have long COVID frequently experience a substantial reduction or impairment in the ability to engage in preillness levels of occupational, educational, social, or personal activities that persist for >6 months (*14*). They might also experience difficulty sticking to daily routines, dealing with stress, getting household tasks done, and caring for/supporting others (*25*). Abnormal scores on mental and cognitive health questionnaires have also been observed among patients who have long COVID (*7*). Our study builds on the existing knowledge base by examining the prevalence and predictors of long COVID among a sample of university members, including students, faculty, and staff, who tested positive for COVID-19 over an 18-month period.

Methods

COVID-19 Case Identification

The George Washington University COVID-19 surveillance and testing program identified 4,800 COVID-19 cases during August 2020–February 2022. COVID-19 positivity at George Washington University was determined on the basis of PCR tests that were performed in the George Washington University Clinical Laboratory Improvement Amendments, or Clinical Laboratory Improvement Amendment–certified, Public Health Laboratory (n = 3,228); other cases were identified through results uploaded to the person's medical portal from external positive tests, either PCRs from an external Clinical Laboratory Improvement Amendment–certified laboratory or self-administered antigen tests (n = 1,572). Only antigen tests approved for emergency use under the Food and Drug Administration emergency use authorization were accepted (*26*).

COVID-19 Case Investigation Data Collection

As COVID-19 cases were identified, the George Washington University Campus COVID-19 Support Team (CCST), which is responsible for campus-related COVID-19 case management (*27*), completed case investigations within 24–48 hours of the person receiving a positive test result. Among the 4,800 positive results during August 2020–February 2022, a total of 133 initial case investigations were incomplete because of loss to follow-up, meaning they could not be reached by telephone or electronic survey; because the case was already cleared by a medical provider (because of not being able to reach the person during their isolation period); or because the person refused to complete the interview. Furthermore, 1,072 persons were missing case investigation data, such as missing data for symptoms or underlying conditions, Those exclusions resulted in 3,595 positive test results (with corresponding completed case investigation data) for which CCST had obtained complete case investigation data (Table 1).

Long COVID Follow-up Data Collection

During July 2021–March 2022, all 4,800 positive COVID-19 test results reported during August 2020–February 2022 were followed up with confidential electronic surveys sent to each patient at least 28 days after their initial positive result that included

Table 1. Initial case investigation and long COVID data collection for postacute sequelae of SARS-CoV-2 in university setting, Washington, DC, USA*

Characteristic	Value
Positive test results reported during 2020 Aug–2022 Feb	4,800
GWU PCR	3,228
External CLIA PCR or self-administered antigen	1,572
Initial case investigation incomplete	133
Initial case investigation data missing	1,072
Total positive test results with case investigation data	3,595
Long COVID surveys sent out, 2021 Jul–2022 Mar	4,800
Repeat infection duplicates	143
Persons surveyed	4,657
Responses received	1,493
Duplicate responses/multiple responses	11
Persons responding	1,482
Response rate, 1,482/4,657	31.8%
Responders with incomplete case investigation	141
Responders with incomplete long COVID questions	3
Total valid responses	1,338

*Values are no. except as indicated. CLIA, Clinical Laboratory Improvement Amendments; GWU, George Washington University.

questions about long COVID. Those data were merged with the COVID-19 case investigation data.

For the long COVID follow-up survey data collection, we determined that 143 persons had ≥2 COVID-19 diagnoses during August 2020–February 2022; those persons were only included once in the long COVID follow-up data collection, resulting in a total of 4,657 persons who were COVID-19 positive during the study period. The follow-up survey had a response rate of 32% (1,482/4,657). We observed major differences in age, university affiliation, underlying conditions, and vaccination status at the time of test between follow-up survey respondents and nonrespondents (Appendix 1, https://wwwnc.cdc.gov/EID/article/29/3/22-1522-App1.pdf). A total of 11 respondents completed the follow-up survey twice but were only counted once for the response rate. Not all responses were usable in the final analysis: 141 did not have a complete initial case investigation, and 3 did not provide responses to the survey questions about long COVID, removing them from the final sample. Thus, the final analytic sample consisted of 1,338 respondents (Table 1).

Instrument and Measures

Survey Instrument

The long COVID survey was designed as a follow-up telephone interview (Appendix 2, https://wwwnc.cdc.gov/EID/article/29/3/22-1522-App2.pdf); interviews were administered by CCST during July 2021–March 2022, and all survey responses were stored on REDCap, a secure web application for online surveys and databases (*28*). Initially, CCST interviewers exclusively administered the follow-up survey by telephone calls. However, after 3 months, a link to an electronic survey was sent to all remaining cases in addition to calling. Three call attempts were made over a period of 5 weeks, prompting case-patients to complete an anonymous survey. The long COVID survey consisted of close-ended questions pertaining to symptoms during the postisolation period and behavior changes from preisolation to postisolation periods (Appendix 1). The survey took ≈15–20 minutes to complete, and at the conclusion, a list of resources to assist with long COVID symptoms was provided.

Measures

We defined long COVID as experiencing ≥1 of the following symptoms lasting for >28 days after a respondent's 10-day isolation period ended (*2*): difficulty driving, difficulty having conversations, difficulty making decisions, difficulty thinking, fatigue, feeling anxious, feeling depressed or sad, loss of smell, loss of taste, memory loss, muscle pain, muscle weakness, shortness of breath or difficulty breathing, trouble sleeping, worsening of symptoms after physical activity, worsening of symptoms after mental activity, or other symptoms. In addition, respondents were considered to have long COVID if they reported still experiencing COVID-19–related symptoms at the time of the long COVID survey.

Sociodemographic Characteristics

We calculated age from the respondent's date of birth extracted from their health record. Sex and race were self-reported at the time of the case investigation. We determined school affiliation by asking respondents their primary university affiliation at the time of the case investigation.

Symptoms and Underlying Conditions

We measured symptoms at the time of the case investigation by asking if respondents experienced any of the following: chest pain, chills, congestion, cough, diarrhea, fatigue, fever, headache, loss of smell, loss of taste, muscle pain, nausea or vomiting, runny nose, shortness of breath, sore throat, or other symptoms. At the time of the case investigation, respondents self-reported any of the following medical conditions: diabetes, asthma, hypertension, obesity, sickle cell disease, cancer, chronic kidney disease, lung diseases, serious heart conditions, or other conditions. Smoking status was self-reported as current/former smoker or vaper.

Vaccination Status and Severity of COVID-19 Infection

Over the course of the study period, COVID-19 vaccine availability and recommendations shifted dramatically. In December 2020, vaccines were first available but only for select groups such as healthcare workers, the elderly, and certain other susceptible populations. During March–April 2021, vaccines were made available to all adults (>16 years of age) across all US states. In June 2021, George Washington University mandated all members of the campus community to be up to date (an up-to-date course of COVID-19 vaccines consisted of either 2 doses of Moderna [https://www.modernatx.com] or Pfizer-BioNTech [https://www.pfizer.com] vaccines or 1 Johnson & Johnson/Janssen [https://www.jnj.com] immunization with the primary series of COVID-19 vaccinations), or to have obtained an exemption. In September 2021, in the United States, COVID-19 booster shots were authorized for administration 6 months after the second dose of Pfizer or Moderna

or 2 months after 1 dose of Johnson & Johnson/Janssen, initially just for persons ≥65 years of age, persons living or working in high-risk settings, or persons who had underlying conditions. In November 2021, booster shots were recommended for all adults >18 years of age. In January 2022, George Washington University mandated all members of the campus community to have a booster shot or to have obtained an exemption. Community members uploaded vaccine information including the type of vaccine(s) and dates of vaccinations and boosters as a condition of employment and access to campus. This information was used to determine vaccine status on the date of first positive COVID-19 test. The case investigation interviews also collected data about whether medical care was sought, hospitalizations, and administration of monoclonal antibodies.

Statistical Analysis

We described continuous variables by using medians and interquartile ranges (IQRs) and categorical variables by using frequencies and percentages. We compared characteristics of survey respondents by using χ^2 tests for categorical variables and Wilcoxon rank-sum tests for continuous variables. We used logistic regression to determine unadjusted associations between characteristics of survey respondents and long COVID status. We included characteristics that were found to be significantly associated with long COVID status in bivariate analyses in multivariable logistic regression models. All hypothesis tests were 2-sided, and statistical significance was set at an α of 0.05. We performed analyses by using SAS version 9.4 (SAS Institute, Inc., https://www.sas.com).

All university community members provided informed consent to participate in the George Washington University COVID-19 surveillance program. The George Washington University Institutional Review Board concluded that these were non–research-related activities.

Results

Overall, the median age of respondents was 23 (IQR 21–32) years, and the median symptom count was 4 (IQR 1–6) (Table 2). More than half of respondents were female (63.4%) and non-Hispanic White (55.7%). Most (73.4%) respondents were students; 26.6% were faculty/staff . The median days from end of isolation to the follow-up survey was 57 QR (39–158) days.

Most respondents had no underlying conditions (75.2%), never smoked (83.0%), had acute COVID-19 symptoms (79.1%), did not seek medical care at the time of their first positive COVID-19 result (96.6%), and did not receive monoclonal antibody treatment (94.5%) (Table 2). Approximately 41.5% of respondents had received a booster vaccine, 29.9% were fully vaccinated with an initial vaccine series, and 28.6% were not fully vaccinated at the time of their first positive COVID-19 test result. The most common acute symptom was upper respiratory (e.g., congestion, cough, sore throat, runny nose) (92.0%), followed by headache (51.2%), fatigue (51.1%), and chills/fever (44.9%).

Nearly 36% of survey respondents reported experiencing symptoms of long COVID (Table 2). Respondents who had underlying conditions (44.7%; $p = 0.003$), who were not fully vaccinated (47.7%; $p<0.0001$), who were female (40.9%; $p = 0.002$), who were former/current smokers (45.3%; $p = 0.028$), who experienced acute COVID-19 symptoms (43.3%; $p<0.0001$), who reported higher symptom counts (mean 5; $p<0.0001$), who sought medical care (73.9%; $p<0.0001$), or who received antibody treatment (72.0%; $p = 0.0012$) were significantly more likely to report symptoms of long COVID. All symptom categories were strongly associated with long COVID status, except for upper respiratory and other symptoms (Table 2; Figure).

Unadjusted associations between characteristics of survey respondents and long COVID status showed that sex, race/ethnicity, underlying conditions, smoking status, vaccination status, any symptoms, symptom type, symptom count, seeking out medical care, and receiving antibody treatment were strongly associated with long COVID (Table 3). Multivariable models adjusting for statistically significant characteristics in the bivariate analyses found several significant associations: smoking history (former/current smokers versus never smokers) (model 1: adjusted odds ratio [aOR] 1.59, 95% CI 1.13–2.25); experiencing any symptoms at the time of positive test (model 1: aOR 1.92, 95% CI 1.01–3.62); experiencing fatigue (model 1: aOR 1.80, 95% CI 1.32–2.47); and experiencing chest pain/shortness of breath (model 1: aOR 2.18, 95% CI 1.48–3.22). Immunization status was significantly associated with long COVID; those fully vaccinated had higher odds of long COVID than those who had also received a booster (model 1: aOR 2.10, 95% CI 1.51–2.90), and those who were not fully vaccinated had higher odds than those fully vaccinated and those given a booster (model 1: aOR 2.71, 95% CI 1.94–3.77). We found similar results after using symptom count in lieu of any symptoms (versus no symptoms) in model 2.

Table 2. Characteristics of survey respondents by long COVID status for postacute sequelae of SARS-CoV-2 in university setting, Washington, DC, USA*

Characteristic	Total, n = 1,338	No long COVID, n = 833	Long COVID,† n = 475	p value
Age, y median (IQR)	23 (21–32)	23 (21–33)	23 (21–30)	0.265
Sex, n = 1,327				0.002
F	841 (63.4)	497 (59.1)	344 (40.9)	
M	486 (36.6)	328 (67.5)	158 (31.5)	
Race/ethnicity, n = 1,319				0.089
Non-Hispanic White	734 (55.7)	439 (59.8)	295 (40.2)	
Asian	175 (13.3)	119 (68.0)	56 (32.0)	
Non-Hispanic Black	175 (13.3)	117 (66.9)	58 (33.1)	
Hispanic	117 (8.9)	77 (65.8)	40 (34.2)	
Other	70 (5.3)	37 (52.9)	33 (47.1)	
Multiracial	48 (3.6)	32 (66.7)	16 (33.3)	
Affiliation				0.115
Students	982 (73.4)	599 (61.0)	383 (39.0)	
Faculty/staff	356 (26.6)	234 (65.7)	122 (34.3)	
Underlying conditions‡, n = 1,262				0.003
No	949 (75.2)	613 (64.6)	336 (35.4)	
Yes	313 (24.8)	173 (55.3)	140 (44.7)	
Smoking status, n = 1,259				0.028
Never	1,045 (83.0)	655 (62.7)	390 (37.3)	
Former/current	214 (17.0)	117 (54.7)	97 (45.3)	
Vaccination status at time of positive test result				<0.0001
Fully vaccinated with booster	555 (41.5)	411 (74.1)	144 (25.9)	
Fully vaccinated	400 (29.9)	213 (55.6)	170 (44.4)	
Not fully vaccinated	383 (28.6)	209 (52.3)	191 (47.7)	
Any symptoms at time of positive test result, n = 1,328				<0.0001
No	278 (20.9)	231 (83.1)	47 (16.9)	
Yes	1,050 (79.1)	595 (56.7)	455 (43.3)	
Symptom type at time of positive test result, n = 1,050				
Congestion/cough/sore throat/runny nose	966 (92.0)	549 (56.8)	417 (43.2)	0.713
Headache	538 (51.2)	275 (51.1)	263 (48.9)	0.0002
Fatigue	537 (51.1)	256 (47.7)	281 (52.3)	<0.0001
Chills/measured fever/subjective fever	471 (44.9)	240 (51.0)	231 (49.0)	0.0008
Muscle pain	326 (31.1)	148 (45.4)	178 (54.6)	<0.0001
Chest pain/shortness of breath	189 (18.0)	67 (35.5)	122 (64.5)	<0.0001
Diarrhea/nausea/vomiting	181 (17.2)	78 (43.1)	103 (56.9)	<0.0001
Loss of taste/smell	180 (17.1)	86 (47.8)	94 (52.2)	0.008
Other	59 (5.6)	28 (47.5)	31 (52.5)	0.142
Symptom count, median (IQR)	4 (1–6)	3 (0–5)	5 (3–8)	<0.0001
Sought medical care, n = 1,336				<0.0001
No	1,290 (96.6)	819 (63.5)	471 (36.5)	
Yes	46 (3.4)	12 (26.1)	34 (73.9)	
Received monoclonal antibodies, n = 1,331				0.0012
No	1,258 (94.5)	788 (62.6)	470 (37.4)	
Unknown	48 (3.6)	33 (68.8)	15 (31.2)	
Yes	25 (1.9)	7 (28.0)	18 (72.0)	

*Values are no. (%) except as indicated. IQR, interquartile range.
†Long COVID was defined as experiencing ≥1 of the following symptoms lasting for >28 d after a respondent's 10-day isolation period ended: difficulty driving, difficulty having conversations, difficulty making decisions, difficulty thinking, fatigue, feeling anxious, feeling depressed or sad, loss of smell, loss of taste, memory loss, muscle pain, muscle weakness, shortness of breath or difficulty breathing, trouble sleeping, worsening of symptoms after physical activity, worsening of symptoms after mental activity, or other symptoms.
‡Includes diabetes, asthma, hypertension, obesity, sickle cell disease, cancer, chronic kidney disease, lung diseases, serious heart conditions, and other conditions.

Discussion

This study aimed to examine the prevalence and predictors of long COVID in a university community. This sample was unique in that it consisted of primarily young adults who had few underlying health conditions and otherwise were considered healthy. Regardless of initial symptoms, nearly 36% of COVID-19 survivors in this study reported experiencing symptoms consistent with long COVID. That result is within ranges found in other studies reporting a prevalence of long COVID of anywhere from 10% to 80% among COVID-19 survivors (*3–5,7,21,29–31*). Our study also found an increased odds of reporting symptoms consistent with long COVID for each additional symptom reported during the initial infection. This finding is consistent with recent studies conducted with a high proportion of young adults that also found a higher number of acute symptoms

during a COVID-19 infection predicted ≥1 long COVID symptom (*32*). Monitoring symptoms of initial cases could help identify persons at risk for long COVID.

Our study also found that persons who had the fewest previous COVID-19 vaccines and boosters were at higher risk for development of symptoms consistent with long COVID, supporting other investigations suggesting that vaccination is associated with reduced risk for long COVID (*33*–*36*). Many colleges and universities required the COVID-19 vaccine before the fall 2021 semester but offered reasonable medical/religious exemptions. Our results further highlight the need for routine short- and long-term follow-up for persons who test positive for COVID-19 while continuing to advocate and monitor for vaccine and booster adherence to published recommendations.

Although prevention efforts are needed for long COVID, the findings from this study support the need to ameliorate consequences of long COVID. Based on symptomatology, recovery strategies for long COVID include physical rehabilitation, management of preexisting conditions, mental health support, social services support, and exercise programs scaled to the ability of the patient (*11*,*37*). Because long COVID can greatly interfere with the ability to learn or work, classroom or job accommodations, such as modifying academic and workplace policies, flexible scheduling, changing workplace environment, enabling remote or alternative learning, and modifying job responsibilities, are recommended for those having long COVID.

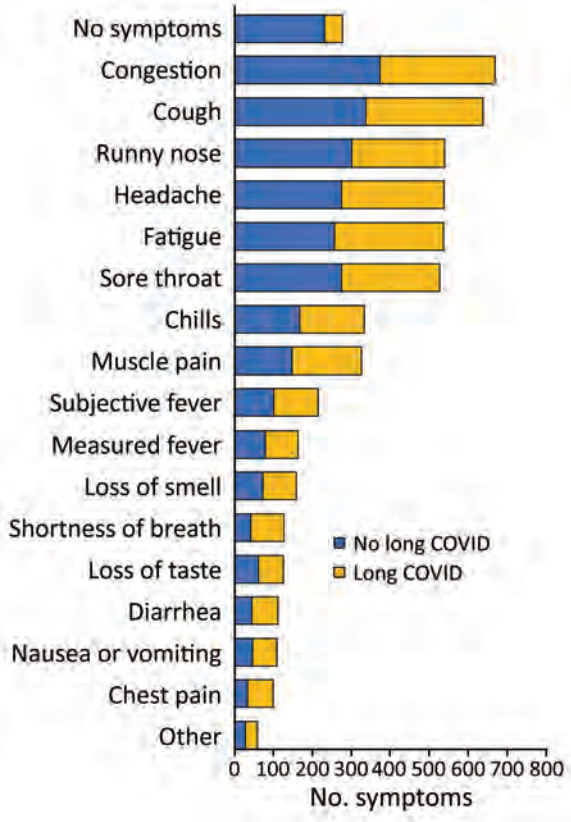

Figure. Frequency of reported acute symptoms among survey respondents for postacute sequelae of SARS-CoV-2 in university setting, by long COVID status, Washington, DC, USA (n = 1,338).

Limitations in conducting this study included the possibility of recall bias, loss to follow-up, and digital literacy challenges, as well as acknowledgment that the results are only for persons who tested positive for SARS-CoV-2. Persons were asked to recall information about their illness after ≥28 days had passed. Considering brain fog is a symptom consistent with long COVID and the length of time between isolation and follow-up, some persons who had long COVID might have forgotten details of their health status during a tumultuous time in their life. Although inevitable, this situation was mitigated by providing the person with dates of their illness when asking them to think back to that time.

Loss to follow-up was also a limitation; some persons never completed a case investigation, which made it more likely for them to forgo a follow-up months later. CCST made >3 attempts at different time points throughout the day to reach as many persons as possible. Those strategies, and our achieved response rate, are consistent with other COVID-19 studies conducted during the pandemic (*38*). Nonetheless, we acknowledge that results could be inflated because persons experiencing symptoms consistent with long COVID might be more likely to respond. Thus, results should be interpreted with caution.

In addition, surveys were conducted by electronic survey and telephone. Although there were no major differences in demographics between telephone and electronic survey completion, some of our participants did not have smartphones, only had landlines, or could not be reached by email, which contributed to loss to follow-up.

Finally, our sample was only of persons who had COVID-19 within our campus community and not of the entire campus population. Thus, it is not possible to know whether symptoms reported in our survey were also increased in the campus population as a whole during this time. Many of the symptoms in our survey are common and might or might not be directly related to SARS-CoV-2 infection or long COVID.

Public health experts and healthcare providers have been gathering data about COVID-19 while simultaneously trying to understand the long-term consequences of SARS-CoV-2 infection. Although preliminary findings of long COVID were anecdotal, researchers continue to gain a clearer picture

Table 3. Association between characteristics of survey respondents and long COVID for postacute sequelae of SARS-CoV-2 in university setting, Washington, DC, USA*

Characteristic	Unadjusted OR (95% CI), n = 1,338	Model 1, aOR† (95% CI), n =1,172	Model 2, aOR† (95% CI), n = 1,175
Age, y	0.99 (0.98–1.00)	–	–
Sex, n = 1,327			
F	1.44 (1.14–1.82)	1.22 (0.92–1.62)	1.16 (0.88–1.54)
M	Referent	Referent	Referent
Race/ethnicity, n = 1,319			
Non-Hispanic White	Referent	Referent	Referent
Asian	0.70 (0.49–0.99)	0.97 (0.64–1.46)	1.00 (0.66–1.50)
Non-Hispanic Black	0.74 (0.52–1.04)	0.79 (0.53–1.19)	0.81 (0.54–1.21)
Hispanic	0.77 (0.51–1.16)	0.82 (0.52–1.19)	0.85 (0.53–1.34)
Other	1.33 (0.81–2.17)	1.54 (0.87–2.74)	1.48 (0.84–2.63)
Multiracial	0.74 (0.40–1.38)	0.78 (0.39–1.59)	0.81 (0.40–1.64)
Affiliation			
Students	1.23 (0.95–1.58)	–	–
Faculty/staff	Referent	–	–
Underlying conditions,‡ n = 1,262			
No	Referent	Referent	Referent
Yes	1.48 (1.14–1.91)	1.23 (0.90–1.66)	1.27 (0.94–1.73)
Smoking status, n = 1,259			
Never	Referent	Referent	Referent
Former/current	1.39 (1.04–1.87)	1.59 (1.13–2.25)	1.60 (1.13–2.25)
Vaccination status at time of positive test result			
Fully vaccinated with booster	Referent	Referent	Referent
Fully vaccinated	2.28 (1.73–3.01)	2.10 (1.51–2.90)	2.19 (1.58–3.03)
Not fully vaccinated	2.61 (1.99–3.43)	2.71 (1.94–3.77)	3.01 (2.16–4.21)
Any symptoms at time of positive test result, n = 1,328			
No	Referent	Referent	–
Yes	3.76 (2.68–5.26)	1.92 (1.04–3.62)	–
Symptom type at time of positive test result			
Fatigue	2.83 (2.25–3.56)	1.80 (1.32–2.47)	1.53 (1.05–2.22)
Chest pain/shortness of breath	3.64 (2.64–5.03)	2.18 (1.48–3.22)	1.70 (1.08–2.67)
Congestion/cough/sore throat/runny nose	2.45 (1.87- 3.21)	0.96 (0.58–1.60)	1.07 (0.69–1.65)
Chills/measured fever/subjective fever	2.08 (1.65–2.62)	0.93 (0.69–1.26)	0.73 (0.49–1.08)
Headache	2.21 (1.76–2.77)	1.11 (0.82–1.50)	0.97 (0.69–1.37)
Loss of taste/smell	1.99 (1.45–2.73)	1.04 (0.72–1.49)	0.83 (0.53–1.29)
Muscle pain	2.52 (1.95–3.25)	1.25 (0.91–1.73)	1.10 (0.78–1.57)
Diarrhea/nausea/vomiting	2.48 (1.80–3.41)	1.24 (0.85–1.81)	1.02 (0.66–1.56)
Other	1.88 (1.11–3.17)	0.89 (0.48–1.64)	0.83 (0.44–1.55)
Symptom count	1.22 (1.18–1.27)	–	1.16 (1.00–1.33)
Sought out medical care, n = 1,336			
No	Referent	Referent	Referent
Yes	4.93 (2.53–9.61)	2.17 (0.98–4.77)	2.07 (0.94–4.55)
Received monoclonal antibodies, n = 1,331			
No	Referent	Referent	Referent
Unknown	0.76 (0.41–1.42)	0.74 (0.34–1.64)	0.72 (0.33–1.59)
Yes	4.31 (1.79–10.40)	1.93 (0.63–5.96)	2.06 (0.68–6.23)

*Long COVID was defined as experiencing ≥1 of the following symptoms lasting for >28 d after a respondent's 10-day isolation period ended: difficulty driving, difficulty having conversations, difficulty making decisions, difficulty thinking, fatigue, feeling anxious, feeling depressed or sad, loss of smell, loss of taste, memory loss, muscle pain, muscle weakness, shortness of breath or difficulty breathing, trouble sleeping, worsening of symptoms after physical activity, worsening of symptoms after mental activity, or other symptoms. aOR, adjusted odds ratio; IQR, interquartile range; OR, odds ratio; –, variable omitted for that model.
†Adjusted for all other variables in the column.
‡Includes diabetes, asthma, hypertension, obesity, sickle cell disease, cancer, chronic kidney disease, lung diseases, serious heart conditions, and other conditions.

on who it affects and how it affects certain populations. From a university standpoint, this analysis is key to understanding how administration can fill the needs of the campus population that has long-term complications caused by COVID-19. Paired with the recommendations presented in this article, universities can strengthen existing services or make referrals to prevention and rehabilitation services (i.e., mental health, exercise programs, long-term health studies) for those who have long COVID that affects their ability to engage in university activities such as classes and work. In addition, universities might benefit from adopting preventive resources for their populations, as well as extended pandemic leave, given the considerable long-lasting effects of long COVID.

Future research avenues should consider following up with long COVID survivors/patients to assess long-term or long-lasting symptoms. Such

analysis could explore the consequences of long COVID for 5–10 years after the initial infection, especially to gain a better understanding of its effect on young, healthy populations. Follow-up could also occur with older populations to assess whether symptoms progress into retirement age and to determine the cost of long-term care resulting from long COVID. Furthermore, research should continue to examine the effect vaccine booster doses have on long COVID symptoms. Such research is vital to clarifying long-term effects of long COVID and how universities can support those dealing with long COVID to promote health and wellness across campus communities.

Acknowledgments

We appreciate our campus community and strive to continue serving our community members. We thank the entire Campus COVID-19 Support Team and their tireless efforts in keeping our community safe. We could not have had a successful return to campus and ongoing surveillance without our team. We also thank the staff of our partners in the Public Health Laboratory, the Student Health Center, and the employee Occupational Health department for their partnership in the successful implementation of the campus surveillance program and their dedication to striving to keep our campus safe and healthy.

About the Author

Dr. Landry is the project director for the Campus COVID-19 Support Team at the George Washington University, Washington, DC. Her primary research interests are public health surveillance and maternal and child health.

References

1. Calabrese L. Long COVID: what do we know and what should we do? Presented at: Basic and Clinical Immunology for the Busy Clinician; February 26, 2022 (virtual meeting) [cited 2022 Dec 15]. https://www.clevelandclinicmeded.com/live/courses/Clinical22/agenda.asp
2. Centers for Disease Control and Prevention. National Center for Immunization and Respiratory Diseases (NCIRD), Division of Viral Diseases. Post-COVID conditions, September 16, 2021 [cited 2022 Dec 15]. https://www.cdc.gov/coronavirus/2019-ncov/long-term-effects/index.html
3. Berger Z, Altiery DE Jesus V, Assoumou SA, Greenhalgh T. Long COVID and health inequities: the role of primary care. Milbank Q. 2021;99:519–41. https://doi.org/10.1111/1468-0009.12505
4. Jason LA, Islam M, Conroy K, Cotler J, Torres C, Johnson M, et al. COVID-19 symptoms over time: comparing long-haulers to ME/CFS. Fatigue. 2021;9:59–68. https://doi.org/10.1080/21641846.2021.1922140
5. Leviner S. Recognizing the clinical sequelae of COVID-19 in adults: COVID-19 long-haulers. J Nurse Pract. 2021;17:946–9. https://doi.org/10.1016/j.nurpra.2021.05.003
6. Parums DV. Editorial: long COVID, or post-COVID syndrome, and the global impact on health care. Med Sci Monit. 2021;27:e933446. https://doi.org/10.12659/MSM.933446
7. van Kessel SA, Olde Hartman TC, Lucassen PL, van Jaarsveld CH. Post-acute and long-COVID-19 symptoms in patients with mild diseases: a systematic review. Fam Pract. 2022;39:159–67. https://doi.org/10.1093/fampra/cmab076
8. Soriano JB, Murthy S, Marshall JC, Relan P, Diaz JV; WHO Clinical Case Definition Working Group on Post-COVID-19 Condition. A clinical case definition of post-COVID-19 condition by a Delphi consensus. Lancet Infect Dis. 2022;22:e102–7. https://doi.org/10.1016/S1473-3099(21)00703-9
9. Phillips S, Williams MA. Confronting our next national health disaster: long-haul COVID. N Engl J Med. 2021;385:577–9. https://doi.org/10.1056/NEJMp2109285
10. Lambert, NJ; Survivor Corps. COVID-19 "long hauler" symptoms survey report, 2020. Indiana University School of Medicine [cited 2022 Dec 15]. https://dig.abclocal.go.com/wls/documents/2020/072720-wls-covid-symptom-study-doc.pdf
11. Aiyegbusi OL, Hughes SE, Turner G, Rivera SC, McMullan C, Chandan JS, et al.; TLC Study Group. Symptoms, complications and management of long COVID: a review. J R Soc Med. 2021;114:428–42. https://doi.org/10.1177/01410768211032850
12. Iqbal FM, Lam K, Sounderajah V, Clarke JM, Ashrafian H, Darzi A. Characteristics and predictors of acute and chronic post-COVID syndrome: a systematic review and meta-analysis. EClinicalMedicine. 2021;36:100899. https://doi.org/10.1016/j.eclinm.2021.100899
13. Anaya JM, Rojas M, Salinas ML, Rodríguez Y, Roa G, Lozano M, et al.; Post-COVID study group. Post-COVID syndrome. A case series and comprehensive review. Autoimmun Rev. 2021;20:102947. https://doi.org/10.1016/j.autrev.2021.102947
14. Mahmud R, Rahman MM, Rassel MA, Monayem FB, Sayeed SKJB, Islam MS, et al. Post-COVID-19 syndrome among symptomatic COVID-19 patients: a prospective cohort study in a tertiary care center of Bangladesh. PLoS One. 2021;16:e0249644. https://doi.org/10.1371/journal.pone.0249644
15. Michelen M, Manoharan L, Elkheir N, Cheng V, Dagens A, Hastie C, et al. Characterising long COVID: a living systematic review. BMJ Glob Health. 2021;6:e005427. https://doi.org/10.1136/bmjgh-2021-005427
16. Nalbandian A, Sehgal K, Gupta A, Madhavan MV, McGroder C, Stevens JS, et al. Post-acute COVID-19 syndrome. Nat Med. 2021;27:601–15. https://doi.org/10.1038/s41591-021-01283-z
17. Sathyamurthy P, Madhavan S, Pandurangan V. Prevalence, pattern and functional outcome of post COVID-19 syndrome in older adults. Cureus. 2021;13:e17189.
18. Sudre CH, Murray B, Varsavsky T, Graham MS, Penfold RS, Bowyer RC, et al. Attributes and predictors of long COVID. Nat Med. 2021;27:626–31. https://doi.org/10.1038/s41591-021-01292-y
19. Taquet M, Dercon Q, Luciano S, Geddes JR, Husain M, Harrison PJ. Incidence, co-occurrence, and evolution of long-COVID features: a 6-month retrospective cohort study of 273,618 survivors of COVID-19. PLoS Med. 2021;18:e1003773. https://doi.org/10.1371/journal.pmed.1003773

20. Tirelli U, Taibi R, Chirumbolo S. Post COVID syndrome: a new challenge for medicine. Eur Rev Med Pharmacol Sci. 2021;25:4422–5.
21. Berg S. What doctors wish patients knew about long COVID, October 22, 2021. American Medical Association [cited 2022 Dec 15]. https://www.ama-assn.org/delivering-care/public-health/what-doctors-wish-patients-knew-about-long-covid
22. Crispo A, Bimonte S, Porciello G, Forte CA, Cuomo G, Montagnese C, et al. Strategies to evaluate outcomes in long-COVID-19 and post-COVID survivors. Infect Agent Cancer. 2021;16:62. https://doi.org/10.1186/ s13027-021-00401-3
23. Singh I, Joseph P, Heerdt PM, Cullinan M, Lutchmansingh DD, Gulati M, et al. Persistent exertional intolerance after COVID-19. Chest. 2022;161:54–63. https://doi.org/10.1016/j.chest.2021.08.010
24. Sojka A, Machniak M, Andrzejewski W, Kosendiak A, Chwałczyńska A. Changes in physical activity and the occurrence of specific symptoms of "long-COVID syndrome" in men aged 18–25. Int J Environ Res Public Health. 2022;19:1199. https://doi.org/10.3390/ijerph19031199
25. Lemhöfer C, Sturm C, Loudovici-Krug D, Best N, Gutenbrunner C. The impact of post-COVID-syndrome on functioning: results from a community survey in patients after mild and moderate SARS-CoV-2-infections in Germany. J Occup Med Toxicol. 2021;16:45. https://doi.org/10.1186/s12995-021-00337-9
26. US Food and Drug Administration. In vitro diagnostic. EUAs: antigen diagnostic tests for SARS-CoV-2, 2021 [cited 2022 Dec 15]. https://www.fda.gov/medical-devices/coronavirus-disease-2019-covid-19-emergency-use-authorizations-medical-devices/in-vitro-diagnostics-euas-antigen-diagnostic-tests-sars-cov-2
27. Towers SA, Gemechu NB, Nagaraj NC, Landry MM, Beane P, Sardon GA Jr, et al.; George Washington University Campus COVID-19 Support Team. SARS-CoV-2 surveillance and outbreak response on an urban American college campus. J Am Coll Health. 2022;Mar 8:1–9. https://doi.org/10.1080/07448481.2022.2034834
28. Harris PA, Taylor R, Thielke R, Payne J, Gonzalez N, Conde JG. Research electronic data capture (REDCap): a metadata-driven methodology and workflow process for providing translational research informatics support. J Biomed Inform. 2009;42:377–81. https://doi.org/10.1016/j.jbi.2008.08.010
29. Lewis D. Long COVID and kids: scientists race to find answers. Nature. 2021;595:482–3. https://doi.org/10.1038/d41586-021-01935-7
30. Lopez-Leon S, Wegman-Ostrosky T, Perelman C, Sepulveda R, Rebolledo PA, Cuapio A, et al. More than 50 long-term effects of COVID-19: a systematic review and meta-analysis. Sci Rep. 2021;11:16144. https://doi.org/10.1038/s41598-021-95565-8
31 Silverberg JI, Zyskind I, Naiditch H, Zimmerman J, Glatt AE, Pinter A, et al. Predictors of chronic COVID-19 symptoms in a community-based cohort of adults. PLoS One. 2022;17:e0271310. https://doi.org/10.1371/journal.pone.0271310
32. Ebell MH, Forgacs D, Shen Y, Ross TM, Hulme C, Bentivegna M, et al. High prevalence of both previous infection with SARS-CoV-2 and persistent symptoms. J Am Board Fam Med. 2022;35:570–8. https://doi.org/10.3122/jabfm.2022.03.210348
33. Antonelli M, Penfold RS, Merino J, Sudre CH, Molteni E, Berry S, et al. Risk factors and disease profile of post-vaccination SARS-CoV-2 infection in UK users of the COVID Symptom Study app: a prospective, community-based, nested, case-control study. Lancet Infect Dis. 2022; 22:43–55. https://doi.org/10.1016/S1473-3099(21)00460-6
34. Kuodi P, Gorelik Y, Zayyad H, Wertheim O, Wiegler KB, Jabal KA, et al. Association between BNT162b2 vaccination and reported incidence of post-COVID-19 symptoms: cross-sectional study 2020-21, Israel. NPJ Vaccines. 2022;7:101. https://doi.org/10.1038/s41541-022-00526-5
35. Hastie CE, Lowe DJ, McAuley A, Winter AJ, Mills NL, Black C, et al. Outcomes among confirmed cases and a matched comparison group in the Long-COVID in Scotland study. Nat Commun. 2022;13:5663. https://doi.org/10.1038/s41467-022-33415-5
36. Ayoubkhani D, Bermingham C, Pouwels KB, Glickman M, Nafilyan V, Zaccardi F, et al. Trajectory of long covid symptoms after covid-19 vaccination: community based cohort study. BMJ. 2022;377:e069676. https://doi.org/10.1136/bmj-2021-069676
37. Morley JE. COVID-19: the long road to recovery. J Nutr Health Aging. 2020;24:917–9. https://doi.org/10.1007/s12603-020-1497-y
38. Amaral S, Dinarte L, Dominguez P, Romero S, Perez-Vincent SM. Talk or text? Evaluating response rates by remote survey method during COVID-19. CESifo working paper no. 9517. 2022 [cited 2022 Dec15]. https://doi.org/10.2139/ssrn.4009417

Address for correspondence: Megan Landry, The George Washington University Milken Institute School of Public Health, 950 New Hampshire Ave NW, 7th Fl, Washington, DC 20052, USA; email: mmlandry@gwu.edu

Clonal Expansion of Multidrug-Resistant *Streptococcus dysgalactiae* Subspecies *equisimilis* Causing Bacteremia, Japan, 2005–2021

Koh Shinohara, Kazunori Murase, Yasuhiro Tsuchido, Taro Noguchi, Satomi Yukawa, Masaki Yamamoto, Yasufumi Matsumura, Ichiro Nakagawa, Miki Nagao

In support of improving patient care, this activity has been planned and implemented by Medscape, LLC and Emerging Infectious Diseases. Medscape, LLC is jointly accredited with commendation by the Accreditation Council for Continuing Medical Education (ACCME), the Accreditation Council for Pharmacy Education (ACPE), and the American Nurses Credentialing Center (ANCC), to provide continuing education for the healthcare team.

Medscape, LLC designates this Journal-based CME activity for a maximum of 1.00 ***AMA PRA Category 1 Credit(s)™***. Physicians should claim only the credit commensurate with the extent of their participation in the activity.

Successful completion of this CME activity, which includes participation in the evaluation component, enables the participant to earn up to 1.0 MOC points in the American Board of Internal Medicine's (ABIM) Maintenance of Certification (MOC) program. Participants will earn MOC points equivalent to the amount of CME credits claimed for the activity. It is the CME activity provider's responsibility to submit participant completion information to ACCME for the purpose of granting ABIM MOC credit.

All other clinicians completing this activity will be issued a certificate of participation. To participate in this journal CME activity: (1) review the learning objectives and author disclosures; (2) study the education content; (3) take the post-test with a 75% minimum passing score and complete the evaluation at http://www.medscape.org/journal/eid; and (4) view/print certificate. For CME questions, see page 677.

Release date: February 22, 2023; Expiration date: February 22, 2024

Learning Objectives

Upon completion of this activity, participants will be able to:

- Assess the microbiologic characteristics of identified bartonellosis cases, based on a series of broad-range and organism-specific molecular assays at a large clinical reference laboratory
- Evaluate demographic and clinical characteristics of patients with bartonellosis, based on a series of broad-range and organism-specific molecular assays at a large clinical reference laboratory
- Determine the clinical implications of the demographic, clinical, and microbiologic characteristics of patients with bartonellosis, based on a series of broad-range and organism-specific molecular assays at a large clinical reference laboratory

CME Editor

Susan Zunino, PhD, Technical Writer/Editor, Emerging Infectious Diseases. *Disclosure: Susan Zunino, PhD, has no relevant financial relationships.*

CME Author

Laurie Barclay, MD, freelance writer and reviewer, Medscape, LLC. *Disclosure: Laurie Barclay, MD, has no relevant financial relationships.*

Authors

David W. McCormick, MD, MPH; Sara L. Rassoulian-Barrett, MS; Daniel R. Hoogestraat, BS, MB(ASCP); Stephen J. Salipante, MD, PhD; Dhruba SenGupta, PhD; Elizabeth A. Dietrich, PhD; Brad T. Cookson, MD, PhD; Grace E. Marx, MD, MPH; Joshua A. Lieberman, MD, PhD.

Authors affiliation: Kyoto University Graduate School of Medicine, Kyoto, Japan

DOI: https://doi.org/10.3201/eid2903.221060

Incidence of *Streptococcus dysgalactiae* subspecies *equisimilis* (SDSE) bacteremia is increasing in the Kyoto-Shiga region of Japan. We retrospectively analyzed clinical features of SDSE bacteremia and conducted comparative genomic analyses of isolates collected from 146 bacteremia episodes among 133 patients during 2005–2021. Of those patients, 7.7% required vasopressor support, and 7.0% died while in the hospital. The prevalence of isolates resistant to erythromycin, minocycline, and clindamycin increased from 8.6% during 2005–2017 to 21.6% during 2018–2021. Our genomic analysis demonstrated that sequence type 525 and clonal complex 25 were predominant in SDSE isolates collected during 2018–2021. In addition, those isolates had acquired 2 antimicrobial-resistance genes, *erm*B and *tet*M, via Tn*916*-like integrative and conjugative elements (ICEs). Phylogenetic analysis revealed clonal distribution of Tn*916*-like ICEs in SDSE isolates. Our findings suggest that Tn*916*-like ICEs contributed to the emergence and recent increase of multidrug-resistant SDSE bacteremia in this region of Japan.

Streptococcus dysgalactiae subspecies *equisimilis* (SDSE) is a member of the pyogenic group of streptococci that typically is agglutinated by serum against Lancefield group G or C antigens (rarely A or L antigens) (*1*). Although SDSE has been considered a part of the commensal flora and is much less virulent than *S. pyogenes*, SDSE increasingly has been recognized as a clinically relevant pathogenic bacterium (*2*–*4*). SDSE can cause a broad range of diseases, from milder illnesses such as pharyngitis and skin and soft-tissue infections to severe conditions such as streptococcal toxic shock syndrome (STSS) and necrotizing fasciitis that can resemble infections caused by *S. pyogenes* (*2*,*4*–*6*).

Invasive SDSE infections mainly affect elderly persons with underlying illnesses (*2*,*4*,*6*); fatality rates of 2%–20% have been reported (*4*,*7*). Moreover, multiple countries, including Israel, Denmark, Norway, and Canada, have reported increasing incidence of invasive diseases caused by SDSE or group C or G Streptococcus (GCGS) (*8*–*11*). In Japan, a single-center study in Tokyo reported a substantial increase in the age-adjusted incidence of invasive group G Streptococcus from 2003–2007 to 2008–2013 (*12*). An aging population with multiple underlying conditions only partially explains those reports (*8*,*12*), and other reasons for the growing prevalence of invasive SDSE infections remain unclear.

SDSE is essentially susceptible to penicillin and other β-lactam antibiotics, but resistance to other antimicrobial agents has emerged. Multiple countries, including the United States, Japan, and Norway, have reported increased prevalence of erythromycin- and clindamycin-resistant isolates (*2*,*5*,*13*). Moreover, recent studies in countries in eastern Asia showed much higher prevalence of resistance to multiple antimicrobial agents, including macrolides, tetracyclines, and lincosamide (*14*,*15*). A multicenter study in China showed resistance rates of 71.4% to erythromycin, 71.4% to clindamycin, and 60.7% to tetracycline (15). The prevalent genes responsible for macrolide resistance in those studies were *mef*A/E, *erm*A, and *erm*B (5,13–15); *erm*A and *erm*B are also responsible for clindamycin resistance and typically confer inducible and constitutive resistance.

We conducted a retrospective, multicenter, surveillance study of SDSE bacteremia cases in the Kyoto-Shiga region of Japan. We also performed a comparative genomic analysis of clinical SDSE isolates preserved in 3 hospitals in the region to explore the phylogenetic relationships and emergence of antimicrobial resistance (AMR).

Materials and Methods

Surveillance Data Collection

We collected the annual number of GCGS and SDSE bacteremia cases and hospital admissions during January 2011–December 2020 in 6 hospitals in the Kyoto-Shiga region of Japan. Four hospitals were in Kyoto, Kyoto University Hospital (KUHP), Kyoto City Hospital (KCH), Kyoto Katsura Hospital (KKH), and Kyoto Min-iren Chuo Hospital (KMCH); 2 hospitals were Shiga, Japanese Red Cross Otsu Hospital (JRCOH) and Shiga General Hospital (SGH) (Figure 1). Among the hospitals, 3 changed their methods of identifying β-hemolytic streptococci during the study period, from the biochemical and Lancefield grouping methods to matrix-assisted laser desorption/ionization time-of-flight (MALDI-TOF) mass spectrometry: KUHP changed in 2016, KCH in 2015, and KMCH in 2019. The other 3 hospitals used the biochemical and Lancefield grouping methods throughout the study period; therefore, we collected the combined incidences of GCGS and SDSE bacteremia.

Bacterial Isolates

We conducted a microbiological and genomic study using the preserved isolates collected from GCGS and SDSE isolates from the bacteremia cases during 2005–2021 in 3 hospitals: KUHP, KKH, and JRCOH. The bacterial isolates from patients' blood samples were identified as GCGS when isolates

Figure 1. Study area for investigation of clonal expansion of multidrug-resistant *Streptococcus dysgalactiae* subspecies *equisimilis* causing bacteremia, Japan, 2005–2021. Shading indicates the Kyoto-Shiga region and hospitals included in the study. Inset shows study area in Japan. KCH, Kyoto City Hospital; KKH, Kyoto Katsura Hospital; KMCH, Kyoto Min-iren Chuo Hospital; KUHP, Kyoto University Hospital; JRCOH, Japanese Red Cross Otsu Hospital; SGH, Shiga General Hospital.

showed large colony size (>0.5 mm), β-hemolysis on 5% sheep blood agar plate after overnight culture, and Lancefield grouping C or G. In some hospitals, GCGS isolates were then identified as SDSE by using phenotypic methods such as API 20 Strep (bioMérieux), BBL Crystal (Becton Dickinson Microbiology Systems), Microscan Walkaway System (Beckman Coulter, Inc.), or MALDI-TOF mass spectrometry. The study comprised 146 SDSE isolates collected during 2005–2021 (Appendix 1, https://wwwnc.cdc.gov/EID/article/29/3/22-1060-App1.xlsx).

Lancefield grouping was performed using the Prolex Streptococcal Grouping Latex Kit (Pro Lab Diagnostics Inc.). Antimicrobial susceptibility testing was conducted by using the MicroScan WalkAway System according to the manufacturers' instructions or by broth microdilution by using customized dry plates (Eiken Chemical Co., Ltd). Susceptibility results were interpreted following Clinical Laboratory Standards Institute recommendations (16). Multidrug-resistant (MDR) was defined as nonsusceptibility to >2 antimicrobial agents; for this study, we refer to MDR as nonsusceptibility to erythromycin, minocycline, and clindamycin.

Clinical Data Collection

We retrospectively reviewed the charts of patients with preserved isolates. Using clinical records from each episode, we collected the age, sex, dates of illness onset and sample collection, underlying illnesses, receipt of chemotherapy or immunosuppressive agents, signs, symptoms, laboratory findings at the first visit, clinical source of the bacteremia, infection type (community-acquired or nosocomial: nosocomial infections were defined as clinical signs and symptoms occurring >48 hours after admission), infection severity parameters, outcomes, and relapses.

Whole-Genome Sequencing and Bioinformatic Analysis

We extracted genomic DNA from isolates by using the MagNA Pure 96 DNA and Viral NA Small Volume Kit on a MagNA Pure 96 Instrument

(Roche). We prepared a short-read library by using the Illumina DNA Prep Kit (Illumina Inc.) and used NextSeq 1000/2000 P1 Reagent Kit version 3 on the NextSeq platform (Illumina) to generate paired-end reads. We used the Rapid Barcoding Kit (Oxford Nanopore Technologies) to prepare a long-read library from unsheared genomic DNA, which we sequenced by using an R9.4.1 Flow Cell on a MinION device (Oxford Nanopore Technologies). We assembled draft genome sequences from the short-reads and complete genome sequences from the long-reads by using Unicycler pipeline version 0.4.8 with default parameters (17). We annotated assembled genomes by using Prokka version 1.14.6 (17) with default settings and used annotated genomes for downstream analysis. We confirmed isolates as SDSE by comparing 16S rRNA gene similarity with the subsequent contigs.

We identified multilocus sequence types (MLSTs) from the assembled contigs by using a BLASTn search (https://blast.ncbi.nlm.nih.gov) against the S. dysgalactiae MLST database in pubMLST (https://pubmlst.org/organisms/streptococcus-dysgalactiae) and then assigned the MLST to a clonal complex (CC) by using global optimal eBURST (goeBURST). We assigned CCs by a single-locus variation from a founding sequence type (ST). We determined *emm* types via BLAST search against the *emm* sequence database curated by the Centers for Disease Control and Prevention (https://www2.cdc.gov/vaccines/biotech/strepblast.asp). We detected AMR genes by using abricate (https://github.com/tseemann/abricate) and the Comprehensive Antibiotic Resistance Database (https://card.mcmaster.ca) (18). We predicted virulence factors of SDSE genomes by using BLASTP against the Virulence Factor Database (http://www.mgc.ac.cn/VFs) (19) set A, a core dataset that covers genes associated with experimentally verified virulence factors, and a cutoff E-value of 1E−5.

We submitted the raw Illumina and MinION read data to the International Nucleotide Sequence Database Collaboration (https://www.insdc.org) under BioProject accession no. PRJDB12179. We summarized the assembly statistics and general genomic information (Appendix 1).

Phylogenetic Analyses

We used Roary version 3.13.0 (*20*) and default parameters to identify the core genomes of the 146 SDSE

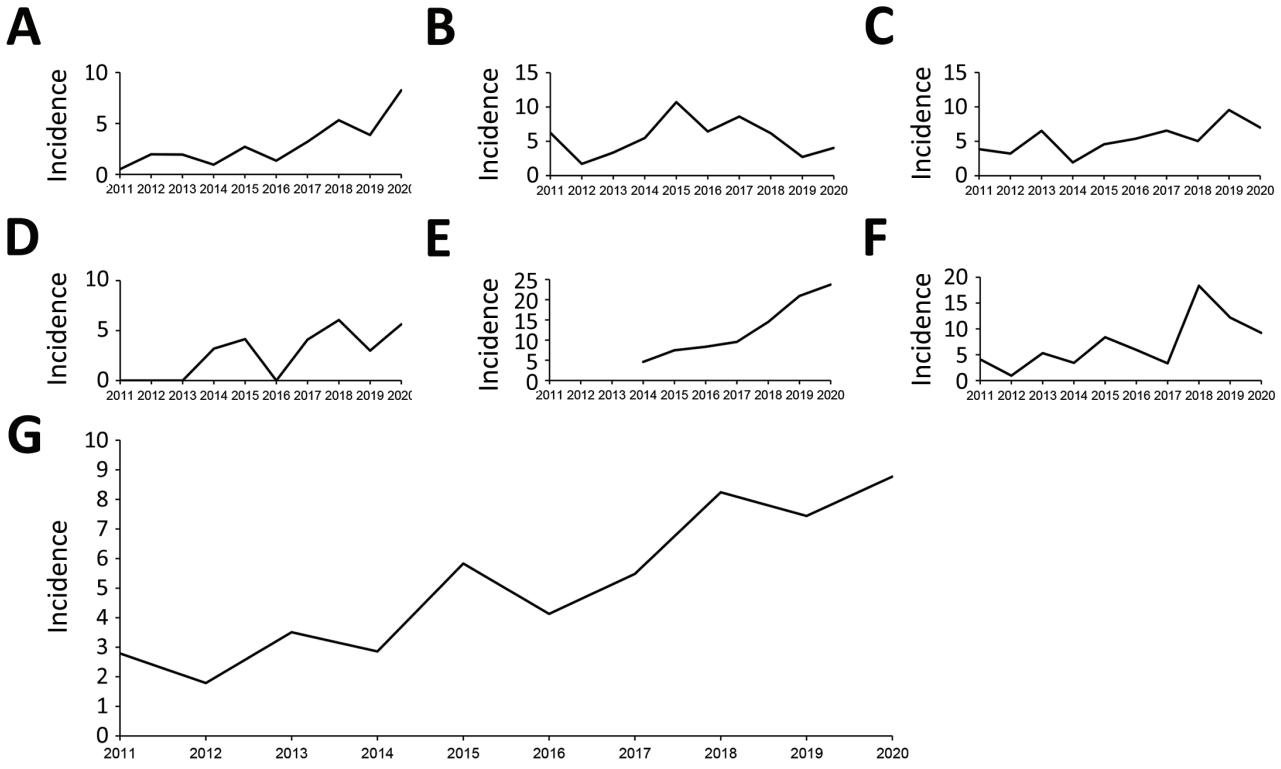

Figure 2. Incidence (cases/10,000 admissions) of multidrug-resistant *Streptococcus dysgalactiae* subspecies *equisimilis* and group C or G *Streptococcus* bacteremia, Kyoto-Shiga region, Japan, 2011–2020. A) Kyoto University Hospital; B) Kyoto City Hospital; C) Japanese Red Cross Otsu Hospital; D) Shiga General Hospital; E) Kyoto Min-iren Chuo Hospital; F) Kyoto Katsura Hospital; G) total for all 6 hospitals included in the study.

Table 1. Characteristics of 133 patients with *Streptococcus dysgalactiae* subspecies *equisimilis* bacteremia, Japan, 2005–2021*

Characteristic	Value
Median age, y (IQR)	81.0 (72.0–88.0)
Age group, y	
<30	1 (0.8)
30–39	4 (3.0)
40–49	5 (3.6)
50–59	6 (4.5)
60–69	12 (9.0)
70–79	29 (21.8)
80–89	50 (37.6)
≥90	26 (19.5)
Sex	
M	72 (54.1)
F	61 (45.9)
Medical history	
No underlying conditions	15 (11.3)
Solid organ tumor†	36 (27.1)
History of surgery, n = 36	15 (41.7)
Active malignancy, n = 36‡	22 (61.1)
Metastasis, n = 36	10 (27.8)
Hematologic malignancy	6 (4.5)
Hematopoietic stem cell transplant, n = 6	
Cardiovascular disease	21 (15.8)
Cerebral artery diseases	38 (28.6)
Chronic kidney diseases	27 (20.3)
Diabetes mellitus	22 (16.5)
Dementia	31 (23.3)
Collagen diseases	8 (6.0)
Chronic lung diseases	7 (5.3)
HIV	0
Chemotherapy	12 (9.0)
Immune suppressive therapy	6 (4.5)
Neutropenia, neutrophil count <500 cells/μL	5 (3.8)

*Values are no. (%) except as indicated. For patients with multiple episodes, variables for the first episode are described.
†Ten patients with prostate cancer; 8 with cervical cancer; 7 with colon, rectal, or anal cancer; 3 with lung cancer; 2 with stomach cancer; 2 with endometrial cancer; 2 with bladder cancer; 2 with breast cancer; and 1 with cancer categorized as other (esophageal cancer, ovarian cancer, pharyngeal cancer, salivary gland cancer, vaginal cancer, and extramammary Paget's disease), including duplicates.
‡Treated within 5 years.

isolates. We generated a maximum-likelihood phylogenetic tree from the core genome alignment by using RAxML-NG version 1.0.3 and a general time-reversible plus gamma distribution DNA substitution model with 100 bootstrap replicates (21). We used FigTree version 1.4.4 (https://github.com/rambaut/figtree) and iTOL version 6 (*22*) to visualize phylogenetic trees.

Tn*916*-Like Integrative and Conjugative Element Analysis

We extracted sequences of the Tn*916*-like integrative and conjugative elements (ICEs) from the assembled contigs by using a BLASTn search (*23*) against the Enterococcus faecalis Tn*916* reference sequence (GenBank accession no. U09422.1). We manually analyzed the region structures by using the Artemis Comparison Tool (24).

Statistical Analyses

We used χ^2 and Fisher exact tests to compare categorical variables, as appropriate, and used Mann-Whitney U tests to analyze continuous, nonparametric data. To assess the time trends in GCGS/SDSE bacteremia incidence during 2011–2020, we calculated the incidence rate ratio and significance of the data by comparing the later cohort (2016–2020) with the early cohort (2011–2015) and considered a 2-sided $p<0.05$ statistically significant. We performed all statistical analyses using R version 3.6.0 (The R Foundation for Statistical Computing, https://www.r-project.org).

The Ethics Committee of Kyoto University Graduate School and Faculty of Medicine approved the study (approval no. R3240). The study was conducted in accordance with the principles expressed in the Declaration of Helsinki.

Results

Temporal Trends in SDSE Bacteremia

The Kyoto-Shiga Region is a metropolitan area in Japan with a population of ≈2.5 million in an area of 70 km. We collected data on 398 episodes of bacteremia caused by GCGS and SDSE in 6 hospitals in Kyoto-Shiga region during 2011–2020 (Figure 1). We investigated the temporal trend in combined incidence of GCGS and SDSE bacteremia per 10,000 admissions (Figure 2). The incidence of GCGS and SDSE bacteremia increased from 2.77/10,000 admissions in 2011 to 8.77/10,000 admissions in 2020. We noted a statistically significant increase in GCGS and SDSE bacteremia incidence between the first and last 5-year periods (incidence rate ratio = 2.03, p = 0.03). During 2018–2020, the average annual incidence of bacteremia reached 13.3 cases/10,000 admissions in KKH and 19.7 cases/10,000 admissions in KMCH.

Clinical Characteristics of Patients with SDSE Bacteremia

We investigated 146 SDSE bacteremia episodes by using preserved isolates from 133 patients at KUHP, KKH, and JRCOH. The study included 118 isolates collected from KUHP, KKH, and JRCOH, representing 50.6% (118/233) of all cases from the 3 hospitals during 2011–2020. KUHP preserved consecutive isolates throughout the study period (2005–2021), but JRCOH and KKH did not. In detail, JRCOH preserved consecutive isolates during 2015–2021 but only preserved 1 isolate during 2013–2014. Similarly, KKH preserved 8 of 20 isolates collected in 2021.

Table 2. Clinical manifestations and severity markers for 146 episodes of multidrug-resistant *Streptococcus dysgalactiae* subspecies *equisimilis* bacteremia, Japan, 2005–2021*

Characteristics	No. (%
Type of infection	
Community-acquired	136 (93
Nosocomial	10 (6.
Clinical source of bacteremia†	
Cellulitis	74 (50
Primary bacteremia without focus	27 (18
Necrotizing fasciitis	10 (6.
Vertebral osteomyelitis and discitis	10 (6.
Psoas abscess	6 (4.1
Septic arthritis	11 (7.
Infectious endocarditis	4 (2.7
Urinary tract infection	7 (4.8
Pneumonia	1 (0.7
Others‡	14 (9.
Clinical characteristics	
Body temperature ≥38°C, n = 143	100 (69
Mean arterial pressure <80 mm Hg, n = 140	42 (30
Heart rate >90 beats/min, n = 138	83 (60
Disturbance of consciousness, n = 141	54 (38
Severe disease, n = 142	
Streptococcus toxic shock syndrome	7 (4.9
Vasopressor support required	11 (7.
Ventilator support required	6 (4.2
Admission to intensive care unit required	9 (6.3
Death	
In-hospital death, n = 143	10 (7.
30-d mortality, n = 138	5 (3.6

*Data include 13 relapse or reinfection episodes among 9 patients (deta are available in Appendix 2 Table 1, (https://wwwnc.cdc.gov/EID/article/29/3/22-1060-App2.pdf).
†Data include ≥1 instance per patient, including 3 case-patients with cellulitis and septic arthritis; 2 with vertebral osteomyelitis and psoas abscess; and 1 with each of the following co-infections: cellulitis and vertebral osteomyelitis; cellulitis and psoas abscess; cellulitis and urina tract infection; necrotizing fasciitis and septic arthritis; vertebral osteomyelitis and septic arthritis; psoas abscess and septic arthritis; infective endocarditis and vertebral osteomyelitis; cellulitis and mycotic aneurysm; vertebral osteomyelitis, psoas abscess, and pyogenic lymphadenitis; vertebral osteomyelitis, psoas abscess, and urinary tract infection; vertebral osteomyelitis, septic arthritis, and empyema.
‡Other infections were 3 cases of catheter-related bloodstream infectio cases of decubitus infection; 2 cases of secondary peritonitis; and 1 cas each of empyema; surgical site infection; retroperitoneal abscess; pyogenic lymphadenitis; and mycotic aneurysm.

Among 133 patients with SDSE bacteremia, most were 80–89 years of age (Table 1). Many patients had underlying conditions, predominantly cerebrovascular disease (28.6%), solid organ cancer (27.1%), and dementia (21.3%) (Table 2). We noted recurrent SDSE bacteremia in 9 patients who had a total of 13 episodes (Appendix 2 Table 1, https://wwwnc.cdc.gov/EID/article/29/3/22-1060-App2.pdf).

Table 3. Temporal changes in clonal complexes and sequence types and antimicrobial nonsusceptibility rates of *Streptococcus dysgalactiae* subspecies *equisimilis* bacteremia, Japan, 2005–2021*

Characteristics	No. (%) patients 2005–2017, n = 58	No. (%) patients 2018–2021, n = 88	p value
CC or ST			
CC17	23 (39.7)	27 (30.7)	0.288
CC25	13 (22.4)	28 (31.8)	0.261
CC29	5 (8.6)	8 (9.1)	1.000
ST525	1 (1.7)	15 (17.1)	0.001
Others	16 (27.6)	10 (11.4)	0.015
Antimicrobial nonsusceptibility			
Erythromycin	16 (27.6)	30 (34.1)	0.469
Minocycline	17 (29.3)	28 (31.8)	0.855
Clindamycin	11 (19.0)	26 (29.5)	0.176
MDR†	5 (8.6)	19 (21.6)	0.042

*CC, clonal complex; MDR, multidrug resistance; ST, sequence type.
†Resistant to erythromycin, minocycline, and clindamycin.

Of the 146 episodes in 133 patients, the most common sources of bacteremia were cellulitis (50.7%) or primary bacteremia (18.5%) (Table 1). Of 142 episodes for which detailed data were available, 7 (4.9%) involved STSS and 11 (7.7%) required vasopressor use; of 143 patients, 10 (7.0%) died during hospitalization.

Of 146 SDSE bacteremia episodes, most (136, 93.2%) were community-acquired; 10 (6.8%) were nosocomial (Appendix 2 Table 2). Of the 10 patients with nosocomial episodes, 7 had active malignancy, 5 received chemotherapy, and 3 had febrile neutropenia. Four patients had multiple pathogen infections: 2 episodes were primary bacteremia occurring in patients with neutropenia, the other 2 catheter-related bloodstream infections. In the neutropenic patients with primary bacteremia, *Escherichia coli* or viridans streptococci were isolated from each patient. In the patients with catheter-related bloodstream infections, *Staphylococcus aureus* or *S. epidermidis* was isolated from each patient. Two nosocomial-onset patients died while hospitalized.

AMR and Virulence Profiles of SDSE Isolates

Of the 146 SDSE isolates identified, 138 were classified as Lancefield group G, 6 as group C, 1 as group

Table 4. Antimicrobial nonsusceptibility rates among *Streptococcus dysgalactiae* subspecies *equisimilis* clonal complexes and sequence types, Japan, 2005–2021*

CC or ST	Penicillin G	Cefotaxime	Meropenem	Erythromycin	Minocycline	Clindamycin
CC17, n = 50	0	0	0	9 (18.0)	2 (4.0)	8 (16.0)
CC25, n = 41	0	0	0	12 (29.3)	16 (39.0)	12 (29.3)
ST525, n = 16	0	0	0	16 (100)	16 (100)	16 (100)
CC29, n = 13	0	0	0	1 (7.7)	1 (7.7)	1 (7.7)
Others, n = 26	0	0	0	8 (30.8)	10 (38.5)	0
Total, n = 146	0	0	0	46 (31.5)	45 (30.8)	37 (25.5)

*Values are no. (%) isolates. CC, clonal complex; ST, sequence type.

Table 5. Prevalence of antimicrobial resistance determinant genes and Tn*916*-like integrative and conjugative elements among *Streptococcus dysgalactiae* subspecies *equisimilis* clonal complexes and sequence types, Japan, 2005–2021*

CC or ST	*erm*B	*erm*A	*mef*(A/E)	*tet*M	*tet*L	Tn*916*-like ICE
CC17, n = 50	2 (4.0)	7 (14.0)	0	2 (4.0)	0	2 (4.0)
CC25, n = 41	12 (29.3)	0	0	18 (43.9)	0	17 (41.5)
ST525, n = 16	16 (100)	0	0	16 (100)	0	16 (100)
CC29, n = 13	0	1 (7.7)	0	0	0	0
Others, n = 26	0	5 (19.2)	5 (19.2)	10 (38.5)	2 (7.7)	3 (11.5)
Total, n = 146	30 (20.5)	13 (8.9)	5 (3.4)	46 (31.5)	2 (1.4)	38 (26.0)

*Values are no. (%) isolates. CC, clonal complex; ICE, integrative and conjugative element; ST, sequence type.

A, and 1 as untypeable; 25 STs were represented, and a goeBURST analysis further classified the 25 STs into 7 CCs and 9 singletons. CC17 (34.2%) was the most prevalent, followed by with CC25 (28.1%), ST525 (11.0%), and CC29 (8.9%). Prevalence of CC17, CC25, and CC29 did not change substantially over time, but after ST525 was first isolated in 2016, its prevalence rate increased significantly, from 1.7% (1/58 isolates) during 2005–2017 to 20.0% (15/88 isolates) during 2018–2020 (p = 0.001) (Table 3; Appendix 2 Figure). Conversely, the prevalence of nonmajor CC and ST isolates (other than CC17, CC25, CC29, and ST525) decreased significantly from 27.6% (16/58 isolates) during 2005–2017 to 11.4% (10/88 isolates) during 2018–2020 (p = 0.015) (Appendix 2 Figure). Patients harboring ST525 strains were significantly older than were patients harboring non-ST525 strains (median age 87.0 years vs. 80.5 years; p = 0.007).

We classified *emm*-type isolates into 19 groups (Appendix 2 Table 3). The most prevalent *emm* type was stG6792 (28.1%), which was predominant in CC17, followed by *stG245* (20.0%), found only in CC25; *stG485* (9.6%), found in CC29 and CC128; and *stG840* (11.0%) found only in *ST525*.

We assessed AMR rates according to CC and ST (Table 4). No isolates showed nonsusceptibility to penicillin G, ceftriaxone, or meropenem. Nonsusceptibility rates were 31.5% to erythromycin, 30.8% to minocycline, and 25.5% to clindamycin; prevalence of isolates nonsusceptible to those 3 antimicrobial agents increased significantly, from 8.6% (5/58 isolates) during 2005–2017 to 21.6% (19/88 isolates) during 2018–2021 (p = 0.042). Of note, all 16 ST525 isolates were MDR and were resistant to those 3 antimicrobial agents. For CC25, nonsusceptibility rates were 29.3% for erythromycin, 29.3% for clindamycin, and 39.0%

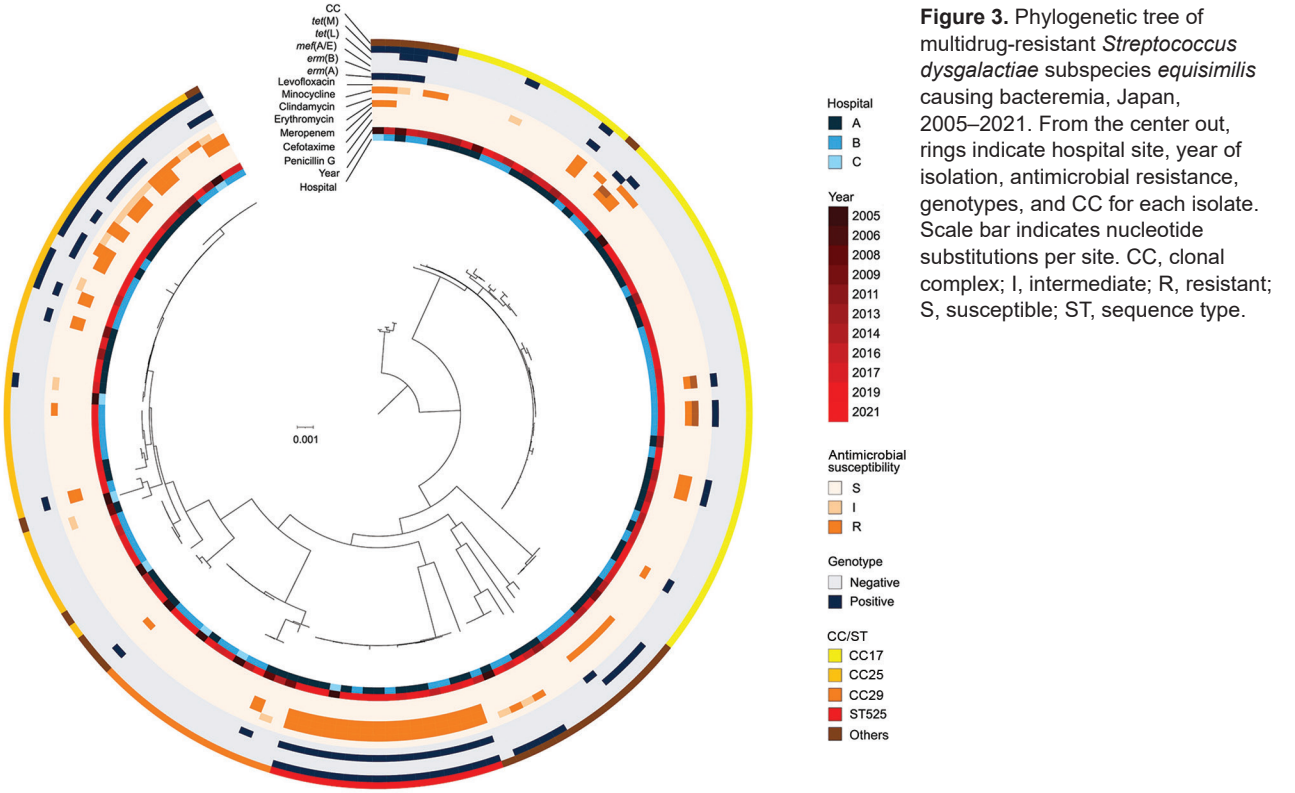

Figure 3. Phylogenetic tree of multidrug-resistant *Streptococcus dysgalactiae* subspecies *equisimilis* causing bacteremia, Japan, 2005–2021. From the center out, rings indicate hospital site, year of isolation, antimicrobial resistance, genotypes, and CC for each isolate. Scale bar indicates nucleotide substitutions per site. CC, clonal complex; I, intermediate; R, resistant; S, susceptible; ST, sequence type.

for minocycline. Nonsusceptibility rates were much lower for CC17 and CC29: 18.0% for CC17 and 7.7% for CC29 for erythromycin; 4.0% for CC17 and 7.7% for CC29 for minocycline; and 16.0% for CC17 and 7.7% for CC29 for clindamycin. Further AMR gene analysis showed that *erm*B was the most prevalent (20.5% of all isolates) resistance gene for macrolide resistance and was predominantly found in CC25 and ST525 isolates, and *erm*A (8.9%) was mainly found in CC17 isolates (Table 5). In addition, *tet*M was the predominant gene for tetracycline resistance (31.5%), and 23 of 24 MDR isolates possessed both *tet*M and *erm*B.

We assessed prevalence of the virulence factor–associated genes according to CC (Appendix 2 Table 4). All SDSE isolates contained virulence factor–associated genes, including *fbp54, lmb, scpA/scpB, slo, ska*, and *has*C. Prevalence of other virulence-related genes, such as *sda, speG*, and pilus island 1–associated genes, differed between CCs. *speG* was significantly associated with STSS (p = 0.026). However, other virulence genes did not have statistically significant correlation with severe disease (defined as STSS, necrotizing fasciitis, or need for vasopressors) or in-hospital death (Appendix 2 Table 4).

Phylogenic Analysis of SDSE Isolates

We visualized a phylogenetic tree of the SDSE isolates based on the 39,258 concatenated single nucleotide polymorphisms of the core genome (Figure 3). Phylogenetic analysis of 146 SDSE strains from Japan revealed no geographic relationships among specific clades or relationships with the year of isolation. However, the CCs reflected phylogenetic relationships, and the phylogenetic tree showed the clonal accumulation of clindamycin, minocycline, and erythromycin resistance in the ST525 clade and a part of the CC25 clade. The isolates possessed both *tet*M and *erm*B AMR genes.

Structure and Genetic Characterization of Tn*916*-Like ICEs on SDSE Genome

To investigate the genetic elements contributing to the clonal accumulation of *tet*M and *erm*B, we performed further sequence analysis by using the complete genome sequences. The *tet*M and *erm*B genes were located on the Tn*916*-like ICEs inserted into the chromosomal backbone. The genomes of 35 (24.0%) of the 146 strains harbored Tn*916*-like ICEs (Table 5). The dendrogram based on prevalence of coding sequences in the elements showed that SDSE-associated Tn*916*-like ICEs were mainly divided into 2 distinct groups (Figure 4). Group A included all 16 ST525 isolates and 1 ST17 (CC17) isolate (Figure 5); group B included all 17 ST127 (CC25) isolates and 1 ST17 isolate (Figures 5, 6).

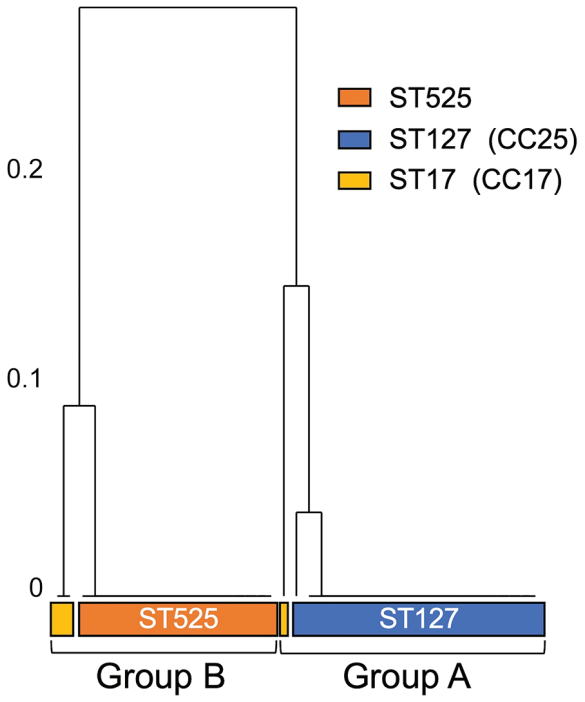

Figure 4. Phylogenetic relationship of group A and group B multidrug-resistant *Streptococcus dysgalactiae* subspecies *equisimilis* causing bacteremia, Japan, 2005–2021. Numbers on left of tree indicate the distance of the clusters. CC, clonal complex; ST, sequence type.

We conducted a further detailed structural and sequence comparison of the Tn*916*-like ICEs. In group B, ST17_B had an identical structure to the original Tn*916*, and a hypothetical protein was inserted on the intergenic region between open reading frame (ORF) 20 and ORF21 in all ST127 isolates (Figures 5, 6). In group A, ST17_A had an identical structure to Tn*3872*, which carries Tn*917* with *erm*B inserted in the form of a splitting ORF9 on Tn*916*, and all ST525 isolates had an additional hypothetical protein inserted similar to those in the ST127 isolates (Figures 5, 6). In the ST127 isolates with *erm*B on a sequence region other than Tn*916*-like ICE, *erm*B was sandwiched between 2 IS*1216*E genes and inserted into a specific site (Figure 5). The Tn*916*-like ICEs were clonally distributed in a phylogenic tree; each type of Tn*916*-like ICE showed the distribution pattern along with phylogenetic relationships and specific insertion sites on the genome (Figure 6). To further investigate Tn*3872*-like ICE in ST525, we performed a BLASTn search against the National Center for Biotechnology Information database using parameters of >90% query coverage and >95% identification. We found almost identical

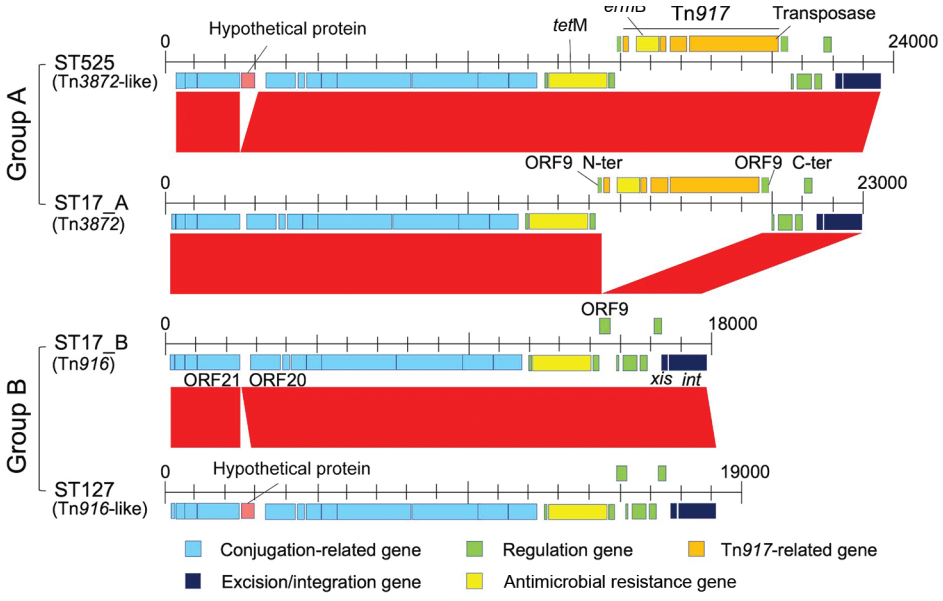

Figure 5. Hypothetical protein substitutions for group A and group B multidrug-resistant *Streptococcus dysgalactiae* subspecies *equisimilis* causing bacteremia, Japan, 2005–2021. CC, clonal complex; ORF, open reading frame; ST, sequence type.

genetic structure with highly conserved sequences in other streptococci and nonstreptococci bacteria (Appendix 2 Table 5).

Discussion

We investigated the genomic characteristics of the SDSE isolates causing increased prevalence of bloodstream infections in the Kyoto-Shiga region of Japan. Our results indicate a recent replacement of the major SDSE CC in this region and increases in isolates that are nonsusceptible to erythromycin, minocycline, and clindamycin. The increased nonsusceptibility rates are mainly because of the emergence of ST525 strains harboring Tn*916*-like ICEs carrying both *tet*M and *erm*B.

The characteristics of SDSE-derived invasive diseases in this study were generally the same as those previously reported (*2*,*4*,*6*,*7*). SDSE predominantly affected elderly patients with underlying diseases, usually skin and soft tissue infections or primary bacteremia, and were sometimes associated with life-threatening STSS or necrotizing fasciitis. Our investigation of clinical information on patients with SDSE bacteremia revealed that 7.7% of patients required vasopressor support and intensive care unit admission, and 7.0% of patients died in the hospital. Those mortality rates indicate the relatively high severity of invasive SDSE disease and are similar to those from previous reports (*4*,*7*), even considering the increasing incidence of SDSE bacteremia. As the global population ages, those findings indicate an increasing burden of invasive SDSE disease in clinical settings.

Invasive SDSE infections can also contribute to nosocomial onset (*2*,*25*), but detailed clinical features of nosocomial cases are unclear. Our study revealed that nosocomial SDSE infections mainly affected patients with malignant disease who were undergoing chemotherapy, as shown in the clinical data for 3 of 10 patients with nosocomial SDSE who had febrile neutropenia (Appendix 2 Table 1). Compared with S. pyogenes and S. agalactiae, SDSE can be carried persistently in the throat (*26*). Nosocomial infections, including those in patients with febrile neutropenia, might be associated with a long duration of SDSE carriage on the skin and in oral mucosa, throat, and gastrointestinal tracts.

Multiple countries have reported increased incidences of invasive SDSE disease (*8*,*9*,*11*,*27*,*28*). One reason for these increases might be the increase in aging populations, as previously reported (2,5,12,14). During 2011–2020, the aging population of Kyoto City increased; the percentage of persons >65 years of age increased by 21.9% and of persons >80 years of age by 41.9% (*29*). Shiga Prefecture is adjacent to Kyoto Prefecture and constitutes the Kyoto metropolitan area (Figure 1), and active commuting between the prefectures could contribute to further spread of SDSE in the region. In this study, KKH and KMCH showed higher incidences of SDSE bacteremia than the other 4 hospitals. KKH and KMCH had higher proportions of inpatients >70 years of age (66.1% for KKH and KMCH vs. 51.6% for the other 4 hospitals). This rapid increase in the older population might have affected the increasing prevalence of SDSE bacteremia. In addition, the trend in antimicrobial drug prescriptions in

Japan is concerning. The proportion of oral macrolide and third-generation cephalosporin consumption to total oral antimicrobial drug consumption is greater in Japan than in Europe or the United States (30). Therefore, high selective pressure by macrolides might be contributing to the emergence of macrolide-resistant SDSE, which acquired the resistance gene through mobile genetic elements, such as Tn916-like ICEs. The possible long-term persistent carriage of SDSE could increase the antimicrobial selective pressure (*26*), leading to the further selection of resistant strains.

Our genomic analysis indicated that the increased prevalence of MDR SDSE isolates was mainly because of emerging ST525 strains, which uniformly had Tn*3872*-like ICE, a Tn*916*-like element with the insertion of Tn*917* (Figure 6). Increasing evidence suggests that mobile genetic elements, including Tn*916*-like ICEs, are involved in disseminating AMR genes among *S. pneumoniae, S. pyogenes, and S. agalactiae*, either by clonal expansion or horizontal gene transfer (*31*–*33*). However, the genetic background of macrolide and lincosamide resistance dissemination in SDSE is unclear. A recent whole-genome sequencing study revealed that ICEs carried resistance genes such as *erm*A and *erm*B (*13*). The authors reported that those ICEs exhibited remarkable intraspecies and interspecies similarities, suggesting possible dissemination of resistance genes via conjugative transfer of the ICEs. Phylogenetic analysis showed shorter genetic distances of isolates with Tn*916*-like ICEs in the ST525 and CC25 clades, implying clonal expansion of those isolates. Although we found no evidence of intraspecies or interspecies transfer of Tn*916*-like ICEs among SDSE, macrolide-resistant SDSE could become widespread, as seen with other streptococci (*31*–*33*). Also, the Tn*3872*-like ICEs found in the ST525 were widely distributed in other bacteria, including other streptococci and enterococci (Appendix 2 Table 5), but not in any *S. dysgalactiae* genomes available in public databases. Although another study reported 1 SDSE isolate with Tn*3872*-like ICE, those elements lacked a transposase Tn*4430* in Tn*917* (*13*).

The first limitation of our study is the retrospective design, which only enabled us to use preserved isolates. Although selection bias among the preserved isolates might have affected the incidence of AMR isolates and the epidemiology of AMR genes, the multicenter study and detailed genomic investigation enabled us to assess regional clonal dynamics, especially the dynamics of ICEs carrying AMR genes. The second limitation was that the strain identification methods, such as MALDI-TOF mass spectrometry and Lancefield group typing,

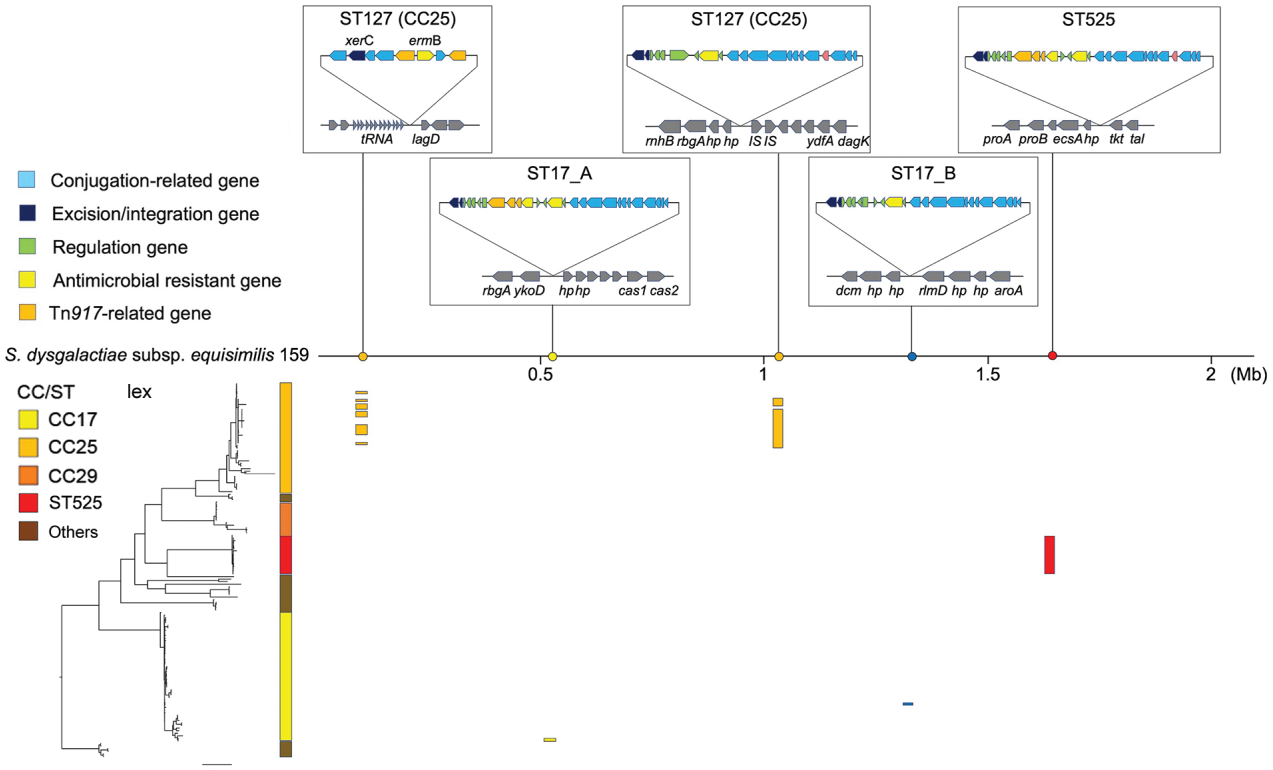

Figure 6. Phylogenetic relationships between clonal complexes of multidrug-resistant *Streptococcus dysgalactiae* subspecies *equisimilis* causing bacteremia, Japan, 2005–2021. Phylogenetic tree is shown in the lower left corner. Scale bar indicates nucleotide substitutions per site. CC, clonal complex; Mb, megabase; ST, sequence type.

varied depending on the facility or year in which the strain was isolated. The strain identification methods might have influenced estimation of SDSE bacteremia incidence because other Streptococcus species belonging to Lancefield group C or G and non-GCGS SDSE have been reported (*1*,*34*,*35*). However, previous studies revealed that SDSE causes most GCGS infections in humans (2,4), and few SDSE isolates represented groups other than C or G in our study. Considering those findings, we believe that estimation of the temporal trend in our study is generally reliable.

In conclusion, our study showed an increasing incidence of SDSE bacteremia in the Kyoto-Shiga region of Japan over the past decade. In addition, clonal expansion of ST525 strains carrying *erm*B and *tet*M on Tn*916*-like ICEs contributed to the emergence of MDR SDSE strains. Continuous surveillance, including whole-genome sequencing, is needed to clarify and predict trends in MDR SDSE strains associated with Tn*916*-like ICEs.

Acknowledgments

We thank Traci Raley from Edanz (https://jp.edanz.com/ac) for editing a draft of this manuscript. We thank Marcos Pinho for assigning the novel sequence types.

K.S., K.M., and M.N. designed and led the study and analyzed the data. K.S., M.Y., T.N., and Y. T. collected the clinical data. K.S., K.M., and Y.M. performed the microbiological examinations, including whole-genome sequencing, with help from I.N., K.S. and K.M. conducted the genomic investigation. K.S. wrote the first draft of the report and performed a literature search with help from K.M. and M.N. I.N. supervised the manuscript preparation. All authors helped interpret the data and revise the article and approved the final version of the article for submission.

About the Author

Dr. Shinohara is a PhD student in the Department of Clinical Laboratory Medicine, Kyoto University Graduate School of Medicine, and an infectious disease physician at the Department of Infection Control and Prevention, Kyoto University Hospital, Kyoto, Japan. His research focuses on clinical management of infectious diseases in immunocompromised hosts and treatment for and molecular epidemiology of antimicrobial drug resistance mechanisms among gram-positive bacteria.

References

1. Facklam R. What happened to the streptococci: overview of taxonomic and nomenclature changes. Clin Microbiol Rev. 2002;15:613–30. https://doi.org/10.1128/CMR.15.4.613-630.2002
2. Broyles LN, Van Beneden C, Beall B, Facklam R, Shewmaker PL, Malpiedi P, et al. Population-based study of invasive disease due to β-hemolytic streptococci of groups other than A and B. Clin Infect Dis. 2009;48:706–12. https://doi.org/10.1086/597035
3. Shimomura Y, Okumura K, Murayama SY, Yagi J, Ubukata K, Kirikae T, et al. Complete genome sequencing and analysis of a Lancefield group G *Streptococcus dysgalactiae* subsp. *equisimilis* strain causing streptococcal toxic shock syndrome (STSS). BMC Genomics. 2011;12:17. https://doi.org/10.1186/1471-2164-12-17
4. Takahashi T, Sunaoshi K, Sunakawa K, Fujishima S, Watanabe H, Ubukata K; Invasive Streptococcal Disease Working Group. Clinical aspects of invasive infections with *Streptococcus dysgalactiae* ssp. *equisimilis* in Japan: differences with respect to *Streptococcus pyogenes* and *Streptococcus agalactiae* infections. Clin Microbiol Infect. 2010;16:1097–103. https://doi.org/10.1111/j.1469-0691.2009.03047.x
5. Wajima T, Morozumi M, Hanada S, Sunaoshi K, Chiba N, Iwata S, et al. Molecular characterization of invasive *Streptococcus dysgalactiae* subsp. *equisimilis*, Japan. Emerg Infect Dis. 2016;22:247–54. https://doi.org/10.3201/eid2202.141732
6. Lother SA, Jassal DS, Lagacé-Wiens P, Keynan Y. Emerging group C and group G streptococcal endocarditis: a Canadian perspective. Int J Infect Dis. 2017;65:128–32. https://doi.org/10.1016/j.ijid.2017.10.018
7. Rantala S. *Streptococcus dysgalactiae* subsp. *equisimilis* bacteremia: an emerging infection. Eur J Clin Microbiol Infect Dis. 2014;33:1303–10. https://doi.org/10.1007/s10096-014-2092-0
8. Sylvetsky N, Raveh D, Schlesinger Y, Rudensky B, Yinnon AM. Bacteremia due to beta-hemolytic *Streptococcus* group G: increasing incidence and clinical characteristics of patients. Am J Med. 2002;112:622–6. https://doi.org/10.1016/S0002-9343(02)01117-8
9. Ekelund K, Skinhøj P, Madsen J, Konradsen HB. Invasive group A, B, C and G streptococcal infections in Denmark 1999–2002: epidemiological and clinical aspects. Clin Microbiol Infect. 2005;11:569–76. https://doi.org/10.1111/j.1469-0691.2005.01169.x
10. Oppegaard O. Beta-haemolytic group A, C and G streptococcal infections in Western Norway: a 15-year retrospective survey. Clin Microbiol Infect. 2015;21:171–8. https://doi.org/10.1016/j.cmi.2014.08.019
11. Schwartz IS, Keynan Y, Gilmour MW, Dufault B, Lagacé-Wiens P. Changing trends in β-hemolytic streptococcal bacteremia in Manitoba, Canada: 2007–2012. Int J Infect Dis. 2014;28:211–3. https://doi.org/10.1016/j.ijid.2014.03.1376
12. Fujiya Y, Hayakawa K, Gu Y, Yamamoto K, Mawatari M, Kutsuna S, et al. Age-related differences in clinical characteristics of invasive group G streptococcal infection: comparison with group A and group B streptococcal infections. PLoS One. 2019;14:e0211786. https://doi.org/10.1371/journal.pone.0211786
13. Oppegaard O, Skrede S, Mylvaganam H, Kittang BR. Emerging threat of antimicrobial resistance in β-hemolytic streptococci. Front Microbiol. 2020;11:797. https://doi.org/10.3389/fmicb.2020.00797
14. Kim S, Byun JH, Park H, Lee J, Lee HS, Yoshida H, et al. Molecular epidemiological features and antibiotic susceptibility patterns of *Streptococcus dysgalactiae* subsp. *equisimilis* isolates from Korea and Japan. Ann Lab Med. 2018;38:212–9. https://doi.org/10.3343/alm.2018.38.3.212
15. Lu B, Fang Y, Huang L, Diao B, Du X, Kan B, et al. Molecular characterization and antibiotic resistance of clinical

Streptococcus dysgalactiae subsp. *equisimilis* in Beijing, China. Infect Genet Evol. 2016;40:119–25. https://doi.org/10.1016/j.meegid.2016.01.030
16. Clinical and Laboratory Standards Institute. Performance standards for antimicrobial susceptibility testing; thirty-second informational supplement (M100-S32). Wayne (PA): The Institute; 2022.
17. Seemann T. Prokka: rapid prokaryotic genome annotation. Bioinformatics. 2014;30:2068–9. https://doi.org/10.1093/bioinformatics/btu153
18. Jia B, Raphenya AR, Alcock B, Waglechner N, Guo P, Tsang KK, et al. CARD 2017: expansion and model-centric curation of the comprehensive antibiotic resistance database. Nucleic Acids Res. 2017;45(D1):D566–73. https://doi.org/10.1093/nar/gkw1004
19. Chen L, Zheng D, Liu B, Yang J, Jin Q. VFDB 2016: hierarchical and refined dataset for big data analysis—10 years on. Nucleic Acids Res. 2016;44(D1):D694–7. https://doi.org/10.1093/nar/gkv1239
20. Page AJ, Cummins CA, Hunt M, Wong VK, Reuter S, Holden MTG, et al. Roary: rapid large-scale prokaryote pan genome analysis. Bioinformatics. 2015;31:3691–3. https://doi.org/10.1093/bioinformatics/btv421
21. Kozlov AM, Darriba D, Flouri T, Morel B, Stamatakis A. RAxML-NG: a fast, scalable and user-friendly tool for maximum likelihood phylogenetic inference. Bioinformatics. 2019;35:4453–5. https://doi.org/10.1093/bioinformatics/btz305
22. Letunic I, Bork P. Interactive Tree Of Life (iTOL) v5: an online tool for phylogenetic tree display and annotation. Nucleic Acids Res. 2021;49(W1):W293–6. https://doi.org/10.1093/nar/gkab301
23. Altschul SF, Gish W, Miller W, Myers EW, Lipman DJ. Basic local alignment search tool. J Mol Biol. 1990;215:403–10. https://doi.org/10.1016/S0022-2836(05)80360-2
24. Carver TJ, Rutherford KM, Berriman M, Rajandream MA, Barrell BG, Parkhill J. ACT: the Artemis Comparison Tool. Bioinformatics. 2005;21:3422–3. https://doi.org/10.1093/bioinformatics/bti553
25. Woo PCY, Fung AMY, Lau SKP, Wong SSY, Yuen KY. Group G beta-hemolytic streptococcal bacteremia characterized by 16S ribosomal RNA gene sequencing. J Clin Microbiol. 2001;39:3147–55. https://doi.org/10.1128/JCM.39.9.3147-3155.2001
26. de O Luiz FB, Alves KB, Barros RR. Prevalence and long-term persistence of beta-haemolytic streptococci throat carriage among children and young adults. J Med Microbiol. 2019;68:1526–33. https://doi.org/10.1099/jmm.0.001054
27. Lambertsen LM, Ingels H, Schønheyder HC, Hoffmann S; Danish Streptococcal Surveillance Collaboration Group 2011. Nationwide laboratory-based surveillance of invasive beta-haemolytic streptococci in Denmark from 2005 to 2011. Clin Microbiol Infect. 2014;20:O216–23. https://doi.org/10.1111/1469-0691.12378
28. Rantala S, Vuopio-Varkila J, Vuento R, Huhtala H, Syrjänen J. Clinical presentations and epidemiology of β-haemolytic streptococcal bacteraemia: a population-based study. Clin Microbiol Infect. 2009;15:286–8. https://doi.org/10.1111/j.1469-0691.2008.02672.x
29. Kyoto City. Kyoto City statistics portal site [cited 2022 Jun 3]. https://www2.city.kyoto.lg.jp/sogo/toukei
30. The Government of Japan. Japan: National action plan on antimicrobial resistance (AMR) [cited 2022 Mar 25]. https://www.who.int/publications/m/item/japan-national-action-plan-on-antimicrobial-resistance-(amr)
31. Schroeder MR, Stephens DS. Macrolide resistance in *Streptococcus pneumoniae.* Front Cell Infect Microbiol. 2016;6:98. https://doi.org/10.3389/fcimb.2016.00098
32. Puopolo KM, Klinzing DC, Lin MP, Yesucevitz DL, Cieslewicz MJY. A composite transposon associated with erythromycin and clindamycin resistance in group B *Streptococcus.* J Med Microbiol. 2007;56:947–55. https://doi.org/10.1099/jmm.0.47131-0
33. Berbel D, Càmara J, González-Díaz A, Cubero M, López de Egea G, Martí S, et al. Deciphering mobile genetic elements disseminating macrolide resistance in *Streptococcus pyogenes* over a 21 year period in Barcelona, Spain. J Antimicrob Chemother. 2021;76:1991–2003. https://doi.org/10.1093/jac/dkab130
34. Chochua S, Rivers J, Mathis S, Li Z, Velusamy S, McGee L, et al. Emergent invasive group A *Streptococcus dysgalactiae* subsp. *equisimilis*, United States, 2015–2018. Emerg Infect Dis. 2019;25:1543–7. https://doi.org/10.3201/eid2508.181758
35. Ikebe T, Okuno R, Kanda Y, Sasaki M, Yamaguchi T, Otsuka H, et al.; Working Group for Beta-Hemolytic Streptococci in Japan. Molecular characterization and antimicrobial resistance of group A streptococcus isolates in streptococcal toxic shock syndrome cases in Japan from 2013 to 2018. Int J Med Microbiol. 2021;311:151496. https://doi.org/10.1016/j.ijmm.2021.151496

Address for correspondence: Miki Nagao, Kyoto University Graduate School of Medicine, 54 Kawahara-cho, Shogoin, Sakyo-ku, Kyoto 606-8507, Japan; email: mnagao@kuhp.kyoto-u.ac.jp

Associations of *Anaplasma phagocytophilum* Bacteria Variants in *Ixodes scapularis* Ticks and Humans, New York, USA

Melissa Prusinski,[1] Collin O'Connor,[1] Alexis Russell, Jamie Sommer, Jennifer White, Lauren Rose, Richard Falco, John Kokas,[2] Vanessa Vinci, Wayne Gall,[3] Keith Tober,[2] Jamie Haight, JoAnne Oliver, Lisa Meehan, Lee Ann Sporn, Dustin Brisson, P. Bryon Backenson

Anaplasmosis, caused by the tickborne bacterium *Anaplasma phagocytophilum*, is an emerging public health threat in the United States. In the northeastern United States, the blacklegged tick (*Ixodes scapularis*) transmits the human pathogenic genetic variant of *A. phagocytophilum* (Ap-ha) and a nonpathogenic variant (Ap-V1). New York has recently experienced a rapid and geographically focused increase in cases of anaplasmosis. We analyzed *A. phagocytophilum*–infected *I. scapularis* ticks collected across New York during 2008–2020 to differentiate between variants and calculate an entomological risk index (ERI) for each. Ap-ha ERI varied between regions and increased in all regions during the final years of the study. Space-time scan analyses detected expanding clusters of Ap-ha located within documented anaplasmosis hotspots. Ap-ha ERI was more positively correlated with anaplasmosis incidence than non-genotyped *A. phagocytophilum* ERI. Our findings help elucidate the relationship between the spatial ecology of *A. phagocytophilum* variants and anaplasmosis.

Anaplasma phagocytophilum is the bacterium capable of causing anaplasmosis (*1*,*2*). Anaplasmosis symptoms include fever, headache, myalgia, and malaise (*3*). Severe illness is reported more commonly in older and immunocompromised patients but is also documented in immunocompetent persons and may result in hospitalization or death if appropriate treatment is not promptly administered (*3*). Patient condition generally improves markedly in the 24–48 hours after initiation of treatment with the antimicrobial drug doxycycline (*3*).

In eastern North America, *A. phagocytophilum* is transmitted to humans through the bite of an infected blacklegged tick (*Ixodes scapularis*) (*2*). *I. scapularis* ticks have 3 active life stages (larva, nymph, and adult); nymphs and adults can carry multiple genetic variants of *A. phagocytophilum*, including the pathogenic human-active variant (Ap-ha) and the nonpathogenic Variant 1 (Ap-V1) (*4*–*6*). Other genetic variants of *A. phagocytophilum* have been documented in the northeastern United States; their prevalence in nature and pathogenicity remains understudied (*7*,*8*). *A. phagocytophilum* is not transmitted transovarially from infected adult female *I. scapularis* ticks to larvae and is maintained in the environment within various host species (*9*,*10*). The most common host reservoir of Ap-ha is the white-footed mouse (*Peromyscus leucopus*) and of Ap-V1 is the white-tailed deer (*Odocoileus virginianus*) (*5*,*8*,*11*).

In New York state, excluding the city of New York, 5,146 anaplasmosis cases were reported dur-

Author affiliations: New York State Department of Health, Albany, New York, USA (M. Prusinski, A. Russell, J. Sommer, J. White, L. Rose, L. Meehan, P.B. Backenson); University at Buffalo Department of Geography, Buffalo, New York, USA (C. O'Connor); New York State Department of Health, Buffalo (C. O'Connor, W. Gall, K. Tober); New York State Department of Health, Armonk, New York, USA (R. Falco, J. Kokas, V. Vinci); New York State Department of Health, Falconer, New York, USA (J. Haight); New York State Department of Health, Syracuse, New York, USA (J. Oliver); Paul Smith's College, Paul Smiths, New York, USA (L.A. Sporn); University of Pennsylvania, Philadelphia, Pennsylvania, USA (D. Brisson)

DOI: https://doi.org/10.3201/eid2903.220320

[1]These authors contributed equally to this article.

[2]Retired.

[3]Current affiliation: US Department of Agriculture, Animal and Plant Health Inspection Service, Buffalo, NY 14213, USA.

ing 2010–2018; the median was 454 (range 220–1,112) cases/year. Anaplasmosis incidence increased statewide nearly 4-fold over a period of a decade, from 2.0 cases/100,000 persons in 2010 to 7.6 cases/100,000 persons during 2018; that increase was not spatially homogenous (*12*,*13*). Specifically, the largest increase in anaplasmosis incidence occurred in the Capital District region of New York, where incidence increased from 3.0/100,000 persons in 2008 to 5.3/100,000 persons in 2018 (*13*). Focal increases in incidence of anaplasmosis may result from a change in the abundance and spatial extent of Ap-ha–infected *I. scapularis* ticks, potentially related to changes in the deer–tick–rodent cycle (*10*); those changes may reflect the relative abundance of Ap-ha competent reservoir hosts, increased contact between host-seeking ticks (unfed ticks of any lifestage actively seeking a host bloodmeal) and small mammal reservoirs of Ap-ha, or a greater overlap between human residential or recreational areas and habitats conducive for the enzootic amplification of Ap-ha. Thus, further examination of the relationship between Ap-ha and Ap-V1 may broaden the understanding of anaplasmosis etiology and *A. phagocytophilum* ecology, refining risk assessment for this emerging disease and enabling targeted prevention efforts to reduce anaplasmosis incidence.

We analyzed *A. phagocytophilum*–infected host-seeking *I. scapularis* tick specimens to elucidate the spatial differences in entomological risk for anaplasmosis in New York. We used a TaqMan single-nucleotide polymorphism (SNP) genotyping assay (ThermoFisher Scientific, https://www.thermofisher.com) to differentiate between the Ap-ha and Ap-V1 variants as previously described (*14*). Next, we calculated a measure of human-infection risk as a function of *I. scapularis* tick density and *A. phagotycophilum* genotype prevalence, known as the entomological risk index (ERI) for both Ap-ha and Ap-V1.We then tested for spatiotemporal differences in counts of Ap-ha– and Ap-V1–infected *I. scapularis* ticks by using statistical modeling and tested for correlations between Ap-ha ERI and anaplasmosis incidence. We also used a scan statistic to search for spatiotemporal clusters of Ap-ha and Ap-V1 in New York tick populations for 2008–2020. We then compared spatiotemporal clusters of Ap-ha and Ap-V1 in *I. scapularis* ticks to documented regions of increased anaplasmosis incidence in New York over the same timeframe (*13*,*15*). The results help to illuminate the relationship between the spatial ecology of each variant and the outcome of human disease.

Methods

Active Tick Sampling

We collected host-seeking ticks primarily from publicly accessible lands across New York during 2008–2020 using standardized drag-cloth or flag surveys of vegetation and forest leaf litter, as previously described (*16*). Generally, we visited 1 site within each county twice annually; we visited additional sites as weather and resources permitted. Collection sites had suitable tick habitat and potential risk for human exposure to ticks. We typically sampled ≥1,000 m^2 of suitable habitat per site during each collection event. In some instances, we did not find suitable habitat for nymphal and adult *I. scapularis* tick sampling at the same collection site; as a result, we sampled some sites for 1 *I. scapularis* lifestage, resulting in separate nymphal and adult *I. scapularis* tick sampling sites (Figure 1). We stored ticks in 70%–100% ethanol at 4°C until they were sorted by developmental stage and identified to species using dichotomous keys (*17*,*18*), placed into sterile microcentrifuge tubes containing 100% ethanol, and stored at −20°C until DNA extraction (*16*,*19*).

Pathogen Detection and Ap-ha/Ap-V1 Differentiation

Individual *I. scapularis* nymphs and adults underwent total genomic DNA extraction as previously described (*16*,*19*). Using a quadplex real-time PCR (*20*), we tested for the following pathogens and target genes: *A. phagocytophilum* (msp 2), *Babesia microti* (18S rDNA), *Borrelia burgdorferi* (16S rDNA), and *Borrelia miyamotoi* (16S rDNA). Samples testing positive for *A. phagocytophilum* by quadplex PCR were further tested using a custom TaqMan SNP genotyping PCR to differentiate between the Ap-ha and Ap-V1 variants of *A. phagocytophilum* as described previously (*14*), with the following modifications: each 25 uL reaction contained 0.625 uL of 80× Custom TaqMan SNP Genotyping Assay primer/probe mix, 12.5 uL TaqMan Universal Master Mix (ThermoFisher), 1.875 uL nuclease-free water, and 10 uL of gDNA template (or nuclease-free water for negative controls). We performed SNP assays and variant assignment and generated allelic discrimination plots using Applied Biosystems 7500 Real-time PCR System version 2.0.5 (ThermoFisher).

ERI Calculation

To estimate risk for human exposure to Ap-ha and Ap-V1 variants of *A. phagocytophilum*, we calculated ERI (*20*) using the equation

$$\mathrm{ERI} = \frac{\text{no. ticks collected}}{\text{distance dragged, m}^2} \times \frac{\text{no. variant-positive ticks}}{\text{no. ticks tested}}$$

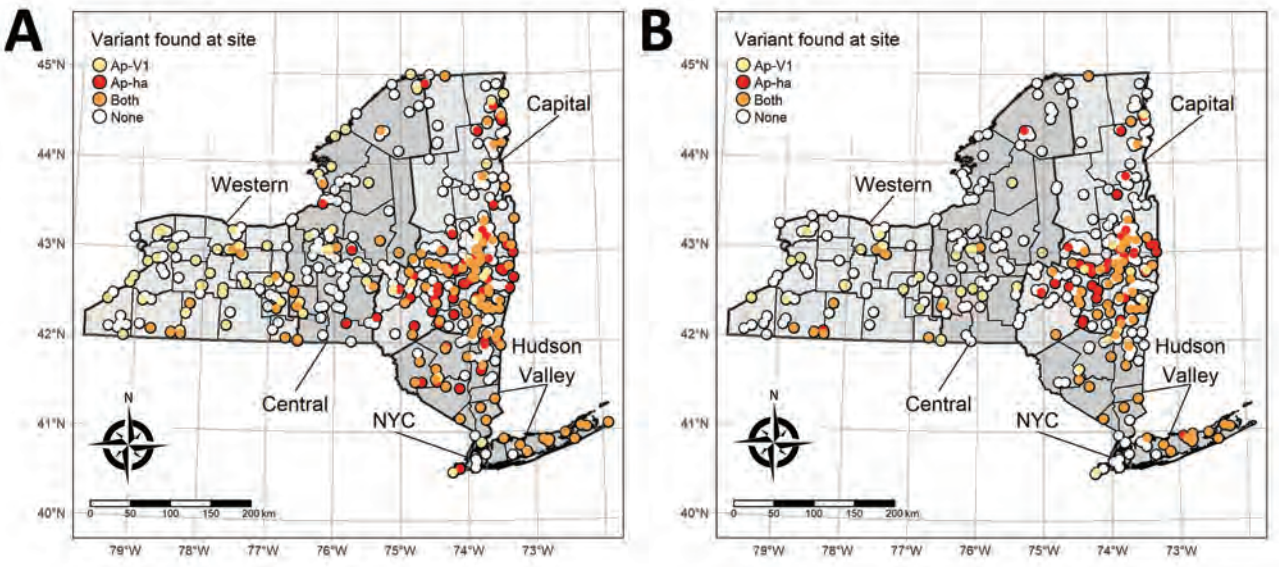

Figure 1. New York State Department of Health (NYSDOH) *Ixodes scapularis* tick sampling sites categorized by the *Anaplasma phagocytophilum* genetic variants found at each site, New York, USA. Thick black outlines indicate NYSDOH regions (labeled). A) Adult sampling sites; B) nymph sampling sites.

for *I. scapularis* nymphs and adults. A high ERI value denotes an increased risk for human exposure to a particular pathogen. Of note, Ap-V1 does not cause disease in humans, so the term entomologic risk index is used only to provide a metric for comparison between Ap-ha and Ap-V1 variants. For sites with multiple sampling events within the same season, we averaged ERIs for all events.

Bernoulli Space-Time Scan Statistic

We compared the spatiotemporal distribution of Ap-ha–infected and Ap-V1–infected *I. scapularis* adults and nymphs by using the Bernoulli space-time scan statistic (*21*), implemented in SaTScan version 9.6 (https://www.satscan.org) (*22*,*23*). SaTScan searched for statistically significant clusters of Ap-ha or Ap-V1; we considered a cluster to be a location at which the relative risk (RR) of the presence of a variant is >1.0 inside a given cluster compared to outside. We selected maximum spatial and temporal cluster sizes a priori for our analysis. We set maximum spatial cluster size as 10% of the collected ticks to allow for new clusters to form as time progressed and to show the movement of each variant. We selected maximum temporal cluster size as 90% of the study period to allow for the identification of established populations of either *A. phagocytophilum* variant.

Table 1. Sampling and genotyping analysis results of adult and nymphal *Ixodes scapularis* ticks collected in New York, USA, 2008–2020*

Characteristic	Adults	Nymphs
No. site visits	2,496	1,595
No. specimens collected	91,163	38,782
Specimens tested, no. (%)	43,520 (47.74)	25,748 (66.39)
A. phagocytophilum positive	3,207 (7.37)	1,183 (4.59)
Specimens genotyped, no. (%)		
Ap-ha positive	2,327 (5.35)	425 (1.65)
Ap-V1 positive	728 (1.67)	669 (2.60)
Ap-ha/Ap-V1 co-infected	18 (0.04)	0 (0.00)
Undetermined	124 (0.28)	87 (0.34)
Missing†	10 (0.02)	2 (0.01)

*Ap-ha, human pathogenic variant of A. phagocytophilum bacteria; Ap-V1, nonpathogenic variant of *A. phagocytophilum* bacteria.
†Refers to samples that were unable to be located in storage for genotyping.

Statistical Analysis

We tested the Spearman rank correlation between mean Ap-ha ERI in *I. scapularis* nymphs and adults and anaplasmosis incidence at the postal (ZIP) code tabulation area level gathered from the New York State Department of Health (NYSDOH) Communicable Disease Electronic Surveillance system as previously described (*13*). We assessed the correlation for each year, 2010–2018. We selected the Spearman rank test because of the underlying count data used to generate anaplasmosis incidence and Ap-ha ERI. We corrected the 18 correlation tests for multiple testing using the Bonferroni-Holm adjustment (*24*). We compared results of the Spearman rank tests with the results from a previous analysis using non–genotype-specific *A. phagocytophilum* ERI (*13*).

We tested for spatiotemporal interaction in the number of Ap-ha– and Ap-V1–infected *I. scapularis* nymphs and adults by year and across latitude and longitude categories using a generalized linear mixed model (GLMM) extension of zero-inflated negative

binomial (ZINB) regression (*25,26*). ZINB regression accounted for overdispersion and excess zero-counts of Ap-ha–and Ap-V1–infected *I. scapularis* ticks, whereas the GLMM extension handled the repeated nature of our sampling scheme by allowing sampling sites to have varying intercepts. We binned tick collection data and corresponding PCR results by year, latitude, and longitude to increase the number of observations within each combination of covariates to fit the model. We binned tick data by year into 4 categories: 2008–2011, 2012–2014, 2015–2017, and 2018–2020. We binned tick collection sites by latitude into 3 categories: sites south of 42°N, at 42°N to 43°N, and north of 43°N. We binned collection sites by longitude into 3 categories: sites east of 74°W, from 74°W to 76°W, and west of 78°W. We built 4 models to analyze Ap-ha and Ap-V1 in *I. scapularis* nymphs and adults separately. We assessed interaction between year and latitude/

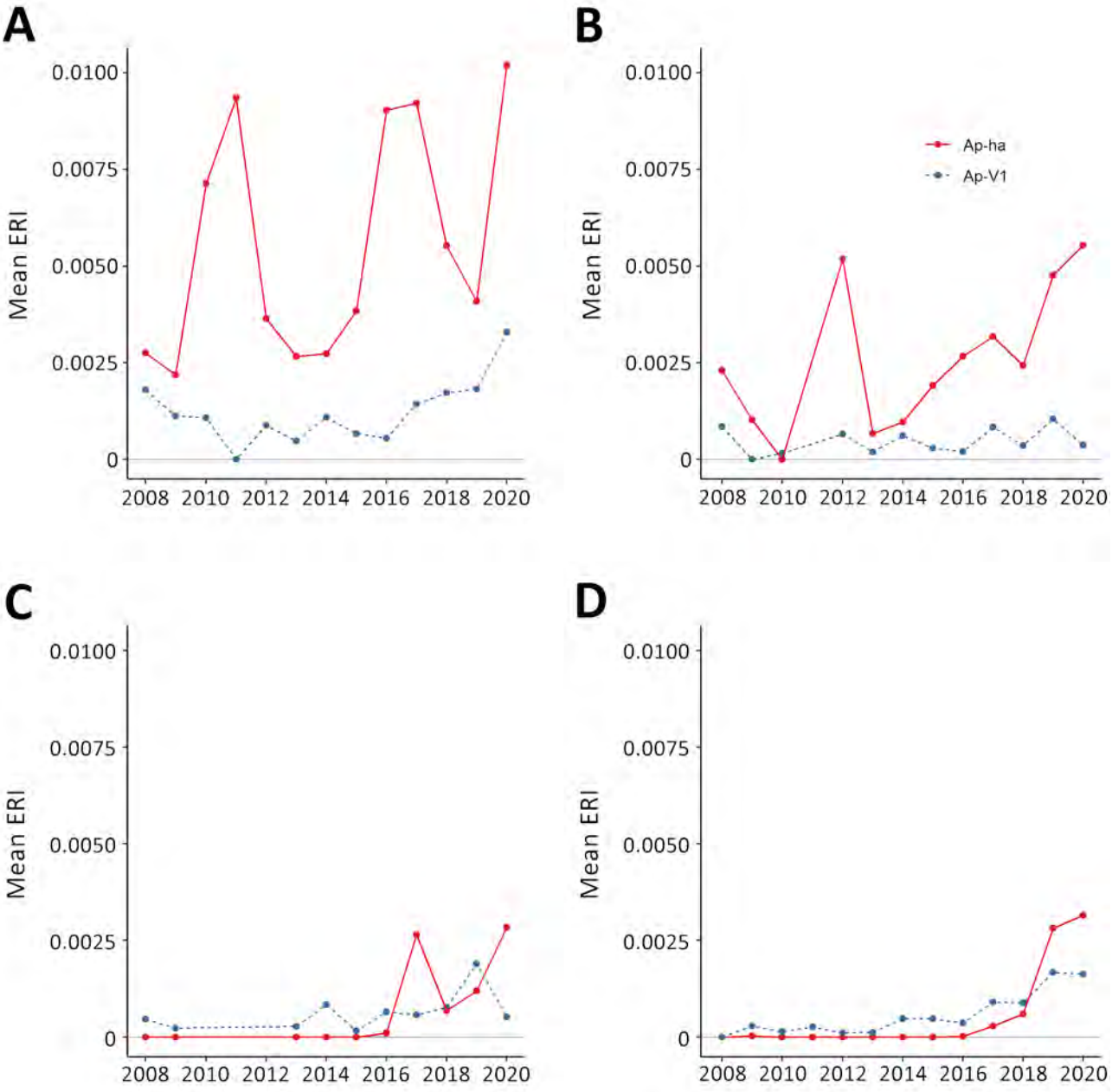

Figure 2. Mean ERI of pathogenic and nonpathogenic genetic variants of *Anaplasma phagocytophilum* bacteria in adult blacklegged ticks aggregated to regions of New York, 2008–2020. A) Hudson Valley region; B) Capital region; C) Central region; D) Western region. Ap-ha, human pathogenic variant of *A. phagocytophilum* bacteria; Ap-V1, nonpathogenic variant of *A. phagocytophilum*; ERI, entomological risk index.

longitude categories using the likelihood ratio test (LRT). We used the natural log of the total number of *I. scapularis* ticks of the target developmental stage (nymphs during sampling events in late May, June, July, and August; adult ticks during April, early May, October, November, and December) as an offset. We conducted data cleaning, generation of summary statistics, and data visualization using R version 4.0.3 (http://www.rstudio.com) and the dplyr (https://CRAN.R-project.org/package=dplyr), sf, ggplot2, and tmap R packages (*27*–*29*). We used the glmmTMB package in R (*30*) for modeling.

Results

Active Tick Sampling and Pathogen Detection

We recorded active tick sampling and *A. phagocytophilum* genotyping results for *I. scapularis* tick specimens (Table 1). We categorized sampling sites according to the presence of *A. phagocytophilum* genetic variants (Figure 1). Of 91,163 adult *I. scapularis* ticks collected during 2008–2020, we tested 43,520 for *A. phagocytophilum*; of 38,782 nymphal ticks, we tested 25,748 (Table 1). Among those tested for *A. phagocytophilum*, 3,207 (7.4%) adults and 1,183 (4.6%)

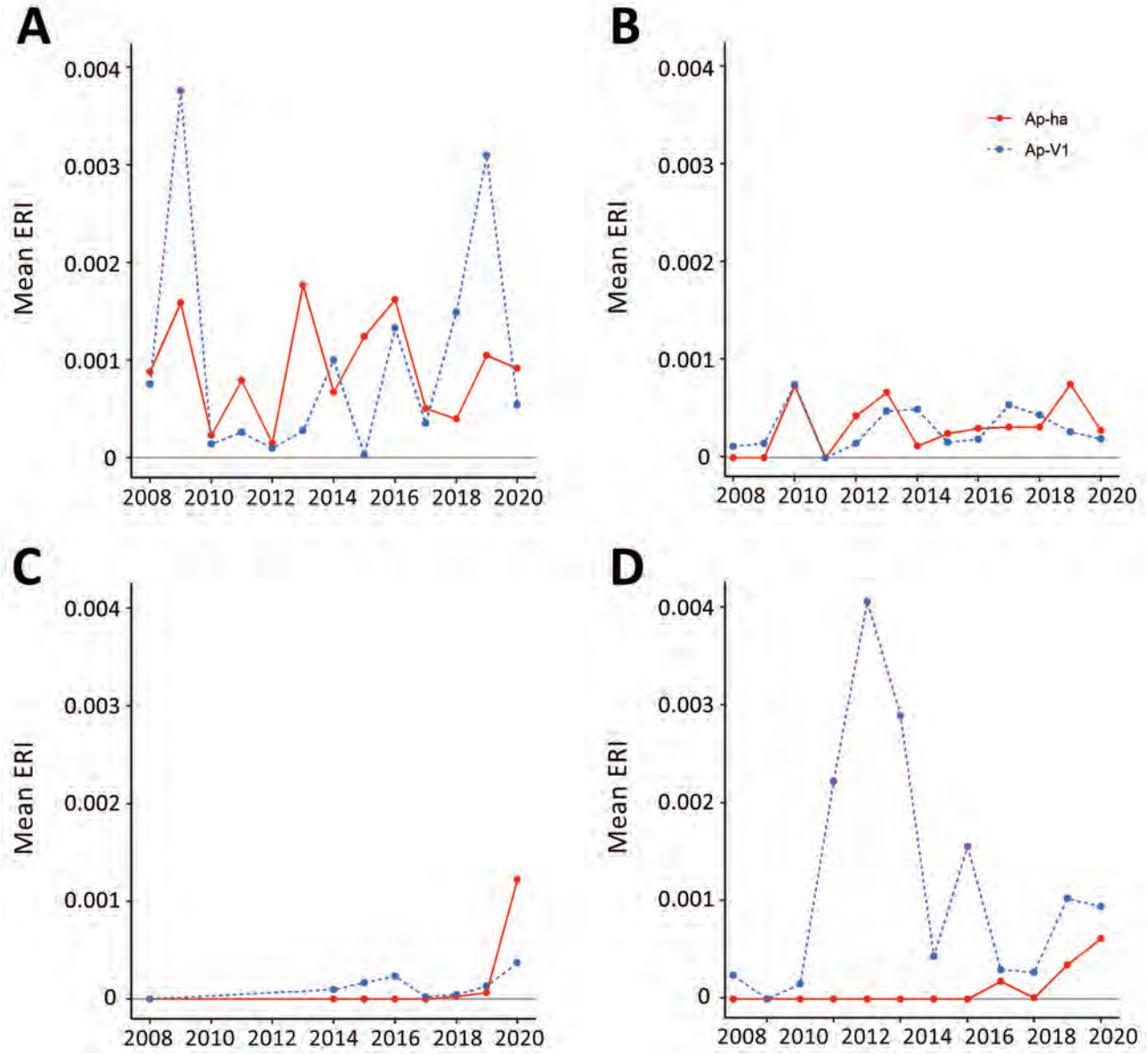

Figure 3. Mean ERI of pathogenic and nonpathogenic genetic variants of *Anaplasma phagocytophilum* bacteria in nymphal blacklegged ticks aggregated to regions of New York, 2008–2020. A) Hudson Valley region; B) Capital region; C) Central region; D) Western region. Ap-ha, human pathogenic variant of *A. phagocytophilum* bacteria; Ap-V1, nonpathogenic variant of *A. phagocytophilum;* ERI, entomological risk index.

Table 2. Distance and relative risks of space-time Bernoulli clusters of pathogenic and nonpathogenic variants of *A. phagocytophilum* bacteria in adult and nymphal *Ixodes scapularis* ticks, New York, USA, 2008–2020*

Cluster no.	Cluster type	Years	Radius, km	RR
Adults				
1	Ap-V1	2008–2018	192.47	4.74†
2	Ap-V1	2008–2015	139.14	4.23†
3	Ap-ha	2011–2016	25.62	1.29
4	Ap-ha	2012–2020	20.64	1.22
5	Ap-ha	2014–2020	31.76	1.26
6	Ap-ha	2014–2017	58.66	1.24
7	Ap-ha	2015–2016	42.41	1.30
8	Ap-ha	2016–2020	36.91	1.28
9	Ap-ha	2016–2020	24.01	1.24
Nymphs				
1	Ap-V1	2009–2019	113.01	1.80†
2	Ap-V1	2016–2019	52.94	1.60†
3	Ap-ha	2011–2020	27.10	1.66
4	Ap-ha	2013–2017	44.28	2.12
5	Ap-ha	2015–2020	39.95	2.02
6	Ap-ha	2017–2020	42.53	2.19

*Ap-ha, human pathogenic variant of *A. phagocytophilum* bacteria; Ap-V1, nonpathogenic variant of *A. phagocytophilum* bacteria; RR, relative risk.
†Case and control groups were reversed to indicate an increased risk of one variant to another.

nymphs were determined to be positive. *A. phagocytophilum* genotyping deterimined that *I. scapularis* adults had a higher prevalence of Ap-ha (5.4%) than Ap-V1 (1.7%), whereas *I. scapularis* nymphs had a higher prevalence of Ap-V1 (2.6%) than Ap-ha (1.7%). We observed co-infection of Ap-ha and Ap-V1 in *I. scapularis* adults (0.04%).

ERI

The Hudson Valley and Capital District regions in the eastern portion of the state generally exhibited higher Ap-ha ERI than the Central and Western regions of New York (Figures 2, 3). Ap-V1 ERI of *I. scapularis* nymphs was generally higher in the Western and Hudson Valley regions than in the Capital District and Central NY regions, but the levels were highly variable and exhibited no obvious temporal trend. Overall, ERI for Ap-ha increased in the later years of the study period for all 4 regions.

Retrospective Bernoulli Space-Time Cluster Analysis

We detected increased RR of Ap-ha or Ap-V1 in 9 clusters of adult (Table 2; Figure 4, panel A) and 6 clusters of nymphal *I. scapularis* (Figure 5, panel A) ticks in the period 2008–2020. Among the 9 clusters of *I. scapularis* adults, 7 exhibited increased RR of Ap-ha and 2 exhibited increased RR of Ap-V1. Among the 6 clusters of *I. scapularis* nymphs, 4 exhibited increased RR of Ap-ha and 2 exhibited increased RR Ap-V1. Clusters of Ap-ha tended to be located in the Hudson Valley and eastern Capital District regions of New York, whereas clusters of Ap-V1 tended to be located in the Western and northern Capital District regions of New York, near the border with Canada. Analysis of *I. scapularis* adults revealed 3 of 13 years in our study period with no clusters of Ap-ha (2008–2010), whereas clusters of Ap-V1 were present in all years but 2019 and 2020 (Figure 4). Analysis of *I. scapularis* nymphs exhibited similar results; clusters of Ap-ha were present in all but 2 years of the study period (2009 and 2010), and 1 year, 2020, was without a cluster of Ap-V1 (Figure 5).

Spearman Rank Correlations and Zero-Inflated Regression Models

Anaplasmosis incidence was significantly correlated with Ap-ha ERI in *I. scapularis* adults for all 9 years analyzed, whereas 6 of the 9 years analyzed were correlated for *I. scapularis* nymphs (Table 3). Statistically significant correlation coefficients in *I. scapularis* adults were 0.36–0.75, an increase in the minimum and maximum correlation coefficients compared with non–variant-specific PCR results (*13*). Statistically significant correlation coefficients in *I. scapularis* nymphs were 0.19–0.68, a decrease in the minimum coefficient and an increase in the maximum coefficient compared with correlations calculated using the non–variant-specific PCR results (*13*).

ZINB regression models of Ap-ha and Ap-V1 in *I. scapularis* nymphs failed to converge, likely because of an insufficient number of observations within the year, latitude, and longitude covariate combinations. We detected notable spatiotemporal interaction only in Ap-ha in *I. scapularis* adults (Table 4). The final model for Ap-ha–infected *I. scapularis* adults indicated high interaction between both year and latitude and year and longitude in the negative binomial portion of the model; however, the LRT indicated the model with year

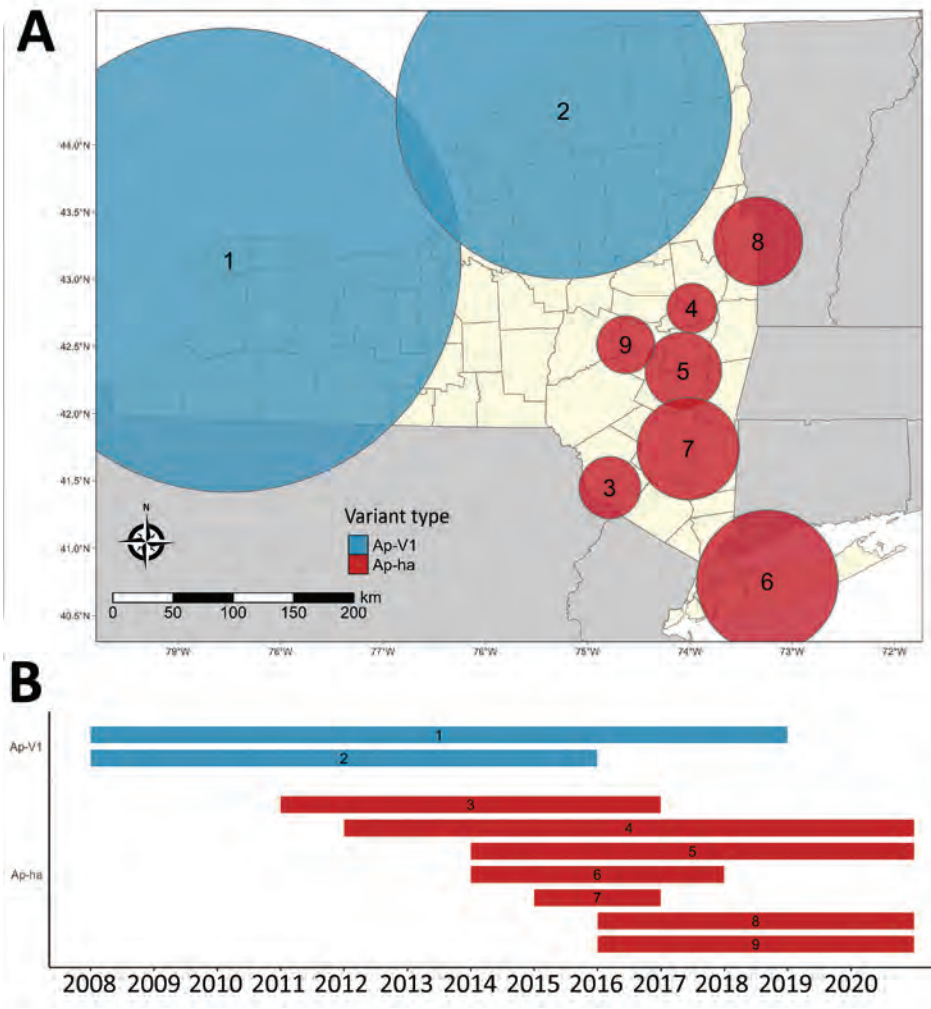

Figure 4. Bernoulli clusters of pathogenic and nonpathogenic genetic variants of *Anaplasma phagocytophilum* bacteria in adult *Ixodes scapularis* ticks in New York, 2008–2020. A) Spatial clusters; B) temporal clusters. Ap-ha, pathogenic variant; Ap-V1, nonpathogenic variant.

and longitude interaction was not better fit than the model without the year and longitude interaction (p = 0.0976). (Table 4). Model coefficients indicate increasing log counts of Ap-ha–infected *I. scapularis* adults north of 43°N as year categories increased: for 2012–2014, β = 2.36 (95% CI 0.32–4.40); 2015–2017, β = 2.76 (95% CI 0.76–4.47); and 2018–2020, β = 3.79 (95% CI 1.77–5.80). log counts of Ap-ha–infected *I. scapularis* adult at latitudes from 42°N to 43°N only increased in the final year category: for 2012–2014, β = 0.27 (95% CI –0.60 to 1.14); 2015–2017, β = 0.50 (95% CI –0.34 to 1.33); and 2018–2020, β = 1.39 (95% CI 0.56– 2.21). In addition, the log counts increased in year category 2018–2020 between 74°W and 76°W (β = 0.78 [95% CI 0.02–1.53]), although the LRT indicated that using the year and longitude interaction did not improve model fit. Of note, the interaction between the 2012–2014 year category and west of 76°W longitude category exhibited a wide 95% CI (–6,096.27 to 6,062.91) because no positive Ap-ha *I. scapularis* ticks were found in all 68 site visits at those latitudes over that period. The zero-inflated portion of the model indicated a significant difference in the log odds of being an excessive zero between all latitude categories and longitude categories. For latitudes between 42°N and 43°N, β = 2.15 (95% CI 0.31–3.99); north of 43°N, β = 3.82 (95% CI 1.92–5.72). For longitudes between 74°W and 76°W, β = 1.30 (95% CI 0.53– 2.08); west of 76°W, β = 3.95 (95% CI 2.96–4.94). Only the 2018–2020 year category significantly differed from the reference group: for that category, β = −1.68 (95% CI –3.31 to –0.06).

Discussion

Our study describes the landscape of Ap-ha and Ap-V1 genetic variants in New York, which has direct public health implications on the incidence of anaplasmosis. Continued geographic expansion of the Ap-ha variant in New York, as shown in this study, will result in a growing area of increased anaplasmosis risk for residents of the impacted regions. The current distribution of *A. phagocytophilum* variants and associated anaplasmosis risk in New York is characterized by elevated risk in the

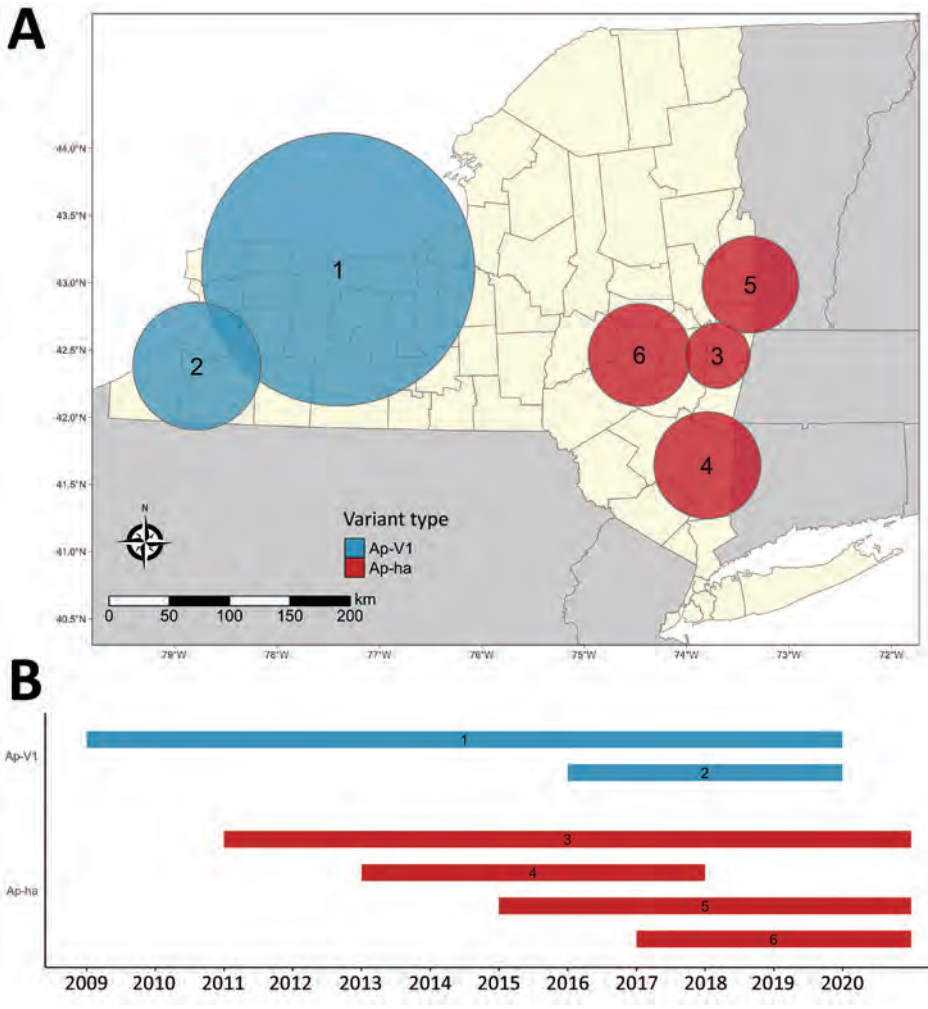

Figure 5. Bernoulli clusters of pathogenic and nonpathogenic genetic variants of *Anaplasma phagocytophilum* bacteria in nymphal *Ixodes scapularis* ticks in New York, 2008–2020. A) Spatial clusters; B) temporal clusters. Ap-ha, pathogenic variant; Ap-V1, nonpathogenic variant.

Hudson Valley and Capital District region predominated by Ap-ha, compared with other geographic regions with low or variable Ap-V1 prevalence (Figure 2). During our study, the range of Ap-ha expanded relative to Ap-V1 over time, whereas Ap-V1 was largely unchanged and remained the dominant variant in the Western and northern Capital District regions. Those regions border the Canada provinces Ontario and Quebec, where Krakowetz et al. (*14*) also found Ap-V1 to be the predominant variant, indicating the range of Ap-V1 may extend from the spatial clusters detected in our analysis northward into both provinces.

The results from the ZINB regression model support our variant cluster detection; Ap-ha expanded northward at an increasing rate over time, and some

Table 3. Spearman correlation results between Ap-ha ERI and anaplasmosis incidence at postal code tabulation area level, New York, USA, 2010–2018*

	Adults		Nymphs	
Year	ρ	p value	ρ	p value
2010	0.75	0.0011†	0.24	0.3591
2011	0.75	0.0185†	−0.21	0.5524
2012	0.62	0.0001†	0.57	0.0233†
2013	0.52	<0.0001†	0.68	0.0001†
2014	0.57	<0.0001†	0.20	0.1225
2015	0.73	<0.0001†	0.56	<0.0001†
2016	0.71	<0.0001†	0.43	0.0001†
2017	0.57	<0.0001†	0.47	0.0001†
2018	0.36	<0.0001†	0.19	0.0407†

*Ap-ha, human pathogenic variant of *A. phagocytophilum* bacteria; ERI, entomological risk index; ρ, Spearman rank correlation coefficient;.
†p<0.05, indicating statistical significance.

Table 4. Final zero-inflated negative binomial regression model for Ap-ha in adult *I. scapularis* in New York, USA, 2010–2018

	Negative binomial model				Zero-inflated model			
Category	β	95% CI	SE	p value	β	95% CI	SE	p value
Intercept	–3.19	–3.69 to –2.69	0.25	**<0.0001**	–3.67	–6.14 to –1.20	1.26	**0.0036**
Year categories								
2008–2011	Referent				Referent			
2012–2014	–0.09	–0.65 to 0.46	0.29	0.7431	–0.18	–1.83 to 1.47	0.84	0.8282
2015–2017	0.33	–0.18 to 0.83	0.26	0.2023	–0.23	–1.80 to 1.35	0.80	0.7783
2018–2020	–0.40	–0.90 to 0.10	0.26	0.1149	–1.68	–3.31 to –0.06	0.83	**0.0421**
Latitude categories								
South of 42°N	Referent				Referent			
42°N–43°N	–0.50	–1.31 to 0.32	0.42	0.2304	2.15	0.31–3.99	0.94	**0.0223**
North of 43°N	–2.91	–4.93 to –0.89	1.03	**0.0048**	3.82	1.92–5.72	0.97	**<0.0001**
Longitude categories								
East of 74°W	Referent							
74°W–76°W	–0.63	–1.39 to 0.14	0.39	0.1071	1.30	0.53–2.08	0.40	**0.0001**
West of 76°W	–1.67	–4.44 to 1.09	1.41	0.2351	3.95	2.96–4.94	0.50	**<0.0001**
Interaction categories								
2012–2014: 42°N–43°N	0.27	–0.60 to 1.14	0.44	0.5456				
2015–2017: 42°N–43°N	0.50	–0.34 to 1.33	0.43	0.2435				
2018–2020: 42°N–43°N	1.39	0.56–2.21	0.42	**0.0010**				
2008–2011: North of 43°N)	Referent							
2012–2014: North of 43°N	2.36	0.32–4.40	1.04	**0.0237**				
2015–2017: North of 43°N	2.76	0.76–4.47	1.02	**0.0069**				
2018–2020: North of 43°N	3.79	1.77–5.80	1.03	**0.0002**				
2012–2014: 74°W–76°W	0.45	–0.38 to 1.27	0.42	0.2915				
2015–2017: 74°W–76°W	0.33	–0.43 to 1.09	0.39	0.3948				
2018–2020: 74°W–76°W	0.78	0.02–1.53	0.38	**0.0437**				
2012–2014: West of 76°W	–16.73	–6,096.37 to 6,062.91	3,101.91	0.9957				
2015–2017: West of 76°W	0.77	–2.06 to 3.60	1.44	0.5917				
2018–2020: West of 76°W	1.25	–1.54 to 4.04	1.42	0.3799				

*Bold indicates statistical significance. Ap-ha, human pathogenic variant of *A. phagocytophilum* bacteria; ERI, entomological risk index.

westward expansion is evident. Of note, these directions are relative only to the spatial extent of New York; our analyses only examined New York data. Including data from Massachusetts, Connecticut, and Vermont could indicate a westward expansion of entomological risk from Ap-ha. If the true spread of Ap-ha is occurring radially from neighboring states east of New York, the phenomenon would appear as the northward and westward increase relative to the borders of New York, as we observed in our results.

The geographic dynamics of Ap-ha and Ap-V1 are also likely linked to the deer–tick–rodent cycle and the varied reservoir competency of key vertebrate hosts. The observed geographic range expansion of Ap-ha, whereas that of Ap-V1 remained stable, indicates that the variants may not have a directly inverse relationship. Furthermore, co-infection of Ap-ha and Ap-V1 within individual ticks was rarely observed in our study and others (*14*), suggesting some competitive interaction between pathogen variants within the vector. The varied *A. phagocytophilum* genotype prevalence across *I. scapularis* tick life stages points to a developmental stage-specific association; the exact ecologic mechanism is unknown. One possibility is that Ap-V1 acquired during a larval tick bloodmeal may be later outcompeted by a subsequent infection of Ap-ha acquired during a nymphal bloodmeal. This phenomenon may be plausible because infection with either variant is maintained within the tick vector from one developmental stage to the next; higher prevalence of Ap-V1 in the nymphal stage did not yield a higher rate of Ap-V1 infection in adult ticks of the same cohort (*31*). Other possibilities include that *I. scapularis* larvae may be more likely to feed on deer than mice in certain geographic regions, that small-mammal populations in certain regions may not harbor Ap-ha, or that another small mammal may serve as an alternate reservoir for Ap-V1 in nature. The difference in Ap-ha prevalence between *I. scapularis* adults and nymphs could cause higher anaplasmosis incidence during the early spring and autumn months, when *I. scapularis* adults are most active, but investigating this possibility was beyond the scope of this study.

It is likely that competition between Ap-V1 and Ap-ha occurs primarily between particular Ap-V1 and Ap-ha clusters (Figures 4, 5). The region between these clusters should be a continued area of focus for epidemiologic research. Competition of variants at the local scale will likely result in spatial changes in the incidence of anaplasmosis; the

expansion of Ap-ha clusters and large but unchanging clusters of Ap-V1 observed in our study match the dynamics of human anaplasmosis incidence depicted in Russell et al. (*13*) (Appendix Figure, https://wwwnc.cdc.gov/EID/article/29/3/22-0320-App1.pdf; Video, https://wwwnc.cdc.gov/EID/article/29/3/22-0320-V1.htm). Our study showed tests for correlation using only Ap-ha in ERI calculations moderately increased the correlation between ERI and reported anaplasmosis incidence; this finding suggests that surveillance testing to detect *A. phagocytophilum* in host-seeking ticks must be variant-specific to yield the most accurate assessment of anaplasmosis risk.

Our study had several limitations, including spatiotemporal variability in tick sampling and the limited spatial extent of our data. Collection sites are more numerous and in closer proximity to one another in the Capital District region than other regions (Figure 1). Heterogenous sampling effort likely resulted in larger clusters of Ap-V1 than Ap-ha (Table 2; Figures 4, 5), because the a priori parameters of the cluster analysis forced clusters to include the same maximum number of ticks, regardless of the distance between sites. Therefore, Ap-V1 clusters in the Western region required a larger radius to include the same number of ticks than Ap-ha clusters in the Capital District region, potentially limiting spatial resolution in western New York. Lower sample sizes at varying latitudes and longitudes also likely reduced statistical power of the ZINB models. In addition, the directionality of the emergence of new clusters and spatiotemporal interaction in the ZINB models are limited by the lack of data outside of New York, possibly biasing results.

Given the changes in spatial distribution of the Ap-ha variant of *A. phagocytophilum,* we suggest medical providers in newly emergent areas familiarize themselves with the signs and symptoms of anaplasmosis to streamline prompt and accurate diagnosis and treatment to ensure the best patient outcomes. Tickborne disease prevention education campaigns should target populations along the leading edge of Ap-ha advancement in New York and elsewhere. Continued differentiation and monitoring of the Ap-ha and Ap-V1 variants of *A. phagocytophilum* to document rate and directionality of spread is critical; further studies will elucidate the ecologic factors driving the expansion of Ap-ha and the resulting increase in anaplasmosis. The results of our study and others can be used to educate medical practitioners and to guide public health policy and disease prevention efforts in New York.

Acknowledgments

We thank the New York State Department of Environmental Conservation, the New York State Department of Parks, Recreation and Historic Preservation, and various county, town and village park managers for granting us use of lands to conduct this research. We thank the following individuals and groups for their assistance in collection, identification, and/or preparation of tick samples for molecular testing: the students of Paul Smith's College, Jake Sporn and the boat launch stewards of the Adirondack Watershed Institute, Elyse Banker, John Howard, James Sherwood, Marly Katz, Anna Perry, Rachel Reichel, Donald Rice, Thomas Mistretta, R.C. Rizzitello, many other NYSDOH employees and student interns, Melissa Fierke and associates with the State University of New York (SUNY) College of Environmental Science and Forestry, Claire Hartl and others from SUNY Brockport, Niagara County DOH, Erie County DOH, Scott Campbell, Michael Santoriello, Christopher Romano, Suffolk County DOH, and Ilia Rochlin, Moses Cucura, and Suffolk County Vector Control.

This work was supported by the New York State Department of Health, US National Institutes of Health (grant nos. AI097137 and AI142572), US Centers for Disease Control and Prevention (award no. U01CK000509) and the CDC Emerging Infections Program TickNET (Cooperative Agreement no. NU50CK000486).

About the Author

Ms. Prusinski is a research scientist and laboratory supervisor with the Vector Ecology Laboratory, Bureau of Communicable Disease Control, New York State Department of Health. Her research focuses on the ecology and epidemiology of tickborne and other arthropod-borne diseases. Mr. O'Connor is a project research assistant with the Bureau of Communicable Disease Control, New York State Department of Health. His research interests include the biogeography and epidemiology of communicable diseases.

References

1. Bakken JS, Dumler JS, Chen SM, Eckman MR, Van Etta LL, Walker DH. Human granulocytic ehrlichiosis in the upper Midwest United States. A new species emerging? JAMA. 1994;272:212–8. https://doi.org/10.1001/jama.1994.03520030054028
2. Chen SM, Dumler JS, Bakken JS, Walker DH. Identification of a granulocytotropic *Ehrlichia* species as the etiologic agent of human disease. J Clin Microbiol. 1994;32:589–95. https://doi.org/10.1128/jcm.32.3.589-595.1994
3. Dumler JS, Madigan JE, Pusterla N, Bakken JS. Ehrlichioses in humans: epidemiology, clinical presentation, diagnosis, and treatment. Clin Infect Dis. 2007;45(Suppl 1):S45–51. https://doi.org/10.1086/518146
4. Massung RF, Mauel MJ, Owens JH, Allan N, Courtney JW, Stafford KC III, et al. Genetic variants of *Ehrlichia*

phagocytophila, Rhode Island and Connecticut. Emerg Infect Dis. 2002;8:467–72. https://doi.org/10.3201/eid0805.010251
5. Massung RF, Courtney JW, Hiratzka SL, Pitzer VE, Smith G, Dryden RL. *Anaplasma phagocytophilum* in white-tailed deer. Emerg Infect Dis. 2005;11:1604–6. https://doi.org/10.3201/eid1110.041329
6. Massung RF, Mather TN, Priestley RA, Levin ML. Transmission efficiency of the AP-variant 1 strain of *Anaplasma phagocytophila.* Ann N Y Acad Sci. 2003;990:75–9. https://doi.org/10.1111/j.1749-6632.2003.tb07340.x
7. de la Fuente J, Massung RF, Wong SJ, Chu FK, Lutz H, Meli M, et al. Sequence analysis of the *msp4* gene of *Anaplasma phagocytophilum* strains. J Clin Microbiol. 2005;43:1309–17. https://doi.org/10.1128/JCM.43.3.1309-1317.2005
8. Reichard MV, Roman RM, Kocan KM, Blouin EF, de la Fuente J, Snider TA, et al. Inoculation of white-tailed deer (*Odocoileus virginianus*) with Ap-V1 Or NY-18 strains of *Anaplasma phagocytophilum* and microscopic demonstration of Ap-V1 in *Ixodes scapularis* adults that acquired infection from deer as nymphs. Vector Borne Zoonotic Dis. 2009;9:565–8. https://doi.org/10.1089/vbz.2008.0106
9. Fishbein DB, Dawson JE, Robinson LE. Human ehrlichiosis in the United States, 1985 to 1990. Ann Intern Med. 1994;120:736–43. https://doi.org/10.7326/0003-4819-120-9-199405010-00003
10. Telford SR III, Dawson JE, Katavolos P, Warner CK, Kolbert CP, Persing DH. Perpetuation of the agent of human granulocytic ehrlichiosis in a deer tick-rodent cycle. Proc Natl Acad Sci U S A. 1996;93:6209–14. https://doi.org/10.1073/pnas.93.12.6209
11. Massung RF, Priestley RA, Miller NJ, Mather TN, Levin ML. Inability of a variant strain of *Anaplasma phagocytophilum* to infect mice. J Infect Dis. 2003;188:1757–63. https://doi.org/10.1086/379725
12. O'Connor C, Prusinski MA, Jiang S, Russell A, White J, Falco R, et al. A comparative spatial and climate analysis of human granulocytic anaplasmosis and human babesiosis in New York State (2013–2018). Hamer S, editor. J Med Entomol. 2021 Jul 21;tjab107.
13. Russell A, Prusinski M, Sommer J, O'Connor C, White J, Falco R, et al. Epidemiology and spatial emergence of anaplasmosis, New York, USA, 2010–2018. Emerg Infect Dis. 2021;27:2154–62. https://doi.org/10.3201/eid2708.210133
14. Krakowetz CN, Dibernardo A, Lindsay LR, Chilton NB. Two *Anaplasma phagocytophilum* strains in *Ixodes scapularis* ticks, Canada. Emerg Infect Dis. 2014;20:2064–7. https://doi.org/10.3201/eid2012.140172
15. Getis A, Ord JK. The analysis of spatial association by use of distance statistics. Geogr Anal. 1992;24:189–206. https://doi.org/10.1111/j.1538-4632.1992.tb00261.x
16. Prusinski MA, Kokas JE, Hukey KT, Kogut SJ, Lee J, Backenson PB. Prevalence of *Borrelia burgdorferi* (Spirochaetales: Spirochaetaceae), *Anaplasma phagocytophilum* (Rickettsiales: Anaplasmataceae), and *Babesia microti* (Piroplasmida: Babesiidae) in *Ixodes scapularis* (Acari: Ixodidae) collected from recreational lands in the Hudson Valley Region, New York State. J Med Entomol. 2014;51:226–36. https://doi.org/10.1603/ME13101
17. Durden LA, Keirans JE. Nymphs of the genus *Ixodes* (Acari: Ixodidae) of the United States: taxonomy, identification key, distribution, hosts, and medical/veterinary importance. Thomas Say publications in entomology. Lanham (MD): Entomological Society of America; 1996.
18. Keirans JE, Clifford CM. The genus *Ixodes* in the United States: a scanning electron microscope study and key to the adults. J Med Entomol Suppl. 1978;15(suppl_2):1–38. https://doi.org/10.1093/jmedent/15.suppl2.1
19. Piedmonte NP, Shaw SB, Prusinski MA, Fierke MK. Landscape features associated with blacklegged tick (Acari: Ixodidae) density and tick-borne pathogen prevalence at multiple spatial scales in central New York state. J Med Entomol. 2018;55:1496–508. https://doi.org/10.1093/jme/tjy111
20. Mather TN, Nicholson MC, Donnelly EF, Matyas BT. Entomologic index for human risk of Lyme disease. Am J Epidemiol. 1996;144:1066–9. https://doi.org/10.1093/oxfordjournals.aje.a008879
21. Jung I, Kulldorff M, Richard OJ. A spatial scan statistic for multinomial data. Stat Med. 2010;29:1910–8. https://doi.org/10.1002/sim.3951
22. Kulldorff M. A spatial scan statistic. Commun Stat Theory Methods. 1997;26:1481–96. https://doi.org/10.1080/03610929708831995
23. Kulldorff M. Prospective time periodic geographical disease surveillance using a scan statistic. J R Stat Soc Ser A Stat Soc. 2001;164:61–72. https://doi.org/10.1111/1467-985X.00186
24. Hochberg Y. A sharper Bonferroni procedure for multiple tests of significance. Biometrika. 1988;75:800–2. https://doi.org/10.1093/biomet/75.4.800
25. Diuk-Wasser MA, Vourc'h G, Cislo P, Hoen AG, Melton F, Hamer SA, et al. Field and climate-based model for predicting the density of host-seeking nymphal *Ixodes scapularis*, an important vector of tick-borne disease agents in the eastern United States. Glob Ecol Biogeogr. 2010;19:504–14.
26. Diuk-Wasser MA, Hoen AG, Cislo P, Brinkerhoff R, Hamer SA, Rowland M, et al. Human risk of infection with *Borrelia burgdorferi*, the Lyme disease agent, in eastern United States. Am J Trop Med Hyg. 2012;86:320–7. https://doi.org/10.4269/ajtmh.2012.11-0395
27. Pebesma E. Simple features for R: standardized support for spatial vector data. R J. 2018;10:439–446. https://doi.org/10.32614/RJ-2018-009
28. Wickham H. ggplot2: elegant graphics for data analysis. 2nd ed. Edinburgh: Springer Cham; 2016.
29. Tennekes M. tmap: thematic maps in *R.* J Stat Soft. 2018;84:1–39. https://doi.org/10.18637/jss.v084.i06
30. Brooks ME, Kristensen K, Benthem KJ, Magnusson A, Berg CW, Nielsen A, et al. glmmTMB balances speed and flexibility among packages for zero-inflated generalized linear mixed modeling. R J. 2017;9:378–400. https://doi.org/10.32614/RJ-2017-066
31. Ross DE, Levin ML. Effects of *Anaplasma phagocytophilum* infection on the molting success of *Ixodes scapularis* (Acari: Ixodidae) larvae. J Med Entomol. 2004;41:476–83. https://doi.org/10.1603/0022-2585-41.3.476

Address for correspondence: Collin O'Connor, New York State Department of Health, Western New York Regional Vector Ecology Laboratory, State University of New York College at Buffalo, SAMC 236/237, Buffalo, NY 14222, USA; email: collin.oconnor@health.ny.gov

Prevalence of *Mycobacterium tuberculosis* Complex among Wild Rhesus Macaques and 2 Subspecies of Long-Tailed Macaques, Thailand, 2018–2022

Suthirote Meesawat, Saradee Warit, Yuzuru Hamada, Suchinda Malaivijitnond

We identified tuberculosis in 1,836 macaques from 6 wild rhesus (*Macaca mulatta*), 23 common long-tailed (*M. fascicularis fascicularis*), and 6 Burmese long-tailed (*M. fascicularis aurea*) macaque populations in Thailand. We captured, anesthetized, and collected throat, buccal, and rectal swab specimens from the macaques. We screened swabs for *Mycobacterium tuberculosis* complex (MTBC) using insertion sequence 6110–specific nested PCR. We found higher MTBC prevalence at both population and individual levels among *M. mulatta* than *M. fascicularis fascicularis* macaques; all 3 *M. fascicularis aurea* macaque populations were positive for tuberculosis. We found that throat swab specimens provided the best sample medium for detecting MTBC. Our results showed no difference in MTBC prevalence between male and female animals, but a higher percentage of adults were infected than subadults and juveniles. Although we detected no association between frequency of human–macaque interaction and MTBC prevalence, bidirectional zoonotic transmission should be considered a possible public health concern.

Climate change and habitat encroachment by humans have led to overlapping of home ranges of wildlife with human settlements. Subsequently, a vast variety of infectious zoonotic diseases have recently emerged or reemerged, transmitted to humans directly from wildlife or indirectly through domestic animals (*1*). Tuberculosis (TB), caused by *Mycobacterium tuberculosis* bacteria, is an airborne chronic infectious disease with zoonotic potential found among both humans and wildlife (*2*). TB has been with humanity for thousands of years and has not been eliminated by modern medical efforts, despite identification of the causative agent 140 years ago by Dr. Robert Koch. A 2021 World Health Organization report ranked Thailand as a country with one of the highest burdens of human TB (*3*).

TB has previously been reported among both wild and captive nonhuman primates. Approximately 75% of TB cases in monkeys are caused by *M. tuberculosis*. Among 500 species of nonhuman primates existing throughout the world, rhesus (*Macaca mulatta*) and long-tailed (*M. fascicularis*) macaques have commonly been used as animal models for TB drug and vaccine research because clinical signs and immune responses after MTB infection are similar to those in humans (*4*–*7*).

Thailand is located at the center of the rhesus and long-tailed macaque distribution ranges, where the 2 species live close together, and comprises part of their interspecific hybridization zone (*8*–*10*). Rhesus macaques are distributed in the north and northeast of Thailand and long-tailed macaques live in central to southern Thailand (*11*–*13*); the hybrid zone, where they cohabit, is within 15°–20°N latitude. It has been proposed that, during earth's glacial periods, male rhesus macaques introgressed southwards into long-tailed macaque population areas and hybridized with female long-tailed macaques (*9*,*10*). Recently, researchers analyzed the level of genetic admixture between rhesus and long-tailed macaque ancestral populations using autosomal single-nucleotide polymorphism markers. Populations of long-tailed macaques from the northern part of their range carry higher levels of genetic admixture of rhesus ancestry than do southern populations (*10*).

Author affiliations: Chulalongkorn University Faculty of Science, Bangkok, Thailand (S. Meesawat, S. Malaivijitnond); National Science and Technology Development Agency, Pathumthani, Thailand (S. Warit); Chulalongkorn University National Primate Research Center of Thailand Saraburi, Thailand (Y. Hamada, S. Malaivijitnond)

DOI: https://doi.org/10.3201/eid2903.221486

Thailand has also been the site of core hybridization between common long-tailed (*M. fascicularis fascicularis*) and Burmese long-tailed (*M. fascicularis aurea*) macaques at 8°10′–12°24′N latitude within Thailand (*11*,*14*,*15*). The natural range of Burmese long-tailed macaques spans southward along the Andaman coast to southwestern Thailand (*11*,*15*). During the past decade, researchers have intensively investigated genetic characteristics of Burmese long-tailed macaques using various genetic markers, including partial and whole mitochondrial DNA, Y-chromosome genes TSPY and SRY (*14*,*16*), whole-genome sequences (*17*), and autosomal single-nucleotide polymorphisms (*15*). Those studies indicated that Burmese long-tailed macaques genetically diverge from common long-tailed and rhesus macaques.

Although both rhesus and long-tailed macaques are widely used for TB research, they differ in their TB pathogenesis, progression, and bacterial burden (*18*). Rhesus macaques are more susceptible than long-tailed macaques to infection after aerosol challenge with *M. tuberculosis* (*19*), and ≈50% of long-tailed macaques showed a clinically latent stage after low-dose exposure to Erdman strain *M. tuberculosis* (*4*). One main concern is that *M. tuberculosis* susceptibility among the 2 macaque species has been tested only in laboratory settings, which do not thoroughly reflect what happens in nature. However, genetic background might also affect levels of susceptibility to *M. tuberculosis* in among different species of macaques. Because of the threat to public health presented by *M. tuberculosis*, we aimed to investigate its prevalence among wild rhesus macaques and 2 subspecies (common and Burmese) of long-tailed macaques whose habitats now overlap with human habitats in Thailand.

Methods

Study Sites and Specimen Collections

During 2018–2022, we captured, sampled, and released 1,836 macaques (189 rhesus, 1,520 common long-tailed, and 127 Burmese long-tailed) from 32 location-defined populations of 2 species of macaques (rhesus and long-tailed), including 2 subspecies of long-tailed macaques (common and Burmese), with distribution ranges in Thailand (*11*,*12*). We identified species and subspecies on the basis of morphologic characteristics, including pelage color, relative tail length, check hair pattern, and head crest (*11*,*12*,*14*,*20*). We recorded the habitat types (temples and tourist attraction sites) where we found them and the frequency of interaction (daily, weekly, monthly, or rarely) with humans (Table 1).

We captured the macaques in iron mesh traps and anesthetized them using an intramuscular injection of 2–5 mg/kg body weight of tiletamine/zolazepam (Virbac, https://us.virbac.com) mixed with 20–50 μg/kg body weight of (dex)medetomidine hydrochloride (Zoetis, https://www.zoetis.com) (*13*,*15*). We recorded sex, body weight, and rectal temperature and estimated age on the basis of dental eruption patterns (*21*); we also attached numeric identification tags to the animals' legs. Using cotton swabs, we took throat swab specimens from between the base of the tongue and the soft palate, buccal swab specimens from the bulge of the cheek pouches, and rectal swab specimens from the anus. We stored swabs at room temperature in 1.5 mL of sterile lysis buffer (0.5% wt/vol sodium dodecyl sulfate, 100 mmol pH 8.0 ethylenediaminetetraacetic acid, 100 mmol pH 8.0 tris aminomethane hydrochloride, and 10 mmol NaCl) (*9*,*10*) until time of genomic DNA extraction. We collected throat and buccal swab specimens from 1,836 macaques in all 32 populations but collected rectal swab specimens from only 1,681 in 28 populations (Table 1). After we had collected all biologic specimens, we administered an intramuscular injection of atipamezole hydrochloride (Zoetis) at the same volume as the (dex) medetomidine hydrochloride anesthetic dose; after their recovery from anesthesia, we released the macaques back to their habitats.

The National Primate Research Center of Thailand-Chulalongkorn University (NPRCT-CU) Animal Care and Use Committees approved all animal procedures (protocol review no. 2075007). The Thailand Department of the National Parks, Wildlife and Plant Conservation approved the protocols for capturing and collecting specimens from macaques.

DNA Extraction and MTB Detection Using Nested PCR

We incubated swab samples at 70°C for 1 h with 50 μL of 30 mg/mL lysozyme solution (SERVA, https://www.serva.de) and extracted genomic DNA using an automated QIAsymphony Virus/Pathogen Mini Kit (QIAGEN, https://www.qiagen.com). We measured the concentration of extracted DNA using QIAGEN QIAxpert. We amplified extracted DNA using nested PCR with MTBC insertion sequence (IS) 6110–specific primers, according to a protocol developed for specimens from humans (*22*). We amplified the MTBC IS6110 DNA (*23*) for 2 rounds. For the first round, we used Tb 294 (5′-GGACAACGCCGAATTGCGAAGGGC-3′) and Tb 850 (5′-TAGGCGTCGGTGACAAAGGCCACG-3′) primers to achieve a 580-bp amplicon. For the second-round nested PCR,

Table 1. Macaque species, locations, geographic coordinates, habitat types, and frequency of interaction with humans from study of macaques infected with *Mycobacterium tuberculosis* complex, Thailand, 2018–2022

Species (common name)	Location	Latitude N, longitude E	Habitat type*	Interaction frequency†
Macaca mulatta (rhesus)	Wat Phra Phutthabat Pha Ruea	20°10′, 100°03′	A	3
	Wat Tham Mueang On	18°47′, 99°14′	B	3
	Wat Tham Thorani Siri Ram	17°11′, 99°33′	C	0
	Ban Sang School	17°51′, 103°57′	B	2
	Ban Phon Kor	17°64′, 104°34′	A	3
	Wat Tham Erawan	17°20′, 101°59′	A	3
M. fascicularis fascicularis (common long-tailed)	Wat Haad Moon	16°30′, 100°16′	C	3
	Wat Ta Sung Tai	15°94′, 99°95′	A	3
	Kao Nor	15°57′, 99°52′	B	2
	Wat Tham Thep Ban Dan	15°44′, 101°02′	C	2
	Wat Mueang Khaen Yai	15°36′, 104°21′	C	3
	Muang Ling Ban Wan	15°38′, 104°18′	B	2
	Wat Ku Phra Ko Na	15°33′, 103°49′	A	3
	Wat Phikun Ngam	15°27′, 100°05′	C	2
	Suan Ling Garden	14°98′, 100°23′	A	3
	Lopburi	14°80′, 100°61′	B	3
	Phar Phothisat	14°57′, 101°14′	A	3
	Wat Kai	14°50′, 100°52′	A	3
	Phra Phutthabat Noi	14°39′, 100°58′	C	2
	Khao Laem Pu Chao	13°39′, 100°52′	B	3
	Wat Tham Khao Chakan	13°39′, 102°05′	A	3
	Wat Tham Khao Cha Ang	13°12′, 101°39′	A	3
	Wat Khao Cha Ang	13°11′, 101°31′	A	3
	Wat Khao Wong Khot	12°52′, 101°49′	A	3
	Kao Ngu	13°34′, 99°46′	B	2
	Wat Kao Tharmon	13°02′, 99°57′	A	3
	Wat Suwan Kuha	8°25′, 98°28′	A	3
	Wat Khao Keaw Wichian	8°12′, 100°05′	C	1
	Khao Chaison	7°27′, 100°07′	B	3
M. fascicularis aurea (Burmese long-tailed)	Tham Pra Khayang	10°19′, 98°45′	B	1
	World War Museum	10°10′, 98°43′	B	0
	Mangrove Forest Research Center	9°87′, 98°60′	B	1

*A, temple (tourist site); B, nontemple tourist site; C, temple (nontourist site).
†0, rarely; 1, monthly; 2, weekly; 3, daily.

we used Tb 505 (5′-ACGACCACATCAACC-3′) and Tb 670 (5′-AGTTTGGTCATCAGCC-3′) primers to achieve a 181-bp amplicon. The 25-μL PCR reaction mixture consisted of 17.4 μL deionized distilled water, 0.5 μL of each primer (0.4 pmol/μL), 2 μL DNA template, 4.6 μL TaKaRa Ex Taq Hot Start Version Kit, 2.5 μL 10X Ex Taq Buffer (Mg^{2+} plus), and 2.0 μL each of 2.5 mmol deoxynucleoside triphosphate and 0.125 μL TaKaRa Ex Taq Hot (TaKaRa Bio, https://www.takarabio.com).

We ran the PCR using Applied Biosystems Verti 96-Well Thermal Cyclers (Thermo Fisher Scientific, https://www.thermofisher.com). For the first round of PCR, we set thermal cycling at 98°C for 1 min, followed by 30 cycles at 93°C for 20 s, 65°C for 30 s, 72°C for 1 min, and 72°C for 10 min. We amplified 1 μL of the first-round PCR product in the second round at 98°C for 1 min, followed by 30 cycles at 93°C for 20 s, 48°C for 30 s, 72°C for 30 s, and 72°C for 10 min. We visualized the 181-bp PCR products using 2% wt/vol agarose gel electrophoresis and stained them with Invitrogen SYBR Safe DNA gel stain (Thermo Fisher).

Specificity and Sensitivity of MTBC Detection Using IS6110 Nested PCR

We validated specificity of the MTBC nested PCR with IS6110-specific primers using granuloma lung tissues from a naturally *M. tuberculosis*–infected long-tailed macaque (Figure 1). We confirmed *M. tuberculosis* infection in the macaque by mycobacterium culture and interferon gamma release assay, using methods reported elsewhere (*24*). We collected and extracted granuloma lung tissues for genomic DNA using a QIAGEN Virus/Pathogen Mini Kit. We purified the products obtained from 181-bp nested PCR testing of the naturally *M. tuberculosis*–infected macaque and the 19 nested PCR–positive samples randomly selected from populations of wild rhesus macaques from Ban Phon Kor and Ban Sang School and Burmese long-tailed macaques from Tham Pra Khayang and Mangrove Forest Research Center using the GenUP Exo Sap Kit (Biotechrabbit, https://www.biotechrabbit.com) and submitted the samples to Macrogen (https://www.macrogen.com) for DNA sequencing. We aligned nucleotide sequences with published *M. tuberculosis* sequences accessed from GenBank using MEGA X software (*25*). After all

amplicons from the *M. tuberculosis* sequences from macaques in our study showed 100% homology with published sequences, we used an IS6110-specific nested PCR protocol to determine the sensitivity of the *M. tuberculosis* nested PCR technique, using genomic DNA of the *M. tuberculosis* H37Rv (ATCC27294) strain, serially diluted (1:10) from 1 ng to 1 fg (*26*). We designated the lowest concentration of *M. tuberculosis* H37Rv that we could detect by nested PCR as the limit of detection (LOD) for this technique.

Data Analyses

We calculated prevalence rate and 95% CIs for differences in MTBC shedding stratified by species and subspecies, sex, and age of macaques. Using Pearson χ^2 tests, we analyzed associations between MTBC prevalence and macaque species and subspecies, sex and age, and between MTBC prevalence and frequency of human–macaque interaction. Using Pearson correlation analysis, we analyzed correlations between MTBC prevalence and bodily site (throat, buccal and rectal) of specimen collection and used SPSS Statistics 28 for Mac (IBM, https://www.ibm.com) to analyze data. We used $p \leq 0.05$ to indicate statistical significance.

Results

Specificity and Sensitivity of MTBC Detection Using IS6110 Nested PCR

The 181-bp nucleotide sequences from granuloma lung tissues and 19 nested PCR–positive samples from a naturally *M. tuberculosis*–infected macaque all showed 100% similarity with the MTB H37Rv complete genome (GenBank accession no. NC_000962.3) (data not shown). A BLASTn (https://blast.ncbi.nlm.nih.gov/Blast.cgi) search using the NCBI-registered complete genomes indicated that the specific 181-bp nucleotide sequence obtained from the IS6110-specific nested PCR (574 *M. tuberculosis*; 8 *M. bovis* BCG; 3 *M. canettii*; 2 each *M. bovis* and *M. africanum*; and 1 each *M. caprae*, *M. microti*, and *M. orygis* strains) could be detected in the MTBC. Thus, we interpreted the results from the IS6110-specific nested PCR in this study as positive for MTBC.

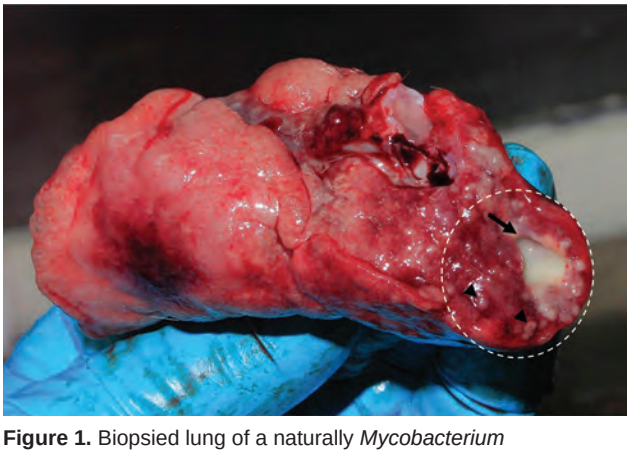

Figure 1. Biopsied lung of a naturally *Mycobacterium tuberculosis*–infected common long-tailed macaque collected in Thailand. Within the white dashed circle, arrow indicates granuloma and arrowheads indicate multiple-sized granulomas diffused within the lung parenchyma.

The optimized MTBC nested PCR conditions of the H37Rv DNA (ATCC27294) strain showed LOD values of 100 fg/μL in the first round (580-bp product) and 10 fg/μL in the second round (181-bp product) (Figure 2). Because MTBC concentration was low in some macaques, we could not visualize 580-bp PCR products from resolved 2% wt/vol agarose gel electrophoresis but detected a positive result from the second-round nested PCR with a 181-bp amplicon. In the second round in this study, we found 71/192 MTBC-positive specimens overall: 21/80 for rhesus, 36/93 for common long-tailed, and 14/19 for Burmese long-tailed macaques.

Prevalence of MTBC in Rhesus Macaques and 2 Subspecies of Long-Tailed Macaques

We detected MTBC IS6110 DNA among all 3 (100%) Burmese long-tailed macaque populations, higher than for either rhesus (5/6, 83.3%) or common long-tailed (10/23, 43.5%) macaque populations (Table 2; Figure 3). We found MTBC IS6110 DNA in 128/1,836 (7.0%) throat, 41/1,836 (2.3%) buccal, and 23/1,681 (1.4%) rectal swab samples (Table 2). When we analyzed specimens from all body collection sites, correlation was significant between 1,836 throat and buccal ($r^2 = 0.04$; $p = 0.01$), 1,681 throat and rectal ($r^2 = 0.01$; $p = 0.01$), and 1,681 buccal and rectal swab samples ($r^2 = 0.07$; $p = 0.01$). However, when we analyzed only MTBC-positive results, we found significant correlations only between 152 throat and buccal ($r^2 = 0.29$; $p = 0.01$), and 99 throat and rectal swab samples ($r^2 = 0.30$; $p = 0.01$), but not between 45 buccal and rectal swab samples ($r^2 = 0.004$; $p = 0.54$).

Because we detected MTBC-positive cases most frequently from throat swab specimens, we further analyzed the 16 location-specific populations that showed MTBC-positive results from throat swab specimens: Wat Phra Phutthabat Pha Ruea, Ban Sang School, Ban Phon Kor, and Wat Tham Erawan for rhesus macaques; Wat Mueang Khaen Yai, Wat Ku Phra Ko Na, Lopburi, Phar Phothisat, Wat Kai, Phra Phutthabat Noi, Khao Laem Pu Chao, Wat Tham Khao Cha Ang, Wat Khao Cha Ang, and Wat Kao Tharmon for common long-tailed macaques; and Tham Pra Khayang and Mangrove

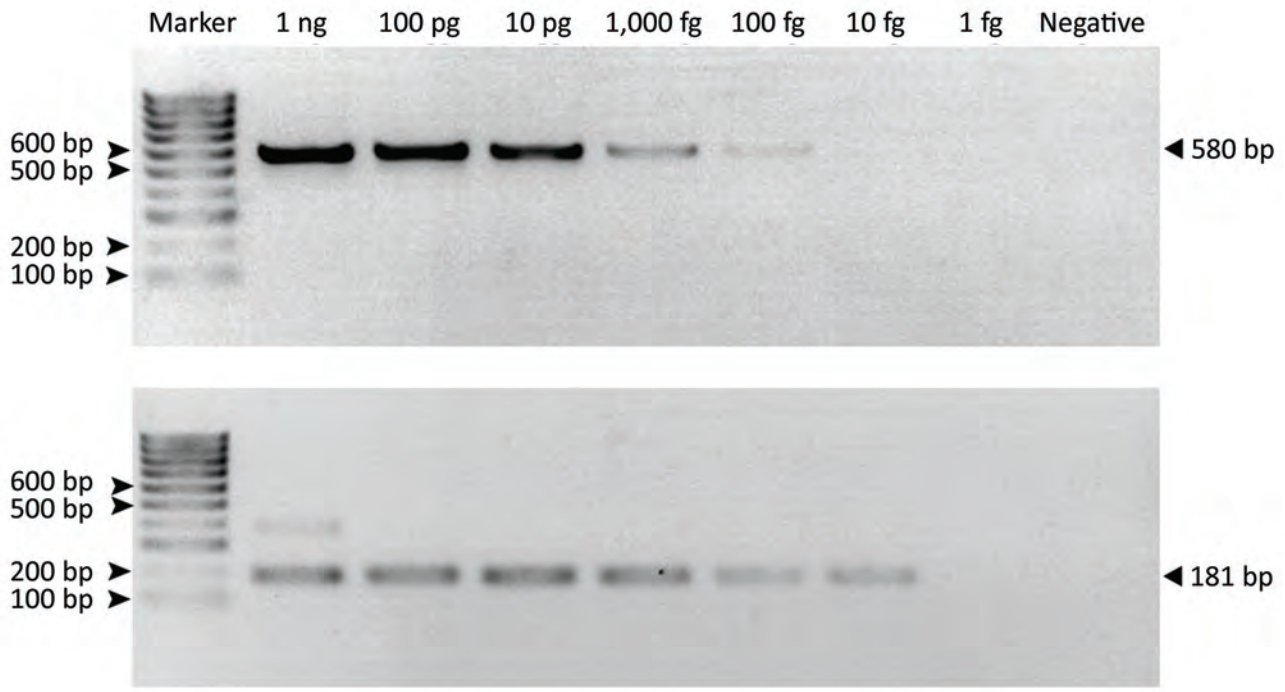

Figure 2. Limit of detection of *Mycobacterium tuberculosis* complex in the first (A) (580-bp) and second (B) (181-bp) rounds of IS6110-specific nested PCR of samples from free-ranging macaques, Thailand, 2018–2022. We could not visualize 580-bp PCR products from resolved 2% wt/vol agarose gel electrophoresis in the first round but detected a positive result from the second-round nested PCR with a 181-bp amplicon.

Forest Research Center for Burmese long-tailed macaques (Tables 2, 3). Based on these data, MTBC prevalence was significantly higher (χ^2 = 253.95; p = 0.01) among rhesus (37.1% [95% CI 30.0%–44.2%]; 66/178 in 4 populations) than Burmese long-tailed (8.0% [95% CI 1.9%–14.1%]; 6/75 in 2 populations) and common long-tailed (6.6% [95% CI 5.0%–8.3%]; 56/843 in 10 populations) macaques. Most MTBC-positive common long-tailed macaques inhabited the central region of Thailand at 13°02′–15°36′N latitude (Figure 3).

We futher analyzed the data for any correlation between MTBC prevalence and age and sex. We stratified data into 3 groups on the basis of age estimated from dental eruption at the time of capture; we classified both male and female macaques >6 years as adults, 3–6 years as subadults, and <3 years as juveniles (Tables 3, 4). MTBC shedding status detected from throat swab specimens was significantly higher among adult positive case-patients than other age groups of the same species: 47.0% (31/66) for adult rhesus macaques, 50.0% (28/56) for adult common long-tailed macaques, and 50.0% (3/6) for adult Burmese long-tailed macaques (χ^2 = 0.14; p = 0.01). When we considered data on MTBC prevalence by sex of positive case-patients, the difference between males (51.6%, 66/128) and females (48.4%, 62/128) was not significant (χ^2 = 0.94; p = 0.33). We also found no significant difference by swab collection site between percentages of MTBC-positive macaques and frequency of human interaction (χ^2 = 6.76, p = 0.08 for throat; χ^2 = 5.41, p = 0.14 for buccal; and χ^2 = 3.27, p value = 0.11 for rectal swab samples).

Discussion

Intradermal tuberculin skin test (TST) is used globally to detect TB in macaques. Testers intradermally inject tuberculin antigens at the edge of the animal's upper eyelid and look for an immune response (erythema or edema) at 24, 48, and 72 hours after injection (*27*). Disadvantages of TST include that it depends on an interpreter's subjective judgment and is time-consuming and impractical for field study in free-ranging or wild macaques. Therefore, we collected swabs of biologic specimens from common sites of MTBC shedding—throat, cheeks, and rectum—for screening. To test samples, we modified a nested PCR technique previously developed for clinical specimens using IS6110-specific primers (*22*) and used it to detect MTBC among free-ranging rhesus and long-tailed macaques. Results in samples taken from multiple sites (*22*,*28*,*29*) revealed a higher prevelance of MTBC DNA in throat than in buccal and rectal swab

Table 2. Detection of MTBC in throat, buccal, and rectal swab specimens tested by using IS6110-specific nested PCR in 32 populations of macaques, by swab site and location found, Thailand, 2018–2022*

Species (common name)	Location	Throat and buccal/rectal specimens	MTBC-PCR detected in swabs, no. (%)							MTBC-positive (%)
			Throat	Buccal	Rectal	Throat + buccal	Throat + rectal	Buccal + rectal	All 3	
Macaca mulatta (rhesus)	Wat Phra Phutthabat Pha Ruea	57/57	2 (3.5)	1 (1.8)	2 (3.5)	0	1 (1.8)	0	0	4 (7.0)
	Wat Tham Mueang On	10/10	0	0	0	0	0	0	0	0
	Wat Tham Thorani Siri Ram	1/1	0	0	1 (100)	0	0	0	0	1 (100.0)
	Ban Sang School	42/0	29 (69.0)	4 (9.5)	NA	4 (9.5)	0	0	0	29 (69.0)
	Ban Phon Kor	19/0	12 (63.2)	3 (15.8)	NA	2 (10.5)	0	0	0	13 (68.4)
	Wat Tham Erawan	60/60	23 (38.3)	3 (5.0)	0	3 (5.0)	0	0	0	23 (38.3)
	Total	189/128	66 (34.9)	11 (5.8)	3 (2.3)	9 (4.8)	1 (0.8)	0	0	70 (37.0)
M. fascicularis fascicularis (common long-tailed)	Wat Haad Moon	34/34	0	0	0	0	0	0	0	0
	Wat Ta Sung Tai	60/60	0	0	0	0	0	0	0	0
	Kao Nor	77/77	0	0	0	0	0	0	0	0
	Wat Tham Thep Ban Dan	55/55	0	0	0	0	0	0	0	0
	Wat Mueang Khaen Yai	60/60	5 (8.3)	12 (20.0)	8 (13.3)	1 (1.7)	0	4 (6.7)	1 (1.7)	20 (33.3)
	Muang Ling Ban Wan	4/4	0	0	0	0	0	0	0	0
	Wat Ku Phra Ko Na	77/77	9 (11.7)	0	2 (2.6)	0	2 (2.6)	0	0	7 (9.1)
	Wat Phikun Ngam	11/11	0	0	0	0	0	0	0	0
	Suan Ling Garden	148/148	0	0	0	0	0	0	0	0
	Lopburi	91/91	2 (2.2)	1 (1.1)	0	1 (1.1)	0	0	0	1 (1.1)
	Phar Phothisat	304/304	7 (2.3)	1 (0.3)	0	0	0	0	0	8 (2.6)
	Wat Kai	60/60	5 (8.3)	0	0	0	0	0	0	5 (8.3)
	Phra Phutthabat Noi	118/118	5 (4.2)	0	0	0	0	0	0	5 (4.2)
	Khao Laem Pu Chao	10/10	1 (10.0)	0	1 (10.0)	0	0	0	0	2 (20.0)
	Wat Tham Khao Chakan	50/50	0	0	0	0	0	0	0	0
	Wat Tham Khao Cha Ang	36/36	9 (25.0)	5 (13.9)	1 (2.8)	2 (5.6)	0	1 (2.8)	0	13 (36.1)
	Wat Khao Cha Ang	15/15	6 (40.0)	4 (26.7)	1 (6.7)	1 (6.7)	0	1 (6.7)	0	9 (60.0)
	Wat Khao Wong Khot	47/47	0	0	0	0	0	0	0	0
	Kao Ngu	71/71	0	0	0	0	0	0	0	0
	Wat Kao Thamon	72/72	7 (9.7)	1 (1.4)	0	0	0	0	0	8 (11.1)
	Wat Suwan Kuha	28/28	0	0	0	0	0	0	0	0
	Wat Khao Keaw Wichian	33/33	0	0	0	0	0	0	0	0
	Khao Chaison	59/59	0	0	NA	0	0	0	0	0
	Total	1,520/1,461	56 (3.7)	24 (1.6)	13 (0.9)	5 (0.3)	2 (0.1)	6 (0.4)	1 (0.1)	78 (5.1)
M. fascicularis aurea (Burmese long-tailed)	Tham Pra Khayang	40/40	2 (5.0)	1 (2.5)	3 (7.5)	0	1 (2.5)	0	0	5 (12.5)
	World War Museum	52/52	0	1 (1.9)	4 (7.7)	0	0	0	0	5 (9.6)
	Mangrove Forest Research Center	35/0	4 (11.4)	4 (11.4)	NA	0	0	0	0	8 (22.9)
	Total	127/92	6 (4.7)	6 (4.7)	7 (7.6)	0	1 (1.1)	0	0	18 (14.2)
All	Total	1,836/1,681	128 (7.0)	41 (2.3)	23 (1.3)	14 (0.8)	4 (0.2)	6 (0.4)	1 (0.1)	166 (9.0)

*MTBC, *Mycobacterium tuberculosis* complex; NA, not available.

specimens. Thus, we determined that, because of their higher efficiency, throat swab specimens should be used for collecting specimens to detect MTBC shedding in free-ranging macaques. Because of low MTBC concentration in the collected specimens, most 580-bp band PCR amplifications in the first round were undetected; however, we could clearly identify the 181-bp PCR amplicons in agarose gel in the second round. LOD for the second-round nested PCR, 10 fg/μL, was 10-fold lower than in the first round, 100 fg/μL, similar

to findings reported elsewhere (*26*). Although this nested PCR had the advantage of higher sensitivity, the possibility of false-positive results from contaminated DNA or DNA carryover, mainly amplicons, should be considered. To avoid cross-contamination or carryover, key processes, such as template preparation, specimen handling, and preparation of PCR mixture, should be performed in different PCR biosafety cabinets and should include negative controls.

In a previous report, laboratory-tested rhesus macaques were more susceptible to MTBC infection than long-tailed macaques (*19*); likewise, in our study, free-ranging rhesus macaques in Thailand showed higher MTBC prevalence than did common long-tailed macaques, both in the number of populations and individual macaques infected. The laboratory-tested rhesus macaques exhibited illness, had respiratory tract granuloma develop, and returned to activity after a short duration. In contrast, free-ranging rhesus macaques in our study showed no signs of illness (*5*,*6*,*30*). One possible explanation for this difference is that the rhesus macaques in Thailand had a genetic admixture of long-tailed macaque ancestry, which made them more resistant to MTBC. For example, rhesus macaques in the population at Ban Sang School, which carried up to an 18% genetic admixture of long-tailed macaque ancestry, had a high percentage, 29%, of MTBC prevalence (*10*). Considering the high MTBC prevalence in rhesus macaques and frequent interaction with humans among some populations, there is a need for practices such as avoiding direct contact with macaques and conveying information to local residents about the spread of TB from macaques. Local residents should also be monitored for bidirectional transmission of MTBC.

In light of usual rates of MTBC infection among long-tailed macaques, it is notable that all 3 populations of Burmese long-tailed macaques were MTBC positive, in spite of less frequent contact with humans, rare or monthly, than for populations of common long-tailed macaques. In particular, the World War Museum and Mangrove Forest Research Center populations in Ranong Province in southern Thailand reside in mangrove forests and roam freely for invertebrate foods. Unique genetic characteristics among Burmese long-tailed macaques, identified through intensive genetic studies (*14*–*17*), might factor into their high MTBC prevalence. More research should be conducted on TB infection among Burmese long-tailed macaques, especially about

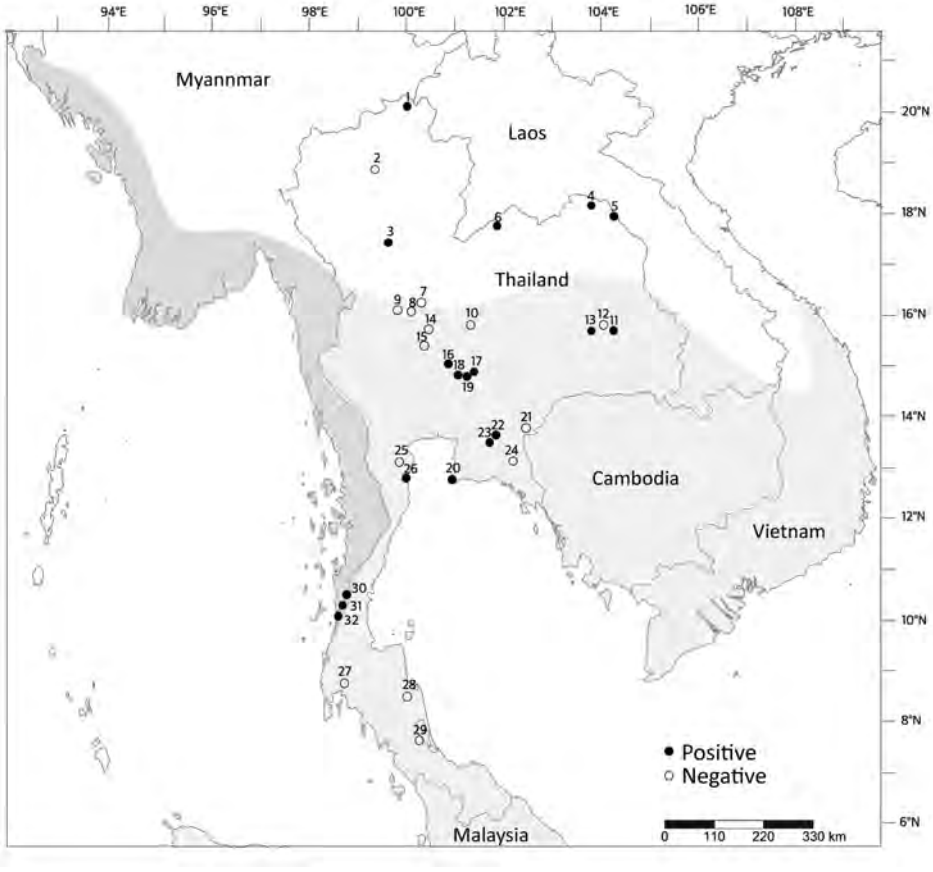

Figure 3. Locations, species, and *Mycobacterium tuberculosis* complex status in free-ranging macaques, Thailand, 2018–2022. White area on map shows the range of rhesus macaques; light gray, common long-tailed macaques; and dark gray, Burmese long-tailed macaque. Numbers indicate locations where we found macaques: 1, Wat Phra Phutthabat Pha Ruea; 2, Wat Tham Mueang On; 3, Wat Tham Thorani Siri Ram; 4, Ban Sang School; 5, Ban Phon Kor; 6, Wat Tham Erawan; 7, Wat Haad Moon; 8, Wat Ta Sung Tai; 9, Kao Nor; 10, Wat Tham Thep Ban Dan; 11, Wat Mueang Khaen Yai; 12, Muang Ling Ban Wan; 13, Wat Ku Phra Ko Na; 14, Wat Phikun Ngam; 15, Suan Ling Garden; 16, Lopburi; 17, Phar Phothisat; 18, Wat Kai; 19, Phra Phutthabat Noi; 20, Khao Laem Pu Chao; 21, Wat Tham Khao Chakan; 22, Wat Tham Khao Cha Ang; 23, Wat Khao Cha Ang; 24, Wat Khao Wong Khot; 25, Kao Ngu; 26, Wat Kao Tharmon; 27, Wat Suwan Kuha; 28, Wat Khao Keaw Wichian; 29, Khao Chaison; 30, Tham Pra Khayang; ; 31, World War Museum; 32, Mangrove Forest Research Center.

Table 3. Detection of MTBC in throat swabs using IS6110-specific nested PCR in 32 populations of macaques, by sex and location found, Thailand, 2018–2022*

Species (common name)	Location	No. positive/total no. (%)	MTBC PCR detected in throat swab specimens, no. positive/total no. (%)					
			M age groups†			F age groups†		
			Adult	Subadult	Juvenile	Adult	Subadult	Juvenile
Macaca mulatta (rhesus)	Wat Phra Phutthabat Pha Ruea	2/57 (3.5)	0/2	0/10	1/18 (5.6)	0/4	0/10	1/13 (7.7)
	Ban Sang School	29/42 (69.0)	6/9 (66.7)	4/5 (80.0)	3/6 (50.0)	11/15 (73.3)	3/5 (60.0)	2/2 (100.0)
	Ban Phon Kor	12/19 (63.2)	4/5 (80.0)	2/3 (66.7)	3/5 (60.0)	1/3 (33.3)	1/1 (100.0)	1/2 (50.0)
	Wat Tham Erawan	23/60 (38.3)	2/3 (66.7)	3/10 (30.0)	2/10 (20.0)	7/11 (63.6)	6/18 (33.3)	3/8 (37.5)
	Total	66/178 (37.1)	12/19 (63.2)	9/28 (32.1)	9/39 23.1)	19/33 (57.6)	10/34 (29.4)	7/25 (28.0)
M. fascicularis fascicularis (common long-tailed)	Wat Mueang Khaen Yai	5/60 (8.3)	0/2	0/15	1/8 (12.5)	3/22 (13.6)	1/11 (9.1)	0/2
	Wat Ku Phra Ko Na	9/77 (11.7)	1/13 (7.7)	3/22 (13.6)	0/11	3/13 (23.1)	1/9 (11.1)	1/9 (11.1)
	Lopburi	2/91 (2.2)	0/21	0/17	0/9	1/29 (3.4)	1/11 (9.1)	0/4
	Phar Phothisat	7/304 (2.3)	3/51 (5.9)	2/35 (5.7)	0/27	1/102 (1.0)	1/57 (1.8)	0/32
	Wat Kai	5/60 (8.3)	3/25 (12.0)	0/15	0/0	2/10 (20.0)	0/9	0/1
	Phra Phutthabat Noi	5/118 (4.2)	2/2 (100.0)	1/5 (20.0)	1/52 (1.9)	0/5	1/12 (8.3)	0/42
	Khao Laem Pu Chao	1/10 (10.0)	1/3 (33.3)	0/3	0/0	0/0	0/2	0/2
	Wat Tham Khao Cha Ang	9/36 (25.0)	1/9 (11.1)	1/2 (50.0)	3/10 (30.0)	0/3	2/6 (33.3)	2/6 (33.3)
	Wat Khao Cha Ang	6/15 (40.0)	4/10 (40.0)	0/0	0/0	0/0	1/2 (50.0)	1/3 (33.3)
	Wat Kao Tharmon	7/72 (9.7)	0/23	2/20 (10.0)	1/6 (16.7)	3/11 (27.3)	1/9 (11.1)	0/3
	Total	56/843 (6.6)	15/159 (9.4)	9/134 (6.7)	6/123 (4.9)	13/195 (6.7)	9/128 (7.0)	4/104 (3.9)
M. fascicularis aurea (Burmese long-tailed)	Tham Pra Khayang	2/40 (5.0)	1/15 (6.7)	0/4	1/5 (20.0)	0/6	0/7	0/3
	Mangrove Forest Research Center	4/35 (11.4)	2/10 (20.0)	1/7 (14.3)	1/9 (11.1)	0/2	0/4	0/3
	Total	6/75 (8.0)	3/25 (12.0)	1/11 (9.1)	2/14 (14.3)	0/8	0/11	0/6
All	Total	128/1,096 (11.7)	30/203 (14.8)	19/173 (11.0)	17/176 (9.7)	32/236 (13.6)	19/173 (11.0)	11/135 (8.1)

*MTBC, *Mycobacterium tuberculosis* complex.
†Adult, >6 y; subadult, 3–6 y; juvenile, <3 y.

mechanisms of infection and disease progression related to genetic factors, because the species might prove to be an alternative animal model for TB research. Of note, we did not see higher MTBC positivity among northern common long-tailed macaques, even though they carry a higher genetic admixture of rhesus ancestry than their southern relatives (*10*). Thus, factors other than hybridization should be

Table 4. Detection of *Mycobacterium tuberculosis* complex in throat swabs using IS6110-specific nested PCR in 32 populations of macaques, Thailand, 2018–2022*

Species (common name)	Age group	Male	Female	Total
		Positive, % (95% CI)	Positive, % (95% CI)	Positive, % (95% CI)
Macaca mulatta (rhesus)	Adult	12, 18.2 (8.9–27.5)	19, 28.8 (17.9–39.7)	31, 47.0 (24.4–47.6)
	Subadult	9, 13.6 (5.4–21.9)	10, 15.2 (6.5–23.8)	19, 28.8 (17.9–39.7)
	Juvenile	9, 13.6 (5.4–21.9)	7, 10.6 (0.8–13.2)	16, 24.2 (13.9–34.6)
	Total	30, 45.5 (33.4–57.5)	36, 54.5 (24.4–47.6)	**66, 100.0 (100.0–100.0)**
M. fascicularis fascicularis (common long-tailed)	Adult	15, 26.8 (15.2–38.4)	13, 23.2 (12.1–34.3)	28, 50.0 (36.9–63.1)
	Subadult	9, 16.1 (6.5–25.7)	9, 16.1 (6.5–25.7)	18, 32.1 (19.9–44.4)
	Juvenile	6, 10.7 (2.6–18.8)	4, 7.1 (0.4–13.9)	10, 17.9 (7.8–27.9)
	Total	30, 53.6 (40.5–66.6)	26, 46.4 (33.4–59.5)	56, 100.0 (100.0–100.0)
M. fascicularis aurea (Burmese long-tailed)	Adult	3, 50.0 (10.0–90.0)	0	3, 50.0 (10.0–90.0)
	Subadult	1, 16.7 (0.0–46.5)	0	1, 16.7 (0.0–46.5)
	Juvenile	2, 33.3 (0.0–71.1)	0	2, 33.3 (0.0–71.1)
	Total	6, 100.0 (100.0–100.0)	0	6, 100.0 (100.0–100.0)
All	Total	66, 51.6 (42.9–60.2)	62, 48.4 (39.8–57.1)	128, 100.0 (100.0–100.0)

*Bold indicates significant difference ($p < 0.05$) from other species

consideredwhen assessing MTBC prevalence among common long-tailed macaques.

MTBC shedding in 10/23 common long-tailed macaques populations in our study differed from a report published elsewhere (*31*), in which *Mycobacterium* spp. were not detected in any of 649 free-living common long-tailed macaques from 26 locations (*31*). This discrepancy might be because of differences between studies in sampling locations, specimen collection methods, DNA extraction processes, and PCR performance. Although the researchers in that study used IS6110-specific primer sets, they did not conduct a nested PCR, so the sensitivity of their method might have been insufficient to detect low-level shedding of MTBC in macaques.

Although nested PCR is highly sensitive and less time-consuming than other methods, it can detect TB only during the active shedding stage of infection (*32*,*33*). Other diagnostic tools, such as TST or TB blood test, are still required to detect TB during latent or nonshedding active stages. Another disadvantage of the nested PCR approach is the invasive methods needed to catch and anesthetize macaques to collect specimens, which in some locations, such as mangrove forests (e.g., Mangrove Forest Research Center) or high cliffs (e.g., Wat Suwan Kuha), are also impractical. A noninvasive technique to collect samples should be developed, such as using a rope bait method to collect pathogens inside the oral cavity (*33*) or analyzing samples from recently dropped feces (*34*). On the basis of our results showing comparable prevalence of MTBC infection between male and female macaques and higher prevalence among adults than other age groups, specimen collection efforts could focus on adults in free-ranging macaque populations if only preliminary results are needed.

Because MTBC-infected wild macaques could be reservoirs of the pathogen and it might be transmitted back to humans, bidirectional zoonotic transmission should be considered, especially for populations in which the MTBC-infected macaques interact with humans on a daily basis. In a worst-case scenario, MTBC bacteria could mutate after infecting a macaque, then be transmitted back to humans; existing commercial antimycobacterial agents might be ineffective for treating the mutated pathogen (*35*). Experience with SARS-CoV-2 virus (*36*) and other emerging and reemerging pathogens transmitted from wildlife to humans has provided lessons about surveilance for and control of emerging public health threats that can be applied to managing potential threats to public health from MTBC.

Acknowledgments

We are grateful to Taratorn Kemthong, Chanatip Kraitat, and Nopparat Kongsombat, NPRCT-CU, for supporting and participating in the field study. We thank all the officers and staff of the Department of the National Parks, Wildlife and Plant Conservation, Thailand for their cooperation and permission to conduct this research.

This research was supported by the Research Fund Senior Scholar (grant no. RTA6280010, to S.M.), the TSRI Fund, (to S.M.), the National Science Research and Innovation Fund through the Program Management Unit for Human Resources and Institutional Development, Research and Innovation (grant no. B05F640122, to S.M.), the 90th Anniversary of Chulalongkorn University Ratchadaphiseksomphot Endowment Fund (to S.M.) and the Chulalongkorn University and National Science and Technology Development Agency doctoral scholarship program.

About the Author

Mr. Meesawat is a PhD student in the Biological Sciences Program, Faculty of Science, Chulalongkorn University, and was a researcher in National Primate Research Center of Thailand–Chulalongkorn University. His interests include developing of methods for detecting tuberculosis among captive and wild macaques and research on dynamics of tuberculosis transmission between human and macaques.

References

1. Cunningham AA, Daszak P, Wood JLN. One Health, emerging infectious diseases and wildlife: two decades of progress? Philos Trans R Soc Lond B Biol Sci. 2017;372:20160167. https://doi.org/10.1098/rstb.2016.0167
2. Cambau E, Drancourt M. Steps towards the discovery of *Mycobacterium tuberculosis* by Robert Koch, 1882. Clin Microbiol Infect. 2014;20:196–201. https://doi.org/10.1111/1469-0691.12555
3. World Health Organization. Global tuberculosis report 2021 [cited 2022 Sep 25]. https://www.who.int/publications/i/item/9789240037021
4. Capuano SV III, Croix DA, Pawar S, Zinovik A, Myers A, Lin PL, et al. Experimental *Mycobacterium tuberculosis* infection of cynomolgus macaques closely resembles the various manifestations of human *M. tuberculosis* infection. Infect Immun. 2003;71:5831–44. https://doi.org/10.1128/IAI.71.10.5831-5844.2003
5. Flynn JL, Capuano SV, Croix D, Pawar S, Myers A, Zinovik A, et al. Non-human primates: a model for tuberculosis research. Tuberculosis (Edinb). 2003;83:116–8. https://doi.org/10.1016/S1472-9792(02)00059-8
6. Peña JC, Ho W-Z. Monkey models of tuberculosis: lessons learned. Infect Immun. 2015;83:852–62. https://doi.org/10.1128/IAI.02850-14
7. Foreman TW, Mehra S, Lackner AA, Kaushal D. Translational research in the nonhuman primate model of tuberculosis. ILAR J. 2017;58:151–9. https://doi.org/10.1093/ilar/ilx015

8. Bonhomme M, Cuartero S, Blancher A, Crouau-Roy B. Assessing natural introgression in 2 biomedical model species, the rhesus macaque (*Macaca mulatta*) and the long-tailed macaque (*Macaca fascicularis*). J Hered. 2009;100:158–69. https://doi.org/10.1093/jhered/esn093
9. Bunlungsup S, Imai H, Hamada Y, Matsudaira K, Malaivijitnond S. Mitochondrial DNA and two Y-chromosome genes of common long-tailed macaques (*Macaca fascicularis fascicularis*) throughout Thailand and vicinity. Am J Primatol. 2017;79:1–13. https://doi.org/10.1002/ajp.22596
10. Bunlungsup S, Kanthaswamy S, Oldt RF, Smith DG, Houghton P, Hamada Y, et al. Genetic analysis of samples from wild populations opens new perspectives on hybridization between long-tailed (*Macaca fascicularis*) and rhesus macaques (*Macaca mulatta*). Am J Primatol. 2017;79:e22726. https://doi.org/10.1002/ajp.22726
11. Fooden J. Systematic review of Southeast Asian longtail macaques, *Macaca fascicularis* (Raffles, [1821]). Fieldiana Zool. 1995;81:1–206.
12. Fooden J. Systematic review of the rhesus macaque, *Macaca mulatta* (Zimmermann, 1780). Fieldiana Zool. 2000;96:1–180.
13. Malaivijitnond S, Hamada Y. Current situation and status of long-tailed macaques (*Macaca fascicularis*) in Thailand. Nat Hist J Chulalongkorn Univ. 2008;8:185–204.
14. Bunlungsup S, Imai H, Hamada Y, Gumert MD, San AM, Malaivijitnond S. Morphological characteristics and genetic diversity of Burmese long-tailed macaques (*Macaca fascicularis aurea*). Am J Primatol. 2016;78:441–55. https://doi.org/10.1002/ajp.22512
15. Phadphon P, Kanthaswamy S, Oldt RF, Hamada Y, Malaivijitnond S. Population structure of *Macaca fascicularis aurea*, and their genetic relationships with *M. f. fascicularis* and *M. mulatta* determined by 868 RADseq-derived autosomal SNPs—a consideration for biomedical research. J Med Primatol. 2022;51:33–44. https://doi.org/10.1111/jmp.12554
16. Matsudaira K, Hamada Y, Bunlungsup S, Ishida T, San AM, Malaivijitnond S. Whole mitochondrial genomic and Y-chromosomal phylogenies of Burmese long-tailed macaque (*Macaca fascicularis aurea*) suggest ancient hybridization between *fascicularis* and *sinica* species groups. J Hered. 2018;109:360–71. https://doi.org/10.1093/jhered/esx108
17. Osada N, Matsudaira K, Hamada Y, Malaivijitnond S. Testing sex-biased admixture origin of macaque species using autosomal and X-chromosomal genomic sequences. Genome Biol Evol. 2020;13:evaa209. https://doi.org/10.1093/gbe/evaa209
18. Maiello P, DiFazio RM, Cadena AM, Rodgers MA, Lin PL, Scanga CA, et al. Rhesus macaques are more susceptible to progressive tuberculosis than cynomolgus macaques: a quantitative comparison. Infect Immun. 2018;86:e00505–17. https://doi.org/10.1128/IAI.00505-17
19. Sharpe S, White A, Gleeson F, McIntyre A, Smyth D, Clark S, et al. Ultra low dose aerosol challenge with *Mycobacterium tuberculosis* leads to divergent outcomes in rhesus and cynomolgus macaques. Tuberculosis (Edinb). 2016;96:1–12. https://doi.org/10.1016/j.tube.2015.10.004
20. Hamada Y, San AM, Malaivijitnond S. Assessment of the hybridization between rhesus (*Macaca mulatta*) and long-tailed macaques (*M. fascicularis*) based on morphological characters. Am J Phys Anthropol. 2016;159:189–98. https://doi.org/10.1002/ajpa.22862
21. Smith BH, Crummett TL, Brandt KL. Ages of eruption of primate teeth: a compendium for aging individuals and comparing life histories. Yearb Phys Anthropol. 1994;37(S19):177–231. https://doi.org/10.1002/ajpa.1330370608
22. Githui WA, Wilson SM, Drobniewski FA. Specificity of IS6110-based DNA fingerprinting and diagnostic techniques for *Mycobacterium tuberculosis* complex. J Clin Microbiol. 1999; 37:1224–6. https://doi.org/10.1128/JCM.37.4.1224-1226.1999
23. Roychowdhury T, Mandal S, Bhattacharya A. Analysis of IS6110 insertion sites provide a glimpse into genome evolution of *Mycobacterium tuberculosis*. Sci Rep. 2015;5:12567. https://doi.org/10.1038/srep12567
24. Warit S, Billamas P, Makhao N, Jaitrong S, Juthayothin T, Yindeeyoungyeon W, et al. Detection of tuberculosis in cynomolgus macaques (*Macaca fascicularis*) using a supplementary monkey interferon Gamma releasing assay (mIGRA). Sci Rep. 2020;10:16759. https://doi.org/10.1038/s41598-020-73655-3
25. Kumar S, Stecher G, Li M, Knyaz C, Tamura K. MEGA X: molecular evolutionary genetics analysis across computing platforms. Mol Biol Evol. 2018;35:1547–9. https://doi.org/10.1093/molbev/msy096
26. Gengvinij N, Pattanakitsakul SN, Chierakul N, Chaiprasert A. Detection of *Mycobacterium tuberculosis* from sputum specimens using one-tube nested PCR. Southeast Asian J Trop Med Public Health. 2001;32:114–25.
27. Stunkard JA, Szatalowicz FT, Sudduth HC. A review and evaluation of tuberculin testing procedures used for *Macaca* species. Am J Vet Res. 1971;32:1873–8.
28. Eisenach KD, Sifford MD, Cave MD, Bates JH, Crawford JT. Detection of *Mycobacterium tuberculosis* in sputum samples using a polymerase chain reaction. Am Rev Respir Dis. 1991;144:1160–3. https://doi.org/10.1164/ajrccm/144.5.1160
29. Eisenach KD. Use of an insertion sequence for laboratory diagnosis and epidemiologic studies of tuberculosis. Ann Emerg Med. 1994;24:450–3. https://doi.org/10.1016/S0196-0644(94)70182-2
30. Scanga CA, Flynn JL. Modeling tuberculosis in nonhuman primates. Cold Spring Harb Perspect Med. 2014;4:a018564. https://doi.org/10.1101/cshperspect.a018564
31. Kaewchot S, Tangsudjai S, Sariya L, Mongkolphan C, Saechin A, Sariwongchan R, et al. Zoonotic pathogens survey in free-living long-tailed macaques in Thailand. Int J Vet Sci Med. 2022;10:11–8. https://doi.org/10.1080/23144599.2022.2040176
32. Mätz-Rensing K, Hartmann T, Wendel GM, Frick JS, Homolka S, Richter E, et al. Outbreak of tuberculosis in a colony of rhesus monkeys (*Macaca mulatta*) after possible indirect contact with a human TB patient. J Comp Pathol. 2015;153:81–91. https://doi.org/10.1016/j.jcpa.2015.05.006
33. Toyoda A, Matsudaira K, Maruhashi T, Malaivijitnond S, Kawamoto Y. Highly versatile, non-invasive method for collecting buccal DNA from free-ranging non-human primates. J Trop Biol Conserv. 2021;18:251–67. https://doi.org/10.51200/jtbc.v18i.3460
34. Wolf TM, Mugisha L, Shoyama FM, O'Malley MJ, Flynn JL, Asiimwe B, et al. Noninvasive test for tuberculosis detection among primates. Emerg Infect Dis. 2015;21:468–70. https://doi.org/10.3201/eid2103.140052
35. Nguyen L. Antibiotic resistance mechanisms in *M. tuberculosis*: an update. Arch Toxicol. 2016;90:1585–604. https://doi.org/10.1007/s00204-016-1727-6
36. Abdel-Moneim AS, Abdelwhab EM. Evidence for SARS-CoV-2 infection of animal hosts. Pathogens. 2020;9:529. https://doi.org/10.3390/pathogens9070529

Address for correspondence: Suchinda Malaivijitnond, National Primate Research Center of Thailand, Chulalongkorn University, Saraburi 18110, Thailand; email: suchinda.m@chula.ac.th

Increase in Colorado Tick Fever Virus Disease Cases and Effect of COVID-19 Pandemic on Behaviors and Testing Practices, Montana, 2020

Raymond A. Soto, Erika Baldry, Grace M. Vahey, Jennifer Lehman, Margaret Silver, Amanda Panella, Aaron C. Brault, Holly R. Hughes, Kelly A. Fitzpatrick, Jason Velez, Brad J. Biggerstaff, Brent Wolff, Jean Randolph, Laird J. Ruth, J. Erin Staples, Carolyn V. Gould

In 2020, Montana, USA, reported a large increase in Colorado tick fever (CTF) cases. To investigate potential causes of the increase, we conducted a case–control study of Montana residents who tested positive or negative for CTF during 2020, assessed healthcare providers' CTF awareness and testing practices, and reviewed CTF testing methods. Case-patients reported more time recreating outdoors on weekends, and all reported finding a tick on themselves before illness. No consistent changes were identified in provider practices. Previously, only CTF serologic testing was used in Montana. In 2020, because of SARS-CoV-2 testing needs, the state laboratory sent specimens for CTF testing to the Centers for Disease Control and Prevention, where more sensitive molecular methods are used. This change in testing probably increased the number of CTF cases detected. Molecular testing is optimal for CTF diagnosis during acute illness. Tick bite prevention measures should continue to be advised for persons doing outdoor activities.

Colorado tick fever (CTF) virus is a coltivirus in the family *Reoviridae* (*1*). The primary vector for CTF virus is the Rocky Mountain wood tick (*Dermacentor andersoni*), which is found at elevations of 4,000–10,000 feet in the western United States and Canada (*2*,*3*). The incubation period of CTF virus is usually 3–4 days (range 1–14 days). Patients with CTF virus disease commonly experience fever, headache, fatigue, myalgias, and a biphasic course (i.e., remission and relapse of symptoms with 1–4 days between remission and relapse). Approximately 15%–30% of patients with CTF are hospitalized, but severe complications such as meningoencephalitis, hepatitis, and epididymoorchitis are uncommon, occurring in <5% of patients; deaths related to CTF are rare (<1%) (*4*–*7*).

CTF virus disease is not nationally notifiable but is reportable in 9 states (Arizona, Colorado, Idaho, Montana, New Mexico, Oregon, South Dakota, Utah, and Wyoming), which voluntarily report cases to the Centers for Disease Control and Prevention (CDC). Because of shifts in reporting and testing practices, the numbers of cases reported from various states has fluctuated over time. During 2002–2019, a total of 108 CTF cases were identified from western states, a median of 5 cases per year, and ≤1 case per year in Montana (*7*,*8*). During 2020, a total of 21 CTF cases were reported among Montana residents.

The COVID-19 pandemic had several potential effects on risk, detection, and reporting of vectorborne diseases, including changes in individual behaviors affecting vector exposures, healthcare-seeking behaviors, healthcare provider test ordering practices, and diagnostic testing procedures, because of increased burden on state laboratories for SARS-CoV-2 testing. For example, CDC guidance recommended that persons engage in outdoor recreation to remain active while maintaining social distancing and reducing transmission of SARS-CoV-2 (*9*). In

Author affiliations: Centers for Disease Control and Prevention, Fort Collins, Colorado, USA (R.A. Soto, G.M. Vahey, J. Lehman, M. Silver, A. Panella, A.C. Brault, H.R. Hughes, K.A. Fitzpatrick, J. Velez, B.J. Biggerstaff, J.E. Staples, C.V. Gould); Montana Department of Health and Human Services, Helena, Montana, USA (E. Baldry); Centers for Disease Control and Prevention, Atlanta, Georgia, USA (B. Wolff, J. Randolph, L.J. Ruth)

DOI: https://doi.org/10.3201/eid2903.221240

2020, a historic number of persons visited national forests for recreation (*10*).

Our aim was to investigate the increase in CTF cases in Montana in 2020, including the potential effect of the COVID-19 pandemic and risk factors for CTF virus disease among residents of Montana. Therefore, we conducted a case–control study, surveyed healthcare providers, and evaluated diagnostic testing practices for CTF virus infection.

Methods

Case–Control Study

Testing for CTF virus infection at CDC's Arbovirus Diagnostic Laboratory (Fort Collins, CO, USA; Division of Vector-Borne Diseases, National Center for Emerging and Zoonotic Infectious Diseases) is performed at the request of state health departments. Testing uses reverse transcription PCR (RT-PCR) on serum or cerebrospinal fluid (CSF) samples collected <14 days after symptom onset and plaque-reduction neutralization test (PRNT) on specimens collected >14 days after symptom onset, as previously described (*11*,*12*). During the period under investigation, we conducted RT-PCR testing using primers targeting segment 3 of the viral genome (*12*). We based neutralizing antibody titers on the highest dilution of serum that reduced viral plaque formation by >90% (we considered a titer >10 to be positive). For specimens collected 8–21 days after symptom onset, we tested using both RT-PCR and PRNT on a case-by-case basis. We defined laboratory-confirmed recent infection as detection of CTF viral nucleic acid in a specimen or a seroconversion with >4-fold change in virus-specific neutralizing antibody titers between paired acute and convalescent serum specimens. We defined a probable infection as detection of virus-specific neutralizing antibodies in a single specimen because the timing of infection cannot be determined. IgM testing typically is not performed because the sensitivity for detection of IgM is lower than for neutralizing antibodies (*11*).

We identified case-patients and controls through a query of the Arbovirus Diagnostic Laboratory database. We defined a case-patient as a Montana resident who had symptom onset and a confirmed or probable CTF virus infection in 2020. We defined a control as a Montana resident who had symptom onset but negative testing for CTF virus infection in 2020. We contacted persons by phone to describe the investigation and offer participation in a survey collecting data on demographics, clinical symptoms, outdoor recreational and occupational exposures, tick exposures and prevention measures, and changes in behavior related to the COVID-19 pandemic. We collected specific location data for recreational activities and tick exposures whenever possible. Survey questions focused on the potential incubation or 2-week period before symptom onset in 2020 and the same period in 2019.

Healthcare Provider Survey

We developed a survey for healthcare providers and distributed them to staff in 13 hospitals in 10 public health jurisdictions in Montana where either a CTF case was reported in the previous 10 years or CTF virus testing was requested in 2020. The survey collected information on healthcare provider type and demographics, awareness and testing practices for CTF virus and other tickborne diseases, patient encounters for tick bites, and healthcare providers' interest in educational resources for CTF.

Diagnostic Testing Evaluation

We reviewed diagnostic laboratory methods used for CTF testing during 2020 and in previous years and calculated the proportion of specimens testing positive. To assess whether other tickborne diseases transmitted by *Dermacentor andersoni* ticks increased in Montana during 2020, we also examined trends in reported cases of Rocky Mountain spotted fever (RMSF) and tularemia.

Data Analysis

We managed data from participant interviews and the healthcare provider survey in Research Electronic Data Capture (Vanderbilt University, https://www.project-redcap.org) (*13*) and analyzed data using SAS (SAS Institute Inc., https://www.sas.com). For categorical variables, we calculated 95% CIs of the odds ratios (ORs) between case-patients and controls by using the score interval (*14*); given the rarity of CTF in the population, we expected OR estimates to provide reliable estimates of relative risk. For quantitative variables, we calculated 95% CIs of the differences in means by using the Welch-Satterthwaite approximation for the Student *t* interval (*15*). We determined statistical significance from the reported 95% CIs by noting whether they contained the null values of 1 for the ORs and 0 for the mean differences, enabling interpretation in a hypothesis-testing context at a significance level of $\alpha = 0.05$. We performed geospatial mapping of tick exposure locations by using ArcGIS 10.7.1 (Environmental Systems Research Institute, https://www.esri.com).

Results

Case–Control Study

Of 107 potential participants identified, including 21 case-patients and 86 controls, we were able to contact 36 (14 [67%] case-patients and 22 [26%] controls) who agreed to participate. Both groups consisted of predominantly non-Hispanic White men and had similar age distributions. Most participants from both groups reported having no underlying medical conditions. About one third of participants reported being tested for SARS-CoV-2 when they sought healthcare for their symptoms, and all reported a negative test result (Table 1).

Symptom onset dates for case-patients occurred during April 1–July 31, 2020; for controls, symptoms occurred during April 1–August 22, 2020. Case-patients were more likely to become symptomatic earlier in the year, having a peak in late April, compared with controls (Figure 1). Symptoms reported by over half of the participants were similar between groups and included fever, fatigue, muscle aches, headache, chills, weakness, and joint pain and swelling (Table 2). Case-patients (11 [79%]) were statistically significantly more likely to report a biphasic illness than controls (3 [14%]).

Almost half of all participants (44% [16/36]) reported spending more time outside in 2020 because of the COVID-19 pandemic compared with the same period in 2019, and we identified no difference between groups. A statistically significantly greater proportion of case-patients (86%) reported spending ≥4 hours outdoors recreating on weekends than controls (50%) (Table 3). Participants reported several outdoor activities; hiking or walking on unpaved trails was most common for both groups. Case-patients reported fewer instances of yardwork or gardening in the 2-week period before symptom onset than did controls and were statistically significantly more likely than controls to report finding a tick crawling on themselves (100% vs. 41%) or a tick attached to themselves (93% vs. 36%) (Table 3).

Among patients who reported finding ticks on themselves, 86% (12/14) of case-patients and 44% (4/9) of controls provided specific information about where they acquired the tick or ticks (Figure 2). Tick exposures occurred in national forests, in state parks, and on private land in several areas of Montana; 6/12 case-patients reported acquiring their tick or ticks in the vicinity of the Bitterroot Valley (5 in Ravalli County and 1 in Mineral County). One Montana resident with CTF reported acquiring a tick in Idaho (Figure 2). Except for 1 case-patient, all other case-patients reported that their tick exposures occurred in locations >4,000-ft elevation.

Healthcare Provider Survey

A total of 36 healthcare providers from 10 public health jurisdictions responded to the survey. Most respondents were physicians (22 [61%]), worked in outpatient clinics (24 [67%]), and had a nonpediatric specialty (26 [72%]). The median number of years practicing was 15

Table 1. Demographic characteristics of participants in a Colorado tick fever case–control study, Montana, USA, 2020*

Characteristic	Case-patients, n = 14	Controls, n = 22	OR (95% CI)
Sex			
M	10 (71)	12 (55)	2.1 (0.5–8.3)
F	4 (29)	10 (45)	0.5 (0.1–2.0)
Age group, y			
<21	5 (36)	4 (18)	2.5 (0.6–11.0)
21–44	3 (21)	10 (45)	0.3 (0.1–1.4)
45–64	5 (36)	5 (23)	1.9 (0.4–7.9)
≥65	1 (7)	3 (14)	0.5 (0.1–3.9)
Median age, y (range)	26 (1–70)	33 (7–84)	NA
Race			
White	14 (100)	22 (100)	0.6 (0.4–11.7)
Ethnicity			
Non-Hispanic or non-Latino	12 (86)	17 (77)	1.8 (0.3–9.2)
Hispanic or Latino	1 (7)	3 (14)	0.5 (0.1–3.9)
Other	1 (7)	2 (9)	0.8 (0.1–6.7)
Underlying medical condition			
None	11 (79)	13 (59)	2.5 (0.6–10.8)
Immunosuppressive condition or medication	0	2 (9)	0.3 (0.0–3.6)
Diabetes mellitus	0	2 (9)	0.3 (0.0–3.6)
Cardiovascular disease	1 (7)	3 (14)	0.5 (0.1–3.9)
Cancer	0	1 (5)	0.1 (0.0–1.3)
Other	2 (14)	2 (9)	1.7 (0.3–10.9)
SARS-CoV-2 testing during illness			
Tested	6 (43)	7 (32)	1.6 (0.4–6.3)
Positive	0	0	1.6 (0.1–28.1)

*Values are no (%) except as indicated. NA, not applicable; OR, odds ratio.

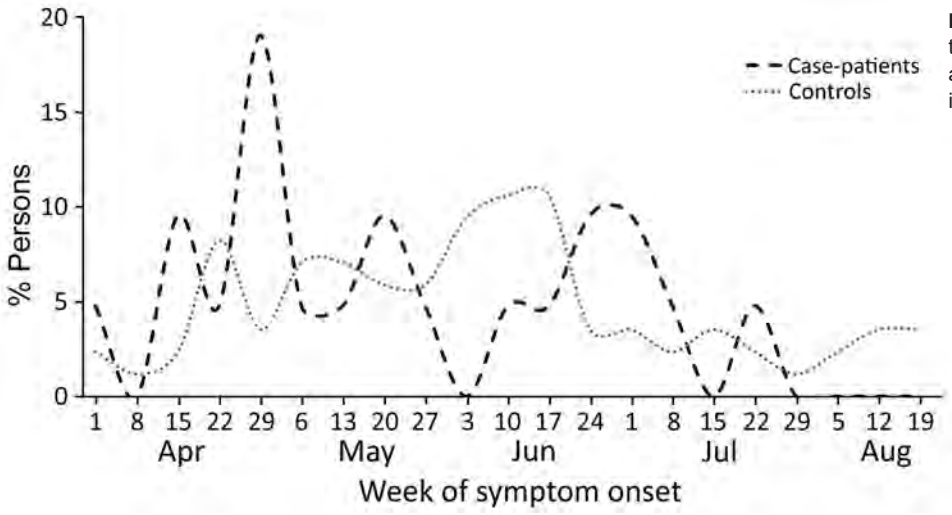

Figure 1. Percentage of Colorado tick fever case-patients (n = 21) and controls (n = 86), by week of illness onset, Montana, USA, 2020.

years (range 1–41 years), including 10 years (range 0.5–40 years) practicing in Montana. Only 2 providers indicated that they had more patients reporting tick bites in 2020 than in 2019, whereas 5 had fewer patients reporting tick bites in 2020 than in 2019. Three healthcare providers reported ordering more CTF virus tests in 2020 than in 2019, and 2 providers ordered fewer CTF tests. Most providers (31 [86%]) reported no change in their awareness of CTF virus in 2020 compared with 2019. Many providers (26 [72%]) were interested in educational resources for CTF.

Laboratory Testing Evaluation

Before 2020, testing for CTF virus in Montana was conducted by the state public health laboratory using an indirect immunofluorescence assay (IFA) to detect CTF virus–specific IgG antibodies (*16*,*17*). Cases were reported as probable if virus-specific IgG was detected in a single serum specimen and confirmed if a 4-fold rise in IgG was detected between paired acute and convalescent serum specimens. During 2011–2019, a median of 156 specimens (range 90–208 specimens) were tested for CTF annually by using IFA, and average positivity was 1.3% (Table 4). We did not have data on the numbers of specimens tested per patient or timing of specimen collection in relation to onset.

In 2020, because of the surge in SARS-CoV-2 testing, Montana began sending specimens for CTF testing to CDC, which primarily used RT-PCR for acute specimens and PRNT for convalescent specimens. A total of 137 CTF tests were performed at CDC on specimens sent on behalf of 107 Montana residents with symptom onset in 2020; of those, 21 tests (15.3%) were positive. Of the RT-PCR tests performed, 18/84 (21.4%) were positive (confirmed cases) on serum specimens collected a median of 3 days (range 0–14

Table 2. Self-reported symptoms leading to Colorado tick fever virus testing of case–control study participants, Montana, USA, 2020*

Symptom	No. (%)		OR (95% CI)
	Case-patients, n = 14	Controls, n = 22	
Fever	13 (93)	14 (64)	7.4 (1.0–50.7)
Fatigue	13 (93)	18 (82)	2.9 (0.4–21.0)
Muscle aches	12 (86)	18 (82)	1.3 (0.2–7.2)
Headache	11 (79)	17 (77)	1.1 (0.2–4.9)
Chills	9 (64)	13 (59)	1.3 (0.3–4.8)
Weakness	9 (64)	17 (77)	0.5 (0.1–2.2)
Nausea	8 (57)	9 (41)	1.9 (0.5–7.3)
Joint pain or swelling	8 (57)	15 (68)	0.6 (0.2–2.4)
Rash	5 (36)	13 (59)	0.4 (0,1–1.5)
Stiff neck	5 (36)	10 (45)	0.7 (0.2–2.6)
Abdominal pain	5 (36)	5 (23)	1.9 (0.4–7.9)
Swollen lymph nodes	4 (28)	11 (50)	0.4 (0.1–1.5)
Confusion	4 (28)	10 (45)	0.5 (0.1–1.9)
Vomiting	4 (28)	3 (14)	2.5 (0.5–12.3)
Diarrhea	3 (21)	5 (23)	0.9 (0.2–4.4)
Sore throat	3 (21)	7 (32)	0.6 (0.1–2.6)
Biphasic illness†	11 (79)	3 (14)	**23.2 (4.2–128.6)**

*Bold indicates statistical significance (α = 0.05). OR, odds ratio.
†Defined as remission and relapse of symptoms with 1–4 d between remission and relapse when dates were provided.

Table 3. Outdoor and tick exposures during the 2 weeks before illness onset for participants in a Colorado tick fever case–control study, Montana, USA, 2020*

Risk factor	Case-patients, n = 14	Controls, n = 22	OR or SD (95% CI)
Employment status			
Employed	7 (50)	12 (55)	0.8 (0.2–3.1)
Retired	2 (14)	4 (18)	0.7 (0.1–4.2)
Student or dependent child	5 (36)	5 (23)	1.9 (0.4–7.9)
Occupational outdoor activities	5/7 (71)	4/12 (33)	5.0 (0.7–33.5)
More outdoor recreation because of COVID-19 pandemic	6 (43)	10 (45)	0.9 (0.2–3.4)
Recreational outdoor activities			
≥4 h outside per weekday	6 (43)	5 (23)	2.5 (0.6–10.5)
≥4 h outside per weekend day	12 (86)	11 (50)	**6.0 (1.2–29.2)**
Average total time outside, h (SD)	83.3 (77.2)	51.3 [47.5)	31.9 (–16.1 to 80.0)
Specific recreational outdoor activities			
Yard work or gardening	8 (58)	15 (68)	0.6 (0.2 to 2.4)
Average no. times (SD)	2.9 (1.7)	7 [4.7)	**–4.0 (–6.8 to –1.2)**
Hunting or fishing	5 (36)	7 (32)	1.2 (0.3 to 4.7)
Average no. times (SD)	2.8 (1.6)	3.1 [1.0)	–0.3 (–2.4 to 1.7)
Hiking/walking/running on unpaved trails	12 (86)	15 (68)	2.8 (0.5 to 13.9)
Average no. times (SD)	5.6 (3.5)	8.9 [6.0)	–3.3 (–7.2 to 0.7)
Camping	6 (43)	6 (27)	2.0 (0.5 to 8.0)
Average no. times (SD)	4.2 (1.7)	2.8 [1.2)	1.3 (–0.6 to 3.3)
Off-road mountain biking	2 (14)	5 (23)	0.6 (0.1 to 3.1)
Average no. (SD)	5 (0)	3.3 [2.2)	1.7 (–1.0 to 4.4)
Personal tick prevention measures			
Used repellent or repellent-treated clothing	3 (21)	10 (45)	0.3 (0.1–1.4)
Checked self for ticks	14 (100)	10 (45)	**34.5 (3.0–365.3)**
Wore long pants	11 (78)	15 (68)	1.7 (0.4–7.5)
Wore long sleeves	12 (86)	14 (64)	3.4 (0.7–16.9)
Found a tick on self	14 (100)	9 (41)	**41.2 (3.5–436.6)**
Found tick attached to self	13 (93)	8 (36)	**22.7 (3.0–156.0)**
Location where tick acquired			
National Forest	8/12 (67)	4/4 (100)	0.2 (0.0–3.0)
State Park	2/12 (17)	0/4 (0)	2.1 (0.1–27.0)
Private land	2/12 (17)	0/4 (0)	2.1 (0.1–27.0)

*Values are no (%) except as indicated. Bold indicates statistical significance ($\alpha = 0.05$). OR, odds ratio.

days) after symptom onset. Of the PRNT tests performed, 3/53 (5.7%) were positive (probable cases) on serum specimens collected 17, 23, and 42 days after symptom onset. For 25 patients, RT-PCR and PRNT were performed on the same specimen; of these, 4 had discordant results, 3 (12%) were RT-PCR-positive and PRNT-negative (collected 8, 12, and 14 days after onset), 1 was RT-PCR-negative and PRNT-positive (collected 17 days after onset), and 21 had concordant negative results (Table 4).

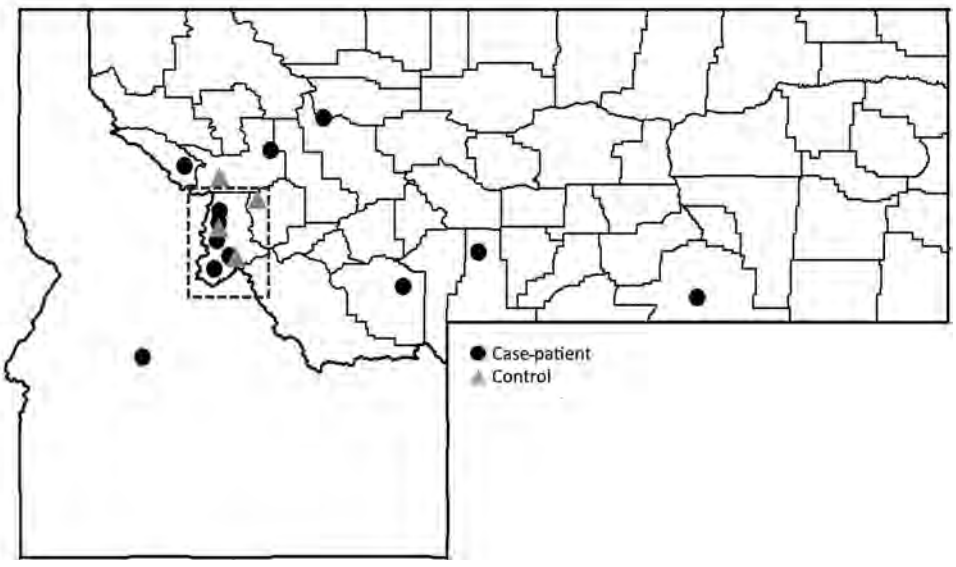

Figure 2. Geographic locations in Montana and Idaho, USA, where case-patients (n = 12) and controls (n = 4) reported tick acquisition during the 2 weeks before symptom onset in a Colorado tick fever case–control study, Montana, USA, 2020. Ravalli County (dashed box) had the most case-patient tick acquisitions (5); Missoula, Mineral, Madison, Park, Big Horn, and Lewis and Clark each had 1 acquisition. One case-patient acquired a tick in Idaho.

Table 4. Laboratory testing for Colorado tick fever virus infection performed on specimens from Montana, USA, 2011–2020*

Year	Assay	No. tests performed	No. (%) tests positive
2011	IFA	90	0
2012	IFA	141	2 (1.4)
2013	IFA	168	0
2014	IFA	143	2 (1.4)
2015	IFA	199	4 (2.0)
2016	IFA	120	3 (2.5)
2017	IFA	172	4 (2.3)
2018	IFA	208	3 (1.4)
2019	IFA	170	3 (1.8)
2020	RT-PCR	84	18 (21.4)
	PRNT	53	3 (5.7)
	Total	137	21 (15.3)

*IFA, indirect immunofluorescence assay for IgG; PRNT, plaque-reduction neutralization test; RT-PCR, reverse transcription PCR.

During 2020, no changes occurred in testing for RMSF or tularemia. The numbers of cases reported were within the range of those reported during previous years in Montana: 2 cases of RMSF reported in 2020 compared with an average of 5 cases (range 1–11 cases) during 2010–2019, and 1 case of tularemia in 2020 compared with an average of 4 cases (range 1–7 cases) during 2010–2019.

Discussion

Using a multifaceted approach, we investigated the effect the COVID-19 pandemic might have had on CTF virus infection risk and diagnosis in Montana in 2020. Because of the pandemic, persons were more likely to spend time outdoors, and many persons with CTF reported acquiring ticks in areas of Montana known to be endemic for CTF virus. However, a switch from serologic to primarily molecular testing on acute-phase specimens that occurred because of the surge in demand for SARS-CoV-2 testing was most likely responsible for the increase in CTF cases detected.

Unlike most domestic arthropodborne viruses, CTF virus infection is characterized by a sustained viremic period caused by infection of hematopoietic progenitor cells and delayed antibody response (*12*). CTF viral RNA can usually be detected by RT-PCR during the first 2 weeks of illness and for up to 6 weeks after illness onset (*1*,*7*,*12*). CTF virus–specific antibodies are undetectable in >50% of patients at 2 weeks after illness onset, but neutralizing antibodies are detectable in >90% of patients by 4 weeks after illness onset (*1*,*7*,*11*,*16*). Therefore, RT-PCR testing is recommended for acute-phase specimens (collected <14 days after symptom onset), and serologic testing (e.g., IFA or PRNT) is recommended for specimens collected ≥2 weeks symptom onset (*11*,*12*,*18*). Previous studies comparing IFA to PRNT assays for serologic diagnosis of CTF demonstrated comparable performance (*16*). As a crude comparison, we found that the proportion of RT-PCR tests positive during 2020 was ≈20-fold higher compared with the proportion of tests positive by IFA in previous years; however, we were unable to test specimens from previous years to directly compare the assay performances.

CTF used to be one of the most frequently reported domestic arboviral diseases. Beginning in the late 1980s, the numbers of CTF cases reported to CDC began decreasing, probably because of changes in land use, testing, and reporting practices (*4*,*7*). Because CTF is not a nationally notifiable condition, reporting is based on individual state requirements, and not all states where CTF virus is known to be endemic have reported consistently over time (*7*). Furthermore, diagnostic testing methods among states are variable; before 2006, most available CTF testing was done by serologic testing only (*4*,*7*). Therefore, historical trends are difficult to assess, and the actual prevalence of CTF is probably underappreciated.

The findings of this investigation are consistent with national trends showing that outdoor recreation increased during the COVID-19 pandemic. More time spent recreating outdoors can increase the likelihood of persons being exposed to vectors that can transmit infections. A recent report on Lyme disease surveillance in the United States found that ≈50% of respondents to a consumer survey reported spending more time outdoors in 2020 than in previous years, similar to our results (*19*). Reports from Switzerland and Germany during the summer of 2020 demonstrated a substantial increase in endemic tickborne encephalitis virus but decreases in travel-related vectorborne diseases such as dengue and malaria (*20*,*21*). Both reports attributed the increase in cases primarily to increased outdoor activity. Although 44% of our participants reported spending more time outdoors in 2020 compared with 2019, case-patients and controls reported a similar change in behavior. Furthermore, we did not see an increase in the number of other diseases

transmitted by the same tick vector for which testing algorithms did not change, including RMSF and tularemia, and providers did not report an increase in patient encounters with tick exposure histories in 2020. Although tularemia can be spread by other routes, the lack of an increase in either of these diseases is supportive evidence that the CTF testing protocol change was the major factor leading to an increase in CTF cases detected.

These findings also indicate that the locations where case-patients spent their time recreating and were exposed to ticks probably contributed to the case-patients becoming infected. In addition, greater awareness of tickborne diseases in highly endemic areas might have led to more testing of patients exposed in these regions. Half (6 of 12) of patients with CTF who knew where they acquired a tick before becoming ill reported acquiring ticks in the Bitterroot Valley. The Bitterroot Valley, located between the Bitterroot and Sapphire Mountains in Ravalli and Missoula Counties, has historically been an endemic area for CTF virus; a survey of ticks collected during 2002–2003 and 2009–2013 in the Bitterroot Valley found a 6.6% prevalence of infection with CTF virus (*22*). On the basis of the specific location data provided by participants, CDC and the Montana Department of Public Health and Human Services worked with partners at the US Forest Service and Montana Department of Fish, Wildlife, and Parks to distribute social media messages and trail signs on tick-prevention measures and CTF awareness to targeted areas identified during this investigation.

The first limitation of our study is that the small number of participants and our convenience sample of controls with suspected tickborne diseases could have limited the precision of our estimates and our power to detect differences. In addition, given the relatively few case-patients able to participate in the study, reliable evaluation of confounding or identification of potential effect modifiers of the identified risk factors was not possible. We report a range of 95% CI estimates for both ORs and mean differences, and several of these are wide, given the context of the application. Although our results are consistent with what is known about the epidemiology of CTF in Montana and are not unexpected, caution should be used when interpreting imprecise results. Further, selection was nonrandom, and participation was self-selected, so our results may be subject to related unmeasurable biases. The results were probably subject to participant recall bias and accentuated by delays in the investigation related to the COVID-19 pandemic. Finally, although the molecular testing performed at CDC might have increased the proportion of specimens identified as positive, we did not test specimens from previous years to directly compare sensitivities of the assays.

To help potentially improve case detection and to address healthcare provider interest in additional CTF resources identified during this investigation, CDC developed and distributed a pocket card with information about CTF, including epidemiology, clinical findings, prevention, and testing recommendations (https://www.cdc.gov/coloradotickfever/diagnostic-testing.html). CDC also created a tickborne viral disease training module for clinicians, which includes information on CTF, Powassan, Heartland, and Bourbon virus diseases and provides continuing education credits (https://tceols.cdc.gov/course/detail2/8642).

In summary, the increase in CTF cases reported by Montana in 2020 was most likely caused by the shift in use of molecular testing for CTF, which is recommended during the acute phase of illness. State public health laboratories should consider molecular testing for CTF, and support for adopting this testing platform can be obtained from CDC on request. Greater outdoor recreation, particularly in areas endemic for CTF, was an identified modifiable risk factor. Although outdoor recreation should be encouraged, persons who work or recreate in CTF-endemic areas should continue to be advised to take precautions to avoid tick exposures, such as using insect repellent approved by the US Environmental Protection Agency, performing tick checks when returning from outdoor activities (https://www.cdc.gov/ticks/avoid/on_people.html), and promptly removing ticks.

E.B. reports an Epidemiology and Laboratory Capacity Cooperative Agreement grant from CDC during the conduct of the study. None of the investigative work was funded by an outside source.

About the Author

Dr. Soto is an Epidemic Intelligence Service officer assigned to the Division of Vector-Borne Diseases, National Center for Emerging and Zoonotic Infectious Diseases, CDC. His primary research interests are vectorborne disease, arboviruses, and surveillance.

References

1. Staples JE. Reoviruses: Colorado tick fever virus and other vector-borne reoviruses. In: Kaslow RA, Stanberry LR, LeDuc JW, editors. Viral infections of humans: epidemiology and control. New York: Springer; 2022.

2. Florio L, Miller MS, Mugrage ER. Colorado tick fever; isolations of virus from *Dermacentar variabilis* obtained from Long Island, New York, with immunological comparisons between Eastern and Western strains. J Immunol. 1950;64:265–72.
3. James AM, Freier JE, Keirans JE, Durden LA, Mertins JW, Schlater JL. Distribution, seasonality, and hosts of the Rocky Mountain wood tick in the United States. J Med Entomol. 2006;43:17–24. https://doi.org/10.1093/jmedent/43.1.17
4. Brackney MM, Marfin AA, Staples JE, Stallones L, Keefe T, Black WC, et al. Epidemiology of Colorado tick fever in Montana, Utah, and Wyoming, 1995–2003. Vector Borne Zoonotic Dis. 2010;10:381–5. https://doi.org/10.1089/vbz.2009.0065
5. Goodpasture HC, Poland JD, Francy DB, Bowen GS, Horn KA. Colorado tick fever: clinical, epidemiologic, and laboratory aspects of 228 cases in Colorado in 1973–1974. Ann Intern Med. 1978;88:303–10. https://doi.org/10.7326/0003-4819-88-3-303
6. Spruance SL, Bailey A. Colorado tick fever. A review of 115 laboratory confirmed cases. Arch Intern Med. 1973;131:288–93. https://doi.org/10.1001/archinte.1973.00320080124018
7. Yendell SJ, Fischer M, Staples JE. Colorado tick fever in the United States, 2002–2012. Vector Borne Zoonotic Dis. 2015;15:311–6. https://doi.org/10.1089/vbz.2014.1755
8. Centers for Disease Control and Prevention. Colorado tick fever: statistics and maps [cited 2022 Dec 6]. https://www.cdc.gov/coloradotickfever/statistics.html
9. Centers for Disease Control and Prevention. COVID-19: how to protect yourself and others [cited 2022 Dec 6]. https://www.cdc.gov/coronavirus/2019-ncov/prevent-getting-sick/prevention.html
10. US Department of Agriculture. National Visitor Use Monitoring Program: 2020 national report [cited 2022 Dec 6]. https://www.fs.usda.gov/about-agency/nvum
11. Calisher CH, Poland JD, Calisher SB, Warmoth LA. Diagnosis of Colorado tick fever virus infection by enzyme immunoassays for immunoglobulin M and G antibodies. J Clin Microbiol. 1985;22:84–8. https://doi.org/10.1128/jcm.22.1.84-88.1985
12. Lambert AJ, Kosoy O, Velez JO, Russell BJ, Lanciotti RS. Detection of Colorado tick fever viral RNA in acute human serum samples by a quantitative real-time RT-PCR assay. J Virol Methods. 2007;140:43–8. https://doi.org/10.1016/j.jviromet.2006.10.014
13. Harris PA, Taylor R, Thielke R, Payne J, Gonzalez N, Conde JG. Research electronic data capture (REDCap)—a metadata-driven methodology and workflow process for providing translational research informatics support. J Biomed Inform. 2009;42:377–81. https://doi.org/10.1016/j.jbi.2008.08.010
14. Miettinen O, Nurminen M. Comparative analysis of two rates. Stat Med. 1985;4:213–26. https://doi.org/10.1002/sim.4780040211
15. Satterthwaite FE. An approximate distribution of estimates of variance components. Biometrics. 1946;2:110–4. https://doi.org/10.2307/3002019
16. Emmons RW, Dondero DV, Devlin V, Lennette EH. Serologic diagnosis of Colorado tick fever. A comparison of complement-fixation, immunofluorescence, and plaque-reduction methods. Am J Trop Med Hyg. 1969;18:796–802. https://doi.org/10.4269/ajtmh.1969.18.796
17. Montana Department of Public Health and Human Services. Montana Public Health Laboratory laboratory services manual [cited 2022 Dec 6]. https://dphhs.mt.gov/assets/publichealth/Lab/PublicHealthLabTesting/PHLLabManual.pdf
18. Piantadosi A, Kanjilal S. Diagnostic approach for arboviral infections in the United States. J Clin Microbiol. 2020;58:e01926–19. https://doi.org/10.1128/JCM.01926-19
19. McCormick DW, Kugeler KJ, Marx GE, Jayanthi P, Dietz S, Mead P, et al. Effects of COVID-19 pandemic on reported Lyme disease, United States, 2020. Emerg Infect Dis. 2021;27:2715–7. https://doi.org/10.3201/eid2710.210903
20. Steffen R, Lautenschlager S, Fehr J. Travel restrictions and lockdown during the COVID-19 pandemic-impact on notified infectious diseases in Switzerland. J Travel Med. 2020;27:27. https://doi.org/10.1093/jtm/taaa180
21. Ullrich A, Schranz M, Rexroth U, Hamouda O, Schaade L, Diercke M, et al.; Robert Koch's Infectious Disease Surveillance Group. Impact of the COVID-19 pandemic and associated non-pharmaceutical interventions on other notifiable infectious diseases in Germany: an analysis of national surveillance data during week 1–2016–week 32–2020. Lancet Reg Health Eur. 2021;6:100103. https://doi.org/10.1016/j.lanepe.2021.100103
22. Williamson BN, Fischer RJ, Lopez JE, Ebihara H, Schwan TG. Prevalence and strains of Colorado tick fever virus in Rocky Mountain wood ticks in the Bitterroot Valley, Montana. Vector Borne Zoonotic Dis. 2019;19:694–702. https://doi.org/10.1089/vbz.2018.2407

Address for correspondence: Carolyn Gould, Centers for Disease Control and Prevention, 3156 Rampart Rd, Mailstop P-02, Fort Collins, CO, 80521, USA; email: cgould@cdc.gov

Comparative Effectiveness of COVID-19 Vaccines in Preventing Infections and Disease Progression from SARS-CoV-2 Omicron BA.5 and BA.2, Portugal

Irina Kislaya,[1] Pedro Casaca,[1] Vítor Borges, Carlos Sousa, Bibiana I. Ferreira, Ana Fonte, Eugénia Fernandes, Carlos Matias Dias, Sílvia Duarte, José Pedro Almeida, Inês Grenho, Luís Coelho, Rita Ferreira, Patrícia Pita Ferreira, Cláudia Medeiros Borges, Joana Isidro, Miguel Pinto, Luís Menezes, Daniel Sobral, Alexandra Nunes, Daniela Santos, António Maia Gonçalves, Luís Vieira, João Paulo Gomes, Pedro Pinto Leite, Baltazar Nunes, Ausenda Machado,[2] André Peralta-Santos[2]

We estimated comparative primary and booster vaccine effectiveness (VE) of SARS-CoV-2 Omicron BA.5 and BA.2 lineages against infection and disease progression. During April–June 2022, we implemented a case–case and cohort study and classified lineages using whole-genome sequencing or spike gene target failure. For the case–case study, we estimated the adjusted odds ratios (aORs) of vaccination using a logistic regression. For the cohort study, we estimated VE against disease progression using a penalized logistic regression. We observed no reduced VE for primary (aOR 1.07 [95% CI 0.93–1.23]) or booster (aOR 0.96 [95% CI 0.84–1.09]) vaccination against BA.5 infection. Among BA.5 case-patients, booster VE against progression to hospitalization was lower than that among BA.2 case-patients (VE 77% [95% CI 49%–90%] vs. VE 93% [95% CI 86%–97%]). Although booster vaccination is less effective against BA.5 than against BA.2, it offers substantial protection against progression from BA.5 infection to severe disease.

The BA.5 lineage of the SARS-CoV-2 Omicron variant emerged in South Africa in February 2022 (*1*) and rapidly spread to other countries (*2*). In Portugal, the first BA.5 case was detected on March 29, 2022, and BA.5 became predominant by epidemiologic week 19 of 2022 (May 9–15) (*3*), leading to a new surge in SARS-CoV-2 infections, hospitalizations, and deaths (*4*).

Early data showed that protection against BA.4/5 conferred by a previous pre–Omicron SARS-CoV-2 variant infection was low (*5*). Studies from the United Kingdom (*6*) and Denmark (*7*) indicated no differences in the odds of having been vaccinated between BA.5 and BA.2 case-patients, suggesting no differences in the vaccine performance against infection. A severity assessment from South Africa indicated no differences in the risk for severe hospitalization or death during the BA.4/5 wave compared with the BA.1 wave (*8*). In contrast, a study from Denmark indicated higher odds of hospitalization among BA.5 case-patients compared with BA.2 case-patients, even among those vaccinated with a booster dose (*7*). Those studies have not addressed potential differences in vaccine effectiveness (VE) against severe outcomes or disease progression between the 2 lineages.

Author affiliations: Instituto Nacional de Saúde Doutor Ricardo Jorge, Lisbon, Portugal (I. Kislaya, V. Borges, C. Matias Dias, S. Duarte, L. Coelho, R. Ferreira, J. Isidro, M. Pinto, D. Sobral, A. Nunes, D. Santos, L. Vieira, J.P. Gomes, B. Nunes, A. Machado); Comprehensive Health Research Centre, Lisbon (I. Kislaya, C. Matias Dias, B. Nunes, A. Machado, A. Peralta-Santos); Direção-Geral da Saúde, Lisbon (P. Casaca, E. Fernandes, P. Pita Ferreira, P. Pinto Leite, A. Peralta-Santos); Unilabs, Porto, Portugal (C. Sousa, J.P. Almeida, L. Menezes, A. Maia Gonçalves); Algarve Biomedical Center Research Institute, Faro, Portugal (B.I. Ferreira, I. Grenho); Administração Central do Sistema de Saúde, Lisbon (A. Fonte, C.M. Borges)

DOI: https://doi.org/10.3201/eid2903.221367

[1]These first authors contributed equally to this article.

[2]These authors contributed equally to this article.

VE against emerging SARS-CoV-2 variants has become a pressing issue (*9*). In the context of highly vaccinated populations and challenges with establishing a negative control group, alternative study designs can be helpful. Case–case studies based on surveillance data that include only infected case-patients have been shown to be feasible for rapid evaluation of changes in VE against SARS-CoV-2 infection in the context of variants replacing other variants (*10*–*12*). Moreover, integrating the surveillance data on COVID-19 outcomes of different severity levels enables timely assessment of changes in VE against severe disease, which can be achieved by estimating VE against disease progression in infected case-patients (*13*,*14*). According to Halloran et al. (*14*), VE against severe outcomes estimated with traditional study designs can be expressed as a product of 2 components, VE against infection and VE against progression from infection to a severe outcome. Therefore, the reduction of VE against disease progression with a new variant would also lead to a decrease in VE against a severe outcome.

Our study builds on previous work to address this knowledge gap (*10*,*15*; A. Peralta-Santos, et al., unpub. data, https://doi.org/10.1101/2022.01.20.22269406). We aimed to measure the comparative VE of complete primary vaccination and first booster dose between Omicron BA.5 and BA.2 lineages against infection and compare lineage-specific VE against progression to severe COVID-19 outcomes that require hospitalization.

Methods

Study Design and Population

First, we conducted a case–case study to compare the odds of vaccination between persons infected with SARS-CoV-2 Omicron lineages BA.5 and BA.2. Second, we followed a cohort of BA.2- and BA.5-infected persons to compare lineage-specific VE against progression from infection to hospitalization (VEp). We estimated VEp by comparing the risk for severe outcomes in vaccinated infected and unvaccinated infected persons (*14*).

We included persons from mainland Portugal who had SARS-CoV-2 diagnosed by an reverse transcription PCR (RT-PCR) test and and had their illness reported to Portugal's national surveillance system during April 25–June 10, 2022. We excluded SARS-CoV-2 case-patients who were not eligible for booster vaccination (i.e., those <18 years of age) and residents in the autonomous regions of Madeira and Azores or for whom residence information was unavailable. Further, we excluded those vaccinated with brands other than the ones used in Portugal; vaccinated with a combination of brands other than the ones recommended by the vaccines' manufacturers; vaccinated with an interval period between the 2 doses shorter than that recommended by the manufacturer; vaccinated with the second booster dose or with an incomplete vaccination scheme; infected with variants other than BA.2 and BA.5 according to whole-genome sequencing (WGS) results. Finally, we excluded those who had suspected cases of nosocomial infection.

The testing policies remained stable during the study period, and all symptomatic patients were eligible for a free diagnostic test. All patients admitted to a hospital were tested at admission, even if asymptomatic. However, during April 29–May 23, 2022, rapid antigen tests were not available free of charge, and some asymptomatic infections might have been undiagnosed. The overall positivity rate during the study period was very high (≈50%) (*16*).

Case Selection and Variant Classification

We classified samples as BA.2 or BA.5 according to spike gene target failure (SGTF) status (BA.5 as SGTF, BA.2 as non-SGTF) or by WGS. WGS data was provided by the National Genomics Surveillance Network, which conducts nationwide random sequencing surveys weekly (*3*). SGTF data was provided by 2 clinical pathology laboratories (UNILABS and Algarve Biomedical Center Laboratory) that operate in mainland Portugal and use the TaqPath COVID-19 RT-PCR (ThermoFisher, https://www.thermofisher.com), enabling identification of samples with SGTF or non-SGTF status. Those 2 laboratories detected ≈3% of diagnosed cases at the national level during the study period. For SGTF-based classification, we considered only samples with both nucleocapsid and open reading frame 1a positive signals and cycle threshold values ≤30.

We defined a COVID-19 hospitalization as any admission (of ≥24 hours' duration) of a patient to the National Health Service (NHS) hospitals in mainland Portugal with a SARS-CoV-2 diagnosis classified as BA.2 or BA.5 infection. We obtained data from Portgual's Integrated Hospital Information System registry, which captures information from NHS hospitals and registers COVID-19 admissions for all the patients with primary or secondary COVID-19 diagnoses hospitalized in COVID-19 dedicated facilities. In Portugal, NHS covers the cost of nearly all COVID-19 hospitalizations.

Exposure Definition

We extracted vaccination status from the nationwide electronic vaccination registry and classified

them as unvaccinated (i.e., no record of COVID-19 vaccine administration), complete primary vaccination received, or booster dose vaccination received. We included a patient in the primary vaccination category if the SARS-CoV-2 infection diagnosis occurred ≥14 days after the complete vaccination regimen according to the product characteristics (i.e., >14 days after the second dose of mRNA BNT162b2 [Comirnaty, https://www.pfizer.com], mRNA-1273 SARS-CoV-2 [Moderna, https://www.modernatx.com] or AstraZeneca [https://www.astrazeneca.com] vaccines or ≥14 days after the single dose of the Johnson & Johnson/Janssen [https://www.jnj.com] COVID-19 vaccine). We included a patient in the booster dose vaccination if a SARS-CoV-2 infection diagnosis occurred ≥14 days after the first mRNA booster dose.

Other Covariates

We collected information on age, sex, region of residence, and swab collection date through Portugal's national surveillance system. We defined a previous infection as a positive RT-PCR or rapid antigen SARS-CoV-2 test result for the same patient >90 days apart. Data extraction and deterministic linkage of electronic health records with laboratory data were performed on July 12, 2022, by the General Directorate of Health team using the National Health Service user number, a unique identifier for health services in Portugal.

Statistical Analysis

We used absolute and relative frequencies to describe BA.2 and BA.5 case characteristics. In a case–case design, we estimated the odds of vaccination (primary and first booster dose) and previous infection in BA.5 case-patients compared with BA.2 case-patients by using a logistic regression model adjusted for sex, age group, region of residence, and week of swab collection.

For interpretation, we expect no differences in VE between 2 lineages if the odds of vaccination in BA.5 case-patients are higher than for BA.2 case-patients, the OR estimate is >1, suggesting that VE is lower for BA.5 lineage compared with BA.2. If the odds of vaccination are similar between BA.2 and BA.5, (i.e., OR = 1), we expect no differences in VE between 2 lineages. The OR for the previous infection can be interpreted similarly; an OR >1 suggests less protection conferred by the previous infection against BA.5 compared with BA.2. In addition, we combined previous infection and vaccination exposure to compare levels of protection conferred by so-called hybrid immunity between BA.5 and BA.2 lineages.

To reduce the bias caused by rare events, we estimated VEp in BA.5 and BA.2 case-patients by using penalized logistic regression (Firth's penalized likelihood method) (*17*), adjusting for sex, age group, region of residency, and week of swab collection. To compare lineage-specific VEp estimates, we included an interaction term between lineage and vaccination status in the models. The OR for the lineage and vaccination status interaction can be interpreted as measure of relative VE to prevent progression to severe outcomes among patients infected with BA.5 compared with BA.2.

We performed all statistical analyses with Stata 15.1 software (StataCorp, https://www.stata.com). All tests were 2-sided, and we considered a p value <0.05 to be statistically significant.

Ethics Considerations

The genomic surveillance of SARS-CoV-2 in Portugal is regulated by the Assistant Secretary of State and Health Executive Order (dispatch no. 331/2021, issued January 11, 2021). The study protocol received clearance from the Ethics Committee of Portugal's Instituto Nacional de Saúde Doutor Ricardo Jorge on June 15, 2022.

Results

Study Participant Characteristics

For the period April 25–June 10, 2022, we included 27,702 SARS-CoV-2–positive case-patients (15,396 with the BA.2 variant and 12,306 with BA.5). A total of 106 COVID-19 hospitalization occurred (54 [0.4%] among patients infected with BA.2 and 52 [0.4%] among those infected with BA.5). Most cases (91.2%) were classified using SGTF. Sex distribution was similar between the 2 groups (BA.5 case-patients were slightly younger than BA.2 case-patients), and BA.5 was more frequent in Alentejo and Centro regions (Table 1). Both groups had a similar percentage of nonvaccinated case-patients (4%–5%), but the BA.5 group had a higher percentage of case-patients who received complete primary vaccination (20.6% vs. 15.8%), and BA.2 case-patients had a higher percentage of patients who had received the first booster dose (80.1% vs. 74.7%). Also, the percentage of case-patients with a previous COVID-19 infection was higher among BA.5 case-patients (10.0%) than among BA.2 case-patients (5.6%).

Case–Case Study

For the case–case study, the odds of complete primary vaccination (aOR 1.07 [95% CI 0.93–1.23]) or first

Table 1. Sociodemographic and clinical characteristics of COVID-19 case-patients in the study sample, by SARS-CoV-2 variant, Portugal, April 25–June 10, 2022

Characteristic	No. (%) patients	
	BA.5, n = 12,306	BA.2, n = 15,396
Sex		
F	7,176 (58.3)	9,043 (58.7)
M	5,130 (41.7)	6,353 (41.3)
Age group, y		
18–29	3,474 (28.2)	3,299 (21.4)
30–39	2,059 (16.7)	2,922 (19.0)
40–49	2,475 (20.1)	3,431 (22.3)
50–59	1,974 (16.0)	2,581 (16.8)
60–69	1,089 (8.9)	1,567 (10.2)
≥70	1,235 (10.0)	1,596 (10.4)
Region		
Alentejo	1,280 (10.4)	752 (4.9)
Algarve	325 (2.6)	487 (3.2)
Centro	1,401 (11.4)	972 (6.3)
Lisboa e Vale do Tejo	1,462 (11.9)	3,396 (22.1)
Norte	7,838 (63.7)	9,789 (63.6)
Epidemiologic week of diagnosis, 2022		
Week 17	980 (8.0)	4,200 (27.3)
Week 18	3,237 (26.3)	5,691 (37.0)
Week 19	5,655 (46.0)	4,763 (30.9)
Week 20	1,080 (8.8)	492 (3.2)
Week 21	799 (6.5)	174 (1.1)
Week 22	348 (2.8)	56 (0.4)
Week 23	207 (1.7)	20 (0.1)
COVID-19 vaccination status		
Not vaccinated	590 (4.8)	631 (4.1)
Complete primary vaccination	2,530 (20.6)	2,434 (15.8)
First booster vaccination	9,186 (74.7)	12,331 (80.1)
Previous SARS-CoV-2 infection		
No	11,073 (90.0)	14,536 (94.4)
Yes	1,233 (10.0)	860 (5.6)
Hospitalization		
No	12,254 (99.6)	15,342 (99.7)
Yes	52 (0.4)	54 (0.4)

booster dose (aOR 0.96 [95% CI 0.84–1.09]) among BA.5 case-patients were similar to those for the BA.2 case-patients, suggesting no relevant differences in VE against infection for the BA.5 lineage compared with the BA.2 lineage (Table 2). We observed higher odds of previous infection in BA.5 case-patients compared with BA.2 case-patients (aOR 1.44 [95% CI 1.30–1.60]).

Cohort VEp Study

For the cohort study, regarding hospitalization (Table 3), for complete primary vaccination, we estimated an aOR of 0.38 (95% CI 0.16–0.89) for BA.2 case-patients and 0.78 (95% CI 0.29–2.09) for BA.5 case-patients, which is equivalent to a VEp of 62% (95% CI 11%–84%) for BA.5 and 22% (95% CI –109%–71%) for BA.2 For the first booster dose, we observed a higher reduction in risk for hospitalization among infected patients for both BA.2 (aOR 0.07 [95% CI 0.03–0.14]) and BA.5 (aOR 0.23 [(95% CI 0.10–0.51]), representing VEp of 93% (95% CI 86%–97%) for BA.2 and 77% (95% CI 49%–90%) for BA.5.

The interaction term that enables comparison between BA.5 and BA.2 lineage-specific VEp was aOR 3.36 (95% CI 1.18–9.63), suggesting reduced protection induced by the first booster dose against hospitalization for BA.5 case-patients compared with BA.2. For complete primary vaccination the difference in VEp between BA.5 and BA.2 case-patients was not statistically significant (aOR 2.06 [95% CI 0.56–7.55]).

Discussion

Using routinely collected data from electronic health records, we found no differences in odds of vaccination between BA.5 and BA.2 infection in the adult population of Portugal, suggesting that VE against BA.5 infection was similar to VE against BA.2. This result corroborates findings from studies conducted in the United Kingdom and Denmark that compared VE against infection between BA.5 and BA.2 by using a similar methods (*6*,*7*).

Our study showed that infection with the SARS-CoV-2 Omicron BA.5 lineage was associated with

Table 2. Crude and adjusted odds ratios of vaccine infection breakthrough in BA.5 case-patients compared with BA.2 SARS-CoV-2 case-patients, Portugal, epidemiologic weeks 17–23, 2022*

Category	BA.5, no. (%)	BA.2, no. (%)	Crude OR (95% CI)	Adjusted† OR (95% CI)
Vaccination status				
Unvaccinated	590	631	Referent	Referent
Complete primary vaccination	2,530	2,434	1.11 (0.98–1.26)	1.07 (0.93–1.23)
Booster dose	9,186	12,331	0.80 (0.71–0.89)	0.96 (0.84–1.09)
Previous infection				
No	11,073	14,536	Referent	Referent
Yes	1,233	860	1.88 (0.71–2.06)	1.44 (1.30–1.60)
Vaccination status accounting for previous infection				
Unvaccinated without previous infection	468 (3.8)	550 (3.6)	Referent	Referent
Unvaccinated with previous infection	122 (1.0)	81 (0.5)	1.77 (1.30–2.41)	1.77 (1.26–2.49)
Complete primary vaccination without previous infection	1,802 (14.6)	1,982 (12.9)	1.07 (0.93–1.23)	1.08 (0.92–1.26)
Complete primary vaccination with previous infection	729 (5.9)	452 (2.9)	1.90 (1.60–2.25)	1.70 (1.40–2.05)
Booster without previous infection	8,805 (71.5)	12,004 (78.0)	0.86 (0.76–0.98)	0.99 (0.86–1.14)
Booster with the previous infection	382 (3.1)	327 (2.1)	1.37 (1.13–1.66)	1.18 (0.95–1.47)

*OR, odds ratio.
†Adjusted for age group, sex, region, and week of diagnosis.

higher odds of previous infection compared with BA.2, suggesting reduced protection conferred by the previous infection against BA.5. The effect of the previous infection on the odds of being infected with BA.4/BA.5 and BA.2 has been investigated in Qatar, where the reported protective effect of previous infection against infection with BA.2 was 46.1% (95% CI 39.5%–51.9%) (*18*). The authors reported a low effect for pre-Omicron infection 14.9% (95% CI −47.5%–50.9%) and higher effectiveness for previous infection with BA.1/2 of 76.1% (95% CI 54.9%–87.3%) in reducing the risk for infection with BA.4/BA.5 (*5*). Although not directly comparable, our results align with these findings.

Moreover, we used a cohort design to compare the risk for hospitalization among vaccinated and unvaccinated patients, conditional on being infected with BA.5 or BA.2. Our results suggest statistically significant differences between BA.5 and BA.2 in VEp after the first booster dose (aOR 3.36 [95% CI 1.18–9.63]). In addition, among BA.5-infected patients, the protective effect of the first booster on reducing the odds of hospitalization was higher (VEp 77% [95% CI 49%–90%]) than for the primary vaccination (VEp 22%–95% [95% CI −109% to 71%]). These findings align with neutralization studies that suggested higher immune evasion for the BA.5 lineage than for BA.2 (*19*) and an improvement in plasma-neutralizing activity after receipt of booster vaccine, highlighting the importance of vaccine boosters for eliciting potent neutralizing antibody responses against Omicron lineages (*20*).

Among the limitations of our study is that, for most included cases, SARS-CoV-2 variant was determined by SGTF, so we cannot exclude the possibility of variant misclassification, given that other contemporary lineages (BA.1 and BA.4) also display SGTF and non-SGTF status. However, genomic surveillance data indicate that this potential bias was largely minimized because BA.1 and BA.4 had a <0.3% weekly relative frequency throughout the study period (*3*). Regarding the non-SGTF profile, only very sporadic sequences were detected beside the dominant BA.2. Both observations support a reduced risk for lineage misclassification.

In addition, the study relies on surveillance data that had some limitations (e.g., lack of information on potential confounders, underlying conditions, and adherence to protective measures such as mask use, social distancing, or other behaviors, which may differ between vaccinated and unvaccinated patients). These differences can be rooted in the risk perception of the disease associated with age or previous exposure to SARS-CoV-2. Although we account for age, sex, and region of residence in the models, which minimize the confounding, we cannot exclude unmeasured confounding bias.

Moreover, we cannot identify the variant from a previous infection, and having a pre-Omicron infection affects the odds of being infected with BA.5, as demonstrated in the Qatar study (*5*,*18*). Time since previous infection was also unknown, so we were not

Table 3. Adjusted odds ratios of hospitalization among COVID-19 case-patients, by SARS-CoV-2 variant, Portugal, 2022*

Vaccination status	BA.5		BA.2		aOR BA.5/BA.2 (95% CI)
	No. (%)	aOR (95% CI)	No. (%)	aOR (95% CI)	
Not vaccinated	9/590 (1.53)	Referent	14/631 (2.2)	Referent	
Complete primary vaccination	9/2,530 (0.36)	0.78 (0.29–2.09)	11/2,434 (0.45)	0.38 (0.16–0.89)	2.06 (0.56–7.55)
1st booster vaccination	34/9,186 (0.37)	0.23 (0.10–0.51)	29/12,331 (0.24)	0.07 (0.03–0.14)	3.36 (1.18–9.63)

*aOR, adjusted odds ratio; OR, odds ratio.

able to address the hypothesis of waning protection. We did not account for the underascertainment of the previous infection, meaning that we are probably underestimating the protective effect of the previous infection. Serologic surveys have estimated postinfection seroprevalence to be higher than the cumulative incidence reported by the national surveillance system in Portugal (*21*,*22*).

The ascertainment bias might be present if the probability of testing is different between vaccinated and unvaccinated case-patients. However, during the study period, the daily testing rate in Portugal was 3.6–4.7 tests/1,000 population, the testing recommendations remained stable, and active community testing was maintained, which meant all symptomatic persons could have a free test and paid sick leave regardless of vaccination status. The variant status is unknown to the person being tested and hence is less likely to be an incentive for different testing behaviors by itself. Although we cannot exclude the effect of ascertainment bias on our results, the robust community testing and the paid sick leave program probably minimize it.

Our approach does not provide a direct measure of VE against infection or severe disease but does provide a rapid assessment of the effects of SARS-CoV-2 variants on VE, which can be helpful in guiding public health measures. Our results suggest no differences in VE against SARS-CoV infection and lower protective effect of previous infection against infection with BA.5 compared with BA.2, which explains the surge in cases observed in countries with high BA.5 prevalence. In addition, we observed that VE against COVID-19 progression to severe disease was lower among patients infected by BA.5 compared with BA.2. Vaccines currently used in Portugal are less effective in reducing the risk for disease progression to severe outcomes for patients infected with BA.5 compared with BA.2. The observed difference between BA.5 and BA.2 lineages emphasizes the importance of high vaccination coverage to prevent severe COVID-19–associated outcomes.

The acquisition of sequencing equipment and reagents used in this study by the Instituto Nacional de Saúde Doutor Ricardo Jorge was partially funded by the HERA project (grant no. 2021/PHF/23776) supported by the European Commission through the European Centre for Disease Control, and also partially funded by the GenomePT project (grant no. POCI-01-0145-FEDER-022184), supported by COMPETE 2020–Operational Programme for Competitiveness and Internationalisation, Lisboa Portugal Regional Operational Programme, Algarve Portugal Regional Operational, under the Portugal 2020 Partnership Agreement, through the European Regional Development Fund, and by the Portuguese Science and Technology Foundation. Algarve Biomedical Center Laboratory received public funding through the Project ALG-D2-2021-06 Variants Screen in Southern Portugal–Monitoring Variants of Concern in Southern Portugal and the Portuguese Science and Technology Foundation national support through the Comprehensive Health Research Center (grant no. UIDP/04923/2020)

Author contributions: A.M., I.K., B.N., C.D., A.P.S., and P.C. designed the study. Data collection was performed by J.P.G., V.B., L.C., R.F., J.I., M.P., D.S., A.N., D.Sa., S.D., L.V., C.S., J.P.A., L.M., B.F., A.F., C.M.B., A.P.S., E.F., and P.P.F.. I.K. completed data analysis. I.K., P.C., and A.P.S. wrote the first draft of the manuscript. Data interpretation was performed by I.K., A.P.S., P.C., and A.M. All authors approved the final version of the manuscript and agreed to be accountable for all aspects of the work in ensuring that questions related to the accuracy or integrity of the work are appropriately investigated and resolved.

The findings, opinions and conclusions described in this article reflect the authors' views only. The European Centre for Disease Control is in no way responsible for the information contained in this article or for any use that may be made of this information.

About the Author

Mrs. Kislaya is a biostatistician in the Department of Epidemiology at Instituto Nacional de Saúde Doutor Ricardo Jorge, Lisbon, Portugal and a researcher at the Comprehensive Health Research Centre, Lisbon, Portugal. Her primary research interests include influenza and COVID-19 vaccine effectiveness, health surveys and the population-level effects of public health interventions.

References

1. Tegally H, Moir M, Everatt J, Giovanetti M, Scheepers C, Wilkinson E, et al.; NGS-SA consortium. Emergence of SARS-CoV-2 Omicron lineages BA.4 and BA.5 in South Africa. Nat Med. 2022;28:1785–90. https://doi.org/10.1038/s41591-022-01911-2
2. European Centre for Disease Prevention and Control. Epidemiological update: SARS-CoV-2 Omicron sub-lineages BA.4 and BA.5. 2022 [cited 2022 Jul 22]. https://www.ecdc.europa.eu/en/news-events/epidemiological-update-sars-cov-2-omicron-sub-lineages-ba4-and-ba5
3. Instituto Nacional de Saúde Doutor Ricardo Jorge. Genetic diversity of the novel coronavirus SARS-CoV-2 (COVID-19) in Portugal. 2022 Aug 23 [cited 2022 Aug 23]. https://insaflu.insa.pt/covid19

4. European Centre for Disease Prevention and Control. COVID-19 situation dashboard [cited 2022 Jul 28]. https://qap.ecdc.europa.eu/public/extensions/COVID-19/COVID-19.html#eu-eea-daily-tab
5. Altarawneh HN, Chemaitelly H, Ayoub HH, Hasan MR, Coyle P, Yassine HM, et al. Protective effect of previous SARS-CoV-2 infection against Omicron BA.4 and BA.5 subvariants. N Engl J Med. 2022;387:1620–2. https://doi.org/10.1056/NEJMc2209306
6. Public Health England. SARS-CoV-2 variants of concern and variants under investigation in England. Technical briefing 43; 24 June 2022. 2022 [cited 2022 Jul 22]. https://assets.publishing.service.gov.uk/government/uploads/system/uploads/attachment_data/file/1103533/Technical-Briefing-43-24June2022.pdf
7. Hansen CH, Friis NU, Bager P, Stegger M, Fonager J, Fomsgaard A, et al. Risk of reinfection, vaccine protection, and severity of infection with the BA.5 omicron subvariant: a nation-wide population-based study in Denmark. Lancet Infect Dis. 2022;S1473-3099(22)00595-3.
8. Davies MA, Kassanjee R, Rousseau P, Morden E, Johnson L, Solomon W, et al.; Western Cape and South African National Departments of Health in collaboration with the National Institute for Communicable Diseases in South Africa Affiliations. Outcomes of laboratory-confirmed SARS-CoV-2 infection in the Omicron-driven fourth wave compared with previous waves in the Western Cape Province, South Africa. Trop Med Int Health. 2022;27:564–73. https://doi.org/10.1111/tmi.13752
9. Cao L, Lou J, Chan SY, Zheng H, Liu C, Zhao S, et al. Rapid evaluation of COVID-19 vaccine effectiveness against symptomatic infection with SARS-CoV-2 variants by analysis of genetic distance. Nat Med. 2022;28:1715–22. https://doi.org/10.1038/s41591-022-01877-1
10. Kislaya I, Rodrigues EF, Borges V, Gomes JP, Sousa C, Almeida JP, et al.; PT-COVID-19 Group. Comparative effectiveness of coronavirus vaccine in preventing breakthrough infections among vaccinated persons infected with Delta and Alpha variants. Emerg Infect Dis. 2022;28:331–7. https://doi.org/10.3201/eid2802.211789
11. Eggink D, Andeweg SP, Vennema H, van Maarseveen N, Vermaas K, Vlaemynck B, et al. Increased risk of infection with SARS-CoV-2 Omicron BA.1 compared with Delta in vaccinated and previously infected individuals, the Netherlands, 22 November 2021 to 19 January 2022. Euro Surveill. 2022;27:2101196. https://doi.org/10.2807/1560-7917.ES.2022.27.4.2101196
12. Pogreba-Brown K, Austhof E, Ellingson K. Methodology minute: an overview of the case-case study design and its applications in infection prevention. Am J Infect Control. 2020;48:342–4. https://doi.org/10.1016/j.ajic.2018.11.024
13. Ioannidis JPA. Estimating conditional vaccine effectiveness. Eur J Epidemiol. 2022;37:885–90. https://doi.org/10.1007/s10654-022-00911-3
14. Halloran ME, Longini IM Jr, Struchiner CJ. Design and interpretation of vaccine field studies. Epidemiol Rev. 1999;21:73–88. https://doi.org/10.1093/oxfordjournals.epirev.a017990
15. Nunes B, Rodrigues AP, Kislaya I, Cruz C, Peralta-Santos A, Lima J, et al. mRNA vaccine effectiveness against COVID-19-related hospitalisations and deaths in older adults: a cohort study based on data linkage of national health registries in Portugal, February to August 2021. Euro Surveill. 2021;26:2100833. https://doi.org/10.2807/1560-7917.ES.2021.26.38.2100833
16. European Centre for Disease Prevention and Control. Data on testing for COVID-19 by week and country. 2022 [cited 2022 Jul 22]. https://www.ecdc.europa.eu/en/publications-data/covid-19-testing
17. Firth D. Bias reduction of maximum likelihood estimates. Biometrika. 1993;80:27–38. https://doi.org/10.1093/biomet/80.1.27
18. Altarawneh HN, Chemaitelly H, Ayoub HH, Tang P, Hasan MR, Yassine HM, et al. Effects of previous infection and vaccination on symptomatic Omicron infections. N Engl J Med. 2022;387:21–34. https://doi.org/10.1056/NEJMoa2203965
19. Hachmann NP, Miller J, Collier AY, Ventura JD, Yu J, Rowe M, et al. Neutralization escape by SARS-CoV-2 Omicron subvariants BA.2.12.1, BA.4, and BA.5. N Engl J Med. 2022;387:86–8. https://doi.org/10.1056/NEJMc2206576
20. Bowen JE, Addetia A, Dang HV, Stewart C, Brown JT, Sharkey WK, et al. Omicron spike function and neutralizing activity elicited by a comprehensive panel of vaccines. Science. 2022;377:890–4. https://doi.org/10.1126/science.abq0203
21. Kislaya I, Gonçalves P, Gómez V, Gaio V, Roquette R, Barreto M, et al.; ISN2COVID-19 Group. SARS-CoV-2 seroprevalence in Portugal following the third epidemic wave: results of the second National Serological Survey (ISN2COVID-19). Infect Dis (Lond). 2022;54:418–24. https://doi.org/10.1080/23744235.2021.2025421
22. Canto E Castro L, Pereira AHG, Ribeiro R, Alves C, Veloso L, Vicente V, et al. Prevalence of SARS-CoV-2 antibodies after first 6 months of COVID-19 pandemic, Portugal. Emerg Infect Dis. 2021;27:2878–81. https://doi.org/10.3201/eid2711.210636

Address for correspondence: Irina Kislaya, Instituto Nacional de Saúde Doutor Ricardo Jorge, Av Padre Cruz, 1649-016 Lisbon, Portugal; email: irina.kislaya@insa.min-saude.pt

Clonal Dissemination of Antifungal-Resistant *Candida haemulonii*, China

Xinfei Chen, Xinmiao Jia, Jian Bing, Han Zhang, Nan Hong, Yun Liu, Haiyang Xi, Weiping Wang, Zhiyong Liu, Qiangqiang Zhang, Li Li, Mei Kang, Yuling Xiao, Bin Yang, Yulan Lin, Hui Xu, Xin Fan, Jingjing Huang, Jie Gong, Juan Xu, Xiuli Xie, Wenhang Yang, Ge Zhang, Jingjia Zhang, Wei Kang, He Wang, Xin Hou, Meng Xiao,[1] Yingchun Xu[1]

Candida haemulonii, a relative of *C. auris*, frequently shows antifungal resistance and is transmissible. However, molecular tools for genotyping and investigating outbreaks are not yet established. We performed genome-based population analysis on 94 *C. haemulonii* strains, including 58 isolates from China and 36 other published strains. Phylogenetic analysis revealed that *C. haemulonii* can be divided into 4 clades. Clade 1 comprised strains from China and other global strains; clades 2–4 contained only isolates from China, were more recently evolved, and showed higher antifungal resistance. Four regional epidemic clusters (A, B, C, and D) were identified in China, each comprising ≥5 cases (largest intracluster pairwise single-nucleotide polymorphism differences <50 bp). Cluster A was identified in 2 hospitals located in the same city, suggesting potential intracity transmissions. Cluster D was resistant to 3 classes of antifungals. The emergence of more resistant phylogenetic clades and regional dissemination of antifungal-resistant *C. haemulonii* warrants further monitoring.

The first case of human infection caused by the yeast *Candida haemulonii* was reported in 1984 (*1*). Recent research has indicated that the previously recognized *C. haemulonii* species is actually a species complex comprising 4 phylogenetically closely related species, *C. haemulonii*, *C. duobushaemulonii*, *C. pseudohaemulonii*, and *C. vulturna* (*1*,*2*). The emerging, highly problematic pathogen *C. auris*, which is also a closely related species of the *C. haemulonii* complex, was first reported in Japan in 2009; it has attracted widespread attention worldwide owing to its multidrug resistance and capacity to cause nosocomial outbreaks (*3*–*5*). Because the overall prevalence of *C. haemulonii* sensu stricto remains low worldwide, less attention has been paid to this species. Like *C. auris*, *C. haemulonii* exhibits notable resistance to various classes of antifungal agents, including azoles and amphotericin B (*6*–*8*), and some reports have described nosocomial outbreaks caused by *C. haemulonii* (*9*). However, although *C. haemulonii* s.s. has been discovered in a broad range of wild environmental and animal sources (*10*–*15*), it has not been isolated from a hospital environment.

Molecular methods play important roles in clinical mycology, including laboratory diagnostics, taxonomic investigations, phylogenetic analysis, and confirmation of outbreaks (*16*). Previous studies on the *C. haemulonii* complex have applied methods such as sequencing of the rDNA internal transcribed spacer (ITS) region, amplified fragment-length polymorphism, and random amplified polymorphic DNA; however, the

Author affiliations: Peking Union Medical College Hospital, Chinese Academy of Medical Sciences and Peking Union Medical College, Beijing, China (X. Chen, X. Jia, H. Zhang, J. Huang, X. Xie, W. Yang, G. Zhang, J. Zhang, W. Kang, M. Xiao, Y. Xu); State Key Laboratory of Complex Severe and Rare Diseases and Beijing Key Laboratory for Mechanisms Research and Precision Diagnosis of Invasive Fungal Diseases, Beijing (X. Chen, X. Jia, H. Zhang, J. Huang, X. Xie, W. Yang, G. Zhang, J. Zhang, W. Kang, M. Xiao, Y. Xu); Fudan University, Shanghai, China (J. Bing, Q. Zhang, L. Li); Nanjing University School of Medicine, Nanjing, China (N. Hong, H. Xi, W. Wang); Changhai Hospital, Shanghai (Y. Liu); Southwest Hospital Affiliated the Third Military Medical University, Chongqing, China (Z. Liu); Sichuan University, Chengdu, China (M. Kang, Y. Xiao); The First Affiliated Hospital of Fujian Medical University, Fuzhou, China (B. Yang, Y. Lin); The First Affiliated Hospital of Zhengzhou University, Zhengzhou, China (H. Xu); Capital Medical University, Beijing (X. Fan); Chinese Center for Disease Control and Prevention, Beijing (J. Gong, J. Xu); Dynamiker Sub-Center of Beijing Key Laboratory for Mechanisms Research and Precision Diagnosis of Invasive Fungal Disease, Tianjin, China (H. Wang); Peking University Third Hospital, Beijing (X. Hou)

DOI: http://doi.org/10.3201/eid2903.221082

[1]These senior authors contributed equally to this article.

discriminatory powers of those methods are limited and only capable of assigning isolates to the species level (*2*). Whole-genome sequencing (WGS) provides a high-resolution alternative. In fact, WGS-based genomic analysis has assisted in tracing the phylogenetic evolution and dissemination of *C. auris* globally (*17*), confirming nosocomial transmission of *C. auris* in healthcare facilities (*5*,*18*,*19*), and analyzing potential antifungal resistance mechanisms (*20*–*22*).

The global phylogeny of *C. haemulonii* remains uncharacterized. The China Hospital Invasive Fungal Surveillance Net (CHIF-NET) program identified several regional clustered cases (n ≥5) in China caused by *C. haemulonii*; however, the overall prevalence of this species remained low (0.8%) (*23*). We performed WGS-based analysis of 94 *C. haemulonii* strains, 58 isolates collected from 23 hospitals by the CHIF-NET study over 8 years in China and 36 previously published international strain genomes (*24*). The primary goal of our study was to illustrate the phylogenetic character of this species worldwide and determine the population relatedness of regional cluster cases in China. In addition, we sought to predict major antifungal resistance mechanisms using bioinformatic analysis. Our study was approved by the Human Research Ethics Committee of the Peking Union Medical College Hospital (protocol S-263).

Materials and Methods

We examined 58 nonduplicated clinical *C. haemulonii* isolates collected from 23 hospitals distributed across 15 provinces in China during August 2009–July 2017 (Figure 1). Of those strains, 31 had been previously reported (*7*). We also included publicly available genomic data for 36 international *C. haemulonii* strains, obtained from the National Center for Biotechnology Information Sequence Read Archive.

Of the strains from China, 69% (40/58) were isolated from the blood and 13.8% (8/58) from the cerebrospinal fluid. The remaining strains were isolated from venous catheters (8.6%, 5/58), secretions (3.4%, 2/58), tissue fluid (1.7%, 1/58), ascitic fluid (1.7%, 1/58), and drainage (1.7%, 1/58) (Appendix 1 Table 1, https://wwwnc.cdc.gov/EID/article/29/3/22-1082-App1.xlsx). Samples came from from patients in medical wards (53.4%, 31/58), surgical wards (22.4%, 13/58), intensive care units (22.4%, 13/58), and emergency departments (1.7%, 1/58).

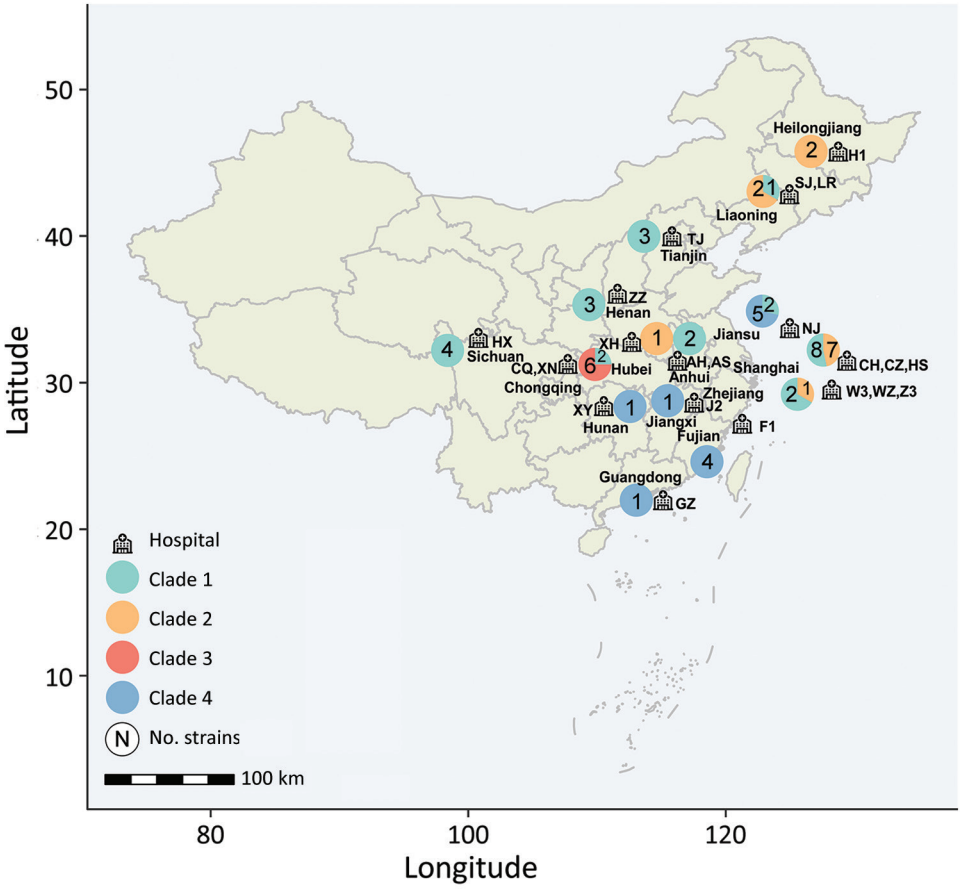

Figure 1. Regional distribution of 58 invasive infections caused by *C. haemulonii* in China during 2010–2017, collected from the China Hospital Invasive Fungal Surveillance Net study. Province names are listed, and hospital locations are marked by icons; the abbreviation codes of hospitals are listed next to each location. The pie charts adjacent to the province names indicate the number of isolates collected; phylogenetic clades are labeled in different colors.

The international strains were isolated from 3 continents: 18 from South America (Venezuela, n = 7; Colombia, n = 11), 17 from North America (United States, n = 13; Panama, n = 4), and 1 from Asia (Israel, n = 1). Of the strains, 94.4% (34/36) were from humans (blood, wounds, bone bronchial wash, foot, vaginal secretion, catheter, urine, or peritoneal fluid), 2.8% (1/36) from animals (fish), and 2.8% (1/36) with no source information (Appendix 1 Table 1).

We identified all strains by using matrix-assisted laser desorption/ionization time-of-flight mass spectrometry and ITS sequencing (Appendix 2, https://wwwnc.cdc.gov/EID/article/29/3/22-1082-App2.pdf). We evaluated in vitro susceptibility and performed WGS to explore the molecular features of the isolates. Raw genome reads are available from the National Center for Biotechnology Information (BioProject no. PRJNA827237).

Results

Collection of Isolates

We identified all strains as *C. haemulonii* by using Autof MS 1000 (Autobio Diagnostics Co., Ltd; https://en.autobio.com.cn) and Vitek MS (bioMerieux; https://www.biomerieux-usa.com/). The phylogenetic tree based on rDNA ITS region sequences revealed that CHIF-NET strains clustered with *C. haemulonii* CBS5149^T rather than other species within the *C. haemulonii* species complex.

C. haemulonii Genome Highly Conserved

We performed single-nucleotide polymorphism (SNP) calling for all 94 isolates. Although derived from vast international geographic regions, we found *C. haemulonii* genomes to be highly conserved. We found 6,807 SNPs among the 94 *C. haemulonii* genomes, which was a considerably smaller number than that first reported for *C. auris* (119,188 SNPs) (*4*). The pairwise SNP differences among all international strains ranged from 6 to 553 (median 269). SNP differences between Chinese and international isolates ranged from 4 to 653 (median 333), and pairwise SNP differences between different Chinese strains ranged from 6 to 581 (median 297).

Four Phylogenetic Clades Identified Worldwide

Fast hierarchical Bayesian analysis of population structure revealed that all strains could be divided into 4 major clades, and principal components analysis results clearly supported the presence of these 4 groups (Figure 2; Appendix 2 Figure 1). We classified 63 isolates (67%) as clade 1, 13 (13.8%) as clade 2, 6 (6.4%) as clade 3, and 12 (12.8%) as clade 4 (Appendix 1 Table 1). From the phylogenetic tree, we observed that clade 1 strains were widely distributed across vast geographic regions (Figure 1). In comparison, all isolates in clades 2, 3, and 4 were exclusively from China (clade 2, n = 13; clade 3, n = 6; clade 4, n = 12), and those 3 branches are suggested to have evolved from clade 1 in the phylogenetic tree. Of note, analysis of the mating-type locus showed that all 94 isolates were *MATa*.

Regional Clustered Cases Associated with Spread of Specific Clones

We observed several clustered regional cases. To investigate potential clonal spreads or outbreaks, we first concentrated on any hospital with ≥5 cases of *C. haemulonii* infections that occurred during the surveillance period. We found that the maximum pairwise SNP differences for isolates within the same clade from the same hospital were all <50 (33 SNPs for clade 1 in hospital HS, 28 for clade 2 in hospital CH, 34 for clade 3 in hospital XN, and 45 for clade 4 in hospital NJ). Except for isolates of clade 3 that were identified in only 1 hospital, the above differences were considerably less than the average intraclade pairwise SNP differences of all isolates within the same clade, which were 301 SNPs for clade 1, 131 for clade 2, and 160 for clade 4. We therefore used a criterion of ≤50 SNPs for defining clonal clusters in our primary analysis. On the basis of those criteria, we identified 4 obvious clusters.

We discovered cluster A, initially, in hospital CH in East China; 6 cases accounted for 85.7% (6/7) of the *C. haemulonii* infection cases found in that institution. Cluster A isolates belonged to clade 2, and SNP differences between any 2 cluster A strains ranged from 10 to 28 bp (median 21). Three strains were isolated from the surgical ward, 2 strains from the medical department, and 1 strain from the intensive care unit. Five strains were isolated from blood and 1 strain from cerebrospinal fluid. The remaining non–cluster A isolates from that hospital belonged to clade 1, which differed from the cluster A strains, ranging from 349 to 399 bp (median 398). Of note, 1 strain isolated from another hospital (hospital CZ, also located in hospital CH's city) fell into cluster A (paired SNPs 13 to 22 versus CH cluster A strains), suggesting intra-city transmission of *C. haemulonii* from August 2016 through April 2017 (Figure 3).

Cluster B, belonging to clade 1, was detected in hospital HS in East China, comprising 6 cases, and the inter-cluster pairwise SNP differences ranged from 6 to 33 bp (median 20). Although hospitals HS, CH,

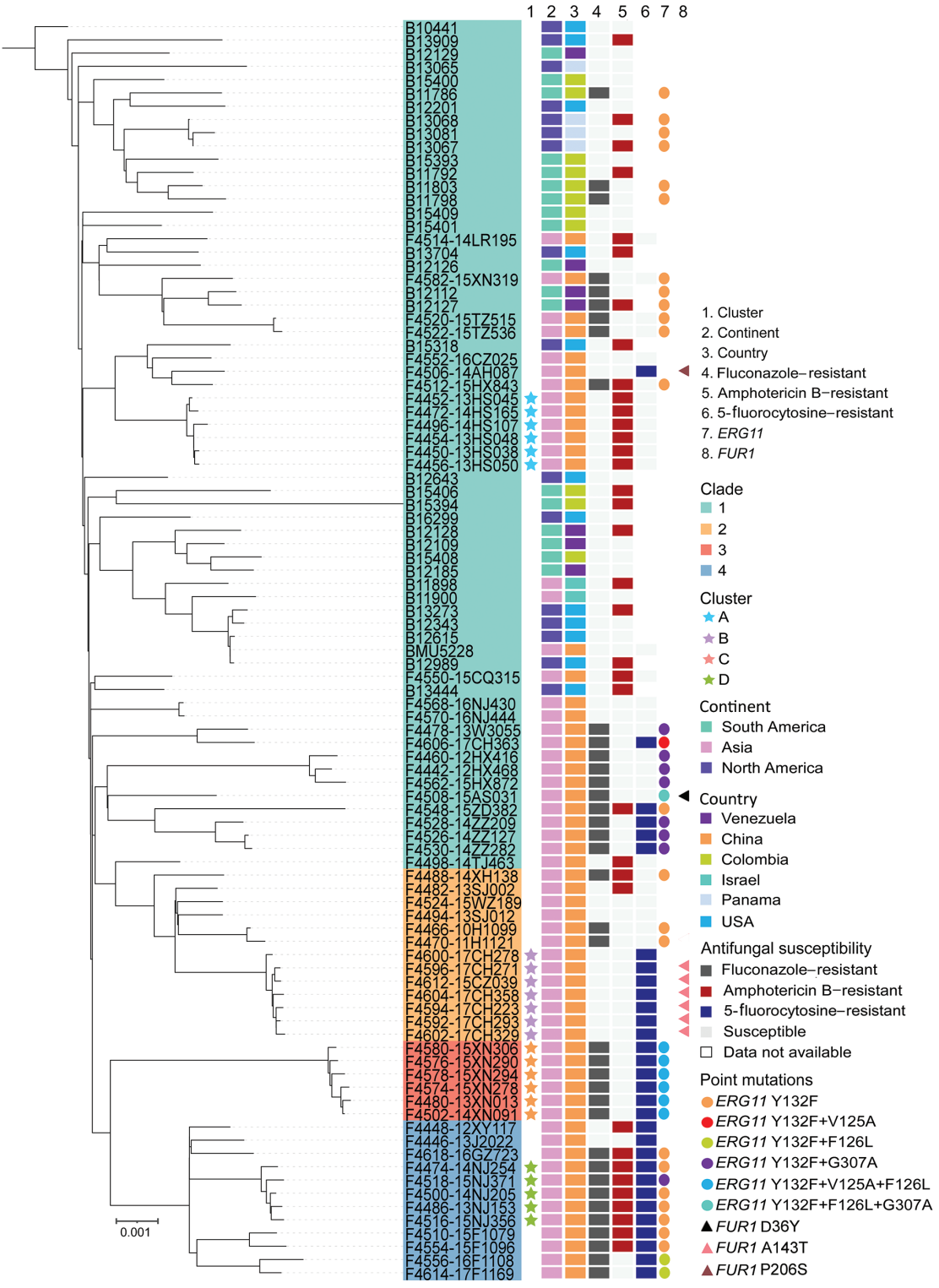

Figure 2. Maximum-likelihood phylogenetic tree constructed based on whole-genome single-nucleotide polymorphisms and phylogenetic clades in a study of antifungal-resistant *Candida haemulonii* in China. Information is labeled for each strain: geographic origin, antifungal susceptibilities for representative drugs of different classes (fluconazole, amphotericin B, and 5-fluorocytosine), and key amino acid substitutions related to antifungal resistance that were observed in genes encoding lanosterol 14-α-demethylase (*ERG11*) and uracil phosphoribosyltransferase (*FUR1*). The tree was rooted to strain B10441 (CBS5149), which is the most ancient *C. haemulonii* strain, identified in 1962 (from *Haemulon sciurus*). All remaining strains were isolated after 2010.

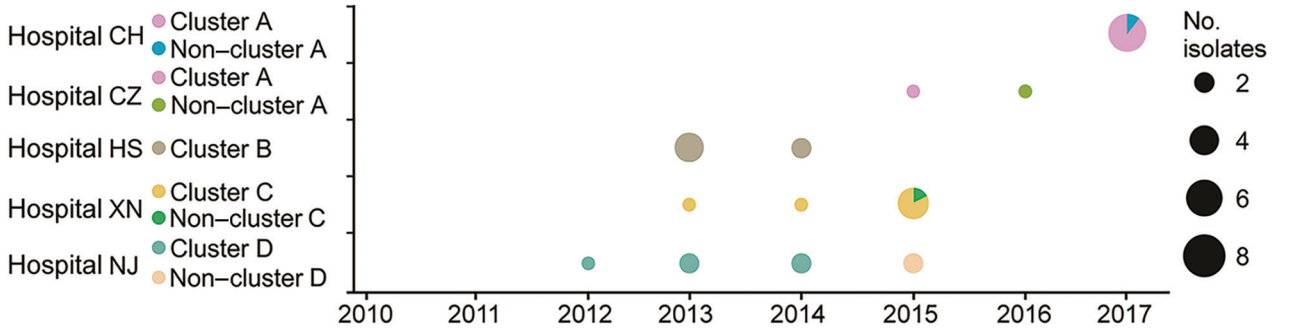

Figure 3. Distribution of 4 regionally disseminated *Candida haemulonii* clusters (clusters A, B, C, and D) in 5 hospitals in China. Isolates not belonging to the 4 major clusters were summarized as noncluster strains. Pie charts indicate number of isolates (indicated by size of pie) and distribution of clusters (distinguished by color).

and CZ were in the same city, cluster B diverged from cluster A (>258 bp differences). Four cluster B isolates were collected from the infectious department ward, 1 isolate was collected from the emergency department, and 1 isolate was collected from the intensive care unit. All strains were isolated from cerebrospinal fluid during October 2013–August 2014 (Figure 3).

Cluster C was detected in hospital XN in Southwest China and belonged to clade 3. Of the 7 strains isolated from hospital XN, 85.7% (6/7) were attributed to cluster C. The remaining isolate was from clade 3 but differed from other cluster C strains by 421–463 bp. Within cluster C strains, pairwise SNP differences ranged from 11 to 34 bp (median 28). All cluster C strains from hospital XN were isolated from the hepatobiliary ward; 3 of those strains were cultured from blood and catheter samples. The timeline for the isolation of cluster C isolates in hospital XN was >2 years (September 2013–October 2015) (Figure 3).

Cluster D isolates belonging to clade 4 were detected from hospital NJ in East China and comprised 5 cases. The number of SNPs in cluster D ranged from 19 to 45 bp (median 37). All 6 cluster D strains were isolated from the general surgery wards. As with cluster C strains, cluster D strains persisted in hospital NJ for >2 years (September 2013–November 2015) (Figure 3). Of interest, 2 additional non–cluster D strains from that hospital belonged to clade 1. Both strains were isolated from the nephrology ward (August 2016–November 2016), and pairwise SNP differences between the 2 strains were only 11, suggesting another potential nosocomial transmission.

In summary, 4 clonal dissemination events of *C. haemulonii* were identified in China. Moreover, evidence suggests the occurrence of an intra-city clonal spread caused by a multidrug-resistant clone.

Notable Antifungal Resistance in *C. haemulonii*

Among the 94 isolates studied, only an international strain from Venezuela was reported to be resistant to caspofungin (MIC = 16 μg/mL) (*24*). All other strains remained susceptible to echinocandins. Of the isolates, 40.4% (38/94) were resistant to fluconazole and 21.2% (20/94) were resistant to voriconazole, including 24.5% (23/94) that were cross-resistant to the 2 azoles. The resistance rate in China was 56.9% (33/58) for fluconazole and 34.5% (20/58) for voriconazole, both rates higher than the rates among international strains, which were 13.9% (5/36) for fluconazole and 0% (0/36) for voriconazole. In comparison, only 9.6% (9/94) of the isolates were resistant to itraconazole, and only 1 isolate had a minimum inhibitory concentration ≥1 μg/mL for posaconazole. Nearly half (44.7%, 42/94) of the isolates were resistant to amphotericin B. Although data for 5-fluorocytosine resistance were not available for the 36 international strains, more than half (53.4%) of the 58 strains from China were 5-fluorocytosine resistant. Moreover, in China, 25.8% (15/58) of the isolates were multidrug resistant, including 15.5% (9/58) that were resistant to 3 classes of antifungal agents.

Antifungal resistance was associated with the clonal background of the strains. For instance, fluconazole resistance rates were above 80% for clade 3 (100%) and clade 4 (83.3%) strains, whereas only 30.2% of clade 1 and 46.2% of clade 2 isolates were fluconazole resistant (Appendix 1 Table 2). In addition, China clade 1 isolates exhibited a higher fluconazole resistance rate (51.9%) than the international strains (13.9%). The amphotericin B resistance rate of strains in clade 1 (49.2%) and in clade 4 (58.3%) were higher compared with other clades (<20%). The 5-fluorocytosine resistance rate was 100% in clades 3 and 4. Strains resistant to 3 classes of antifungals were mainly

distributed in clade 4 (66.7%), including all cluster D isolates (Appendix 1 Table 2).

Potential Resistance Mechanisms of *C. haemulonii*

We used the genome of strain BMU5228 as a wild-type sequence to annotate gene mutations in 25 known important antifungal resistance genes (Appendix 1 Table 3). Among the 33 fluconazole-resistant strains in China, 100% harbored the Y132F substitution in Erg11p (Table). We also found the Y132F substitution in 11.1% (4/36) of the international strains, and 2 of them were fluconazole resistant. We found 54.5% (18/33) of fluconazole-resistant strains in China harbored ≥1 of the substitutions V125A, F126L, and G307A (Table; Appendix 1 Table 3). We screened other genes reported to cause azole resistance and found that 6 cluster C strains had the substitution M589L in Tac1Bp, the transcriptional regulator of the efflux pump Cdr1. Our analysis of the distribution of copy number variations revealed that 13 (22.4%) strains in China had >1 copy of the *ERG11* gene, and those strains were all resistant to fluconazole (Appendix 2 Figure 2). For strains with >1 copy of *ERG11*, 6 strains were from clade 3 and 7 strains were from other clades (Appendix 2 Figure 2). Isolates with >1 copy of *ERG11* had significantly higher MICs against fluconazole than did isolates with 1 copy ($p<0.05$ by Mann–Whitney test). For 5-fluorocytosine, of the 31 resistant isolates, 25.8% (8/31) had noteworthy mutations in the *FUR1* gene, including 7 strains carrying the substitution A143T (all of which were cluster C) and 1 strain carried the substitution P206S. Although 42.6% (40/94) of the strains were resistant to amphotericin B, we observed no mutations of note in the previously described resistance-related genes, including *ERG2*, *ERG3*, or *ERG6* (Appendix 1 Table 3).

Discussion

In recent years, the number of human infections caused by emerging pathogens has increased gradually (*24*). Among those pathogens, *C. haemulonii* and its closely related species *C. auris*, belonging to the family Metschnikowiaceae, have received great public attention because of their notable trends of antifungal resistance and capacity to cause nosocomial transmission (*5*,*9*,*25*).

Genome-based phylogenetic studies of *C. auris* have revealed that 5 distinct clades (I, II, III, IV, and V) are distributed in East Asia, South Asia, South Africa, and South America (*17*,*26*), whereas the population structure of *C. haemulonii* has not been previously defined. In this study, we found that *C. haemulonii* can also be divided into 4 phylogenetic clades. Rooted by the most ancient *C. haemulonii* strain B10441 (CBS5149) that was isolated in 1962, strains from clades 2–4 emerged more recently, with isolates identified exclusively in China and antifungal resistance observed more notably compared with clade 1. We found that 46.2% of clade 2 isolates were fluconazole resistant versus 30.2% in clade 1, all clade 3 isolates were cross-resistant to fluconazole and 5-fluorocytosine, and 66.7% of clade 4 isolates were resistant to 3 classes of antifungals.

Although *C. haemulonii* can be divided into 4 clades, the total number of SNPs identified in the 13.31 Mb whole genome of *C. haemulonii* was only 6,807 (<0.005%), which was considerably less than that in *C. auris*, which has a similar genome size (>210,000 SNPs in a 12.4 Mb genome) (*27*–*29*). When we compared the most ancient *C. haemulonii* strains identified to date (strain ID no. CBS5149, isolated from *Haemulon sciurus* fish in 1962) with the other strains in our study, the maximum genome sequence difference was only 384 bp. Those factors indicate that the genome of *C. haemulonii* is highly conserved. In some *Candida* species, mating can lead to an increase in genetic diversity, and opposite mating types have been observed in *C. auris* (*17*,*29*). However, all *C. haemulonii* isolates identified were of the same mating type (type α), and a sexual cycle has not been observed in this species (*2*), which is a possible reason for the conservation of the species' genome found in previous studies (*24*,*29*).

Although the global prevalence of *C. haemulonii* remains low, nosocomial outbreaks have been reported (*9*,*24*). Nosocomial transmission of *C. haemulonii* was first reported in Kuwait in 2006 (*9*). Because bloodstream infection caused by *C. haemulonii* was rare at the time of the report, the outbreaks were determined by successive isolations of *C. haemulonii* with identical phenotypic characteristics made in the

Table. Distribution of noteworthy Erg11p substitutions among 4 clades of *Candida haemulonii* strains studied as part of an investigation of antifungal-resistant *C. haemulonii*, China

Clade/ geographic origin	Erg11p substitutions				No. isolates
	Y132F	V125A	F126L	G307A	
Clade 1					
International	Y	N	N	N	8
China	Y	N	N	N	5
	Y	N	N	Y	7
	Y	Y	N	N	1
	Y	N	Y	Y	1
Clade 2					
China	Y	N	N	N	3
Clade 3					
China	Y	Y	Y	N	6
Clade 4					
China	Y	N	N	N	7
	Y	N	Y	N	2
	Y	N	N	Y	1

same ward (a neonatal intensive care unit) within a short period of time (3 months), but the outbreaks were not verified by molecular typing. Such molecular methods as ITS sequence typing, random amplified polymorphic DNA analysis, amplified fragment length polymorphism analysis, and, more recently, matrix-assisted laser desorption/ionization time-of-flight mass spectrometry have been applied in *C. haemulonii* studies (*2*,*30*); however, all of those methods have limitations in discriminatory power. Considering the low genetic diversity of *C. haemulonii*, traditional molecular typing assays are not suitable for providing solid evidence for the dissemination of *C. haemulonii*.

WGS-based analysis provides a high-resolution alternative for confirming bacterial and fungal outbreak transmission (*16*,*31*,*32*). Even for species with low genetic diversity, such as *Saprochaete clavata*, this approach can clearly distinguish between sporadic cases and epidemic outbreaks (SNPs <400) (*33*). In this study, we proposed a pairwise SNP difference of ≤50 bp as a criterion for determining clonal cluster cases in *C. haemulonii*, and identified 4 regional clusters that met the criterion. In the absence of medical record evidence, we could not determine whether the case clusters were outbreaks. A previous study by Chow et al. used a 12-bp SNP difference as a cutoff value for interpreting *C. auris* outbreaks (*25*). We suggest that an equally strict pairwise difference might be needed to characterize *C. haemulonii* outbreak events; however, this hypothesis requires further investigation.

C. auris has a potent ability to colonize humans and persist in the hospital environment, and biofilm formation is considered the main contributor (*34*). *C. haemulonii* can form dense biofilms (*35*,*36*), which are thought to enhance its capacity to cause regional dissemination and nosocomial transmission. The epidemic cluster events of *C. haemulonii* identified in China had further implications. Several studies have reported that *C. haemulonii* has a low susceptibility to triazoles and amphotericin B (*9*,*37*,*38*). Our study further revealed that antifungal resistance was more obvious among *C. haemulonii* strains from China than among those from other geographic regions (*24*). Moreover, the 4 regional clusters we identified were all caused by antifungal-resistant clones: cluster A was caused by a clone resistant to amphotericin B, cluster B by a clone resistant to 5-fluorocytosine, cluster C by a clone cross-resistant to fluconazole and 5-fluorocytosine, and cluster D by a clone resistant to 3 classes of antifungals. Cluster A was recovered from 2 hospitals located in the same city, suggesting interfacility transmission. Gade et al. reported that 2 strains of *C. haemulonii* isolated from different healthcare facilities in Valencia, Venezuela, were closely related (with only 32 SNPs) (*24*). As with the closely related species *C. auris*, which presents a serious global health threat (*5*,*25*), the emergence of *C. haemulonii* clones with high rates of both transmission and antifungal resistance should be taken as a warning.

A potential limitation of this study is that only a limited number of publicly available genomes were available for *C. haemulonii*, and they were derived from systematic epidemiology surveillances. These isolates, therefore, may not represent real-world *C. haemulonii* distributions globally. To this end, further genomic-based studies need to be conducted with more isolates from different geographic regions.

In conclusion, we studied a total of 94 *C. haemulonii* genomes, including 36 international strains (38.2%) from the National Center for Biotechnology Information Sequence Read Archive database and 58 strains (61.7%) from 23 hospitals in China. We observed 4 phylogenetic clades, 3 of which were identified exclusively in China and exhibited higher antifungal resistance. All fluconazole-resistant strains carried the Y132F substitution in Erg11p. WGS confirmed that the 4 regional cluster cases were caused by specific clones. We additionally noted a potential interfacility transmission within the same city and the spread of multidrug-resistant clones. As with its close relative *C. auris*, *C. haemulonii* should be recognized as a potential threat to global health, and further monitoring and stewardship steps to limit excessive antifungal usage are warranted.

Acknowledgments

We thank principal investigators and co–principal investigators and the 23 hospitals who contributed clinical *C. haemulonii* isolates in collaboration with the China Hospital Invasive Fungal Surveillance Net (CHIF-NET) Study Group (CHIF-NET 2010 to 2017): Yun Liu, Changhai Hospital, Shanghai; Hai-Yan Xi and Wei-Ping Wang, General Hospital of Nanjing Military Area Command, Nanjing, Jiangsu Province; Zhi-Yong Liu, Southwest Hospital Affiliated the Third Military Medical University (First Affiliated Hospital of Third Military Medical University), Chongqing; Qiang-Qiang Zhang, Huashan Hospital, Fudan University, Shanghai; Bin Yang and Yu-Lan Lin, First Affiliated Hospital of Fujian Medical University, Fuzhou, Fujian Province; Mei Kang and Yu-Ling Xiao, West China Hospital of Sichuan University, Chengdu, Sichuan Province; Xiao-Gai Li, The First Affiliated Hospital of Zhengzhou University, Zhengzhou,

Henan Province; Ting-Ying Zhou, Shanghai Changzheng Hospital, Shanghai; (Da-Wen Guo and Lan-Ying Cui, The First Clinic College of Harbin Medical University, Harbin, Heilongjiang Province; Yong Liu, Zhi-Jie Zhang, The 2nd Hospital Affiliated to China Medical University (Shengjing Hospital of China Medical University), Shenyang, Liaoning Province; Zhi-Dong Hu, General Hospital of Tianjin Medical University, Tianjin; Yuan-Hong Xu and Ying Huang, The First Affiliated Hospital of Anhui Medical University, Hefei, Anhui Province; Huai-Wei Lu and Zheng-Chao Nie, The First Affiliated Hospital of University of Science and Technology of China (Anhui Provincial Hospital), Hefei, Anhui Province; Xiu-Yu Xu and Yun Xia, The First Affiliated Hospital of Chongqing Medical Hospital, Chongqing; Long-Hua Hu and Xiao-Yan Hu, The Second Affiliated Hospital of Nanchang University, Nanchang, Jiangxi Province; Hong-Mei Zhao and Yu-Guang Guo, The People's Hospital of Liaoning Province, Shenyang, Liaoning Province; Ke-Cheng Li and Fei Xia, Ruian People's Hospital, Wenzhou, China. Third Affiliated Hospital of Wenzhou Medical College, Wenzhou, Zhejiang Province; Zi-Yong Sun and Zhong-Ju Chen, Tongji Hospital, Tongji Medical College, Huazhong University of Science and Technology, Wuhan, Hubei Province; Ling Ma and Shuai-Xian Du, Union Hospital, Tongji Medical College of Huazhong University of Science and Technology, Wuhan, Hubei Province; Tie-Li Zhou and Qing Wu, The First Affiliated Hospital of Wenzhou Medical University, Wenzhou, Zhejiang Province; Wen-En Liu and Hong-Ling Li, Xiangya Hospital, Central South University, Changsha, Hunan Province; Hai-Shen Kong and Qing Yang, The First Affiliated Hospital, College of Medicine, Zhejiang University, Hangzhou, Zhejiang Province; Kang Liao and Peng-Hao Guo, The First Affiliated Hospital, Sun Yat-sen University, Guangzhou, Guangdong Province. We also thank Hao Zhang and Vladimir Gritsenko for their valuable suggestions.

This work was supported by the National Key Research and Development Program of China (grant no. 2022YFC2303002), National Natural Science Foundation of China (grant no. 82002178), National High Level Hospital Clinical Research Funding (grant no. 2022-PUMCH-B-074), Beijing Nova Program (grant no. Z201100006820127), and the Beijing Key Clinical Specialty for Laboratory Medicine-Excellent Project (grant no. ZK201000).

About the Author

Dr. Chen is a doctoral student in clinical laboratory diagnostics at the Peking Union Medical College Hospital whose research interests are genomic epidemiology of clinical *Candida* isolates.

References

1. Lavarde VDF, Saez H, Arnold M, Faguer B. Peritonite mycosique a *Torulopsis haemulonii*. Bull Soc Fr Mycol Med. 1984;13:173–6.
2. Cendejas-Bueno E, Kolecka A, Alastruey-Izquierdo A, Theelen B, Groenewald M, Kostrzewa M, et al. Reclassification of the Candida haemulonii complex as *Candida haemulonii* (*C. haemulonii* group I), *C. duobushaemulonii* sp. nov. (*C. haemulonii* group II), and *C. haemulonii var. vulnera* var. nov.: three multiresistant human pathogenic yeasts. J Clin Microbiol. 2012;50:3641–51. https://doi.org/10.1128/JCM.02248-12
3. Satoh K, Makimura K, Hasumi Y, Nishiyama Y, Uchida K, Yamaguchi H. *Candida auris* sp. nov., a novel ascomycetous yeast isolated from the external ear canal of an inpatient in a Japanese hospital. Microbiol Immunol. 2009;53:41–4. https://doi.org/10.1111/j.1348-0421.2008.00083.x
4. Lockhart SR, Etienne KA, Vallabhaneni S, Farooqi J, Chowdhary A, Govender NP, et al. Simultaneous emergence of multidrug-resistant *Candida auris* on 3 continents confirmed by whole-genome sequencing and epidemiological analyses. Clin Infect Dis. 2017;64:134–40. https://doi.org/ 10.1093/cid/ciw691
5. Eyre DW, Sheppard AE, Madder H, Moir I, Moroney R, Quan TP, et al. A *Candida auris* outbreak and its control in an intensive care setting. N Engl J Med. 2018;379:1322–31. https://doi.org/10.1056/NEJMoa1714373
6. Ben-Ami R, Berman J, Novikov A, Bash E, Shachor-Meyouhas Y, Zakin S, et al. Multidrug-resistant *Candida haemulonii* and *C. auris*, Tel Aviv, Israel. Emerg Infect Dis. 2017;23:195–203. https://doi.org/10.3201/eid2302.161486
7. Hou X, Xiao M, Chen SC, Wang H, Cheng JW, Chen XX, et al. Identification and antifungal susceptibility profiles of *Candida haemulonii* species complex clinical isolates from a multicenter study in China. J Clin Microbiol. 2016;54:2676–80. https://doi.org/10.1128/JCM.01492-16
8. Lima SL, Francisco EC, de Almeida Júnior JN, Santos DWCL, Carlesse F, Queiroz-Telles F, et al. Increasing prevalence of multidrug-resistant *Candida haemulonii* species complex among all yeast cultures collected by a reference laboratory over the past 11 years. J Fungi (Basel). 2020;6:110. https://doi.org/10.3390/jof6030110
9. Khan ZU, Al-Sweih NA, Ahmad S, Al-Kazemi N, Khan S, Joseph L, et al. Outbreak of fungemia among neonates caused by *Candida haemulonii* resistant to amphotericin B, itraconazole, and fluconazole. J Clin Microbiol. 2007;45:2025–7. https://doi.org/10.1128/JCM.00222-07
10. Kolipinski MC; van UDEN. *Torulopsis haemulonii* nov. spec., a yeast from the Atlantic Ocean. Antonie van Leeuwenhoek. 1962;28:78–80. https://doi.org/10.1007/BF02538724
11. Antony SP, Singh IS, Sudheer NS, Vrinda S, Priyaja P, Philip R. Molecular characterization of a crustin-like antimicrobial peptide in the giant tiger shrimp, *Penaeus monodon*, and its expression profile in response to various immunostimulants and challenge with WSSV. Immunobiology. 2011;216:184–94. https://doi.org/10.1016/j.imbio.2010.05.030
12. Pagani DM, Heidrich D, Paulino GV, de Oliveira Alves K, Dalbem PT, de Oliveira CF, et al. Susceptibility to antifungal agents and enzymatic activity of *Candida haemulonii* and *Cutaneotrichosporon dermatis* isolated from soft corals on the Brazilian reefs. Arch Microbiol. 2016;198:963–71. https://doi.org/10.1007/s00203-016-1254-0
13. Buck JD. Occurrence of human-associated yeasts in the feces and pool waters of captive bottlenosed dolphins (*Tursiops truncatus*). J Wildl Dis. 1980;16:141–9. https://doi.org/10.7589/0090-3558-16.1.141

14. Ferreira N, Belloch C, Querol A, Manzanares P, Vallez S, Santos A. Yeast microflora isolated from Brazilian cassava roots: taxonomical classification based on molecular identification. Curr Microbiol. 2010;60:287–93. https://doi.org/10.1007/s00284-009-9539-z
15. Glushakova AM, Zheltikova TM, Chernov II. Groups and sources of yeasts in house dust. Mikrobiologiia. 2004;73:111–7.
16. Sabat AJ, Budimir A, Nashev D, Sá-Leão R, van Dijl J, Laurent F, et al.; ESCMID Study Group of Epidemiological Markers (ESGEM). Overview of molecular typing methods for outbreak detection and epidemiological surveillance. Euro Surveill. 2013;18:20380. https://doi.org/10.2807/ese.18.04.20380-en
17. Muñoz JF, Gade L, Chow NA, Loparev VN, Juieng P, Berkow EL, et al. Genomic insights into multidrug-resistance, mating and virulence in *Candida auris* and related emerging species. Nat Commun. 2018;9:5346. https://doi.org/10.1038/s41467-018-07779-6
18. Theodoropoulos NM, Bolstorff B, Bozorgzadeh A, Brandeburg C, Cumming M, Daly JS, et al. *Candida auris* outbreak involving liver transplant recipients in a surgical intensive care unit. Am J Transplant. 2020;20:3673–9. https://doi.org/10.1111/ajt.16144
19. Prestel C, Anderson E, Forsberg K, Lyman M, de Perio MA, Kuhar D, et al. *Candida auris* outbreak in a COVID-19 specialty care unit—Florida, July–August 2020. MMWR Morb Mortal Wkly Rep. 2021;70:56–7. https://doi.org/10.15585/mmwr.mm7002e3
20. Bing J, Hu T, Zheng Q, Muñoz JF, Cuomo CA, Huang G. Experimental evolution identifies adaptive aneuploidy as a mechanism of fluconazole resistance in *Candida auris*. Antimicrob Agents Chemother. 2020;65:e01466-20. https://doi.org/10.1128/AAC.01466-20
21. Rybak JM, Sharma C, Doorley LA, Barker KS, Palmer GE, Rogers PD. Delineation of the direct contribution of *Candida auris ERG11* mutations to clinical triazole resistance. Microbiol Spectr. 2021;9:e0158521. https://doi.org/10.1128/Spectrum.01585-21
22. Rybak JM, Barker KS, Muñoz JF, Parker JE, Ahmad S, Mokaddas E, et al. In vivo emergence of high-level resistance during treatment reveals the first identified mechanism of amphotericin B resistance in *Candida auris*. Clin Microbiol Infect. 2022;28:838–43. https://doi.org/10.1016/j.cmi.2021.11.024
23. Xiao M, Chen SC, Kong F, Xu XL, Yan L, Kong HS, et al. Distribution and antifungal susceptibility of *Candida* species causing candidemia in China: An update from the CHIF-NET Study. J Infect Dis. 2020;221(Suppl 2):S139–47. https://doi.org/10.1093/infdis/jiz573
24. Gade L, Muñoz JF, Sheth M, Wagner D, Berkow EL, Forsberg K, et al. Understanding the emergence of multidrug-resistant *Candida*: using whole-genome sequencing to describe the population structure of *Candida haemulonii* species complex. Front Genet. 2020;11:554. https://doi.org/10.3389/fgene.2020.00554
25. Chow NA, Gade L, Tsay SV, Forsberg K, Greenko JA, Southwick KL, et al.; US Candida auris Investigation Team. Multiple introductions and subsequent transmission of multidrug-resistant *Candida auris* in the USA: a molecular epidemiological survey. Lancet Infect Dis. 2018;18:1377–84. https://doi.org/10.1016/S1473-3099(18)30597-8
26. Chow NA, de Groot T, Badali H, Abastabar M, Chiller TM, Meis JF. Potential fifth clade of *Candida auris*, Iran, 2018. Emerg Infect Dis. 2019;25:1780–1. https://doi.org/10.3201/eid2509.190686
27. Tian S, Bing J, Chu Y, Chen J, Cheng S, Wang Q, et al. Genomic epidemiology of *Candida auris* in a general hospital in Shenyang, China: a three-year surveillance study. Emerg Microbes Infect. 2021;10:1088–96. https://doi.org/10.1080/22221751.2021.1934557
28. Naicker SD, Maphanga TG, Chow NA, Allam M, Kwenda S, Ismail A, et al. Clade distribution of *Candida auris* in South Africa using whole genome sequencing of clinical and environmental isolates. Emerg Microbes Infect. 2021;10:1300–8. https://doi.org/10.1080/22221751.2021.1944323
29. Chow NA, Muñoz JF, Gade L, Berkow EL, Li X, Welsh RM, et al. Tracing the evolutionary history and global expansion of *Candida auris* using population genomic analyses. MBio. 2020;11:e03364-19. https://doi.org/10.1128/mBio.03364-19
30. Lehmann PF, Lin D, Lasker BA. Genotypic identification and characterization of species and strains within the genus *Candida* by using random amplified polymorphic DNA. J Clin Microbiol. 1992;30:3249–54. https://doi.org/10.1128/jcm.30.12.3249-3254.1992
31 Etienne KA, Gillece J, Hilsabeck R, Schupp JM, Colman R, Lockhart SR, et al. Whole genome sequence typing to investigate the *Apophysomyces* outbreak following a tornado in Joplin, Missouri, 2011. PLoS One. 2012;7:e49989. https://doi.org/10.1371/journal.pone.0049989
32. Lee SC, Billmyre RB, Li A, Carson S, Sykes SM, Huh EY, et al. Analysis of a food-borne fungal pathogen outbreak: virulence and genome of a *Mucor circinelloides* isolate from yogurt. MBio. 2014;5:e01390–14. https://doi.org/10.1128/mBio.01390-14
33. Vaux S, Criscuolo A, Desnos-Ollivier M, Diancourt L, Tarnaud C, Vandenbogaert M, et al.; Geotrichum Investigation Group. Multicenter outbreak of infections by *Saprochaete clavata*, an unrecognized opportunistic fungal pathogen. MBio. 2014;5:e02309-14. https://doi.org/10.1128/mBio.02309-14
34. Horton MV, Johnson CJ, Kernien JF, Patel TD, Lam BC, Cheong JZA, et al. *Candida auris* forms high-burden biofilms in skin niche conditions and on porcine skin. MSphere. 2020;5:e00910-19. https://doi.org/10.1128/mSphere.00910-19
35. Ramos LS, Mello TP, Branquinha MH, Santos ALS. Biofilm formed by *Candida haemulonii* species complex: structural analysis and extracellular matrix composition. J Fungi (Basel). 2020;6:46. https://doi.org/10.3390/jof6020046
36. Sherry L, Ramage G, Kean R, Borman A, Johnson EM, Richardson MD, et al. Biofilm-forming capability of highly virulent, multidrug-resistant *Candida auris*. Emerg Infect Dis. 2017;23:328–31. https://doi.org/10.3201/eid2302.161320
37. de Almeida JN Jr, Motta AL, Rossi F, Abdala E, Pierrotti LC, Kono AS, et al. First report of a clinical isolate of *Candida haemulonii* in Brazil. Clinics (São Paulo). 2012;67:1229–31. https://doi.org/10.6061/clinics/2012(10)18
38. Kim MN, Shin JH, Sung H, Lee K, Kim EC, Ryoo N, et al. *Candida haemulonii* and closely related species at 5 university hospitals in Korea: identification, antifungal susceptibility, and clinical features. Clin Infect Dis. 2009;48:e57–61. https://doi.org/10.1086/597108

Address for correspondence: Yingchun Xu and Meng Xiao, Peking Union Medical College Hospital, Peking Union Medical College, Chinese Academy of Medical Sciences, Department of Laboratory Medicine, No.1 Shuaifuyuan Wangfujing Dongcheng District, Beijing, 100730 China; email: xycpumch@139.com and cjtcxiaomeng@aliyun.com

Extended Viral Shedding of MERS-CoV Clade B Virus in Llamas Compared with African Clade C Strain

Jordi Rodon, Anna Z. Mykytyn, Nigeer Te,[1] Nisreen M.A. Okba, Mart M. Lamers, Lola Pailler-García, Guillermo Cantero, Irina Albulescu, Berend-Jan Bosch, Malik Peiris, Albert Bensaid, Júlia Vergara-Alert, Bart L. Haagmans, Joaquim Segalés

Middle East respiratory syndrome coronavirus (MERS-CoV) clade B viruses are found in camelids and humans in the Middle East, but clade C viruses are not. We provide experimental evidence for extended shedding of MERS-CoV clade B viruses in llamas, which might explain why they outcompete clade C strains in the Arabian Peninsula.

Middle East respiratory syndrome coronavirus (MERS-CoV) infections cause severe pneumonia, acute respiratory distress syndrome, and even lethal disease in humans. High case-fatality rates are reported in the Middle East (*1*), where the virus is endemic and represents a major human health threat. Although major travel-associated outbreaks have occurred and nosocomial transmissions have been documented, MERS-CoV is primarily carried and transmitted to humans by dromedary camels, which are the natural reservoirs and main source of zoonotic events (*2*). All primary cases of MERS-CoV in humans reported during July–December 2021 occurred in persons who had been exposed to dromedary camels (*3*). Susceptible camelid species, such as dromedaries, llamas, and alpacas (*4*), as opposed to humans, do not experience severe disease upon MERS-CoV infection. Infection in camelids is characterized by upper respiratory tract replication, abundant infectious viral shedding, and high transmission potential (*2*). Furthermore, robust and transient innate immune responses in alpacas correlate with virus clearance in the respiratory epithelia (*5*,*6*).

High seroprevalences and active circulation of MERS-CoV have been determined in dromedary camels from the Arabian Peninsula and Africa (*7*). Although >80% of the global camel population is found in Africa (https://www.fao.org/faostat) and MERS-CoV infection is widespread in dromedaries in Africa, zoonotic disease has only been reported in the Arabian Peninsula. Serologic and molecular evidence of MERS-CoV infection in camel handlers exists (*8*–*11*), but no zoonotic transmission has been reported in Africa. Despite continuous trade of dromedaries into the Arabian Peninsula, African clade C MERS-CoV strains have not been detected in the region. One explanation for the dominance of clade B strains in the Middle East could be their increased fitness compared with African clade C viruses. A recent study demonstrated increased replication competence of MERS-CoV clade B Arabian viruses compared with different clade C African strains in human lung ex vivo cultures and in a transgenic mouse model expressing the human cell receptor for MERS-CoV (human dipeptidyl peptidase-4 [hDPP4]) (*12*). However, the replication and

Author affiliations: Unitat Mixta d'Investigació IRTA-UAB en Sanitat Animal, Centre de Recerca en Sanitat Animal (CReSA), Campus de la Universitat Autònoma de Barcelona, Bellaterra, Spain (J. Rodon, N. Te, L. Pailler-García, G. Cantero, A. Bensaid, J. Vergara-Alert, J. Segalés); IRTA, Programa de Sanitat Animal, CReSA, Campus de la Universitat Autònoma de Barcelona, Bellaterra (J. Rodon, N. Te, L. Pailler-García, G. Cantero, A. Bensaid, J. Vergara-Alert); Erasmus Medical Centre, Rotterdam, the Netherlands (A.Z. Mykytyn, N.M.A. Okba, M.M. Lamers, B.L. Haagmans); Utrecht University, Utrecht, the Netherlands (I. Albulescu, B.-J. Bosch); The University of Hong Kong, Hong Kong, China (M. Peiris); Facultat de Veterinària, Universitat Autònoma de Barcelona, Bellaterra (J. Segalés)

DOI: https://doi.org/10.3201/eid2903.220986

[1]Current affiliation: The University of Hong Kong, Hong Kong, China

transmission competence of Arabian and African viruses in camelid reservoir species remains unknown.

The kinetics by which llamas shed infectious MERS-CoV are similar to those of dromedary camels, so they are considered a reliable surrogate model for transmission experiments (*2*,*4*). Therefore, we experimentally investigated transmission of MERS-CoV viruses in llamas.

The Study

We used a previously developed direct-contact model in which the transmission of a MERS-CoV clade B isolate (Qatar15/2015) was assessed in llamas (*13*,*14*). In brief, we kept a group of 5 llamas inside an experimental enclosure (Appendix Figure 1, panel A, https://wwwnc.cdc.gov/EID/article/29/3/22-0986-App1.pdf) to study the transmission capabilities of a MERS-CoV clade C isolate (MERS-CoV/Egypt2013) that was obtained from an infected dromedary (*15*). We inoculated 2 llamas with MERS-CoV and placed them in direct contact with 3 sentinels at 2 days postinoculation (dpi) (Appendix). We monitored clinical signs and body temperature and collected nasal swab specimens for virologic studies. In addition, we retrieved experimental data from MERS-CoV Qatar15/2015-inoculated and in-contact llamas (*13*,*14*) and performed comparative analyses.

We specifically selected the animals used in the transmission studies to be 6-to-10-month-old juveniles of similar geographic origin, sex, and health status background. All animal experimentation and MERS-CoV handling were conducted at the Biosafety Level 3 facilities of the Biocontainment Unit of IRTA CReSA (Barcelona, Spain). Animal handling and experimental procedures were approved by the Ethical and Animal Welfare Committee of IRTA and by the Ethical Commission of Animal Experimentation of the Autonomous Government of Catalonia (approval nos. FUE-2017–00561265 and CEA-OH/10942/1).

Rectal temperatures of all animals remained at basal levels (37°C–40°C), and no animals displayed clinical signs during the study. We detected no gross or microscopic lesions in the upper or lower respiratory tracts of any studied llama, independent of their experimental group. Animals inoculated with a high dose of either MERS-CoV Egypt/2013 (clade C) or Qatar15/2015 (clade B) had similar levels of genomic and subgenomic viral RNA in nasal swab specimens for 2 weeks (Figure 1, panels A, B). They also shed

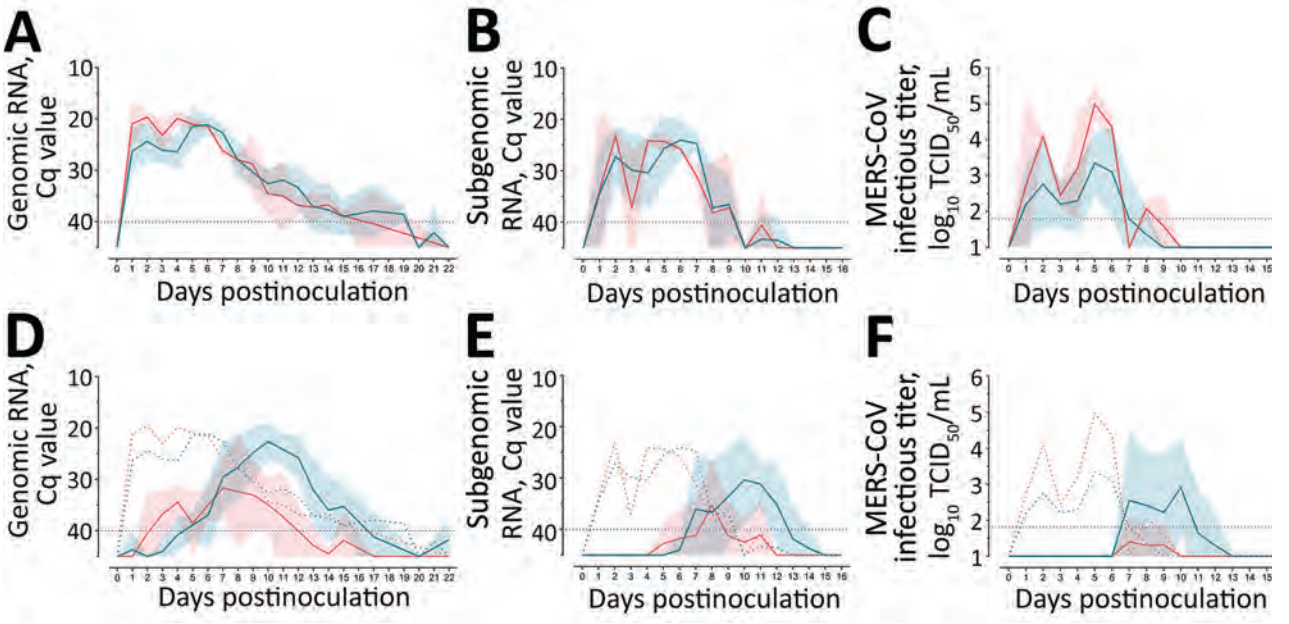

Figure 1. MERS-CoV RNA and infectious virus shedding in llamas experimentally infected with MERS-CoV Egypt/2013 (red) or Qatar15/2015 (blue) strains. A–C) Viral RNA and infectious MERS-CoV shedding of inoculated animals. Genomic (A) and subgenomic (B) viral RNA were quantified in nasal swab samples collected at different times after MERS-CoV inoculation. Infectious MERS-CoV titers (C) were demonstrated in nasal swab specimens collected on different days after MERS-CoV inoculation. Solid lines indicate mean values determined for different MERS-CoV–inoculated groups; shadings represents SD intervals. D–F) Infection profile of naive in-contact llamas). Genomic (D) and subgenomic (E) viral RNA quantified in nasal swab samples collected at different times after MERS-CoV inoculation. Infectious MERS-CoV titers (F) were demonstrated in nasal swab samples collected on different days after MERS-CoV inoculation. Solid lines indicate mean values of the groups of animals infected by contact; shaded areas represent SD intervals. Colored dashed lines indicate mean values calculated for MERS-CoV–inoculated animals. Horizontal dashed lines depict detection limits of assays. Cq, quantification cycle; MERS-CoV, Middle East respiratory syndrome coronavirus; $TCID_{50}$, 50% tissue culture infective dose.

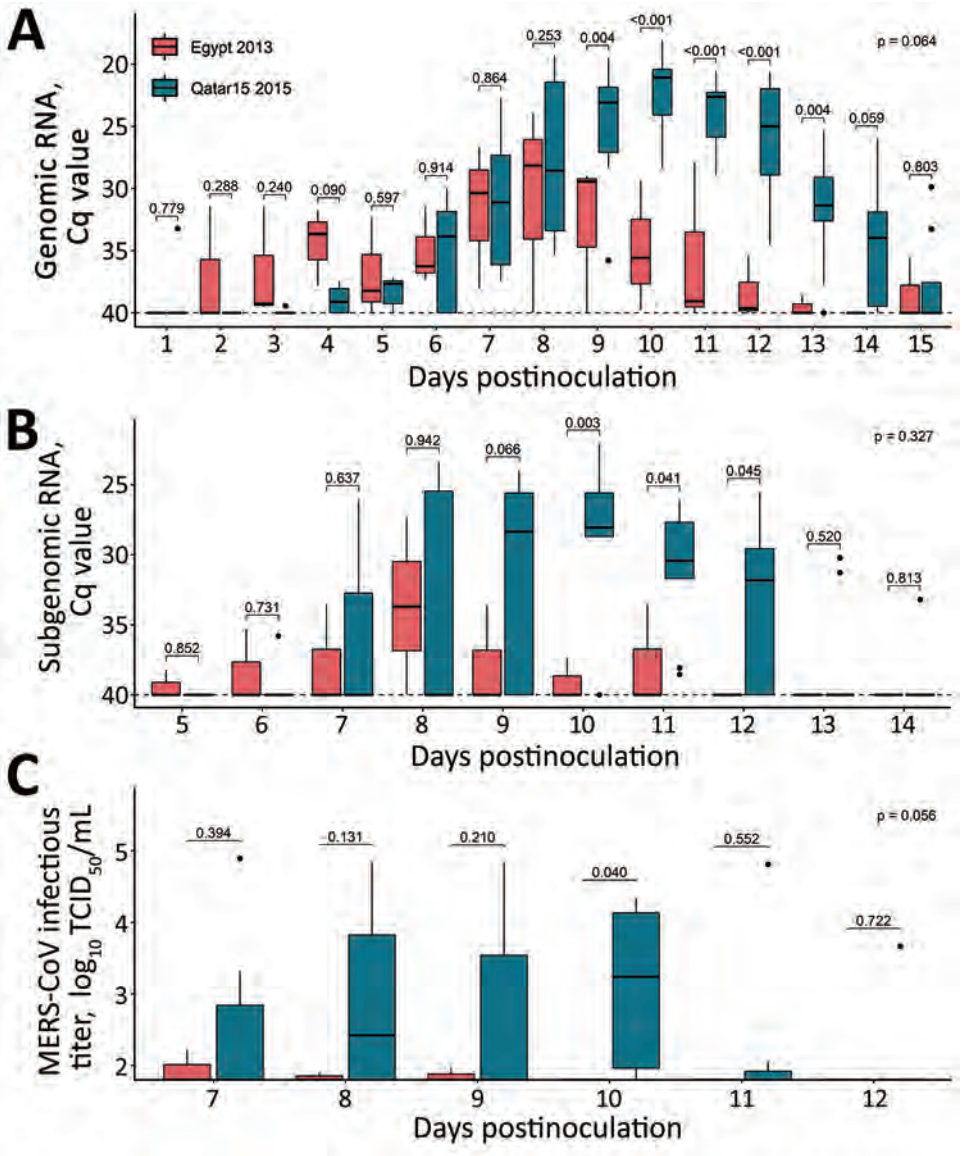

Figure 2. Mixed model analyzing the transmission competence of each MERS-CoV strain over time in investigation of llamas experimentally infected with MERS-CoV. Boxplots show daily virus shedding of sentinel llamas infected with MERS-CoV Egypt/2013 (red) or Qatar15/2015 strains (blue) after direct exposure to inoculated llamas. A, B) Genomic (A) and subgenomic (B) viral RNA quantification in nasal swabs collected throughout the study. C) Infectious MERS-CoV titers. Only the time points considered in the mixed models are represented. Horizontal lines within boxes indicate medians; box tops and bottoms indicate interquartile ranges; error bars indicate 95% CIs; black dots indicate outliers. p values are indicated above the boxes; p values indicate statistical differences between areas under the curve of the experimental groups, as calculated by Wilcoxon test. Cq, quantification cycle; MERS-CoV, Middle East respiratory syndrome coronavirus; $TCID_{50}$, 50% tissue culture infective dose.

high titers of infectious virus during the first week after inoculation in a similar biphasic pattern (Figure 1, panel C), indicating that the doses used to inoculate the animals caused productive infection with both strains. Although viral shedding was comparable between both experimental groups, higher infectious titers were detected in Egypt/2013-inoculated llamas. The infection was characterized by a first peak of shedding at 2 dpi and a subsequent reduction in MERS-CoV viral loads, followed by a secondary peak before viral clearance.

The African MERS-CoV isolate was transmitted to 2 of 3 in-contact animals in this study, as determined by quantitative reverse transcription PCR (Figure 1, panels D, E), but infectious virus shedding in contact animals largely remained below threshold levels (Figure 1, panel F). Infectious MERS-CoV Egypt/2013 could only be isolated sporadically and at titers close to the limit of detection. In contrast, the Arabian MERS-CoV Qatar15/2015 isolate was transmitted to all direct-contact llamas, leading to productive infection (Figure 1, panels D–F). Of note, genomic and subgenomic MERS-CoV Egypt/2013 RNA was detected at lower levels and cleared faster in direct-contact llamas than in sentinels infected with the MERS-CoV Qatar15/2015 strain (Figure 1, panels D, E). In the remaining sentinel, a productive infection did not develop, but the animal was naturally exposed to MERS-CoV Egypt/2013, as indicated by traces of genomic RNA in NS at 3–7, 10, and 12 dpi (cycle quantitation values >37) and development of serum neutralizing antibodies (nAbs) to MERS-CoV (Appen-

dix Figure 2). Subgenomic RNA analyses indicated no evidence for either viral replication or shedding in this llama throughout the study. Statistical analyses in sentinel animals showed a significant reduction in MERS-CoV Egypt/2013 replication and shedding period compared with those observed in llamas exposed to MERS-CoV Qatar15/2015 strain (Figure 2). Regardless of the MERS-CoV strain investigated, nAbs were detected starting at 2 weeks after infection in all inoculated animals and in-contact sentinels (Appendix Figure 2). We did not find statistical differences in serum nAb levels among experimental groups.

Altogether, our data demonstrated transmission of both MERS-CoV strains, which resulted in decreased viral replication and shedding capabilities of the Egypt/2013 strain compared with the Qatar15/2015 strain in sentinel llamas infected by contact. Therefore, the Egypt/2013 strain might have a lower potential of transmission than the Qatar15/2015 strain.

Conclusions

The results of our experimental investigation might explain why MERS-CoV clade C strains have not been established in the Arabian Peninsula after being introduced through imported camels and competing with enzootic clade B viruses. However, further studies are needed to determine whether this potentially reduced transmissibility is a common feature of the diverse MERS-CoV lineages found in dromedaries in Africa. Specific amino acid substitutions in the spike protein or in other genomic regions of African clade C viruses might be determinant of the low replication phenotype observed in the in-contact animals in our study, as has been previously observed in human cells (*12*). However, viral or host factors that play a key role in conferring replication and transmission competence remain to be explored in camelid reservoirs. High MERS-CoV genome stability was previously described in llamas infected with the Qatar15/2015 strain (*13*). Thus, eventual mutations arising from animals infected with the Egypt/2013 strain were not expected, and no sequencing was performed in those infected animals. Nonetheless, our study provides in vivo experimental data demonstrating reduced MERS-CoV fitness of 1 African clade C isolate to in-contact camelids compared with an Arabian clade B isolate. In addition, reduced MERS-CoV shedding from infected camelids might limit spillover to humans. Introducing MERS-CoV clade B strains to Africa through infected camelids must be avoided, because these strains might outcompete African MERS-CoV clade C strains and pose a greater zoonotic and pandemic threat in Africa.

This study was performed as part of the Zoonotic Anticipation and Preparedness Initiative (ZAPI project) (Innovative Medicines initiative [IMI] grant 115760), with assistance and financial support from IMI and the European Commission and contributions from EFPIA partners. J.R. was partially supported by the VetBioNet project (EU Grant Agreement INFRA-2016-1 N°731014) and the crowdfunding initiative #Yomecorono, available online at https://www.yomecorono.com (accessed on June 16, 2022). IRTA is supported by CERCA Programme/Generalitat de Catalunya.

About the Author

Dr. Rodon conducted his doctoral research at the Animal Health Department of IRTA-CReSA, Barcelona, Spain. His primary research interest is reemerging viral zoonotic diseases with pandemic potential, with particular focus on the One Health approach.

References

1. World Health Organization. MERS situation update—August 2021 [cited 2022 Jun 15]. https://applications.emro.who.int/docs/WHOEMCSR451E-eng.pdf
2. Te N, Ciurkiewicz M, van den Brand JMA, Rodon J, Haverkamp A-K, Vergara-Alert J, et al. Middle East respiratory syndrome coronavirus infection in camelids. Vet Pathol. 2022;59:546–55. https://doi.org/10.1177/03009858211069120
3. Food and Agriculture Organization Of the United Nations. MERS-CoV situation update. 2021 [cited 2022 Jun 15]. https://www.fao.org/ag/againfo/programmes/en/empres/mers/situation_update.html
4. Vergara-Alert J, Vidal E, Bensaid A, Segalés J. Searching for animal models and potential target species for emerging pathogens: experience gained from Middle East respiratory syndrome (MERS) coronavirus. One Health. 2017;3:34–40. https://doi.org/10.1016/j.onehlt.2017.03.001
5. Te N, Rodon J, Ballester M, Pérez M, Pailler-García L, Segalés J, et al. Type I and III IFNs produced by the nasal epithelia and dimmed inflammation are features of alpacas resolving MERS-CoV infection. PLoS Pathog. 2021;17:e1009229. https://doi.org/10.1371/journal.ppat.1009229
6. Te N, Rodon J, Pérez M, Segalés J, Vergara-Alert J, Bensaid A. Enhanced replication fitness of MERS-CoV clade B over clade A strains in camelids explains the dominance of clade B strains in the Arabian Peninsula. Emerg Microbes Infect. 2021;1–51.
7. Reusken CBEM, Messadi L, Feyisa A, Ularamu H, Godeke G-J, Danmarwa A, et al. Geographic distribution of MERS coronavirus among dromedary camels, Africa. Emerg Infect Dis. 2014;20:1370–4. https://doi.org/10.3201/eid2008.140590
8. Munyua PM, Ngere I, Hunsperger E, Kochi A, Amoth P, Mwasi L, et al. Low-level Middle East respiratory syndrome coronavirus among camel handlers, Kenya, 2019. Emerg Infect Dis. 2021;27:1201–5. https://doi.org/10.3201/eid2704.204458
9. Liljander A, Meyer B, Jores J, Müller MA, Lattwein E, Njeru I, et al. MERS-CoV antibodies in humans, Africa,

2013–2014. Emerg Infect Dis. 2016;22:1086–9. https://doi.org/10.3201/eid2206.160064
10. Kiyong'a AN, Cook EAJ, Okba NMA, Kivali V, Reusken C, Haagmans BL, et al. Middle East respiratory syndrome coronavirus (MERS-CoV) seropositive camel handlers in Kenya. Viruses. 2020;12:396. https://doi.org/10.3390/v12040396
11. Mok CKP, Zhu A, Zhao J, Lau EHY, Wang J, Chen Z, et al. T-cell responses to MERS coronavirus infection in people with occupational exposure to dromedary camels in Nigeria: an observational cohort study. Lancet Infect Dis. 2021;21:385–95. https://doi.org/10.1016/S1473-3099(20)30599-5
12. Zhou Z, Hui KPY, So RTY, Lv H, Perera RAPM, Chu DKW, et al. Phenotypic and genetic characterization of MERS coronaviruses from Africa to understand their zoonotic potential. Proc Natl Acad Sci U S A. 2021;118:e2103984118. https://doi.org/10.1073/pnas.2103984118
13. Rodon J, Okba NMA, Te N, van Dieren B, Bosch B-J, Bensaid A, et al. Blocking transmission of Middle East respiratory syndrome coronavirus (MERS-CoV) in llamas by vaccination with a recombinant spike protein. Emerg Microbes Infect. 2019;8:1593–603. https://doi.org/10.1080/22221751.2019.1685912
14. Rodon J, Mykytyn A, Martinez S, Cantero G, Albulescu IC, Bosch B-J, et al. Protective efficacy of an RBD-based Middle East respiratory syndrome coronavirus (MERS-CoV) particle vaccine in llamas. One Health Outlook. 2022;4:12. PMID 35739576
15. Chu DKW, Poon LLM, Gomaa MM, Shehata MM, Perera RAPM, Abu Zeid D, et al. MERS coronaviruses in dromedary camels, Egypt. Emerg Infect Dis. 2014;20:1049–53. https://doi.org/10.3201/eid2006.140299

Address for correspondence: Bart L. Haagmans, Department of Viroscience, Erasmus Medical Centre, 3000 CA Rotterdam, The Netherlands; email: b.haagmans@erasmusmc.nl; Joaquim Segalés, Centre de Recerca en Sanitat Animal (CReSA, IRTA-UAB), Campus de la UAB, 08193 Bellaterra, Spain; email: joaquim.segales@irta.cat

etymologia revisited

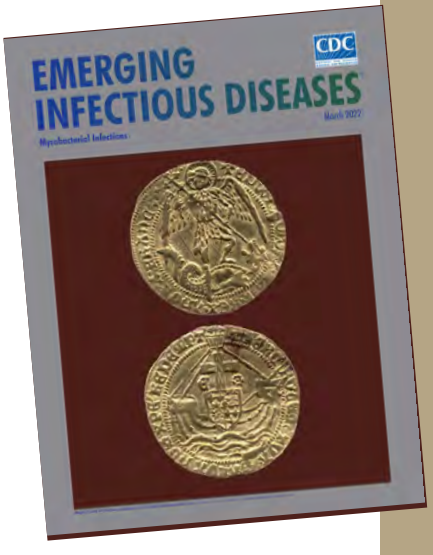

Originally published in March 2022

Schizophyllum commune

[skiz-of'-ĭ-ləm kom'-yoon]

Schizophyllum commune, or split-gill mushroom, is an environmental, wood-rotting basidiomycetous fungus. *Schizophyllum* is derived from "*Schíza*" meaning split because of the appearance of radial, centrally split, gill like folds; "*commune*" means common or shared ownership or ubiquitous. Swedish mycologist, Elias Magnus Fries (1794–1878), the Linnaeus of Mycology, assigned the scientific name in 1815. German mycologist Hans Kniep in 1930 discovered its sexual reproduction by consorting and recombining genomes with any one of numerous compatible mates (currently >2,800).

Sources

1. Chowdhary A, Kathuria S, Agarwal K, Meis JF. Recognizing filamentous basidiomycetes as agents of human disease: a review. Med Mycol. 2014;52: 782–97. https://doi.org/10.1093/mmy/myu047
2. Cooke WB. The genus *Schizophyllum*. Mycologia. 1961;53:575–99. https://doi.org/10.1080/00275514.1961.12017987
3. Greer DL. Basidiomycetes as agents of human infections: a review. Mycopathologia. 1978;65:133–9. https://doi.org/10.1007/BF00447184
4. O'Reilly P. *Schizophyllum commune*, split gill fungus, 2016 [cited 2021 Aug 23]. https://www.first-nature.com/fungi/schizophyllum-commune.php
5. Raper CA, Fowler TJ. Why study *Schizophyllum*? Fungal Genet Rep. 2004;51:30–6. https://doi.org/10.4148/1941-4765.1142

Seroprevalence of Specific SARS-CoV-2 Antibodies during Omicron BA.5 Wave, Portugal, April–June 2022

Irina Kislaya, Aryse Melo, Marta Barreto, Camila Henriques, Carlos Aniceto, Carla Manita, Sara Ramalhete, João Almeida Santos, Sofia Soeiro, Ana Paula Rodrigues; ISN4COVID-19 Group[1]

After the rapid spread of SARS-CoV-2 BA.5 Omicron lineage in Portugal, we developed a seroepidemiologic survey based on a sample of 3,825 residents. Results indicated that from April 27 through June 8, 2022, the estimated seroprevalence of SARS-CoV-2 nucleocapsid or spike IgG was 95.8%, which indicates a high level of protection.

Serial seroepidemiologic surveys contribute information about pandemic dynamics; monitoring population-level SARS-CoV-2 antibody distribution establishes trends in postinfection and vaccine-induced immunity. Such surveys are essential to integrated surveillance systems for respiratory infections (*1*).

During May 2020–June 2022, the National Health Institute Doutor Ricardo Jorge, in partnership with the National Clinical Pathology Laboratories Association, the Portuguese Association of Clinical Analysts, and a nationwide network of public hospitals, conducted 4 serial seroepidemiologic surveys (ISN1COVID-19, ISN2COVID-19, ISN3COVID-19, and ISN4COVID-19). Number of study participants ranged from 2,301 to 8,463 residents of Portugal (*2*–*4*) (Figure 1). The fourth survey (ISN4COVID-19) was conducted from April 27, 2022, through June 8, 2022, after the mandatory mask mandate was lifted and during rapid spread of the SARS-CoV-2 BA.5 Omicron lineage (*5*) (Appendix Figure 1, https://wwwnc.cdc.gov/EID/article/29/3/22-1546-App1.pdf) and the ongoing second booster vaccination campaign (*6*) (Appendix Figure 2). We estimated SARS-CoV-2 seroprevalence, distinguishing between antibodies against the spike (S) and nucleocapsid (N) proteins. This distinction is relevant because currently deployed vaccines elicit an immune response against the S protein, so the presence of N antibodies could be interpreted as a proxy for postinfection seroprevalence in highly vaccinated populations.

The study was approved by the Ethics Committee of the National Health Institute Doutor Ricardo Jorge. The need for participants' informed consent was waived by the Ethics Committee because of the irreversible anonymization of the data at collection sites.

The Study

Using a 2-stage nonprobability quota sampling design, we collected 3,825 irreversibly anonymized residual serum samples from persons who had undergone blood testing for reasons unrelated to COVID-19 in a nationwide network of participating clinical pathology laboratories and public hospitals (Figure 2; Appendix). For each sample, we qualitatively determined the type of IgG against SARS-CoV-2 N protein and quantitatively determined IgG against S protein by using Abbott SARS-CoV-2 Chemiluminescent Microparticle Immunoassays in the ARCHITECT i1000SR (https://www.abbott.com). We considered samples with S IgG levels >50 arbitrary units (AU)/mL to be positive. Total seroprevalence was defined as positivity for S or N IgG.

We stratified seroprevalence by patient sex, age group, and region of residence. To compare seroprevalence between population subgroups, we used a design-adjusted χ^2 test (*7*). We described the distribution of quantitative S IgG in terms of geometric means and respective 95% CIs (Appendix). We stratified estimates by patient age group, and sex. To account for

Author affiliation: Instituto Nacional de Saúde Doutor Ricardo Jorge, Lisbon, Portugal

DOI: https://doi.org/10.3201/eid2903.221546

[1]Group members are listed at the end of this article.

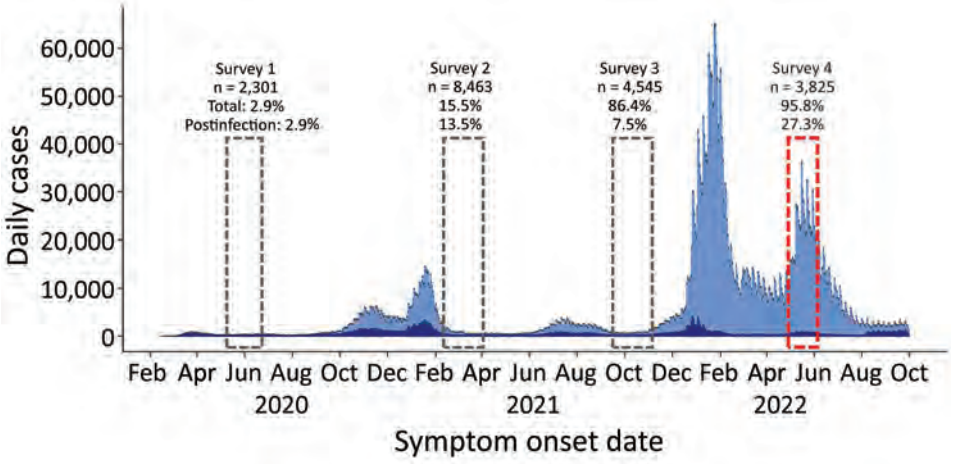

Figure 1. Daily number of cases and percentages of SARS-CoV-2 seroprevalence in 4 serial seroepidemiologic surveys in Portugal, May 2020–June 2022. Tick marks correspond to the first day of the month.

sampling design, we weighted all estimates to match the distribution of the Portugal population by sex, age group, and region of residence. We conducted statistical analyses by using Stata 15.1 software (StataCorp LLC, https://www.stata.com).

From 3,825 collected residual serum samples, 27.3% were positive for N IgG, 95.0% for S IgG, and 95.8% for either N or S IgG (Table 1). Seroprevalence of N IgG was similar by sex but varied significantly by age group, highest among children (39.2% among those 0–4 years of age and 40.0% among those 10–19 years of age) and lowest (17.3%) among adults ≥70 years of age. The age-related pattern for seroprevalence of S IgG differed; estimated rates were lower among those 0–4 years of age (71.2%) and 5–9 years of age (78.2%) than for those in the remaining age groups. S IgG seroprevalence also was lower in Algarve (91.0%) than in other regions of Portugal. Total seroprevalence also varied by region and age group, showing patterns similar to those of S IgG.

We observed lower S IgG levels among children <10 years of age (geometric mean 180.4 AU/mL for 0–4 and 426.6 AU/ml for 5–9 years of age). S IgG levels were also lower among persons ≥70 years of age (geometric mean 4,558.5 AU/mL) than among middle-aged adults. Higher S IgG levels were observed among those positive for N IgG (Table 2).

Conclusions

The fourth observational nationwide study (ISN-4COVID-19) estimated that during the early Omicron BA.5 circulation period, most residents of Portugal (95.5%, 95% CI 95.0–96.4%) had specific SARS-CoV-2 antibodies resulting from infection or vaccination. Total seroprevalence increased by ≈10 percentage points compared with findings from a previous survey developed during September–November 2021 (Figure 1) (*4*). Seropositivity in Portugal during April–June 2022 was comparable to the reported seroprevalence in Scotland during May–June 2022 (95.7%) (*8*) and to that in Navarra, Spain, during May–July 2022 (S IgG 92.7%) (*9*). Seropositivity in Portugal was also in line with the high vaccination coverage achieved in Portugal (Appendix Figure 2) (*6*).

Our results reveal a steep increase in N IgG seroprevalence for all age groups between the third and

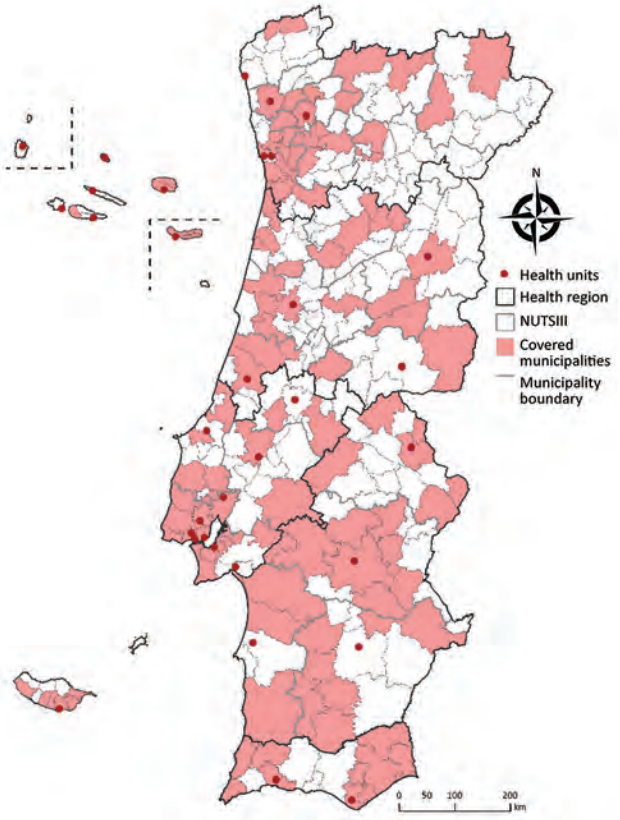

Figure 2. Data collection sites for study of seroprevalence of specific SARS-CoV-2 antibodies during the Omicron BA.5 wave, Portugal, April–June 2022 (ISN4COVID-19 study). NUTSIII, territorial units for statistics level III.

Table 1. Seroprevalence of specific SARS-CoV-2 antibodies, stratified by sex, age group, and region of residence, Portugal, April 27–June 8, 2022*

Characteristic	N IgG positive, % (95% CI)	S IgG positive, % (95% CI)	N or S IgG positive, % (95% CI)
Overall	27.3 (25.5–29.1)	95.0 (94.2–95.7)	95.8 (95.0–96.4)
Sex	p = 0.8789	p = 0.9801	p = 0.8544
M	27.4 (25.0–30.0)	95.0 (93.9–95.9)	95.7 (94.6–96.6)
F	27.1 (24.7–29.7)	95.1 (93.7–96.1)	95.8 (94.6–96.8)
Age group, y	p<0.001	p<0.001	p<0.001
0–4	39.2 (32.3–46.5)	71.2 (64.4–77.2)	76.2 (69.6–81.7)
5–9	32.9 (26.6–39.9)	78.2 (71.5–83.6)	78.7 (72.1–84.1)
10–19	40.0 (35.0–45.2)	95.2 (92.5–97.0)	96.2 (93.7–97.7)
20–29	29.7 (24.8–35.2)	97.9 (95.7–99.0)	98.6 (96.5–99.5)
30–39	30.3 (25.2–36.0)	96.3 (93.4–98.0)	96.9 (94.1–98.4)
40–49	27.2 (22.3–32.7)	96.6 (93.8–98.2)	97.7 (95.3–98.9)
50–59	27.0 (22.2–32.4)	97.5 (95.0–98.8)	97.7 (95.1–98.9)
60–69	21.0 (16.7–26.0)	97.0 (94.4–98.4)	97.4 (94.8–98.7)
≥70	17.3 (13.5–21.7)	96.7 (94.2–98.2)	97.2 (94.8–98.6)
Region of residence	p = 0.1465	p = 0.0141	p = 0.0315
Norte	24.8 (21.6–28.3)	96.4 (94.9–97.5)	96.8 (95.3–97.8)
Centro	28.2 (24.3–32.6)	95.2 (93.0–96.7)	95.9 (93.8–97.3)
Lisboa e Vale do Tejo	29.3 (26.3–32.6)	94.2 (92.5–95.6)	95.3 (93.7–96.5)
Alentejo	25.4 (21.7–29.5)	95.3 (93.1–96.9)	96.0 (93.9–97.3)
Algarve	27.6 (23.2–32.5)	91.0 (87.6–93.5)	91.7 (88.4–94.1)
Madeira	31.0 (26.8–35.5)	94.1 (92.0–95.7)	95.6 (93.7–97.0)
Açores	24.4 (20.6–28.6)	93.7 (91.1–95.6)	95.9 (93.8–97.3)

*ISN4COVID-19 study. Weighted to match the distribution of the resident population of Portugal (Census 2021) by sex, age group, and region. p values indicate design-adjusted χ^2 testing used to compare seroprevalence by sex, age group, and region. N, nucleocapsid protein; S, spike protein.

fourth surveys (Appendix Figure 3) (*4*), comparable to intensive epidemic activity in Portugal during January–June 2022 (*10*). The age-related pattern of lower N IgG seroprevalence in older age groups observed in our study is in line with age-specific SARS-COV-2 notifications to the National Epidemiological Surveillance Information System in early 2022 (*10*) and similar to results from Canada (*11*) and Navarra (*9*), which reported lower postinfection seroprevalence for the older than younger age groups.

Table 2. Geometric mean of specific antibodies against SARS-CoV-2 spike protein IgG, stratified by patient sex, age group, and region of residence, Portugal, April 27–June 8, 2022*

Characteristic	Geometric mean, AU/mL (95% CI)
Sex	
M	4,344.8 (3,909.5–4,828.6)
F	4,662.3 (4,150.5–5,237.1)
Age group, y	
0–4	180.4 (118.9–273.6)
5–9	426.6 (285.4–637.7)
10–19	4,750.8 (3,795.5–5,946.5)
20–29	6,011.5 (5,050.5–7,155.4)
30–39	5,433.3 (4,342.8–6,797.6)
40–49	6,940.7 (5,645.7–8,532.9)
50–59	7,669.3 (6,297.5–9,340.0)
60–69	5,484.6 (4,420.3–6,805.2)
≥70	4,558.5 (3,708.4–5,603.4)
Region of residence	
Norte	5,020.5 (4,358.0–5,783.6)
Centro	5,020.9 (4,158.3–6,062.4)
Lisboa e Vale do Tejo	3,998.1 (3,451.9–4,630.9)
Alentejo	5,038.9 (4,177.2–6,078.3)
Algarve	2,970.2 (2,294.2–3,845.3)
Madeira	5,070.6 (4,188.3–6,138.8)
Açores	4,339.1 (3,523.1–5,344.1)
Positivity for nucleocapsid IgG	
Positive	9,233.6 (8,099.1–10,527.0)
Negative	3,452.8 (3,146.7–3,788.6)

*ISN4COVID-19 study. Weighted to match the distribution of the resident population of Portugal (Census 2021) by sex, age group, and region.

Regarding the pediatric population, our results demonstrate high postinfection seroprevalence among children not eligible for COVID-19 vaccination. Among children 0–4 years of age, seroprevalence was >75%, higher than estimates reported for unvaccinated pediatric populations by European Union countries at the beginning of the Omicron BA.1 wave: 28.8% among children 1–4 years of age in Ireland in January 2022 (*12*); 45% among preschool children in Italy in February 2022 (*13*); and >4-fold as high as seroprevalence among children recruited in our previous seroepidemiologic study conducted during September–October 2021 in Portugal (ISN-3COVID-19) (Appendix Figure 3) (*4*). The percentage of persons seropositive for N IgG in the 0–4 year age group was lower (39.2%) than for those positive for S IgG (71.2%). This finding may be associated with a previously reported shorter half-life of N IgG (*14*). The results regarding N IgG positivity should be interpreted with caution because they may reflect only the most recent infections.

Antibody levels were lower among those at the extremes of age distribution. This finding may be related to the course of the vaccination campaign and age-related immunosenescence. Since September 2021, the first booster vaccinations were rolled out by age criteria; those in the older age groups were vaccinated earlier and experienced a more

pronounced wane of antibody levels (*15*) compared with middle-aged adults who were vaccinated more recently. Although starting May 15, 2022, a second booster was offered for persons ≥80 years of age and for institutionalized persons, our results have not yet reflected the effect of that change. The second booster recommendation was issued during collection of ISN4COVID-19 data, and at the end of the study period, only 4.4% of the population had received the second booster (*6*).

Lower antibody levels in children may be associated with postinfection immunity; antibody levels that were lower after infection than after vaccination have been reported (*14*,*15*). Furthermore, at the time of data collection, a booster was not recommended for the pediatric population, which may also explain lower antibody levels.

Among the limitations of our study, the nonrandom sampling and recruitment strategy can result in selection bias because participants seeking clinical care might differ from the general population. Also, the study might not capture reinfections, and because seroreversion occurs without recent vaccination or infection, we were unable to estimate a cumulative number of SARS-CoV-2 infections in Portugal.

In summary, almost all persons in the Portugal population have specific antibodies against SARS-CoV-2. Even among children not eligible for vaccination, ≈75% have SARS-CoV-2 antibodies. Among adults, IgG values are higher for those in age groups who received their vaccine booster more recently.

Members of ISN4COVID-19 Group: Paulo Gonçalves, Rita Matos, Inês Costa, Nuno Verdasca, Fátima Martins, Jorge Machado, Raquel Guiomar, Ana Rita Torres, Carlos Matias Dias, Ana Loureiro, Filomena Caldeira, Adriana Coutinho, M. Paula Falcão, Alzira Louro, Igor Filipciuc, Marisa Isabel da Conceição Belchior, Claudia Sofia Barão Ferreira, Ingrid Villanueva, Sara Moura, Marlene Silva, Rita Paulino, Conceição Cardoso, Ana Margarida Casaca, Maria Vitória Antunes de Matos, Lúcia Coimbra, Nazaré Boavida, Paula Cristina Justino Gama, Afonso Tavares Leite Barros dos Santos, Ana Maria Cabrita Frota Fernandes, Bela Jerónima Nogueira, Rui Pedro Vieira Ferreira, Rui Manuel Borges Vassal, Paula Barbeiro, Aurora Direito, Ana Paula Peleta Marques, Margarida Freitas, Gil Sequeira, Sandra Vieira, Gil Ferreira, Teresa Reis, Lucilia Araujo, Teresa Rodrigues, Lurdes Correia, Susana Gomes, Sílvia Campos, Maira João Cardoso, Angélica Ramos, Carlos Caldas, Eliana Costa, Joana Costa, José Alves, Jácome Bruges Armas, Ana Rita Couto, Paula Genuína de la Cerda Sarmento Escobar, Sónia Oliveira Dias Ávila, Luís Silva, Patricia Vargas, Maria Noia, Vanessa Cordeiro, Teresa Damião, Rita Pinto, Helena Rodrigues, Filomena Reis, André Ferreira Pinto, Fátima Vale, Ricardo Rodrigues, Ricardo Castro, Bernardo Silva, Jesuína Duarte, Isabel Santos, Ana Miranda Rosa, Adilia Vicente, José Alves, Raquel Sebastião, Patrícia Pereira, Gizela Ferreira Alves dos Santos, Ana Catarina Faria Guerreiro, Armindo Miguel Rosado Gonçalves, Maria de Fátima Narciso Rolo Raimundo, Manuel Cirne Carvalho, Mário João Santos, Nuno Aguiar, Rui Campaínha, Ana Margarida Godinho, João Pedro Freitas, Rita Batista Coelho, Maria Conceição Miranda Senra Furtado, Miguel Eduardo Magalhães Gouveia, Laura Brum, Ana Paula Farto, Susana Agostinho, Luísa Ponte, Maria Beatriz Tomaz, Joana Ramos, Alexandra Santos, Isabel Forjaz Sampaio, Ana Abreu, Paulo Aguiar, Rita Ribeiro, Ana Guia Pereira, Sandra Vieira, Jorge Nunes Oliveira, Inês Stilwell, Sandra Nóbrega, Iolanda Rodrigues, Marco Marques, Sofia Jorge, Jorge Queiroz, Mavilde Vargues, Carlos Cardoso, Rui Pinto, Ana Filipa Alves, João Fernandes.

I.K. collaborated in the study design and implementation, performed the statistical analysis, and wrote the first draft of the manuscript. A.M., C.H., C.M., S.S., and J.A.S. collaborated on the study design, samples processing, results interpretation, and critically reviewed the manuscript. C.A. and S.R. collaborated in the study implementation, data collection, results interpretation, and critically reviewed the manuscript. A.P.R. coordinated the study, was responsible for the study design and implementation, interpreted the results, and critically reviewed the manuscript. ISN4COVID-19 group members collaborated in the data collection, samples processing, results interpretation and critically reviewed the manuscript. All authors approved the final version of the manuscript and agree to be accountable for all aspects of this work

About the Author

Mrs. Kislaya is a biostatistician in the Department of Epidemiology at Instituto Nacional de Saúde Doutor Ricardo Jorge, Lisbon, Portugal. Her primary research interests include influenza and COVID-19 vaccine effectiveness, health surveys, and population-level impact of public health interventions.

References

1. Operational considerations for respiratory virus surveillance in Europe. [cited 2023 Jan 3]. https://www.ecdc.europa.eu/sites/default/files/documents/Operational-considerations-respiratory-virus-surveillance-euro-2022.pdf
2. Kislaya I, Gonçalves P, Gómez V, Gaio V, Roquette R, Barreto M, et al. SARS-CoV-2 seroprevalence in Portugal following the third epidemic wave: results of the second National Serological Survey (ISN2COVID-19). Infect Dis (Lond). 2022;54:418–24.

3. Kislaya I, Gonçalves P, Barreto M, Sousa R, Garcia AC, Matos R, et al.; ISNCOVID-19 Group. Seroprevalence of SARS-CoV-2 infection in Portugal in May-July 2020: results of the first national serological survey (ISNCOVID-19). Acta Med Port. 2021;34:87–94. https://doi.org/10.20344/amp.15122
4. Kislaya I, Gonçalves P, Ramalhete S, Barreto M, Torres AR, Gaio V, et al. SARS-CoV-2 seroprevalence following a large-scale vaccination campaign in Portugal: results of the National Serological Survey, September–November 2021. Acta Med Port. 2023;36:5–14. https://doi.org/a0.20344/amp.18528
5. National Institute of Health Doutor Ricardo Jorge. Genetic diversity of the novel coronavirus SARS-CoV-2 (COVID-19) in Portugal. August 23th 2022 report. Lisbon (Portugal): The Institute; 2022.
6. European Centre for Disease Prevention and Control. COVID-19 vaccine tracker [cited 2022 Feb 6]. https://vaccinetracker.ecdc.europa.eu/public/extensions/COVID-19/vaccine-tracker.html
7. Rao JNK, Scott AJ. On simple adjustments to chi-square tests with sample survey data. Ann Stat. 1987;15:385–97. https://doi.org/10.1214/aos/1176350273
8. Public Health Scotland. Enhanced surveillance of COVID-19 in Scotland—population-based seroprevalence surveillance [cited 2022 Aug 5]. https://publichealthscotland.scot/id/83780
9. Glück V, Grobecker S, Köstler J, Tydykov L, Bertok M, Weidlich T, et al. Immunity after COVID-19 and vaccination: follow-up study over 1 year among medical personnel. Infection. 2022;50:439–46. https://doi.org/10.1007/s15010-021-01703-9
10. Directorate-General for Health, National Institute of Health Doctor Ricardo Jorge. Monitoring of epidemiological situation on COVID-19. Report nº13—June 8, 2022 [cited 2022 Aug 10]. https://www.insa.min-saude.pt/wp-content/uploads/2022/06/20220608_Monitorizacao_COVID-19.pdf
11. Skowronski DM, Kaweski SE, Fraser M, Reyes RC, Henry B, Levett N, et al.. Serial cross-sectional estimation of vaccine- and infection-induced SARS-CoV-2 seroprevalence in British Columbia, Canada CMAJ. 2022;194 :E1599–609. https:doi.org/10.1503/cmaj.221335
12. HSE Health Protection Surveillance Centre, Dublin. Seroprevalence of antibodies to SARS-CoV-2 in children aged 1–12 years and adults aged 18+ years: results from National Serosurveillance Programme Collection Cycle 1 [cited 2022 Aug 10]. https://www.hpsc.ie/a-z/nationalserosurveillance programme/reports/NSP%20combined%20adult%20paeds%20cycle%201%20report_final.pdf
13. Mari A, Garancini N, Barcellini L, Zuccotti GV, Alberti L, Gaia P, et al. SARS-CoV-2 seroprevalence among school-age children in Milan: how has it changed with the fourth pandemic wave? Pediatr Infect Dis J. 2022;41:e344–5. https://doi.org/10.1097/INF.0000000000003583
14. Stone M, Grebe E, Sulaeman H, Di Germanio C, Dave H, Kelly K, et al. Evaluation of commercially available high-throughput SARS-CoV-2 serologic assays for serosurveillance and related applications Emerg Infect Dis. 2022;28:672–83. https://doi.org/10.3201/eid2803.211885
15. Guiomar R, Santos AJ, Melo AM, Costa I, Matos R, Rodrigues AP, et al. Monitoring of SARS-CoV-2 specific antibodies after vaccination. Vaccines (Basel). 2022;10:154. PMID: 35214613

Address for correspondence: Irina Kislaya, Instituto Nacional de Saúde Doutor Ricardo Jorge, Av. Padre Cruz, 1649-016 Lisbon, Portugal; email: irina.kislaya@insa.min-saude.pt

SARS-CoV-2 Incubation Period during the Omicron BA.5–Dominant Period in Japan

Tsuyoshi Ogata, Hideo Tanaka

The mean virus incubation period during the SARS-CoV-2 Omicron BA.5–dominant period in Japan was 2.6 (95% CI 2.5–2.8) days, which was less than during the Delta-dominant period. Incubation period correlated with shared meals and adult infectors. A shorter incubation suggests a shorter quarantine period for BA.5 than for other variants.

BA.5 is a subvariant of the SARS-CoV-2 Omicron variant (*1*). Since July 2022, Omicron BA.5 has been the dominant variant in Japan (*2*,*3*). According to Japan's Infectious Diseases Control Law, public health centers (PHCs) must be notified of all COVID-19 cases and conduct contact tracing (*4*). The first patient infected with SARS-CoV-2 Omicron BA.5 was reported on July 4, 2022, to the Itako PHC in Ibaraki Prefecture, Japan. The number of confirmed COVID-19 cases from July 4 through August 19, 2022, was 12,577 in the PHC's jurisdiction, which has a population of ≈265,000 persons (*5*). In our study, we estimated the incubation period (period between virus exposure and symptom onset) of SARS-CoV-2 Omicron BA.5, determined potential correlations with demographic data and transmission settings, and compared the BA.5 subvariant with other subvariants.

The Study

We enrolled COVID-19 infector/infectee pairs who lived within the Itako PHC jurisdiction and had a single definite close contact date with patients who had COVID-19 without other potential transmission settings. We calculated the incubation period by using the calendar dates of contact and symptom onset, regardless of duration or number of contacts. If a pair shared meals on July 4 and the infectee had COVID-19 symptoms on July 7, we calculated an incubation period of 3 days. If the pair shared meals on both July 4 and 5, we excluded all data from this pair. Other transmission settings included conversations in the home, a building or car, or outdoors. Procedures used for contact tracing and data collection for patient pairs with COVID-19 were similar to those described previously (*6*,*7*). Persons exposed to SARS-CoV-2 in household, workplace, or school settings were excluded if they might have been exposed at another time. We defined the patient with the later symptom onset in each pair as the infected patient.

We defined patients in the Omicron BA.5–dominant period as those who had symptoms during July 4–August 19, 2022. Genomic sequencing of 528 samples collected in Ibaraki showed 481 (91%) samples were BA.5, 40 were BA.2, and 7 were BA.1 subvariants. We defined patients in the BA.1–dominant period as those who had symptom onset during January 1–February 2, 2022. Of the 1,216 samples collected during January 3–February 6 in Ibaraki, a total of 1,158 (95%) were negative for the SARS-CoV-2 spike protein mutation L452R (*8*). Genomic sequencing showed that 92% of 22,953 variants of concern sampled in Japan during January 3–February 6 were BA.1 (*9*). We defined patients in the Delta-dominant period as those who had symptom onset during July 23–September 14, 2021, and either they or their contacts were confirmed to have L452R-positive SARS-CoV-2. Genomic sequencing detected variants of concern in Japan from July 19–September 13, 2001, as follows: 26,963 cases of B.1.617.2 (Delta), 15,009 cases of B.1.1.7 (Alpha), and 5 cases of other variants (*9*); the L452R mutation was found mostly in the Delta variant.

We extracted data for 266 infector/infectee pairs who had 1 definite date of SARS-CoV-2 exposure as follows: 122 infectees from 108 infectors during the Omicron BA.5–dominant period, 68 infectees from 49 infectors during the BA.1–dominant period, and 76 infectees from 51 infectors during the Delta-dominant period. Patient data during the BA.1–dominant

Author affiliations: Itako Public Health Center of Ibaraki Prefectural Government, Ibaraki, Japan (T. Ogata); Public Health Center of Neyagawa City, Osaka, Japan (H. Tanaka)

DOI: https://doi.org/10.3201/eid2903.221360

Table 1. Estimated overall mean incubation periods and means within percentiles for Omicron and Delta variants in study of SARS-CoV-2 incubation period during the Omicron BA.5-dominant period in Japan*

Distribution†	BA.5-dominant period, n = 122	BA.1-dominant period, n = 68	Delta-dominant period, n = 76
Overall mean	2.6 (2.5–2.8)	2.9 (2.6–3.2)	3.7 (3.4–4.0)
5th percentile	1.2 (1.1–1.4)	1.2 (1.0–1.5)	1.8 (1.5–2.1)
25th percentile	1.9 (1.8–2.0)	2.0 (1.8–2.3)	2.7 (2.4–3.0)
50th percentile (median)	2.5 (2.3–2.7)	2.7 (2.5–3.0)	3.5 (3.2–3.8)
75th percentile	3.2 (3.0–3.5)	3.6 (3.3–4.0)	4.5 (4.1–4.9)
95th percentile	4.5 (4.1–4.9)	5.2 (4.6–5.9)	6.1 (5.5–6.8)

*Values are mean no. days (95% CI). Means were calculated by fitting to gamma distribution model for SARS-CoV-2 infections during Omicron BA.5–dominant and BA.1–dominant and Delta-dominant periods.
†Distribution of patients within incubation period.

and Delta-dominant periods were obtained from previous studies (*6*,*7*). The mean (±SD) incubation periods were 2.6 (±1.0) days during the BA.5–dominant period, 2.9 (±1.3) days during the BA.1–dominant period, and 3.7 (±1.6) days during the Delta-dominant period.

When we fitted incubation period data from the BA.5–dominant period to parametric distribution models, the Akaike information criterion for gamma distribution was smaller than that for Gaussian, log-normal, and Weibull distribution models. We fitted incubation period data for each subvariant to the gamma distribution model and calculated parameters and 95% CI within a Bayesian inference framework.

The estimated mean incubation period for patients during the BA.5–dominant period was 2.6 (95% CI 2.5–2.8) days, and the median was 2.5 (95% CI 2.3–2.7) days. The mean during the BA.1–dominant period was 2.9 (95% CI 2.6–3.2) days, and the median was 2.7 (95% CI 2.5–3.0) days. During the Delta-dominant period, the mean incubation period was 3.7 (3.4–4.0) days, and the median was 3.5 (3.2–3.8) days. The estimated mean incubation period was shorter for patients during the BA.5–dominant period than during the Delta-dominant period. The 95th percentile distribution for incubation period was estimated at 4.5 (95% CI 4.1–4.9) days during the BA.5–dominant period, 5.2 (95% CI 4.6–5.9) days during the BA.1–dominant period, and 6.1 (95% CI 5.5–6.8) days during the Delta-dominant period (Table 1; Figure).

We estimated the monovariable mean incubation period of 122 patients during the BA.5–dominant period. The mean incubation period was 2.5 days for patients infected during shared meals, 2.9 days for patients without transmission during shared meals, 3.0 days for patients with infectors who were ≤19 years of age, and 2.5 days for patients with infectors who were ≥20 years of age (2.6 days for 79 patients with infectors who were 20–59 years of age and 2.1 days for 16 patients with infectors who were ≥60 years of age). We performed multivariate gamma regression analyses; transmission during shared meals (p = 0.03) and age of infector (p = 0.007) correlated significantly with incubation period (Table 2).

Conclusions

The estimated mean incubation period for patients during the Omicron BA.5–dominant period in this region was 2.6 days. Incubation periods for Omicron BA.1 were reported to be 3.3 days in Norway, 4.6

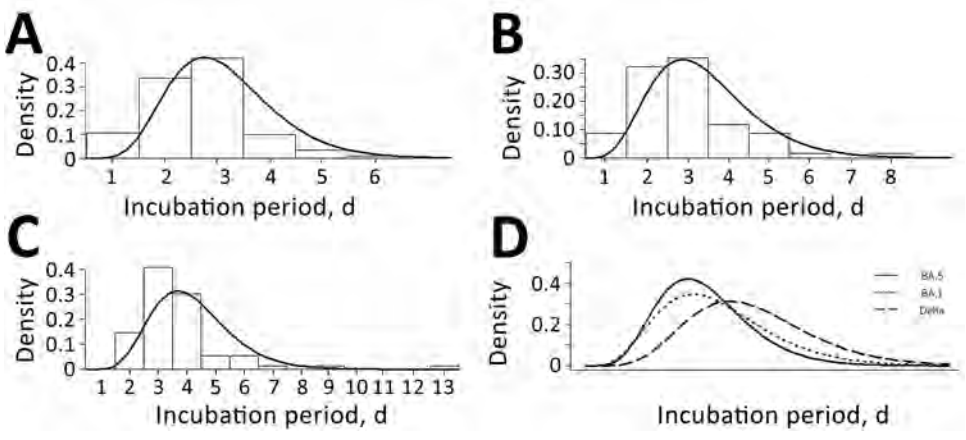

Figure. Probability densities for incubation period distribution during different SARS-CoV-2 variant-dominant periods in study of SARS-CoV-2 incubation period during the Omicron BA.5–dominant period in Japan. A–C) Histograms show probability densities for estimated gamma distribution of virus incubation periods for patients during the Omicron BA.5–dominant period (A), Omicron BA.1–dominant period (B), and Delta-dominant period (C). D) Comparison of probability densities for estimated gamma distribution of virus incubation periods among patients during the BA.5-dominant period (solid line), BA.1–dominant period (short-dashed line), and Delta-dominant period (long-dashed line).

Table 2. Correlations between incubation period and different patient characteristics in study of SARS-CoV-2 incubation period during the Omicron BA.5-dominant period in Japan*

Variables	No. patients	Incubation period, mean no. d (SD)	p value
Total no. patients	122	2.6 (1.0)	NA
Infectee variables			
Sex			0.07
M	55	2.8 (1.0)	NA
F	67	2.5 (1.0)	NA
Age, y			0.13
≤19	32	2.8 (1.2)	NA
≥20	90	2.6 (0.9)	NA
No. vaccinations			0.66
0–2	54	2.6 (1.0)	NA
3	68	2.6 (1.0)	NA
Transmission—shared meals			0.03
Yes	90	2.5 (0.9)	NA
No	32	2.9 (1.1)	NA
Infector variables			
Sex			0.68
M	68	2.7 (1.0)	NA
F	54	2.5 (1.0)	NA
Age, y			0.007
≤19	27	3.0 (1.2)	NA
≥20	95	2.5 (0.9)	NA
No. vaccinations			0.83
0–2	59	2.7 (1.0)	NA
3	63	2.6 (0.9)	NA

*We performed multivariable gamma regression analyses of patients during the SARS-CoV-2 Omicron BA.5–dominant period in Japan. NA, not applicable.

days in South Korea, 3.2 days in the Netherlands, 3.1 days in Spain, and 2.9 days in Japan (*6*,*10*,*11*); incubation period for BA.2 was 4.4 days in Hong Kong (*12*).

Reports on incubation periods for BA.5 are sparse. The incubation period in this study for patients during the BA.5–dominant period was markedly shorter than that for patients during the Delta-dominant period; this result is supported by those from previous studies (*10*,*11*). The 95th percentile distribution for incubation period among patients during the BA.5–dominant period appeared shorter than that during the BA.1–dominant period, although the difference was not statistically significant. Our results might warrant a reduction of the quarantine period from 7 to 5 days during the BA.5–dominant period in Japan (*13*).

The incubation period was shorter among patients who had transmission occur during shared meals and those with adult infectors. The incubation period might be influenced by various factors, such as viral load, environmental setting, patient immune response, severity of disease, and selection biases. Infectees exposed while eating do not normally wear masks and may share longer exposure times, so they might be exposed to a higher viral load than those exposed through conversations while wearing a mask. Exposure in restaurants has been shown to increase COVID-19 infection risk (*14*). Furthermore, children usually have mild symptoms, and average viral shedding might be less than that of an adult (*15*).

The first limitation of our study is that the infector and infectee might have been mutually misclassified, leading to overestimation. Second, patient pairs with long incubation periods might be censored during observational periods, and selection bias might result in underestimation. Third, exposures from sources other than the infector of the pair might have been missed. Fourth, the incubation period was calculated by the calendar date and not by real-time intervals. Fifth, the variant type was not confirmed by using genomic sequencing. Finally, increasing patient numbers might have influenced the quality of contact tracing by the PHC.

In summary, our results indicate that the SARS-CoV-2 Omicron BA.5 subvariant has a shorter incubation period than other variants. Shorter incubation time for this variant suggests the quarantine period could be reduced.

Acknowledgments

We thank the staff of the Itako Public Health Center, Ibaraki Prefectural Institute of Public Health, and government of Ibaraki Prefecture for their contributions to our study.

About the Author

Dr. Ogata has been engaged in the field of public health for 40 years as a medical officer and is the director of the Itako Public Health Center. His interests focus on evaluating data on and responding to epidemics in the Itako PHC jurisdiction and Japan.

References

1. World Health Organization. Tracking SARS-CoV-2 variants [cited 2022 Aug 31]. https://www.who.int/en/activities/tracking-SARS-CoV-2-variants
2. National Institute of Infectious Diseases. Current situation of infection, Aug 10, 2022 [cited 2022 Aug 31]. https://www.niid.go.jp/niid/en/2019-ncov-e/11411-covid19-ab94th-en.html
3. Ministry of Health, Labor and Welfare. Visualizing the data: information on COVID-19 infections [cited 2022 Aug 31]. https://covid19.mhlw.go.jp
4. National Institute of Infectious Diseases. Manual for active epidemiological surveillance of patients with novel coronavirus infection [cited 2022 Aug 31]. https://www.niid.go.jp/niid/en/2019-ncov-e/2484-idsc/9472-2019-ncov-02-en.html
5. Ibaraki Prefectural Government. Outbreak status of patients with new coronavirus infection in the prefecture (in Japanese) [cited 2022 Aug 31]. https://www.pref.ibaraki.jp/1saigai/2019-ncov/shiryouteikyou.html
6. Tanaka H, Ogata T, Shibata T, Nagai H, Takahashi Y, Kinoshita M, et al. Shorter incubation period among COVID-19 cases with the BA.1 Omicron variant. Int J Environ Res Public Health. 2022;19:6330. https://doi.org/10.3390/ijerph19106330
7. Ogata T, Tanaka H, Irie F, Hirayama A, Takahashi Y. Shorter incubation period among unvaccinated Delta variant coronavirus disease 2019 patients in Japan. Int J Environ Res Public Health. 2022;19:1127. https://doi.org/10.3390/ijerph19031127
8. Ibaraki Prefectural Government. Status of new coronavirus tests (Prefectural Institute of Public Health and Mito City Health Center inspections) (in Japanese) [cited 2022 Aug 31]. https://www.pref.ibaraki.jp/hokenfukushi/eiken/kikaku/covid-19_ibarakieiken_kensa.html
9. Ministry of Health, Labour and Welfare. Materials of the Advisory Board for Countermeasures against novel coronavirus infections (66th–80th) [in Japanese] [cited 2022 Aug 31]. https://www.mhlw.go.jp/stf/seisakunitsuite/bunya/0000121431_00333.html
10. Du Z, Liu C, Wang L, Bai Y, Lau EHY, Wu P et al. Shorter serial intervals and incubation periods in SARS-CoV-2 variants than the SARS-CoV-2 ancestral strain. J Travel Med. 2022;29:taac052. PubMed https://doi.org/10.1093/jtm/taac052
11. Wu Y, Kang L, Guo Z, Liu J, Liu M, Liang W. Incubation period of COVID-19 caused by unique SARS-CoV-2 strains: a systematic review and meta-analysis. JAMA Netw Open. 2022;5:e2228008. https://doi.org/10.1001/jamanetworkopen.2022.28008
12. Mefsin YM, Chen D, Bond HS, Lin Y, Cheung JK, Wong JY et al. Epidemiology of infections with SARS-CoV-2 Omicron BA.2 Variant, Hong Kong, January–March 2022. Emerg Infect Dis. 2022;28:1856–8. PubMed https://doi.org/10.3201/eid2809.220613
13. Ministry of Health Labor and Welfare. The identification of close contacts, restrictions of behavior, and implementation of contact tracing by each transmission setting based on the characteristics of the B.1.1.529 (Omicron variant) while it is the mainstream (in Japanese) [cited 2022 Aug 31]. https://www.mhlw.go.jp/content/000968056.pdf
14. Fisher KA, Tenforde MW, Feldstein LR, Lindsell CJ, Shapiro NI, Files DC, et al.; IVY Network Investigators; CDC COVID-19 Response Team. Community and close contact exposures associated with COVID-19 among symptomatic adults ≥18 years in 11 outpatient health care facilities—United States, July 2020. MMWR Morb Mortal Wkly Rep. 2020;69:1258–64. https://doi.org/10.15585/mmwr.mm6936a5
15. Chen PZ, Bobrovitz N, Premji ZA, Koopmans M, Fisman DN, Gu FX. SARS-CoV-2 shedding dynamics across the respiratory tract, sex, and disease severity for adult and pediatric COVID-19. Elife. 2021;10:e70458. https://doi.org/10.7554/eLife.70458

Address for correspondence: Tsuyoshi Ogata, Itako Public Health Center of Ibaraki Prefectural Government, Osu1446-1, Itako, Ibaraki, 311-2422, Japan; e-mail: kenkoukikikanri@gmail.plala.or.jp

Risk Factors for Reinfection with SARS-CoV-2 Omicron Variant among Previously Infected Frontline Workers

Katherine D. Ellingson, James Hollister, Cynthia J. Porter, Sana M. Khan, Leora R. Feldstein, Allison L. Naleway, Manjusha Gaglani, Alberto J. Caban-Martinez, Harmony L. Tyner, Ashley A. Lowe, Lauren E.W. Olsho, Jennifer Meece, Sarang K. Yoon, Josephine Mak, Jennifer L. Kuntz, Natasha Schaefer Solle, Karley Respet, Zoe Baccam, Meredith G. Wesley, Matthew S. Thiese, Young M. Yoo, Marilyn J. Odean, Flavia N. Miiro, Steve L. Pickett, Andrew L. Phillips, Lauren Grant, James K. Romine, Meghan K. Herring, Kurt T. Hegmann, Julie Mayo Lamberte, Brian Sokol, Krystal S. Jovel, Mark G. Thompson, Patrick Rivers, Tamara Pilishvili, Karen Lutrick, Jefferey L. Burgess, Claire M. Midgley, Ashley L. Fowlkes

In a cohort of essential workers in the United States previously infected with SARS-CoV-2, risk factors for reinfection included being unvaccinated, infrequent mask use, time since first infection, and being non-Hispanic Black. Protecting workers from reinfection requires a multipronged approach including up-to-date vaccination, mask use as recommended, and reduction in underlying health disparities.

Essential and frontline workers experience repeated occupational exposure to SARS-CoV-2 (*1*). The variant B.1.1.529 (Omicron) is characterized by unprecedented transmissibility and potential for immune evasion, which led to a surge in first-time infections and reinfections in the United States beginning in December 2021 (*2*). Before Omicron predominance, previous infection had been highly protective against reinfection, but protection waned as Omicron emerged (*3*–*5*). Compared with results for pre-Omicron variants, reports of mRNA vaccine effectiveness against first-time Omicron infections were lower (46% after 2 doses and 60% after 3 doses) (*6*). Early reports on vaccine effectiveness against hospitalization related to reinfection with Omicron demonstrated 35% risk reduction with 2 doses of mRNA vaccine and 68% with 3 doses (*6*,*7*).

Little is known about the constellation factors that put persons who had previous infections at risk for reinfection with Omicron (*8*). In this study, we examined a prospective cohort of essential and frontline workers who had previous SARS-CoV-2 infections to identify risk factors for reinfection during Omicron predominance.

The Study

Beginning in July 2020, frontline workers in 8 US locations were enrolled in the Arizona Healthcare, Emergency Response, and Other Essential Workers Study (AZ-HEROES) and the Research on the Epidemiology of SARS-CoV-2 in Essential Response Personnel (RECOVER) Study (*9*,*10*). Participants self-collected weekly mid-turbinate nasal specimens regardless of symptoms and upon the date of onset of any COVID-19–like illness symptoms. All specimens were tested at Marshfield

Author affiliations: University of Arizona, Tucson, Arizona, USA (K.D. Ellingson, J. Hollister, C.J. Porter, S.M. Khan, A.A. Lowe, Z. Baccam, F.N. Miiro, J.K. Romine, K.S. Jovel, P. Rivers, K. Lutrick, J.L. Burgess); Centers for Disease Control and Prevention, Atlanta, Georgia, USA (L.R. Feldstein, J. Mak, Y.M. Yoo, J. Mayo Lamberte, M.G. Thompson, T. Pilishvili, C.M. Midgley, A.L. Fowlkes); Kaiser Permanente Northwest, Portland, Oregon, USA (A.L. Naleway, J.L. Kuntz); Baylor Scott and White Health, Temple, Texas, USA (M. Gaglani); A.J. Caban-Martinez, N. Schaefer Solle); St. Luke's Regional Health Care System, Duluth, Minnesota, USA (H.L. Tyner, K. Respet, M.J. Odean); Abt Associates Inc., Rockville, Maryland, USA (L.E.W. Olsho, M.G. Wesley, S.L. Pickett, M.K. Herring, B. Sokol); Marshfield Clinic, Marshfield, Wisconsin, USA (J. Meece); University of Utah Health, Salt Lake City, Utah, USA (S.K. Yoon, M.S. Thiese, A.L. Phillips, K.T. Hegmann)

DOI: https://doi.org/10.3201/eid2903.221314

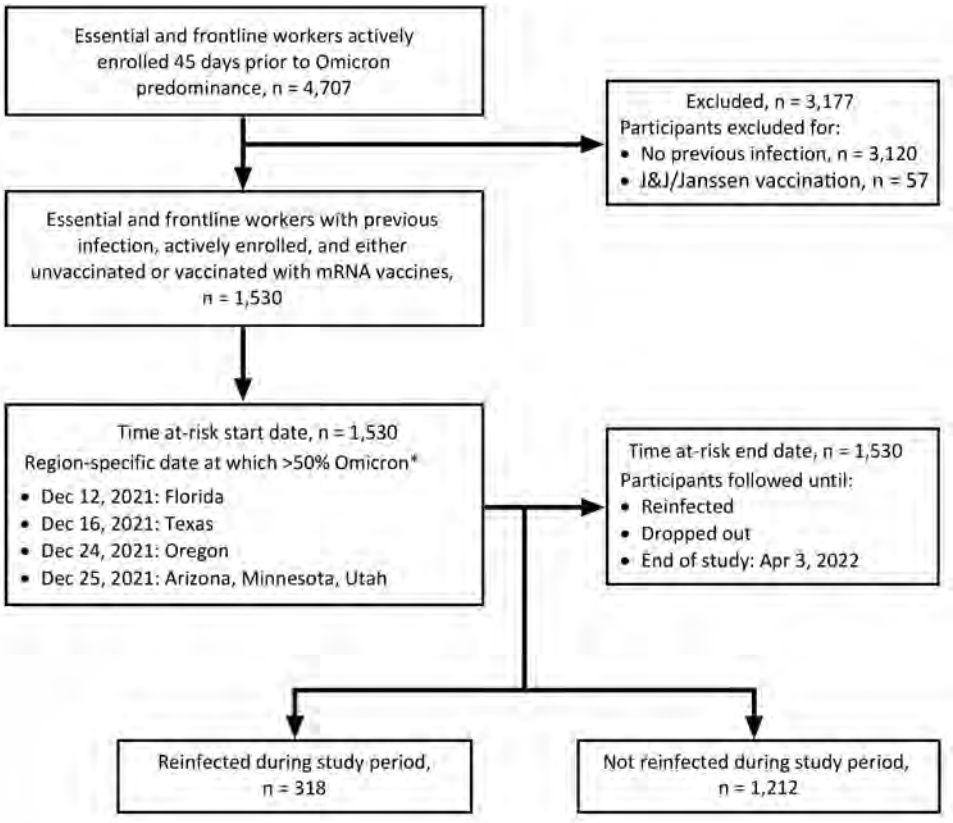

Figure. Sample inclusion criteria and site-specific study timeline for risk factor analyses for reinfection with SARS-CoV-2 Omicron variant among previously infected frontline workers, United States.

Clinical Research Laboratories (Marshfield, WI, USA) for SARS-CoV-2 RNA by reverse transcription PCR (RT-PCR) testing. Specimens positive by RT-PCR with a cycle threshold (Ct) value <30 underwent whole-genome sequencing to determine SARS-CoV-2 variant. (Ct is defined as the number of cycles required for the fluorescent signal to cross the threshold [i.e., exceeds background level].)

If the specimen was ineligible (Ct ≥30) for sequencing, the date of incident infection was used to estimate variant predominance by using the state-specific date at which >50% of specimens sequenced were of the Delta or Omicron variants according to Centers for Disease Control and Prevention data (Figure) (*11*). Only participants who were actively enrolled in the study during site-specific Omicron predominance, and those who had 1 previous infection at least 45 days before Omicron predominance, were included (Figure).

We identified first infections on the basis of participant-reported positive viral test results before enrollment or positive study-based RT-PCR results after enrollment. We defined reinfections as the second incident infection with >90 days between last date of positivity for first infection and first date of positivity for the second infection, or a second infection after 45 days from a distinct SARS-CoV-2 variant. We collected demographic and underlying health information at enrollment. Participants self-reported vaccination at enrollment, quarterly, and more frequently when new vaccines became available; study staff subsequently verified self-reports through vaccine card uploads, state vaccine registries or electronic medical records. We collected exposure variables, including self-reported mask use and number of hours worked per week, monthly and averaged them over the study period (*12*). All participants provided written consent, and protocols were approved by institutional review boards at all participating sites, including Abt Associates and the Centers for Disease Control and Prevention.

We estimated unadjusted and adjusted hazard ratios for Omicron reinfection with Cox proportional-hazards models by using the Andersen–Gill extension to account for time-varying vaccination status described previously (*13*). Adjusted models included demographic information, preexisting health conditions, time-varying vaccination status, self-reported mask use in the community, and time since previous infection. All statistical analyses were conducted in R version 4.0.4 (The R Project for Statistical Computing, https://www.r-project.org) and SAS university edition 9.4 (SAS Institute, Inc., https://www.sas.com).

Of 4,707 actively enrolled HEROES-RECOVER participants, 1,587 (33.7%) had a previous SARS-CoV-2 infection ≥45 days before Omicron predominance. We excluded from the study population persons who had received J&J/Janssen (https://www.jnj.com) vaccination (n = 57) (Figure). From the location-specific date of Omicron predominance through April 3, 2022, a total of 1,530 participants who had previous SARS-CoV-2 infections contributed 124,665 person-days at risk for reinfection (Table).

Table. Composition of study sample at risk for reinfection with SARS-CoV-2 during Omicron predominance, United States, December 2021–April 2022*

Characteristic	No. participants, n = 1,530†	No. reinfected, n = 318	No. person-days at risk, n = 124,665	Reinfection incidence/1,000 days at risk (95% CI)	Unadjusted HR (95% CI)‡	Adjusted HR (95% CI)§
Site, no. (%)						
Tucson, AZ	579 (37.8)	109	47,933	2.27 (1.85–2.70)	Referent	Referent
Phoenix, AZ	211 (13.8)	40	17,054	2.35 (1.62–3.07)	1.03 (0.72–1.49)	0.99 (0.66–1.48)
Other areas in AZ	123 (8.0)	21	10,389	2.02 (1.16–2.89)	0.88 (0.56–1.42)	0.75 (0.46–1.35)
Temple, TX	93 (6.1)	20	8,003	2.50 (1.40–3.59)	1.15 (0.71–1.85)	1.12 (0.68–1.82)
Portland, OR	59 (3.9)	9	4,851	1.86 (0.64–3.07)	0.84 (0.42–1.65)	0.99 (0.48–2.01)
Miami, FL	151 (9.9)	43	11,834	3.63 (2.55–4.72)	1.66 (1.17–2.37)	1.28 (0.86–1.91)
Duluth, MN	135 (8.8)	24	11,271	2.13 (1.28–2.98)	0.92 (0.59–1.43)	1.08 (0.67–1.74)
Salt Lake City, UT	179 (11.7)	52	13,330	3.90 (2.84–4.96)	1.65 (1.19–2.30)	1.61 (1.09– 2.37)
Age category, y, no. (%)						
18–34	360 (23.5)	83	28,112	2.95 (2.32–3.59)	Referent	Referent
35–49	662 (43.3)	135	54,065	2.50 (2.08–2.92)	0.86 (0.66–1.13)	0.88 (0.65–1.20)
50–77	508 (33.2)	100	42,488	2.35 (1.89–2.81)	0.82 (0.61–1.10)	0.89 (0.63–1.27)
Sex, no. (%)						
M	605 (39.5)	144	47,929	3.00 (2.51–3.50)	Referent	Referent
F	925 (60.5)	174	76,736	2.27 (1.93–2.60)	0.76 (0.61–0.95)	0.95 (0.72–1.25)
Race/ethnicity, no. (%)¶#						
Non-Hispanic/White	1,023 (66.9)	197	84,350	2.34 (2.01–2.66)	Referent	Referent
Non-Hispanic/Black	44 (2.9)	15	3,058	4.91 (2.42–7.39)	2.02 (1.19–3.41)	2.14 (1.17–3.92)
Non-Hispanic/Asian	30 (2.0)	5	2,636	1.90 (0.23–3.56)	0.81 (0.33–1.96)	1.02 (0.43–2.43)
Hispanic	375 (24.9)	88	29,837	2.95 (2.33–3.57)	1.26 (0.98–1.62)	1.30 (0.98–1.72)
Other	18 (1.2)	3	1,605	1.87 (0.00–3.98)	0.81 (0.26–2.56)	0.56 (0.18–1.78)
Comorbid conditions, no. (%)#**						
0	970 (63.4)	206	78,492	2.62 (2.27–2.98)	Referent	Referent
>1	489 (32.0)	106	39,704	2.67 (2.16–3.18)	1.02 (0.80–1.29)	1.17 (0.90–1.53)
Occupation, no. (%)††						
Heathcare personnel	650 (42.5)	126	53,745	2.34 (1.94–2.75)	Referent	Referent
First responder	400 (26.1)	111	30,557	3.63 (2.96–4.31)	1.52 (1.18–1.96)	1.13 (0.78–1.63)
Other essential worker	480 (31.4)	81	40,363	2.01 (1.57–2.44)	0.86 (0.65–1.13)	0.82 (0.60–1.13)
Time-varying vaccination status, no.‡‡						
0 doses	441	125	32,879	3.80 (3.14–4.47)	Referent	Referent
1 dose	34	5	2,605	1.92 (0.24–3.60)	0.56 (0.22–1.40)	0.56 (0.22–1.42)
2 doses	646	107	48,039	2.23 (1.81–2.65)	0.58 (0.45–0.75)	0.57 (0.43–0.75)
3 doses	513	81	42,726	1.90 (1.48–2.31)	0.55 (0.41–0.72)	0.54 (0.39–0.75)
Mask use in community, no. (%)#§§						
Above mean (47%)	766 (50.1)	126	64,630	1.95 (1.61–2.29)	Referent	Referent
Below mean	735 (48.0)	189	57,595	3.28 (2.81–3.75)	1.64 (1.31–2.06)	1.39 (1.07–1.82)
Weekly work hours, no. (%)#						
Below mean (30 hours)	781 (51.0)	154	64,077	2.40 (2.02–2.78)	Referent	Referent
Above mean	741 (48.5)	164	59,901	2.74 (2.32–3.16)	1.14 (0.91–1.41)	1.09 (0.87–1.37)
Time elapsed since first infection, y, no. (%)						
≤1	781 (51.0)	133	65,239	2.04 (1.69–2.39)	Referent	Referent
>1	749 (49.0)	185	59,426	3.13 (2.66–3.56)	1.53 (1.23–1.91)	1.63 (1.28–2.07)

*HR, hazard ratio.
†Column percentage reported.
‡Each covariate listed was entered into a Cox proportional hazard model as a single predictor to generate unadjusted hazard ratios
§All covariates were entered into a fully adjusted model.
¶Other includes American Indian or Alaska Native, Asian/Pacific Islander, or multiracial.
#Missing values for this variable but <5% of study sample; persons who had missing values were excluded from hazard ratio analyses.
**Includes asthma, other chronic lung disease, cancer, diabetes, heart disease or condition, hypertension, immunosuppression, kidney disease, liver disease, neurologic disease or disorder, autoimmune disease, or other medical problem requiring clinical care for ≥6 months.
††Includes inpatient, ambulatory, and institutional healthcare personnel; First responders include nonfire emergency medical service workers, fire services, law enforcement and corrections personnel; other essential workers include persons who work in the hospitality, retail, food service, education, government, or grocery sectors and persons who work in essential infrastructure and operations.
‡‡Vaccination status was allowed to vary over the time period at risk by using the Andersen–Gill extension methods; column percentages are not provided because they do not add up to 100%.
§§Refers to the reported percentage of time masks were worn while in public but not at work in the past 7 days averaged across the study period.

More than half of the participants were from Arizona (59.7%), female (60.5%), and non-Hispanic White (66.9%). In this study sample, 42.5% were healthcare personnel, 26.1% first responders, and 31.4% other essential workers.

Of all mRNA vaccines received, 71.2% were BNT162b2 (Pfizer-BioNTech, https://www.pfizer.com) and 28.8% were mRNA-1273 (Moderna, https://www.modernatx.com). About half (51.0%) of participants experienced their first infection within a year of location-specific Omicron predominance. Reinfections were identified among 318 (20.8%) participants; 27.0% of those reinfected were asymptomatic.

The proportional hazards assumption was met for all models. Participants who had 2 or 3 doses of mRNA vaccine had lower risk for reinfection with Omicron than persons who were unvaccinated (adjusted HR [aHR] 0.57 [95% CI 0.43–0.75] for those with 2 doses; aHR 0.54 [95% CI 0.39–0.75] for those with 3 doses) (Table). Although age and sex did not significantly predict reinfection in this sample, residence in Utah (aHR 1.61, 95% CI 1.09–2.37; referent Tucson, AZ, USA) and self-identification as non-Hispanic Black (aHR 2.14, 95% CI 1.17–3.92; referent non-Hispanic White) were risk factors for reinfection. Participants who wore masks in community settings less frequently, defined as wearing less than the mean reported percentage of time of 47% (interquartile range 8%–83%), had higher risk for reinfection (aHR 1.39, 95% CI 1.07–1.82). Finally, participants for whom >1 year had elapsed since their first infection had increased risk for reinfection compared with persons who had ≤1 year since their first infection (aHR 1.63, 95% CI 1.28–2.07).

Conclusions

In this prospective cohort of previously infected frontline workers, mRNA vaccination with 2 or 3 doses reduced the risk for reinfection by >40%. Risk for reinfection was increased by low self-reported mask use and for persons who had an initial infection >1 year before the study period. Those findings are consistent with risk factor studies for primary infections and suggest that infection-induced immunity wanes over time (*12*,*14*). Given that 27% of reinfections were asymptomatic, our findings suggest that vaccination might have been protective against infections that workers would have acquired unknowingly. Non-Hispanic Black participants had increased risk for reinfection, which underscores the need for addressing health disparities, especially because racial and ethnic minority groups are overrepresented among essential and frontline workers (*15*).

The first limitation of this study is that sparse data contributed from certain geographic sites and demographic groups reduced the precision of estimates. Second, it is possible that some persons who were reinfected during the early phases of Omicron predominance (when Omicron and Delta were co-circulating) and who also had high Ct values that precluded whole-genome sequencing were misclassified as Omicron reinfections (instead of Delta), although that number is probably negligible, given the rapid acceleration of Omicron dominance. Third, although inclusion of self-reported mask use in community settings was a strength of the study, we were unable to account for venue-specific mask mandates, which might have been variable among participants or changed throughout the study period. Fourth, findings suggesting the need for second and third doses of mRNA vaccines are less relevant as recommendations for additional and variant-specific boosters emerge. Nonetheless, those findings suggest the role of time since immune-modifying events, including most recent mRNA vaccination or previous infection, in reducing risk for reinfection. Overall, our findings underscore the need for maintaining a multipronged approach, including vaccines, nonpharmaceutical interventions, and efforts to reduce disparities, to protect frontline workers as the pandemic enters a period in which reinfections are increasingly common.

Acknowledgments

On behalf of HEROES-RECOVER Network, we thank the cohort participants and the following collaborators: Eduardo Azziz-Baumgartner, Melissa L. Arvay, William Brannen, Stephanie Bialek, Allison Ciesla, Alicia M. Fry, Aron Hall, Adam MacNeil, Clifford McDonald, Sue Reynolds, Robert Slaughter, Matthew J. Stuckey, Rose Wang, Ryan Wiegand, CDC; Danielle R. Hunt, Laura J. Edwards, Robin Bloodworth, Claire Douglas, Jazmin Duque, Jini Etolue, Deanna E. Fleary, Jessica Flores, Isaiah Gerber, Kimberly Groover, Louise Hadden, Jenna Harder, Nancy McGarry, Peenaz Mistry, Tyler C. Morrill, Kelly Patlan, Brandon P. Poe, Khaila Prather, Meghan Shea, John Thacker, Pearl Zheng, Abt Associates; Kayan Dunnigan, Spencer Rose, Nicole Calhoun, Leah Odame-Bamfo, Clare Mathenge, Michael E. Smith, Kempapura Murthy, Tnelda Zunie, Eric Hoffman, Martha Zayed, Ashley Graves, Joel Blais, Jason Ettlinger, Sharla Russell, Natalie Settele, Tiya Searcy, Rupande Patel, Elisa Priest, Jennifer Thomas, Muralidhar Jatla, Madhava Beeram, Javed Butler, Alejandro Arroliga, Baylor Scott and White Health; Holly Groom, Yolanda Prado, Daniel Sapp, Mi Lee, Chris Eddy, Matt Hornbrook, Donna Eubanks, Danielle Millay, Dorothy Kurdyla, Kristin Bialobok, Ambrosia Bass, Kristi

Bays, Kimberly Berame, Cathleen Bourdoin, Rashyra Brent, Carlea Buslach, Lantoria Davis, Stephen Fortmann, Jennifer Gluth, Kenni Graham, Tarika Holness, Kelley Jewell, Enedina Luis, Abreeanah Magdaleno, DeShaun Martin, Joyce Smith-McGee, Martha Perley, Sam Peterson, Aaron Peipert, Krystil Phillips, Joanna Price, Ana Reyes, Sperry Robinson, Katrina Schell, Emily Schield, Natosha Shirley, Anna Shivinsky, Valencia Smith, Britta Torgrimson-Ojerio, Brooke Wainwright, Shawn Westaway, Kaiser Permanente NW; Saydee Benz, Adam Bissonnette, Krystal Boese, Emily Botten, Jarod Boyer, Michaela Braun, Julianne Carlson, Caleb Cravillion, Amber Donnerbauer, Tim Dziedzic, Joe Eddy, Heather Edgren, Alex Ermeling, Kelsey Ewert, Connie Fehrenbach, Rachel Fernandez, Wayne Frome, Sherri Guzinski, Mitch Hertel, Garrett Heuer, Erin Higdon, Cressa Huotari, Lynn Ivacic, Lee Jepsen, Steve Kaiser, Bailey Keffer, Tammy Koepel, Sarah Kohn, Alaura Lemieux, Carrie Marcis, Megan Maronde, Isaac McCready, Nidhi Mehta, Dan Miesbauer, Collin Nikolai, Brooke Olson, Jeremy Olstadt, Lisa Ott, Cory Pike, Nicole Price, Chris Reardon, Alex Slenczka, Elisha Stefanski, Lydia Sterzinger, Kendra Stoltz, Melissa Strupp, Lyndsay Watkins, Roxann Weigel, Ben Zimmerman, Marshfield Clinic Research Laboratory; Damena Gallimore-Wilson, Roger Noriega, Cynthia Beaver, Alexandra Cruz, Annabel Reyes, Brigitte Madan, Addison Testoff, John Jones, University of Miami; Jennifer Viergutz, Angela Hunt, Jessica Lundgren, Tyna O'Connor, Daniel Stafki, Jill Dolezilek, Bethany Brunner, Leiah Hoffman, Kate Diluzio O'Connor, Daniel Stafki, Jill Dolezilek, Bethany Brunner, Leiah Hoffman, Kate Diluzio, St. Luke's; Ariyah Armstrong, Nora Baccam, Shawn Beitel, Tatum Butcher, Shelby Capell, Andrea Carmona, Karysa Carson, Alissa Coleman, Hannah Cowling, Carly Deal, Kiara Earley, Sophie Evans, Julia Fisher, Ashlyn Flangos, Joe K. Gerald, Lynn Gerald, Anna Giudici, Erika Goebert, Taylor Graham, Sofia Grijalva, Hanna Hanson, Olivia Healy, Chloe Hendrix, Katherine Herder, Adrianna Hernandez, Raven Hilyard, Rezwana Islam, Caroline Klinck, Karl Krupp, Karla Ledezma, Sally Littau, Amelia Lobos, Jeremy Makar, Natalya Mayhew, Kristisha Mevises, Cierra Morris, Sarah Murray, Janko Nikolich-Žugich, Assumpta Nsengiyunva, Kennedy Obrien, Mya Pena, Riley Perlman, Celia Pikowski, Ferris A. Ramadan, Jen Scott, Priyanka Sharma, Alison Slocum, Saskia Smidt, Lili Steffen, Jayla Sowell, Danielle Stea, Xiaoxiao Sun, Nicholas Tang, Gianna Taylor, Ta'Nya Tomas, Heena Timsina, Italia Trejo, April Yingst, University of Arizona; Rachel T. Brown, Camie Schaefer, Arlyne Arteaga, Matthew Bruner, Daniel Dawson, Emilee Eden, Jenna Praggastis, Joseph Stanford, Jeanmarie Mayer, Marcus Stucki, Riley Campbell, Kathy Tran, Madeleine Smith, Braydon Black, Christina Pick, Madison Tallman, Chapman Cox, Derrick Wong, Michael Langston, Adriele Fugal, Fiona Tsang, Maya Wheeler, Gretchen Maughan, Megan Wilson, Pasha Stinson, Jesse Williams, Seon Reed, Jinyi Mao, Nikki Gallacher, Kendal Chatard, Jenna Vo, Katie Luong, Ryder Jordin, Grace Stewart, Brock Bourdelle, Timina Powaukee, Max Minoughan, University of Utah. The Florida research team thanks the firefighters, healthcare workers, and frontline and essential workers for participating in this occupational cohort study.

This study was supported by the National Center for Immunization and Respiratory Diseases, Centers for Disease Control and Prevention under contract numbers 75D30120R68013 awarded to the Marshfield Clinic Research Laboratory and 75D30120C08379 to the University of Arizona.

ALN reports receiving support from Pfizer and Vir Biotechnology for unrelated studies.

About the Author

Dr. Ellingson is an associate professor of epidemiology at the Mel and Enid Zuckerman College of Public Health at the University of Arizona, Tucson, AZ. Her primary research interest is infectious diseases in high-risk occupational and congregate settings.

References

1. Michaels D, Wagner GR. Occupational Safety and Health Administration (OSHA) and worker safety during the COVID-19 pandemic. JAMA. 2020;324:1389–90. https://doi.org/10.1001/jama.2020.16343
2. Pulliam JR, van Schalkwyk C, Govender N, von Gottberg A, Cohen C, Groome MJ, et al. Increased risk of SARS-CoV-2 reinfection associated with emergence of Omicron in South Africa. Science. 2022;376:eabn4947. https://doi.org/10.1126/science.abn4947
3. Altarawneh HN, Chemaitelly H, Hasan MR, Ayoub HH, Qassim S, AlMukdad S, et al. Protection against the Omicron variant from previous SARS-CoV-2 infection. N Engl J Med. 2022;386:1288–90. https://doi.org/10.1056/NEJMc2200133
4. Hall VG, Al-Alahmadi G, Solera JT, Marinelli T, Cardinal H, Prasad GV, et al. Outcomes of SARS-CoV-2 infection in unvaccinated compared with vaccinated solid organ transplant recipients: a propensity matched cohort study. Transplantation. 2022;106:1622–8. https://doi.org/10.1097/TP.0000000000004178
5. Hansen CH, Michlmayr D, Gubbels SM, Mølbak K, Ethelberg S. Assessment of protection against reinfection with SARS-CoV-2 among 4 million PCR-tested individuals in Denmark in 2020: a population-level observational study. Lancet. 2021;397:1204–12. https://doi.org/10.1016/S0140-6736(21)00575-4
6. Yoon SK, Hegmann KT, Thiese MS, Burgess JL, Ellingson K, Lutrick K, et al.; HEROES-RECOVER Network Investigators; HEROES-RECOVER Network Investigators. Protection with a third dose of mRNA vaccine against SARS-CoV-2 variants in frontline workers. N Engl J Med. 2022;386:1855–7. https://doi.org/10.1056/NEJMc2201821

7. Plumb ID, Feldstein LR, Barkley E, Posner AB, Bregman HS, Hagen MB, et al. Effectiveness of COVID-19 mRNA vaccination in preventing COVID-19-associated hospitalization among adults with previous SARS-CoV-2 infection—United States, June 2021–February 2022. MMWR Morb Mortal Wkly Rep. 2022;71:549–55. https://doi.org/10.15585/mmwr.mm7115e2
8. Helfand M, Fiordalisi C, Wiedrick J, Ramsey KL, Armstrong C, Gean E, et al. Risk for reinfection after SARS-CoV-2: a living, rapid review for American College of Physicians practice points on the role of the antibody response in conferring immunity following SARS-CoV-2 infection. Ann Intern Med. 2022;175:547–55. https://doi.org/10.7326/M21-4245
9. Edwards LJ, Fowlkes AL, Wesley MG, Kuntz JL, Odean MJ, Caban-Martinez AJ, et al. Research on the epidemiology of SARS-CoV-2 in essential response personnel (RECOVER): protocol for a multisite longitudinal cohort study. JMIR Res Protoc. 2021;10:e31574. https://doi.org/10.2196/31574
10. Lutrick K, Ellingson KD, Baccam Z, Rivers P, Beitel S, Parker J, et al. COVID-19 infection, reinfection, and vaccine effectiveness in a prospective cohort of Arizona frontline/essential workers: the AZ HEROES research protocol. JMIR Res Protoc. 2021;10:e28925. https://doi.org/10.2196/28925
11. Centers for Disease Control and Prevention. COVID data tracker: variant proportions [cited 2022 Dec 28]. https://covid.cdc.gov/covid-data-tracker/#variant-proportions
12. Naleway AL, Grant L, Caban-Martinez AJ, Wesley MG, Burgess JL, Groover K, et al. Incidence of SARS-CoV-2 infection among COVID-19 vaccinated and unvaccinated healthcare personnel, first responders, and other essential and frontline workers: eight US locations, January–September 2021. Influenza Other Respir Viruses. 2022;16:585–93. https://doi.org/10.1111/irv.12956
13. Thompson MG, Burgess JL, Naleway AL, Tyner H, Yoon SK, Meece J, et al. Prevention and attenuation of COVID-19 with the BNT162b2 and mRNA-1273 vaccines. N Engl J Med. 2021;385:320–9. https://doi.org/10.1056/NEJMoa2107058
14. Goldberg Y, Mandel M, Bar-On YM, Bodenheimer O, Freedman LS, Ash N, et al. Protection and waning of natural and hybrid immunity to SARS-CoV-2. N Engl J Med. 2022;386:2201–12. https://doi.org/10.1056/NEJMoa2118946
15. Lopez L III, Hart LH III, Katz MH. Racial and ethnic health disparities related to COVID-19. JAMA. 2021;325:719–20. https://doi.org/10.1001/jama.2020.26443

Address for correspondence: Katherine D. Ellingson, Department of Epidemiology and Biostatistics, Zuckerman College of Public Health, University of Arizona, Tucson, AZ 85724, USA; email: kellingson@arizona.edu

etymologia revisited

Originally published in June 2020

Scrapie
[skra'pe]

Scrapie is a fatal neurodegenerative disease of sheep and goats that was the first of a group of spongiform encephalopathies to be reported (1732 in England) and the first whose transmissibility was demonstrated by Cuille and Chelle in 1936. The name resulted because most affected sheep develop pruritis and compulsively scratch their hides against fixed objects. Like other transmissible spongiform encephalopathies, scrapie is associated with an alteration in conformation of a normal neural cell glycoprotein, the prion protein. The scrapie agent was first described as a prion (and the term coined) by Stanley Prusiner in 1982, work for which he received the Nobel Prize in 1997.

Sources:

1. Brown P, Bradley R. 1755 and all that: a historical primer of transmissible spongiform encephalopathy. BMJ. 1998;317:1688–92.
2. Cuillé J, Chelle PL. The so-called "trembling" disease of sheep: is it inoculable? [in French]. Comptes Rendus de l'Académie Sciences. 1936;203:1552.
3. Laplanche J-L, Hunter N, Shinagawa M, Williams E. Scrapie, chronic wasting disease, and transmissible mink encephalopathy. In: Prusiner SB, editor. Prion biology and diseases. Cold Spring Harbor (NY): Cold Spring Harbor Laboratory Press; 1999. p. 393–429.
4. Prusiner SB. Novel proteinaceous infectious particles cause scrapie. Science. 1982;216:136–44.

https//wwwnc.cdc.gov/eid/article/26/6/et-2606_article

Correlation of High Seawater Temperature with *Vibrio* and *Shewanella* Infections, Denmark, 2010–2018

Yaovi Mahuton Gildas Hounmanou, Jørgen Engberg, Karsten Dalsgaard Bjerre, Hanne Marie Holt, Bente Olesen, Marianne Voldstedlund, Anders Dalsgaard, Steen Ethelberg

During 2010–2018 in Denmark, 638 patients had *Vibrio* infections diagnosed and 521 patients had *Shewanella* infections diagnosed. Most cases occurred in years with high seawater temperatures. The substantial increase in those infections, with some causing septicemia, calls for clinical awareness and mandatory notification policies.

Vibrio and *Shewanella* spp. bacteria cause a variety of human infections, including wound infections, ear infections, septicemia, and gastroenteritis (*1*). Domestically acquired *Vibrio* and *Shewanella* infections occur only sporadically in countries in northern Europe because the coastal seawater temperature tends to be too cold to support growth and high bacterial pathogen concentration levels (*2*,*3*). However, the warming of low-salinity coastal waters of the Baltic Sea has promoted the growth of *Vibrio* and *Shewanella* spp. and consequently increased the risk of disease for humans exposed to such seawater (*4*). In the unusually warm summer of 1994 in Denmark, several *V. vulnificus* and *S. algae* infections were seen among patients who reported bathing in seawater (*5*,*6*). Furthermore, during 2014–2018, more than 1,055 cases of vibriosis were reported in northern Europe countries, including Denmark (*7*).

Considering the annual increase in infections during recent summer seasons in Denmark and the recurring heatwaves across Europe, this emerging public health threat requires more investigation to provide decision-makers with evidence for action. The aim of our nationwide study was to describe the distribution of *Vibrio* and *Shewanella* infections in Denmark during 2010–2018 and investigate a possible correlation between infections and sea surface temperature.

The Study

We studied cases of *Vibrio* and *Shewanella* infections during 2010–2018 in the summer months in Denmark (June to August); in the decade spanning 2010–2020, 2018 was the warmest registered summer in the country. We obtained information about the cases from the Danish Microbiology Database, a national database containing all clinical microbiology reports from Denmark (*8*). We extracted identification results, confirmed by matrix-assisted laser desorption/ionization time-of-flight mass spectrometry, on *Vibrio* and *Shewanella* spp. cultured from blood, wound swabs, deep soft tissue, ear, trachea, urine, and feces as well as information about date of sampling. We also extracted the person identification number of each patient studied from Denmark's Central Person Registry (CPR) (*9*). Clinical patient information was not available, but sample types were used as a proxy for type of infection. We registered cases by month per patient (Appendix 1, https://wwwnc.cdc.gov/EID/article/29/3/22-1568-App1.pdf). We counted the number of cases by calendar year and stratified them by the genus of isolated bacterial pathogen. Using the CPR number, we eliminated duplicate positive results. By linking to data from the CPR register, we retrieved information on address of residence for each case at the time of sampling. We performed geomapping and geocoding in QGIS 1.8.0 Lisboa (https://www.qgis.org) for the spatial analysis of *Shewanella* and *Vibrio* cases and plotting of number of infections per municipality, which we further interpreted based on seawater salinity in the mapped areas. We obtained sea surface temperatures of

Author affiliations: University of Copenhagen, Copenhagen, Denmark (Y.M.G. Hounmanou, A. Dalsgaard, S. Ethelberg); Zealand University Hospital, Køge, Denmark (J. Engberg); Statens Serum Institut, Copenhagen (K.D. Bjerre, M. Voldstedlund, S. Ethelberg); Odense University Hospital, Odense, Denmark (H.M. Holt); Herlev and Gentofte University Hospital, Herlev, Denmark (B. Olesen).

DOI: http://doi.org/10.3201/eid2903.221568

the coastal waters of Denmark during summer from the Danish Meteorological Institute (Appendix 1; Appendix 2, https://wwwnc.cdc.gov/EID/article/29/3/22-1568-App2.xlsx). We performed the Pearson correlation test in R version 4.2.1 (The R Foundation for Statistical Computing, https://www.r-project.org) to determine correlation between annual summer seawater temperatures and number of *Vibrio* and *Shewanella* cases.

We found a positive correlation between average summer seawater temperatures (15°C–22°C) and the number of cases of *Vibrio* (29–172) and *Shewanella* (18–134) infections diagnosed in Denmark during 2010–2018 ($p<0.0001$; Figure 1, panels A, B). Results showed a higher number of infections during warmer summers compared with colder summers. Ear infections (n = 595) and wound infections (n = 424) were the most frequent clinical manifestations (Table); *V. alginolyticus* and *S. algae* were predominant in ear infections. *V. parahaemolyticus* was the most frequently isolated from wounds (n = 103, 24%), *V. vulnificus* (n = 14, 36%) and *S. putrefaciens* (n = 10, 26%) were predominant in septicemia cases, and *S. putrefaciens* was the species most associated with deep soft tissue infections (Table). Clinical manifestations varied by bacterial species. More than one third of *V. vulnificus* infections manifested as septicemia, supporting evidence of the high virulence of this species (*10*–*12*).

Vibrio and *Shewanella* infections increased during every summer in the study period. The summers of 2014 and 2018 were characterized by particularly high sea surface temperatures and showed an association to higher incidence in infections (Figure 1, panels A, B). In all studied years, the frequency of *Vibrio* and *Shewanella* spp. infections increased beginning in week 23, reaching a peak in the warmest months (July and August), followed by a tail of decreasing number in subsequent months (Appendix 1 Figure, panel A). A recent study on 2018 data alone reported that most human vibriosis cases reported in the Nordic region were likely linked to exposure to the warm seawater that year (*7*). We found that infections were more prevalent in men and boys 10–19 years of age and in elderly

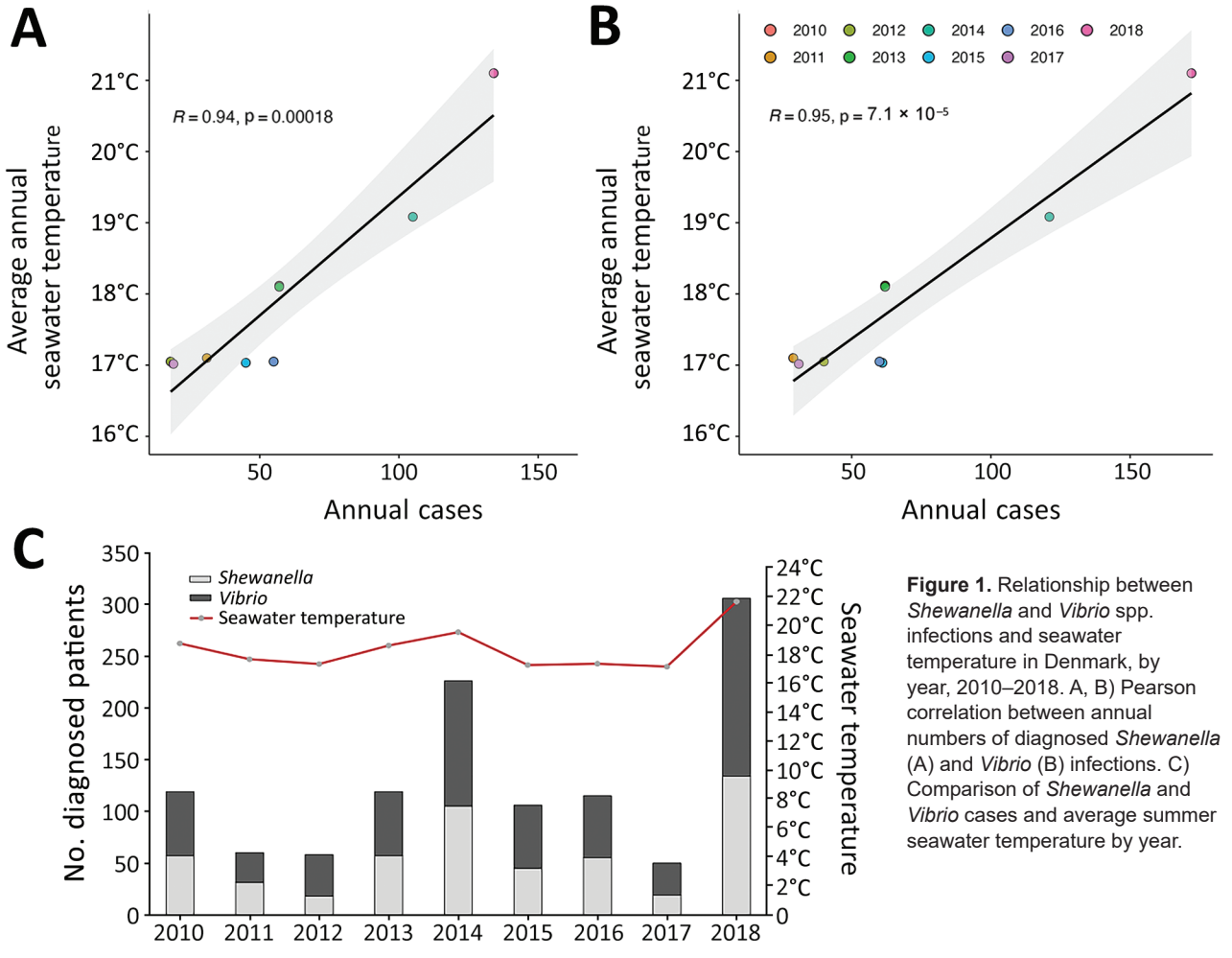

Figure 1. Relationship between *Shewanella* and *Vibrio* spp. infections and seawater temperature in Denmark, by year, 2010–2018. A, B) Pearson correlation between annual numbers of diagnosed *Shewanella* (A) and *Vibrio* (B) infections. C) Comparison of *Shewanella* and *Vibrio* cases and average summer seawater temperature by year.

Table. Distribution of species per type of *Vibrio* and *Shewanella* infections, Denmark 2010–2018*

Bacterial species	Type of manifestation or site of infection, no. (%)							
	Ear	Wound and shallow soft tissue	Septicemia	Feces†	Deep soft tissue	Respiratory tract	Urine	Other
Shewanella algae	99 (16.6)	82 (19.3)	4 (10.3)	NA	3 (12.5)	6 (30)	1 (7.7)	2 (9.5)
S. putrefaciens	86 (14.5)	80 (18.9)	10 (25.6)	NA	12 (50)	7 (35)	8 (61.5)	10 (47.6)
Shewanella spp.‡	58 (9.7)	41 (9.7)	1 (2.6)	NA	1 (4.2)	6 (30)	2 (15.4)	2 (9.5)
Total *Shewanella*	243	203	15	NA	16	19	11	14
Vibrio alginolyticus	248 (41.7)	72 (17)	2 (5.1)	2 (8.7)	4 (16.7)	1 (5)	0	4 (19)
V. cholerae	12 (2)	1 (0.2)	0	4 (17.4)	0	0	0	1 (4.8)
V. fluvialis	9 (1.5)	3 (0.7)	1 (2.6)	4 (17.4)	0	0	0	0
V. parahaemolyticus	36 (6.1)	103 (24.3)	5 (12.8)	9 (39.1)	2 (8.3)	0	0	1 (4.8)
V. vulnificus	2 (0.3)	11 (2.6)	14 (35.9)	1 (4.3)	2 (8.3)	0	2 (15.4)	0
Vibrio spp.‡	45 (7.6)	31 (7.3)	2 (5.1)	3 (13)	0	0	0	1 (4.8)
Total *Vibrio*	352	221	24	23	8	1	2	7
Total	595	424	39	23	24	20	13	21

*NA, not applicable.
†*S. algae*, *S. putrefaciens*, *S. spp.* found in feces samples (n = 24) were excluded from all analyses.
‡Not identified to species level.

persons, 60–80 years of age (Appendix 1 Figure, panel B). We suspect that those results are likely because active adolescents may have scratches or wounds while performing recreational water activities (e.g., swimming, rowing, windsurfing, or fishing) and because of the vulnerability of elderly persons in general.

We found a marked geographic distribution in results obtained from 2018, when most cases were in persons who lived near coastal areas with brackish waters characterized by low saline levels (<30 parts per thousand; Figure 2) (*13*). In contrast, along the west coast of Jutland, where the salinity of the North Sea is high and the water colder, the frequency of infections was lower. This difference suggests that increased temperature of low-salinity water favors the growth of *Vibrio* and *Shewanella* bacteria. It is important to consider that the association between place of residence and number of cases is challenged because geographic distances are short in Denmark and multiple exposures at different geographic sites during a summer season are to be expected. The lack of information on prior seawater exposure and information on international travel for each case is a limitation for the correlation between number of *Vibrio* and *Shewanella* infections and seawater exposure.

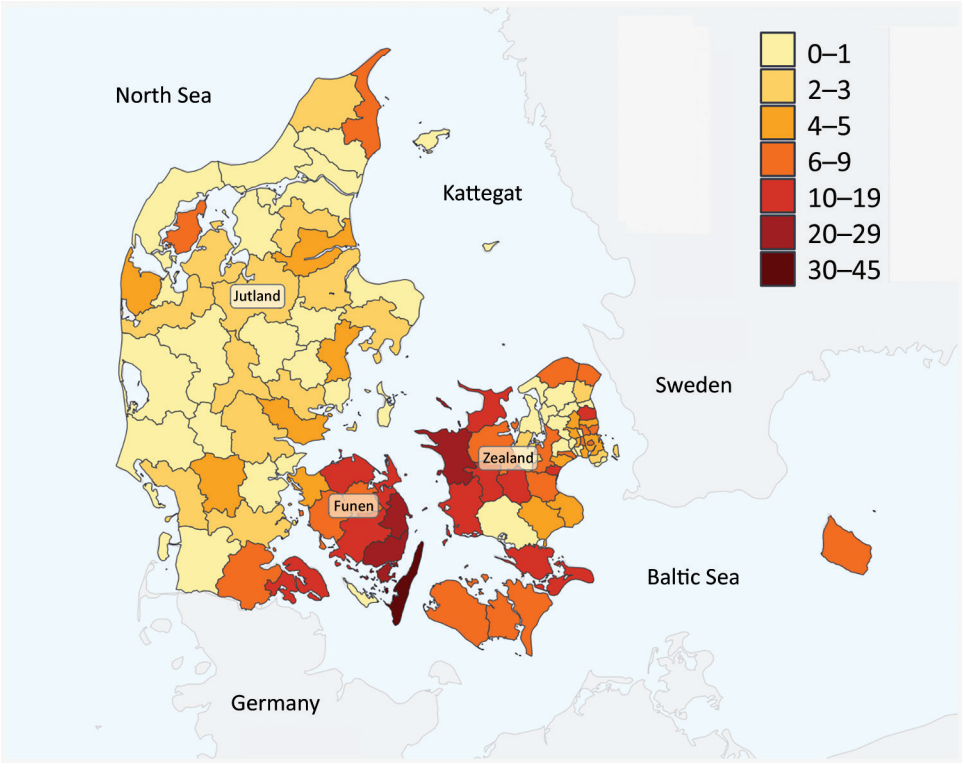

Figure 2. Number of cases of *Shewanella* and *Vibrio* spp. infection (n = 98), by municipality, Denmark, 2018.

Nevertheless, the observed geographic distribution of cases and the presented correlation between the number of cases in cold and warm summers strongly supports a relationship between higher-temperature/low-saline seawater exposure and risk of infection.

Conclusions

In this nationwide study, we show a correlation between number of *Vibrio* and *Shewanella* human infections and coastal summer water temperature in Denmark during 2010–2018. In addition, we were able to map residency of most cases to geographic areas with coastlines of low salinity. A combination of climate change effects (i.e., increasing coastal sea surface temperature at higher latitudes during summer) and a more elderly population indicates the need for increased awareness of the risk of these emerging infections and their public health impact. Rising temperatures will lead to an increase in burden of disease for these marine infections in an expanding area of the northern hemisphere (*14*). We propose that persons in Denmark who are exposed to seawater in summer should consider covering open wounds with a waterproof bandage, particularly the elderly and immunocompromised. We also recommend that persons thoroughly wash new cuts exposed to seawater and inform healthcare professionals of recent seawater exposure when seeking medical attention. Persons with defected eardrums should use earplugs. Our study lends support to categorizing all *Vibrio* and *Shewanella* infections in humans as mandatory notifiable diseases in Denmark and other countries in Europe that have seawater borders to monitor the incidence of these infections.

Acknowledgments

The authors thank the Danish Microbiology Database board of representatives and the departments of clinical microbiology in Denmark. We also extend our gratitude to Naja Stolberg Bahrenscheer for assistance with drawing the map.

This study was conducted based on administrative register data. According to Denmark law, ethics approval is not needed for such research. The study is covered by the legal acts regulating national surveillance of infectious diseases.

About the Author

Dr. Hounmanou is a postdoctoral fellow at the University of Copenhagen. He conducts research in microbial genomics on human pathogens that arise from animals and the aquatic environment and addresses questions related to climate change implications on disease transmission between humans and waterbodies, such as cholera and other *Vibrio* infections.

References

1. Tantillo GM, Fontanarosa M, Di Pinto A, Musti M. Updated perspectives on emerging vibrios associated with human infections. Lett Appl Microbiol. 2004;39:117–26. https://doi.org/10.1111/j.1472-765X.2004.01568.x
2. Baker-Austin C, Trinanes JA, Taylor NGH, Hartnell R, Siitonen A, Martinez-Urtaza J. Emerging *Vibrio* risk at high latitudes in response to ocean warming. Nat Clim Chang. 2013;3:73–7. https://doi.org/10.1038/nclimate1628
3. Gram L, Bundvad A, Melchiorsen J, Johansen C, Fonnesbech Vogel B. Occurrence of *Shewanella algae* in Danish coastal water and effects of water temperature and culture conditions on its survival. Appl Environ Microbiol. 1999;65:3896–900. https://doi.org/10.1128/AEM.65.9.3896-3900.1999
4. Baker-Austin C, Trinanes JA, Salmenlinna S, Löfdahl M, Siitonen A, Taylor NGH, et al. Heat wave-associated vibriosis, Sweden and Finland, 2014. Emerg Infect Dis. 2016;22:1216–20. https://doi.org/10.3201/eid2207.151996
5. Dalsgaard A, Frimodt-Møller N, Bruun B, Høi L, Larsen JL. Clinical manifestations and molecular epidemiology of *Vibrio vulnificus* infections in Denmark. Eur J Clin Microbiol Infect Dis. 1996;15:227–32. https://doi.org/10.1007/BF01591359
6. Holt HM, Søgaard P, Gahrn-Hansen B. Ear infections with *Shewanella* alga: a bacteriologic, clinical and epidemiologic study of 67 cases. Clin Microbiol Infect. 1997;3:329–34. https://doi.org/10.1111/j.1469-0691.1997.tb00622.x
7. Amato E, Riess M, Thomas-Lopez D, Linkevicius M, Pitkänen T, Wołkowicz T, et al. Epidemiological and microbiological investigation of a large increase in vibriosis, northern Europe, 2018. Euro Surveill. 2022;27:2101088. https://doi.org/10.2807/1560-7917.ES.2022.27.28.2101088
8. Voldstedlund M, Haarh M, Mølbak K; MiBa Board of Representatives. The Danish Microbiology Database (MiBa) 2010 to 2013. Euro Surveill. 2014;19:20667. https://doi.org/10.2807/1560-7917.ES2014.19.1.20667
9. Schmidt M, Pedersen L, Sørensen HT. The Danish civil registration system as a tool in epidemiology. Eur J Epidemiol. 2014;29:541–9. https://doi.org/10.1007/s10654-014-9930-3
10. Frank C, Littman M, Alpers K, Hallauer J. *Vibrio vulnificus* wound infections after contact with the Baltic Sea, Germany. Euro Surveill. 2006;11:E060817.1.
11. Li G, Wang MY. The role of *Vibrio vulnificus* virulence factors and regulators in its infection-induced sepsis. Folia Microbiol (Praha). 2020;65:265–74. https://doi.org/10.1007/s12223-019-00763-7
12. Horseman MA, Surani S. A comprehensive review of *Vibrio vulnificus*: an important cause of severe sepsis and skin and soft-tissue infection. Int J Infect Dis. 2011;15:e157–66. https://doi.org/10.1016/j.ijid.2010.11.003
13. Kniebusch M, Meier HEM, Radtke H. Changing salinity gradients in the Baltic Sea as a consequence of altered freshwater budgets. Geophys Res Lett. 2019;46:9739–47. https://doi.org/10.1029/2019GL083902
14. Trinanes J, Martinez-Urtaza J. Future scenarios of risk of *Vibrio* infections in a warming planet: a global mapping study. Lancet Planet Health. 2021;5:e426–35. https://doi.org/10.1016/S2542-5196(21)00169-8

Address for correspondence: Yaovi Mahuton Gildas Hounmanou, Department of Veterinary and Animal Sciences, University of Copenhagen, Stigbøjlen 4, 1870 Frederiksberg, Denmark; gil@sund.ku.dk

Tuberculosis Preventive Therapy among Persons Living with HIV, Uganda, 2016–2022

Deus Lukoye, Gail Gustavson, Proscovia M. Namuwenge, Simon Muchuro, Estella Birabwa, Seyoum Dejene, Julius Ssempiira, Julius N. Kalamya, Steven Baveewo, Odile Ferroussier-Davis, Lisa A. Mills, Emilio Dirlikov, Lisa J. Nelson, Stavia Turyahabwe

During October 2016–March 2022, Uganda increased tuberculosis (TB) preventive therapy coverage among persons living with HIV from 0.6% to 88.8%. TB notification rates increased from 881.1 to 972.5 per 100,000 persons living with HIV. Timely TB screening, diagnosis, and earlier treatment should remain high priorities for TB/HIV prevention programming.

Tuberculosis (TB) is the leading cause of illness and death globally among persons living with HIV (PLHIV) (*1*,*2*). In 2021, among ≈38.4 million PLHIV worldwide, 703,000 TB cases and 187,000 TB-related deaths were reported (*3*,*4*). HIV antiretroviral therapy (ART) and TB preventive therapy (TPT) reduce TB incidence and death among PLHIV (*5*,*6*). TPT is administered to persons at high risk for TB and who do not have symptoms of active disease; positive tuberculin skin tests or interferon gamma release assays are not required. Although increased ART coverage has coincided with declines in TB-related deaths worldwide, since the early 2000s, TPT scale-up has been limited (*3*,*7*,*8*).

Uganda is a World Health Organization–designated TB and HIV high-burden country (*3*). By 2020, ≈1,400,000 PLHIV were reported in Uganda; in 2021, a total of 29,000 TB cases and 6,200 TB-related deaths among PLHIV were reported (*9*,*10*). In 2015, Uganda accelerated efforts to provide TPT to PLHIV who had no TB symptoms and received support from the US President's Emergency Plan for AIDS Relief (PEPFAR) (*11*,*12*). Further efforts included a 100-day scale-up campaign in 2019, adopting TPT as standard of care for all eligible PLHIV in 2021 (*13*), and a last-mile campaign launched in June 2022. Therefore, despite the COVID-19 pandemic, TPT scale-up continued. We analyzed data describing TPT scale-up among PLHIV in Uganda and highlight next steps to further reduce TB-related illness and death and reach global targets for treatment coverage.

The Study

We sourced semiannual aggregate data during October 2016–March 2022 from the centralized PEPFAR DATIM Monitoring, Evaluation, and Reporting database (Uganda DATIM version 1.31 MER 2.5, updated January 4, 2021; https://ug.datim4u.org). We analyzed trends among PLHIV receiving PEPFAR-supported ART across 5 areas: TPT initiation, defined as beginning any TPT regimen, such as 6-month daily isoniazid or 3-month 1 time/week isoniazid plus rifapentine; TPT completion, defined as receiving a full course of TPT according to data capture tools; TPT completion rates, calculated as the number of TPT completions divided by the number of TPT initiations in the previous semiannual period × 100; TPT coverage, calculated as the number of TPT completions divided by the total number of PLHIV eligible for TPT; and TB notification among PLHIV on ART, calculated as the number of registered new and relapsed TB patients with documented HIV-positive status divided by the total number of PLHIV on ART. TPT eligibility was defined as 95% of total PLHIV on ART; TPT ineligibility (5%) accounts for PLHIV with active TB and PLHIV

Author affiliations: US Centers for Disease Control and Prevention, Kampala, Uganda (D. Lukoye, G. Gustavson, J. Ssempiira, J.N. Kalamya, S. Baveewo, L.A. Mills, E. Dirlikov, L.J. Nelson); Uganda Ministry of Health, Kampala (P.M. Namuwenge, S. Muchuro, S. Turyahabwe); US Department of Defense, Kampala (E. Birabwa); US Agency for International Development, Kampala (S. Dejene); US Centers for Disease Control and Prevention, Atlanta, Georgia, USA (O. Ferroussier-Davis)

DOI: https://doi.org/10.3201/eid2903.221353

discontinuing TPT because of loss to follow-up, death, or adverse events. Since October 2019, PLHIV have been considered to be on ART until ≤27 days after their last missed clinical appointment; clients whose last missed appointment was ≥28 days earlier are not considered to be receiving ART. Before October 2019, PLHIV were considered to be on ART until ≤90 days after their last missed appointment.

We used R software version 4.1.1 (The R Project for Statistical Computing, https://www.r-project.org) to analyze age groups, sex, and region. We described semiannual trends by using time series plots. We used nonparametric Cuzick tests to analyze TB notification rates across periods.

The total number of PLHIV on ART in Uganda increased from 890,938 in March 2017 to 1,283,662 in September 2022. Most (1,226,266; 95.5%) PLHIV were ≥15 years of age, and 822,864 (65.5%) were women. Age and sex distribution remained stable over time.

TPT completions increased from 28.6% (5,264/18,394) during October 2016–March 2017 to 94.0% (75,173/79,949) during October 2021–March 2022 (Table 1; Figure 1). We observed a steady increase in TPT completion rates except for a decline from 71.1% during April–September 2017 to 63.6% during October 2017–March 2018. The average regional TPT completion rate increased from 27.2% (interquartile range [IQR] 12.9%–41.9%) during October 2016–March 2017 to 93.8% (IQR 91.85%–96.25%) during October 2021–March 2022. The lowest regional average completion rate across all periods was 69.9% in the Kigezi region, and the highest average completion rate was 85.2% in the Lango region.

From October 2016–March 2017 through October 2021–March 2022, TPT coverage increased from 0.6% to 88.8% (Figure 2). In all periods, TPT coverage was higher for men. After October 2017–March 2018, TPT coverage increased steadily for both age groups; the largest increases were among PLHIV who were <15 years of age. The median regional TPT coverage during October 2021–March 2022 was 88.0% (IQR 84.5%–92.9%); the lowest rate (68.8%) was in the Karamoja region, and the highest rate (100.0%) was in the West Nile region.

TB notification rates increased from 881.1 cases/100,000 PLHIV during October 2016–March 2017 to 972.5 cases/100,000 PLHIV during October 2021–March 2022 (Table 2). Across all periods, TB notification rates were higher among men and PLHIV who were <15 years of age. During October 2021–March 2022, the highest regional TB notification rate was 1,819.2/100,000 PLHIV in the Karamoja region, and the lowest rate was 665.5/100,000 PLHIV in the Acholi region. The average regional TB notification rate during October 2016–March 2017 was 935.0 (IQR 715.4–1,069.9)/100,000 PLHIV compared with 1,032.72 (IQR 876.7–1,095.2)/100,000 PLHIV during October 2021–March 2022. Across all regions except Karamoja, TB notification rates declined during October 2019–March 2020.

Conclusion

In 6 years, Uganda successfully scaled up TPT coverage among a large cohort of PLHIV on ART. Key enablers of success were strong country leadership and ownership, integration of HIV and TB programs, data-driven stakeholder engagement, stable supply chains, and data use for continuous program improvement. However, TB notification rates increased, likely reflecting improvements in TB case reporting

Table 1. Tuberculosis preventive therapy completion and coverage among persons living with HIV who received antiretroviral therapy during semiannual periods, Uganda, October 2016–March 2022*

Semiannual periods	Initiated TPT	Completed TPT	Receiving ART†	TPT eligible‡	Cumulative completion	Completion rate, %§	TPT coverage, %¶
2016 Oct–2017 Mar	18,394	5,264	890,938	846,391	5,264	28.6	0.6 (5,264/846,391)
2017 Apr–2017Sep	17,391	12,360	993,070	943,417	17,624	71.1	1.9 (17,624/943,417)
2017 Oct–2018 Mar	8,162	5,188	1,030,756	979,218	22,812	63.6	2.3 (22,812/979,218)
2018 Apr–2018 Sep	18,836	13,272	1,101,716	1,046,630	36,084	70.5	3.4 (36,084/1,046,630)
2018 Oct–2019 Mar	99,602	85,954	1,097,366	1,042,498	122,038	86.3	11.7 (122,038/1,042,498)
2019 Apr–2019 Sep	443,900	391,514	1,148,258	1,090,845	513,552	88.2	47.1 (513,552/1,090,845)
2019 Oct–2020 Mar	111,898	98,399	1,201,166	1,141,108	611,951	87.9	53.6 (611,951/1,141,108)
2020 Apr–2020 Sep	172,862	158,546	1,218,006	1,157,106	770,497	91.7	66.6 (770,497/1,157,106)
2020 Oct–2021 Mar	122,969	113,296	1,239,829	1,177,838	883,793	92.1	79.1 (883,793/1,117,838)
2021 Apr–2021 Sep	134,387	124,525	1,266,588	1,203,259	1,008,318	92.7	83.8 (1,008,318/1,203,259)
2021 Oct–2022 Mar	79,949	75,173	1,283,662	1,219,479	1,083,491	94.0	88.8 (1,083,491/1,219,479)

*Patients received ART at PEPFAR-supported facilities. ART, antiretroviral therapy; PEPFAR, US President's Emergency Plan for AIDS Relief; TPT, tuberculosis preventive therapy.
†Number of adults and children receiving ART was reported quarterly; we used the number reported during the final quarter of each 6-month period.
‡TPT eligible was defined as 95% of total persons living with HIV who were receiving ART; TPT ineligibility (5%) accounts for PLHIV with active TB disease and PLHIV discontinuing TPT because of loss to follow-up, death, or adverse events.
§Number of patients who completed TPT divided by the number of patients who initiated TPT × 100.
¶TPT coverage was calculated as cumulative number of persons living with HIV who completed TPT divided by the number of TPT eligible patients × 100.

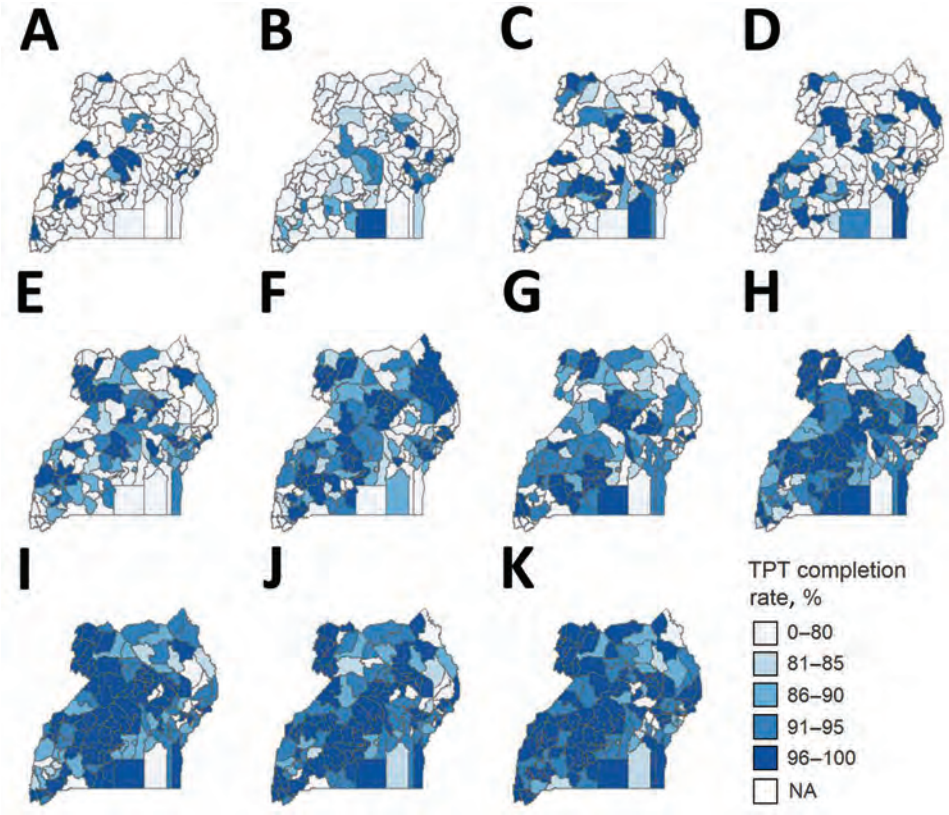

Figure 1. Completion rate percentages for tuberculosis preventive therapy by district among persons living with HIV in Uganda during 2016–2022. Completion rates in different districts in Uganda for 11 semiannual periods: A) October 2016–March 2017; B) April 2017–September 2017; C) October 2017–March 2018; D) April 2018–September 2018; E) October 2018–March 2019; F) April 2019–September 2019; G) October 2019–March 2020; H) April 2020–September 2020; I) October 2020–March 2021; J) April 2021–September 2021; and K) October 2021–March 2022. TPT, tuberculosis preventive therapy.

as part of efforts to provide TPT to all eligible PLHIV. Over time, TPT completion rates increased, especially during October 2019–March 2020, after the 100-day scale-up campaign (Appendix, https://wwwnc.cdc.gov/EID/article/29/3/22-1353-App1.pdf) (*14*). Although TPT coverage has continued to expand since 2020, negative effects of the COVID-19 pandemic are reflected by declines in TPT initiations and completions during the October 2019–March 2020 and April–September 2020 periods (*3*).

Considering available evidence (*6*–*8*), reducing the burden of TB among PLHIV in Uganda is feasible given high TPT coverage and if the following priorities are continued. First, full TPT coverage should be maintained, including among newly identified eligible PLHIV; shorter TPT regimens should be leveraged for high initiation and completion rates (*15*), and data should be routinely collected for close program monitoring. Second, enhanced TB case reporting is warranted, including among the general population,

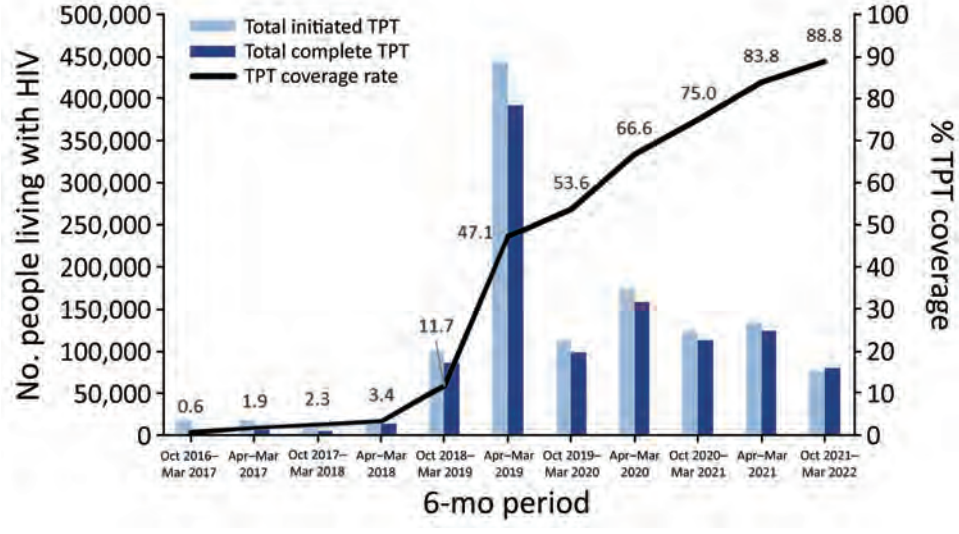

Figure 2. Number of persons initiating and completing tuberculosis preventive therapy among persons living with HIV and overall percentage coverage rate in Uganda, 2016–2022. Numbers are given for 11 semiannual periods; values along line indicate percentage coverage for that period. TPT, tuberculosis preventive therapy.

Table 2. Tuberculosis notification rates per 100,000 persons living with HIV during semiannual periods in study of tuberculosis preventive therapy among persons living with HIV, Uganda, October 2016–March 2022*

Semiannual periods	Overall	Patient age		Patient sex	
		<15 y	≥15 y	M	F
2016 Oct–2017 Mar†	881.1 (7,850/890,938)	NA	NA	NA	NA
2017 Apr–2017 Sep‡	523.4 (5,198/993,070)	465.6 (290/62,279)	331.2 (3,083/930,791)	642.0 (2,106/328,026)	201.0 (1,267/630,451)
2017 Oct–2018 Mar†	860.1 (8,866/1,030,756)	NA	NA	NA	NA
2018 Apr–2018 Sep‡	1,015.3 (11,186/1,101,716)	1,633.7 (1,035/63,353)	294.1 (3,054/1,038,363)	547.9 (2,128/388,410)	274.9 (1,961/713,306)
2018 Oct–2019 Mar	1,028.3 (11,284/1,097,366)	1,553.2 (929/59,812)	998.0 (10,355/1,037,554)	1,694.1 (6,528/385,331)	667.9 (4,756/712,035)
2019 Apr–2019 Sep	1,094.4 (12,566/1,148,258)	1,607.6 (985/61,273)	1,065.4 (11,581/1,086,985)	1,774.4 (7,195/405,491)	723.1 (5,371/742,767)
2019 Oct–2020 Mar	918.9 (11,037/1,201,166)	1,182.6 (730/61,731)	904.6 (10,307/1,139,435)	1,489.6 (6,336/425,358)	605.9 (4,701/775,808)
2020 Apr–2020 Sep	710.2 (8,650/1,218,006)	756.6 (462/61,062)	707.7 (8,188/1,156,944)	1,148.3 (4,956/431,584)	469.7 (3,694/786,422)
2020 Oct–2021 Mar	866.8 (10,747/1,239,829)	1,144.3 (678/59,249)	854.1 (10,083/1,180,580)	1,356.2 (5,921/436,577)	602.6 (4,840/803,252)
2021 Apr–2021 Sep	908.8 (11,511/1,266,588)	1,175.1 (703/59,925)	895.6 (10,808/1,206,763)	1,388.7 (6,185/445,390)	648.6 (5,326/821,198)
2021 Oct–2022 Mar	972.5 (12,483/1,283,662)	1,416.5 (813/57,396)	951.7 (11,670/1,226,266)	1,504.8 (6,788/451,092)	684.0 (5,695/832,570)

*Values are no./100,000 population (actual number of notifications among PLHIV/total PLHIV population). Tuberculosis notification rate is defined as the number of registered new and relapsed TB cases with documented HIV-positive status during the reporting period divided by the total number of PLHIV currently receiving antiretroviral treatment at PEPFAR-supported sites in Uganda. NA, not applicable; PEPFAR, US President's Emergency Plan for AIDS Relief.
†Total number of tuberculosis cases disaggregated by age and sex were not available.
‡Disaggregated totals for age groups and sex do not equal the overall totals in periods 2 and 4 because of synchronization issues between DATIM (Uganda DATIM version 1.31 MER 2.5, updated January 4, 2021; https://ug.datim4u.org) and the national reporting system; only the sites in which disaggregated totals were consistent with the national reporting system were included.

because the effects of high TPT coverage have not yet translated into declining TB notification rates among PLHIV. Ensuring early identification and treatment initiation for confirmed patients could include quality TB screening, testing, and prompt treatment. Third, newly recommended shorter TB treatment regimens should be considered standards of care to improve patient outcomes.

The first limitation of our study is that discrepancies were observed during some periods between disaggregated and overall totals because the national reporting systems integrated PEPFAR reporting requirements for TB-related data. Second, aggregate patient data are prone to ecologic fallacy and limited our ability to analyze person-level factors affecting TPT initiation and completion. Third, disaggregated data for TB cases during October 2016–March 2017 and October 2017–March 2018 were missing because of changes in data reporting requirements.

In summary, programmatic data indicate that almost all PLHIV in Uganda have received TPT, accelerating progress toward global targets for treatment coverage. Investments in timely TB screening, diagnosis, and earlier treatment during disease course should remain high priorities for TB/HIV prevention programming.

Acknowledgments

We thank Fatumah Nalubega for technical advice and assisting in data analysis.

This project was reviewed in accordance with human research protection procedures at the CDC and was determined to be nonresearch. A waiver for informed consent was obtained from the Makerere University Institutional Review Board in Uganda to use programmatic data.

This publication was supported by cooperative agreement no. NU2GGH002093 (G.G.) from the CDC and the Public Health Institute. This study was supported by PEPFAR through CDC through a cooperative agreement (no. GH002221). PEPFAR attribution statement: This publication has been supported by PEPFAR through CDC. The findings and conclusions in this presentation are those of the author(s) and do not necessarily represent the official position of the funding agencies.

About the Author

Dr. Lukoye is an epidemiologist in the Division of Global HIV and TB, Center for Global Health, US Centers for Disease Control and Prevention, Uganda. He serves as the public health expert for TB prevention, TB/HIV co-infections, and MDR TB and supports the Uganda Ministry of Health and implementing partners to achieve TB elimination.

References

1. Gupta RK, Lucas SB, Fielding KL, Lawn SD. Prevalence of tuberculosis in post-mortem studies of HIV-infected adults and children in resource-limited settings: a systematic review and meta-analysis. AIDS. 2015;29:1987–2002. https://doi.org/10.1097/QAD.0000000000000802
2. Granich R, Akolo C, Gunneberg C, Getahun H, Williams P, Williams B. Prevention of tuberculosis in people living with HIV. Clin Infect Dis. 2010;50:S215–22. https://doi.org/10.1086/651494
3. World Health Organization. Global tuberculosis report 2022 [cited 2022 Aug 5]. https://www.who.int/teams/global-tuberculosis-programme/tb-reports/global-tuberculosis-report-2022
4. UNAIDS: Joint United Nations Programme on HIV/AIDS. UNAIDS data 2021 [cited 2022 Aug 5]. https://www.unaids.org/sites/default/files/media_asset/JC3032_AIDS_Data_book_2021_En.pdf
5. Ayele HT, van Mourik MSM, Debray TPA, Bonten MJM. Isoniazid prophylactic therapy for the prevention of tuberculosis in HIV infected adults: a systematic review and meta-analysis of randomized trials. PLoS One. 2015;10:e0142290. PubMed https://doi.org/10.1371/journal.pone.0142290
6. Briggs MA, Emerson C, Modi S, Taylor NK, Date A. Use of isoniazid preventive therapy for tuberculosis prophylaxis among people living with HIV/AIDS: a review of the literature. J Acquir Immune Defic Syndr. 2015;68:S297–305. https://doi.org/10.1097/QAI.0000000000000497
7. Oxlade O, Rochon H, Campbell JR, Menzies D. Tuberculosis preventive treatment in people living with HIV-is the glass half empty or half full? PLoS Med. 2021;18:e1003702. https://doi.org/10.1371/journal.pmed.1003702
8. Pathmanathan I, Ahmedov S, Pevzner E, Anyalechi G, Modi S, Kirking H, et al. TB preventive therapy for people living with HIV: key considerations for scale-up in resource-limited settings. Int J Tuberc Lung Dis. 2018;22:596–605. https://doi.org/10.5588/ijtld.17.0758
9. World Health Organization. Tuberculosis profile: Uganda. Estimates of TB burden, 2021 [cited 2022 Aug 5]. https://worldhealthorg.shinyapps.io/tb_profiles/?_inputs_&entity_type=%22country%22&lan=%22EN%22&iso2=%22UG%22
10. UNAIDS: Joint United Nations Programme on HIV/AIDS. Country factsheets Uganda 2021 [cited 2022 Aug 5]. https://www.unaids.org/en/regionscountries/countries/uganda
11. Ministry of Health Republic of Uganda. Manual for management and control of tuberculosis and leprosy in Uganda, 3rd edition [cited 2022 Aug 5]. https://www.health.go.ug/cause/manual-for-management-and-control-of-tuberculosis-and-leprosy-in-uganda-3rd-edition
12. Dirlikov E, Kamoga J, Talisuna SA, Namusobya J, Kasozi DE, Akao J, et al. Scale-up of HIV antiretroviral therapy and estimation of averted infections and HIV-related deaths—Uganda, 2004–2022. MMWR Morb Mortal Wkly Rep. 2023;72:90–4. PubMed https://doi.org/10.15585/mmwr.mm7204a2
13. The Republic of Uganda Ministry of Health. Guidelines for programmatic management of TB preventive treatment in Uganda: a health worker guide. Kampala (Uganda): Government of Uganda, Ministry of Health; 2020.
14. Ministry of Health Republic of Uganda.100-Day accelerated isoniazid preventive therapy scale up plan, 2019 [cited 2022 Aug 5]. https://www.health.go.ug/cause/100-day-accelerated-isoniazid-preventive-therapy-scale-up-plan
15. Semitala FC, Musinguzi A, Ssemata J, Welishe F, Nabunje J, Kadota JL, et al. Acceptance and completion of rifapentine-based TB preventive therapy (3HP) among people living with HIV (PLHIV) in Kampala, Uganda—patient and health worker perspectives. Implement Sci Commun. 2021;2:71. https://doi.org/10.1186/s43058-021-00173-2

Address for correspondence: Deus Lukoye, US Centers for Disease Control and Prevention Uganda, US Embassy, 1577 Ggaba Rd, Nsambya, PO Box 7007, Kampala, Uganda; email: oju0@cdc.gov

Nosocomial Severe Fever with Thrombocytopenia Syndrome in Companion Animals, Japan, 2022

Hirohisa Mekata, Kazumi Umeki, Kentaro Yamada, Kunihiko Umekita, Tamaki Okabayashi

In Japan, 2 cats that underwent surgery in a room where a sick dog had been euthanized became ill within 9 days of surgery. Severe fever with thrombocytopenia syndrome virus was detected in all 3 animals; nucleotide sequence identity was 100%. Suspected cause was an uncleaned pulse oximeter probe used for all patients.

Severe fever with thrombocytopenia syndrome (SFTS) is an emerging and mostly fatal tickborne zoonosis in eastern Asia. The causative agent is *Dabie bandavirus*, of the family Phenuiviridae and genus *Bandavirus*, and is generally known as SFTS virus (SFTSV). In Japan, SFTS-related mortality rates are reported to be 27% among humans and 62% among domestic cats (*1*,*2*). Although dogs can become infected with SFTSV, the mortality rate is unclear because infection of healthy dogs tends be subclinical (*3*).

SFTSV is transmitted to humans and animals primarily through tick bites. However, nosocomial infection without a tick bite can occur via contact with blood and body fluids (*4*). Human-to-human transmission from an index patient to healthcare workers has been reported (*4*). Animal-to-human transmission from an index animal to veterinary personnel has also been reported (*5*,*6*). We report a nosocomial animal-to-animal transmission of SFTSV.

The Cases

On January 8, 2022, a 13-year-old female dog (dog 1) with a high fever (39.9°C [reference range 38.0°C–39.0°C]) and anorexia was examined at animal hospital A (Table; Figure 1). The next day, dog 1 exhibited diarrhea and neurologic symptoms (unsteadiness and wandering). When the animal's condition did not improve, on January 11, the dog was transferred to animal hospital B. On the basis of a high concentration of pancreas-specific lipase and pancreatic ultrasonography findings, veterinarians in animal hospital B diagnosed pancreatitis. Infectious disease was not suspected because the dog had no signs of a tick bite and had been vaccinated against most of the severe canine diseases in Japan. At 11:00 A.M. the next day, the dog was unresponsive to stimuli. The dog underwent tracheal intubation and mechanical ventilation, and a pulse oximeter probe was placed on the tongue. The dog did not respond to treatment and was euthanized and returned to the owner at approximately 3:00 P.M.

On January 12, at approximately 10 A.M., a healthy 7-month-old female domestic cat (cat 1) was hospitalized at animal hospital B for ovariohysterectomy (Figure 1). At approximately 4:00 P.M., the ovariohysterectomy was performed under anesthesia on the same operating table and with the same ventilator used for dog 1. Cat 1 was discharged in healthy condition the next day.

Also on January 12, at approximately 6 P.M., a 21-month-old male domestic cat (cat 2) was urgently hospitalized at animal hospital B for ingestion of a foreign body. Cat 2 underwent endoscopic surgery under anesthesia in the same operating room and was discharged in healthy condition the next day.

Cats 1 and 2 had no contact with dog 1 in the hospital. After surgery, the cats were kept in the same hospital room but in different cages and had no contact with each other. All 3 animals had different owners, and no contact before hospitalization was reported.

On January 19, a high fever (40.8°C [reference range 38.0°C–39.0°C]), vomiting, and inappetence developed in cat 1. Its condition worsened; on January 21, leukopenia and thrombocytopenia were confirmed (Table), and on January 22, the cat

Author affiliations: University of Miyazaki, Miyazaki, Japan (H. Mekata, K. Yamada, K. Umekita, T. Okabayashi); Kyushu University of Health and Welfare, Nobeoka, Japan (K. Umeki); University of Miyazaki Hospital, Miyazaki (K. Umekita)

DOI: https://doi.org/10.3201/eid2903.220720

Table. Hematologic results and outcomes for 3 companion animals with severe fever with thrombocytopenia syndrome virus infection, Japan, 2022*

Characteristic	Reference ranges†		Dog 1		Cat 1	Cat 2
	Canine	Feline	Jan 8	Jan 12	Jan 21	Jan 21
Real-time RT-PCR, copies/mL	NA		1.99×10^6‡	ND§	1.53×10^6	6.37×10^6
Virus isolation	NA		ND	ND	+	+
ELISA (absorbance at 405 nm)	(<0.04)§		ND	ND	+ (0.39)	+ (2.92)
Temperature, °C	38.0–39.0	38.0–39.0	39.9	ND	37.2¶	39.8
Leukocytes, $\times 10^2$ cells/mL	40–155	30–148	81.0	49.4	13.1	73.7
Hemoglobin, g/dL	12.1–20.3	9.3–15.9	14.4	11.4	15.1	35.1
Platelets, $\times 10^4$/mL	17–40	20–50	10.6	1.4	0.9	6.4
Total bilirubin, mg/dL	0.1–0.3	0.1–0.4	0.2	3.2	5.5	5.1
Alanine transaminase, U/L	12–118	10–100	157	189	566	148
Alkaline phosphatase, U/L	5–131	10–50	>1225	>1225	<10	16
Creatinine, mg/dL	0.5–1.6	0.6–2.4	0.8	5.1	1.3	1.5
Outcome			Euthanasia		Death	Recovery

*NA, not applicable; ND, not done; RT-PCR, reverse transcription PCR.
†Standard canine and feline hematology parameters were selected according to (*7*).
‡Poorly preserved blood was used for real-time RT-PCR and virus isolation.
§Cutoff value selected according to (*8*).
¶Temperature was 40.8°C on January 19.

died. On January 21, high fever (39.8°C) with bilirubinuria developed in cat 2. Despite vomiting on January 22, cat 2 recovered by January 26. Both cats were kept indoors only, and neither had a history of a tick bite.

The director of animal hospital B suspected nosocomial infections because severe symptoms developed in the 2 cats that had undergone surgery on the same day. Serum samples from the cats were sent to the Center for Animal Disease Control, University of Miyazaki, where real-time reverse transcription PCR for SFTSV, feline calicivirus, and feline parvovirus was performed (*9*–*11*).

High copy numbers of SFTSV RNA were detected in both samples (cat 1 = 1.53×10^6 copies/mL; cat 2 = 6.37×10^6 copies/mL). Also confirmed by using double-antigen ELISA were IgG, IgM, or both against SFTSV nucleoprotein (absorbance at 405 nm) (cat 1 = 0.39; cat 2 = 2.92) (*8*). Blood collected from dog 1 on January 8 had been discarded in the medical waste box but was retrieved and sent to the Center for Animal Disease Control after results for the cats were confirmed. Although the blood had been kept at room temperature for >2 weeks, a high copy number of SFTSV RNA was detected (1.99×10^6 copies/mL). ELISA was not performed because the blood was in

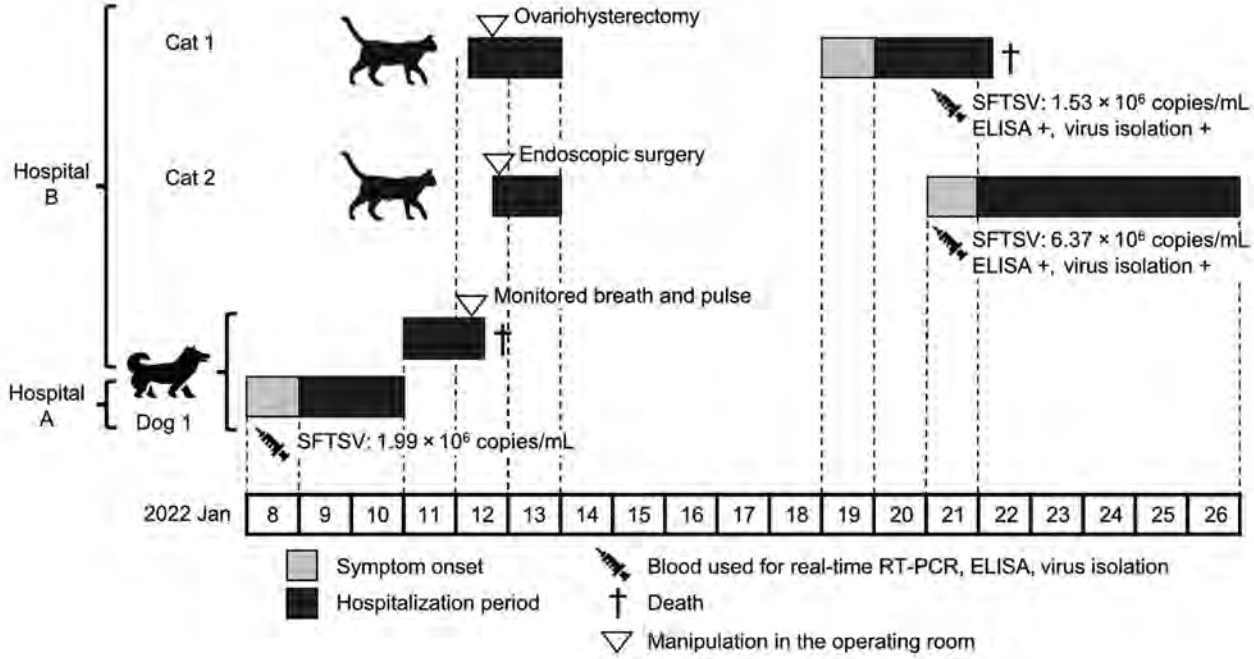

Figure 1. Timeline of dog-to-cat nosocomial transmission of SFTSV, Japan, 2022. Cat 1 was 7 months of age; cat 2 was 21 months of age; dog 1 was 13 years of age. RT-PCR, reverse transcription PCR; SFTSV, severe fever with thrombocytopenia syndrome virus; +, positive.

poor condition. For veterinary personnel, body temperature and real-time reverse transcription PCR were monitored daily by the Oita City Public Health Center, but SFTSV infection was not detected.

SFTSV isolation was performed by using serum from cats 1 and 2 and hemolyzed blood from dog 1. The virus isolation procedure has been previously described (*12*). SFTSV was isolated from both cats but not from the dog because of poor preservation of the dog sample. Next, the entire sequences of the SFTSV medium (M) segment from the animals were compared. The M segment encoding Gn and Gc glycoproteins is a more diverse segment than the small and large segments (*13*). Almost the entire sequence (SFTSV M segment, nt 9–3378) was successfully amplified and determined by using the reported primers (*13*) and submitted to the DNA Data Bank of Japan (accession no. LC705155-7). The virus sequences from the index dog and the 2 secondarily affected cats showed 100% homology (Figure 2). Furthermore, the sequences were most closely related (99.8%) to the SFTSV SPL105A Miyazaki 2013 strain (accession no. AB985315), which was obtained from a person with SFTS infection in an adjacent prefecture in 2013.

The operating room was a sanitary environment. The operating table was disinfected after each use; repeated use of contaminated instruments was prohibited; and all staff wore disposable gowns, masks, and gloves during operations. Although most medical instruments do not cause nosocomial infection, we determined that the pulse oximeter probe posed the highest risk for virus transmission between the dog and the cats because a disposable paper towel was placed between the probe and tongue, with saliva contaminating the probe, and the staff were unable to confirm whether the inner surface of the probe was wiped with hypochlorous acid between patients. A previous study detected high levels of viral RNA in the saliva of animals with SFTS (*14*,*15*). Because the same ventilator was used with the 3 animals reported here, aerosol transmission is another suspected source. Although the tracheal tubes

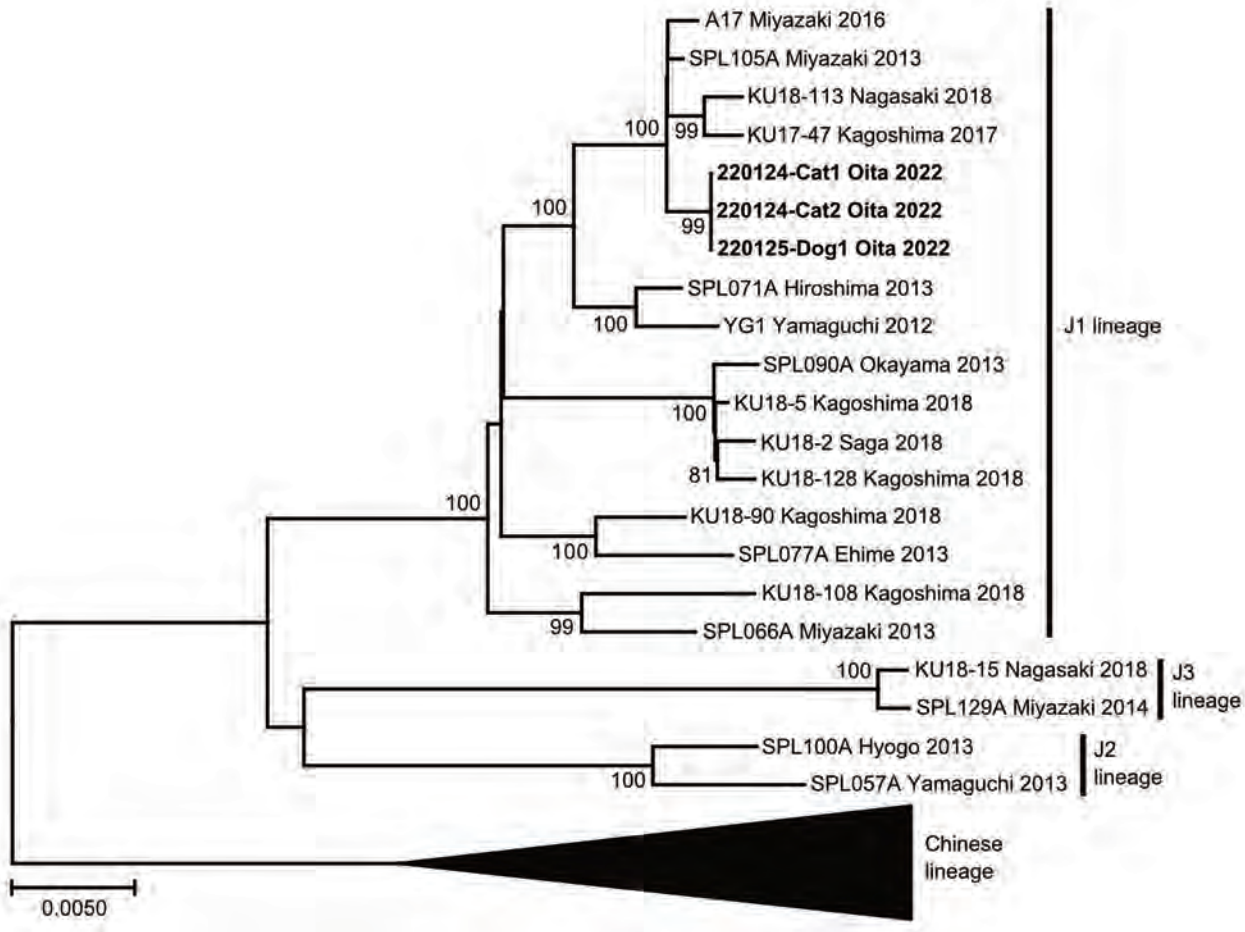

Figure 2. Phylogenetic analysis of severe fever with thrombocytopenia syndrome virus obtained from dog with index infection and 2 cats with nosocomial infection, Japan, 2022. The phylogenetic tree is shown for the viral genomic RNA of the medium segment. Boldface indicates viruses isolated from the animals in this study. Scale bar indicates nucleotide substitutions per site.

and attached equipment were changed after each use, other parts (e.g., the breathing tube) were not changed and disinfected because infectious disease was not suspected.

Conclusions

We report molecular evidence of nosocomial transmission of SFTSV among companion animals in an animal hospital in Japan. Veterinary personnel should be aware of the risk that this emerging zoonotic disease poses for their safety as well as the safety of patients and clients. To prevent nosocomial infections, veterinary staff should be educated about basic infection prevention and control practices in animal hospitals.

Acknowledgments

We thank the veterinarians and clients for permission to report this study. We also thank Mari Yamamoto and Saori Kusakari for their technical assistance.

This study was supported by the Japan Society for the Promotion of Science, KAKENHI (grant no. 21H02361).

About the Author

Dr. Mekata is an associate professor with the Center for Animal Disease Control, University of Miyazaki, Miyazaki, Japan. His research interests are epidemiology, prevention measures, and the viral evolution of animal infectious diseases.

References

1. Kobayashi Y, Kato H, Yamagishi T, Shimada T, Matsui T, Yoshikawa T, et al.; SFTS Epidemiological Research Group Japan. Severe fever with thrombocytopenia syndrome, Japan, 2013–2017. Emerg Infect Dis. 2020;26:692–9. https://doi.org/10.3201/eid2604.191011
2. Matsuu A, Momoi Y, Nishiguchi A, Noguchi K, Yabuki M, Hamakubo E, et al. Natural severe fever with thrombocytopenia syndrome virus infection in domestic cats in Japan. Vet Microbiol. 2019;236:108346. https://doi.org/10.1016/j.vetmic.2019.06.019
3. Park SC, Park JY, Choi JY, Oh B, Yang MS, Lee SY, et al. Experimental infection of dogs with severe fever with thrombocytopenia syndrome virus: pathogenicity and potential for intraspecies transmission. Transbound Emerg Dis. 2022;69:3090–6. https://doi.org/10.1111/tbed.14372
4. Jung IY, Choi W, Kim J, Wang E, Park SW, Lee WJ, et al. Nosocomial person-to-person transmission of severe fever with thrombocytopenia syndrome. Clin Microbiol Infect. 2019;25:633.e1–4. https://doi.org/10.1016/j.cmi.2019.01.006
5. Yamanaka A, Kirino Y, Fujimoto S, Ueda N, Himeji D, Miura M, et al. Direct transmission of severe fever with thrombocytopenia syndrome virus from domestic cat to veterinary personnel. Emerg Infect Dis. 2020;26:2994–8. https://doi.org/10.3201/eid2612.191513
6. Kida K, Matsuoka Y, Shimoda T, Matsuoka H, Yamada H, Saito T, et al. A case of cat-to-human transmission of severe fever with thrombocytopenia syndrome virus. Jpn J Infect Dis. 2019;72:356–8. https://doi.org/10.7883/yoken.JJID.2018.526
7. Klaassen JK. Reference values in veterinary medicine. Lab Med. 1999;30:194–7. https://doi.org/10.1093/labmed/30.3.194
8. Umeki K, Yasuda A, Umekita K, Megumi R, Nomura H, Kawaguchi T, et al. Detection of anti-SFTSV nuclear protein antibody in the acute phase sera of patients using double-antigen ELISA and immunochromatography. J Virol Methods. 2020;285:113942. https://doi.org/10.1016/j.jviromet.2020.113942
9. Takahashi T, Maeda K, Suzuki T, Ishido A, Shigeoka T, Tominaga T, et al. The first identification and retrospective study of severe fever with thrombocytopenia syndrome in Japan. J Infect Dis. 2014;209:816–27. https://doi.org/10.1093/infdis/jit603
10. Streck AF, Rüster D, Truyen U, Homeier T. An updated TaqMan real-time PCR for canine and feline parvoviruses. J Virol Methods. 2013;193:6–8. https://doi.org/10.1016/j.jviromet.2013.04.025
11. Brunner C, Kanellos T, Meli ML, Sutton DJ, Gisler R, Gomes-Keller MA, et al. Antibody induction after combined application of an adjuvanted recombinant FeLV vaccine and a multivalent modified live virus vaccine with a chlamydial component. Vaccine. 2006;24:1838–46. https://doi.org/10.1016/j.vaccine.2005.10.030
12. Sato Y, Mekata H, Sudaryatma PE, Kirino Y, Yamamoto S, Ando S, et al. Isolation of severe fever with thrombocytopenia syndrome virus from various tick species in area with human severe fever with thrombocytopenia syndrome cases. Vector Borne Zoonotic Dis. 2021;21:378–84. https://doi.org/10.1089/vbz.2020.2720
13. Yoshikawa T, Shimojima M, Fukushi S, Tani H, Fukuma A, Taniguchi S, et al. Phylogenetic and geographic relationships of severe fever with thrombocytopenia syndrome virus in China, South Korea, and Japan. J Infect Dis. 2015;212:889–98. https://doi.org/10.1093/infdis/jiv144
14. Park E-S, Shimojima M, Nagata N, Ami Y, Yoshikawa T, Iwata-Yoshikawa N, et al. Severe fever with thrombocytopenia syndrome phlebovirus causes lethal viral hemorrhagic fever in cats. Sci Rep. 2019;9:11990. https://doi.org/10.1038/s41598-019-48317-8
15. Yu K-M, Jeong H-W, Park S-J, Kim Y-I, Yu M-A, Kwon H-I, et al. Shedding and transmission modes of severe fever with thrombocytopenia syndrome phlebovirus in a ferret model. Open Forum Infect Dis. 2019;6:ofz309. https://doi.org/10.1093/ofid/ofz309

Address for correspondence: Tamaki Okabayashi, Center for Animal Disease Control, University of Miyazaki, 1-1 Gakuen-Kibanadai-Nishi, Miyazaki, 889-2192, Japan; email: okbys81@cc.miyazaki-u.ac.jp

Burkholderia thailandensis Isolated from the Environment, United States

Carina M. Hall, Nathan E. Stone, Madison Martz, Shelby M. Hutton, Ella Santana-Propper, Lora Versluis, Kieston Guidry, Marielisa Ortiz, Joseph D. Busch, Trevor Maness, Jonathan Stewart, Tom Sidwa, Jay E. Gee, Mindy G. Elrod, Julia K. Petras, Maureen C. Ty, Christopher Gulvik, Zachary P. Weiner, Johanna S. Salzer, Alex R. Hoffmaster, Sarai Rivera-Garcia, Paul Keim, Amanda Kieffer, Jason W. Sahl, Fred Soltero, David M. Wagner

Burkholderia thailandensis, an opportunistic pathogen found in the environment, is a bacterium closely related to *B. pseudomallei*, the cause of melioidosis. Human *B. thailandensis* infections are uncommon. We isolated *B. thailandensis* from water in Texas and Puerto Rico and soil in Mississippi in the United States, demonstrating a potential public health risk.

Burkholderia thailandensis, a gram-negative bacterium found in the environment, poses a public health threat both because of its ability to cause infections as an opportunistic pathogen and potential misidentification as the more pathogenic *B. pseudomallei*, its closest phylogenetic relative (*1*–*4*). *B. pseudomallei*, designated a Select Agent by the US Federal Select Agents Program and the causative pathogen of melioidosis, and *B. thailandensis* are found in the environment in some tropical regions, including Southeast Asia and northern Australia. *B. thailandensis*, a Biosafety Level 2 organism not classified as a Select Agent (*3*), has fewer safety restrictions than *B. pseudomallei*, and because it can be handled outside of Biosafety Level 3 laboratories, it is used by researchers as a surrogate in some experiments (*5*). In laboratory analyses, *B. thailandensis* is challenging to distinguish from *B. pseudomallei* because of their similar biochemical phenotypes, the only difference being that *B. thailandensis* can assimilate L-arabinose (*1*,*3*). *B. thailandensis* was described after researchers observed reduced virulence in an environmental isolate thought to be *B. pseudomallei*. Subsequent 16S rRNA gene analysis revealed a novel *Burkholderia* species named *B. thailandensis* after the geographic origin of the type strain (*3*).

Human *B. thailandensis* infections are uncommon (*1*,*4*), especially in the Western Hemisphere. Three previous clinical cases in that region have been reported, all from the southern United States: Louisiana in 1997, Texas in 2003 (*1*), and Arkansas in 2017 (*4*). Environmental sampling related to the 2003 case in Texas and previous environmental sampling for *B. pseudomallei* complex members did not recover *B. thailandensis* (*6*). *B. thailandensis* has been described primarily from the environment in Southeast Asia and Australia (*3*,*7*) and, recently, Africa (*8*). Occurrence of *B. thailandensis* in the environment in the Western Hemisphere remains poorly understood. We used a systematic approach to detect and isolate *B. thailandensis* from soil and water samples collected in Texas in November 2019 and November 2020 (*9*) and Puerto Rico during December 2018–March 2020.

The Study

We collected 2,540 environmental samples, 370 (280 soil, 80 water, 10 environmental water tank scrapes) from Texas and 2,170 (1,650 soil, 520 water) from throughout Puerto Rico. From the collected samples, we detected *B. thailandensis* DNA in 10 complex broth

Author affiliations: Northern Arizona University, Flagstaff, Arizona, USA (C.M. Hall, N.E. Stone, M. Martz, S. Hutton, E. Santana-Propper, K. Guidry, J.D. Busch, P. Keim, J.W. Sahl, D.M. Wagner); US Department of Agriculture, San Juan, Puerto Rico, USA (M. Ortiz, S. Rivera-Garcia, F. Soltero); Texas Department of State Health Services, San Antonio, Texas, USA (T. Maness, J. Stewart, A. Kieffer); Texas Department of State Health Services, Austin, Texas, USA (T. Sidwa); Centers for Disease Control and Prevention, Atlanta, Georgia, USA (J.E. Gee, M.G. Elrod, J.K. Petras, M.C. Ty, C. Gulvik, Z.P. Weiner, J.S. Salzer, A.R. Hoffmaster)

DOI: https://doi.org/10.3201/eid2903.221245

samples, 4 from Texas and 6 from Puerto Rico (Appendix, https://wwwnc.cdc.gov/EID/article/29/3/22-1245-App1.pdf). Culturing (*10*) yielded *B. thailandensis* isolates from 5 samples, 1 from Texas and 4 from Puerto Rico. In addition, we isolated *B. thailandensis* from a soil sample collected in Mississippi in July 2022 during a melioidosis cluster investigation (*11*). Further, in 2021, we identified *B. thailandensis* infection in a 4th case-patient in the United States (Oklahoma) (Table). The patient was suspected to have aspirated water after a motor vehicle rollover into water; he died because of multiple complications (Appendix).

We used whole-genome analysis of those 7 isolates (National Center for Biotechnology Information BioProject nos. PRJNA575701, PRJNA818328, PRJNA908850) to place them within a larger phylogeographic context, including other *B. thailandensis* isolates from the United States and other global locations (Table; Figure). Environmental *B. thailandensis* isolates from Texas and Mississippi grouped in the same clade with clinical isolates from Texas and Louisiana and 2 environmental isolates from Asia. The 2021 clinical isolate from Oklahoma was most closely related to the isolate from the 2003 clinical case in Texas. Environmental isolates from Texas and Mississippi differed by more (4,639 single-nucleotide polymorphisms [SNPs]) than environmental isolates from Thailand and Australia (2,671 SNPs); *B. pseudomallei* isolates found in Australia and Asia are more diverse than isolates in the Americas (*10*). We observed little diversity among the 4 *B. thailandensis* isolates from Puerto Rico; total diversity was 62 SNPs, and distance between any 2 isolates was 28–36 SNPs.

Among the isolates identified in our study, in silico multilocus sequence type analysis (https://pubmlst.org/organisms/burkholderia-pseudomallei) revealed novel *ace* allele 106 in the 4 isolates from Puerto Rico and the clinical isolate from Oklahoma, assigning all 5 to novel sequence type (ST) 1772. Novel *gltB* allele 175 was identified in the isolate from Texas, which was assigned to novel ST1785. The isolate from Mississippi, which had a unique combination of alleles, was assigned to novel ST2019.

Conclusions

Our study confirms *B. thailandensis* endemicity in the environment in the United States, albeit of rare occurrence and low abundance, requiring extensive sampling to detect; we found *B. thailandensis* at only 3.7% of collection sites in Puerto Rico and 8% in Texas. However, the pathogen could be present in other unsampled areas in the southern United States and Puerto Rico. Substantial culturing was required to isolate bacteria from PCR-positive samples, suggesting low abundance or its presence being outcompeted by other bacteria. *B. thailandensis* abundance might vary seasonally or on the basis of precipitation levels.

Table. Genomes from global isolates used to generate whole-genome phylogeny in study of *Burkholderia thailandensis* from the environment in the United States*

Isolate	Alternative ID	Country (state/territory)	Sample type (source)	Year	MLST	GenBank accession no.
Bt10009†	165–01_P1_S7	USA (TX)	Environmental (water)	2019	1758	JALGJD00000000
Bt10013†	203–09_P1_S27	USA (PR)	Environmental (water)	2020	1772	JALGJC00000000
Bt9795†	61_10_S54_S1 copy3	USA (PR)	Environmental (water)	2018	1772	WCIR00000000
Bt9920†	89–06_P1_S1	USA (PR)	Environmental (water)	2018	1772	WCIQ00000000
Bt9942†	91–08_P2_S1	USA (PR)	Environmental (water)	2018	1772	WCIP00000000
BtMS2022a†		USA (MS)	Environmental (soil)	2022	2019	SRR22548212
BtOK2021a†		USA (OK)	Clinical (human)	2021	1772	SRR22548210
2.1		Vietnam	Environmental (soil)	2017	696	GCA_002803565.1
82172	34; 2002721621	France	Veterinary (horse)	1982	73	GCA_001555485.1
Bt4	49639	Australia	Environmental	Unknown	699	GCA_000170395.1
BtAR2017		USA (AR)	Clinical (human)	2017	101	GCA_004684955.1
E1		Papua New Guinea	Environmental	1995	669	GCA_001524325.1
E254		Thailand	Environmental (soil)	1992	345	GCA_000765375.1
E264	ATCC 700388	Thailand	Environmental (soil)	1994	80	GCA_003568605.1
E444	E0444	Thailand	Environmental (soil)	2002	79	GCA_000567945.1
E555		Cambodia	Environmental	2005	696	GCF_000179515.1
H0587	2002721121	USA (LA)	Clinical (human)	1997	101	GCA_000567905.1
MSMB59		Australia	Environmental (soil)	2006	669	GCA_001718595.1
MSMB60		Australia	Environmental (soil)	2006	669	GCA_001524345.1
Phuket 4W-1		Thailand	Environmental (water)	1965	80	GCA_000877335.1
TXDOH	CDC3015869; 2003015869	USA (TX)	Clinical (human)	2003	101	GCA_002888425.1
USAMRU Malaysia no. 20	2002721744	Malaysia	Unknown	Unknown	80	GCA_000706745.1

*Phylogeny shown in Figure. MLST, multilocus sequence type; USAMRU, US Army Medical Research Unit; TXDOH, Texas Department of Health.
†Isolated in this study.

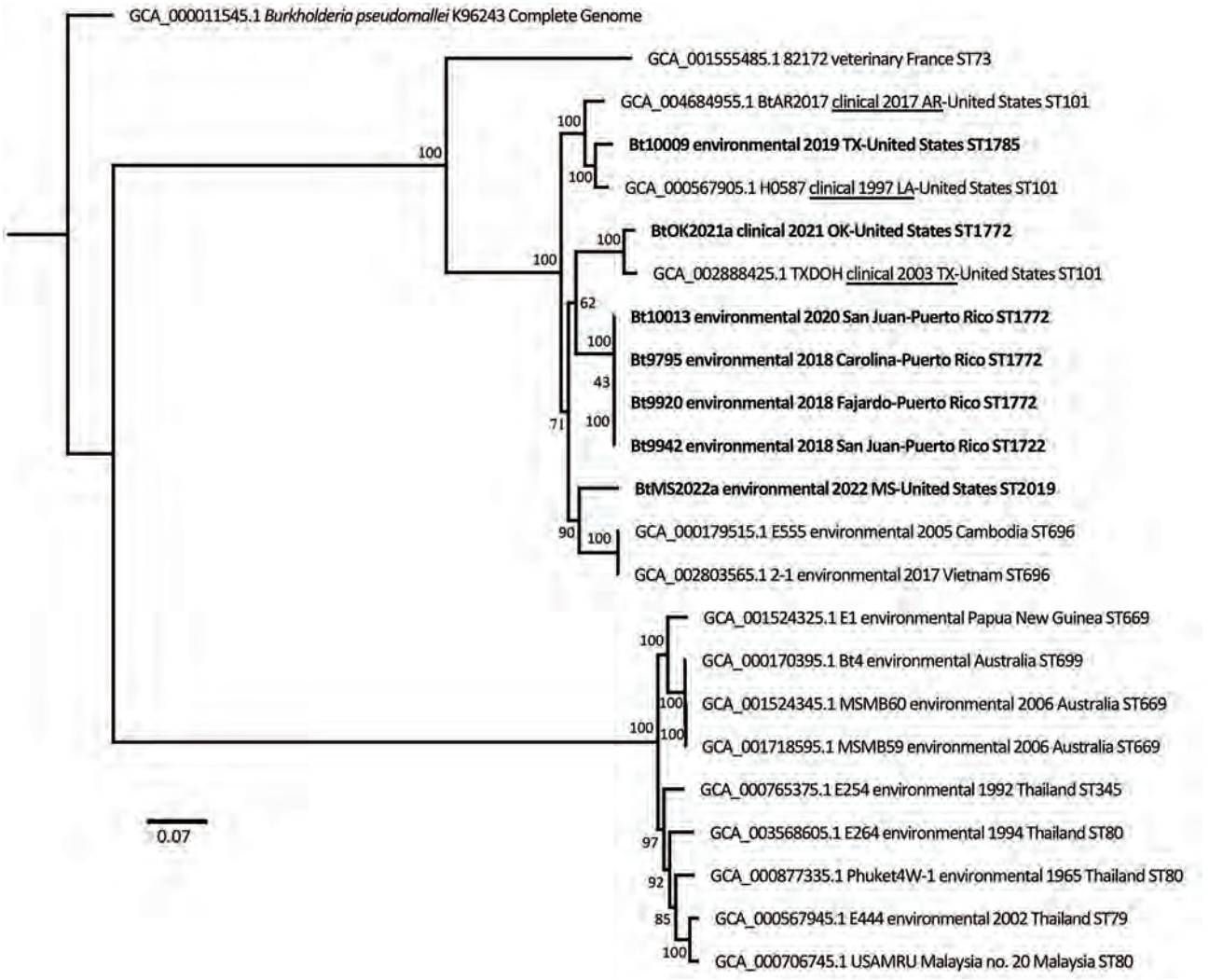

Figure. Wholegenome maximum-likelihood phylogeny of global isolates in study of *Burkholderia thailandensis* from the environment in the United States (Table). Tree was constructed with 1,000 bootstrap replicates and rooted with *B. pseudomallei*. Bold indicates *B. thailandensis* genomes generated from isolates collected in this study; other *B. thailandensis* from the Western Hemisphere have epidemiologic information underlined. Scale bar indicates 3,000 SNPs.

We detected *B. thailandensis* in Texas and Puerto Rico only from water samples, although they comprised only 24% of total (water and soil) samples collected at positive sites; all soil samples were negative for *B. thailandensis*. In contrast, in Thailand, *B. thailandensis* is most commonly isolated from soil (*12*). All 4 clinical cases from the United States were associated with traumatic injuries (*1*,*4*), 3 involving water (*1*), demonstrating the public health risk for disease from traumatic injuries related to contaminated water. This risk is especially relevant in Puerto Rico where *B. thailandensis* was detected within neighborhoods of the largest city, San Juan. Puerto Rico and the southeastern United States are prone to hurricane-induced flooding, which could increase the risk for infection by both *B. thailandensis* and *B. pseudomallei* (*13*).

Although samples were collected from 3 municipalities in northeastern Puerto Rico during a 1-year period, we found little phylogenetic diversity among the isolates, suggesting *B. thailandensis* may be widespread but rare in the environment in Puerto Rico and the result of a single introduction, as previously suggested for *B. pseudomallei* in Puerto Rico (*10*). We found evidence of possible local adaptation in Puerto Rico, which supports this hypothesis. We identified 113 genes unique to *B. thailandensis* isolates from Puerto Rico (Appendix), many of them potentially colocated in genomic islands, a pattern similar to one previously observed among *B. pseudomallei* isolates from Puerto Rico (*10*). Of note, 2 genes common to all *B. thailandensis* from Puerto Rico were present in some *B. pseudomallei* isolates from Puerto

Rico but absent from all other global *B. pseudomallei* genomes (Appendix). In contrast, thousands of SNPs were found among *B. thailandensis* strains in the continental United States (Arkansas, Louisiana, Mississippi, Oklahoma, and 2003 clinical and 2019 environmental isolates from Texas). This finding suggests a long-term but cryptic presence of *B. thailandensis* in the southern United States, perhaps in water. It is unknown how long *B. thailandensis* can persist in water, but *B. pseudomallei* can survive in water for ≥16 years without nutrients (*14*).

Our study provides valuable information regarding *B. thailandensis* occurrence and the potential of water to serve as a reservoir and source of infection for this opportunistic pathogen in the southern United States and Puerto Rico, especially following flooding events. Because likely autochthonous melioidosis cases also have been reported from Texas (*15*), Puerto Rico (*10*), and Mississippi (*11*), clinicians should be aware of the potential of misidentifying *B. thailandensis* as *B. pseudomallei* because of their morphologic and biochemical similarities.

Acknowledgments

We thank the Mississippi State Health Department, the Oklahoma Department of Health, animal health technicians from the US Department of Agriculture Animal and Plant Health Inspection Service, Veterinary Services in Puerto Rico, and undergraduate researchers at Northern Arizona University.

Funding for this project was provided by the Centers for Disease Control and Prevention through award nos. 75D30118C00594 and 75D30119P05696.

About the Author

Dr. Hall is a research scientist at the Pathogen and Microbiome Institute in Flagstaff, Arizona, USA, and has conducted research on *Burkholderia pseudomallei* for 10 years. She has conducted environmental surveys for *B. pseudomallei* and other *Burkholderia* spp. in the United States in Arizona, Louisiana, Florida, Puerto Rico, Texas, and the US Virgin Islands, and in Australia.

References

1. Glass MB, Gee JE, Steigerwalt AG, Cavuoti D, Barton T, Hardy RD, et al. Pneumonia and septicemia caused by *Burkholderia thailandensis* in the United States. J Clin Microbiol. 2006;44:4601–4. https://doi.org/10.1128/JCM.01585-06
2. Wu B, Tong X, He H, Yang Y, Chen H, Yang X, et al. Misidentification of *Burkholderia pseudomallei*, China. Emerg Infect Dis. 2021;27:964–6. https://doi.org/10.3201/eid2703.191769
3. Brett PJ, DeShazer D, Woods DE. *Burkholderia thailandensis* sp. nov., a *Burkholderia pseudomallei*-like species. Int J Syst Bacteriol. 1998;48:317–20. https://doi.org/10.1099/00207713-48-1-317
4. Gee JE, Elrod MG, Gulvik CA, Haselow DT, Waters C, Liu L, et al. *Burkholderia thailandensis* isolated from infected wound, Arkansas, USA. Emerg Infect Dis. 2018;24:2091–4. https://doi.org/10.3201/eid2411.180821
5. Morici LA, Heang J, Tate T, Didier PJ, Roy CJ. Differential susceptibility of inbred mouse strains to *Burkholderia thailandensis* aerosol infection. Microb Pathog. 2010;48:9–17. https://doi.org/10.1016/j.micpath.2009.10.004
6. Hall CM, Busch JD, Shippy K, Allender CJ, Kaestli M, Mayo M, et al. Diverse *Burkholderia* species isolated from soils in the southern United States with no evidence of *B. pseudomallei*. PLoS One. 2015;10:e0143254. https://doi.org/10.1371/journal.pone.0143254
7. Ginther JL, Mayo M, Warrington SD, Kaestli M, Mullins T, Wagner DM, et al. Identification of *Burkholderia pseudomallei* near-neighbor species in the Northern Territory of Australia. PLoS Negl Trop Dis. 2015;9:e0003892. https://doi.org/10.1371/journal.pntd.0003892
8. Birnie E, van 't Hof S, Bijnsdorp A, Mansaray Y, Huizenga E, van der Ende A, et al. Identification of *Burkholderia thailandensis* with novel genotypes in the soil of central Sierra Leone. PLoS Negl Trop Dis. 2019;13:e0007402. https://doi.org/10.1371/journal.pntd.0007402
9. Hall CM, Romero-Alvarez D, Martz M, Santana-Propper E, Versluis L, Jiménez L, et al. Low risk of acquiring melioidosis from the environment in the continental United States. PLoS One. 2022;17:e0270997. https://doi.org/10.1371/journal.pone.0270997
10. Hall CM, Jaramillo S, Jimenez R, Stone NE, Centner H, Busch JD, et al. *Burkholderia pseudomallei*, the causative agent of melioidosis, is rare but ecologically established and widely dispersed in the environment in Puerto Rico. PLoS Negl Trop Dis. 2019;13:e0007727. https://doi.org/10.1371/journal.pntd.0007727
11. Centers for Disease Control and Prevention. Melioidosis locally endemic in areas of the Mississippi Gulf Coast after *Burkholderia pseudomallei* isolated in soil and water and linked to two cases—Mississippi, 2020 and 2022 [cited 2022 Jul 27]. https://emergency.cdc.gov/han/2022/han00470.asp
12. Hantrakun V, Thaipadungpanit J, Rongkard P, Srilohasin P, Amornchai P, Langla S, et al. Presence of *B. thailandensis* and *B. thailandensis* expressing *B. pseudomallei*-like capsular polysaccharide in Thailand, and their associations with serological response to *B. pseudomallei*. Plos Neglect Trop D. 2018;12. https://doi.org/10.1371/journal.pntd.0006193
13. Hodgetts K, Kleinecke M, Woerle C, Kaestli M, Budd R, Webb JR, et al. Melioidosis in the remote Katherine region of northern Australia. PLoS Negl Trop Dis. 2022;16:e0010486. https://doi.org/10.1371/journal.pntd.0010486
14. Pumpuang A, Chantratita N, Wikraiphat C, Saiprom N, Day NPJ, Peacock SJ, et al. Survival of *Burkholderia pseudomallei* in distilled water for 16 years. Trans R Soc Trop Med Hyg. 2011;105:598–600. https://doi.org/10.1016/j.trstmh.2011.06.004
15. Cossaboom CM, Marinova-Petkova A, Strysko J, Rodriguez G, Maness T, Ocampo J, et al. Melioidosis in a resident of Texas with no recent travel history, United States. Emerg Infect Dis. 2020;26:1295–9. https://doi.org/10.3201/eid2606.190975

Address for correspondence: Dave Wagner, Northern Arizona University, 1395 S Knoles Dr, Flagstaff, AZ 86011, USA; email: dave.wagner@nau.edu

Mycobacterium leprae in Armadillo Tissues from Museum Collections, United States

Daniel Romero-Alvarez, Daniel Garzon-Chavez, Mary Jackson, Charlotte Avanzi, A. Townsend Peterson

We examined armadillos from museum collections in the United States using molecular assays to detect leprosy-causing bacilli. We found *Mycobacterium leprae* bacilli in samples from the United States, Bolivia, and Paraguay; prevalence was 14.8% in nine-banded armadillos. US isolates belonged to subtype 3I-2, suggesting long-term circulation of this genotype.

Hansen disease (leprosy) is an ancient pathology caused by 2 slow-growing intracellular bacilli, *Mycobacterium leprae* and *M. lepromatosis* (*1*). Both pathogens have the ability to damage peripheral nerves of hosts, producing a broad spectrum of clinical outcomes. Routes of disease transmission have been hypothesized for >100 years but are still actively debated (*2*); traditionally, human-to-human transmission has been considered the dominant route of infection. Evidence incriminates *M. leprae* as a zoonotic pathogen; the nine-banded armadillo (*Dasypus novemcinctus*) is its main wildlife reservoir in the southern United States (*2*). *M. leprae* also has been found in *D. novemcinctus* armadillos outside the United States (e.g., in Brazil), in the six-banded armadillo (*Euphractus sexcinctus*), and in nonhuman primates including chimpanzees, macaques, and sooty mangabeys (*2*). In addition, *M. leprae* and *M. lepromatosis* have been reported in red squirrels (*Sciurus vulgaris*) in the British Isles (*3*). Those data strongly suggest broad zoonotic transmission dynamics for both bacilli.

Natural history collections represent a neglected resource for biomedical research despite their known utility (*4*). We examined armadillo (family Dasypodidae) tissues deposited in museum collections across the United States to identify *M. leprae* and *M. lepromatosis* across space and time. We report presence of *M. leprae* in armadillo tissue samples from endemic and nonendemic areas of the Americas, suggesting that public health policy should contemplate zoonotic leprosy transmission routes carefully.

Author affiliations: Universidad de las Américas, Quito, Ecuador (D. Romero-Alvarez); University of Kansas, Lawrence, Kansas, USA (D. Romero-Alvarez, A.T. Peterson); Universidad San Francisco de Quito, Quito, Ecuador (D. Garzon-Chavez); Colorado State University, Fort Collins, Colorado, USA (M. Jackson, C. Avanzi)

DOI: https://doi.org/10.3201/eid2903.221636

The Study

We assembled a database of museum armadillo tissue samples using the biodiversity information portals VertNet (http://portal.vertnet.org) and Arctos (https://arctos.database.museum/home.cfm), queried during December 2018–April 2019. Ten US museums included armadillo samples in their datasets. The samples were collected during 1974–2017 (Appendix 1 Figure 4, https://wwwnc.cdc.gov/EID/article/29/3/22-1636-App1.pdf) from 8 countries across the Americas; 68.6% (n = 109) came from the United States (Table 1; Figure 1). Each museum contributed ≈1 mm^3 of armadillo tissue (Appendix 1; Appendix 2, https://wwwnc.cdc.gov/EID/article/29/3/22-1636-App2.xlsx). The 159 samples processed corresponded to 10 armadillo species; *D. novemcinctus*, the nine-banded armadillo, was the most common (n = 122 [76.7%]). Most samples were liver tissues (n = 66 [41.5%]), followed by muscle (n = 37 [23.3%]) and spleen (n = 31 [19.5%]) (Table 1). The specimens were frozen or preserved in 10% dimethyl sulfoxide or 70%, 90%, or 95% ethanol; most were either frozen (n = 77 [48.4%]) or in 95% ethanol (n = 55 [34.6%]) (Table 1).

We processed tissues using an in-house DNA extraction method based on magnetic beads (Appendix 1). We applied standardized PCR protocols using specific primers to detect *M. leprae* and *M. lepromatosis* (*5*,*6*). For *M. leprae*, we implemented typification and subtypification as described previously (*7*). We performed quantitative real-time PCR (qPCR) on all samples for which genotyping was successful as a proxy of *M. leprae* DNA quantity with cycle threshold

(Ct) <26 as a threshold for whole-genome sequencing. We multiplexed and sequenced libraries on an Illumina NextSeq 500 instrument (https://www.illumina.com) (Appendix 1).

We found *M. leprae* in 18/159 (11.3%) samples. All positives were in *D. novemcinctus* armadillos, for prevalence in that species of 14.8% (n = 18/122). We detected positive results mainly in muscle tissue (n = 13/18 [72.2%]) and in 95% ethanol–preserved specimens (n = 13/18 [72.2%]) (Tables 1, 2). *M. lepromatosis* was not detected in the tissues examined. PCR subtyping was successful in 5/18 (27.8%) positive samples; 4 belonged to subtype 3I, as expected for armadillos from Texas, USA (*8*) (Table 2). The remaining sample was characterized only to type (3 or 4), because we found low amounts of *M. leprae* DNA (Table 2). After RLEP qPCR, 2 samples had a Ct<26 (i.e., 109 and 209) and were suitable for whole-genome sequencing. The genomes of *M. leprae* National Center for Biotechnology Information BioSample no. SAMN31421191 (https://www.ncbi.nlm.nih.gov/biosample) had coverage of 18.2× and of BioSample SAMN31421192, 4.9× (Appendix 1). Phylogenetic analysis showed that both *M. leprae* strains belonged to genotype 3I-2 (*8*,*9*). The 2 *M. leprae* genomes clustered specifically with other isolates previously identified in armadillos (i.e., I-30) and humans (i.e., NHDP-55 and NHDP-63) from the United States (Figure 2). Isolate 109 harbored 3 specific single-nucleotide polymorphisms, including 1 missense mutation in *argD* (i.e., C1691069T; Arg61Cys), encoding a probable acetylornithine aminotransferase. Sequence data are available from the National Center for Biotechnology Information Sequence Read Archive under accession no. PRJNA893376.

Conclusions

We identified *M. leprae* in *D. novemcinctus* armadillos only; prevalence was 14.8%. Positive samples were mainly detected from muscle and from ethanol-preserved specimens (Table 1). Infected armadillos were found in the United States, Paraguay, and Bolivia. *M. leprae* has not been reported in other wildlife in Paraguay or Bolivia. In our study, tissues from Paraguay were collected in 1996 and from Bolivia in 1993 (Table 2). Hansen disease is prevalent in humans in both countries (*10*); presence of infected armadillos should prompt research to explore their role as a potential zoonotic source of leprosy (*2*). In Bolivia, a previous survey of *D. novemcinctus* and *T. matacus* armadillos conducted during 1999–2001 found 0 positive animals (*2*). We found 7 *M. leprae*–negative armadillo tissues in the United States: 1 from Florida in 1974 and 6 from Texas collected during 1982–1990 (Appendix 2). No evidence for *M. leprae* was reported in Florida before 2009 (*8*). In Texas, although immunologic detection studies suggested the presence of *M. leprae* in armadillos before the 2000s, evidence was restricted to 1 area (*2*). Thus, our molecular identification of *M. leprae* in Texas armadillos from 1996, 1999, and 2000 are novel records (Table 2; Figure 1).

Table 1. Characteristics of armadillo tissues from US museum collections examined for *Mycobacterium leprae and M. lepromatosis**

Category	No. (%) animals	No. (%) positive for *M. leprae*
Species		
Dasypus novemcinctus	122 (76.7)	18 (100)
Tolypeutes matacus	20 (12.6)	0
Cabassous unicinctus	5 (3.1)	0
Chaetophractus vellerosus	3 (1.9)	0
Zaedypus pichiy	3 (1.9)	0
Chaetophractus villosus	2 (1.3)	0
Cabassous tatouay	1 (0.6)	0
Chaetophractus sp.	1 (0.6)	0
Euphractus sexcinctus	1 (0.6)	0
Priodontes maximus	1 (0.6)	0
Total	159 (100)	18 (100)
Sex		
M	72 (45.3)	4 (22.2)
F	71 (44.7)	12 (66.7)
Unknown†	16 (10.1)	0
Total	159 (100)	18 (100)
Tissues tested		
Liver	66 (41.5)	2 (11.1)
Muscle	37 (23.3)	13 (72.2)
Spleen	31 (19.5)	3 (16.7)
Unknown	16 (10.1)	0
Lysate	4 (2.5)	0
Heart and kidney	2 (1.3)	0
Kidney	2 (1.3)	0
Heart	1 (0.6)	0
Total	159 (100)	18 (100)
Preservation method		
Frozen	77 (48.4)	4 (22.2)
Ethanol 95%	55 (34.6)	13 (72.2)
Ethanol 70%	17 (10.7)	0
DMSO	9 (5.7)	1 (5.6)
Ethanol 90%	1 (0.6)	0
Total	159 (100)	18 (100)
DNA concentration, ng/μL		
Mean	19	15.63
SD	27.3	12.2
Range	0.0041–218	0.0041–43
Country of origin		
United States	109 (68.6)	16 (88.9)
Paraguay	24 (15.1)	1 (5.6)
Argentina	10 (6.3)	0
Bolivia	7(4.4)	1 (5.6)
Peru	3 (1.9)	0
Brazil	2 (1.3)	0
Unknown	2 (1.3)	0
Costa Rica	1 (0.6)	0
Panama	1 (0.6)	0
Total	159 (100)	18 (100)

*All samples tested negative for *M. lepromatosis*. DMSO, dimethyl sulfoxide.
†Unknown indicates no data were available.

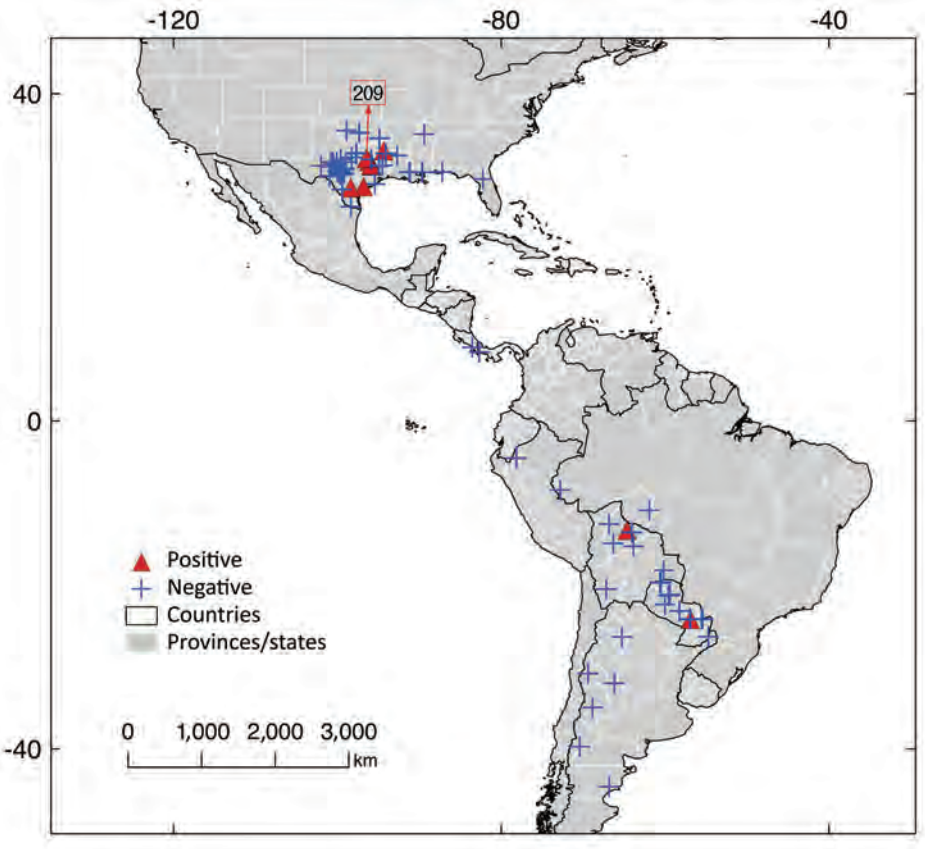

Figure 1. Geographic origin of samples analyzed in study of *Mycobacterium leprae* in armadillo tissue samples from US museums (n = 8 countries). We obtained coordinates from the tissue metadata or georeferenced them manually by using Google Earth (https://earth.google.com). Of the 2 samples suitable for whole-genome sequencing, 1, USA-am-109, lacked spatial detail from which to obtain coordinates and is not included on the map, along with 4 additional samples. The other sample that was sequenced, USA-am-209, is indicated with an arrow and the number in a red square.

M. lepromatosis has been reported in multiple countries of the Americas, including the United States, Mexico, and Colombia, but as of 2022, only in humans (*11*,*12*). Although this species has been detected in *Sciurus vulgaris* squirrels in the British Isles, broader surveillance in rodents across Europe and Mexico identified 0 positive samples (*13*). From our dataset we obtained only negative results. *M. lepromatosis* is seldom screened as a Hansen disease–causing pathogen because of lack of awareness, which has impeded understanding of its incidence. Thus, in countries endemic for Hansen disease, *M. lepromatosis*

Table 2. Characteristics of armadillo tissue samples from US museums identified as positive by standard PCR for *Mycobacterium leprae**

Voucher/tissue no.	Sample ID	Tissue type	Preservation (%)	DNA con.	Country	State	Sex	Year	Type	Subtype	Ct
YPM 16952	63	Muscle	Ethanol (95)	20	USA	Texas	F	2014	ND	ND	ND
YPM 15982	66	Muscle	Ethanol (95)	13	USA	Texas	F	2015	ND	ND	ND
YPM 15294	80	Muscle	Ethanol (95)	2.89	USA	Texas	F	2013	3	3I	34.41
YPM 16954	95	Muscle	Ethanol (95)	11	USA	Texas	M	2014	ND	ND	ND
YPM 15295	97	Muscle	Ethanol (95)	14	USA	Texas	F	2013	ND	ND	ND
YPM 15292	99	Muscle	Ethanol (95)	5.7	USA	Texas	F	2013	ND	ND	ND
YPM 15296	103	Muscle	Ethanol (95)	8.9	USA	Texas	F	2013	ND	ND	ND
YPM 15293	105	Muscle	Ethanol (95)	4.76	USA	Texas	M	2013	ND	ND	ND
YPM 14944	**109**	**Muscle**	**Ethanol (95)**	**9.3**	**USA**	**Texas**	**NA**	**2014**	**3**	**3I**	**23.15**
YPM 15315	110	Muscle	Ethanol (95)	0.0041	USA	Texas	F	2013	ND	ND	ND
YPM 15298	111	Muscle	Ethanol (95)	27	USA	Texas	F	2013	ND	ND	ND
YPM 15299	115	Muscle	Ethanol (95)	43	USA	Texas	F	2012	ND	ND	ND
UAM 46589	118	Liver	DMSO	11	Paraguay	Canindeyu	F	1996	ND	ND	ND
MSB 140243	138	Liver	Ethanol (95)	37	Bolivia	Beni	NA	1993	ND	ND	ND
TTU 75235	158	Spleen	Frozen	19	USA	Texas	F	1996	3 or 4	ND	35.12
TTU 82457	194	Muscle	Frozen	3.82	USA	Texas	M	2000	3	3I	31.58
TTU 75360	**209**	**Spleen**	**Frozen**	**20**	**USA**	**Texas**	**F**	**1996**	**3**	**3I**	**25.83**
TTU 80673	212	Spleen	Frozen	31	USA	Texas	M	1999	ND	ND	ND

*We identified a total of 18 *M. leprae*-positive samples. Bold text indicates samples suitable for whole-genome sequencing (n = 2). Samples negative for subtyping were determined unsuitable for whole-genome sequencing. Ct determined by quantitative PCR. Ct, cycle threshold; DNA con., concentration of total DNA per sample; NA, no data available; ND, not determined

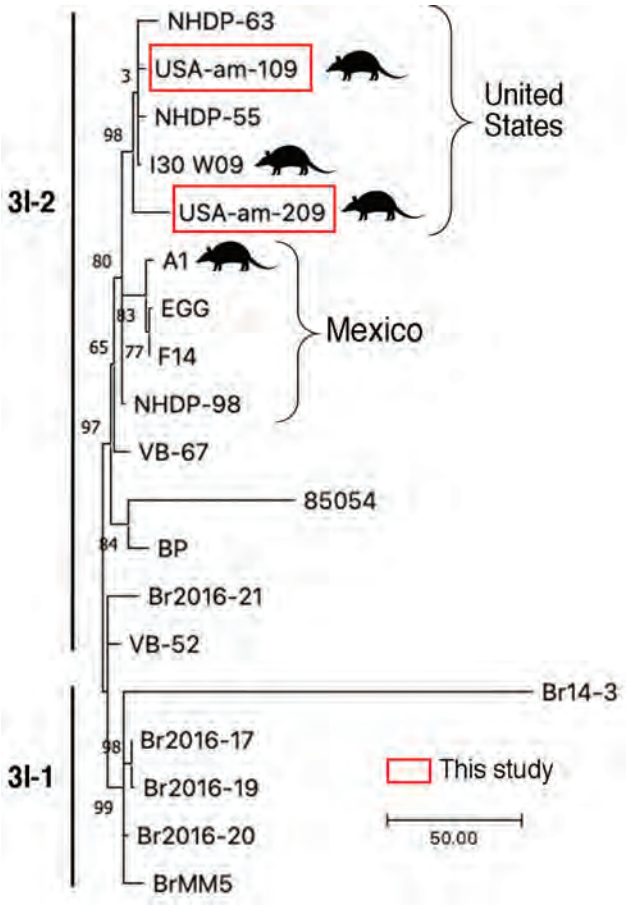

Figure 2. Comparative genomics of the *Mycobacterium leprae* sequenced this study from armadillo tissues from US museums and those from humans and armadillos from the United States and Mexico. Samples subjected to whole-genome sequencing, USA-am-109 and USA-am-209, clustered among genomes from humans and armadillos from the United States (branch 3I). The tree represents a zoom into the *M. leprae* genotypes 3I-1 and 3I-2 from a maximum-parsimony tree of 302 *M. leprae* genomes rooted with *M. lepromatosis* as outgroup. The tree was built in MEGA version 11 software (https://www.megasoftware.net). Support values were obtained by bootstrapping 500 replicates. Scale bar indicates number of nucleotide substitutions.

should be also screened systematically in humans and potential animal reservoirs.

We were able to identify *M. leprae* subtypes in 4 armadillos (Table 2) and to sequence 2 entire genomes. Those 2 strains clustered with armadillo and human isolates from the United States, all belonging to subtype 3I-2, on branch 3 of the genetic tree (Figure 2). Of interest, our isolates differed by several nonsynonymous sites from those isolated previously. Our findings corroborate that several strains of *M. leprae* are circulating in armadillo populations in the southern United States (*8*,*9*,*14*). As predicted (*15*), our data also confirm that the strains circulating in armadillos today are close to those infecting animals ≥30 years ago, highlighting the promise of using preserved animal tissues to study epizootic dynamics of leprosy and other diseases.

Information on pathogen biodiversity in wildlife is much needed. We suggest that specimens in natural museums can play a role in infectious disease monitoring; our study relied on the global museum initiative and the large digital repositories of relevant specimen data in the United States. Protocols for using museum repositories for infectious disease research are still in development (*4*); parameters to optimal pathogen identification should be explored for *M. leprae* and other pathogens. We recognize that no single best way to study the diversity of pathogens exists; any approach should consider the specific nuances of each zoonotic system.

The reagent genomic DNA from *Mycobacterium leprae*, strain Thai-53, NR-19352 was obtained through BEI Resources, US National Institute of Allergy and Infectious Diseases, National Institutes of Health. Genomic DNA for *Mycobacterium lepromatosis* was provided by Ramanuj Lahiri (National Hansen's Disease Program, Baton Rouge, Louisiana, USA).

C.A. and M.J. are supported by the Fondation Raoul Follereau, the Heiser Program of the New York Community Trust for Research in Leprosy (grant no. P21-000127), the European Union's Horizon 2020 Research and Innovation Program (C.A. by Marie Sklodowska-Curie grant no. 845479).

About the Author

Dr. Romero-Alvarez is an MD and PhD candidate at the Biodiversity Institute and the Department of Ecology & Evolutionary Biology at the University of Kansas and is affiliated with the Universidad de las Américas, Quito, Ecuador. His research is focused on the eco-epidemiology and geographic distribution of infectious diseases.

References

1. Singh P, Benjak A, Schuenemann VJ, Herbig A, Avanzi C, Busso P, et al. Insight into the evolution and origin of leprosy bacilli from the genome sequence of *Mycobacterium lepromatosis*. Proc Natl Acad Sci U S A. 2015;112:4459–64. https://doi.org/10.1073/pnas.1421504112
2. Ploemacher T, Faber WR, Menke H, Rutten V, Pieters T. Reservoirs and transmission routes of leprosy; a systematic review. PLoS Negl Trop Dis. 2020;14:e0008276. https://doi.org/10.1371/journal.pntd.0008276
3. Avanzi C, del Pozo J, Benjak A, Stevenson K, Simpson VR, Busso P, et al. Red squirrels in the British Isles are infected with leprosy bacilli. Science. 2016;354:744–7.
4. Colella JP, Bates J, Burneo SF, Camacho MA, Carrion Bonilla C, Constable I, et al. Leveraging natural history biorepositories as a global, decentralized,

pathogen surveillance network. PLoS Pathog. 2021; 17:e1009583. https://doi.org/10.1371/journal.ppat.1009583
5. Sharma R, Singh P, McCoy RC, Lenz SM, Donovan K, Ochoa MT, et al. Isolation of *Mycobacterium lepromatosis* and development of molecular diagnostic assays to distinguish *Mycobacterium leprae* and *M. lepromatosis*. Clin Infect Dis. 2020;71:e262–9. https://doi.org/10.1093/cid/ciz1121
6. Tió-Coma M, Wijnands T, Pierneef L, Schilling AK, Alam K, Roy JC, et al. Detection of *Mycobacterium leprae* DNA in soil: multiple needles in the haystack. Sci Rep. 2019;9:3165. https://doi.org/10.1038/s41598-019-39746-6
7. Monot M, Honoré N, Garnier T, Zidane N, Sherafi D, Paniz-Mondolfi A, et al. Comparative genomic and phylogeographic analysis of *Mycobacterium leprae*. Nat Genet. 2009;41:1282–9. https://doi.org/10.1038/ng.477
8. Sharma R, Singh P, Loughry WJ, Lockhart JM, Inman WB, Duthie MS, et al. Zoonotic leprosy in the southeastern United States. Emerg Infect Dis. 2015;21:2127–34. https://doi.org/10.3201/eid2112.150501
9. Vera-Cabrera L, Ramos-Cavazos CJ, Youssef NA, Pearce CM, Molina-Torres CA, Avalos-Ramirez R, et al. *Mycobacterium leprae* infection in a wild nine-banded armadillo, Nuevo León, Mexico. Emerg Infect Dis. 2022;28:747–9. https://doi.org/10.3201/eid2803.211295
10. Schaub R, Avanzi C, Singh P, Paniz-Mondolfi A, Cardona-Castro N, Legua P, et al. Leprosy transmission in Amazonian countries: current status and future trends. Curr Trop Med Rep. 2020;7:79–91. https://doi.org/10.1007/s40475-020-00206-1
11. Cardona-Castro N, Escobar-Builes MV, Serrano-Coll H, Adams LB, Lahiri R. *Mycobacterium lepromatosis* as cause of leprosy, Colombia. Emerg Infect Dis. 2022;28:1067–8. https://doi.org/10.3201/eid2805.212015
12. Deps P, Collin SM. *Mycobacterium lepromatosis* as a second agent of Hansen's disease. Front Microbiol. 2021;12:698588. https://doi.org/10.3389/fmicb.2021.698588
13. Schilling AK, Avanzi C, Ulrich RG, Busso P, Pisanu B, Ferrari N, et al. British red squirrels remain the only known wild rodent host for leprosy bacilli. Front Vet Sci. 2019;6:8. https://doi.org/10.3389/fvets.2019.00008
14. Truman RW, Andrews PK, Robbins NY, Adams LB, Krahenbuhl JL, Gillis TP. Enumeration of *Mycobacterium leprae* using real-time PCR. PLoS Negl Trop Dis. 2008;2:e328. https://doi.org/10.1371/journal.pntd.0000328
15. Schuenemann VJ, Singh P, Mendum TA, Krause-Kyora B, Jäger G, Bos KI, et al. Genome-wide comparison of medieval and modern *Mycobacterium leprae*. Science. 2013;341:179–83. https://doi.org/10.1126/science.1238286

Address for correspondence: Daniel Romero-Alvarez, Biodiversity Institute and Department of Ecology & Evolutionary Biology, University of Kansas, 1345 Jayhawk Blvd, Lawrence, KS 66044, USA; email: daromero88@gmail.com

etymologia revisited

Originally published in January 2021

Petri Dish
[pe'tre 'dish]

The Petri dish is named after the German inventor and bacteriologist Julius Richard Petri (1852–1921). In 1887, as an assistant to fellow German physician and pioneering microbiologist Robert Koch (1843–1910), Petri published a paper titled "A minor modification of the plating technique of Koch." This seemingly modest improvement (a slightly larger glass lid), Petri explained, reduced contamination from airborne germs in comparison with Koch's bell jar.

Sources:

1 Central Sheet for Bacteriology and Parasite Science [in German]. Biodiversity Heritage Library. Volume 1, 1887 [cited 2020 Aug 25]. https://www.biodiversitylibrary.org/item/210666#page/313/mode/1up
2. Petri JR. A minor modification of the plating technique of Koch [in German]. Cent für Bacteriol und Parasitenkd. 1887;1:279–80.
3. Shama G. The "Petri" dish: a case of simultaneous invention in bacteriology. Endeavour. 2019;43:11–6. DOIExternal
4. The big story: the Petri dish. The Biomedical Scientist. Institute of Biomedical Science [cited 2020 Aug 25]. https://thebiomedicalscientist.net/science/big-story-petri-dish

https//wwwnc.cdc.gov/eid/article/27/1/et-2701_article

New Detection of Locally Acquired Japanese Encephalitis Virus Using Clinical Metagenomics, New South Wales, Australia

Joel Maamary, Susan Maddocks, Yael Barnett, Stephen Wong, Michael Rodriguez, Linda Hueston, Neisha Jeoffreys, John-Sebastian Eden, Dominic E. Dwyer, Tony Floyd, Marshall Plit, Jen Kok, Bruce Brew[1]

In the context of an emerging Japanese encephalitis outbreak within Australia, we describe a novel locally acquired case in New South Wales. A man in his 70s had rapidly progressive, fatal meningoencephalitis, diagnosed as caused by Japanese encephalitis virus by RNA-based metagenomic next-generation sequencing performed on postmortem brain tissue.

Japanese encephalitis virus (JEV) is a single-stranded, positive-sense, RNA flavivirus endemic to tropical regions of South and Southeast Asia and is the most common cause of vaccine-preventable encephalitis in the Asia-Pacific region (*1*). As for Murray Valley encephalitis virus and Kunjin virus, 2 other flaviviruses endemic in Australia, most JEV infections are asymptomatic, but severe meningoencephalitis can occur in up to 1% (*2*) of cases. Although incidence varies geographically, ≈100,000 cases are estimated annually worldwide, resulting in 709,000 disability-adjusted life years through severe neurologic disease complications (*3*). Nonspecific febrile illness is the typical clinical manifestation, but in severe cases, rapidly progressive neurologic deterioration, reduced consciousness, movement disorders, seizures, and coma can occur. Neuroinvasive JEV mortality can reach 30%, and major neurologic disability approaches 50% (*4*).

Culex tritaeniorhynchus mosquitoes are the primary vector for JEV transmission in Asia. Although previously thought absent from Australia, this species was recently detected in the Darwin and Katherine regions of the Northern Territory (*5*). The *Cx. annulirostris* mosquito, which is the primary vector for Flaviviridae transmission in Australia, has also been implicated in JEV transmission globally. JEV has previously been isolated from subspecies of *Aedes* and *Anopheles* mosquitoes, both present in Australia. Wading and water birds are the virus's natural host; feral and domestic pigs are particularly susceptible. Transmission between pigs occurs through mucosal and microdroplet contacts, enabling disease amplification and acting as a protective reservoir for the virus. However, humans are dead-end hosts, probably because of low levels of or short-lived viremia (*6*).

In Australia, sporadic human cases and virus isolation in pigs and mosquitoes have all been confined to the tropical north of the country (*7*,*8*). Since February 2022, however, JEV has been found in 4 states in Australia (New South Wales [NSW], Victoria, Queensland, and South Australia), thousands of kilometers from previously detected cases. We describe a locally acquired case of fatal JEV meningoencephalitis in a NSW resident in January 2022. The infection was diagnosed by RNA-based metagenomic next-generation sequencing (RNA-mNGS) performed on postmortem brain tissue.

Author affiliations: St Vincent's Health Australia, Sydney, New South Wales, Australia (J. Maamary, Y. Barnett, M. Plit, B. Brew); Centre for Infectious Diseases and Microbiology Laboratory Services, NSW Health Pathology-Institute of Clinical Pathology and Medical Research, Westmead, New South Wales, Australia (S. Maddocks, L. Hueston, N. Jeoffreys, D.E. Dwyer, J. Kok); Sydpath, St Vincent's Health Network, Sydney (S. Wong, M. Rodriguez); University of Sydney Institute for Infectious Diseases, Westmead Institute for Medical Research, Westmead (J.-S. Eden); Griffith Base Hospital, Griffith, New South Wales, Australia (T. Floyd); University of New South Wales, Sydney (M. Plit, B. Brew); St Vincent's Centre for Applied Medical Research, Sydney (B. Brew); The University of Notre Dame Australia, Sydney (B. Brew)

DOI: https://doi.org/10.3201/eid2903.220632

[1]All authors contributed equally to this article.

The Case

A man in his 70s sought care at a rural hospital after 3 days of fever and progressive confusion. Results of septic screen, chest radiography and computed tomography brain scan were unremarkable. Despite empiric intravenous flucloxacillin and gentamicin, the patient experienced progressive neurologic deterioration and required intubation. Cerebrospinal fluid (CSF) testing revealed a lymphocyte predominant pleocytosis of 126 × 10^6 cells/L (50 × 10^6 cells/L polymorphs and 76 × 10^6 cells/L mononuclear cells) and elevated protein of 0.96 g/L (reference range 0.15–0.45). No organisms were isolated. Results of CSF nucleic acid testing (NAT) were negative for *Neisseria meningitidis*, *Streptococcus pneumoniae*, herpes simplex virus types 1 and 2, enterovirus, varicella zoster virus, parechovirus, cytomegalovirus, and Epstein-Barr virus. CSF and serum samples tested negative for antineuronal antibodies (PCA-1/PCA-2/ANNA-1/ANNA-2/Ma1/Ma2/Amphiphysin/SOX-1/CRMP-5/Tr) and limbic encephalitis panel (anti-NMDA/CASPR-2/LGI-1/GABA-B/DPPX/IgLON5/AMPA-1/AMPA-2). Empiric treatment was changed to intravenous ceftriaxone, benzylpenicillin, and aciclovir. Magnetic resonance brain imaging showed an equivocal T2/FLAIR hyperintensity in the dorsal midbrain and pons with sparing of both thalami and basal ganglia (Figure 1). Electroencephalogram demonstrated encephalopathic features. Repeat CSF examination on day 10 demonstrated lymphocytic pleocytosis (57 × 10^6 cells/L mononuclear cells), and results of repeat culture, NAT, and antineuronal/limbic encephalitis panels were negative. CSF protein remained elevated at 0.86 g/L.

Despite supportive management and broadening of antimicrobial therapy with meropenem, the patient showed no neurologic improvement and, after discussion with his family, ventilator support was withdrawn; he died 22 days after symptom onset. In the absence of a definitive diagnosis, a noncoronial limited brain autopsy was performed. Twenty-four brain tissue samples were sent for neuropathologic examination; 10 were sent for RNA-mNGS analysis (*9*). Initial sequencing of the right anterior hippocampus, amygdala, and left striatum returned only host-derived sequences. Additional pooled samples of libraries of the left hippocampus, left upper midbrain, pons, medulla, right cerebellum, and dentate nucleus identified 4 JEV genotype IV sequences. We detected JEV RNA by real-time reverse transcription PCR targeting the JEV NS1 region (*10*) in all 10 samples (cycle threshold values 34.3–38.3). Neuropathology showed widespread meningoencephalitis, more marked in gray matter and most severe in the thalamus, hippocampus, and substantia nigra, with perivascular and interstitial lymphocytes (predominantly CD8+ T-cells), macrophages/activated microglia, and loose microglial nodules (Figure 2). Retrospective testing of stored serum samples demonstrated JEV-specific IgM and IgG seroconversion. JEV-specific IgM, but not RNA, was detected in CSF. Further history revealed the patient had recently visited a neighboring town containing numerous domestic pig farms, where JEV was detected and subsequently confirmed.

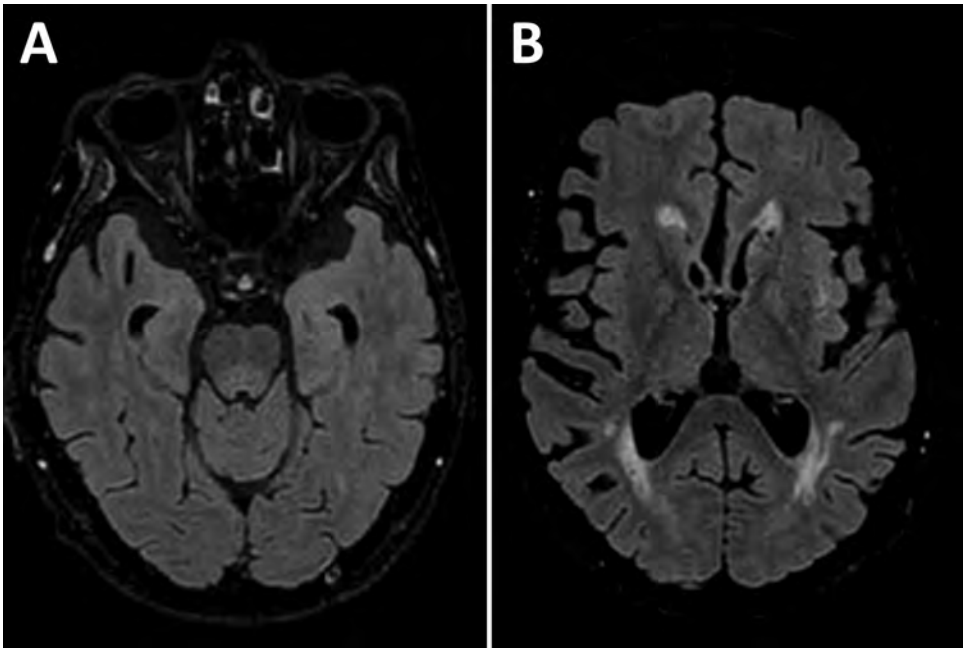

Figure 1. Axial FLAIR magnetic resonance imaging brain sequence in a patient with locally acquired Japanese encephalitis virus detected using clinical metagenomics, New South Wales, Australia. A) Equivocal hyperintensity in the dorsal midbrain and pons; B) sparing of the thalamus and basal ganglia.

Discussion

JEV was detected for the first time across southeastern Australia in 2022 and, as of January 5, 2023, a total of 45 human cases of JEV had been notified in Australia since January 1, 2021 (of which 14 were from NSW), including 7 deaths (*11*). The described case was undiagnosed premortem; JEV was not known to be present in NSW at the time of the patient's admission. RNA-mNGS enabled a definitive diagnosis postmortem through the detection of JEV-specific sequences in brain tissue, confirmed by NAT and seroconversion on retrospective serum testing. The diagnosis was further corroborated by the concurrent detection of JEV in piggeries across 4 Australia states. Similar to other reported cases of infection with fatal genotype IV (*12*), this case evidenced profound neurologic deterioration 3–4 days after symptom onset with CSF lymphocyte predominant pleocytosis and JEV-specific IgM in CSF. However, unlike other case reports, some typical markers of JEV, such as T2/FLAIR hyperintense signal change in both thalami, basal ganglia, and substantia nigra, occasionally associated with hemorrhage, were not present in this case. The lack of JEV RNA detected in CSF is not uncommon because of the relatively brief viremia in humans, although prolonged viruria of 26 days and viremia of 28 days have been reported (*13*). JEV is typically diagnosed by the detection of JEV-specific IgM in CSF or through JEV-specific IgG seroconversion in serum samples, but false-positive results of serologic testing for JEV might occur because of cross-reactivity to other flaviviruses.

This case highlights the diagnostic value of pathogen-agnostic mNGS for pathogens not identified through traditional testing, known but unexpected pathogens, or novel pathogens. Recent public health alerts should prompt clinicians to interrogate a patient's history for animal or mosquito exposures and request specific JEV or other flavivirus (such as Murray Valley encephalitis virus and Kunjin virus) testing accordingly when treating undifferentiated meningoencephalitis. The case also demonstrates the new incursion of a pathogen across a broad, previously nonendemic geographic area and into a largely nonimmune population. The origins remain unclear but, given the widespread geographic area of infected piggeries and human cases, JEV has likely been circulating undetected in wild birds, mosquitoes, and pigs for some time. Whole-genome sequencing has demonstrated that this outbreak is caused by genotype IV, previously thought to be restricted to Indonesia, Papua New Guinea, and the Tiwi Islands.

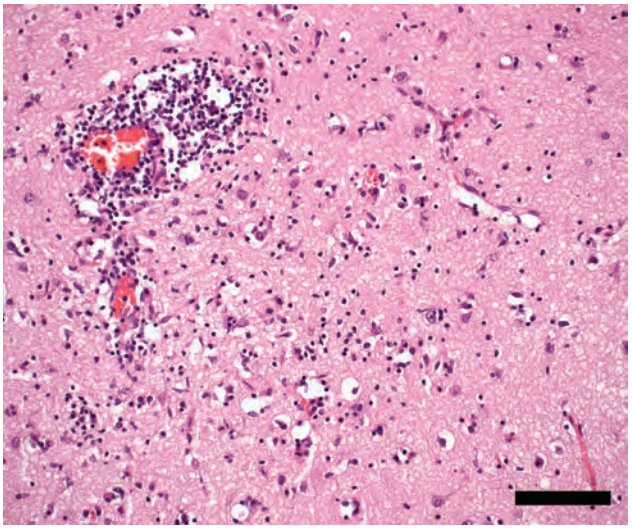

Figure 2. Temporal neocortex showing encephalitis with perivascular and interstitial lymphocytes, macrophages/activated microglia, and neuronophagia in patient with locally acquired Japanese encephalitis virus detected using clinical metagenomics, New South Wales, Australia. Hematoxylin and eosin stain; scale bar indicates 100 μm.

Changes in vector distribution have been associated with changes in climate, destruction of natural habitats altering bird migratory patterns, agricultural practices, and periurban growth (*14*). Floodwater-mediated or windblown movement of JEV-infected mosquito vectors into new regions has been previously reported in Australia (*15*). The movement of other infected vertebrates could also be implicated. Mosquito, human and animal surveillance in areas where JEV is detected will inform the extent of JEV incursion in mainland Australia and guide vector control, vaccination efforts, and research priorities, including vector competence studies to limit further disease and vector spread.

About the Author

Dr. Maamary is a movement disorders fellow at the St. Vincent's Health Network, Sydney, Australia. He is pursuing a PhD at the University of New South Wales and has an interest in translational research, novel therapeutics, and neural pathway mapping.

References

1. Kwak BO, Hong YJ, Kim DH. Changes in age-specific seroprevalence of Japanese encephalitis virus and impact of Japanese encephalitis vaccine in Korea. Clin Exp Pediatr. 2022;65:108–14. https://doi.org/10.3345/cep.2020.01984
2. Southam CM. Serological studies of encephalitis in Japan. II. Inapparent infections by Japanese B encephalitis virus. J Infect Dis. 1956;99:163–9. https://doi.org/10.1093/infdis/99.2.163

3. Mathers CD, Ezzati M, Lopez AD. Measuring the burden of neglected tropical diseases: the global burden of disease framework. PLoS Negl Trop Dis. 2007;1:e114. https://doi.org/10.1371/journal.pntd.0000114
4. Solomon T, Dung NM, Kneen R, Gainsborough M, Vaughn DW, Khanh VT. Japanese encephalitis. J Neurol Neurosurg Psychiatry. 2000;68:405–15. https://doi.org/10.1136/jnnp.68.4.405
5. Lessard BD, Kurucz N, Rodriguez J, Carter J, Hardy CM. Detection of the Japanese encephalitis vector mosquito *Culex tritaeniorhynchus* in Australia using molecular diagnostics and morphology. Parasit Vectors. 2021;14:411. https://doi.org/10.1186/s13071-021-04911-2
6. Filgueira L, Lannes N. Review of emerging Japanese encephalitis virus: new aspects and concepts about entry into the brain and inter-cellular spreading. Pathogens. 2019;8:111. https://doi.org/10.3390/pathogens8030111
7. Pyke AT, Williams DT, Nisbet DJ, van den Hurk AF, Taylor CT, Johansen CA, et al. The appearance of a second genotype of Japanese encephalitis virus in the Australasian region. Am J Trop Med Hyg. 2001;65:747–53. https://doi.org/10.4269/ajtmh.2001.65.747
8. Van Den Hurk AF, Montgomery BL, Northill JA, Smith IL, Zborowski P, Ritchie SA, et al. Short report: the first isolation of Japanese encephalitis virus from mosquitoes collected from mainland Australia. Am J Trop Med Hyg. 2006;75:21–5. https://doi.org/10.4269/ajtmh.2006.75.21
9. Annand EJ, Horsburgh BA, Xu K, Reid PA, Poole B, de Kantzow MC, et al. Novel Hendra virus variant detected by sentinel surveillance of horses in Australia. Emerg Infect Dis. 2022;28:693–704. https://doi.org/10.3201/eid2803.211245
10. Shao N, Li F, Nie K, Fu SH, Zhang WJ, He Y, et al. TaqMan real-time RT-PCR assay for detecting and differentiating Japanese encephalitis virus. Biomed Environ Sci. 2018;31:208–14. https://doi.org/10.3967/bes2018.026
11. Australian Government Department of Health and Aged Care. Japanese encephalitis virus (JEV) [cited 2023 Jan 24]. https://www.health.gov.au/health-alerts/japanese-encephalitis-virus-jev/japanese-encephalitis-virus-jev
12. Pyke AT, Choong K, Moore F, Schlebusch S, Taylor C, Hewitson G, et al. A case of Japanese encephalitis with a fatal outcome in an Australian who traveled from Bali in 2019. Trop Med Infect Dis. 2020;5:133. https://doi.org/10.3390/tropicalmed5030133
13. Huang GKL, Tio SY, Caly L, Nicholson S, Thevarajan I, Papadakis G, et al. Prolonged detection of Japanese encephalitis virus in urine and whole blood in a returned short-term traveler. Open Forum Infect Dis. 2017;4:ofx203. https://doi.org/10.1093/ofid/ofx203
14. Connor B, Bunn WB. The changing epidemiology of Japanese encephalitis and new data: the implications for new recommendations for Japanese encephalitis vaccine. Trop Dis Travel Med Vaccines. 2017;3:14. https://doi.org/10.1186/s40794-017-0057-x
15. Ritchie SA, Rochester W. Wind-blown mosquitoes and introduction of Japanese encephalitis into Australia. Emerg Infect Dis. 2001;7:900–3. https://doi.org/10.3201/eid0705.017524

Address for correspondence: Joel Maamary, Department of Neurology, St Vincent's Health Network Sydney, 390 Victoria St, Darlinghurst, NSW 2010, Australia; email: joel.maamary@svha.org.au

Reemergence of Lymphocytic Choriomeningitis Mammarenavirus, Germany

Calvin Mehl, Claudia Wylezich, Christina Geiger, Nicole Schauerte, Kerstin Mätz-Rensing, Anne Nesseler, Dirk Höper, Miriam Linnenbrink, Martin Beer, Gerald Heckel, Rainer G. Ulrich

Lymphocytic choriomeningitis mammarenavirus (LCMV) is a globally distributed zoonotic pathogen transmitted by house mice (*Mus musculus*). We report the reemergence of LCMV (lineages I and II) in wild house mice (*Mus musculus domesticus*) and LCMV lineage I in a diseased golden lion tamarin (*Leontopithecus rosalia*) from a zoo in Germany.

Lymphocytic choriomeningitis mammarenavirus (LCMV) is an enveloped virus with a bisegmented genome of single-stranded, ambisense RNA (*1*). The small (S) segment of ≈3,400 nt encodes structural components, including the glycoprotein (GP) and nucleocapsid protein (NP), whereas the large (L) segment of ≈7,200 nt encodes the L (RNA polymerase) and Z proteins (*1*,*2*). First identified in St. Louis, Missouri, USA, in 1933 (*3*), LCMV is a zoonotic pathogen transmitted through contact with excreta and secretions of infected house mice (*Mus musculus*), the reservoir host (*4*). More recently, LCMV RNA was also detected in wild wood mice (*Apodemus sylvaticus*) from Spain (*5*).

In humans, LCMV can cause symptoms ranging from influenza-like illness to meningitis and encephalitis (*6*). Infection during pregnancy may lead to neurologic and developmental problems in infants (*7*). New World primates (family Callitrichidae) are also susceptible to infection, resulting in callitrichid hepatitis, a lethal infection exhibiting histopathologic lesions in the brain, liver, and lymphoid tissues (*8*).

During 1968–1973, a total of 48 human cases of LCMV infection were reported in Germany, many of which originated from pet hamsters (*Mesocricetus auratus*) (*6*,*7*,*9*). Thereafter, 6 prenatal or postnatal infections were reported during 1991–1997 in Germany, most of which were believed to have originated from pet rodents (*10*). During 1999–2000, a total of 4 callitrichid hepatitis cases were reported in Germany: 1 in a Goeldi's monkey (*Callimico goeldii*) and 3 in pygmy marmosets (*Cebuella pygmaea*) (*8*).

Very little is known on the distribution and prevalence of LCMV in mice from Germany, the most comprehensive study being from Ackermann et al. (*11*) in 1964, which only surveyed the western federal states of Germany (former West Germany). That study found the highest prevalence among house mice in North Rhine–Westphalia, in the western part of West Germany. Most recently, Fornůsková et al. (*12*) screened nearly 800 mice from the Czech Republic and eastern Germany sampled during 2008–2019 but detected LCMV-positive mice only in the Czech Republic.

Four lineages of LCMV are recognized (I–IV). Lineages I and II are the most common sequences worldwide. Lineage III consists of a single strain from Georgia, USA. Only S-segment sequences exist for lineage IV, entirely comprising sequences obtained from wood mice (*Apodemus sylvaticus*) from Spain. Fornůsková et al. (*12*) recently proposed that LCMV lineages I and II are host-specific, whereby lineage I is harbored by the house mouse subspecies *M. m. domesticus* and lineage II by the subspecies *M. m. musculus*. This hypothesis is of particular importance in Europe because *M. m. domesticus* and *M. m. musculus* meet

Author affiliations: Friedrich-Loeffler-Institut, Greifswald–Insel Riems, Germany (C. Mehl, C. Wylezich, D. Höper, M. Beer, R.G. Ulrich); German Center for Infection Research, Hamburg–Lübeck–Borstel–Riems, Germany (C. Mehl, R.G. Ulrich); Zoo Frankfurt, Frankfurt, Germany (C. Geiger, N. Schauerte); German Primate Center, Leibniz Institute for Primate Research, Göttingen, Germany (K. Mätz-Rensing); Landeslabor Hessen, Giessen, Germany (A. Nesseler); Max Planck Institute for Evolutionary Biology, Plön, Germany (M. Linnenbrink); University of Bern, Institute of Ecology and Evolution, Bern, Switzerland (G. Heckel)

DOI: https://doi.org/10.3201/eid2903.221822

in the house mouse hybrid zone, a ≈2,500-km-long stretch from Scandinavia to the Black Sea. The hybrid zone acts as a barrier to gene flow and the spread of pathogens between the subspecies (*12*,*13*), and, as a consequence, *M. m. domesticus* populations in Germany would be expected to harbor only lineage I.

Although house mice are strongly associated with human settlements, LCMV surveillance in wild mice in Europe is lacking. This study examines the re-emergence of LCMV in a golden lion tamarin (*Leontopithecus rosalia*; family Callitrichidae) and wild house mice (*M. m. domesticus*) from a zoo in Germany.

The Study

In late 2021, an adult golden lion tamarin from a zoo in western Germany died (Appendix, https://ww-

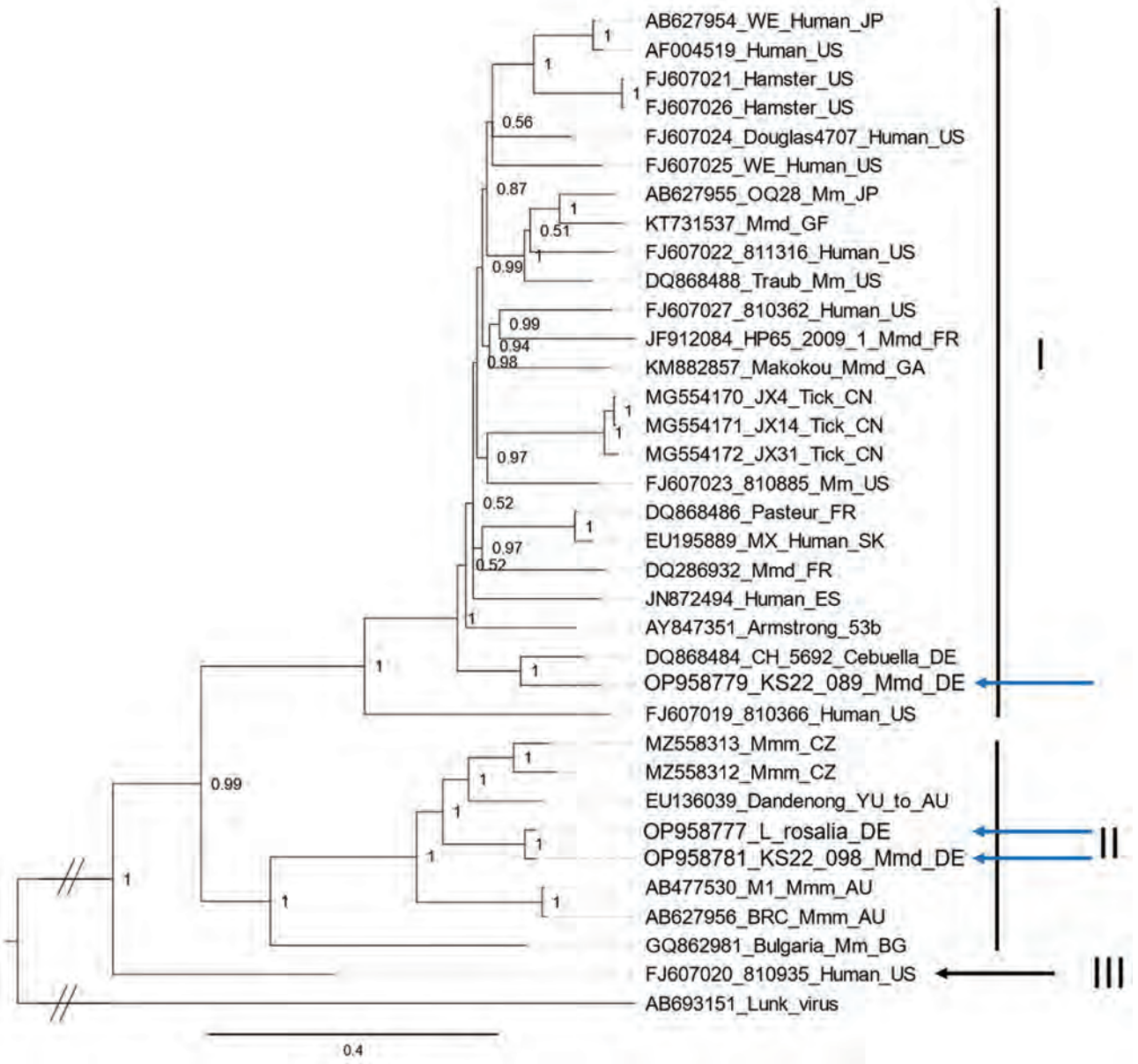

Figure. Phylogeny of the L protein encoding nucleotide sequences of lymphocytic choriomeningitis virus (LCMV) identified in Germany (blue arrows) and reference sequences, constructed by using Bayesian inference. Lunk virus from *Mus minutoides* mice was used as an outgroup. Sequence names are comprised of the GenBank accession number, strain name, host species and country of origin (wherever known). Countries are represented by their International Organization for Standardization code (AU, Australia; BG, Bulgaria; CN, China; DE, Germany; ES, Spain; FR, France; GA, Gabon; GF, French Guiana; JP, Japan; SK, Slovakia; US, USA; YU, former Yugoslavia). Roman numerals (I–IV) represent the different LCMV lineages defined according to Albariño et al. (*2*); WE and Armstrong refer to laboratory strains of LCMV. Mm, *Mus musculus*; Mmm, *Mus musculus musculus*; Mmd, *Mus musculus domesticus.*

wnc.cdc.gov/EID/article/29/3/22-1822-App1.pdf). On the basis of the symptoms and an initial diagnosis by the Hessian State Laboratory (Landeslabor Hessen, Giessen, Germany), we conducted further screening for LCMV. The Hessian State Laboratory and the zoo sent tissue samples from the golden lion tamarin and wild mice from the zoo (taken in 2009, 2021, and 2022) to the Friedrich-Loeffler-Institut (Greifswald–Insel Riems, Germany) for molecular and epidemiologic investigations. We extracted and screened nucleic acids for LCMV using conventional reverse transcription PCR (*14*). We detected LCMV RNA in the brain of the golden lion tamarin and in the kidneys of 55% of wild house mice (*M. m. domesticus*) from 2021 and 2022 (n = 53) but not in any of the house mice from 2009 (n = 82). On the basis of ≈340 nt sequences from the L segment of the virus (GenBank accession nos. OP938541–68), we selected 2 mice with the most dissimilar LCMV sequences and, together with brain tissue from the diseased golden lion tamarin, used them for high-throughput sequencing of complete genomes (GenBank accession nos. OP958777–82) (Appendix).

We used the new complete coding-region sequences (L, GP, and NP) together with all published LCMV genomes to reconstruct phylogenetic trees using the general time reversible substitution model with invariable sites and gamma distribution (MrBayes 3.2.7, https://nbisweden.github.io/MrBayes) (*15*). LCMV sequences of the full coding regions of the L, NP, and GP proteins were almost identical between the golden lion tamarin and 1 of the mice, forming a monophyletic clade within LCMV lineage II (Figure; Appendix Figure). The sequences obtained from the other mouse fell within lineage I (Figure; Appendix Figure). According to the L segment sequences (≈340 nt) obtained from the remaining 27 LCMV-positive mice, both lineages were nearly equally represented in the zoo population (lineage I for 16 mice, lineage II for 11 mice).

We obtained sequences from the mitochondrial DNA d-loop of all LCMV-positive mice and several LCMV-negative mice from 2009 (n = 32), 2021 (n = 12), and 2022 (n = 41). All those sequences identified exclusively the house mouse subspecies *M. m. domesticus* (data not shown).

Conclusions

The high similarity between LCMV lineage II in a golden lion tamarin and a wild house mouse indicates that the virus was passed between wild and captive animals in the zoo. The large number of LCMV lineage I and II strains in the wild house mouse population at this site suggests either an outbreak after recent introduction from 2 different sources or long-term persistence in the local house mouse population but with very low prevalence in 2009.

Despite considerable effort by researchers to detect LCMV in Germany, the virus remains mostly elusive. Although the route through which LCMV entered the zoo is not known, this event most likely occurred after 2009. The virus may have been brought in through naturally occurring wild animals in the region (e.g., wild house mice) or, although unlikely, through infected zoo animals.

We provide evidence for LCMV lineage II in Germany within an area naturally occupied only by the *M. m. domesticus* subspecies of house mice. The occurrence of both LCMV lineages I and II in *M. m. domesticus* mice does not support the subspecies host specificity proposed by Fornůsková et al. (*1*). Further evaluation of LCMV association with house mouse subspecies in Germany and other parts of the world will help clarify potential expanded risk to animal and human health.

Acknowledgments

We thank Hartmut Egdmann and zookeepers for collecting the rodents; Patrick Schuhmacher, Dörte Kaufmann, Edyta Janik-Karpińska, Viola Haring, Stephan Drewes, Maria Justiniano Suarez, and Marieke de Cock for help with dissections; and Lukas Wessler, Patrick Zitzow, and Florian Schröder for technical assistance.

The investigations were funded through German Center for Infection Research, Thematic Translational Unit "Emerging Infections" (grant no. 01.808_00).

About the Author

Mr. Mehl is a doctoral candidate at the Friedrich-Loeffler-Institut in Greifswald–Insel Riems, Germany. His research interests include small-mammal ecology, microbiome diversity, and ecotoxicology, and how these influence disease ecologies.

References

1. Meyer BJ. Arenaviruses: Genomic RNAs, transcription, and replication. In: Oldstone MBA, editor. Arenaviruses I. Berlin: Springer; 2002. p. 139–57.
2. Albariño CG, Palacios G, Khristova ML, Erickson BR, Carroll SA, Comer JA, et al. High diversity and ancient common ancestry of lymphocytic choriomeningitis virus. Emerg Infect Dis. 2010;16:1093–100. https://doi.org/10.3201/eid1607.091902
3. Armstrong C, Lillie RD. Experimental lymphocytic choriomeningitis of monkeys and mice produced by a virus

encountered in studies of the 1933 St. Louis encephalitis epidemic. Public Health Reports (1896–1970). 1934;49(35):1019–27.
4. Goldwater PN. A mouse zoonotic virus (LCMV): a possible candidate in the causation of SIDS. Med Hypotheses. 2021;158:110735. https://doi.org/10.1016/j.mehy.2021.110735
5. Ledesma J, Fedele CG, Carro F, Lledó L, Sánchez-Seco MP, Tenorio A, et al. Independent lineage of lymphocytic choriomeningitis virus in wood mice (*Apodemus sylvaticus*), Spain. Emerg Infect Dis. 2009;15:1677–80. https://doi.org/10.3201/eid1510.090563
6. Ackermann R, Stille W, Blumenthal W, Helm EB, Keller K, Baldus O. Syrian hamsters as vectors of lymphocytic choriomeningitis [in German]. Dtsch Med Wochenschr. 1972;97:1725–31. https://doi.org/10.1055/s-0028-1107638
7. Ackermann R, Körver G, Turss R, Wönne R, Hochgesand P. Prenatal infection with the virus of lymphocytic choriomeningitis: report of two cases [in German]. Dtsch Med Wochenschr. 1974;99:629–32. https://doi.org/10.1055/s-0028-1107814
8. Asper M, Hofmann P, Osmann C, Funk J, Metzger C, Bruns M, et al. First outbreak of callitrichid hepatitis in Germany: genetic characterization of the causative lymphocytic choriomeningitis virus strains. Virology. 2001;284:203–13. https://doi.org/10.1006/viro.2001.0909
9. Ackermann R, Stammler A, Armbruster B. Isolation of the lymphocytic choriomeningitis virus from curettage material after contact of the pregnant woman with a Syrian gold hamster (*Mesocricetus auratus*) [in German]. Infection. 1975;3:47–9. https://doi.org/10.1007/BF01641281
10. Enders G, Varho-Göbel M, Löhler J, Terletskaia-Ladwig E, Eggers M. Congenital lymphocytic choriomeningitis virus infection: an underdiagnosed disease. Pediatr Infect Dis J. 1999;18:652–5. https://doi.org/10.1097/00006454-199907000-00020
11. Ackermann R, Bloedhorn H, Küpper B, Winkens I, Scheid W. Spread of the lymphocytic choriomeningitis virus among West German mice [in German]. Zentralbl Bakteriol Orig. 1964;194:407–30.
12. Fornůsková A, Hiadlovská Z, Macholán M, Piálek J, de Bellocq JG. New perspective on the geographic distribution and evolution of lymphocytic choriomeningitis virus, central Europe. Emerg Infect Dis. 2021;27:2638–47. https://doi.org/10.3201/eid2710.210224
13. Wasimuddin BJ, Bryja J, Ribas A, Baird SJ, Piálek J, Goüy de Bellocq J. Testing parasite 'intimacy': the whipworm *Trichuris muris* in the European house mouse hybrid zone. Ecol Evol. 2016;6:2688–701. https://doi.org/10.1002/ece3.2022
14. Vieth S, Drosten C, Lenz O, Vincent M, Omilabu S, Hass M, et al. RT-PCR assay for detection of Lassa virus and related Old World arenaviruses targeting the L gene. Trans R Soc Trop Med Hyg. 2007;101:1253–64. https://doi.org/10.1016/j.trstmh.2005.03.018
15. Ronquist F, Teslenko M, van der Mark P, Ayres DL, Darling A, Höhna S, et al. MrBayes 3.2: efficient Bayesian phylogenetic inference and model choice across a large model space. Syst Biol. 2012;61:539–42. https://doi.org/10.1093/sysbio/sys029

Address for correspondence: Rainer G. Ulrich, Friedrich-Loeffler-Institut, Südufer 10, Greifswald–Insel Riems 17493, Germany; email: rainer.ulrich@fli.de

Emergomyces pasteurianus in Man Returning to the United States from Liberia and Review of the Literature

Jacob Pierce, Sadia Sayeed, Christopher D. Doern, Alexandra L. Bryson

A 65-year-old man with HIV sought treatment for fever, weight loss, and productive cough after returning to the United States from Liberia. Fungal cultures grew *Emergomyces pasteurianus*, and the patient's health improved after beginning voriconazole. We describe the clinical case and review the literature, treatment, and susceptibilities for *E. pasteurianus.*

In March 2019, a 65-year-old man sought treatment at an emergency department in Virginia, USA, for fever, odynophagia, weight loss, and productive cough after returning from a 2-year stay in Liberia. In January 2019, he had been treated in Liberia for malaria, typhoid, and thrush. The patient already had an HIV diagnosis at the time he sought treatment, which we confirmed; he was taking lamivudine/zidovudine/nevirapine (150/300/200 mg/d) combination tablets, trimethoprim/sulfamethoxazole (160/800 mg/d) for pneumocystis prophylaxis, and fluconazole (100 mg/d) for thrush. Despite self-reported perfect compliance with his medication regimen, the patient lost 14 kg body weight and reported worsening fatigue over the 5-month period before he sought care in Virginia. The patient's social history revealed smoking 30 packs/year and drinking up to 6 beers/day.

At initial workup, his CD4 T lymphocyte count was 16 cells/mm^3 and HIV-1 viral RNA was 359 copies/mL. We excluded malaria during differential diagnosis with 3 thin/thick smears. Because the patient exhibited fever and was an immunocompromised returning traveler, we admitted him for further evaluation. Computed tomography (CT) of the chest revealed ground glass opacifications at bases, tree-in-bud nodularity within posterior, lateral, and anterior right upper lobes, and a central necrotic nodule at the left lower lung base measuring 1.3 × 2.1 cm (Appendix Figure, https://wwwnc.cdc.gov/EID/article/29/3/22-1683-App1.pdf). We found associated hilar and aortopulmonic lymphadenopathy measuring up to 8 mm in diameter. He was evaluated by infectious disease clinicians and started on amoxicillin/clavulanic acid (875/125 mg every 12 h) and doxycycline (100 mg every 12 h). We increased fluconazole to 200 mg/d and continued trimethoprim/sulfamethoxazole prophylaxis and antiretroviral therapy. The patient displayed night sweats and fever on days 2 (100.9°F) and 3 (101.5°F). He was afebrile on day 4 and for the remainder of his hospital stay.

A needle core biopsy of the lung nodule on day 4 revealed necrotizing granulomatous inflammation consisting of epithelioid histiocytes associated with intracellular narrow-based budding yeast (Figure 1, panels B, C) and multinucleated giant cells (Figure 1, panel A). Yeast forms 2–5 μm in size were visible on the hematoxylin and eosin smears. Both histochemical stains for Grocott methenamine silver and periodic acid–Schiff performed on the core biopsy were positive, but a mucicarmine stain was negative. Among the serologic fungal markers tested, serum cryptococcal antigen was negative. The Platelia Aspergillus galactomannan assay (Bio-Rad Laboratories, https://www.bio-rad.com) was elevated at 2.10 (reference range <0.49), and beta-D-glucan (Fungitell; Associates of Cape Cod, https://www.fungitell.com) was negative at 35 pg/mL (reference range <60 pg/mL). The patient was discharged on voriconazole (200 mg 2×/d) in addition to his HIV medication.

On day 17, the biopsy culture grew a fungus initially reported on the basis of morphology as

Author affiliation: Virginia Commonwealth University Medical Center, Richmond, Virginia, USA

DOI: https://doi.org/10.3201/eid2903.221683

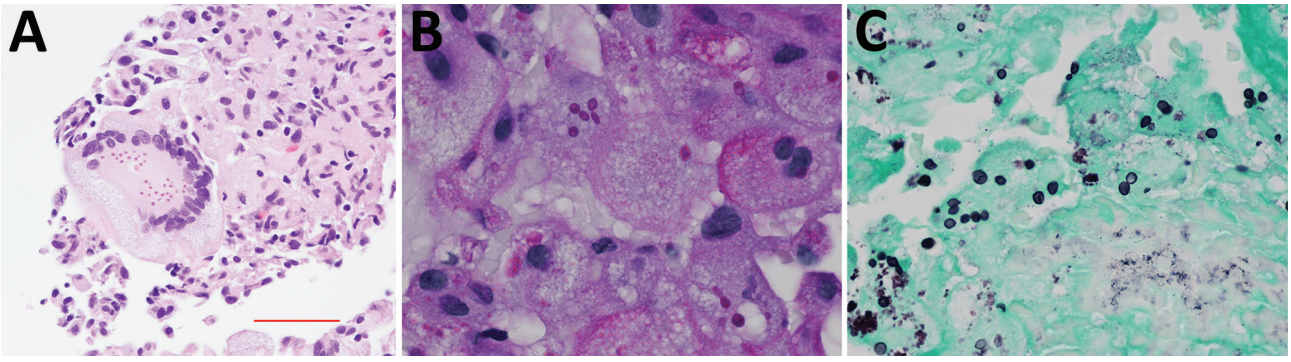

Figure 1. Left lower lobe needle core biopsy histology of *Emergomyces pasteurianus* infection in a patient returning to the United States from Liberia. A) Numerous yeast within a multinucleated giant cell shown by hematoxylin and eosin stain; original magnification ×600. B) Narrow budding yeast shown by periodic acid–Schiff stain; original magnification ×1,000. C) Yeast shown by Grocott methenamine sliver stain; range 2–5 μm.

presumptive *Emmonsia* sp., which was further identified through sequencing. We saw the patient for follow-up in the clinic on day 31; his appetite had returned, and he had gained 4 kg. We simplified his antiretroviral therapy to bictegravir/emtricitabine and tenofovir alafenamide. Day 37 culture results (LabCorp, https://www.labcorp.com) confirmed *Emergomyces pasteurianus* (formerly *Emmonsia pasteuriana*) through sequencing of internal transcribed spacer regions 1 and 2. MICs for antifungal agents were determined at the University of Texas Health Science Center (San Antonio, Texas, USA) by susceptibility tests at 23°C by broth microdilution (Table 1).

At day 81 follow-up, the patient reported that his cough had resolved. His CD4 was 54 cells/mm^3 and viral load was 129 copies/mL. Our plan was to continue prescribing voriconazole for 12 weeks, then repeat the chest CT scan; however, the patient did not return for follow-up.

The geographic distribution of *E. pasteurianus* is still being described. *Emergomyces* is a dimorphic fungus related to *Emmonsia*, *Histoplasma*, and *Blastomyces* (*1*). This organism is an emerging pathogen among immunocompromised persons, especially those with HIV. *E. pasteurianus* was originally classified within the genus *Emmonsia.* However, the formation of yeast rather than adiaconidia (formerly adiaspores) and the clinical manifestations of emergomycosis suggested that *E. pasteurianus* belongs in a different genus from *Emmonsia* spp. (*1*). Subsequent genetic sequencing supported this relationship (*2*). There is evidence that the number of diagnosed emergomycosis cases are increasing, possibly because of more sensitive diagnostic techniques (*1*). We definitively diagnosed the infection in this patient through fungal cultures developed from lung biopsy samples, in which the organism readily grew as a filamentous fungi on Sabouraud dextrose agar, Mycocel agar, and brain–heart infusion agar at 25˚C. Colonies on Sabouraud dextrose agar incubated at 25˚C appeared white and compact and became domed/heaped over time (Figure 2, panel A). The reverse side started as white/cream and progressed to tan.

The microscopic appearance of the mold form of *E. pasteurianus* has been described as septate, hyaline hyphae, with short conidiophores arising at right angles that may show a slight swelling at the tip and

Table 1. MIC/MEC (μg/mL)Antimicrobial susceptibility of antifungal agents for *Emergomyces pasteurianus* isolate from a patient returning to the United States from Liberia and reported cases from the literature*

Case (ref)	AMB	MICA	ANID	FLC	ITC	VOR	POS	ISA	5-FC
This study	0.25	0.03	<0.015	>64	0.06	0.25	0.25	1.0	>64
1 (*9*)	0.031	0.031	0.5	>64	0.125	0.25	0.125	2.0	NA
2 (*10*)	NA	NA	NA	NA	NA	NA	NA	NA	NA
3 (*4*)	1.0	0.05	NA	2.0	0.125	0.25	0.125	NA	NA
4 (*11*)	0.125	0.063	0.0031	>64	0.25	0.25	0.063	1.0	NA
5 (*12*)	NA	NA	NA	NA	NA	NA	NA	NA	NA
6 (*5*)	0.031	<0.008	NA	64	0.063	0.25	0.063	1.0	NA
7 (*5*)	NA	NA	NA	NA	NA	NA	NA	NA	NA
8 (*13*)	NA	NA	NA	NA	NA	NA	NA	NA	NA
9 (*14*)	1.0	0.5†	NA	4.0	0.125	0.25	0.125	NA	NA
10 (*15*)	NA	NA	NA	NA	NA	NA	NA	NA	NA

*Values are MICs (μg/mL), except as indicated. 5-FC, 5-fluorocytosine; AMB, amphotericin B; ANID, anidulafungin; FLC, fluconazole; ISA, isavuconazole; ITC, itraconazole; MICA, micafungin; POS, posaconazole; ref, reference; VOR, voriconazole.
†Caspofungin minimal effective concentration.

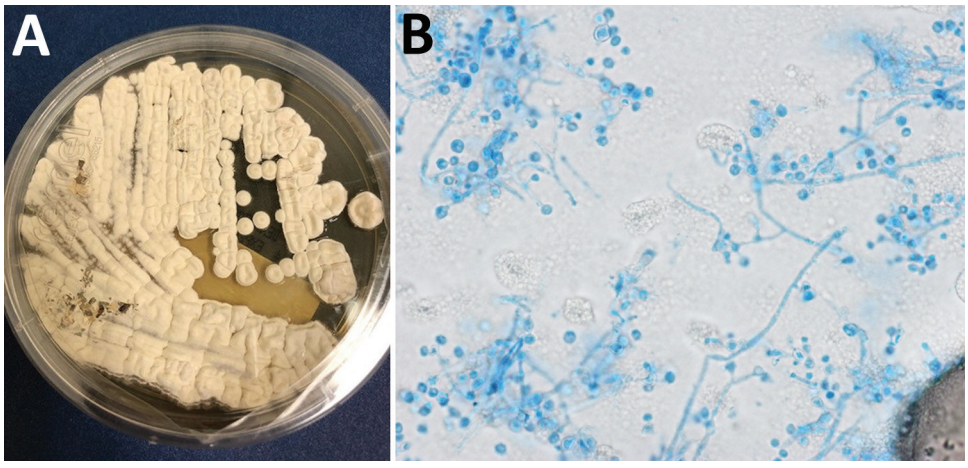

Figure 2. Lung nodule biopsy and fungal culture isolate of *Emergomyces pasteurianus* infection in a patient returning to the United States from Liberia. A) Colony morphology on Sabouraud dextrose agar at 14 days. B) Lactophenol cotton blue tape prep; original magnification ×1,000.

typically produce ≥1 round conidia on short thin denticles. Conidia may also appear directly off the hyphae. The conidia are described as hyaline, thin-walled, 2–4 μm in size (*2*,*3*), which mirrors our experience. The yeast form (grown at 37˚C or present in tissue) is described as 2–5 μm with narrow budding.

Table 2. Reported cases of *Emergomyces pasteurianus* (formerly *Emmonsia pasteuriana*) from the literature*

Case (ref)	Year	Location	Patient age, y/sex	Patient medical history	Clinical features	Specimen cultured	Treatment	Outcome
1 (*9*)	1998	Italy	40/F	HIV/AIDS	Skin ulcerations, weight loss	Skin biopsy	Amphotericin	Died from unrelated cause
2 (*10*)	2008	Spain	46/M	HIV (CD4 134 cells/μL, HCV, liver transplant	Nodular skin lesions (ulcerating), bilateral pulmonary infiltrates, liver failure	Skin biopsy	Liposomal amphotericin B (2 wk), decreased immunosuppression	Died
3 (*4*)	2012	India (Nepal native)	38/F	HIV (CD4 <10 cells/μL)	Nodular skin lesions, weight loss, dyspnea, bilateral pulmonary infiltrates (LUL necrotizing lesion),	Pulmonary nodule biopsy	HAART, 2 wk, amphotericin B, then itraconazole, 12 mo	Survived
4 (*11*)	2015	China	43/M	Renal transplant	Nodular skin lesions (painful, ulcerating), bilateral pulmonary nodules, fungitell negative at first then up to 339 pg/mL	Skin biopsy	Amphotericin B, voriconazole, and caspofungin, 2 wk (ongoing)	Survived
5 (*12*)	2015	China	30/F	CMV enteritis, urticaria (on prednisone), HIV negative	Nodular skin lesions	Skin biopsy	Oral voriconazole, 2 mo	Survived
6 (*5*)	2016	Netherlands (Moroccan ancestry)	62/F	B cell non-Hodgkin lymphoma, cirrhosis, CKD, T2DM, AIHA; 50 mg/d prednisone	Nodular skin lesions, dyspnea, RUL nodule	Skin biopsy	Posaconazole, decreased steroid dosing, 14 mo	Survived
7 (*5*)	2017	Netherlands (Iraqi nationality)	80/M	B-CLL, CKD	Encephalopathy, fever, respiratory failure, sepsis	BAL	Amphotericin B	Died
8 (*13*)	2019	Uganda	38/F	HIV (CD4 140 cells/μL)	Nodular skin lesions	Skin biopsy	Fluconazole, 6 wk, with clinical worsening followed by itraconazole, 8 wk	Survived
9 (*14*)	2020	India	27/F	HIV/AIDS	Weight loss, cough, skin lesions	Skin biopsy	Amphotericin, 2 wk, itraconazole, 12 mo	Survived
10 (*15*)	2020	Hong Kong	61/M	Renal transplant	Pneumonia	Lung biopsy	Amphotericin, 8 wk voriconazole, 10 wk	Died

*AIHA, autoimmune hemolytic anemia; B-CLL, B cell chronic lymphocytic lymphoma; CKD, chronic kidney disease; CMV, cytomegalovirus; HAART, highly active antiretroviral therapy; HCV, hepatitis C virus; LUL, left upper lobe; RUL, right upper lobe; T2DM, type 2 diabetes mellitus; ref, reference.

Bipolar budding and formation of giant cells with broad-based budding have also been reported (*3*–*5*); however, we did not definitively observe those forms in this case (Figure 2, panel B).

Clinical manifestations of emergomycosis may include dyspnea, pleuritic chest pain, and pink to purple nodular skin lesions (*4*). One study reported rapid progression of respiratory failure and death (*5*). Skin rash has been reported in some cases, but frequency of this clinical sign is unknown. CT imaging may show necrotizing cavitary lesions (*4*) or diffuse pulmonary infiltrates (*5*). Histopathology of skin lesions have shown yeast forms (*4*). Risk factors for emergomycosis include HIV (CD4 count <10 cells/mm^3) (*4*), B-cell chronic lymphocytic leukemia with neutropenia, and chronic prednisone therapy (*5*). Chronic kidney disease was present in 2 case-patients, but association was uncertain (*5*).

Data are limited on antifungal susceptibilities for *E. pasteurianus*. The organism appears to have low MICs for itraconazole, posaconazole, and voriconazole but higher MICs for fluconazole and flucytosine (*4*). Although echinocandins generally have low MICs for the mold form of *Emergomyces*, activity in the pathogenic yeast form is less well known and significant discrepancies have been noted in other dimorphic fungi (*6*). A study of 50 clinical isolates of *E. africanus* demonstrated consistently low MICs to voriconazole, posaconazole, and itraconazole for both yeast and mold forms, with consistently elevated MICs for echinocandins and fluconazole (*7*). Although no guidelines exist to direct treatment for emergomycosis, multiple treatment courses have been used with varying outcomes (Table 2).

Serologic markers have been shown insufficient for diagnosing *E. pasteurianus* infection. The galactomannan assay was positive in the only previous case reporting a result and in our case (*5*). Beta-d-glucan testing was negative in our patient but was reported positive in 1/4 cases in other studies (*8*). Cross-reactivity with the histoplasma urine antigen has been reported (*8*). However, none of those tests are specific for *Emergomyces*, and they have not been systematically studied as markers for this specific pathogen.

Conclusions

Our study provides evidence of possible *E. pasteurianus* endemicity in Liberia and adds to the literature on susceptibilities for this emerging pathogen. We provide further evidence of low MICs to newer generation triazoles, suggesting their utility in empiric therapy, but additional data is needed to clarify formal breakpoints. Given the gaps in our knowledge about *E. pasteurianus*, public health providers should be aware of clinical manifestations of emergomycosis and consider it in the differential diagnosis, especially in regions where its presence is known.

About the Author

Dr. Pierce was an infectious diseases fellow at Virginia Commonwealth University at the time of this work. He is currently a clinical assistant professor of medicine and serving as medical director of Infection Prevention for the Brody School of Medicine at East Carolina University, Greenville, North Carolina, USA. His research interests include mechanisms to decrease hospital-acquired infections and antimicrobial stewardship.

References

1. Schwartz IS, Kenyon C, Feng P, Govender NP, Dukik K, Sigler L, et al. 50 years of *Emmonsia* disease in humans: the dramatic emergence of a cluster of novel fungal pathogens. PLoS Pathog. 2015;11:e1005198. https://doi.org/10.1371/journal.ppat.1005198
2. Dukik K, Muñoz JF, Jiang Y, Feng P, Sigler L, et al. Novel taxa of thermally dimorphic systemic pathogens in the Ajellomycetaceae (Onygenales). 2018;60:296–309. https://doi.org/10.1111/myc.12601
3. Samaddar A, Sharma A. Emergomycosis, an emerging systemic mycosis in immunocompromised patients: current trends and future prospects. Front Med (Lausanne). 2021;8:670731. https://doi.org/10.3389/fmed.2021.670731
4. Malik R, Capoor MR, Vanidassane I, Gogna A, Singh A, Sen B, et al. Disseminated *Emmonsia pasteuriana* infection in India: a case report and a review. Mycoses. 2016;59:127–32. https://doi.org/10.1111/myc.12437
5. Gast KB, van der Hoeven A, de Boer MGJ, van Esser JWJ, Kuijper EJ, Verweij JJ, et al. Two cases of *Emergomyces pasteurianus* infection in immunocompromised patients in the Netherlands. Med Mycol Case Rep. 2018;2019:5–8. https://doi.org/10.1016/j.mmcr.2019.01.005
6. Dukik K, Al-Hatmi AMS, Curfs-Breuker I, Faro D, de Hoog S, Meis JF. Antifungal susceptibility of emerging dimorphic pathogens in the family Ajellomycetaceae. Antimicrob Agents Chemother. 2017;62:e01886-17. https://doi.org/10.1128/AAC.01886-17
7. Maphanga TG, Britz E, Zulu TG, Mpembe RS, Naicker SD, Schwartz IS, et al. In vitro antifungal susceptibility of yeast and mold phases of isolates of dimorphic fungal pathogen *Emergomyces africanus* (formerly *Emmonsia* sp.) from HIV-infected South African patients. J Clin Microbiol. 2017;55:1812–20. https://doi.org/10.1128/JCM.02524-16
8. Gori S, Drouhet E, Guého E, Huerre MR, Lofaro A, Parenti M, et al. Cutaneous disseminated mycosis in a patient with AIDS due to a new dimorphic fungus [in French]. J Mycol Med. 1998;8:57–63.
9. Pelegrín I, Ayats J, Xiol X, Cuenca-Estrella M, Jucglà A, Boluda S, et al. Disseminated adiaspiromycosis: case report of a liver transplant patient with human immunodeficiency infection, and literature review. Transpl Infect Dis. 2011;13:507–14. https://doi.org/10.1111/j.1399-3062.2011.00611.x

10. Feng P, Yin S, Zhu G, Li M, Wu B, Xie Y, et al. Disseminated infection caused by *Emmonsia pasteuriana* in a renal transplant recipient. J Dermatol. 2015;42:1179–82. https://doi.org/10.1111/1346-8138.12975
11. Tang XH, Zhou H, Zhang XQ, Han JD, Gao Q. Cutaneous disseminated emmonsiosis due to *Emmonsia pasteuriana* in a patient with cytomegalovirus enteritis. JAMA Dermatol. 2015;151:1263–4. PubMed https://doi.org/10.1001/jamadermatol.2015.1792
12. Rooms I, Mugisha P, Gambichler T, Hadaschik E, Esser S, Rath PM, et al. Disseminated emergomycosis in a person with HIV infection, Uganda. Emerg Infect Dis. 2019;25:1750–1. https://doi.org/10.3201/eid2509.181234
13. Capoor MR, Mishra N, Kolte S, Singla G, Gogna A, Rudramurthy S, et al. Disseminated *Emergomyces pasteurianus* infection in India: a case report and a review. Mycopathologia. 2020;185:193–200.
14. Chik KK, To WK. Autochthonous *Emergomyces pasteurianus* pneumonia in an immunocompromised patient in Hong Kong: a case report. Hong Kong Med J. 2020;26:446–8. https://doi.org/10.12809/hkmj198280

Address for correspondence: Jacob Pierce, East Carolina University, 2390 Hemby Lane, Greenville, NC 27834, USA; email: piercejac22@ecu.edu

Recurrent Cellulitis Revealing *Helicobacter cinaedi* in Patient on Ibrutinib Therapy, France

Anne-Laure Roupie, Emmanuel Lafont, Sylvie Fraitag, Agnès Ferroni, Hervé Lécuyer, Olivia Boccara, Emilie Bessède, Philippe Lehours, François Lefrère, Olivier Lortholary

Author affiliations: University Hospital Necker for Sick Children, Assistance Publique-Hôpitaux de Paris, Paris, France (A.-L. Roupie, E. Lafont, S. Fraitag, A. Ferroni, H. Lécuyer, O. Boccara, F. Lefrère, O. Lortholary); Paris-Cité University, Paris (A.-L. Roupie, E. Lafont, S. Fraitag, A. Ferroni, H. Lécuyer, O. Boccara, F. Lefrère, O. Lortholary); French National Reference Center for Campylobacters & Helicobacters, Bordeaux, France (E. Bessède, P. Lehours); Bordeaux Institute of Oncology, INSERM UMR1312, Bordeaux (E. Bessède, P. Lehours)

DOI: http://doi.org/10.3201/eid2903.221329

Helicobacter cinaedi bacteremia caused recurring multifocal cellulitis in a patient in France who had chronic lymphocytic leukemia treated with ibrutinib. Diagnosis required extended blood culture incubation and sequencing of the entire 16S ribosomal RNA gene from single bacterial colonies. Clinicians should consider *H. cinaedi* infection in cases of recurrent cellulitis.

A 61-year-old man who had been treated for 4 years with the Bruton's tyrosine-kinase (BTK) inhibitor ibrutinib as a first-line therapy for chronic lymphocytic leukemia (CLL) sought treatment for a painful rash. He reported 6 previous episodes in the previous 5 months and had been treated with short courses of amoxicillin, amoxicillin/clavulanate, or pristinamycin. The patient denied fever. We noted, on physical examination, 3 painful, infiltrated erythematous lesions with sharp borders: 1 on his left thigh, 1 on his left tibia, and 1 on the right side of his abdomen (Figure 1).

Laboratory results revealed an abnormal leukocyte count of 13.5 G/L (reference range 4–10 G/L) and a neutrophil count of 10 G/L. We noted normal laboratory findings for C-reactive protein and gammaglobulin levels and found no evidence of progressive CLL. Skin biopsy showed eosinophilic spongiosis leading to spongiotic vesicles, perivascular/interstitial inflammatory infiltrates composed of eosinophilic and lymphocytic cells without atypical cells, mostly located in the superficial and mid dermis (Figure 2, panels A, B, https://wwwnc.cdc.gov/EID/article/29/3/22-1329-F2.htm). Grocott methenamine silver stain, Gram stain, and periodic acid–Schiff stain showed no bacterial or fungal

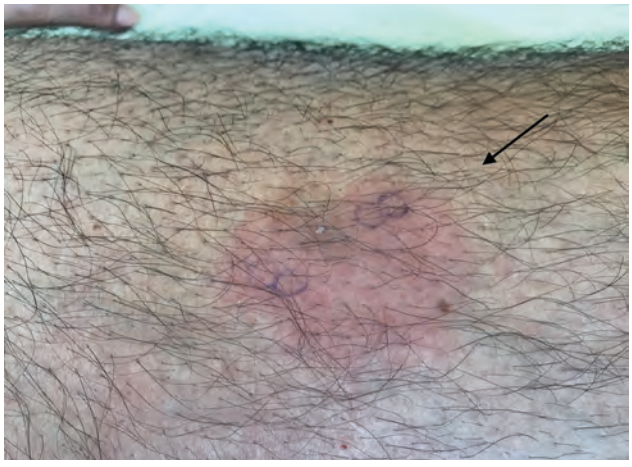

Figure 1. Recurrent skin manifestations revealing *Helicobacter cinaedi* bacteremia in a man on ibrutinib therapy for chronic lymphocytic leukemia, France. A bright red, slightly painful lesion with a sharp border was localized on the left thigh.

element. We performed 16S PCR testing directly on skin biopsy; results were negative. Two different aerobic blood culture bottles showed helical gram-negative rods after 96 hours of incubation; however, we could not identify the strain based on the blood culture broth. We obtained single colonies of fresh bacterial culture and performed matrix-assisted laser/desorption ionization time-of-flight (MALDI-TOF) mass spectrometry without success. We finally identified the strain as *Helicobacter cinaedi* by sequencing the entire 16S ribosomal RNA gene using 2 pairs of primers.

We treated the patient with amoxicillin/clavulanate for 6 weeks and discontinued ibrutinib. During the patient's antibiotic therapy, we performed 3 consecutive blood cultures on 3 different days, all of which remained negative, confirming the efficiency of our antibiotic strategy. The patient achieved complete clinical remission without relapse 6 months after antibiotic discontinuation and was able to restart ibrutinib therapy at that time.

Helicobacter is a gram-negative spiral bacillus belonging to the Helicobacteriaceae family (*1*,*2*). It has been considered an opportunistic infection in patients with either acquired or primary immunodeficiencies (*3*,*4*). Cases of *H. cinaedi* bacteremia have been reported very rarely in immunocompetent persons (*5*). Reported clinical manifestations of *H. cinaedi* infection have included fever, proctitis, enteritis, cellulitis, and arthritis (*1*). Cutaneous manifestations are encountered mainly in the setting of *H. cinaedi* bacteremia, typically presenting as mild but painful cellulitis of the extremities (*6*).

H. cinaedi is a slow-growing bacterium and is difficult to identify. Traditional bacterial identification systems bear numerous limitations. As demonstrat-

ed in our report, a molecular approach is helpful in identifying the strain. Although MALDI-TOF mass spectrometry was insufficient to establish a diagnosis for this patient, others have used it successfully (*7*). A more efficient strategy would be combining a prolonged blood culture incubation time with MALDI-TOF mass spectrometry and a molecular approach. *H. cinaedi* is usually susceptible to carbapenems, tetracyclines, and aminoglycosides (*1*,*8*), as well as to amoxicillin and ceftriaxone (with intermediate MICs) (*1*,*6*). However, this species is resistant to macrolides, such as erythromycin and clarithromycin, and to ciprofloxacin (*1*,*8*). To avoid recurrence, prolonged therapies (2–8 weeks) are preferable (*6*).

H. cinaedi pathogenicity has not been clearly identified. The bacterium's cytolethal distending toxin is reported as a potential virulence factor (*9*). Compared with other *Helicobacter* species, *H. cinaedi* might have a stronger ability to translocate from the intestinal tract to the vascular system, resulting in a greater chance for bacteremia (*1*). *H. cinaedi* is a known cause of bacteremia in patients with humoral immunodeficiency, especially X-linked agammaglobulinemia (*4*).

For our patient, given that CLL was quiescent and gammaglobulins levels were normal, ibrutinib may have promoted the occurrence of *H. cinaedi* bacteremia. Infections are common adverse events in patients receiving ibrutinib, especially pneumonia and invasive fungal infections (*10*). Because BTK inhibition in patients treated with ibrutinib does not generally result in immunoglobulin depletion (*10*), the increased risk for infection might be explained by other putative mechanisms associated with BTK. For example, ibrutinib's disruption of chemokine-controlled B cell migration, trafficking, and homing to lymphoid organs might impair the humoral response to *H. cinaedi* (*10*). Furthermore, ibrutinib's off-target inhibition of interleukin 2–inducible T-cell kinase could weaken the adaptive response against *H. cinaedi* (*10*). In addition, BTK is involved in Toll-like receptor signaling and is found in other immune cell subsets, such as neutrophils and macrophages. Thus, BTK inhibition could lead to a defect in host innate immune response or proliferation and function of myeloid cells.

The case we report illustrates 2 problems associated with *H. cinaedi* infections. First, patients must often endure prolonged courses of antibiotic therapy to avoid recurrence. Second, bacterial strains grow very slowly and often demand a molecular approach to establish microbiological diagnosis. Clinicians should add *H. cinaedi* infection to the diagnostic list when treating recurrent cellulitis, especially in patients with humoral immunodeficiency and those treated with ibrutinib.

About the Author

Dr. Roupie is an adult internal medicine and clinical immunology resident, pursuing a PhD in immunology in Dr. Sylvain Latour's laboratory at Imagine Institute, which is part of the University Hospital Necker for Sick Children in Paris, France. She is interested in pursuing a career in the immunological field and particularly in the research and care of patients with primary immunodeficiencies.

References

1. Kawamura Y, Tomida J, Morita Y, Fujii S, Okamoto T, Akaike T. Clinical and bacteriological characteristics of *Helicobacter cinaedi* infection. J Infect Chemother. 2014; 20:517–26. https://doi.org/10.1016/j.jiac.2014.06.007
2. Fennell CL, Totten PA, Quinn TC, Patton DL, Holmes KK, Stamm WE. Characterization of *Campylobacter*-like organisms isolated from homosexual men. J Infect Dis. 1984;149:58–66. https://doi.org/10.1093/infdis/149.1.58
3. Kiehlbauch JA, Tauxe RV, Baker CN, Wachsmuth IK. *Helicobacter cinaedi*–associated bacteremia and cellulitis in immunocompromised patients. Ann Intern Med. 1994;121:90–3. https://doi.org/10.7326/0003-4819-121-2-199407150-00002
4. Inoue K, Sasaki S, Yasumi T, Imai K, Kusunoki T, Morio T, et al. *Helicobacter cinaedi*-associated refractory cellulitis in patients with X-Linked agammaglobulinemia. J Clin Immunol. 2020;40:1132–7. https://doi.org/10.1007/s10875-020-00830-6
5. Shimizu Y, Gomi H, Ishioka H, Isono M. Refractory to treat *Helicobacter cinaedi* bacteremia with bilateral lower extremities cellulitis in an immunocompetent patient. IDCases. 2016;5:9–11. https://doi.org/10.1016/j.idcr.2016.05.001
6. Shimizu S, Shimizu H. Cutaneous manifestations of *Helicobacter cinaedi*: a review. Br J Dermatol. 2016;175:62–8. https://doi.org/10.1111/bjd.14353
7. Taniguchi T, Sekiya A, Higa M, Saeki Y, Umeki K, Okayama A, et al. Rapid identification and subtyping of *Helicobacter cinaedi* strains by intact-cell mass spectrometry profiling with the use of matrix-assisted laser desorption ionization–time of flight mass spectrometry. J Clin Microbiol. 2014;52:95–102. https://doi.org/10.1128/JCM.01798-13
8. Rimbara E, Mori S, Matsui M, Suzuki S, Wachino J, Kawamura Y, et al. Molecular epidemiologic analysis and antimicrobial resistance of *Helicobacter cinaedi* isolated from seven hospitals in Japan. J Clin Microbiol. 2012;50:2553–60. https://doi.org/10.1128/JCM.06810-11
9. Taylor NS, Ge Z, Shen Z, Dewhirst FE, Fox JG. Cytolethal distending toxin: a potential virulence factor for *Helicobacter cinaedi*. J Infect Dis. 2003;188:1892–7. https://doi.org/10.1086/ 379837
10. Byrd JC, Furman RR, Coutre SE, Flinn IW, Burger JA, Blum KA, et al. Targeting BTK with ibrutinib in relapsed chronic lymphocytic leukemia. N Engl J Med. 2013;369:32–42. https://doi.org/10.1056/NEJMoa1215637

Address for correspondence: Anne-Laure Roupie, University Hospital Necker for Sick Children, Assistance Publique-Hôpitaux de Paris, 149, rue de Sèvres 75015 Paris, France; email: anne-laure.roupie@inserm.fr

Inquilinus limosus Bacteremia in Lung Transplant Recipient after SARS-CoV-2 Infection

Eric Farfour, Mathilde Zrounba, Antoine Roux, Hélène Revillet, Alexandre Vallée, Marc Vasse

Author affiliations: Hôpital Foch, Suresnes, France (E. Farfour, M. Zrounba, A. Roux, A. Vallée, M. Vasse); CHU de Toulouse, Toulouse, France (H. Revillet); Observatoire National Burkholderia cepacia, Toulouse (H. Revillet); UMRS 1176, le Kremlin-Bicêtre, Paris-Saclay, France (M. Vasse)

DOI: https://doi.org/10.3201/eid2903.221564

Inquilinus limosus is an environmental bacterium associated with respiratory tract colonization in cystic fibrosis patients. We report a case of *I. limosus* bacteremia in a patient in France who received a lung transplant and experienced chronic graft dysfunction and SARS-CoV-2 infection. This case suggests *I. limosus* displays virulence factors associated with invasion.

A 45-year-old woman in France who had received a lung transplant in 2016 for end-stage cystic fibrosis (CF) sought care for rhinorrhea on March 1, 2022. Her immunosuppressive regimen included mycophenolate mofetil (750 mg 2×/d) and cyclosporine A (200 mg 2×/d). She received oral azithromycin (250 mg/d) and trimethoprim/sulfamethoxazole 400 (80 mg/d) for pneumocystosis prophylaxis. In 2021, she experienced progressive graft dysfunction with no obvious trigger and was treated with alemtuzumab in June 2021. Her forced expiratory volume decreased from 78% in January 2021 to 57% in May 2021 and 30% in January 2022.

At the visit, the patient tested positive for SARS-CoV-2 by reverse transcription PCR. She returned home with treatment for symptoms; she had a productive cough with greenish sputum, for which she received 7 days of amoxicillin/clavulanate. Because her condition did not improve, she continued the treatment for 14 more days. On April 11, we isolated a strain of *P. aeruginosa* (10^6 CFU/mL) from her sputum and prescribed cefepime (2 g/d). However, her condition worsened, and she was hospitalized on April 20. A chest computed tomography showed bilateral nodular condensations in the lungs; we switched cefepime for piperacillin/tazobactam and tobramycin. Several respiratory samples grew *Inquilinus limosus* and *Pseudomonas aeruginosa* (Table 1). We recovered *A. fumigatus* from bronchoalveolar liquid and started the patient on posaconasole (300 mg/d). No mycobacteria were recovered.

An aerobic vial of a blood culture set sampled on April 26 was positive for *I. limosus* after 87 hours of incubation. We identified *I. limosus* using matrix-assisted laser desorption/ionization time-of-flight mass spectrometry after subculture and formic acid extraction. We replaced the treatment with ceftolozane/tazobactam. We determined MIC as follows: piperacillin/tazobactam, >32 mg/L; cefepime, 256 mg/L; ceftolozane/tazobactam, 256 mg/L; imipenem, 0.047 mg/L; meropenem, 0.012 mg/L; and ciprofloxacin, 0.016 mg/L. Ceftolozane/tazobactam was switched for meropenem plus amikacin and then ciprofloxacin on May 4. The patient improved but remained colonized with *I. limosus*, displaying a similar pattern of resistance, 3 months later. Of interest, she was colonized before the lung transplantation, but *I. limosus* has not been isolated since then.

I. limosus is a fastidious, gram-negative rod from environmental sources (*1*) that has rarely been associated with colonization of the respiratory tract of CF patients (*2*). The airways of CF are susceptible to colonization by respiratory pathogens (*3*), a condition that is improved in lung transplant recipients. Nevertheless, *I. limosus* infection has been reported twice in lung transplant recipients (*4*,*5*). In 1 case, a 22 year-old woman had pulmonary infiltrates develop within a month after lung transplantation (*4*). She completely recovered with antimicrobial drug treatment; *I. limosus* was not isolated during 1 year of follow-up. In the second case, a 31-year-old man experienced a bacteremic lung empyema 1 month posttransplant and a contralateral lung empyema 7 months later (*5*). He recovered from each episode with surgery and antimicrobial treatment with ciprofloxacin and meropenem. Both patients were lung transplant recipients for end-stage cystic fibrosis (CF); they were colonized with *I. limosus* before lung transplantation. Indeed, the lung graft microbiome is affected by donor and recipient factors (*6*), but early posttransplant infections mainly involve the bacteria of the recipient rather than those of the donor (*7*).

In contrast to those patients, the case-patient we describe experienced a late infection several years after *I. limosus* clearance. Unfortunately, the pretransplant strain was not preserved, and we could not determine whether she was infected with the strain she was colonized with before the lung transplantation or another strain. It is possible that the chronic graft dysfunction, the recent intensification of immunosuppression, and the SARS-CoV-2 infection could have led to a modification of the graft microbiome and enabled colonization with *I. limosus*. In CF patients, colonization with *I. limosus* induces a specific

Table. Timeline of events in study of *Inquilinus limosus* bacteremia in lung transplant recipient with history of chronic graft dysfunction and prolonged SARS-CoV-2 infection, France, 2022*

Date	Symptoms and clinical conditions	CT scan findings	Microbiologic findings	Treatment
Mar 1	Rhinorrhea		SARS-CoV-2 RT-PCR positive (Ct = 18.5)	Symptomatic treatment
Mar 14	Productive cough with greenish sputum		SARS-CoV-2 RT-PCR positive (Ct = 17.0)	Amoxicillin/clavulanate 1.5 g/d for 7 d
Mar 29	No improvement			Amoxicillin/clavulanate 1.5 g/d continued for 14 d; oseltamivir added for 5 d
Apr 11	No improvement	Bilateral nodular opacities	Sputum grew 10^6 CFU/mL of *Pseudomonas aeruginosa,* resistant to ticarcillin, piperacillin, and carbapenem and susceptible to ceftazidime, cefepime, tobramycin, and ciprofloxacine (EUCAST 2021 guidelines); SARS-CoV-2 RT-PCR positive (Ct = 23.2)	Cefepime 2 g/d for 11 d
Apr 22	Condition worsened; patient hospitalized	Discordant evolution with reduction of some lesions but appearance of new condensations and ground-glass opacities	SARS-CoV-2 RT-PCR positive (Ct = 26.4)	Piperacillin/tazobactam 8 g/d for 5 d; tobramycin 5 mg/kg, 1 shot
Apr 23			Sputa grew 10^6 CFU/mL of *I. limosus* and 10^3 CFU/mL of a cephalosporin-susceptible *P. aeruginosa*	
Apr 24			Sputa grew 10^6 CFU/mL of *I. limosus* and 10^3 CFU/mL a cephalosporin-susceptible *P. aeruginosa*	
Apr 25			BAL grew 10^4 CFU/mL of *I. limosus*, 10^2 CFU/mL, cephalosporin-susceptible *P. aeruginosa,* and few colonies of *Aspergillus fumigatus*	
Apr 26	Persistent cough and colored sputum		SARS-CoV-2 RT-PCR positive (Ct = 23.1)	Ceftolozane/tazobactam 0.75 g d
Apr 29			Sputa grew 10^6 CFU/mL of *I. limosus* and 10^5 CFU/mL of *P. aeruginosa*	
Apr 30	Fever, no respiratory improvement		1 vial of a blood culture set sampled on April 26 was positive for a gram-negative rod after 87 h of incubation	Posaconazole 300 mg/d
May 2	Apyrexia			Meropenem 2 g/d for 2 d; amikacin 0.75 g, 1 shot
May 3			Gram-negative rod isolated from the blood culture identified as *I. limosus*; antimicrobial susceptibility testing results	
May 4		Increased ground-glass opacities and bilateral condensations		Ciproflxoacin 1 g/d
May 5			SARS-CoV-2 RT-PCR positive (Ct = 27.6); BAL grew 10^4 CFU/mL of *I. limosus*	
May 12	Respiratory improvement		SARS-CoV-2 RT-PCR positive (Ct = 29.8)	
July 21			Sputa grew 10^6 CFU/mL of *I. limosus* and 10^6 CFU/mL of *P. aeruginosa*	

*Blank cells indicate no report. CT, computed tomography; Ct, cycle threshold; EUCAST, European Committee on Antimicrobial Susceptibility Testing; RT-PCR, reverse transcription PCR.

serum antibody response (*8*). The intensification of immunosuppression and the clearance of *I. limosus* after lung transplantation could have reduced humoral immunity. Furthermore, the bacteremia suggested virulence factors involved in the invasion. Two other cases of *I. limosus* bacteremia have been reported previously (*5*,*9*).

Because *I. limosus* is a rarely encountered microorganism and because its colonies are of a mucoid morphotype, it could be misidentified using phenotypic characteristics as *P. aeruginosa* (*8*,*10*). The biochemical methods used previously provided inconsistent identification, and neither European Committee on Antimicrobial Susceptibility Testing nor

Clinical and Laboratory Standards Institutes guidelines include standardized *I. limosus* antimicrobial susceptibility testing. However, matrix-assisted laser desorption/ionization time-of-flight mass spectrometry accurately identifies *I. limosus*. *I. limosus* displays high MICs for colistin and almost all β-lactams, except imipenem and meropenem (*9*). It has been suggested that the multidrug resistance of *I. limosus* enhances its selection in CF patients (*2*). In our case, successive treatment with drugs that were ineffective against *I. limosus* could have enabled its selection.

In conclusion, we emphasize a pathogenic role of *I. limosus* in lung transplant recipients several years after respiratory clearance of the bacteria. Chronic graft dysfunction, intensifying immunosuppression, and SARS-CoV-2 infection in this patient could have favored colonization with *I. limosus*. Characteristics of the bacterium such as colony morphotypes and multidrug resistance could delay effective therapy.

About the Author

Dr. Farfour is a medical microbiologist at Foch Hospital clinical laboratory, Suresnes, France. His primary research interests are emerging pathogens and antimicrobial drug resistance.

References

1. Peeters C, Depoorter E, Praet J, Vandamme P. Extensive cultivation of soil and water samples yields various pathogens in patients with cystic fibrosis but not *Burkholderia multivorans*. J Cyst Fibros. 2016;15:769–75 https://doi.org/10.1016/j.jcf.2016.02.014
2. Bittar F, Leydier A, Bosdure E, Toro A, Reynaud-Gaubert M, Boniface S, et al. *Inquilinus limosus* and cystic fibrosis. Emerg Infect Dis. 2008;14:993–5. https://doi.org/10.3201/eid1406.071355
3. Garnett JP, Kalsi KK, Sobotta M, Bearham J, Carr G, Powell J, et al. Hyperglycaemia and *Pseudomonas aeruginosa* acidify cystic fibrosis airway surface liquid by elevating epithelial monocarboxylate transporter 2 dependent lactate-H + secretion. Sci Rep. 2016;6:37955. https://doi.org/10.1038/srep37955
4. Pitulle C, Citron DM, Bochner B, Barbers R, Appleman MD. Novel bacterium isolated from a lung transplant patient with cystic fibrosis. J Clin Microbiol. 1999;37:3851.
5. Goeman E, Shivam A, Downton TD, Glanville AR. Bacteremic *Inquilinus limosus* empyema in an Australian lung transplant patient with cystic fibrosis. J Heart Lung Transplant. 2015;34:1220–3. https://doi.org/10.1016/j.healun.2015.06.013
6. McGinniss JE, Whiteside SA, Simon-Soro A, Diamond JM, Christie JD, Bushman FD, et al. The lung microbiome in lung transplantation. J Heart Lung Transplant. 2021;40:733–44. https://doi.org/10.1016/j.healun.2021.04.014
7. Konishi Y, Miyoshi K, Kurosaki T, Otani S, Sugimoto S, Yamane M, et al. Airway bacteria of the recipient but not the donor are relevant to post–lung transplant pneumonia. Gen Thorac Cardiovasc Surg. 2020;68:833–40. https://doi.org/10.1007/s11748-019-01273-6
8. Schmoldt S, Latzin P, Heesemann J, Griese M, Imhof A, Hogardt M. Clonal analysis of *Inquilinus limosus* isolates from six cystic fibrosis patients and specific serum antibody response. J Med Microbiol. 2006;55:1425–33. https://doi.org/10.1099/jmm.0.46466-0
9. Kiratisin P, Koomanachai P, Kowwigkai P, Pattanachaiwit S, Aswapokee N, Leelaporn A. Early-onset prosthetic valve endocarditis caused by *Inquilinus* sp. Diagn Microbiol Infect Dis. 2006;56:317–20. https://doi.org/10.1016/j.diagmicrobio.2006.05.005
10. Hogardt M, Ulrich J, Riehn-Kopp H, Tümmler B. EuroCareCF quality assessment of diagnostic microbiology of cystic fibrosis isolates. J Clin Microbiol. 2009;47:3435–8. https://doi.org/10.1128/JCM.01182-09

Address for correspondence: Eric Farfour, Service de biologie Clinique, Hôpital Foch, 40 rue Worth, 92150 Suresnes, France; email: e.farfour@hopital-foch.com, ericf6598@yahoo.fr

Genomic Analysis of Early Monkeypox Virus Outbreak Strains, Washington, USA

Pavitra Roychoudhury,[1] Jaydee Sereewit,[1] Hong Xie, Ethan Nunley, Shah M. Bakhash, Nicole A.P. Lieberman, Alexander L. Greninger

Author affiliations: University of Washington, Seattle, Washington, USA (P. Roychoudhury, J. Sereewit, H. Xie, E. Nunley, S.M. Bakhash, N.A.P. Lieberman, A.L. Greninger); Fred Hutchinson Cancer Research Center, Seattle (P. Roychoudhury, A.L. Greninger)

DOI: https://doi.org/10.3201/eid2903.221446

We conducted a genomic analysis of monkeypox virus sequences collected early in the 2022 outbreak, during July–August , in Washington, USA. Using 109 viral genomes, we found low overall genetic diversity, multiple introductions into the state, ongoing community transmission, and potential for co-infections by multiple strains.

[1]These first authors contributed equally to this article.

The World Health Organization declared the 2022 mpox (formerly monkeypox) outbreak a public health emergency of international concern on July 23, 2022, after cases were identified in nearly 80 countries (*1*). By August 26, 2022, a total of 411 mpox cases had been confirmed in Washington, USA (*2*), and 17,432 cases had been confirmed in the United States (https://www.cdc.gov/poxvirus/monkeypox/response/2022/us-map.html).

Viral whole-genome sequencing (WGS) can augment contact tracing efforts and identify emerging variants, which potentially could affect infectivity, virulence, vaccine escape, and treatment resistance. By late August 2022, Washington had deposited more monkeypox virus (MPXV) sequences into public databases than any other state in the country. Here, we describe the Washington outbreak by using 109 MPXV genomes collected in the state.

We attempted WGS on 140 residual clinical specimens, primarily lesion swabs, that were PCR-positive for MPXV and had a cycle threshold (Ct) value <31 (range 15.9–30.4). We performed sequencing by using a hybridization probe-capture–based approach, as previously described (*3*), and probes designed by using the MPXV 2022/MA001 strain (Genbank accession no. ON563414) (Appendix, https://wwwnc.cdc.gov/EID/article/29/3/22-1446-App1.pdf). We generated consensus genomes by using Revica (https://github.com/greninger-lab/revica), a custom pipeline that performs trimming, filtering, and iterative remapping (Appendix). Sequences with <1% ambiguous bases (Ns) were deposited to GenBank under BioProject accession no. PRJNA862948 (Appendix Table). We used Augur, Auspice, and Nextclade to perform phylogenetic analysis (*4*,*5*), and we used UShER (*6*) to perform phylogenetic placement on a global tree (Appendix). This study was approved by the University of Washington Institutional Review Board STUDY00000408.

The analysis comprised a total of 109 sequences from 98 persons whose specimens were collected during July 6–August 19, 2022, primarily from King and Pierce Counties. Of the 98 patients, 90 (91.84%) were male and 1 (1.02%) female; 7 (7.14%) had unknown or undeclared sex. Median age at specimen collection was 36.0 (range 19–57) years.

We identified multiple identical genomes from different persons, suggesting ongoing community transmission (Figure, panel A). All 109 genomes fell within the predominant 2022 outbreak lineage B.1 (*7*), and sublineages included B.1.1 (n = 18), B.1.2 (n = 6), B.1.3 (n = 10), B.1.4 (n = 2), and B.1.8 (n = 2), suggesting separate MPXV introductions into the state. Among sublineages, we identified the nearest neighbor sequences from Germany (B.1.1); Connecticut, USA (B.1.2); Canada (B.1.4); Florida, USA (B.1.8); and multiple countries in Europe (B.1.3) (Appendix).

Overall, we observed low genetic diversity and a median of 1 aa (range 0–7 aa) mutation (substitutions or deletions) across the genome relative to the

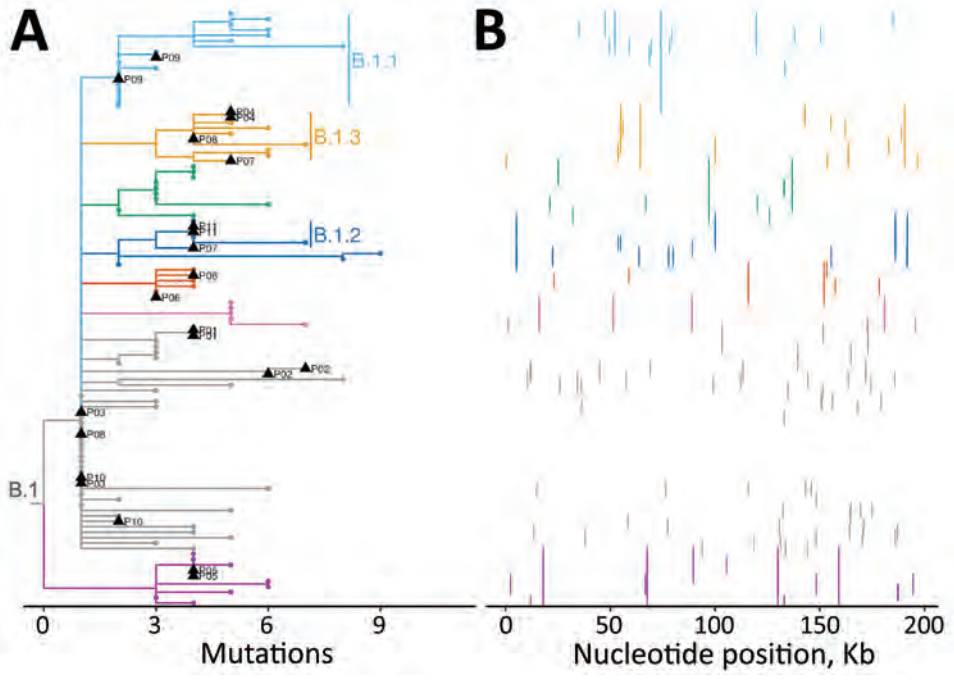

Figure. Phylogenomic analysis of 109 early monkeypox virus outbreak strains, Washington, USA. A) Phylogenetic tree showing that all Washington sequences fall within the major outbreak lineage B.1. The many identical sequences suggest community transmission; distinct sublineages suggest multiple MPXV introductions into the state. Black triangles indicate sequences from multiple swabs from the same patient, which were available for 11 persons, patients P01–P11. Clades with ≥5 sequences were assigned a color for tips and branches, and have text labels for the major sublineages, B.1.1, B.1.2, and B.1.3. All other tips and smaller clades are indicated in gray. B) Single nucleotide polymorphisms from each sample in panel A arrayed across the MPXV genome. Colors correspond to lineage coloring in panel A. MPXV, monkeypox virus.

B.1 ancestor (genome MPXV_USA_2022_MA001; Genbank accession no. ON563414). We identified 138 unique SNPs across the genome in the 109 sequences (Figure, panel B), producing 66 unique mutations (amino acid substitutions or deletions) in 51 genes. Of these, 5 unique aa substitutions (S553N, A1232V, D1546N, D1604N, and S1633L) occurred in surface glycoprotein OPG210, and 3 (E306K, D441Y, and E553K) in OPG189, which encodes one of several ankyrin-repeat proteins (Appendix Figure 1). We noted an abundance of G to A and C to T nucleotide substitutions (Appendix Figure 2), indicative of apolipoprotein B mRNA editing catalytic polypeptide-like3 activity consistent with other reports (*8*). We did not identify any substitutions or deletions in OPG057, a membrane glycoprotein homologous to F13L in vaccinia virus and the putative target of the therapeutic antiviral tecovirimat currently used to treat mpox (*9*).

Sequences from multiple swabs from the same person at the same time point had a median pairwise nucleotide difference of 1 (range 0–10 for 11 sample pairs) outside of labile tandem repeat regions (*10*). We observed even greater similarity in protein sequences with 0 (range 0–6) median pairwise aa differences. Among sample pairs from 3 patients, patient 06 (P06) had 1 aa difference, P07 had 6 aa differences, and P08 had 2 aa differences. Relative to the B.1 ancestral strain MA001, one of the P06 pair featured a V195I mutation in OPG079. One of the P08 pair had synonymous mutations in OPG073 and OPG083, and an OPG003:R84K substitution. Finally, differences in repeat samples from P07 suggest possible co-infection with strains from the B.1.2 and B.1.3 lineages, consistent with the patient's clinical history indicating multiple sexual partners. Relative to the MA001 B.1 reference strain, one of the P07 samples had synonymous mutations in OPG083 and OPG189, OPG180:D325N, and OPG016:R84K. The other of the P07 pair shared none of those SNPs, but had OPG015:V261A, OPG109:I66V, and the B.1.2-defining OPG210:D1604N. These mutations remained after re-extracting and re-sequencing the original specimens and, compared with interhost variation, suggest the possibility of co-infection with different MPXV strains (Appendix Table).

Overall, our data showed ongoing community MPXV transmission in Washington. The limited MPXV genetic diversity makes it challenging to use WGS data for contact tracing. However, continued genomic surveillance will be crucial for tracking viral evolution and identifying mutations associated with vaccine escape or antiviral treatment resistance.

This article was preprinted at https://doi.org/10.1101/2022.09.19.22280115.

About the Author

Dr. Roychoudhury is an acting instructor and director of COVID-19 next-generation sequencing in the Department of Laboratory Medicine and Pathology at the University of Washington, Seattle, Washington, USA, and an associate in the Vaccine and Infectious Disease Division at the Fred Hutchinson Cancer Research Center, Seattle. Her primary research interests are pathogen genomics and mathematical modeling of viral evolution and host-pathogen interactions.

References

1. Kozlov M. Monkeypox declared a global emergency: will it help contain the outbreak? Nature. 2022 Jul 25 [Epub ahead of print]. https://doi.org/10.1038/d41586-022-02054-7
2. Washington State Department of Health. Monkeypox (MPV) [cited 28 Aug 2022]. https://doh.wa.gov/you-and-your-family/illness-and-disease-z/monkeypox
3. Greninger AL, Roychoudhury P, Xie H, Casto A, Cent A, Pepper G, et al. Ultrasensitive capture of human herpes simplex virus genomes directly from clinical samples reveals extraordinarily limited evolution in cell culture. MSphere. 2018;3:e00283-18. https://doi.org/10.1128/mSphereDirect.00283-18
4. Aksamentov I, Roemer C, Hodcroft E, Neher R. Nextclade: clade assignment, mutation calling and quality control for viral genomes. J Open Source Softw. 2021;6:3773. https://doi.org/10.21105/joss.03773
5. Hadfield J, Megill C, Bell SM, Huddleston J, Potter B, Callender C, et al. Nextstrain: real-time tracking of pathogen evolution. Bioinformatics. 2018;34:4121–3. https://doi.org/10.1093/bioinformatics/bty407
6. Turakhia Y, Thornlow B, Hinrichs AS, De Maio N, Gozashti L, Lanfear R, et al. Ultrafast Sample placement on Existing tRees (UShER) enables real-time phylogenetics for the SARS-CoV-2 pandemic. Nat Genet. 2021;53:809–16. https://doi.org/10.1038/s41588-021-00862-7
7. Wang L, Shang J, Weng S, Aliyari SR, Ji C, Cheng G, et al. Genomic annotation and molecular evolution of monkeypox virus outbreak in 2022. J Med Virol. 2022.
8. Gigante CM, Korber B, Seabolt MH, Wilkins K, Davidson W, Rao AK, et al. Multiple lineages of monkeypox virus detected in the United States, 2021–2022. Science. 2022;378:560–5. https://doi.org/10.1126/science.add4153
9. Merchlinsky M, Albright A, Olson V, Schiltz H, Merkeley T, Hughes C, et al. The development and approval of tecoviromat (TPOXX®), the first antiviral against smallpox. Antiviral Res. 2019;168:168–74. https://doi.org/10.1016/j.antiviral.2019.06.005
10. Hatcher EL, Wang C, Lefkowitz EJ. Genome variability and gene content in chordopoxviruses: dependence on microsatellites. Viruses. 2015;7:2126–46. https://doi.org/10.3390/v7042126

Address for correspondence: Pavitra Roychoudhury, Department of Laboratory Medicine and Pathology, University of Washington, 1100 Fairview Ave N, E5-110, Seattle, WA 98109-1024, USA; email: proychou@uw.edu

Sustained Mpox Proctitis with Primary Syphilis and HIV Seroconversion, Australia

Rachel M. Burdon, David Atefi, Jainoor Rana, Arun Parasuraman, Andie S. Lee, Blake Nield

Author affiliations: Sydney Local Health District, Sydney, New South Wales, Australia (R.M. Burdon, D. Atefi, J. Rana, A. Parasuraman); Royal Prince Alfred Hospital, Sydney (A.S. Lee, B. Nield)

DOI: https://doi.org/10.3201/eid2903.221845

A 26-year-old man in Australia who has sex with men had severe perianal ulceration, proctitis, and skin lesions develop. Testing revealed primary syphilis, mpox, and primary HIV infection. Recent publications have documented severe mpox associated with HIV infection. Disruption of mucosal integrity by mpox lesions could enable HIV transmission and vice versa.

Human mpox (formerly monkeypox) is a viral zoonosis caused by monkeypox virus (MPXV). As of December 8, 2022, a total of 144 reported infections had occurred in Australia, all in men who have sex with men (MSM); no mpox-related deaths had been reported.

A 26-year-old overseas-born MSM with no comorbidities sought care at the Sydney Local Health District (SLHD; Sydney, NSW, Australia) Department of Sexual Health Medicine (DSHM), 20 days after becoming unwell with severe perianal ulceration, dyschezia, tenesmus, purulent bloody anal discharge, and skin lesions on his trunk and limbs. His symptoms were initially accompanied by a fever and prodrome, although those had resolved by the time he was examined. He had not received MPXV vaccination and had not taken HIV preexposure prophylaxis.

The patient spoke limited English and had traveled to Australia approximately 3 weeks earlier. He sought care from a local doctor 5 days after onset of symptoms and was prescribed valaciclovir for a clinical diagnosis of herpes simplex virus (HSV). He was unresponsive to treatment and returned to the same doctor 2 weeks later with more extensive perianal lesions and rectal symptoms and new truncal and limb lesions. This doctor contacted the SLHD Public Health Unit, which recommended referral to SLHD DSHM.

Physical examination showed large, superficial, ulcerated lesions with surrounding erythema perianally extending to the buttocks and 2 smaller, deep, indurated ulcers on the anal verge consistent with syphilitic chancres. The patient had purulent discharge from the anus; anoscopy was not attempted because of pain. Several umbilicated, papular lesions with necrotic centers and surrounding erythema were present on the hand, thigh, and trunk. The papular and perianal lesions were swabbed for MPXV, HSV, and syphilis PCR. We performed testing for HIV, chlamydia, and gonorrhea on urine, throat, and rectal specimens and took additional rectal swab specimens for PCR testing for lymphogranuloma venereum, syphilis, HSV, and *Mycoplasma genitalium*. He was treated with 4.8 million units of benzathine benzylpenicillin for presumptive primary syphilis and asked to isolate at home until MPXV results were known.

The patient reported his most recent sexual activity (receptive anal intercourse using a condom) was with a casual partner overseas 7–10 days before his arrival in Australia. The next most recent sexual encounter was 3 months earlier with his regular male partner of 1 year. He had not been to any nightclubs, sex-on-premises venues, or festivals and reported no other intimate contact. His last sexual health screening (including an HIV test) 7 months before detected no sexually transmitted infections.

Results of an HIV antigen/antibody assay were reactive (signal-to-cutoff ratio of 74.2 and a positive p24 antigen), whereas Western blot results were indeterminate (positive band at p24 and gp160), consistent with seroconversion. MPXV was detected at all sites by PCR, and results of syphilis enzyme immunoassay and *Treponema pallidum* particle agglutination assays were positive (rapid plasma reagin test result of 16). Syphilis PCR results were negative, but clinical signs and serologic testing were consistent with primary syphilis. Test results for gonorrhoea, chlamydia, *Mycoplasma genitalium*, HSV, varicella zoster, and hepatitis B and C were all negative.

We began antiretroviral treatment (bictegravir/emtricitabine/tenofovir alafenamide) in anticipation that immune reconstitution would improve the patient's severe and sustained mpox (*1*). His rectal symptoms and perianal lesions improved dramatically after benzylpenicillin administration, and he began oral cefalexin for empirical treatment of secondarily infected mpox lesions. His HIV viral load was found to be 7,120,000 RNA copies/mL and CD4 count was 370×10^6 cells/L (12%) with a fully sensitive genotype. He continued to

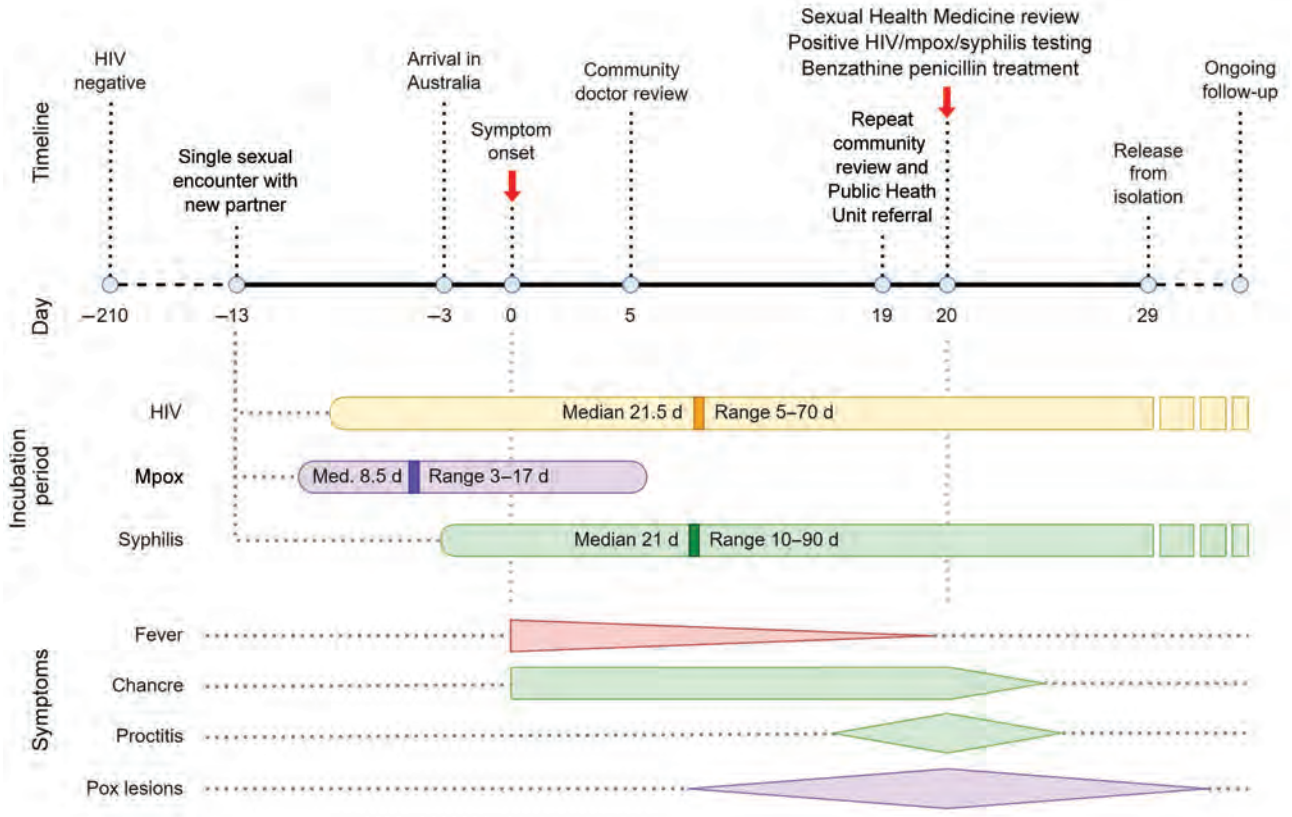

Figure. Timeline of symptom development and infectious vector incubation periods in case of patient with sustained mpox proctitis with primary syphilis and HIV seroconversion, Australia

improve and was deisolated once his skin lesions had resolved.

Severe and protracted mpox infection in persons living with HIV has been described previously (*2*–*5*). Publications have reported mpox co-occurring with HIV (*5*–*7*), syphilis (*8*), COVID-19 (*9*), and varicella zoster (*10*) in up to 15% of mpox cases (*3*). Boesecke et al. (*6*) report a case of severe mpox in the setting of advanced HIV and syphilis. However, no case reports have described mpox in the context of primary syphilis and primary HIV infection. The incubation periods for mpox, HIV infection, and syphilis aligned with the patient's symptom onset 13 days after his only sexual encounter in the preceding 3 months, suggest co-infection likely acquired from a single encounter (Figure 1). This finding could indicate increased transmissibility of ≥1 infection from a partner with multiple infections, especially if the person had active syphilis or mpox skin lesions. Brundu et al. (*5*) postulated a disruption of mucosal integrity by mpox lesions could enable HIV transmission and that HIV infection also enables mpox acquisition. Previous publications have hypothesized local inoculation of the virus aggravated by an immune system dysfunction in the setting of acute HIV infection as a potential mechanism. HIV can result in atypical clinical manifestations of mpox and higher rates of secondary bacterial infections (*2*,*6*,*7*,*9*), consistent with this case-patient's clinical course. This case highlights the need for comprehensive clinical assessment, a broad differential diagnosis, and syndromic testing for MPXV when evaluating patients with anogenital lesions.

Acknowledgments

We thank the New South Wales (NSW) Ministry of Health and Institute of Clinical Pathology and Medical Research for coordination of NSW MPX response and NSW Health Pathology Randwick for diagnostic support.

About the Author

Dr. Burdon is staff specialist at the Sydney Local Health District Department of Sexual Health Medicine. Her research interests include the management and prevention of HIV infection in high-risk and resource-limited settings, sexually transmitted infections, and primary health care of the LGBTQI population.

References:

1. Zhao AV, Crutchley RD, Guduru RC, Ton K, Lam T, Min AC. A clinical review of HIV integrase strand transfer inhibitors (INSTIs) for the prevention and treatment of HIV-1 infection. Retrovirology. 2022;19:22. https://doi.org/10.1186/s12977-022-00608-1
2. Ghazvini K, Keikha M. Human Monkeypox resurgence 2022; a new presentation as a sexual pathogen. Ann Med Surg (Lond). 2022;80:104267. https://doi.org/10.1016/j.amsu.2022.104267
3. Angelo KM, Smith T, Camprubí-Ferrer D, Balerdi-Sarasola L, Díaz Menéndez M, Servera-Negre G, et al.; GeoSentinel Network Collaborators. Epidemiological and clinical characteristics of patients with monkeypox in the GeoSentinel Network: a cross-sectional study. Lancet Infect Dis. 2022;S1473-3099(22)00651-X. https://doi.org/10.1016/S1473-3099(22)00651-X
4. Patrocinio-Jesus R, Peruzzu F. Monkeypox genital lesions. N Engl J Med. 2022;387:66–66. https://doi.org/10.1056/NEJMicm2206893
5. Brundu M, Marinello S, Scaglione V, Ferrari A, Franchin E, Mazzitelli M, et al. The first case of monkeypox virus and acute HIV infection: should we consider monkeypox a new possible sexually transmitted infection? J Dermatol. 2022;1346-8138.16556. https://doi.org/10.1111/1346-8138.16556
6. Boesecke C, Monin MB, van Bremen K, Schlabe S, Hoffmann C. Severe monkeypox-virus infection in undiagnosed advanced HIV infection. Infection. 2022;50:1633–4. https://doi.org/10.1007/s15010-022-01901-z
7. de Sousa D, Patrocínio J, Frade J, Correia C, Borges-Costa J, Filipe P. Human monkeypox coinfection with acute HIV: an exuberant presentation. Int J STD AIDS. 2022;33:936–8. https://doi.org/10.1177/09564624221114998
8. Bížová B, Veselý D, Trojánek M, Rob F. Coinfection of syphilis and monkeypox in HIV positive man in Prague, Czech Republic. Travel Med Infect Dis. 2022;49:102368. https://doi.org/10.1016/j.tmaid.2022.102368
9. Nolasco S, Vitale F, Geremia A, Tramuto F, Maida CM, Sciuto A, et al. First case of monkeypox virus, SARS-CoV-2 and HIV co-infection. J Infect. 2022;S0163-4453(22)00479-0. https://doi.org/10.1016/j.jinf.2022.08.014
10. Hughes CM, Liu L, Davidson WB, Radford KW, Wilkins K, Monroe B, et al. A tale of two viruses: coinfections of monkeypox and varicella zoster virus in the Democratic Republic of Congo. Am J Trop Med Hyg. 2020;104:604–11. https://doi.org/10.4269/ajtmh.20-0589

Address for correspondence: Rachel Burdon, Department of Sexual Health Medicine, Sydney Local Health District, 16 Marsden St, Camperdown, NSW 2050, Australia; email: Rachel.Burdon@health.nsw.gov.au

Intrahost Monkeypox Virus Genome Variation in Patient with Early Infection, Finland, 2022

Hanna Vauhkonen, Hannimari Kallio-Kokko, Eija Hiltunen-Back, Lasse Lönnqvist, Jaana Leppäaho-Lakka, Laura Mannonen, Ravi Kant, Tarja Sironen, Satu Kurkela, Maija Lappalainen, Tomaž Mark Zorec, Samo Zakotnik, Doroteja Vlaj, Miša Korva, Tatjana Avšič-Županc, Mario Poljak, Teemu Smura, Olli Vapalahti

Author affiliations: University of Helsinki, Helsinki, Finland (H. Vauhkonen, R. Kant, T. Sironen, T. Smura, O. Vapalahti); University of Helsinki and Helsinki University Hospital, Uusimaa, Finland (H. Kallio-Kokko, L. Mannonen, S. Kurkela, M. Lappalainen, T. Smura, O. Vapalahti); University of Helsinki and Helsinki University Hospital, Helsinki (E. Hiltunen-Back, L. Lönnqvist); Hospital Nova of Central Finland, Helsinki (J. Leppäaho-Lakka); University of Ljubljana, Ljubljana, Slovenia (T.M. Zorec, S. Zakotnik, D. Vlaj, M. Korva, T. Avšič-Županc, M. Poljak)

DOI: https://doi.org/10.3201/eid2903.221388

Monkeypox virus was imported into Finland during late May–early June 2022. Intrahost viral genome variation in a sample from 1 patient comprised a major variant with 3 lineage B.1.3–specific mutations and a minor variant with ancestral B.1 nucleotides. Results suggest either ongoing APOBEC3 enzyme–mediated evolution or co-infection.

During 2022, an unprecedented multicountry outbreak of monkeypox virus (MPXV) infection among humans was detected. The first verified mpox cases in Europe were reported in mid-May 2022 with no apparent link to MPXV-endemic countries, but patients shared travel history to Lisbon, Portugal, and Gran Canaria, Canary Islands, as well as sexual behavior (men who have sex with men [MSM]) (*1*). The first draft sequence of the outbreak-related genome from Portugal was published on May 19, 2022 (J. Isidro, unpub. data, https://virological.org/t/first-draft-genome-sequence-of-monkeypox-virus-associated-with-the-suspected-multi-country-outbreak-may-2022-confirmed-case-in-portugal/799). During the following weeks, several closely related MPXV genomes were reported from other countries in Europe, resulting from travel-associated and community-transmitted infections. The clinical picture of those infections (anogenital lesions or rash and enlarged

inguinal lymph nodes) (*2*), together with the epidemiologic data, suggested human-to-human transmission by sexual contact, mainly among MSM (*3*); however, other routes of transmission may also have played roles (*4*). As the number of verified mpox cases increased, on July 23, 2022, the World Health Organization declared MPXV a Public Health Emergency of International Concern (https://www.who.int/director-general/speeches), although the epidemic has since waned. We describe the molecular and clinical characteristics of MPXV introduced to Finland during late May–early June 2022 (Table). The patients provided written informed consent for use of their case details and medical images in this study.

We investigated 4 patients who exhibited systemic mpox symptoms, such as fever and skin lesions (Appendix, https://wwwnc.cdc.gov/EID/article/29/3/22-1388-App1.pdf). The patients were epidemiologically unrelated to each other; however, all reported travel in southern Europe, declared themselves to be MSM, and declared recent unprotected sexual exposure with previously unknown partners (Table). Two patients were HIV positive. Orthopoxvirus real-time PCR of individual skin lesion samples detected orthopoxvirus, which was later verified as MPXV by hemagglutinin gene sequencing with MinION (Oxford Nanopore Technologies, https://nanoporetech.com) (Appendix). The sample from patient 1 was also sequenced by MinION and on May 27, 2022, produced an MPXV draft genome. The whole genomes of all samples were subsequently sequenced by using Illumina NovaSeq (https://www.illumina.com). As of November 8, 2022, the total number of verified cases in Finland reached 42, but no further virus transmission from those patients has been reported.

We obtained complete MPXV genomes from 3 of the 4 patients: patient 1 (penis, quantitative cycle [Cq] 19.77), patient 2 (face, Cq 26.29), and patient 4 (perianal skin, Cq 23.4); we could obtain only a fragmental genome from patient 3 (hand, Cq 33.38). In the phylogenetic analysis, the consensus sequence of MPXV genome from patient 1 (GenBank accession no. ON782021) clustered with lineage B.1.3 genomes (Figure). The members of that cluster share 3 substitutions: nonsynonymous G55133A (R665C in OPG074 protein), synonymous C64426T, and nonsynonymous G190660A (R84K in NTB03_gb174 protein), according to National Center for Biotechnology Information reference sequence NC_063383 coordinates (equivalent to the mutations addressed as G55142A, C64435T, G190675A [*5*]). The sequence from patient 2 (GenBank accession no. ON782022) was identical to the early sequences first detected in Portugal (*6*) and thereafter in various other countries. The sequence from patient 4 (GenBank accession no. ON959143) had 4 nt substitutions: C89906T (OPG110: S92F), G94798A (OPG115: E47K), C150831T, and C188491T. Two of those sequences (C89906T and G94798A) were shared with genomes from the United Kingdom, Portugal, Spain, and Germany.

The 3 nt substitutions detected in the patient 1 sequence were not fixed but rather contained minority variants with the frequencies of 10% (G55133A, depth 2231; nucleotide counts G = 233, A = 1997), 12% (C64426T, depth 2685; C = 308, T = 2364), and 13% (G190660A, depth 2685; G = 280, A = 1872). On the other hand, in the members of the same clade from Slovenia (GenBank accession no. ON609725) and France (GenBank accession no. ON622722), all 3 mutations were fixed (allele frequency >99.7%). The mutational signature of the major and minor intralesion single-nucleotide variant (SNV) findings in patient 1 is consistent with the effects of the human apolipoprotein B mRNA-editing catalytic polypeptide-like 3 (APOBEC3) enzyme, which has been suggested to drive the CT>TT and GA>AA conversions

Table. Patient data from study of intrahost viral genome variation from 4 patients with early monkeypox virus infection, Finland, 2022*

Data	Patient no. 1	2	3	4
Age, y	30s	20s	30s	30s
Onset of symptoms	May 19	May 21	Jun 1	Jun 13
Systemic signs/symptoms	Fever, enlarged inguinal lymph nodes	Fever, headache, exhaustion, enlarged inguinal lymph nodes	Fever, myalgia, lymphadenopathy, nausea, myalgia	Fever, headache, anal itch
Lesion sites	Penis	Penis, neck, trunk, face	Trunk, hands, feet, anus	Perianal skin
Evolution of lesions	Synchronous	Asynchronous	Asynchronous	Synchronous
Swab sample lesion sites (C_q value)	Penis (19.77)	Face (26.29), trunk (31.94)	Hand (33.38)	Perianal skin (23.4)
Monkeypox virus sequence†	ON782021‡	ON782022 (face)	NA	ON959143
Sample date	May 24, D5	May 31, D10	Jun 5, D4	Jun 16, D3

*All 4 patients were men who have sex with men who had recent sexual exposure and who had traveled to southern Europe. Cq value, quantitative cycle value of diagnostic orthopoxvirus PCR (Appendix, https://wwwnc.cdc.gov/EID/article/29/3/22-1388-App1.pdf); D, day after first symptom onset; NA, not available.
†GenBank accession numbers.
‡Majority sequence.

in recent MPXV evolution (*6*; A. O'Toole et al., unpub. data, https://virological.org/t/initial-observations-about-putative-apobec3-deaminase-editing-driving-short-term-evolution-of-mpxv-since-2017/830). A similar phenomenon, the fixation of minor intralesion SNVs along the transmission chain, was observed in 5 of the 15

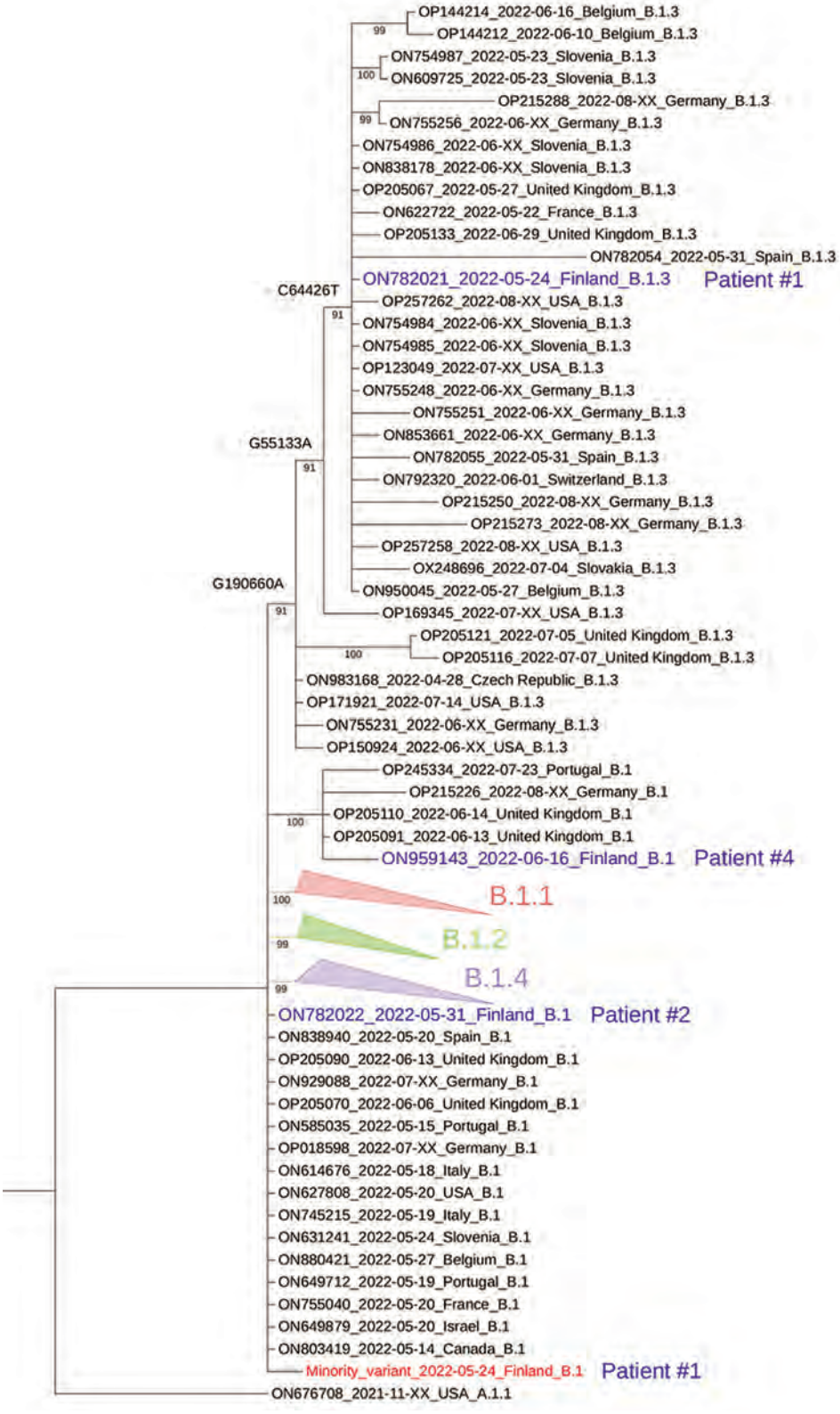

Figure. Phylogenetic tree of monkeypox virus (MPXV) sequences used in study of intrahost viral genome variation in patient with early monkeypox virus infection, Finland, 2022. The tree was inferred by the maximum-likelihood method implemented in IQtree2 software (www.iqtree.org), using 1,000 bootstrap replicates and the Hasegawa-Kishino-Yano plus empirical base frequencies plus invariate sites substitution model (Appendix, https://wwwnc.cdc.gov/EID/article/29/3/22-1388-App1.pdf). The curated dataset of MPXV reference genomes was downloaded from Nextstrain and aligned by using Nextalign (*5*). The reference dataset was downsampled to include only genomes with <5,000 ambiguous genome sites. For the sake of visualization, nodes with bootstrap values <70, as well as clusters with no lineage designation and no representatives from Finland, were deleted; only a subset of nearly identical genomes in the B.1 lineage is shown. Blue indicates the consensus sequences from the 4 patients from Finland; red indicates the hypothetical minority variant sequence (differing from the consensus sequence at sites G55133, C64426, and G190660) from patient 1. Lineage nomenclature (MPXV-1 clade 3, lineage B.1) is as suggested (C. Happi, unpub. data, https://virological.org/t/urgent-need-for-a-non-discriminatory-and-non-stigmatizing-nomenclature-for-monkeypox-virus/8537). The tapering bars indicate clusters of B.1.1 (pink), B.1.2 (green), and B.1.3 (blue), collapsed for clarity. Sequences are identified by GenBank accession number, date, and country of origin.

samples from Portugal sequenced in May 2022 (*6*) and in a publicly available MPXV sequence dataset (A. Nekrutenko et al., unpub. data, https://virological.org/t/mpxv-intrahost-variation-in-the-context-of-apobec-deamination-an-initial-look/856), suggesting that this pattern might be a general pattern of evolution for the 2022 MPXV outbreak. However, in contrast to the previous findings (*6*; A. Nekrutenko et al., unpub. data, https://virological.org/t/mpxv-intrahost-variation-in-the-context-of-apobec-deamination-an-initial-look/856), both the major and minor SNV genotypes from patient 1 could be found fixed in previously reported MPXV sequences.

In conclusion, we demonstrate intrahost MPXV variation within a single lesion from one of the patients with infection introduced to Finland. Most of the sequence reads in that sample contained APOBEC3-related mutations, which may have emerged from the ancestral minor variant present in this sample. However, because the majority and minority nucleotides in that sample are also found fixed in sequences from other countries, we cannot resolve whether this observation relates to contemporary APOBEC3-driven evolution or to co-infection.

Acknowledgments

We gratefully acknowledge the patients for providing consent. We acknowledge the CSC-IT Center for Science, Finland, for providing computational resources.

This study was supported by the Finnish Scientific Advisory Board for Defense, the Academy of Finland (grant no. 336490, 339510), VEO—European Union's Horizon 2020 (grant no. 874735), the Finnish Institute for Health and Welfare, the Jane and Aatos Erkko Foundation, and Helsinki University Hospital Funds (TYH2021343). The study was also supported by the Slovenian Research Agency (research program no. P3-0083).

About the Author

Dr. Vauhkonen is a laboratory coordinator in the Department of Virology at the University of Helsinki. Her research interests include molecular epidemiology of viral zoonoses and next-generation sequencing.

References

1. Perez Duque M, Ribeiro S, Martins JV, Casaca P, Leite PP, Tavares M, et al. Ongoing monkeypox virus outbreak, Portugal, 29 April to 23 May 2022. Euro Surveill. 2022;27:2200424. https://doi.org/10.2807/1560-7917.ES.2022.27.22.2200424
2. Thornhill JP, Barkati S, Walmsley S, Rockstroh J, Antinori A, Harrison LB, et al. Monkeypox virus infection in humans across 16 countries—April–June 2022. N Engl J Med. 2022;387:679–91. https://doi.org/10.1056/NEJMoa2207323
3. Iñigo Martínez J, Gil Montalbán E, Jiménez Bueno S, Martín Martínez F, Nieto Juliá A, Sánchez Díaz J, et al. Monkeypox outbreak predominantly affecting men who have sex with men, Madrid, Spain, 26 April to 16 June 2022. Euro Surveill. 2022;27:2200471. https://doi.org/10.2807/1560-7917.ES.2022.27.27.2200471
4. Karan A, Styczynski AR, Huang CH, Sahoo MK, Srinivasan K, Pinsky BA, et al. Human monkeypox without viral prodrome or sexual exposure, California, USA, 2022. Emerg Infect Dis. 2022;28:2121–3. https://doi.org/10.3201/eid2810.221191
5. Hadfield J, Megill C, Bell SM, Huddleston J, Potter B, Callender C, et al. Nextstrain: real-time tracking of pathogen evolution. Bioinformatics. 2018;34:4121–3. https://doi.org/10.1093/bioinformatics/bty407
6. Isidro J, Borges V, Pinto M, Sobral D, Santos JD, Nunes A, et al. Phylogenomic characterization and signs of microevolution in the 2022 multi-country outbreak of monkeypox virus. Nat Med. 2022;28:1569–72. https://doi.org/10.1038/s41591-022-01907-y

Address for correspondence: Hanna Vauhkonen and Olli Vapalahti, Department of Virology, University of Helsinki, Haartmaninkatu 3, 00014, Helsinki, Uusimaa, Finland; email: hanna.vauhkonen@helsinki.fi and olli.vapalahti@helsinki.fi

New Postmortem Perspective on Emerging SARS-CoV-2 Variants of Concern, Germany

Fabian Heinrich,[1] Tobias Huter,[1] Sophie Mertens, Philine Lange, Jessica Vering, Axel Heinemann, Dominik Sebastian Nörz, Armin Hoffmann, Martin Aepfelbacher, Benjamin Ondruschka,[1] Susanne Krasemann,[1] Marc Lütgehetmann[1]

Author affiliation: University Medical Center Hamburg-Eppendorf, Hamburg, Germany

DOI: https://doi.org/10.3201/eid2903.221297

We performed autopsies on persons in Germany who died from COVID-19 and observed higher nasopharyngeal SARS-CoV-2 viral loads for variants of concern (VOC) compared with non-VOC lineages. Pulmonary inflammation and damage appeared higher in non-VOC than VOC lineages until adjusted for vaccination status, suggesting COVID-19 vaccination may mitigate pulmonary damage.

[1]These authors contributed equally to this article.

SARS-CoV-2 emerged in 2020, and after rapid global spread, virus variants emerged that had adaptation or immune evasion mutations and were classified as variants of concern (VOCs). Although the first VOCs, Alpha (B.1.1.7) and Delta (B.1.617.2), showed enhanced transmissibility (*1*), Omicron (B.1.1.529) lineages carry mutations that provide strong immune evasion after infection with previous lineages or mRNA vaccination (*2*). Because autopsy data are lacking, differences in SARS-CoV-2–related pulmonary disease and tropisms have not been well studied. In this study, we performed full autopsies of persons

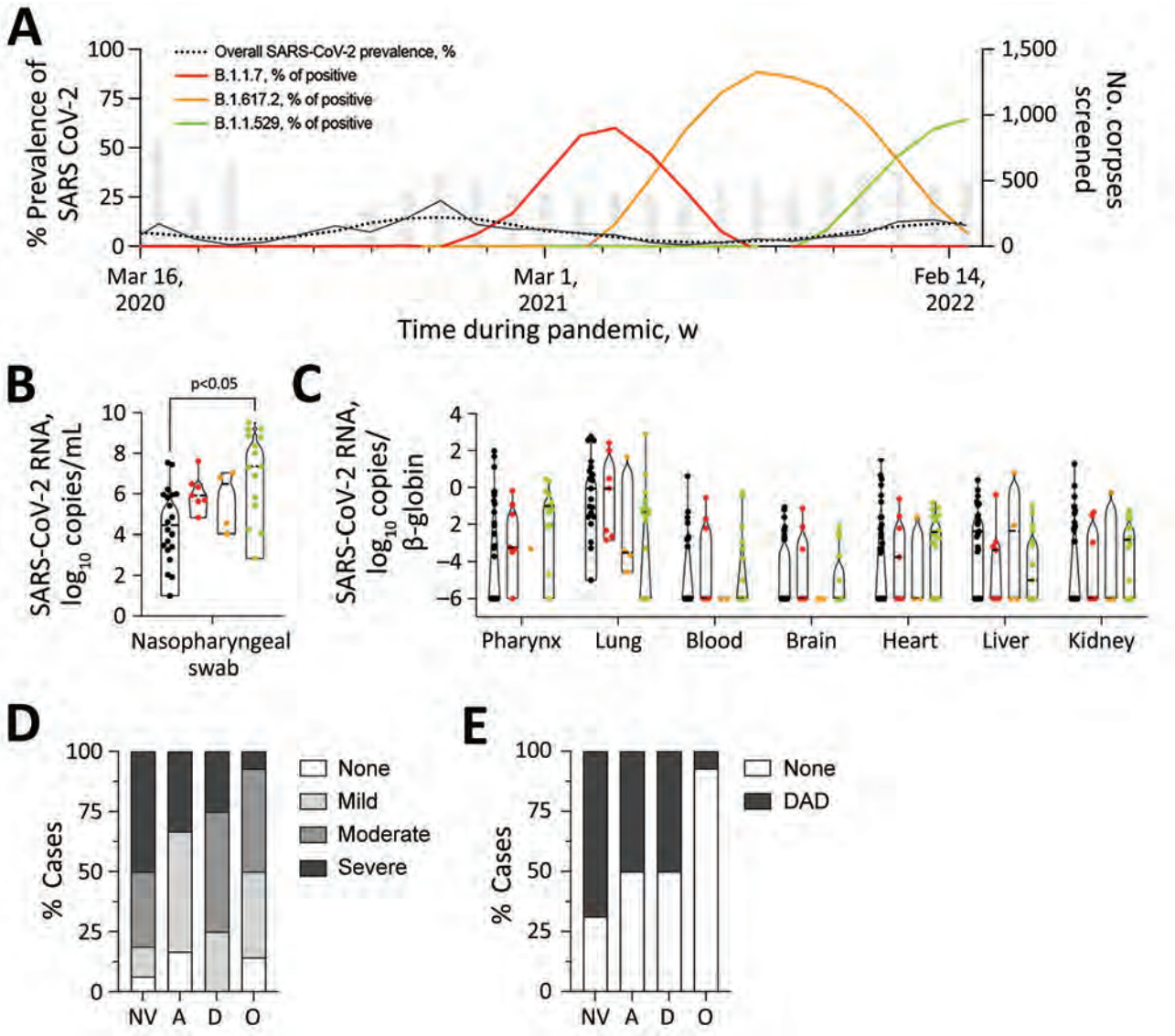

Figure. Prevalence of SARS-CoV-2 variants, pulmonary inflammation, and diffuse alveolar damage in corpses autopsied during 2020 and 2022 at the Institute of Legal Medicine and crematoria in Hamburg, Germany. A) Overall prevalence of corpses positive for SARS-CoV-2 mRNA and prevalence of B.1.1.7 (Alpha), B.1.617.2 (Delta), and B.1.1.529 (Omicron) variants of concern as the percentage of SARS-CoV-2 mRNA-positive corpses are depicted; 3-point centered moving averages are shown. Gray bars indicate monthly number of corpses screened for SARS-CoV-2 mRNA. B, C) Number of SARS-CoV-2 mRNA copies in different autopsy specimens. Median and interquartile ranges of viral mRNA loads were stratified according to virus variants in nasopharyngeal swabs (B) and different organs (C). Nasopharyngeal and organ viral loads for non-VOC and B.1.1.7 were published in part previously (*7*,*8*). Black dots are non-VOC lineages. Pairwise comparisons were performed by using the Kruskal-Wallis H test and Dunn post-hoc analysis. D, E) Percentage of cases that had pulmonary inflammation or alveolar damage caused by different SARS-CoV-2 lineages: NV, Non-VOC lineage; A, Alpha B.1.1.7 lineage; D, Delta B.1.617.2 lineage; O, Omicron B.1.1.529 lineage. D) We scored microscopic pulmonary inflammation as follows: none, 0; mild, 1; moderate, 2; or severe, 3 on the basis of a Likert-like scale and calculated percentages of cases within each group for each SARS-CoV-2 variant. E) Percentage of corpses infected with non-VOC lineages (n = 16) and the VOC lineages B.1.1.7 (Alpha, n = 6), B.1.617.2 (Delta, n = 4), and B.1.1.529 (Omicron, n = 14) that had DAD in lungs. DAD, diffuse alveolar damage; VOC, variant of concern.

Table. Baseline characteristics of persons whose deaths were associated with SARS-CoV-2 infection, grouped according to SARS-CoV-2 virus variant in study of new postmortem perspective on emerging SARS-CoV-2 variants of concern, Germany*

Variable	Non-VOC lineages	B.1.1.7†	B.1.617.2†	B.1.1.529†	p value	Cohort total
No. corpses	23	7	4	15	NA	49
Age, y, median (IQR)	76.0 (70.0–85.0)	75.0 (52.0–77.0)	50.5 (42.5–70.0)	75.0 (58.0–87.0)	0.29	75.0 (63.0–85.0)
Sex					0.31	
M	15 (65.2)	4 (57.1)	2 (50.0)	5 (33.3)	NA	26 (53.1)
F	8 (34.8)	3 (42.9)	2 (50.0)	10 (66.7)	NA	23 (46.9)
BMI, kg/m^2, median (IQR)	25.3 (20.7–31.9)	29.5 (26.1–34.8)	38.4 (16.5–42.9)	22.6 (18.8–23.6)	0.02	24.8 (20.7–31.0)
COVID-19 deaths	20 (87.0)	6 (85.7)	3 (75.0)	3 (20.0)	<0.0001	32 (65.3)
No. underlying conditions, median (IQR)	4.0 (3.0–4.0)	2.0 (2.0–3.0)	3.0 (2.0–5.0)	4.0 (2.0–5.0)	0.24	3.5 (2.0–4.0)
Place of death					0.23	
Home	5 (21.7)	3 (42.9)	0 (0.0)	5 (33.3)	NA	13 (26.5)
Normal ward	9 (39.1)	2 (28.6)	2 (50.0)	2 (13.3)	NA	15 (30.6)
ICU	5 (21.7)	2 (28.6)	2 (50.0)	2 (13.3)	NA	11 (22.4)
Other	4 (17.4)	0 (0.0)	0 (0.0)	6 (40.0)	NA	10 (20.4)
PMI, d, median (IQR)	1.0 (0.0–1.0)	3.0 (1.0–6.0)	1.0 (1.0–1.5)	0.0 (0.0–1.0)	0.03	1.0 (0.0–2.0)
Vaccination	0 (0.0)	1 (7.7)	1 (7.7)	11 (84.6)	<0.0001	13 (27.1)

*Corpses were admitted to the Institute of Legal Medicine, University Medical Center Hamburg-Eppendorf, Hamburg, Germany, for autopsy during 2020–22. Values are no. (%) unless otherwise noted. BMI, body mass index; ICU, intensive care unit; IQR, interquartile range; NA, not applicable; PMI, postmortem interval (time elapsed from death until cooling at 4°C); VOC, variant of concern.
†VOC lineages B.1.1.7 (Alpha), B.1.617.2 (Delta), and B.1.1.529 (Omicron).

who died from COVID-19 and conducted comprehensive analyses to characterize COVID-19–related cases macroscopically and microscopically.

All corpses admitted to the Institute of Legal Medicine (n = 8,578) and crematoria (n = 1,705) in Hamburg, Germany, during March 3, 2020–March 31, 2022, were screened for SARS-CoV-2 mRNA by quantitative reverse transcription PCR (*3*). We found a total of 808 SARS-CoV-2 RNA-positive corpses; median monthly prevalence was 6.54% in 2020, 5.28% in 2021, and 12.50% in 2022 (Figure, panel A). In comparison, the median monthly prevalence of SARS-CoV-2 in Hamburg's general population was 0.10% in 2020, 0.37% in 2021, and ≈5.20% in 2022 (https://de.statista.com/statistik/daten/studie/1106006/umfrage/entwicklung-der-fallzahl-des-coronavirus-in-hamburg). A considerably higher prevalence of virus in deceased persons than in the general population can be explained by an older age in postmortem cohorts, targeted transport of clinically suspected or confirmed COVID-19 deaths to the Institute of Legal Medicine in 2020, and underreporting of overall SARS-CoV-2 prevalence because of limited availability of molecular testing.

We further characterized SARS-CoV-2 RNA-positive samples by using multiplexed typing quantitative reverse transcription PCR (*4*,*5*). The occurrence of VOCs among corpses (B.1.1.7 for December 2020–March 2022, B.1.617.2 beginning in May 2021, and B.1.1.529 beginning in November 2021) reflected their occurrence within the general population but had a 2–4 week delay (https://www.leibniz-liv.de/de/aktuelles/covid-19/daten-der-hamburg-surveillance-plattform).

Of the 808 COVID-19–associated deaths (determined by postmortem SARS-CoV-2 RNA detection), we autopsied 49 corpses and collected multiorgan tissue samples for more detailed analyses. We included 23/49 consecutive deceased persons infected with non-VOC lineages and 26/49 consecutive deceased persons infected with VOCs (B.1.1.7, n = 7; B.1.617.2, n = 4; and B.1.1.529, n = 15) (Table). We processed formalin-fixed paraffin-embedded tissue for histologic and immunohistochemical staining and cryopreserved tissue for molecular analysis as previously described (*3*,*6*).

The median nasopharyngeal SARS-CoV-2 RNA load was 5.82 (interquartile range [IQR] 4.08–7.31) $\log_{10}$ copies/mL (Figure, panel B). Nasopharyngeal and organ viral loads for non-VOC and B.1.1.7 were published in part previously (*7*,*8*). We observed strong evidence for a difference in mean nasopharyngeal viral loads by virus variant (p = 0.01); by using multiple comparisons, we observed a difference in means between B.1.1.529 and non-VOC lineages (p = 0.002; Figure, panel B). This result supports increased infectivity of B.1.1.529 compared with non-VOC lineages (*9*). An association between nasopharyngeal virus load and virus variant at the 5% significance level did not persist in a multivariable

model adjusted for the deceased's vaccination status, which might be because of the small sample size (Appendix Tables 1, 2, https://wwwnc.cdc.gov/EID/article/29/3/22-1297-App1.pdf). Of note, the pulmonary virus load was strongly associated with viremia (odds ratio 2.21, 95% CI 1.34–3.63; p = 0.002) and mRNA detection in peripheral organs (odds ratio 1.54, 95% CI 1.10–2.16; p = 0.01) in univariable logistic regression models. However, normalized SARS-CoV-2 RNA loads in peripheral organs did not differ between virus variants (Figure, panel C).

Experienced pathologists performed single-blind histologic assessments. We detected SARS-CoV-2 nucleocapsid protein in the lungs of 25/41 (61%) cases. Using a Likert-like scale, we found the median abundance of SARS-CoV-2 nucleocapsid protein (0, not detected; 1, low abundance; 2, intermediate abundance; 3, high abundance) was 1 (IQR 0–2) for non-VOC lineage, 1.5 (IQR 1–2) for B.1.1.7, 0.5 (IQR 0–1) for B.1.617.2, and 0 (IQR 0–1) for B.1.1.529 cases (p = 0.03) (Appendix Figure).

We detected mild to strong inflammatory changes in the lungs of 36/40 (90%) cases and microscopic signs of diffuse alveolar damage (DAD), indicating acute respiratory distress syndrome, in 17/40 (43%) cases (Figure, panels D, E). As in recent animal experiments (*10*), pulmonary changes, such as inflammation and DAD, were associated with virus variant at the 5% level (Appendix Tables 3, 4) but not with nasopharyngeal or pulmonary viral load (inflammatory changes, p>0.05; DAD, p>0.05). An association between virus variants and inflammatory changes or DAD at the 5% level did not persist in a multivariable model adjusted for the deceased's vaccination status (Appendix Tables 5–7).

In conclusion, our data confirm higher SARS-CoV-2 mRNA loads in nasopharynges of deceased persons who were infected with the B.1.1.529 VOC lineage, but we observed no differences in pulmonary or tertiary organ viral loads. However, pulmonary inflammation appeared higher and DAD more frequent in non-VOC than VOC lineages until adjustment for vaccination status. Our results suggest that prior vaccination, rather than reduced virulence of virus variants, might convey protection against pulmonary inflammation and acute respiratory distress syndrome during SARS-CoV-2 infections.

Acknowledgments

We thank Christiane Stark and Kristin Hartmann for technical support and Daniela Fröb for managing the logistics of SARS-CoV-2–associated incoming corpses within the Institute of Legal Medicine.

We offer condolences to the families and friends of all the patients whose deaths were attributed to COVID-19.

This work was funded by the research consortium NATON. The NATON project (grant no. 01KX2121) is part of the National Network University Medicine funded by the Federal Ministry of Education and Research, Germany. The National Network University Medicine is coordinated at the Charité–Universitätsmedizin Berlin and supervised by the German Aerospace Center (DLR Project Management Agency). The funders had no role in study design, data collection, and analysis, decision to publish, or preparation of the manuscript.

About the Author

Dr. Heinrich is a medical doctor at the Institute of Legal Medicine, University Medical Center Hamburg-Eppendorf, Germany. His primary research interests focus on infectious disease and immunology.

References

1. Choi JY, Smith DM. SARS-CoV-2 variants of concern. Yonsei Med J. 2021;62:961–8. PubMed https://doi.org/10.3349/ymj.2021.62.11.961
2. Pulliam JRC, van Schalkwyk C, Govender N, von Gottberg A, Cohen C, Groome MJ, et al. Increased risk of SARS-CoV-2 reinfection associated with emergence of Omicron in South Africa. Science. 2022;376:eabn4947. PubMed https://doi.org/10.1126/science.abn4947
3. Heinrich F, Romich C, Zimmermann T, Kniep I, Fitzek A, Steurer S, et al. Dying of VOC-202012/01—multimodal investigations in a death case of the SARS-CoV-2 variant. Int J Legal Med. 2022;136:193–202. https://doi.org/10.1007/s00414-021-02618-8
4. Nörz D, Grunwald M, Olearo F, Fischer N, Aepfelbacher M, Pfefferle S, et al. Evaluation of a fully automated high-throughput SARS-CoV-2 multiplex qPCR assay with built-in screening functionality for del-HV69/70- and N501Y variants such as B.1.1.7. J Clin Virol. 2021;141:104894 https://doi.org/10.1016/j.jcv.2021.104894
5. Nörz D, Grunwald M, Tang HT, Weinschenk C, Günther T, Robitaille A, et al. Clinical evaluation of a fully-automated high-throughput multiplex screening-assay to detect and differentiate the SARS-CoV-2 B.1.1.529 (Omicron) and B.1.617.2 (Delta) lineage variants. Viruses. 2022;14:608. PubMed https://doi.org/10.3390/v14030608
6. Krasemann S, Dittmayer C, von Stillfried S, Meinhardt J, Heinrich F, Hartmann K, et al. Assessing and improving the validity of COVID-19 autopsy studies—a multicentre approach to establish essential standards for immunohistochemical and ultrastructural analyses. EBioMedicine. 2022;83:104193 https://doi.org/10.1016/j.ebiom.2022.104193
7. Puelles VG, Lütgehetmann M, Lindenmeyer MT, Sperhake JP, Wong MN, Allweiss L, et al. Multiorgan and renal tropism of SARS-CoV-2. N Engl J Med. 2020;383:590–2. PubMed https://www.nejm.org/doi/10.1056/NEJMc2011400
8. Ondruschka B, Heinrich F, Lindenmeyer M, Edler C, Möbius D, Czogalla J, et al. Multiorgan tropism of

SARS-CoV-2 lineage B.1.1.7. Int J Legal Med. 2021;135:2347–9. PubMed https://link.springer.com/article/10.1007/s00414-021-02691-z
9. Walsh KA, Jordan K, Clyne B, Rohde D, Drummond L, Byrne P, et al. SARS-CoV-2 detection, viral load and infectivity over the course of an infection. J Infect. 2020;81:357–71. https://doi.org/10.1016/j.jinf.2020.06.067
10. Mohandas S, Yadav PD, Sapkal G, Shete AM, Deshpande G, Nyayanit DA, et al. Pathogenicity of SARS-CoV-2 Omicron (R346K) variant in Syrian hamsters and its cross-neutralization with different variants of concern. EBioMedicine. 2022;79:103997. https://doi.org/10.1016/j.ebiom.2022.103997

Address for correspondence: Fabian Heinrich, Center for Diagnostics, Institute of Legal Medicine, University Medical Center Hamburg Eppendorf, Butenfeld 34, 20259 Hamburg, Germany; email: fa.heinrich@uke.de

Possible Mpox Protection from Smallpox Vaccine–Generated Antibodies among Older Adults

Iván Sanz-Muñoz, Laura Sánchez-dePrada, Javier Sánchez-Martínez, Silvia Rojo-Rello, Marta Domínguez-Gil, Cristina Hernán-García, Virginia Fernández-Espinilla, Raúl Ortiz de Lejarazu-Leonardo,[1] Javier Castrodeza-Sanz,[1] José María Eiros[1]

DOI: https://doi.org/10.3201/eid2903.221231

Author affiliations: National Influenza Centre, Valladolid, Spain (I. Sanz-Muñoz, L. Sánchez-dePrada, J. Sánchez-Martínez, S. Rojo-Rello, M. Domínguez-Gil, C. Hernán-García, V. Fernández-Espinilla, R. Ortiz de Lejarazu-Leonardo, J. Castrodeza-Sanz, J.M. Eiros); Instituto de Estudios de Ciencias de la Salud de Castilla y León, Soria, Spain (I. Sanz-Muñoz, J. Sánchez-Martínez); Hospital Clínico Universitario de Valladolid Microbiology Unit, Valladolid (S. Rojo-Rello, J.M. Eiros); Hospital Universitario Río Hortega Microbiology Unit, Valladolid (M. Domínguez-Gil, J.M. Eiros); Hospital Clínico Universitario de Valladolid Preventive Medicine and Public Health Unit, Valladolid (C. Hernán-García, V. Fernández-Espinilla, J. Castrodeza-Sanz)

[1]These senior authors contributed equally to this article.

Smallpox vaccination may confer cross-protection to mpox. We evaluated vaccinia virus antibodies in 162 persons ≥50 years of age in Spain; 68.5% had detectable antibodies. Highest coverage (78%) was among persons 71–80 years of age. Low antibody levels in 31.5% of this population indicates that addressing their vaccination should be a priority.

As the 2022 mpox outbreak spread worldwide, protection against smallpox has become a focus of interest because smallpox vaccination might provide some protection against monkeypox virus (*1*). Massive vaccination with live vaccinia virus vaccines was conducted in most countries before smallpox was eradicated in 1980 (*2*), meaning a substantial proportion of persons ≥50 years of age as of 2022 might be protected against both diseases. One suggested approach to mpox protection during the current outbreak has been to administer smallpox vaccine to close contacts of infected persons (*3*,*4*). However, before taking this approach if the outbreak spreads to additional persons, concerns need to be addressed about whether smallpox vaccination provides real cross-protection and, if so, whether protection has waned over time.

We conducted a serologic study among 162 persons ≥50 years of age in Spain who had probably received smallpox vaccination to determine the seroprevalence of vaccinia virus antibodies (VVAbs). We included 10 unvaccinated persons <40 years of age as controls, avoiding persons 40–49 years of age to eliminate possible interference in findings from persons of those ages possibly having been immunized against smallpox in the final years of vaccination. Our aim was to ascertain the presence of residual vaccinia virus immunity among adult/elderly persons. The study was approved by the ethics committee of the Eastern Health Area of Valladolid (cod: PI 22–2798) and research performed according to the Declaration of Helsinki. We obtained written informed consent from participants before sampling.

We used the Anti-Vaccinia virus IMV/Envelop protein/H3L/p35 IgG ELISA (Alpha Diagnostic International, https://www.4adi.com) to detect IgG against the vaccinia envelope protein H3L/p35, following manufacturer specifications (Appendix, https://wwwnc.cdc.gov/EID/article/29/3/22-1231-App1.pdf). VVAb levels were expressed in units per milliliter. We stratified results by age group: 50–60, 61–70, 71–80, and >80 years.

Seroprevalence differed by age group. We found no VVAbs among the control group. Seroprevalence increased with age, until it dropped dramatically

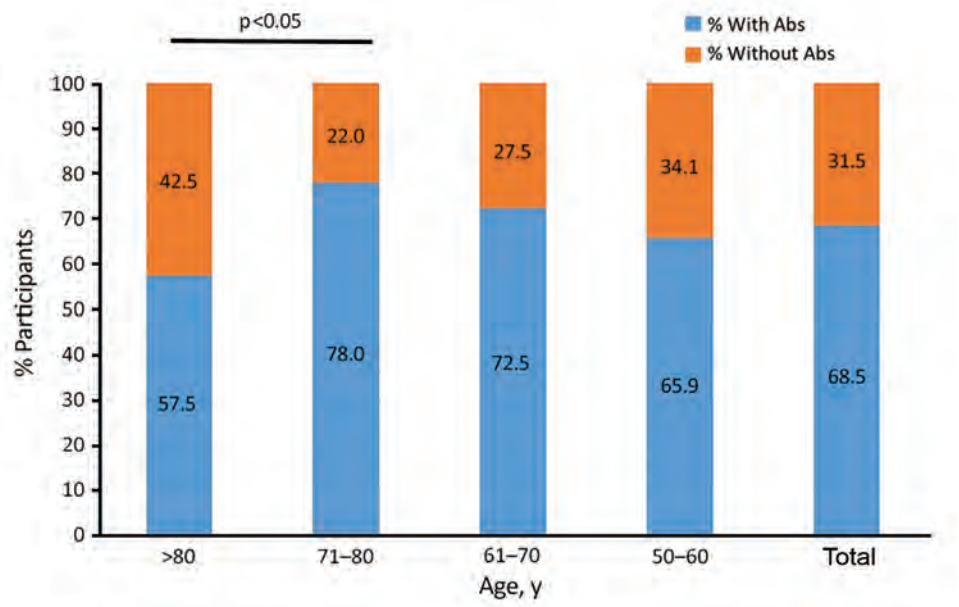

Figure. Seroprevalence of smallpox vaccine–generated antibodies among older adults, Spain. Detectable vaccinia virus antibody levels in the different age groups analyzed and for the total study population are given.

among participants >80 years of age (Figure). The 71–80 year age group exhibited the highest seroprevalence (78.0%), the >80 year group the lowest (57.5%) ($p < 0.05$ by χ^2 test). We found no significant differences in median VVAbs levels between the other age groups.

The relevance of these findings is that, 42 years after the end of routine smallpox vaccination in Spain, 68.5% of persons ≥50 years of age that we tested had detectable antibodies to vaccinia. That the highest seroprevalence was among participants in the 71–80-year age group and gradually decreased among younger age groups is probably explained by declines in smallpox vaccination coverage in Europe over time, rather than by decreased immune response.

Although guidelines for recommended smallpox vaccination did not change during 1937–1980 in most countries in Europe, vaccination coverage in Spain and other countries declined continuously as disease eradication progressed (*5*,*6*). For example, a 2019 article reported that smallpox vaccination coverage in Guinea-Bissau fell dramatically during the 1970s, from 75% to 10%–25% (*7*). Another study, conducted in Denmark, reported that vaccination coverage dropped from 95% in 1965 to 5%–20% among persons born during the 1970s (*8*). In Spain, >6 million smallpox vaccinations were administered in 1961 but only 725,371 in 1970 and 105,573 in 1979 (*5*,*6*). Furthermore, endemic cases in high-income countries declined greatly during the 1950s (*9*). Taken together, those data illustrate that smallpox vaccination coverage steadily declined in most high-income Western countries as smallpox was increasingly confined to low-income countries (*7*). Although an imported outbreak in Yugoslavia in 1972 caused 175 cases and 35 deaths, the last non-imported case in Europe was declared in 1953 (*10*); after that date, persons became less likely to receive smallpox vaccination.

The main limitation of our study is that we did not know the vaccination status of participants and thus could not determine whether lack of VVAbs was because of absence of vaccination or waning of antibodies. In addition, VVAbs levels might not correlate with immune protection against other orthopox viruses. The low number of participants might have affected statistical differences in results between groups. Finally, the absence of conserved cells precluded analysis of cellular immunity.

Our findings suggest that a substantial percentage (31.5%) of persons in Spain born before 1972, especially persons born during the years when routine smallpox vaccination use waned, have either not been vaccinated against smallpox or have lost the VVAbs induced by the vaccine. Assuming 85% maximum cross-protection against monkeypox virus conferred by smallpox vaccination (*1*) and 68.5% of the population ≥50 years of age having detectable VVAbs, we estimated that only 58.2% of persons in those age groups would be protected. Through September 2022, a total of 813 (12.4%) mpox cases in Spain had been reported in persons ≥50 years of age (*11*). Limited vaccine coverage might be one cause of these cases, so vaccination against mpox or with new smallpox vaccines should be a priority in this population.

I.S.M., R.O.L., J.C.S., and J.M.E. designed the study; J.S.M., L.S.D.P., S.R.R., and M.D.D.G. performed the experiments; I.S.M., L.S.D.P., C.H.G., and V.F.E. analyzed the data; I.S.M., L.S.D.P., R.O.L., J.C.S., and J.M.E. wrote the manuscript; R.O.L., J.C.S., and J.M.E. revised the manuscript; all authors edited and revised the final version of the manuscript.

About the Author

Dr. Sanz-Muñoz is a virologist, responsible for science and virological surveillance at the National Influenza Center of Valladolid, Spain. His main interests are virologic and epidemiologic surveillance of influenza viruses, as well as serological studies in diverse populations.

References

1. Centers for Disease Control and Prevention. Interim clinical considerations for use of JYNNEOS and ACAM2000 vaccines during the 2022 U.S. mpox outbreak [cited 2022 Jun 21]. https://www.cdc.gov/poxvirus/monkeypox/clinicians/smallpox-vaccine.html
2. Centers for Disease Control and Prevention. Smallpox [cited 2022 Jul 20]. https://www.cdc.gov/smallpox/index.html
3. World Health Organization. Multi-country monkeypox outbreak in non-endemic countries. 2022 [cited 2022 Jul 20]. https://www.who.int/emergencies/disease-outbreak-news/item/2022-DON385
4. European Centre for Disease Prevention and Control. Monkeypox multi-country outbreak—first update [cited 2022 Jul 20]. https://www.ecdc.europa.eu/sites/default/files/documents/Monkeypox-multi-country-outbreak-first-update-8-July-FINAL3.pdf
5. Carlos III Health Institute. Analysis of healthcare in Spain throughout the 20th century [in Spanish] [cited 2022 Jul 26]. http://gesdoc.isciii.es/gesdoccontroller?action=download&id=19/10/2012-3c0cfd4ca3#page=228
6. Comité Asesor de Vacunas de la Asociación Española de Pediatría. Vaccination against smallpox in Spain in the years prior to its eradication [in Spanish] [cited 2022 Jul 26]. https://vacunasaep.org/profesionales/noticias/la-vacunacion-contra-la-viruela-en-espana-en-los-anos-anteriores-su-erradicacion
7. Rieckmann A, Villumsen M, Hønge BL, Sørup S, Rodrigues A, da Silva ZJ, et al. Phase-out of smallpox vaccination and the female/male HIV-1 prevalence ratio: an ecological study from Guinea-Bissau. BMJ Open. 2019; 9:e031415. https://doi.org/10.1136/bmjopen-2019-031415
8. Sørup S, Villumsen M, Ravn H, Benn CS, Sørensen TIA, Aaby P, et al. Smallpox vaccination and all-cause infectious disease hospitalization: a Danish register-based cohort study. Int J Epidemiol. 2011;40:955–63. https://doi.org/10.1093/ije/dyr063
9. Belongia EA, Naleway AL. Smallpox vaccine: the good, the bad, and the ugly. Clin Med Res. 2003;1:87–92. https://doi.org/10.3121/cmr.1.2.87
10. Centers for Disease Control and Prevention. History of smallpox [cited 2022 Jul 26]. https://www.cdc.gov/smallpox/history/history.html
11. Ministerio de Sanidad. Carlos III Health Institute. Epidemiological situation of monkeypox cases in Spain [in Spanish] [cited 2022 Oct 31]. https://www.isciii.es/QueHacemos/Servicios/VigilanciaSaludPublicaRENAVE/EnfermedadesTransmisibles/Documents/archivos%20A-Z/MPOX/SITUACION%20EPIDEMIOLOGICA%20DE%20LOS%20CASOS%20DE%20VIRUELA%20DEL%20MONO-30082022.pdf

Address for correspondence: Iván Sanz-Muñoz, Centro Nacional de Gripe, Edificio Rondilla, Hospital Clínico Universitario de Valladolid, Calle Rondilla de Santa Teresa s/n, 47009, Valladolid, Spain; email: isanzm@saludcastillayleon.es

SARS-CoV-2 Infection in a Hippopotamus, Hanoi, Vietnam

Vuong Nghia Bui,[1] Tung Duy Dao,[1] Long Hoang Tran, Thanh Thi Vu, Trang Huyen Nguyen, Giang Hoang Nguyen, Kien Viet Dung Tran, Huyen Xuan Nguyen,Anh Ngoc Bui, Fred Unger, Hung Nguyen-Viet, Hu Suk Lee

Author affiliations: National Institute of Veterinary Research, Hanoi, Vietnam (V.N. Bui, T.D. Dao, L.H. Tran, T.T. Vu, T.H. Nguyen, G.H. Nguyen, K.V.D. Tran, A.N. Bui); International Livestock Research Institute, Hanoi (F. Unger, H.S. Lee); International Livestock Research Institute, Nairobi, Kenya (H. Nguyen-Viet); Chungnam National University College of Veterinary Medicine, Daejeon, South Korea (H.S. Lee)

DOI: https://doi.org/10.3201/eid2903.220915

While investigating the death of a hippopotamus at a zoo in Hanoi, Vietnam, we isolated SARS-CoV-2 and sequenced the RNA-dependent RNA polymerase gene from different organs. Phylogenetic analysis showed that the SARS-CoV-2 strain was closely related to 3 human SARS-CoV-2 strains in Vietnam.

On December 4, 2021, a 20-year-old female hippopotamus (*Hippopotamus amphibius*) at a zoo in Hanoi, Vietnam, was treated for lethargy, depression, and reduced appetite. Veterinary staff initiated antimicrobial drug treatment on the basis of the clinical signs.

[1]These first authors contributed equally to this article.

Table. Identification and isolation of SARS-CoV-2 from tissue samples of a hippopotamus, Vietnam

	Real-time RT-PCR result		Virus isolation	
Tissue	All betacoronaviruses	SARS-CoV-2	Vero cells	Real-time RT-PCR result
Lung	27.09	26.67	Positive	26.30
Spleen	33.96	33.53	Positive	33.91
Liver	32.29	31.8	Positive	38.34
Intestine	37.84	36.96	Negative	NA
Blood	Negative	Negative	NA	NA

*NA, not applicable; RT-PCR, reverse transcription PCR.

Six days after onset of clinical signs, the hippopotamus was anorexic; she died 17 days after onset. Zoo staff conducted necropsy; the main finding was severe pneumonia. Tissue samples from the liver, spleen, lung, intestine, and blood were collected and sent to the National Institute of Veterinary Research in Hanoi for further diagnosis of viral and bacterial diseases.

We screened the samples by real-time PCR to detect SARS-CoV-2, in accordance with World Health Organization (WHO) PCR protocol (*1*). The lung, spleen, liver, and intestine samples tested positive; cycle threshold (Ct) values for tissue types were 26.67 for lung, 33.53 for spleen, 31.8 for liver, and 36.96 for intestine. No other viral testing was pursued, and tissues were not examined histologically (data not shown).

To obtain the viral isolate, we inoculated the samples into Vero cells according to a method described previously (*2*). After 3 days, we successfully recovered the virus from the lung, spleen, and liver samples (Table). We confirmed that the recovered viruses from Vero cells were SARS-CoV-2 by real-time PCR. We gave the virus the temporary designation SARS-CoV-2/hippo/zoo/Vietnam/2021.

To further characterize and compare the virus isolated from the hippopotamus and the recent human SARS-CoV-2, we used a seminested reverse transcription PCR assay (*3*) to amplify 599–602 bp of the conserved RNA-dependent RNA polymerase (RdRp) genome sequence of 3 human SARS-CoV-2 strains from COVID-19 patients in Vietnam (selected at the same time as the hippopotamus isolate and afterwards) and the isolates from the dead hippopotamus. We sent the purified PCR products to 1st BASE Company (http://www.base-asia.com), Singapore, to sequence the 599–602-bp nucleotide of the RdRp genome. We submitted the sequences to GenBank (hippopotamus, accession no. ON365747; human, ON365835–7. We conducted multiple alignments of the obtained sequences of the dead hippopotamus and 3 human COVID-19 patients, together with representative nucleotide sequences of SARS-CoV-2 and other betacoronaviruses available in GenBank, using ClustalW in BioEdit version 7.2.5 as previously described (*4*). We performed phylogenetic analysis in MEGA-X software using the maximum-likelihood method with the best-fit model general time reversible plus gamma 4 plus invariate sites and 1,000 bootstrap replicates (*5*). We constructed a Bayesian maximum-clade credibility host discrete traits tree by using BEAST version 1.10.4 (http://tree.bio.ed.ac.uk/software/beast).

Phylogenetic analysis indicated that the sequences obtained from the dead hippopotamus and 3 human COVID-19 patients were SARS-CoV-2 (Figure; Appendix, https://wwwnc.cdc.gov/EID/article/29/3/22-0915-App1.pdf).. The source of the hippopotamus' infection was difficult to pinpoint because the zoo had been open to the public; a visitor or staff member could have been transmitted the virus. As a precaution, all zoo staff were required to wear uniforms, facemasks, and gloves and to disinfect their boots when servicing the animal areas. However, those biosecurity measures were not sufficient to prevent the airborne transmission of the virus from humans to animals. To prevent anthroponotic disease, zoos must closely monitor the health status of zoo staff to eliminate virus transmission from humans to animals. Active surveillance using nasal or oral swab specimens, or fecal samples from animals, is needed for early detection of viral infection. In addition, stricter biosecurity measures are required in zoo exhibit areas to reduce the potential transmission of viruses by visitors to animals. For example, zoos should install glass barriers to separate exhibit areas from pathways for visitors.

This study highlights an urgent need to establish comprehensive monitoring systems for SARS-CoV-2 in animals. Our findings underscore hippopotamuses' susceptibility to SARS-CoV-2 and further contribute to the knowledge of the epidemiology of SARS-CoV-2, especially regarding the virus's host range. Whole-genome sequencing will provide information about SARS-CoV-2 lineage to help track transmission pathways.

Acknowledgments

We thank Ngo Thi Minh Quyen and other members of our laboratory in the Department of Virology at the National Institute of Veterinary Research for technical support. We thank Tezira Lore for language editing work.

Figure. Maximum-likelihood tree constructed for 600-bp RNA-dependent RNA polymerase gene SARS-CoV-2 nucleotide sequences from a hippopotamus (red circle) and 3 human SARS-CoV-2 strains from COVID-19 patients in Vietnam (red triangles) compared with reference betacoronavirus strains obtained from GenBank. Betacoronavirus lineages are indicated on the right of the figure. Scale bar denotes evolutionary distance. MERS, Middle Eastern respiratory syndrome.

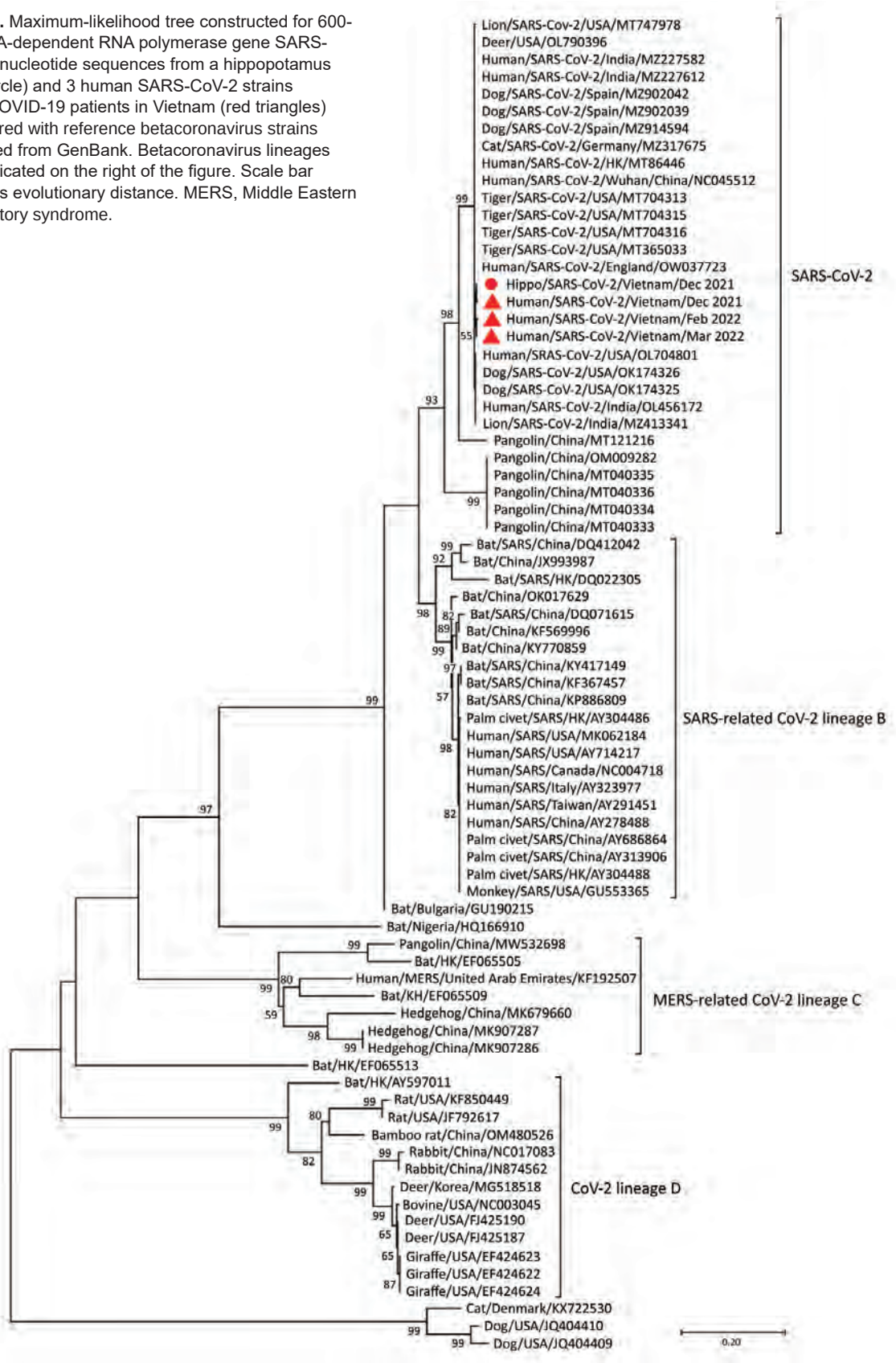

This study was funded by the Consultative Group for International Agricultural Research (CGIAR) COVID-19 Hub and the CGIAR Initiative "Protecting human health through a One Health approach."

About the Author

Dr. Bui is a research scientist and leader in the Department of Virology, National Institute of Veterinary Research, Hanoi, Vietnam. His research interests are molecular epidemiology, pathogenesis of viruses, and viral diseases. Dr. Dao is a research scientist in the Department of Virology, National Institute of Veterinary Research. His research interests include molecular epidemiology, biology, and bioinformatics analysis of influenza virus, coronavirus, foot-and-mouth disease virus, classical swine fever, African swine fever, porcine reproductive and respiratory syndrome, porcine circovirus type 2, hepatitis E virus, dengue virus, and other viruses.

References

1. World Health Organization. Protocol: real-time RT-PCR assays for the detection of SARS-CoV-2. 2020 [cited 2023 Jan 20]. https://www.who.int/docs/default-source/coronaviruse/real-time-rt-pcr-assays-for-the-detection-of-sars-cov-2-institut-pasteur-paris.pdf?sfvrsn=3662fcb6_2
2. Killington RA. Stokes A, Hierholzer JC. Virus purification. In: Mahy BWJ, Kangro HO, editors. Virology method manual. New York: Academic Press; 1996. p. 71–89 [cited 2023 Jan 20]. https://www.sciencedirect.com/book/9780124653306/virology-methods-manual
3. Xiu L, Binder RA, Alarja NA, Kochek K, Coleman KK, Than ST, et al. A RT-PCR assay for the detection of coronaviruses from four genera. J Clinical Virol. 2020; 128:104391.
4. Thompson JD, Higgins DG, Gibson TJ. CLUSTAL W: improving the sensitivity of progressive multiple sequence alignment through sequence weighting, position-specific gap penalties and weight matrix choice. Nucleic Acids Res. 1994;22:4673–80. https://doi.org/10.1093/nar/22.22.4673
5. Kumar S, Stecher G, Li M, Knyaz C, Tamura K. MEGA X: molecular evolutionary genetics analysis across computing platforms. Mol Biol Evol. 2018;35:1547–9. https://doi.org/10.1093/molbev/msy096

Address for correspondence: Hu Suk Lee, International Livestock Research Institute, Regional Office for East and Southeast Asia, Room 301-302, B1 Building, Van Phuc Diplomatic Compound, 298 Kim Ma St, Ba Dinh District, Hanoi, Vietnam; email: H.S.Lee@cgiar.org; or Hu Suk Lee, College of Veterinary Medicine, Chungnam National University, Daejeon, South Korea; email: hs.lee@cnu.ac.kr

Emergence of *Mycobacterium orygis*–Associated Tuberculosis in Wild Ruminants, India

Megha Sharma, Karikalan Mathesh, Premanshu Dandapat, Asok Kumar Mariappan, Ravi Kumar, Soni Kumari, Vivek Kapur, Sushila Maan, Naresh Jindal, Nitish Bansal, Riyaz Kadiwar, Abhishek Kumar, Nitin Gupta, A.M. Pawde, A.K. Sharma

Author affiliations: Indian Council of Agricultural Research—Indian Veterinary Research Institute, Izatnagar, India (M. Sharma, K. Mathesh, A.K. Mariappan, R. Kumar, S. Kumari, A.M. Pawde, A.K. Sharma); Indian Council of Agricultural Research—Indian Veterinary Research Institute, Eastern Regional Station, Kolkata, India (P. Dandapat); Pennsylvania State University, University Park, Pennsylvania, USA (V. Kapur); Lala Lajpat Rai University of Veterinary and Animal Sciences, Hisar, India (S. Maan, N. Jindal, N. Bansal); Sakkarbaug Zoological Garden, Junagarh, India (R. Kadiwar, A. Kumar); Bandhavgarh National Park, Madhya Pradesh, India (N. Gupta)

DOI: https://doi.org/10.3201/eid2903.221228

Tuberculosis caused by *Mycobacterium orygis* was detected in 2 spotted deer from a wildlife sanctuary in western India and an Indian bison from a national park in central India. Nationwide surveillance is urgently required to clarify the epidemiology of the *Mycobacterium tuberculosis* complex at the human–livestock–wildlife interface.

Tuberculosis (TB) caused by *Mycobacterium orygis* has been reported in humans, cattle, and, rarely, wild animals in India (*1*–*3*). We report 3 cases of *M. orygis*–associated TB in wild animals from among 85 unexplained deaths screened as part of disease investigations during February 2016–March 2020, which also revealed cases of suppurative bronchopneumonia (n = 32), TB caused by *M. tuberculosis* or *M. bovis* (n = 29), verminous pneumonia (n = 9), fungal granulomas (n = 6), and neoplasms (n = 6).

In February 2016, two adult free-range spotted deer (a male [case 1] and a female [case 2]) were found dead in Girnar Wildlife Sanctuary, Gujarat, western India. Postmortem examination revealed nonuniform, multifocal, coalescing pale-yellow nodules embedded in the parenchyma of the lungs with caseated yellowish-white material and enlarged liver and mesenteric lymph nodes with surface nodules. In January 2017, an emaciated adult male bison (case 3) was found dead at Bandhavgarh National Park, Madhya Pradesh, central

India. Similar to the deer, the bison had variable-sized white caseous nodules on the visceral pleura, superficial lung parenchyma, and pulmonary lymph nodes.

To investigate the causative agent, tissues from the lungs, liver, and lymph nodes were collected on ice and 10% neutral buffered formalin and processed for histopathology, Ziehl-Neelsen staining, and culture isolation. Histopathologic examination of these tissues revealed large granulomas with extensive caseous necrosis and multiple calcified areas surrounded by epithelioid cells, lymphocytes, giant cells, and fibroblasts (most abundant in case 3). Acid-fast bacilli were abundant (50–75/oil immersion field), both extracellularly and within the macrophages. We cultured all samples in triplicate in Löwenstein–Jensen media with glycerol and in Löwenstein–Jensen with sodium pyruvate, which revealed moist, smooth, and granular colonies (*4*). Primary screening of bacterial isolates by single-tube multiplex PCR that targets the 16S rRNA, specific for the *Mycobacterium* genus, and MPB70 genes, specific for members of MTBC, confirmed that the isolates were MTBC (*5*). We performed further PCR on the MTBC-positive samples to determine the presence or absence of genomic regions of difference (RD4 and RD9) using published primers (*6*); this testing indicated the absence of RD9 and presence of RD4, thus excluding the possibility of *M. tuberculosis*, *M. canetti*, *M. bovis*, or *M. bovis* BCG in all 3 cases.

To determine the exact species of MTBC involved and their genetic similarities with strains affecting livestock and humans circulating in India, we performed paired-end whole-genome sequencing on the Illumina MiSeq platform (https://www.illumina.com). The presence of standard genetic markers for *M. orygis* (RD1, RD4, and Rv044c) and the absence of RD9 and RD12 confirmed our sequences as *M. orygis*. We submitted the whole-genome data generated to the National Center for Biotechnology Information Sequence Read Archive database under accession nos. SRX15482219 (case 1), SRX6969199 (case 2), and SRX6969201 (case 3).

We phylogenetically compared the sequences generated in this study with other available *M. orygis* sequences. The phylogenetic branching patterns

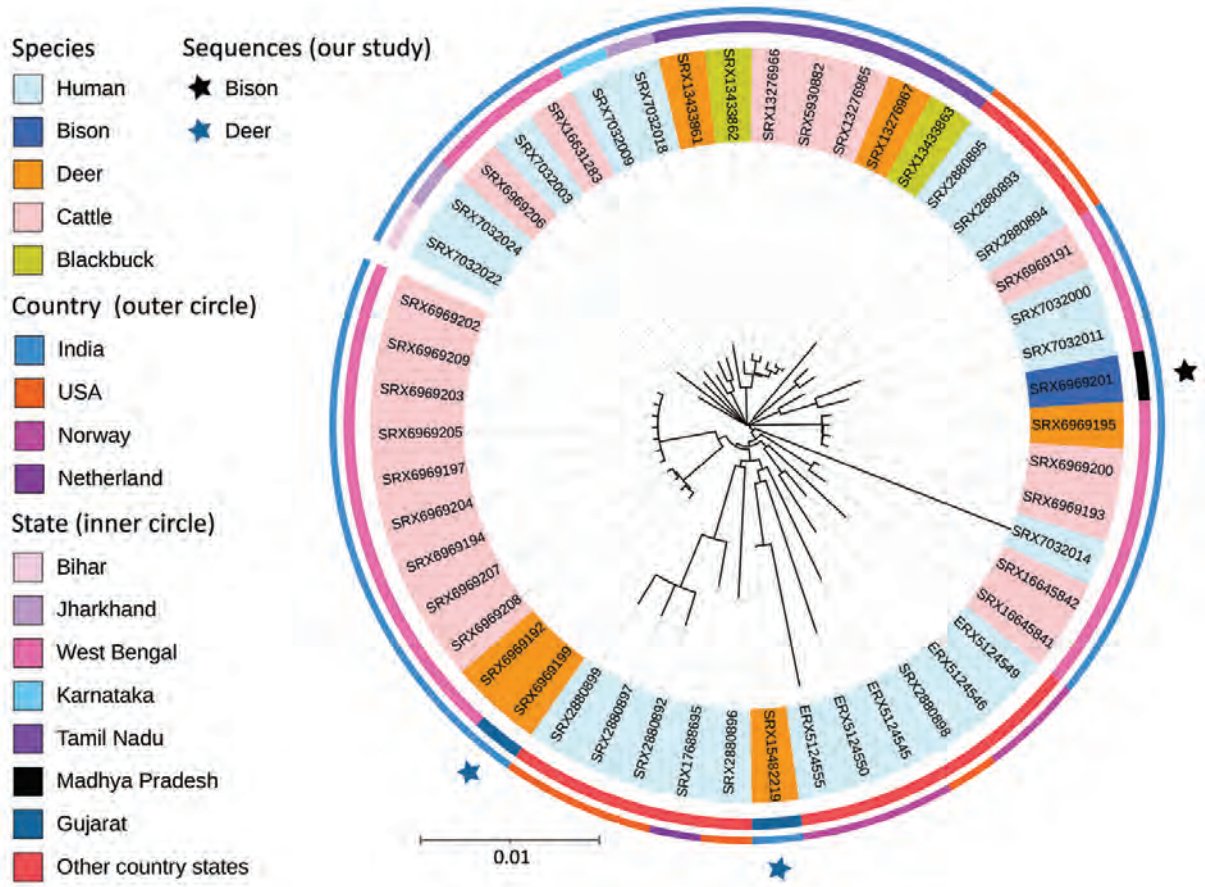

Figure. Phylogeny of newly sequenced *Mycobacterium orygis* wildlife isolates from 3 wild animals in India (black star, bison; blue stars, deer) and reference sequences. The outer circle shows the distribution of isolates in India, Norway, the Netherlands, and the United States. The inner circle shows the statewise distribution within countries. Shading of branch labels corresponds to different species. Scale bar of 0.01 indicates 1 change for every 100 nucleotides.

suggest that the isolate from the case 1 spotted deer was genetically closer to the isolate recovered from the bison (case 3) than the case 2 deer isolate (Figure 1). The average pairwise difference across all the isolates in this study was 272; it was 73 between the isolates. The restricted diversity observed among several of the newly described isolates, including those recovered from among free-living wildlife, is noteworthy and requires future investigations.

Recently, *M. orygis* has emerged as a zoonotic threat in south Asia (*7*); multispecies cases have been reported in India involving humans, dairy cattle, and wild ungulates (*1*–*3*,*7*,*8*). Studies from Nepal and Bangladesh have also revealed the circulation of *M. orygis* in free-ranging wild animals and cattle, which indicates the possibility of *M. orygis* in the India multihost wildlife system (*9*). Reports on the transmission of *M. orygis* infection from an India-origin farm worker to cattle in New Zealand (*10*) and the confirmation of *M. orygis* in 10 human patients in south Asia (*2*) imply endemicity in the region, highlighting the urgent need for genomic epidemiologic investigations.

We report the circulation of *M. orygis* in free-ranging wildlife populations in India, suggesting an unexplored threat to wildlife conservation in regions where various endangered species coexist. In this study, the transmission dynamics of *M. orygis* are unknown; however, spillover and spillback episodes might have occurred because of the shared space and resources at the livestock-wildlife-human interface. In India, human population explosion has led to encroachment on forest areas and shrinking wildlife habitats, which has increased the threat of pathogen transmission among wildlife, livestock, and humans. Although the epidemiology has not been defined, phylogenetic analysis in our study and previous reports indicate that *M. orygis* appears to be circulating in wild animal, human, and livestock populations in India. In light of the World Health Organization End TB Strategy, nationwide screening and continuous surveillance under the umbrella of the One Health approach should be conducted to combat this deadly zoonotic disease.

Acknowledgments

We thank the director of the Indian Council of Agricultural Research—Indian Veterinary Research Institute, the forest departments of Madhya Pradesh and Gujarat and Central Zoo Authority, Government of India for providing necessary permission to conduct this research.

This study received financial contribution from the Department of Biotechnology, Ministry of Science and Technology, Government of India (grant no. BT/ADV/Bovine Tuberculosis/2018).

About the Author

Dr. Sharma is pursuing a PhD in the division of Veterinary Pathology at the Indian Council of Agricultural Research—Indian Veterinary Research Institute (IVRI). Her primary research interests are livestock, poultry, and wildlife disease epidemiology and pathology.

References

1. Refaya AK, Kumar N, Raj D, Veerasamy M, Balaji S, Shanmugam S, et al. Whole-genome sequencing of a *Mycobacterium orygis* strain isolated from cattle in Chennai, India. Microbiol Resour Announc. 2019;8:e01080–19. https://doi.org/10.1128/MRA.01080-19
2. Duffy SC, Srinivasan S, Schilling MA, Stuber T, Danchuk SN, Michael JS, et al. Reconsidering *Mycobacterium bovis* as a proxy for zoonotic tuberculosis: a molecular epidemiological surveillance study. Lancet Microbe. 2020;1:e66–73. https://doi.org/10.1016/S2666-5247(20)30038-0
3. Refaya AK, Ramanujam H, Ramalingam M, Rao GVS, Ravikumar D, Sangamithrai D, et al. Tuberculosis caused by *Mycobacterium orygis* in wild ungulates in Chennai, South India. Transbound Emerg Dis. 2022;69:e3327–33. https://doi.org/10.1111/tbed.14613
4. Thapa J, Nakajima C, Maharjan B, Poudell A, Suzuki Y. Molecular characterization of *Mycobacterium orygis* isolates from wild animals of Nepal. Jpn J Vet Res. 2015;63:151–8.
5. Wilton S, Cousins D. Detection and identification of multiple mycobacterial pathogens by DNA amplification in a single tube. PCR Methods Appl. 1992;1:269–73. https://doi.org/10.1101/gr.1.4.269
6. Warren RM, Gey van Pittius NC, Barnard M, Hesseling A, Engelke E, de Kock M, et al. Differentiation of *Mycobacterium tuberculosis* complex by PCR amplification of genomic regions of difference. Int J Tuberc Lung Dis. 2006;10:818–22.
7. Rahim Z, Thapa J, Fukushima Y, van der Zanden AGM, Gordon SV, Suzuki Y, et al. Tuberculosis caused by *Mycobacterium orygis* in dairy cattle and captured monkeys in Bangladesh: a new scenario of tuberculosis in South Asia. Transbound Emerg Dis. 2017;64:1965–9. https://doi.org/10.1111/tbed.12596
8. van Ingen J, Rahim Z, Mulder A, Boeree MJ, Simeone R, Brosch R, et al. Characterization of *Mycobacterium orygis* as *M. tuberculosis* complex subspecies. Emerg Infect Dis. 2012;18:653–5. https://doi.org/10.3201/eid1804.110888
9. Thapa J, Nakajima C, Gairhe KP, Maharjan B, Paudel S, Shah Y, et al. Wildlife tuberculosis: an emerging threat for conservation in South Asia. In: Lameed GA, editor. Global exposition of wildlife management. London: InTechOpen Limited; 2017. p. 73–90.
10. Dawson KL, Bell A, Kawakami RP, Coley K, Yates G, Collins DM. Transmission of *Mycobacterium orygis* (*M. tuberculosis* complex species) from a tuberculosis patient to a dairy cow in New Zealand. J Clin Microbiol. 2012;50:3136–8. https://doi.org/10.1128/JCM.01652-12

Address for correspondence: Karikalan Mathesh, Center for Wildlife, ICAR-Indian Veterinary Research Institute, Izatnagar-243122, Uttar Pradesh, India; email: karyvet11@gmail.com; Premanshu Dandapat, ICAR-Indian Veterinary Research Institute, Eastern Regional Station, Kolkata (WB), India; email: pdandapat@gmail.com

SARS-CoV-2 Spillback to Wild Coatis in Sylvatic–Urban Hotspot, Brazil

Ana Gabriella Stoffella-Dutra, Bruna Hermine de Campos, Pedro Henrique Bastos e Silva, Karolina Lopes Dias, Iago José da Silva Domingos, Nadja Simbera Hemetrio, Joilson Xavier, Felipe Iani, Vagner Fonseca, Marta Giovanetti, Leonardo Camilo de Oliveira, Mauro Martins Teixeira, Zelia Ines Portela Lobato, Helena Lage Ferreira, Clarice Weis Arns, Edison Durigon, Betânia Paiva Drumond, Luiz Carlos Junior Alcantara Marcelo Pires Nogueira de Carvalho, Giliane de Souza Trindade

Author affiliations: Universidade Federal de Minas Gerais, Belo Horizonte, Brazil (A.G. Stoffella-Dutra, B.H. de Campos, P.H.B. e Silva, K.L. Dias, I.J.S. Domingos, J. Xavier, L.C. de Oliveira, M.M. Teixeira, Z.I.P. Lobato, B.P. Drumond, M.P.N. de Carvalho, G. de Souza Trindade); Fundação de Parques Municipais e Zoobotânica de Belo Horizonte, Belo Horizonte (N.S. Hemetrio); Fundação Ezequiel Dias, Belo Horizonte (F. Iani); Organização Pan-Americana da Saúde, Brasília, Brazil (V. Fonseca); University of Campus Bio-Medico di Roma, Rome, Italy (M. Giovanetti); Fundação Oswaldo Cruz, Rio de Janeiro, Brazil (M. Giovanetti, L.C.J. Alcantara); Universidade de São Paulo, São Paulo, Brazil (H.L. Ferreira, E. Durigon); Universidade de Campinas, Campinas, Brazil (C.W. Arns)

DOI: https://doi.org/10.3201/eid2903.221339

We tested coatis (*Nasua nasua*) living in an urban park near a densely populated area of Brazil and found natural SARS-CoV-2 Zeta variant infections by using quantitative reverse transcription PCR, genomic sequencing, and serologic surveillance. We recommend a One Health strategy to improve surveillance of and response to COVID-19.

By November 2022, the COVID-19 pandemic had resulted in >630 million cases of disease worldwide (*1*). During the outbreak, natural occurrence of SARS-CoV-2 infections in animals was a hallmark; infections have been reported mainly in companion, domestic, captive, and farmed animals but also in wildlife (*2*,*3*). As of September 2022, the World Organisation for Animal Health had recorded 26 animal species infected with SARS-CoV-2 in 36 countries (*2*), indicating that the virus is able to cross the species barrier, thereby increasing risk of new transmission cycles and animal reservoirs (*2*,*3*).

Coatis (*Nasua nasua*) from South America are small diurnal mammals (family Procyonidae) that are omnivorous, terrestrial, synanthropic, and opportunistic. Coatis interact easily with humans and are often seen foraging for human food, especially from trash (*4*,*5*). We investigated the transmission of SARS-CoV-2 to a coati population living in an urban park near a large anthropized area of Brazil.

We collected serum samples and anal and oral swab samples during February–August 2021 from 40 free-living coatis inhabiting Mangabeiras Municipal Park in Belo Horizonte, Brazil (Appendix Table, Figure 1, https://wwwnc.cdc.gov/EID/article/29/3/22-1339-App1.pdf). Trained professionals captured coatis during 4 periods (February, June, July, and August), using appropriate personal protective equipment (laboratory coats, gloves, N95 face masks, and face shields) in accordance with all biosafety guidelines. Ethics approval was obtained for this study (Appendix).

Coatis were captured in Tomahawk Live Traps (https://www.livetrap.com/index.php) (70 cm × 35 cm × 40 cm) baited with banana pieces. Animals were anesthetized with Zoletil 100 (Virbac, https://vet-uk.virbac.com) by intramuscular injection (7–10 mg/kg body weight), clinically evaluated, identified, and marked with polypropylene earrings and microchips. After anesthesia recovery, each coati was released at their capture site.

We stored anal and oral swab specimens by using RNAlater (ThermoFisher Scientific, https://www.thermofisher.com) and extracted RNA by using QIAmp Viral RNA Mini Kits (QIAGEN, https://www/qiagen.com). We performed quantitative reverse transcription PCR targeting the nucleocapsid N1 and N2 regions (*6*) and sequenced PCR positive samples by using nanopore technology. We performed phylogenetic analysis by using IQ–TREE2 (*7*) and maximum-likelihood reconstruction.

We detected SARS-CoV-2 RNA in 2 (5%) female coatis that had no clinical signs of infection (Table). We obtained a complete genomic sequence from the anal swab specimen from coati 535 (99% average coverage). The genomic sequence of SARS-CoV-2 obtained from the anal swab specimen from coati 535 indicated this variant belonged to the Zeta lineage (B.1.1.28.2, P.2) (Figure). The P.2 variant was initially detected in the state of Rio de Janeiro, Brazil, in July 2020 and was considered a variant of interest (*9*).

We performed plaque reduction neutralization tests (PRNT) on serum samples from all captured coatis to detect SARS-CoV-2 neutralizing antibodies (*8*). We serially diluted serum samples to obtain 1:20,

Table. Specimens from 2 SARS-CoV-2 RNA–positive coatis in study of SARS-CoV-2 spillback to wild coatis in sylvatic–urban hotspot, Brazil*

Coati ID	Collection date	Sex	Sample	SARS-CoV-2†	N1 Count‡	N2 Count‡
C341	2021 Feb 17	F	Oral swab	Positive	33	37
			Anal swab	Negative	NA	NA
			Serum	Negative	NA	NA
C535	2021 Feb 18	F	Oral swab	Positive	20	24
			Anal swab	Positive	30	33
			Serum	Negative	NA	NA

*Oral and anal swab and serum samples were collected from 40 wild coatis inhabiting Mangabeiras Municipal Park in Belo Horizonte, Brazil. We performed quantitative reverse transcription PCR targeting the nucleocapsid N1 and N2 regions of SARS-CoV-2 RNA for each sample. ID, identification, NA, not applicable.
†Specimens positive or negative for SARS-CoV-2 RNA by PCR.
‡PCR cycle threshold count.

1:40, and 1:80 dilutions and measured 50% and 90% neutralizing activity against SARS-CoV-2. Twenty (50%) coatis had SARS-CoV-2 neutralizing antibodies in ≥1 dilution at the 50% level; at the 90% level, 13 (32.5%) coatis had detectable neutralizing antibodies in ≥1 dilutions and 7 (17.5%) coatis had SARS-CoV-2 neutralizing antibodies in all 3 dilutions. We observed neutralizing antibodies in all 3 serum dilutions for coati 535 (Appendix Figure 2).

We were unable to confirm the mode of SARS-CoV-2 transmission to the coati population. However, we found evidence for human-to-animal transmission; the P.2 genomic sequence from coati 535 was the same variant circulating in humans within the area during the study period. Furthermore, 50% of the coati population had antibodies against SARS-CoV-2, suggesting a cluster of natural exposure and infections within this population. Our results support indirect

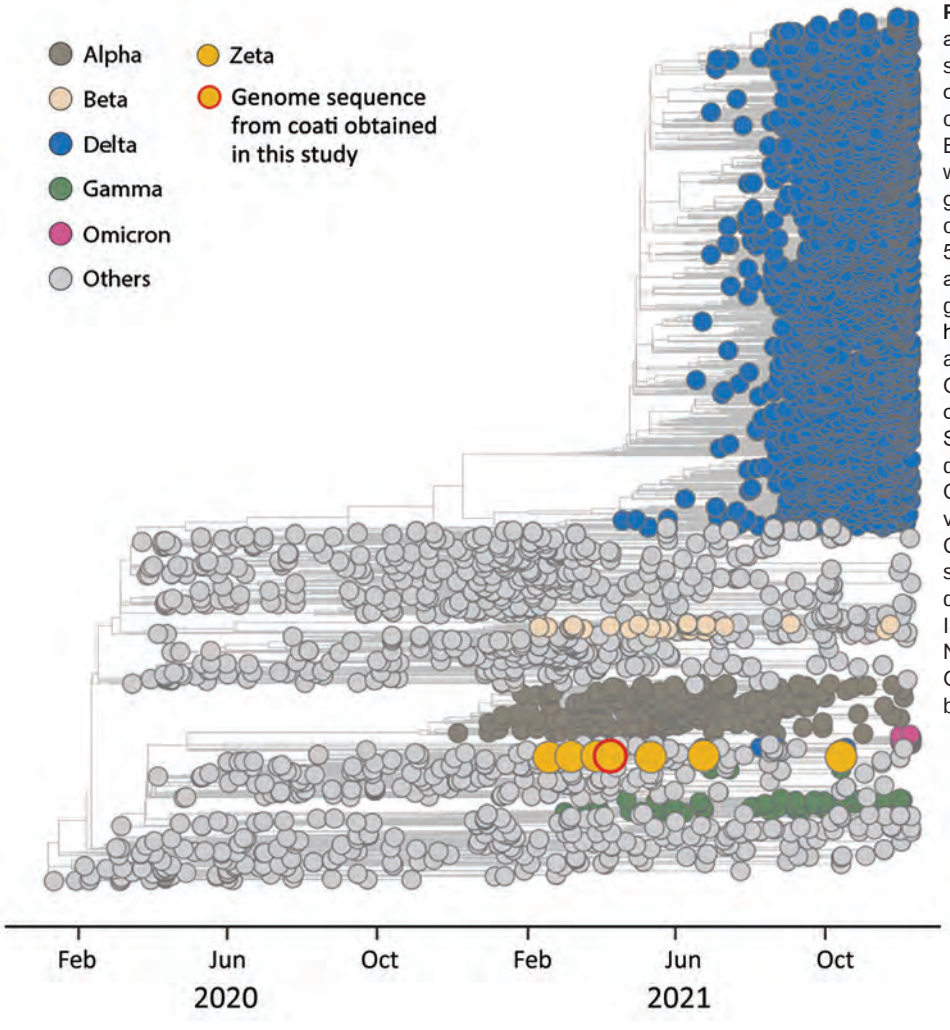

Figure. Time-scaled phylogenetic analysis of SARS-CoV-2 sequences, by variant type, in study of SARS-CoV-2 spillback to wild coatis in sylvatic–urban hotspot, Brazil. Maximum-likelihood method was used to compare the complete genomic sequence of SARS-CoV-2 obtained from coati (*Nasua nasua*) 535 (red-outlined yellow circle) and 3,441 SARS-CoV-2 reference genomic sequences (GISAID, https://www.gisaid.org) from around the world collected through October 2021. Colors represent clades corresponding to different SARS-CoV-2 variants of concern described by the World Health Organization; yellow indicates Zeta variant sequences. The SARS-CoV-2 sequence generated in this study was deposited in the GISAID database (accession no. EPI_ISL_8800460) and SisGen (Sistema Nacional de Gestão do Patrimônio Genético, https://www.sisgen.gov.br; no. A627307).

contact of coatis with contaminated human trash and food scraps in dumpsters and in the bordering urban areas of the park or potential direct close contact with infected human visitors (Appendix Figure 1).

Our findings agree with results from a zoo in Illinois, USA, that also confirmed SARS-CoV-2 in a coati by using molecular methods (*2*,*10*). Those results reinforce the susceptibility of coatis to SARS-CoV-2 infection and suggest possible virus shedding and transmission capacity of coatis. Viral RNA detection in both oral and anal swab specimens from coati 535 (Table) and presence of neutralizing antibodies indicate that viral replication occurred in this host. Therefore, our findings highlight possible SARS-CoV-2 enzootic maintenance in nature, including in fragmented green areas close to urban settings. Because of the potential for SARS-CoV-2 interspecies transmission, we recommend establishing a One Health strategy to improve surveillance and ability to respond to COVID-19 emergency health events.

Acknowledgments

We thank colleagues from the Laboratório de Vírus Instituto de Ciências Biológicas for their excellent technical support; Andrea Garcia de Oliveira, Marcelo Camargos, Kelly Nascimento, and Laboratório Federal de Defesa Agropecuária, Ministry of Agriculture Livestock and Food Supply (MAPA), for supporting our activities in the Biosafety Level Office International des Epizooties laboratory; Fundação de Parques Municipais e Zoobotânica of Belo Horizonte and Sérgio Augusto Domingues for allowing the field work; Augusto Gomes for coati photographs; Brazilian Post and Telegraph Company (Correios) for transporting our samples; and Jônatas Abrahão for excellent scientific discussions.

This study was funded by National Council for Scientific and Technological Development (CNPq) (grant nos. 440593/2016-6 and 403761/2020-4); Coordenação de Aperfeiçoamento de Pessoal de Nível Superior (CAPES), process no. 88882.348380/2010-1; DECIT (Departamento de Ciência e Tecnologia)/MS (Brazilian Ministry of Health) no. 14/2016, Prevenção e Combate ao vírus Zika, FAPEMIG (Fundação de Amparo à Pesquisa do estado de Minas Gerais); PRPq-UFMG (Pró Reitoria de Pesquisa) and Finep/RTR/PRPq/Rede (Financiadora de Estudos e Projetos) COVID-19 (no. 0494/20-0120002600). This work was partially funded by the Ministry of Science, Technology, and Innovation (MCTI-Brazil); US National Institutes of Health (grant no. U01 AI151698) for the United World Antiviral Research Network; CRP- ICGEB RESEARCH GRANT 2020 (project no. CRP/BRA20-03, contract no. CRP/20/03); Oswaldo Cruz Foundation (no. VPGDI-027-FIO-20-2-2-30); and Brazilian Ministry of Health (no. SCON2021-00180). L.C.D.O. and M.M.T. were supported by a grant from MCTI/CNPQ/CAPES and FAPEMIG (project no. 465425/2014-3, Dengue and host-microbial interactions), M.G. and L.C.J.A. were supported by Fundação de Amparo a Pesquisa do Estado do Rio de Janeiro (FAPERJ), and M.G. was funded by PON "Ricerca e Innovazione" 2014–2020. Findings reported herein are the sole deduction, view, and responsibility of the researchers and do not reflect the official positions and sentiments of the funders.

G.S.T., B.P.D., M.G., M.M.T., H.L.F., C.W.A., and L.C.J.A are CNPq researchers; M.M.T., C.W.A., and E.L.D. are members of the Redevirus-MCTI; and H.L.F., Z.I.P.L., B.P.D., C.W.A., and E.L.D. are members of the Previr-MCTI.

About the Author

Ms. Stoffella-Dutra is a PhD student in microbiology at the Federal University of Minas Gerais. Her primary research interests focus on virology, viral zoonoses, epidemiology, and wildlife disease ecology.

References

1. World Health Organization. WHO coronavirus (COVID-19) dashboard, 2022 [cited 2022 Nov 1]. https://covid19.who.int
2. World Organisation for Animal Health. SARS-CoV-2 in animals—situation report 17, 2022 [cited 2022 Nov 1]. https://www.woah.org/app/uploads/2022/10/sars-cov-2-situation-report-17.pdf
3. Delahay RJ, de la Fuente J, Smith GC, Sharun K, Snary EL, Flores Girón L, et al. Assessing the risks of SARS-CoV-2 in wildlife. One Health Outlook. 2021;3:7. https://doi.org/10.1186/s42522-021-00039-6
4. Rodrigues DH, Calixto E, Cesario CS, Repoles RB, de Paula Lopes W, Oliveira VS, et al. Feeding ecology of wild brown-nosed coatis and garbage exploration: a study in two ecological parks. Animals (Basel). 2021;11:2412. https://doi.org/10.3390/ani11082412
5. Projeto Quatis. Parque das Mangabeiras [cited 2022 Jun 6]. https://sites.google.com/site/projetoquatis/parque-das-mangabeiras
6. Centers for Disease Control and Prevention. CDC 2019-novel coronavirus (2019-nCoV) real-time RT-PCR diagnostic panel [cited 2022 Jun 8]. https://www.fda.gov/media/134922/download
7. Minh BQ, Schmidt HA, Chernomor O, Schrempf D, Woodhams MD, von Haeseler A, et al. IQ-TREE 2: new models and efficient methods for phylogenetic inference in the genomic era. Mol Biol Evol. 2020;37:1530–4. https://doi.org/10.1093/molbev/msaa015
8. Chaves DG, de Oliveira LC, da Silva Malta MCF, de Oliveira IR, Barbosa-Stancioli EF, Teixeira MM, et al. Pro-inflammatory immune profile mediated by TNF and IFN-γ and regulated by IL-10 is associated to IgG anti-SARS-CoV-2 in asymptomatic blood donors. Cytokine. 2022;154:155874. https://doi.org/10.1016/j.cyto.2022.155874
9. Voloch CM, da Silva Francisco R Jr, de Almeida LGP,

Cardoso CC, Brustolini OJ, Gerber AL, et al.; Covid19-UFRJ Workgroup, LNCC Workgroup, Adriana Cony Cavalcanti. Genomic characterization of a novel SARS-CoV-2 lineage from Rio de Janeiro, Brazil. J Virol. 2021;95:e00119-21. https://doi.org/10.1128/JVI.00119-21

10. US Department of Agriculture, Animal and Plant Health Inspection Service. Confirmation of COVID-19 in a coatimundi at an Illinois zoo, 2021 [cited 2022 Jun 6]. https://www.aphis.usda.gov/aphis/newsroom/stakeholder-info/sa_by_date/sa-2021/sa-10/covid-coatimundi

Address for correspondence: Giliane de Souza Trindade, Universidade Federal de Minas Gerais, Av Antônio Carlos, 6627, Campus Pampulha, Belo Horizonte, 31270-901, Minas Gerais, Brazil; email: giliane@icb.ufmg.br

Babesia microti Causing Intravascular Hemolysis in Immunocompetent Child, China

Jiafeng Yao,[1] Guoging Liu,[1] Yang Zou, Jin Jiang, Shaogang Li, Heng Wang, Xiaoling Cheng, Rui Zhang, Kaige Zhang, Chunyan Wei, Runhui Wu

Author affiliations: Beijing Children's Hospital, Beijing, China (J. Yao, G. Liu, J. Jiang, X. Cheng, R. Zhang, K. Zhang, R. Wu); Capital Medical University, Beijing (Y. Zou, S. Li); Peking Union Medical College School of Basic Medicine, Beijing (H. Wang, C. Wei)

DOI: https://doi.org/10.3201/eid2903.220888

We report a case of *Babesia microti* infection in an immunocompetent child <5 years of age that caused fever and severe intravascular hemolysis. Physicians in China should be aware of babesiosis, especially in the differential diagnosis of immune hemolytic anemia with negative results for antiglobulin tests.

Babesiosis, caused by tickborne zoonotic protozoa of the genus *Babesia*, is an emerging health risk to humans. Among the known *Babesia* species infecting humans, *B. microti* is the most common cause of human babesiosis (*1*). In China, *B. microti* has caused >100 human cases of babesiosis (*2*), but nearly all have been reported in adults, particularly the elderly.

B. microti babesiosis has rarely been reported in immunocompetent children in China. We reported a case of severe intravascular hemolysis caused by *B. microti* infection in an immunocompetent preschooler from Shandong Province, China.

The patient, a girl 4 years and 9 months of age, had fever develop (highest temperature 39°C) on September 30, 2021. Antimicrobial drug treatment was not effective. Four days later, her urine became dark, and she had abdominal pain. On October 9, 2021, she was admitted to the hospital because of severe anemia and abnormal laboratory test results (Table). She had shock after a discharge of dark brown urine.

To stabilize her vital signs, we began repeated blood transfusion for supportive treatment. Azithromycin and immune regulatory treatment (high-dose methylprednisolone, 10 mg/kg/d for 3 days, and intravenous immunoglobulin, 1 g/kg/d for 2 d) were not effective. Her symptoms worsened, and her hemoglobin level remained at <60 g/L (Appendix Figure, panel A, https://wwwnc.cdc.gov/EID/article/29/3/22-0888-App1.pdf). On the basis of those findings, we excluded congenital hemolytic anemia and autoimmune hemolytic anemia.

We examined her blood smear and observed parasites in the erythrocytes (Appendix Figure, panel B). We used a genus-specific 18S rRNA PCR described previously (*3*) to confirm *Babesia* infection by amplification of a 515-bp fragment (Appendix Figure, panel C). Test results for malaria infection was negative. Subsequent sequencing of the fragment and BLAST analysis (https://blast.ncbi.nlm.nih.gov/Blast.cgi) of the nucleotide sequence showed 100% similarity with *B. microti* RI strain. Those results confirmed the diagnosis as a *B. microti* infection causing severe intravascular hemolytic anemia.

The girl's parents recalled that the child had been in a wild chestnut forest in a suburb of Zaozhuang City, Shandong Province, on September 14, 2021. They found ≈20 red papules and an itching sensation on the trunk and limbs. The papules subsided within 3 days. There were no other complications of babesiosis, such as splenic infarction, acute respiratory distress syndrome, or disseminated intravascular coagulation.

The child was given atovaquone and azithromycin (*4*) for 21 days, and the urine color became clear within 24 hours. The frequency of erythrocyte transfusion was reduced gradually, and the hemolysis was controlled (Appendix Figure, panel A). On the 10th day after the treatment began, molecular detection

[1]These authors contributed equally to this article.

Table. Laboratory test results for *Babesia microti* causing intravascular hemolysis in immunocompetent child, China*

Variable	Age-adjusted reference value or range	Value
Epstein-Barr virus	Negative	Negative
Mycoplasma pneumoniae	Negative	Positive
IgM titer	<1:80	1:80
Drug-resistance gene	Negative	Negative
Leukocyte count, × 10^9 cells/L	4.9–12.7	4.36
Erythrocyte count, × 10^{12} cells/L	4.1–5.5	2
Hemoglobin, g/L	115–150	57
Mean corpuscular volume, μm^3	76–88	83
Mean corpuscular hemoglobin concentration, g/L	309–359	343
Platelet count, × 10^9/L	187–475	100
% Reticulocytes	0.5%–2.5%	2.07%
Clotting function	NA	Normal
Bilirubin, μmol/L		
Total	3.42–20.5	55.98
Direct	0–3.42	13.76
Indirect	0–17.1	42.22
Aspartate aminotransferase, U/L	14–44	196.2
Alanine aminotransferase, U/L	7–30	187.6
Lactate dehydrogenase, U/L	110–295	2,899
Antiglobulin tests		
IgG	Negative	Negative
C3d	Negative	Negative
DAT	Negative	Negative
Control	Negative	negative
Spot urine sample		
Urine color	Light yellow	Brown
Ketone body	Negative	1+
Protein	Negative	2+
Urinary bilirubin	Negative	1+
Occult blood	Negative	3+
Centrifugal microscopy for erythrocytes, HPF	0–3	0
Centrifugal microscopy for leukocytes, HPF	0–3	0
Chest computed tomography	NA	Few shadows in lower lobe of right lung, no exudative lesion
Abdominal ultrasound	NA	Splenomegaly

*DAT, direct antiglobulin test; HPF, high-power field; NA, not applicable.

of *B. microti* showed a negative result. The child has been monitored for >6 months and is in good health.

In this case, we confirmed the severe intravascular hemolysis caused by *B. microti* infection in an immunocompetent child <5 years of age. For children in China, although babesiosis caused by *B. venatorum* and *B. crassa*–like parasites was detected in epidemiologic surveys (*5*,*6*), few children who have babesiosis caused by *B. microti* and severe hemolysis have been reported. Thus, babesiosis is still unfamiliar to pediatricians. This case implied that *Babesia* infection might be underdiagnosed in China. It is imperative for pediatricians and clinicians to be aware of babesiosis, which has become a newly emerging public health threat globally.

In Shandong Province, where this child lived, only 2 adults who had babesiosis and severe anemia caused by *B. divergence* were documented (*7*), but *B. microti*2positive (0.58%) hard ticks from the Jiaodong Peninsula in Shandong Province were reported (*8*). Given that the child did not have a splenectomy, take immunosuppressive drugs, receive previous blood transfusions, or have other travel histories, her travel history to the wild chestnut forest and subsequent red, itching papules provided strong evidence for *B. microti* infection by tick bites. Detailed epidemiologic survey of *Babesia* infection in tick vectors and reservoir animals in local areas is necessary to provide guidelines for better prevention and control of babesiosis.

Severe babesiosis in immunocompetent persons <50 years of age is rare; only 2 cases have been reported (*9*,*10*). We report a case of *B. microti* infection causing severe illness in an immunocompetent child. Better understanding of the pathogenesis of this parasite is necessary. This case indicates that babesiosis cannot be ignored in severe intravascular hemolysis. For patients who have intermittent fever and intravascular hemolysis but negative results for antiglobulin tests, babesiosis should be considered in the differential diagnosis, especially in areas where the tick vector is present. A timely and appropriate treatment for patients who have severe disease that is recognized early is needed.

About the Authors

Dr. Yao is an associate chief physician at Beijing Children's Hospital, Beijing, China. His primary research interest is pediatric hematology. Dr. Liu is a physician at Beijing Children's Hospital, Beijing, China. His primary research interest is pediatric hematology.

References

1. Puri A, Bajpai S, Meredith S, Aravind L, Krause PJ, Kumar S. *Babesia microti*: pathogen genomics, genetic variability, immunodominant antigens, and pathogenesis. Front Microbiol. 2021;12:697669. https://doi.org/10.3389/fmicb.2021.697669
2. Zhao GP, Wang YX, Fan ZW, Ji Y, Liu MJ, Zhang WH, et al. Mapping ticks and tick-borne pathogens in China. Nat Commun. 2021;12:1075. PubMed https://doi.org/10.1038/s41467-021-21375-1
3. Wei CY, Wang XM, Wang ZS, Wang ZH, Guan ZZ, Zhang LH, et al. High prevalence of *Babesia microti* in small mammals in Beijing. Infect Dis Poverty. 2020;9:155. https://doi.org/10.1186/s40249-020-00775-3
4. Krause PJ, Auwaerter PG, Bannuru RR, Branda JA, Falck-Ytter YT, Lantos PM, et al. Clinical practice guidelines by the Infectious Diseases Society of America (IDSA): 2020 guideline on diagnosis and management of babesiosis. Clin Infect Dis. 2021;72:e49–64. https://doi.org/10.1093/cid/ciaa1216
5. Jiang JF, Zheng YC, Jiang RR, Li H, Huo QB, Jiang BG, et al. Epidemiological, clinical, and laboratory characteristics of 48 cases of "*Babesia venatorum*" infection in China: a descriptive study. Lancet Infect Dis. 2015;15:196–203. https://doi.org/10.1016/S1473-3099(14)71046-1
6. Jia N, Zheng YC, Jiang JF, Jiang RR, Jiang BG, Wei R, et al. Human babesiosis caused by a *Babesia crassa*–like pathogen: a case series. Clin Infect Dis. 2018;67:1110–9. https://doi.org/10.1093/cid/ciy212
7. Qi C, Zhou D, Liu J, Cheng Z, Zhang L, Wang L, et al. Detection of *Babesia divergens* using molecular methods in anemic patients in Shandong Province, China. Parasitol Res. 2011;109:241–5. https://doi.org/10.1007/s00436-011-2382-8
8. Zhang H, Sun Y, Jiang H, Huo X. Prevalence of severe febrile and thrombocytopenic syndrome virus, *Anaplasma* spp. and *Babesia microti* in hard ticks (Acari: Ixodidae) from Jiaodong Peninsula, Shandong Province. Vector Borne Zoonotic Dis. 2017;17:134–40. https://doi.org/10.1089/vbz.2016.1978
9. Gonzalez LM, Rojo S, Gonzalez-Camacho F, Luque D, Lobo CA, Montero E. Severe babesiosis in immunocompetent man, Spain, 2011. Emerg Infect Dis. 2014;20:724–6. https://doi.org/10.3201/eid2004.131409
10. Selig T, Ilyas S, Theroux C, Lee J. Fatal babesiosis in an immunocompetent patient. R I Med J (2013). 2022;105:20–3.

Address for correspondence: Chunyan Wei, Department of Microbiology and Parasitology, Institute of Basic Medical Sciences Chinese Academy of Medical Sciences, School of Basic Medicine, Peking Union Medical College, 5# Dong Dan San Tiao, Dongcheng District, Beijing 100005, China; email: weicy@pumc.edu.cn; Runhui Wu, Beijing Children's Hospital, Capital Medical University, National Center for Children's Health, Beijing, China; email: runhuiwu@hotmail.com

Tick-Borne Encephalitis in Pregnant Woman and Long-Term Sequelae

Aurélie Velay, Ralf Janssen-Langenstein, Stéphane Kremer, Elodie Laugel, Maximilian Lutz, Anne Laure Pierson, Marie-Josée Wendling, Francis Schneider, Samira Fafi-Kremer

Author affiliations: Strasbourg University Hospital, Strasbourg, France (A. Velay, R. Janssen-Langenstein, S. Kremer, E. Laugel, A.L. Pierson, M.-J. Wendling, F. Schneider, S. Fafi-Kremer); Université de Strasbourg, Strasbourg (A. Velay, E. Laugel, S. Fafi-Kremer); Charité Universitätsmedizin Berlin, Berlin, Germany (M. Lutz)

DOI: https://doi.org/10.3201/eid2903.221328

We report a case of severe tick-borne encephalitis in a pregnant woman, leading to a prolonged stay in the intensive care unit. She showed minor clinical improvement >6 months after her presumed infection. The patient was not vaccinated, although an effective vaccine is available and not contraindicated during pregnancy.

Tick-borne encephalitis (TBE), an emerging infectious disease, has shown a deeply evolving epidemiology during the past decade, especially in Europe (*1*). TBE virus (TBEV) is transmitted mainly to humans by tick bites and occasionally by consumption of contaminated dairy products (*1*). Although most infections caused by the TBEV European subtype are asymptomatic, some patients' conditions could worsen to show severe encephalitis, associated with long-term sequelae (*1*). Data dealing with TBEV infection during pregnancy are scarce. We report a case of severe TBE and long-term sequelae in a pregnant woman.

In July 2020, a 34-year-old woman at 20 weeks of gestation was admitted to an emergency department in Strasbourg, France, because of meningismus associated with nystagmus. The patient lived in Berlin, Germany, traveled to the Black Forest (Germany), and visited Provence (southeastern France) and Alsace (northeastern France) on the way home before symptom onset.

On day 3, TBEV serologic results were positive for IgM and negative for IgG (Figure). The patient progressed to severe hyperactive delirium, requiring sedation and intubation. After a second lumbar puncture, results of reverse transcription PCR testing of cerebrospinal fluid (CSF) was positive for TBEV (Figure). A second MRI showed signs of diffuse leptomeningitis

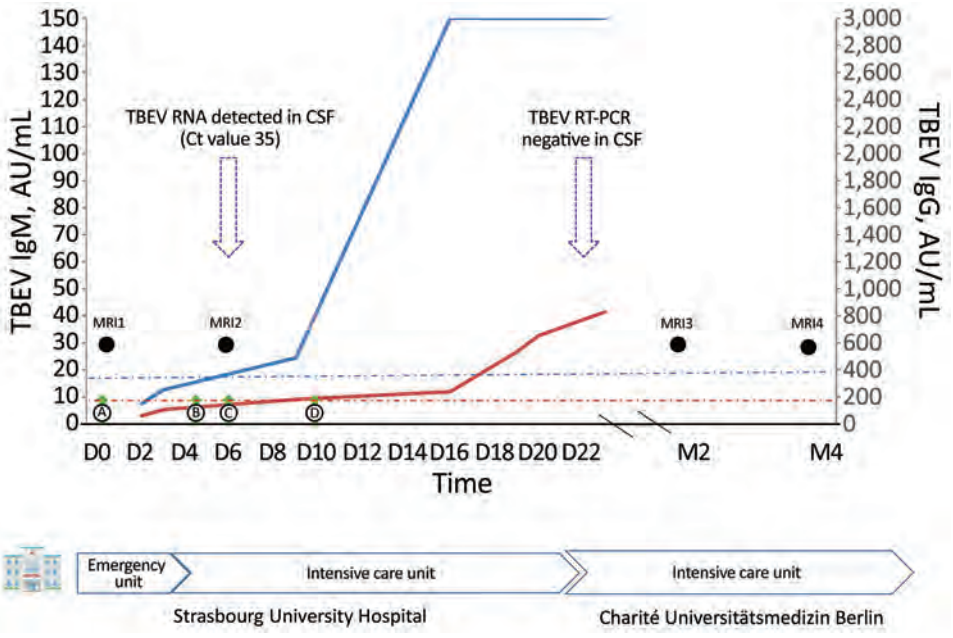

Figure. Tick-borne encephalitis in pregnant woman and long-term sequelae showing relevant clinical and laboratory findings, including TBEV antibody kinetics in serum samples. TBEV IgM (blue curve) and IgG (red curve) were detected in serum samples by using the Serion ELISA Classic TBE Virus IgG/IgM Kit (https://www.serion-immunologics.com) according to the manufacturer's instructions. Results are expressed in arbitrary units (AU) per milliliter, with a positive threshold of 15 AU/mL for IgM (blue dot-dash line) and 150 AU/mL for IgG (red dot-dash line). Green arrows indicate clinical findings; black circles indicate timing of MRIs; purple arrows indicate TBE real-time RT-PCR performed for CSF, with the Ct value for a positive result. An in-house RT-PCR for TBEV nucleic acid was performed on CSF samples. Primer and probe sequences targeted the 3′-untranslated region of the viral genome as described by Cassinoti and Swchaiger (*2*). A positive control, a negative control, and an internal control were included to monitor overall efficiency of the RT-PCR. CSF, cerebrospinal fluid; Ct, cycle threshold; D, day after admission; M, month after admission; MRI, magnetic resonance imaging; RT-PCR, reverse transcription-PCR; TBEV, tick-borne encephalitis virus.

with deep cerebral nuclei involvement (Appendix Figure, https://wwwnc.cdc.gov/EID/article/29/3/22-1328-App1.pdf). At cessation of sedation (day 7), the patient remained in a coma. Iterative TBEV serologic results showed appearance of specific IgG (Figure).

At admission (day 0), lumbar puncture showed pleocytosis (70 cells/mm^3) and 55 mg/dL of protein, and all virologic molecular tests results and bacterial culture results were negative. Lyme borreliosis serologic test results were negative. Results of magnetic resonance imaging (MRI) of the brain were unremarkable. Faced with a worsening of her condition, she was transferred to the intensive care unit 2 days later and showed aseptic meningoencephalitis. Given her recent history of travel, we tested for West Nile virus, dengue virus, Zika virus, Toscana virus, and chikungunya virus; all results were negative. An autoimmune etiology was ruled out by biologic testing.

At the beginning of August 2020, the patient was transferred to Charité Universitätsmedizin in Berlin, Germany. The next 2 MRIs, performed in September and November 2020, showed progression to deep cerebral nuclei and thalamic hemorrhagic transformation and cerebral atrophy (Appendix Figure). She was discharged to a neurologic rehabilitation center after 85 days of hospitalization and had tetraparesis and polyradiculitis. A tracheostomy and a gastrostomy were performed. After intensive rehabilitation, the patient showed slow and minor clinical improvement. She was not vaccinated against TBE and did not recall either a tick bite or consumption of raw milk products. All uterine ultrasounds performed during her hospitalization showed development of the fetus on schedule. The patient gave birth to a healthy boy by cesarean delivery at term.

Six previous cases of TBEV infection occurring during pregnancy have been published (*2*,*3*). For this case, as well as for 2 previously reported cases, pregnancy proceeded normally despite severe maternal infection (*4*). However, for 2 cases reported in 1966 (*3*), premature birth and fetal or neonatal intracranial hemorrhage occurred after the mother was infected. Although vertical transmission is known to occur with other arboviruses, such as Zika virus, to date, it has not been demonstrated for TBEV in humans (*4*) and has only been described in some animal models (*5*,*6*). Transplacental transmission seems unlikely because of the barrier function of the placenta and the short time of TBEV viremia in natural infection (*1*).

Pregnancy-associated changes in the immune system probably influenced the critical state of the patient. Usually, during the phase involving central nervous system symptoms, specific TBEV antibodies appear in blood or CSF samples, but viral RNA cannot be detected

in those biologic fluids. TBEV RNA is rarely detected in CSF samples, as for our patient, corresponding to severe or fatal cases occurring in immunosuppressed patients (*7*,*8*). Relative to pregnancy-related immunotolerance, this patient also showed development of a delayed humoral immune response to TBEV because the first serologic results were negative at the onset of clinical central nervous system disease (*1*,*7*).

Cellular immune response is also required for the clearance of TBEV infection (*1*,*6*,*9*,*10*). We did not explore the cell-mediated response of our patient, but it was potentially also weakened by her pregnancy condition, which could explain the prolonged viral replication in CSF.

Concordant with the severe disease progression of this patient, iterative MRI showed cerebral meningo-radiculoencephalitis evolving to deep cerebral nuclei and thalamic hemorrhagic transformation and cerebral atrophy. Abnormalities on brain MRI are reported in only 20% of TBE patients (*7*).

As for all previously reported cases, this patient was not vaccinated against TBE. However, an effective vaccine is available and not contraindicated during pregnancy.

Further research is warranted to assess the course of TBEV infection during pregnancy. In this context, our case study offers relevant information and highlights the need for vaccination against TBE in disease-endemic areas.

About the Author

Dr. Velay is an assistant professor in the Department of Virology at Strasbourg University Hospital, Strasbourg, France. Her primary research interest is vectorborne diseases with a focus on tick-borne encephalitis.

References

1. Velay A, Paz M, Cesbron M, Gantner P, Solis M, Soulier E, et al. Tick-borne encephalitis virus: molecular determinants of neuropathogenesis of an emerging pathogen. Crit Rev Microbiol. 2019;45:472–93. https://doi.org/10.1080/1040841X.2019.1629872
2. Schwaiger M, Cassinotti P. Development of a quantitative real-time RT-PCR assay with internal control for the laboratory detection of tick borne encephalitis virus (TBEV) RNA. J Clin Virol. 2003;27:136–45. https://doi.org/10.1016/S1386-6532(02)00168-3
3. Weinmayr LM, Kanz D, Eckenweiler M, Bormann T, Huzly D, Bardutzky J, et al. Acute tick-borne encephalitis during pregnancy: an alarming combination. Ticks Tick Borne Dis. 2020;11:101512. https://doi.org/10.1016/j.ttbdis.2020.101512
4. Divé I, Veje M, Dobler G, Bergström T, Buxmann H, Paul B, et al. Tick-borne encephalitis virus (TBEV) infection in pregnancy: absence of virus transmission to the fetuses despite severe maternal disease—a case study. Ticks Tick Borne Dis. 2020;11:101491. https://doi.org/10.1016/j.ttbdis.2020.101491
5. Charlier C, Beaudoin M-C, Couderc T, Lortholary O, Lecuit M. Arboviruses and pregnancy: maternal, fetal, and neonatal effects. Lancet Child Adolesc Health. 2017;1:134–46. https://doi.org/10.1016/S2352-4642(17)30021-4
6. Bakhvalova VN, Potapova OF, Panov VV, Morozova OV. Vertical transmission of tick-borne encephalitis virus between generations of adapted reservoir small rodents. Virus Res. 2009;140:172–8. https://doi.org/10.1016/j.virusres.2008.12.001
7. Taba P, Schmutzhard E, Forsberg P, Lutsar I, Ljøstad U, Mygland Å, et al. EAN consensus review on prevention, diagnosis and management of tick-borne encephalitis. Eur J Neurol. 2017;24:1214–e61. https://doi.org/10.1111/ene.13356
8. Lipowski D, Popiel M, Perlejewski K, Nakamura S, Bukowska-Osko I, Rzadkiewicz E, et al. A cluster of fatal tick-borne encephalitis virus infection in organ transplant setting. J Infect Dis. 2017;215:896–901. https://doi.org/10.1093/infdis/jix040
9. Silasi M, Cardenas I, Kwon J-Y, Racicot K, Aldo P, Mor G. Viral infections during pregnancy. Am J Reprod Immunol. 2015;73:199–213. https://doi.org/10.1111/aji.12355
10. Blom K, Cuapio A, Sandberg JT, Varnaite R, Michaëlsson J, Björkström NK, et al. Cell-mediated immune responses and immunopathogenesis of human tick-borne encephalitis virus-infection. Front Immunol. 2018;9:2174. https://doi.org/10.3389/fimmu.2018.02174

Address for correspondence: Aurélie Velay, Virology Laboratory, University Hospital of Strasbourg, Strasbourg F-67000, France; email: aurelie.velay@chru-strasbourg.fr

Phantom Plague: How Tuberculosis Shaped History

Vidya Krishnan

PublicAffairs Books, New York, New York, USA, 2022; ISBN-10: 1541768469; ISBN-13: 978-1541768468; Pages: 320; Price: US $27.00 (hardcover), US $16.99 (eBook)

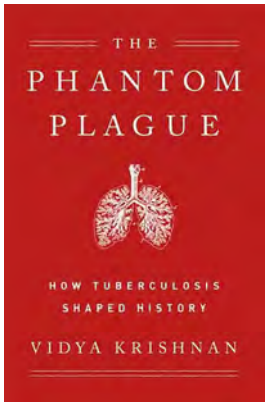

Although the subtitle of Phantom Plague by Vidya Krishnan is How Tuberculosis Shaped History, the book is actually about how history shaped tuberculosis (TB) and how TB transmission and disease has surged and persisted because of conditions such as poverty, crowding, a lack of political commitment, and poor public policies. As noted in the book, "poverty is the disease, TB the symptom." The author focuses largely on the TB epidemic in India, especially in Mumbai, India, and provides heartbreaking narratives of several persons with TB, including Shreya Tripathi, who had drug-resistant TB and whose life inspired the book. The book is an indictment of the healthcare system in India, care provided to patients with TB (often by private providers) in India and elsewhere, and TB control and prevention program bureaucracy, notably India's current government efforts and a somewhat farcical declaration that TB would be ended in India by 2025.

The book also singles out "the rise of the Hindu supremacist movement [in India which] has brought with it a tsunami of misinformation and science denialism"; misinformation and science denialism have been similarly unleashed in the United States during the COVID-19 pandemic. The author highlights many challenges ahead that limit achieving the World Health Organization (WHO) End TB strategy without substantial additional investments and development of new tools to combat TB (the WHO End TB strategy targets a 90% reduction in TB cases and 95% reduction in TB-related deaths by 2035). The book is titled Phantom Plague because ≥30% of global TB cases are never detected, highlighting the urgent need for simple, effective point-of-care TB testing. TB case detection has only worsened during the COVID-19 pandemic, as outlined in the recent WHO Global Tuberculosis Report 2022 (*1*).

The book follows several tangential threads to provide some historical perspective on pandemics. The author, a writer and journalist based in Goa, India, uses those analogies to make her case for the problems and challenges in diagnosing and treating patients, especially those with drug-resistant TB. She takes the reader on journeys to discover how TB was viewed in the late 19th century in America and how historical figures, such as Semmelweis, Pasteur, and Koch, dealt with other challenges and epidemics (and how Koch dealt with TB specifically). Despite being an enjoyable read and journey, several small errors exist that someone with a science or medical background, especially in TB, might find pestiferous and could have been corrected by further editorial review. For example, dexamethasone (a steroid drug) is listed as an antibiotic, efficacies of bedaquiline and delamanid are likely not equivalent as claimed, and patients with drug-resistant TB are not treated with 10–15 drugs/day, although a substantial number of pills might be required.

The author also tackles racism issues suggested by the lack of an adequate global response to TB. She indicates that her book "is an attempt to show how often social misery inflicted on black and brown nations is quantified into 'targets'" that never reflect the pain and suffering experienced by Shreya and others with drug-resistant TB. In addition to India's government, the book is critical of a whole host of entities that include the "West [that] is simply unable to reimagine global health without a role for itself as the savior," other governments, WHO's stewardship of TB, and "Big Pharma, Big Tech, and Big Philanthropy." The author criticizes the Gates Foundation, in part because of Bill Gates' strong support for intellectual property laws. A considerable portion of the book is spent criticizing patent laws, which the author asserts are responsible for restricting availability of newer drugs in low- and middle-income countries where TB is most prevalent. What is not discussed or emphasized in the book is the lack of new drug development for TB treatment. In the past 35 years, 58 new drugs or drug combination have been approved by the US Food and Drug Administration for HIV treatment, yet only 2 new TB drugs have received approval (bedaquiline and pretomanid; pretomanid in conjunction with bedaquiline and linezolid as part of the BPaL regimen). The market forces that support drug development have not been conducive for TB because 99.9% of TB cases occur outside the United States (mainly in low- and middle-income coun-

tries with high TB prevalence), resulting in sparse interest by the pharmaceutical industry in developing new TB drugs. New models to support drug development for TB are urgently needed, but this issue is not discussed in the book. Finally, perhaps the book ends prematurely, because after it was written, new treatments were developed for highly drug-resistant TB that shifted to all oral regimens (WHO recommendation); a ≈90% favorable outcome was recently reported for the BPaL regimen used to treat highly drug-resistant TB (*2*).

In summary, despite some flaws, this book is an interesting, easy read about some of the many challenges on the long road ahead toward the ultimate goal of TB elimination. The book also reminds us of the importance of community engagement: "listening to the voices of the affected community in the development and implementation of treatment options for drug-resistant tuberculosis is paramount" (*3*).

References

1. World Health Organization. Global tuberculosis report 2022 [cited 2022 Nov 30]. https://www.who.int/teams/global-tuberculosis-programme/tb-reports/global-tuberculosis-report-2022
2. Conradie F, Bagdasaryan TR, Borisov S, Howell P, Mikiashvili L, Ngubane N, et al.; ZeNix Trial Team. Bedaquiline-pretomanid-linezolid regimens for drug-resistant tuberculosis. N Engl J Med. 2022;387:810–23. https://doi.org/10.1056/NEJMoa2119430
3. Furin J, Isaakidis P. Being heard on all-oral therapy for resistant tuberculosis. Lancet Infect Dis. 2022;22:923–4. https://doi.org/10.1016/S1473-3099(22)00027-5

Henry M. Blumberg

Author affiliation: Emory University School of Medicine and Rollins School of Public Health, Atlanta, Georgia, USA

DOI: https://doi.org/10.3201/eid2903.221676

Address for correspondence: Henry M. Blumberg, Division of Infectious Diseases, Emory University, 49 Jesse Hill Jr Dr, Atlanta, GA 30303, USA; email: henry.m.blumberg@emory.edu

Félix-Joseph Barrias (1822–1907, *Death of Chopin*, 1885 (detail). Oil on canvas, 43.3 in × 51.6 in/ 110 cm × 131 cm. The National Museum in Krakow, Poland. Muzeum Narodowe w Krakowie, digital collection (https://mnk.pl)

Ars Longa, Vita Brevis

Terence Chorba

"Life is short, art is long, opportunity is ephemeral..."
—Hippocrates, *Aphorisms*

Frédéric François Chopin (born Fryderyk Franciszek Chopin; 1810–1849) was a prolific Poland-born composer and pianist of outstanding technical ability and talent. Although his public career was limited to 30 performances, his contribution as a composer of significant works for piano is unparalleled in its vast array of genres, including ballades, études, impromptus, mazurkas, nocturnes, polonaises, préludes, scherzi, sonatas, and waltzes. All his works included piano and, although he wrote 2 piano concertos and some chamber music, most of his works were written for solo piano.

Chopin was said to have been a sickly child; his younger sister Emilia died at the age of 14 from a rapidly progressive respiratory disease. Drawn by its identity as a center for the arts, he moved to Paris at age 21 and thrived as a master pianist and composer. Chopin continued in ill health throughout adulthood, suffering from shortness of breath, cervical lymphadenitis, night sweats, a persistent cough with copious sputum, and later hemoptysis. His physicians were reluctant to give a diagnosis of tuberculosis, a stigma-laden but probable diagnosis in the 19th century.

Without bacteriology or radiography, a definitive diagnosis of tuberculosis would not have been possible. It was not until March 1882 that Robert Koch announced his discovery of the causative organism of tuberculosis, *Mycobacterium tuberculosis*, and not until late 1895 that Wilhelm Roentgen developed the first radiograph. Thus, the definitive cause of Chopin's death has remained speculative. Given that the composer's sister had died with a similar respiratory affliction, a genetic condition has been proposed as an alternative, the most popular being cystic fibrosis, with its autosomal recessive inheritance pattern. Numerous other diagnoses considered have included aspergillosis, alpha-1 antitrypsin deficiency, granulomatosis with polyangiitis, hypogammaglobulinemia, idiopathic bronchiectasis, mitral stenosis, primary ciliary dyskinesia, tricuspid valve incompetence, pulmonary arteriovenous malformation, pulmonary hemosiderosis, and sarcoidosis, all of which may result in general weakness and nonspecific respiratory symptoms, such as dyspnea and chronic cough.

In 1885, Félix-Joseph Barrias (1822–1907) painted *Death of Chopin*, featured on this month's cover. Barrias was a Paris native whose father was a successful painter on porcelain. Barrias learned the trade and its skills from his father but then became an illustrator and instructor in his own art school. Edgar Degas, a founder of Impressionism, was among Barrias' many distinguished students. Like the works of his younger brother, Louis-Ernest Barrias, a well-renowned sculptor, most of Félix-Joseph Barrias' known canvases have elements of Neoclassicism and Romanticism. Neoclassism is characterized as using the most attractive stylistic elements of the arts and culture of Graeco-Roman antiquity; Romanticism is characterized by emphasis on emotion, individualism, and idealization of heroic figures and their surroundings or environment, as in this portrayal of the death of the composer.

When painting *Death of Chopin*, Barrias may have been inspired by a setting shortly before Chopin's death, described vividly by Hungarian composer Franz

Author affiliation: Centers for Disease Control and Prevention, Atlanta, Georgia, USA

DOI: https://doi.org/10.3201/eid2903.230009

Liszt, also a close friend of Chopin: "[Countess Potocka's] tears were flowing fast when [Chopin] observed her standing at the foot of his bed, tall, slight, draped in white, resembling the beautiful angels created by the imagination of the most devout among the painters… He requested her to sing… The piano was rolled from his parlor to the door of his chamber, while, with sobs in her voice, and tears streaming down her cheeks, his gifted countrywoman sang…. He seemed to suffer less as he listened. She sang the famous Canticle to the Virgin [putatively from Stradella's oratorio for St. John the Baptist (https://youtu.be/qO6i-0AbUGU)]… 'How beautiful it is!' he exclaimed. 'My God, how very beautiful! Again – again!'... Chopin again feeling worse, everybody was seized with fright—by a spontaneous impulse all who were present threw themselves upon their knees—no one ventured to speak; the sacred silence was only broken by the voice of the Countess, floating, like a melody from heaven, above the sighs and sobs which formed its mournful earth accompaniment… A dying light lent its shadows to this sad scene. Chopin's [older] sister [Ludwika] prostrated near his bed, wept, and prayed—and never quitted his attitude of supplication while the life of the brother she so cherished lasted." Most, if not all, of those present would have known that Chopin had dedicated several enlivened, optimistic pieces to the singer including Waltz in D-flat major, Op. 64 (Minute Waltz; https://www.youtube.com/watch?v=3H0SRv8QNwk) and Prelude Op. 28, No 7 (https://www.youtube.com/watch?v=U6vJmHiHBMo), although the somber progressions of Prelude Op. 28, No. 4 (https://www.youtube.com/watch?v=Hj3daBN5F-o) would have been more appropriate to the moment.

Near death, Chopin reportedly asked that his heart not be interred with his body but rather entombed in his native Poland. Ludwika commissioned an autopsy in which his heart was removed and put into a preservative liquid, probably brandy, which was often used for tissue preservation.

Although the rest of Chopin's remains were interred in Paris, Ludwika took the heart back to Poland, where it has remained in the preservative at the Church of the Holy Cross (*Bazylika Świętego Krzyża*) in Warsaw, except when briefly removed from the church under Nazi rule. In April 2014, a team of clergy, scientists, and 2 physicians—1 from the Polish Academy of Sciences' Institute of Human Genetics and 1 from the Institute of Forensic Medicine at Wroclaw Medical University—were allowed to examine the composer's heart visually, without opening its original jar of embalming liquid. Not surprisingly, their assessment was that Chopin had "a serious fibrinoid epicarditis embodied by foci of epicardial hyalinization in the left ventricular front wall and with dilatation, mainly of the right ventricle and right atrium (*cor pulmonale*) with pronounced features of chronic heart failure, predominantly of the right ventricle," consistent with end-stage constrictive pericarditis with fibrosis, and "several glossy, whitish-pearl nodules, slightly protruding from the surface of the myocardium," consistent with myocardial tuberculomas. Those findings are most probably the result of longstanding infection with *M. tuberculosis*.

Other clues to cause of death were provided by sculptor Auguste Clésinger, who shortly after Chopin's death made both a death mask and several casts of his left hand. The bronzes made from the hand casts do not show clubbed fingers—thickening of the distal phalanges caused by hypoxia, characteristic of pulmonary cystic fibrosis. No other physical evidence supports or excludes any potential diagnosis for Chopin other than tuberculosis, a disease for which there was no effective pharmacologic treatment until 1944, when Albert Schatz, Elizabeth Bugie, and Selman Waksman identified streptomycin with bactericidal activity against mycobacteria.

Bibliography

1. Güell-Baró M. A la découverte d'un peintre décorateur oublié: première approche de la vie et de l'oeuvre de Félix Joseph Barrias (1822–1907) [cited 2023 Jan 17]. https://www.latribunedelart.com/margarida-guell-baro-felix-barrias-1822-1907
2. Liszt F. Life of Chopin. 1863 (fourth edition, 1880). Translated from the French by Martha Walker Cook [cited 2023 Jan 6]. https://www.gutenberg.org/files/4386/4386-h/4386-h.htm
3. Pauwels EK. Ten famous composers of the Romantic era and their causes of death. Med Princ Pract. 2022;31:20–8. https://doi.org/10.1159/000521537
4. Rosen C. The romantic generation. Cambridge (MA): Harvard University Press; 1995.
5. Schatz A, Bugie E, Waksman SA, Hanssen AD, Patel R, Osmon DR. Streptomycin, a substance exhibiting antibiotic activity against gram-positive and gram-negative bacteria. 1944. Clin Orthop Relat Res. 2005;437:3–6. https://doi.org/10.1097/01.blo.0000175887.98112.fe
6. Witt M, Dobosz T. Inheritance vs. infectivity as a mechanism of malady and death of Frederic Chopin. J Appl Genet. 2021;62:607–11. https://doi.org/10.1007/s13353-021-00651-2
7. Witt M, Szklener A, Kawecki J, Rużyłło W, Negrusz-Kawecka M, Jeleń M, et al. A closer look at Frederic Chopin's cause of death. Am J Med. 2018;131:211–2. https://doi.org/10.1016/j.amjmed.2017.09.039
8. Witt M, Szklener A, Marchwica W, Dobosz T, Witt M, Szklener A, et al. Disease not genetic but infectious: multiple tuberculomas and fibrinous pericarditis as symptoms pathognomonic for tuberculosis of Frederic Chopin. J Appl Genet. 2018;59:471–3. https://doi.org/10.1007/s13353-018-0456-3

Address for correspondence: Terence Chorba, Centers for Disease Control and Prevention, 1600 Clifton Rd NE, Mailstop US12-4, Atlanta, GA 30329-4027, USA; email: tlc2@cdc.gov

Upcoming Issue

EMERGING INFECTIOUS DISEASES®

April 2023 • Vectorborne Infections

- Challenges in Forecasting Antimicrobial Resistance
- Pediatric Invasive Meningococcal Disease in Auckland, New Zealand, 2004–2020
- *Nocardia pseudobrasiliensis* Co-infection in SARS-CoV-2 Patients
- Monitoring Temporal Changes in SARS-CoV-2 Spike Antibody Levels and Variant-Specific Risk for Infection, Dominican Republic, March 2021–August 2022
- Use of High-Resolution Geospatial and Genomic Data to Characterize Recent Tuberculosis Transmission, Botswana
- Detection of Adeno-Associated Virus 2 and Human Adenovirus Type 41 in Wastewater Coincident to Pediatric Cases of Severe Acute Hepatitis of Unknown Etiology
- Conditions that Facilitated Extensive Spread of SARS-CoV-2 Delta Variant among Vaccinated Persons during 7-Day River Cruise, the Netherlands
- Effectiveness of BNT162b2 Vaccine against Omicron Variant Infection in Children, 5–11 Years of Age, Israel
- Experimental Infection and Transmission of SARS-CoV-2 Delta and Omicron Variants among Beagle Dogs
- Monkeypox Virus Infection in 2 Female Travelers Returning to Vietnam from Dubai, United Arab Emirates, 2022
- Serial Intervals and Incubation Periods of SARS-CoV-2 Omicron and Delta Variants, Singapore
- Reported and Sampling Data for SARS-CoV-2, Verona, Italy, May 2020–2022
- Serial Interval and Incubation Period Estimates of Monkeypox Virus Infection in 12 Jurisdictions, United States, May–August 2022
- Emergence and Persistent Dominance of Omicron BA.2.3.7 Variant, Taiwan
- Ocular Trematodiasis in Children, Sri Lanka
- Highly Pathogenic Avian Influenza A(H5N1) Virus Outbreak in New England Seals, United States
- Yezo Virus Infection in Tick-Bitten Patient and Ticks, Northeastern China
- Tularemia in Pregnant Woman, Serbia, 2018
- Mpox in Young Woman with No Epidemiologic Risk Factors, Massachusetts, USA
- Fatal Infection of Highly Pathogenic Avian Influenza A (H5N1) Virus in *Phocoena phocoena* Harbor Porpoise
- Preventing *Thelazia callipaeda* Reinfection among Humans
- Powassan Virus Infection Detected by Metagenomic Next-Generation Sequencing, Ohio, USA
- Human Metapneumovirus Infections during COVID-19 Pandemic, Spain
- Experimental Infection of North American Deer Mice with Clade 1 and 2 Monkeypox Virus Isolates
- Genomic Characterization of Respiratory Syncytial Virus during 2022–2023 Outbreak, Washington, USA
- Harbor Porpoise Deaths Associated with *Erysipelothrix rhusiopathiae*, the Netherlands, 2021
- SARS-CoV-2 Molecular Evolutionary Dynamics in the Greater Accra Region, Ghana
- Orf Nodule with Erythema Multiforme in Monkeypox Infection Area, France, 2022
- Emergence of SARS-CoV-2 Omicron Variant and Replacement of Delta as Predominate Variant, Puerto Rico
- Model Map of Global Bushmeat Activities to Improve Zoonotic Spillover Surveillance

Complete list of articles in the April issue at https://wwwnc.cdc.gov/eid/#issue-297

Earning CME Credit

To obtain credit, you should first read the journal article. After reading the article, you should be able to answer the following, related, multiple-choice questions. To complete the questions (with a minimum 75% passing score) and earn continuing medical education (CME) credit, please go to http://www.medscape.org/journal/eid. Credit cannot be obtained for tests completed on paper, although you may use the worksheet below to keep a record of your answers.

You must be a registered user on http://www.medscape.org. If you are not registered on http://www.medscape.org, please click on the "Register" link on the right hand side of the website.

Only one answer is correct for each question. Once you successfully answer all post-test questions, you will be able to view and/or print your certificate. For questions regarding this activity, contact the accredited provider, CME@medscape.net. For technical assistance, contact CME@medscape.net. American Medical Association's Physician's Recognition Award (AMA PRA) credits are accepted in the US as evidence of participation in CME activities. For further information on this award, please go to https://www.ama-assn.org. The AMA has determined that physicians not licensed in the US who participate in this CME activity are eligible for AMA PRA Category 1 Credits™. Through agreements that the AMA has made with agencies in some countries, AMA PRA credit may be acceptable as evidence of participation in CME activities. If you are not licensed in the US, please complete the questions online, print the AMA PRA CME credit certificate, and present it to your national medical association for review.

Article Title

Bartonella spp. Infections Identified by Molecular Methods, United States

CME Questions

1. Your patient is a 35-year-old man with suspected bartonellosis. On the basis of the series of broad-range and organism-specific molecular assays at a large clinical reference laboratory by McCormick and colleagues, which one of the following statements about microbiologic characteristics of identified bartonellosis cases is correct?

A. *Bartonella quintana* was the most commonly detected Bartonella spp.
B. No novel *Bartonella* species were detected
C. *Bartonella* spp. were identified from a higher proportion of specimens submitted as formalin-fixed paraffin embedded (FFPE) than as unfixed tissue
D. The total median number of annual specimens submitted for *B. quintana*–specific (bispecies-specific) polymerase chain reaction testing increased over time, going from 18 during 2003–12 to 225 during 2013–21

2. According to the series of broad-range and organism-specific molecular assays at a large clinical reference laboratory by McCormick and colleagues, which one of the following statements about demographic and clinical characteristics of patients with bartonellosis is correct?

A. Most patients were elderly women
B. *B. quintana* was most often identified in lymph node and *B. henselae* in cardiac specimens
C. *B. henselae* was detected in various clinical specimens, including cardiac, hepatic, and bone specimens
D. Of all US states from which specimens were sent, New York and Massachusetts reported the highest number of cases

3. On the basis of the series of broad-range and organism-specific molecular assays at a large clinical reference laboratory by McCormick and colleagues, which one of the following statements about clinical implications of the demographic, clinical, and microbiologic characteristics of patients with bartonellosis is correct?

A. Molecular methods may rapidly identify *Bartonella* spp. infections, which are difficult to diagnose with culture or serology
B. Serology is still preferred for diagnosis of *Bartonella* endocarditis
C. There may be cross-reactivity of antibodies among *Bartonella* spp., but not among non-*Bartonella* pathogens
D. Preanalytical factors such as formalin fixation are the only factors known to limit the sensitivity of molecular methods

Earning CME Credit

To obtain credit, you should first read the journal article. After reading the article, you should be able to answer the following, related, multiple-choice questions. To complete the questions (with a minimum 75% passing score) and earn continuing medical education (CME) credit, please go to http://www.medscape.org/journal/eid. Credit cannot be obtained for tests completed on paper, although you may use the worksheet below to keep a record of your answers.

You must be a registered user on http://www.medscape.org. If you are not registered on http://www.medscape.org, please click on the "Register" link on the right hand side of the website.

Only one answer is correct for each question. Once you successfully answer all post-test questions, you will be able to view and/or print your certificate. For questions regarding this activity, contact the accredited provider, CME@medscape.net. For technical assistance, contact CME@medscape.net. American Medical Association's Physician's Recognition Award (AMA PRA) credits are accepted in the US as evidence of participation in CME activities. For further information on this award, please go to https://www.ama-assn.org. The AMA has determined that physicians not licensed in the US who participate in this CME activity are eligible for AMA PRA Category 1 Credits™. Through agreements that the AMA has made with agencies in some countries, AMA PRA credit may be acceptable as evidence of participation in CME activities. If you are not licensed in the US, please complete the questions online, print the AMA PRA CME credit certificate, and present it to your national medical association for review.

Article Title

Clonal Expansion of Multidrug-Resistant *Streptococcus dysgalactiae* Subspecies *equisimilis* Causing Bacteremia, Japan, 2005–2021

CME Questions

1. Your patient is a 83-year-old man with lung cancer and invasive *Streptococcus dysgalactiae* subspecies *equisimilis* (SDSE) infection. According to the retrospective analysis of 146 bacteremia episodes in 133 patients from 2005 to 2021 by Shinohara and colleagues, which of the following statements about clinical features of SDSE bacteremia and temporal trends in incidence in hospitals in Kyoto-Shiga Region, Japan, is correct?

A. In-hospital mortality was 3.3%
B. Prevalence of multidrug-resistant (MDR) isolates to erythromycin, minocycline, and clindamycin remained stable from 2005–2017 to 2018–2021
C. Most patients were elderly (aged 80–89 years) with underlying diseases and presented with skin and soft-tissue infections or primary bacteremia
D. Overall incidence of group C and group G streptococci (GCGS) and SDSE bacteremia increased by 50% from 2011 to 2020

2. According to the retrospective analysis of 146 bacteremia episodes in 133 patients from 2005 to 2021 by Shinohara and colleagues, which of the following statements about comparative genomic analyses for phylogenetic relationships and recent antimicrobial resistance (AMR) emergence is correct?

A. The most prevalent clonal complex (CC) was CC29, with prevalence increasing over the study period
B. Prevalence of sequence type (ST) ST525 decreased from 2005–2017 to 2018–2020
C. Antibiotic nonsusceptibility rates were much lower for CC25 than for CC17 and CC29
D. In 2018-2021, SDSE isolates acquired 2 AMR genes, ermB and tetM, via Tn916-like integrative and conjugative elements (ICEs)

3. According to the retrospective analysis of 146 bacteremia episodes in 133 patients from 2005 to 2021 by Shinohara and colleagues, which of the following statements about clinical implications of clinical features of SDSE bacteremia and comparative genomic analyses for phylogenetic relationships and AMR emergence is correct?

A. Tn916-like ICEs did not affect emergence and recent increase of MDR SDSE isolates in the Kyoto-Shiga region
B. Ongoing surveillance with whole-genome sequencing is needed to understand and predict trends in MDR SDSE strains linked to Tn916-like 368 ICEs
C. Trends in antimicrobial prescriptions in Japan are likely to reduce prevalence of macrolide-resistant SDSE
D. Demographic trends in Japan and other countries are likely to reduce prevalence of macrolide-resistant SDSE